

Molecular indicators of colorectal cancer cellular response to omega-3 polyunsaturated fatty acids

Catriona Susanne Marshall

Submitted in accordance with the requirements for the degree of
Doctor of Philosophy

The University of Leeds

Faculty of Medicine and Health

May 2021

Intellectual Property and Publication Statements

The candidate confirms that the work submitted is her own, except where work which has formed part of jointly authored publications has been included. The contribution of the candidate and the other authors to this work has been explicitly indicated below. The candidate confirms that appropriate credit has been given within the thesis where reference has been made to the work of others.

The stage of LC-ESI-MS/MS sample analysis detailed in Chapter 3.10.7 was performed by Ms. Amanda Race.

Ms Amanda Race completed the first stages of FA data analysis detailed in Chapter 3.10.8, which included: generating standard calibration curves, measuring sample peak areas and calculating ratio to internal standard and FA percentage ratio calculations. Further data analysis, and all figures relating to this data included within Chapter 5 of this thesis were completed by the candidate.

Reference to MRGPRF work which formed the basis for the hypothesis tested in Chapter 6 (particularly Table 6.3), was carried out by Dr. Milene Volpato and is fully and explicitly indicated as such. Prior to the start of this PhD project, MRGPRF and control vectors were purified and linearised by Dr. Milene Volpato. Any subsequent generation of stable and transient transfectants was completed by myself and Dr. Adam Davidson was responsible for running the sterile cell sort.

Jointly Authored Publication:

Volpato, M., Ingram, N., Perry, S.L., Spencer, J., Race, A.D., Marshall, C., Hutchinson, J.M., Nicolaou, A., Loadman, P.M., Coletta, P.L. and Hull, M. 2020. Cyclooxygenase activity mediates colorectal cancer cell resistance to the omega-3 polyunsaturated fatty acid eicosapentaenoic acid. *Cancer Chemotherapy and Pharmacology*. **87**(2): 173 – 184.

Work attributed to the candidate: acquisition of data. Data used in Figure 1 and supplementary figures S2, S4 and S5 of the publication are included within this thesis.

This copy has been supplied on the understanding that it is copyright material and that no quotation from the thesis may be published without proper acknowledgement.

Acknowledgements

This research was carried out under the supervision of Dr Milene Volpato and Professor Mark Hull. I would like to thank both for answering questions, providing technical and scientific insight, and giving advice over the course of my studentship.

Many thanks to the academics, students, and staff who are / were part of the wider Molecular Gastroenterology team, particularly Dr Louise Coletta, Dr Nicola Ingram and Ms. Sarah Perry who have discussed data and provided feedback during lab meetings.

Many thanks to Professor Paul Loadman and Ms Amanda Race, from the Institute of Cancer Therapeutics (University of Bradford), for providing training, assisting with experiments, and for in-depth data analysis discussions. Thanks to the Beech lab group, in particular Alan Burnett, for the training and support whilst visiting their facility.

I would like to acknowledge Dr Adam Davison and Dr Rachel Barlow who trained me on kit and give thanks the Wellcome Trust Brenner Building (WTBB) infrastructure assistants.

I would like to thank the PGR students who I have worked alongside in the WTBB at St James's University Hospital, for their friendship both in and out of the lab.

Finally, I would like to thank my family and friends. They have been my biggest supporters over the last 4 years... and have never complained about looking after my dog whilst I was at the lab.

Abstract

Colorectal cancer (CRC), the UK's second most lethal cancer, has limited treatment options for unresectable and metastatic tumours. An unmet clinical need for alternative treatments exists. Omega-3 polyunsaturated fatty acids (*n*-3 PUFAs), eicosapentaenoic acid (EPA) and docosahexaenoic acid (DHA) are safe and well tolerated. EPA is licenced for prophylaxis of cardiovascular events in high risk individuals and shows promise as an anti-cancer agent to prevent and treat CRC. *n*-3 PUFA anti-cancer mechanisms are not understood. I aimed to identify biomarkers associated with, or predictive of, CRC cell line response to *n*-3 PUFAs.

To study intrinsic resistance, *n*-3 PUFA responses were characterised for 17 human CRC (hCRC) cell lines by concentration-response viability assays. The cell line panel represented key molecular characteristics; CIN, MSI and CIMP. mRNA expression of *PTGS1* and *PTGS2* were measured by RT-qPCR. FA content was measured by LC-ESI-MS/MS. Relationships between hCRC cell *n*-3 PUFA response, molecular characteristics, and fatty acid (FA) content were examined. To study acquired *n*-3 PUFA resistance, cells were chronically exposed to individual *n*-3 PUFAs and, separately, MRGPRF was overexpressed.

EPA and DHA sensitivity were not correlated. DHA was effective at inhibiting cell growth at lower concentrations than EPA. CIMP+ cell lines were more EPA-sensitive than CIMP- cells. FA analysis found no association between EPA/DHA content before/after *n*-3 PUFA supplementation and hCRC cell *n*-3 PUFA sensitivity. Percentage FA data complement published reports of decreased arachidonic acid (AA) content following *n*-3 PUFA supplementation. Preliminary analysis investigating cellular FA absolute amounts, may indicate that AA content was not reduced in all cell lines. Furthermore, EPA-resistant cells may have increased DPA compared to EPA-sensitive cells.

Overall, data indicated potential benefits of using DHA *in vivo* and clinically. CIMP+ tumour responses to EPA require further investigation to identify mechanisms, or genes downregulated by methylation, that drive resistance.

Table of Contents

Intellectual Property and Publication Statements	ii
Acknowledgements	iii
Abstract	iv
Table of Contents	v
List of Tables	x
List of Figures	xii
Chapter 1: Colorectal cancer and omega-3 polyunsaturated fatty acids	1
1.1. The structure and function of the colon and rectum	1
1.2. Colorectal Cancer	2
1.2.1. Clinical presentation of colorectal cancer	2
1.2.2. Molecular pathology of CRC	5
1.2.3. CRC Treatments	11
1.3. Omega-3 Polyunsaturated Fatty Acids	17
1.3.1. What are nutrients?	17
1.3.2. Biochemistry of <i>n</i> -3 PUFAs	17
1.3.3. Cellular metabolism of <i>n</i> -3 PUFAs	19
1.3.4. Clinical use of <i>n</i> -3 PUFAs	23
1.4. Evidence supporting anti-CRC activity of <i>n</i> -3 PUFAs	23
1.4.1. Epidemiological evidence supporting anti-cancer <i>n</i> -3 PUFA activity	23
1.4.2. Preclinical evidence supporting anti-cancer <i>n</i> -3 PUFA activity	24
1.4.3. Clinical evidence supporting anti-cancer <i>n</i> -3 PUFA activity	26
1.5. <i>N</i> -3 PUFAs anti-cancer mechanisms of action	27
1.5.1. Direct effects of <i>n</i> -3 PUFA on cellular response	28
1.5.2. Modulation of COX metabolism	29
1.5.3. G protein coupled receptor signalling	30
1.5.4. Indirect anti-CRC effects of <i>n</i> -3 PUFAs	31
Chapter 2: Aims and hypotheses	33
2.1. Aim	33
2.2. Hypotheses	33
Chapter 3: Materials and Methods	35
3.1. Stock preparation	35
3.1.1. Fatty acids	35
3.1.2. Epigenetic drugs	35
3.2. Cell Culture	36
3.2.1. Cell Lines Used	36
3.2.2. Routine passage and growth conditions	36
3.2.3. Routine cell cryopreservation	36
3.3. Molecular Profiling of Cell Lines	38
3.3.1. Genomic DNA extraction	38
3.3.2. Short tandem repeat profiling of human CRC cell lines	38
3.3.3. Microsatellite Stability Testing	39

3.4.	Cell viability assays	41
3.4.1.	MTT Assay	41
3.4.2.	Crystal Violet Assay (alternative to MTT)	42
3.4.3.	Cell Treatments	43
3.4.4.	Cell viability assay analysis	43
3.4.5.	Growth rate of hCRC cell lines	44
3.4.6.	EPA and DHA interaction analysis	44
3.5.	Generating Resistance: Chronic Exposure Experiments	45
3.5.1.	IC ₅₀ and escalating dose treatment	45
3.5.2.	High concentration range selection	45
3.6.	<i>PTGS1</i> and <i>PTGS2</i> gene expression model	47
3.6.1.	Developing a <i>PTGS1</i> and <i>PTGS2</i> gene overexpression positive control	47
3.7.	Mammalian cell MRGPRF overexpression model	50
3.8.	RNA Extraction Methods	52
3.9.	Real-time PCR: quantitative polymerase chain reaction	52
3.9.1.	Primer details	52
3.9.2.	RNA processing for qPCR analysis	53
3.9.3.	qPCR: quantitative polymerase chain reaction	55
3.10.	Fatty Acid Content Analysis by LC-ESI-MS/MS	57
3.10.1.	Reagents	57
3.10.2.	Sample preparation	58
3.10.3.	Fatty Acid Extraction	58
3.10.4.	Fatty Acid Hydrolysis for total fatty acids	60
3.10.5.	Derivatisation of Fatty Acids	60
3.10.6.	Standard Curve Preparation	60
3.10.7.	LC-ESI-MS/MS Sample Analysis	61
3.10.8.	LC-ESI-MS/MS Data Analysis	61
3.11.	MRGPRF protein analysis	62
3.11.1.	Cell Lysate Preparation	62
3.11.2.	MRGPRF protein expression detection by Immunofluorescence	63
3.11.3.	MRGPRF protein expression detection by dot blot	64
3.11.4.	MRGPRF Protein detection by Flow Cytometry	65
3.11.5.	Calcium Assay: Assessment of MRGPRF functionality in overexpression models.	66
3.12.	Exploitation of public databases	71
3.12.1.	Development Therapeutics Program	71
3.13.	Statistical analysis	71
Chapter 4:	Characterising human colorectal cancer cell lines and response to EPA and DHA	72
4.1.	Introduction	72
4.1.1.	Sensitivity of CRC cell lines to <i>n</i> -3 PUFAs	72
4.1.2.	Metabolism of <i>n</i> -3 PUFAs: <i>PTGS</i> activity	73
4.1.3.	Modelling CRC <i>in vitro</i>	74
4.1.4.	Associations between molecular phenotypes, CRC and response to <i>n</i> -3 PUFAs	74

4.1.5.	Epigenetics	75
4.2.	Objectives	77
4.3.	Results	78
4.3.1.	Characterisation of the CRC cell line panel	78
4.3.2.	Optimisation of a gene expression assay to study <i>PTGS</i> 1 and 2 expression in human CRC cell lines	79
4.3.3.	<i>PTGS1</i> and <i>PTGS2</i> gene expression in hCRC cell lines	82
4.3.4.	Sensitivity of CRC cell lines to <i>n</i> -3 PUFAs	83
4.3.5.	Relationships between cellular properties and <i>n</i> -3 PUFA sensitivity	92
4.3.6.	Investigating the effect of epigenetic drug treatment on cell sensitivity to <i>n</i> -3 PUFAs	101
4.3.7.	Impact of epigenetic drug pre-treatment on <i>n</i> -3 PUFA sensitivity of CIMP+ and CIMP- hCRC cell lines	103
4.4.	Discussion	108
4.4.1.	Key Findings	108
4.4.2.	Strengths and Limitations	112
4.4.3.	Future directions	114
Chapter 5: Investigating the relationship between human CRC cell line sensitivity to <i>n</i> -3 PUFAs and cellular FA content		117
5.1.	Using LC-ESI-MS/MS to measure fatty acid content in colorectal cancer cell lines	117
5.1.1.	Presence of FAs in cells	117
5.1.2.	How FAs are measured in biological systems	117
5.1.3.	FA content measured in CRC cell lines	118
5.1.4.	FA content measured in human CRC tissues	118
5.2.	Chapter objectives	119
5.3.	Results	120
5.3.1.	Inter-assay variability	120
5.3.2.	FA profiles of hCRC cell lines treated with EPA or DHA	123
5.3.3.	Assessing the relationship between <i>PTGS1</i> and <i>PTGS2</i> gene expression and FA content	133
5.3.4.	Relationship between FA content and cell line sensitivity to <i>n</i> -3 PUFAs	136
5.3.5.	Evaluating whether the cell ability to metabolise EPA to DPA and DHA has any effect on cell sensitivity	140
5.3.6.	Comparison of cells <i>n</i> -3 PUFA content in CIMP+ and CIMP- cell lines	144
5.3.7.	Impact of decitabine pre-treatment on <i>n</i> -3 PUFA content of hCRC cell lines in the presence or absence of EPA supplementation	146
5.4.	Discussion	148
5.4.1.	Key findings	148
5.4.2.	Strengths and Limitations	152
5.4.3.	Future Directions	153
Chapter 6: Investigating CRC cell response to <i>n</i> -3 polyunsaturated fatty acids using isogenic clones with acquired resistance		154
6.1.	Introduction	154
6.1.1.	Identification of <i>Mrgprf</i> , a novel orphan G protein coupled receptor (GPCR)	154
6.1.2.	Mas-related G protein coupled receptor, F (<i>Mrgprf</i>)	155

6.1.3.	G protein coupled receptors	156
6.1.4.	Drug resistance in colorectal cancer	157
6.1.5.	Investigating <i>n</i> -3 PUFA resistance in colorectal cancer cell lines	158
6.2.	Chapter Objectives:	159
6.3.	Results I: Investigating the potential role of MRGPRF in EPA sensitivity	160
6.3.1.	Selection of MRGPRF overexpressing clones	160
6.3.2.	Characterisation of MRGPRF overexpressing clones	162
6.3.3.	Validation of stable <i>Mrgprf</i> overexpressing clones by RT-qPCR	165
6.3.4.	Validation of the stable <i>Mrgprf</i> overexpressing clones by interrogating protein expression	172
6.3.5.	MRGPRF overexpression does not alter CRC cell response to EPA	182
6.3.6.	Assessing the effect of EPA exposure on calcium mediated signalling in MRGPRF overexpressing clones	185
6.4.	Results II: Generating resistance to <i>n</i> -3 PUFAs in hCRC cell lines	191
6.4.1.	CRC cell lines have variable sensitivities to EPA and DHA	191
6.4.2.	The effect of ethanol exposure on cell morphology	191
6.4.3.	Using high concentrations of <i>n</i> -3 PUFAs to place selective pressure on CRC cells to generate resistance	193
6.4.4.	Using incremental selective pressure to induce the emergence of a resistant population	196
6.5.	Discussion	204
6.5.1.	MRGPRF	204
6.5.2.	Generating resistance	211
Chapter 7: General Discussion		213
7.1.	Challenges of understanding resistance to <i>n</i> -3 PUFAs which act via multiple direct and indirect mechanisms of action	214
7.1.1.	Studying direct effects using <i>in vitro</i> cell models of CRC	215
7.1.2.	Limitations of <i>in vitro</i> models for study of <i>n</i> -3 PUFA effects	216
7.2.	Limitations of cell lines for studying indirect <i>n</i> -3 PUFA effects	217
7.2.1.	Tumour microenvironment	217
7.2.2.	The microbiome	219
7.3.	Biomarker discovery to improve CRC outcomes	221
7.3.1.	Comparing <i>n</i> -3 PUFA measurements <i>in vitro</i> and patient samples	222
7.4.	Towards clinical use of <i>n</i> -3 PUFAs for treatment of CRC	222
7.4.1.	Combination with traditional chemotherapy	226
7.4.2.	Combination with nutraceuticals	226
7.5.	Challenges of stratifying use of <i>n</i> -3 PUFAs for CRC treatment	226
7.6.	Conclusion	227
List of References		I
List of Abbreviations		XXIII
Appendix		XXVII
A4.1.	STR profiling	XXVII
A4.2.	Microsatellite status confirmed of HT29, HCT116 and HCA-7 cells	XXIX
A4.3.	Associations between molecular phenotypes and <i>n</i> -3 PUFA sensitivity	XXX
A4.4.	DAC pre-treatment effect on DHA concentration response curves	XXXI

A5.1.	Standard Curves	XXXII
A5.2.	LC-ESI-MS/MS Chromatograms	XXXIII
A5.3.	IC ₅₀ concentrations.	XXXVI
A5.4.	FA profiles (%) of all cell lines	XXXVII
A5.5.	FA profiles (absolute amount) of all cell lines	XLIII
A5.6.	DPA and DHA content at following treatment with ethanol carrier control and 5µM EPA	XLIX
A5.7.	Statistical analysis of FA content analysis by molecular subgroup and following DAC exposure	L
A6.1.	Fluorescence Activated Cell Sorting: GFP gating	LI
A6.2.	RNA quantity and RT-qPCR output data for HEK293 clones	LII
A6.3.	Assessing whether EPA stimulation of MRGPRF clones induced cAMP signalling	LIII

List of Tables

Table 1.1.	TNM and Dukes' staging criteria for CRC	5
Table 1.2.	In vitro studies investigating n-3 PUFA activity in hCRC cells	25
Table 3.1.	Cell line general information	37
Table 3.2.	Primer sequences for BAT-25 and BAT-26 microsatellite stability markers	39
Table 3.3.	n-3 PUFA IC ₁₀ and IC ₅₀ concentrations	45
Table 3.4.	Restriction enzymes used	49
Table 3.5.	Primers to amplify human target mRNA sequences	54
Table 3.6.	Primers to amplify mouse target mRNA sequences	54
Table 3.7.	Fatty acid standards	57
Table 3.8.	Standard Buffer Solution (SBS)	68
Table 3.9.	Compound plate contents	70
Table 3.10.	Flex station settings	70
Table 4.1.	Human colorectal cancer cell line molecular classifications	78
Table 4.2.	Cell line categorised by CIN, MSI and CIMP status	79
Table 4.3.	Human colorectal cancer cell line sensitivity to n-3 PUFAs	83
Table 4.4.	Cell lines exhibiting a biphasic response to EPA	84
Table 4.5.	Cell viability in cells exposed to combination treatment and corresponding individual n-3 PUFA concentrations	91
Table 4.6.	Sensitivity of hCRC cell lines to epigenetic agents TMZ, 5-AZA and DAC	102
Table 4.7.	Sensitivity of CIMP- cell lines to EPA following pre-treatment with TMZ	103
Table 4.8.	Sensitivity of hCRC cell lines to EPA and DHA in presence and absence of 5-AZA and DAC	106
Table 5.1.	Standard curve concentration measurements	121
Table 5.2.	Fatty acid profile of fetal calf serum	122
Table 5.3.	FA concentration in different media supplemented with 10% FCS	122
Table 6.1.	Candidate genes identified by microarray analysis of mouse CRC cells	155
Table 6.2.	Characteristics of HEK293-CT _{VL} clones and parental HEK293 cells	163
Table 6.3.	Characteristics of HEK293-MF _{VL} clones	164
Table 6.4.	RNA quantity and RT-qPCR output data of MC38r stable clones	169
Table 6.5.	Clone selection for protein expression, EPA sensitivity and functionality studies	171
Table 6.6.	Summary of EPA and DHA IC ₅₀ data of CRC cell lines	191
Table 6.7.	Effect of chronic EPA exposure upon EPA sensitivity (IC ₅₀)	195
Table 6.8.	Effect of chronic DHA exposure upon DHA sensitivity (IC ₅₀)	196
Table 7.1.	Prescription n-3 PUFA products for cardiovascular disease	223
Table A4.1.	Loci detected by STR profiling and the expected base pair ranges	XXVII
Table A4.2.	Summary STR trace matches to database profiles	XXVII
Table A5.1.	Cell line dependent IC ₅₀ equivalent concentrations	XXXVI
Table A5.2.	Relative percentage FA profile of EPA ethanol control treated cells	XXXVII
Table A5.3.	Relative percentage FA profile of 5µM EPA treated cells	XXXVIII
Table A5.4.	Relative percentage FA profile of high concentration EPA treated cells	XXXIX
Table A5.5.	Relative percentage FA profile of DHA ethanol control treated cells	XL
Table A5.6.	Relative percentage FA profile of 5µM DHA treated cells	XLI
Table A5.7.	Relative percentage FA profile of high concentration DHA treated cells	XLII
Table A5.8.	FA profile of EPA ethanol control treated cells expressed as absolute amount	XLIII
Table A5.9.	FA profile of 5µM EPA treated cells expressed as absolute amount	XLIV
Table A5.10.	FA profile of high concentration EPA treated cells expressed as absolute amount	XLV
Table A5.11.	FA profile of DHA ethanol control treated cells expressed as absolute amount	XLVI
Table A5.12.	FA profile of 5µM DHA treated cells expressed as absolute amount	XLVII
Table A5.13.	FA profile of high concentration DHA treated cells expressed as absolute amount	XLVIII
Table A5.14.	Differences in n-3 PUFA content of carrier and 5µM EPA (or 5µM DHA) treated CRC cells between molecular subtypes	L

Table A5.15.	Differences in n-3 PUFA content of carrier, DAC, EPA, and combined DAC + EPA treated HCT116 and LS174T cells	L
Table A6.1.	RNA quantity and RT-qPCR output data of HEK293 stable clones	LII

List of Figures

Figure 1.1.	Structure of the colon and CRC tumour staging	1
Figure 1.2.	Pathogenesis of CRC: the adenoma-carcinoma sequence	6
Figure 1.3.	Consensus molecular subtypes of CRC	11
Figure 1.4.	Clinical, molecular, CMS and treatment differences between CRC tumour sites ..	16
Figure 1.5.	N-3 and n-6 polyunsaturated fatty acids (PUFAs)	18
Figure 1.6.	Activity of elongase and desaturase enzymes in the metabolism of LA and LNA ..	20
Figure 1.7.	Metabolic fate of AA, EPA and DHA	22
Figure 1.8.	Mechanisms through which n-3 PUFAs exert anti-cancer effects on hCRC cells ..	32
Figure 3.1.	Reduction of MTT to crystal formazan salt.	41
Figure 3.2.	Vector insert containing selected amplicons	47
Figure 3.3.	MRGPRF expression vector map	50
Figure 3.4.	The process of sample preparation for FA analysis by LC-ESI-MS/MS	59
Figure 3.5.	Fluorescence excitation spectrum of Fura2-AM	67
Figure 4.1	GAPDH Standard curve	80
Figure 4.2	PTGS1 Standard curve	80
Figure 4.3	PTGS2 Standard curve	81
Figure 4.4	Expression of PTGS1 and -2 genes in human CRC cell lines	82
Figure 4.5	CRC cell line concentration response curves to n-3 PUFAs	88
Figure 4.6	Extrapolation of n-3 PUFA concentration response curves	90
Figure 4.7	Correlation between growth rate and n-3 PUFA sensitivity	93
Figure 4.8	Associations between PTGS1 expression and n-3 PUFA sensitivity	95
Figure 4.9	Associations between PTGS2 expression and n-3 PUFA sensitivity	96
Figure 4.10	Associations between combined PTGS expression and n-3 PUFA sensitivity ...	97
Figure 4.11	Associations between n-3 PUFA sensitivity and CIN status	98
Figure 4.12	Associations between n-3 PUFA sensitivity and MS status	99
Figure 4.13	Associations between n-3 PUFA sensitivity and CIMP status	99
Figure 4.14	EPA sensitivity (IC ₅₀) of cell lines grouped by molecular phenotype	100
Figure 4.15	TMZ hCRC concentration response curves	101
Figure 4.16	5-AZA and DAC hCRC concentration response curves	102
Figure 4.17	EPA concentration response curves in hCRC cell lines pre-treated with varied concentrations of TMZ	104
Figure 4.18	EPA concentration response curves in hCRC cell lines pre-treated with varied concentrations of demethylating drugs, 5-AZA and DAC	107
Figure 5.1.	Standard curves for EPA and DHA quantification	121
Figure 5.2.	The effect of EPA exposure on EPA content of human colorectal cancer cell lines	124
Figure 5.3.	The effect of DHA exposure on DHA content of human colorectal cancer cell lines	125
Figure 5.4.	Fatty acid profile of ethanol control samples	129
Figure 5.5.	The effect of EPA supplementation on arachidonic acid (AA) content of CRC cell lines	131
Figure 5.6.	The effect of DHA supplementation on arachidonic acid (AA) content of CRC cell lines	132
Figure 5.7.	PTGS gene expression and EPA content in hCRC cells	134
Figure 5.8.	PTGS gene expression and DHA content in hCRC cells	135
Figure 5.9.	The effect of n-3 PUFA treatment concentration on absolute amount measured ..	136
Figure 5.10.	Correlation between EPA sensitivity and absolute EPA content	137

Figure 5.11.	Correlation between EPA sensitivity and EPA content relative to content in carrier-treated controls	138
Figure 5.12.	Correlation between DHA sensitivity and absolute DHA content	139
Figure 5.13.	Correlation between DHA sensitivity and DHA content relative to carrier-treated cell content	139
Figure 5.14.	Impact of EPA supplementation on hCRC cell DHA absolute amount	140
Figure 5.15.	Impact of EPA supplementation on hCRC relative DHA content	141
Figure 5.16.	Impact of EPA supplementation on hCRC cell DPA absolute amount	141
Figure 5.17.	Impact of EPA supplementation on DPA content measured in hCRC cell lines	143
Figure 5.18.	Relationship between CIMP status and n-3 PUFA content in hCRC cells	145
Figure 5.19.	Effect of DAC pre-treatment on EPA, DPA and DHA content	147
Figure 6.1	G protein coupled receptor signaling pathways	157
Figure 6.2	Generating n-3 PUFA resistant cell lines	158
Figure 6.3	Generation of MRGPRF stable overexpressing cell lines.....	161
Figure 6.4	MC38r cells in culture.....	165
Figure 6.5	Transient transfected HEK293 cell characteristics	166
Figure 6.6	mRNA Mrgprf expression in transient and stably transfected HEK293 cells	168
Figure 6.7	mRNA Mrgprf expression in transient and stably transfected MC38r cells	170
Figure 6.8	Using N-14 to detect MRGPRF protein expression in HEK293 and MF _{VL} clone C3 cells.....	173
Figure 6.9	Confirmation of Stable transfectants GFP expression by flow cytometry	174
Figure 6.10	The effect of variable antibody concentrations on median fluorescent intensity shifts calculated between HEK293-CT _{VL} clone B4 and HEK293-MF _{VL} clone C3 cells	175
Figure 6.11	The effect of MRGPRF overexpression on fluorescence intensity	176
Figure 6.12	Comparison of fluorescence detected in unfixed and fixed cells	176
Figure 6.13	MRGPRF protein expression in stable transfectants.....	177
Figure 6.14	Antibody optimisation of anti-MRGPRF antibody, HPAMF to visualise MRGPRF protein in stable transfected cells.....	179
Figure 6.15	Immunofluorescent labelling of the MRGPRF receptor in HEK293 stably transfected clones	180
Figure 6.16	Immunofluorescent labelling of MC38r stably transfected clones	181
Figure 6.17	Sensitivity of stable HEK293 transfectants to EPA	183
Figure 6.18	Sensitivity of stable MC38r transfectants cell lines to EPA.....	184
Figure 6.19	Intracellular Ca ²⁺ response to Tg	186
Figure 6.20	Comparing F340/390 in Fura-2AM loaded and non-loaded cells expressing eGFP.....	187
Figure 6.21	Effect of EPA exposure on intracellular calcium levels	188
Figure 6.22	Measurement of F340/380 ratio for 200s to monitor response of cell lines to Thapsigargin, ATP and EPA.	190
Figure 6.23	Impact of chronic ethanol exposure on cell growth.....	192
Figure 6.24	The impact of high concentration EPA and DHA exposure for 1 week on CRC cell lines	193
Figure 6.25	Impact of prolonged 200µM EPA on HCT116 cell morphology	194
Figure 6.26	EPA concentration response curves of CRC cell lines which were selected following exposure to high concentrations of EPA.....	195
Figure 6.27	DHA concentration response curves of CRC cell lines which were selected following exposure to high concentrations of DHA	196
Figure 6.28	Effect of chronic EPA exposure on cell morphology	197
Figure 6.29	The effects of EPA and DHA chronic exposure on DLD-1 cells	199
Figure 6.30	The effect of chronic DHA exposure on HCA-7 cells.....	200
Figure 6.31	The effect of chronic EPA and DHA exposure on HCT116 cells	201
Figure 6.32	The effect of chronic EPA and DHA exposure on HT29 cells.....	202
Figure 6.33	Chronic exposure of LoVo cells to IC ₅₀ DHA	203
Figure 6.34	The effect of DHA chronic exposure on MC38 cells	203
Figure 6.35	MRGPRF localization determined by Human Protein Atlas.....	206

Figure 7.1. Key immune cells found in the microenvironment surrounding a CRC tumour 220

Figure A4.1	Representative STR trace for Colo205 cells.....	XXVIII
Figure A4.2	Representative traces of HT29, HCT116 and HCA-7 cells.....	XXIX
Figure A4.3	DHA IC ₅₀ sensitivity of cell lines grouped by molecular phenotype	XXX
Figure A4.4	EPA:DHA (2:1) sensitivity of cells grouped molecular phenotype	XXX
Figure A4.5	DHA concentration response curves for cells following DAC pre-treatment.....	XXXI
Figure A5.1	Standard curves for all FAs measured.....	XXXII
Figure A5.2	Chromatograms of 10000 ng/ml standard	XXXIII
Figure A5.3	Chromatograms of ethanol treated HT29 cells	XXXIV
Figure A5.4	Chromatograms of high concentration EPA treated HT29 cells	XXXV
Figure A5.5	Absolute content of DPA and DHA following treatment with ethanol carrier and 5µM EPA	XLIX
Figure A6.1	eGFP gating in MC38r stable transfectants	LI
Figure A6.2	cAMP production in stable transfectants.....	LIII

Chapter 1: Colorectal cancer and omega-3 polyunsaturated fatty acids

1.1. The structure and function of the colon and rectum

To understand clinical presentation and staging descriptions of colorectal cancer (CRC), basic structure and functions of the colon and rectum need to be understood. The colon and rectum are parts of the digestive system, and are components of the large intestine along with the cecum and anal canal (1). They have a role in enabling the body to obtain energy through food and with excreting waste products.

The colon and rectum are tubes built up by layers of tissue [Figure 1.1]. First, the mucosa is an inner lining made up of a thin layer of epithelial cells (epithelium), a layer of connective tissue (lamina propria) and a thin muscle layer (muscularis mucosa) (2). Surrounding the mucosa is connective tissue named the submucosa, containing mucous glands, blood vessels, lymph vessels and nerves. Next, a thick layer of muscle named the muscularis propria, comprising an inner ring of circular muscle fibres and an outer ring of long muscle fibres, surrounds the wall of the colon and rectum. Finally, the serosa is the outer layer of the colon, however this layer is not found on the rectum (2).

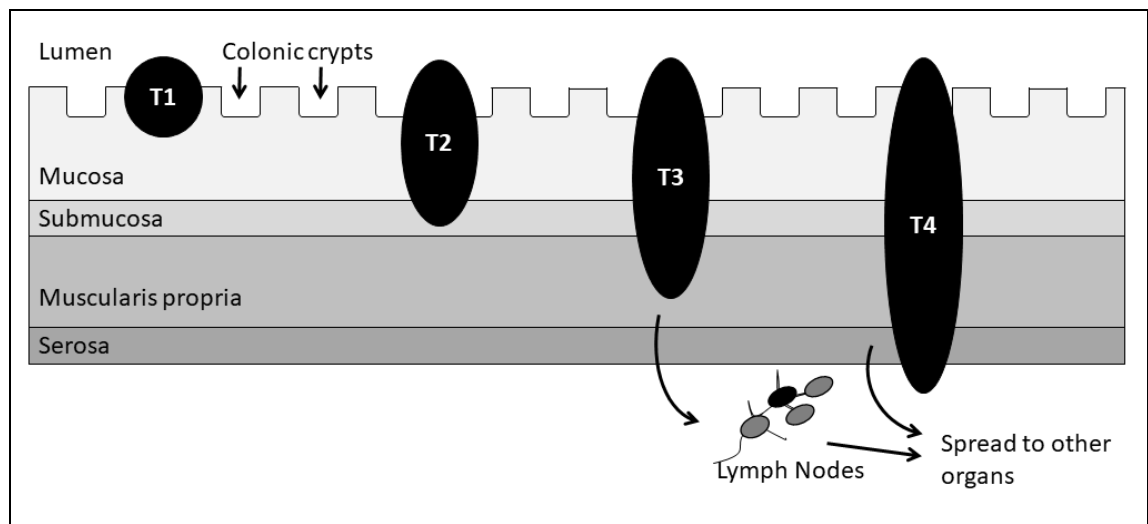


Figure 1.1. Structure of the colon and CRC tumour staging

A cross-sectional representation of the layered structure of the colon wall, which consists of the mucosa, submucosa, muscularis propria and serosa (the rectum does not include the serosa layer). The black shapes represent the growth and development of cancer, and the staging (T1 – T4) is shown as the adenoma invades the various layers. T3 and T4 tumours are more likely to have metastasized to other regions of the body such as the lymph nodes and / or distant organs such as the liver. Image is adapted from (3, 4).

The gastrointestinal tract is colonised by bacteria. The microbiome is composed of between 10^{13} and 10^{14} microorganisms (5) and is found to be imbalanced (dysbiosis) in

CRC patients, with increased presence of *Fusobacterium*, *Peptostreptococcus*, *Prophyromonas*, *Prevotella*, *Parvimonas*, *Bacteroides* and *Gemella* in the diseased state (6). Increase presence of 'harmful' bacteria corresponds with decreased butyrate-producing bacteria and altered levels of gut microbial metabolites such as short-chain fatty acids (SCFAs) and polyamines, both of which are associated with cancer progression and metastasis (7, 8).

Partially digested food from the cecum is moved into the colon. Removal of water and further breakdown of food, aided by bacteria, allows for the absorption of nutrients and electrolytes (2).

1.2. Colorectal Cancer

In 2000 and 2010, Hanahan and Weinberg published 'The Hallmarks of Cancer' and 'Hallmarks of cancer: the next generation' in Cell. These reviews outline key features of cancer cells; self-sufficiency in growth signals, insensitivity to anti-growth signals, tissue invasion and metastasis, limitless replicative potential, sustained angiogenesis, evasion of apoptosis (9), deregulation of cellular energetics, avoidance of immune destruction, genomic instability and mutations and tumour promoting inflammation (10). Elucidating these hallmarks furthered understanding of the complex biology of cancer, explaining how cancer cells are able to acquire growth-promoting capabilities during a multi-step developmental process (10). Targeting molecular pathways that allow for the modification of normal cells to become cancer cells, or the pathways that allow cancer cells survival advantages, have become the focus of anti-cancer therapeutics.

1.2.1. Clinical presentation of colorectal cancer

CRC develops from epithelial cells within the colon or rectum (11, 12). Right-sided (proximal) tumours tend to be mucinous adenocarcinomas (13) or arise from sessile serrated adenomas (14). Mucinous tumours secrete large quantities of mucous (15) and serrated tumours have a characteristic serrated appearance evident when histologically examined (16). Left-sided (distal) tumours tend to be tubular, villous adenocarcinomas (17). Approximately, one third of CRC cases are rectal cancer (18).

1.2.1.1. Symptoms of CRC

Diagnosis of CRC can be challenging, as it can be asymptomatic or symptoms that arise may be attributed to other conditions such as irritable bowel syndrome, diverticulitis,

haemorrhoids, or infections. As normal function of the colon and rectum are involved in digestion of food resulting in the production and removal of stool from the body, symptoms of CRC arise from abnormalities in these processes. Symptoms include; a change in bowel habits (diarrhea or constipation), feeling like a bowel movement is needed (with no relief if there is one), rectal bleeding with bright red blood, blood in the stool, cramping and abdominal pain, weakness and fatigue and unintended weight loss (19).

1.2.1.2. Population Incidence

In 2016, CRC was the fourth most common cancer in the United Kingdom (UK), accounting for 12 % of all cancer cases (20). Within the UK, incidence of CRC differs between females and males, with it remaining stable for the former and declining for the latter. Reduced CRC incidence can be attributed to screening which facilitates pre-cancerous lesion removal and risk factor reduction (21).

1.2.1.3. CRC risk factors

CRC risk has been associated with age, genetic, dietary, and environmental factors. Risk increases with age, 14 % of new cancer cases in males and females is attributed to CRC in elderly patients aged 75 and over, in comparison to 10 % and 5 % in males and females respectively in patients aged between 25 and 49 (22). Although current predictions estimate that incidence rates for colon and rectal cancers will fall by 11 % between 2014 and 2035 (23), patients aged 20 to 34 will increase by 90.0 % to 124.2 % (24). In the UK, CRC is attributed to 10 % of cancer-related deaths, making it the second most common cause of cancer associated mortality (23). One report estimates that by 2030 the global burden of CRC will increase by 60 %, to over 2.2 million new cases and 1.1 million annual deaths (25).

Sporadic CRCs develop in patients with no inherited genetic predisposition or family history of the disease and account for 95 to 98 % of all new diagnoses. Hereditary colorectal cancers account for 2 to 5 % of all colon cancers, and arise due to well-defined inherited syndromes including; Lynch syndrome, familial adenomatous polyposis (FAP), mutY DNA glycosylase (MUTYH)-associated polyposis and hamartomatous polyposis conditions (26). Lynch syndrome and FAP are associated with earlier onset of disease and are associated with mutations in deoxyribonucleic acid (DNA) mismatch repair (MMR) genes and germline adenomatous polyposis coli (APC) gene mutation respectively (26).

An increased risk of CRC development has also been associated with inflammatory bowel diseases (IBD), particularly Ulcerative colitis (UC), obesity, red and processed meat consumption, alcohol intake, immunosuppressive medication, diabetes mellitus and abdominal radiation exposure (24).

1.2.1.4. Clinical staging

The National Institute for Health and Care Excellence (NICE) produce evidence-based guidance and advice for doctors as well as developing quality standards and performance metrics for health care providers (27). An adult with suspected CRC should be provided with information and support and undergo diagnostic investigations which may include colonoscopy, computed tomographic (CT) colonoscopy, flexible sigmoidoscopy or barium enema (28). When CRC is diagnosed, molecular testing is offered, whereby immunohistochemistry (IHC) is used to detect mismatch repair (MMR) proteins (MLH1, MSH2, MSH6 and PMS2) or microsatellite instability (MSI) (28).

Staging is used to classify the cancer and can be informative for treatment options and regimens. CT, magnetic resonance imaging (MRI) and endorectal ultrasounds can be used as part of the staging assessment. The recommended staging system is the Tumour Node Metastases (TNM) staging system, the most recent guidelines of which are outlined in the TNM Classification of Malignant Tumours staging system (Fifth Edition) in line with the Royal College of Pathologists. **Table 1.1** (below) outlines TNM staging and how it corresponds with the historically used Dukes' staging system. In addition, **Figure 1.1** (above) shows how the staging system relates to tumour growth and invasion of tissues.

1.2.1.5. Disease progression

Metastasis is the process whereby cancer cells originating at a primary site migrate, via the bloodstream or lymphatic system (29), to colonise and invade adjacent or distant tissues (9). For many cancers, metastatic spread reduces patient prognosis. Metastatic disease is more difficult to treat and thus more likely to be fatal (30). Approximately 20 % of patients with CRC present with synchronous metastatic disease (30) at diagnosis and 33 % of patients develop distant metachronous metastases in the five year period following a primary tumour resection (31). CRC metastases are commonly found in the brain, lungs, bone, and peritoneum. Development of CRC metastases in the liver (CRCLM) is most common, with the portal venous system suspected in facilitating disease spread. Pathology of development of CRCLM is poorly understood

mechanistically (30). Unfortunately, due to the proximity of tumours to major blood vessels, small scattered metastases and likelihood of a CRCLM patient having cytotoxic anti-cancer therapy induced pre-existing liver damage, only a quarter of CRCLM tumours are suited to curative liver resection surgery, and many display resistance to chemotherapies (29). Consequentially, prognosis of CRCLM patients is bleak with five-year survival statistics reporting a 25 to 50 % survival rate (32).

Table 1.1. TNM and Dukes' staging criteria for CRC

TNM Stage	Description
Tumour	
T1	Tumour confined to submucosa
T2	Tumour has grown into muscularis propria
T3	Tumour has grown into the serosa
T4	Tumour has penetrated through serosa and peritoneal surface
Nodes	
N0	No lymph nodes contain tumour cells
N1	Tumour cells in up to 3 regional lymph nodes
N2	Tumour cells in 4 or more regional lymph nodes
Metastases	
M0	No metastasis to distant organs
M1	Metastasis to distant organs
Dukes' Stage	
A	T1N0M0 or T2N0M0
B	T3N0M0 or T4N0M0
C	Any T, N1M0 or N2,M0
D	Any T, any N, M1

TNM: tumour node metastases. Information source: (4)

1.2.2. Molecular pathology of CRC

CRC is a heterogeneous disease. Molecular mechanisms and pathobiological characteristics underlying CRC development are of clinical significance, as there are links between the molecular phenotypic tumour properties and patient prognosis and treatment response (33). Cancer arises due to an accumulation of genetic changes in a multistep process, and in the case of CRC these genetic abnormalities are acquired over years and sometimes decades (34). At the time of diagnosis, three different, partially overlapping, forms of DNA instability can be used to describe CRC pathology: chromosomal instability (CIN), microsatellite instability (MSI) and CpG island methylation

phenotype (CIMP) (35). CIN, MSI and CIMP phenotypes are not mutually exclusive and thus, some tumours will display characteristics of multiple pathways. Approximately a quarter of MSI CRCs would also be classified as CIN+ and whilst CIMP-positivity is associated with most MSI, CIN- CRCs, roughly a third of CIMP+ tumours will exhibit CIN positivity (36).

1.2.2.1. APC gene: the classic adenoma-carcinoma sequence

The adenoma-carcinoma sequence is a fundamental concept in CRC, originally described by Vogelstein *et al*, in 1988 (37).

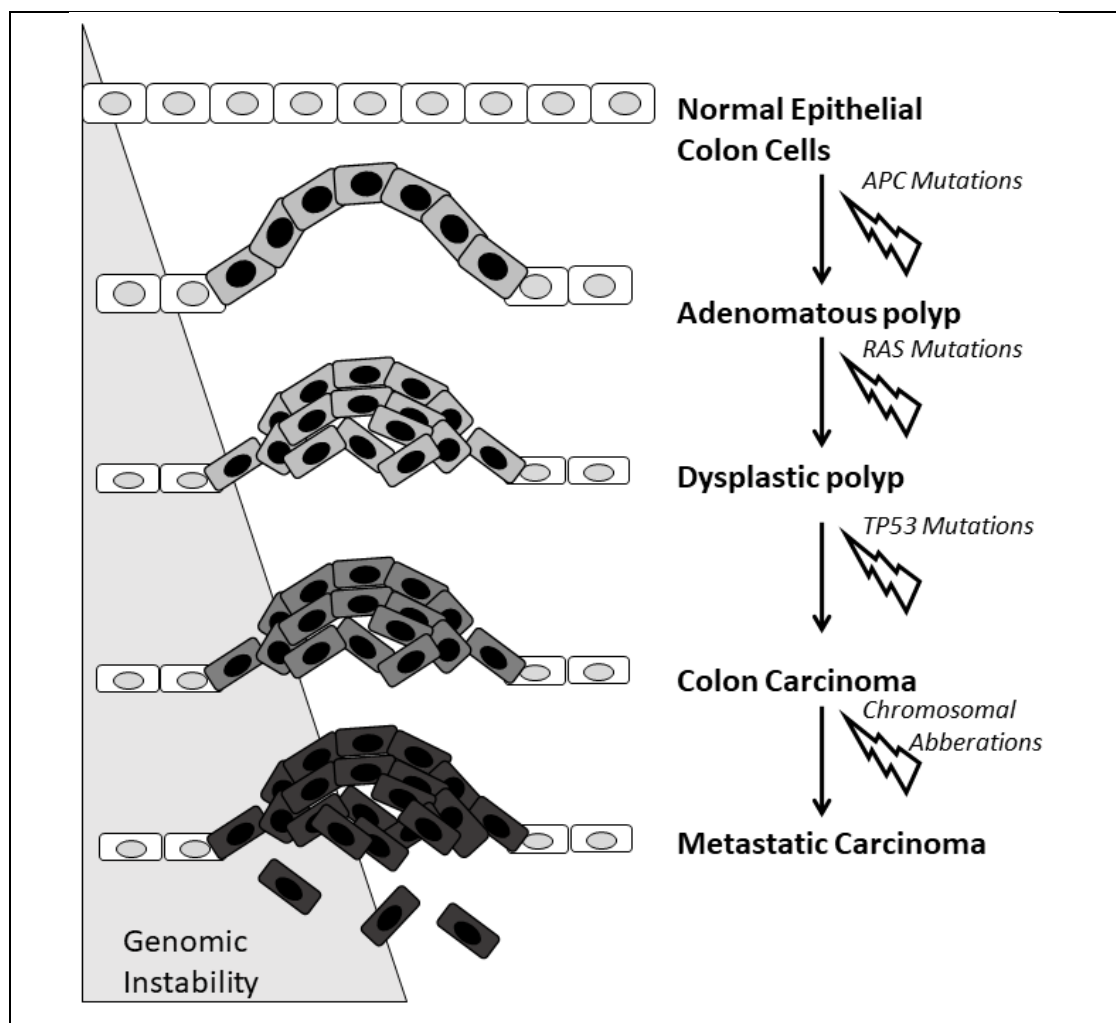


Figure 1.2. Pathogenesis of CRC: the adenoma-carcinoma sequence

Development of CRC via the adenoma-carcinoma sequence. Following an initiating mutation of APC gene, genomic instability accelerates development of CRC. Metastatic cancer is caused by the cells that detach from the primary tumour. Degree of genomic instability is indicated by the triangle on the left-hand side of the figure. Image adapted from (33).

It describes the progression from normal tissue to dysplastic epithelium to carcinoma (38) [Figure 1.2]. The adenoma-carcinoma sequence is caused by the CIN pathway (39), which underlies most colon cancers (36).

The adenomatous polyposis coli (*APC*) tumour suppressor gene is found to be altered early in the sequence of events that ultimately result in malignant colorectal tumours and has been considered a 'gatekeeper' of colonic epithelial cell proliferation (34). A mutated gatekeeper leads to imbalance and an abnormal increase in cell growth and dysregulation of cell death (34). Premalignant lesions display mutated forms of the *APC* gene and *APC* genetic changes are thought to be an initiating event in up to 85 % of sporadic CRCs (40). In addition, germline mutation of *APC* is causative of FAP (34).

Mutated *APC* results in premature stop codons which lead to the production of stable truncated gene products or missense mutations rather than complete *APC* protein loss (40). The genetic instability that results from abnormal expression of *APC* can lead to further cancer-promoting events, such as accumulation of activating mutations of oncogenic Kirsten rat sarcoma (*KRAS*) or inactivation of the tumour protein P53 (*TP53*) tumour suppressor gene (33). The loss of *APC* can lead to stimulation of cell migration, activation of proliferation, inhibition of differentiation, induction of chromosomal instability and promotion of cellular survival (40).

1.2.2.2. Chromosomal instability (CIN)

Malignant cells in CIN tumours are typically aneuploid (stable or unstable alterations in chromosome number), reveal large-scale chromosomal rearrangements (41) and are characterised by a loss of heterozygosity (LOH) and by amplification of sub-chromosomal genomic regions (42).

In order to determine whether a tumour has arisen through the CIN pathway, many approaches have been utilised in order to measure chromosomal instability, although challenges have arisen when trying to standardise the quantitative criteria that defines a 'CIN-positive' (CIN+) tumour as with some techniques the interpretation of data between multiple lab groups would vary and in addition opinions on assigning CIN+ or CIN-negative (CIN-) status is complicated by some proposals of further categorising CIN+ tumours into CIN-low and CIN-high subgroups (42). Methods used to test CIN status have included; cytometry, karyotyping, loss of heterozygosity analysis, fluorescent in situ hybridization (FISH) and comparative genomic hybridization (CGH) (42).

A meta-analysis including 63 eligible studies that reported patient outcome in relations to a CIN+ status determined that there was a worse prognosis associated with this molecular phenotype (43)

1.2.2.3. *Microsatellite instability (MSI)*

In the 15 % of sporadic CRC cases that are considered CIN- and don't present with mutated *APC*, the alternative molecular drivers are usually attributed to activating proto-oncogene B-raf (*BRAF*) oncogenic mutations. These cancers tend to be characterised by high levels of MSI and abnormal DNA MMR gene activity and are often CIMP+ (33, 35, 41)

The microsatellite instability hallmark is observed in nearly all hereditary nonpolyposis colorectal cancer (HNPCC) tumours and some sporadic CRCs. It is characterised by extensive instability of simple short tandem repeat (STR) nucleotide sequences known as microsatellites as the direct result of ineffective DNA mismatch repair machinery (44). Inactivation of genes such as MutL Homolog 1 (*hMLH1*), MutS Homolog 2 (*hMSH2*), MutS Homolog 6 (*hMSH6*) and PMS1 Homolog 2 (*hPMS2*) can result in MSI (45). The genetic instability due to inactive DNA MMR genes causes altered microsatellite lengths as bases are deleted or inserted during DNA replication, which results in somatic frameshift mutations and silencing of the affected genes (45). MSI is associated with CIMP status and is most prevalent in tumours located on the right-hand side of the colon (45). Detecting microsatellite status is of clinical importance, not only for identification of patients with HNPCC and Lynch syndrome, but also for prognostic and therapeutic decision-making purposes. The literature reports that prognosis is better for patients with MSI tumours compared to those with MSS tumours (46).

There are, in fact, hundreds of thousands of microsatellite loci which could be utilised for MSI analysis (45). In 1997, it was recommended that the Bethesda Panel was used as the reference panel through which to determine MS status, comprising five microsatellite loci: *BAT-25*, *BAT-26*, *D2D123*, *D5S346* and *D17*. *BAT-25* and *BAT-26* loci are mononucleotide markers, and the remaining three are dinucleotide loci markers (45). Using the Bethesda panel markers, tumours were classified as MSI-high when they displayed instability, most often products which are smaller in size than the germline allele, at 2 or more loci and MSS when no instability was identified at any loci. The National Institute for Health and Care Excellence (NICE) guidelines stipulate that MSI testing should be offered as part of the diagnostic investigations to all patients with newly diagnosed CRC (28).

Limitations have been reported for using the Bethesda Panel for assigning microsatellite status, particularly as the three dinucleotide repeats are less sensitive and specific than *BAT-25* and *BAT-26*. It has been reported that the mononucleotide repeats undergo significant deletions in a large majority of MSI CRCs (44), with the average shift in allele size for *BAT-25* ranging from -5.3 to -5.4 bases and for *BAT-26*; -8.8 to -9 bases (45).

1.2.2.4. CpG Island Methylation Phenotype (CIMP)

In human cells, DNA methylation is the biochemical addition of a methyl (-CH₃) group to cytosines that are part of symmetrical dinucleotides, 5'-C-phosphate-G-3' (CpG) (47). It is an epigenetic mechanism to control expression of genes. It is known that approximately 1 % of the human genome consists of CpG sites, which are most frequently found to be methylated in healthy adult cells (47). In addition, the promoter region of 50 % of all genes contain a CpG island (repeated CpG dinucleotide clusters), however these are normally unmethylated regardless of whether the gene is expressed or not (47).

Cancers which are classified as CIMP positive (CIMP+) show aberrantly high levels of DNA methylation which leads to the concordant promoter hypermethylation of multiple genes (41). CIMP is not a feature exclusive to CRC, it is also observed in gastric, liver, pancreatic and ovarian cancers (47). CIMP-positivity and microsatellite instability overlap to a large extent (35), hypermethylation of DNA MMR gene promoters inactivates the gene and consequentially allows the accumulation of microsatellite DNA. Of all sporadic MSI CRCs, it is estimated that 70 to 80 % can be attributed to CIMP and the associated *MLH1* methylation (47). Alongside the silencing of DNA MMR genes, the CIMP phenotype can also result in the transcriptional silencing of tumour suppressor genes, such as *APC*, cyclin-dependent kinase inhibitor 2A (*CDKN2A*), *MLH1*, *cadherin 1* (*CDH1*), and Von Hippel-Lindau tumour suppressor (*VHL*) (48, 49). A large body of evidence shows that CIMP-positivity is associated with MSI, female gender, high *BRAF* mutation rates, proximal colon location, poor tumour differentiation and the presence of mucinous features(48).

Following the bisulfite-mediated conversion of genomic DNA, quantitative methylation-specific polymerase chain reaction (PCR) is often used to assess CIMP status (35). CIMP status is assigned upon the evaluation of the methylation status of promoter regions of specific genes and therefore there can be some false reporting of status by groups using different marker panels. Two distinct panels that have been used by multiple sources (35, 41, 50) were proposed by Issa (47) and Weisenberger (51). The Issa panel consists

of *CDKN2A* (*p16*), Amyloid Beta Precursor Protein Binding Family A Member 1 (*MINT1*), Amyloid Beta Precursor Protein Binding Family A Member 2 (*MINT2*), *MINT31* and *MLH1* and CIMP-positivity is defined as 3 or 4 markers being methylated whilst CIMP-negativity is zero to 2 methylated markers (47). Weisenberg's panel is comprised of Calcium Voltage-Gated Channel Subunit Alpha1 G (*CACNA1G*), Insulin Like Growth Factor 2 (*IGF2*), Neurogenin 1 (*NEUROG1*), RUNX Family Transcription Factor 3 (*RUNX3*) and Suppressor Of Cytokine Signalling 1 (*SOCS1*) with $\geq 3/5$ methylated markers and negative samples having a maximum of 2 markers showing hypermethylation (51). Lothe *et al* found that, in a panel of 27 cell lines, promoter hypermethylation of *MINT2* was ubiquitous and thus proved an irrelevant marker for determining CIMP status (35).

As an independent prognostic marker, a meta-analysis of 19 studies found that CIMP+ status was associated with shorter disease free survival and overall survival for CRC (52). Although a majority of CIMP+ CRC tumours also exhibit MSI, a study in which CIMP and microsatellite stability were characterised in 460 tumours shows that 3.9 % MSS tumours were CIMP+ (53). In the aforementioned meta-analysis to assess CIMP as a prognostic marker, subgroup analysis of MSS CRC patients found a significant association between shorter overall survival and CIMP+ (52). The study reported that associations were more prominent in stage 2 and stage 3 CRCs compared to stage 4 disease (52).

1.2.2.5. Consensus molecular subtypes (CMS)

As the biology underpinning CRC development increases, the molecular classification has developed from the classic adenoma-carcinoma CIN pathway (37), to classifications incorporating CIMP and microsatellite status. More recently, considerations of localisation and microenvironment are incorporated. The CRC consensus molecular subtypes (CMS) were described in 2015 as a potential classification of tumours based on their molecular characteristics (54). As such, it encompasses MSI, CIMP and CIN statuses of tumours as well as key tumour microenvironment features, grouping CRC tumours into 4 categories.

The CMS classification system was proposed by the CRC Subtyping Consortium (CRCSC), who assessed core subtype patterns among pre-existing gene expression-based CRC subtyping algorithms. It combines transcriptomic, key biological features, mutation profiles, copy number, methylation statuses, microRNA expression and

proteomic properties (54). The final stage of CMS disease stratification is the correlation of well-defined genomic and epigenetic CRC traits with patient outcome (54, 55).

The 4 CMS of CRC are displayed in **Figure 1.3**. In brief, CMS 1 tumours are MSI and CIMP+, CMS 2 tumours follow the traditional adenoma-carcinoma sequence, CMS 3 tumours are characterized by enriched KRAS mutations and metabolic deregulation and CMS 4 shows aberrant TGF β activation which in turn induces epithelial mesenchymal transition (EMT) giving rise to more motile and invasive cancer cells (35, 41, 55). Pre-clinical models have been shown to recapitulate tumour CMS subgroups (35, 50, 56), (details provided in **Chapter 4.1.3**). Further work is required before the CMS can be utilised in a diagnostic and / or treatment setting.

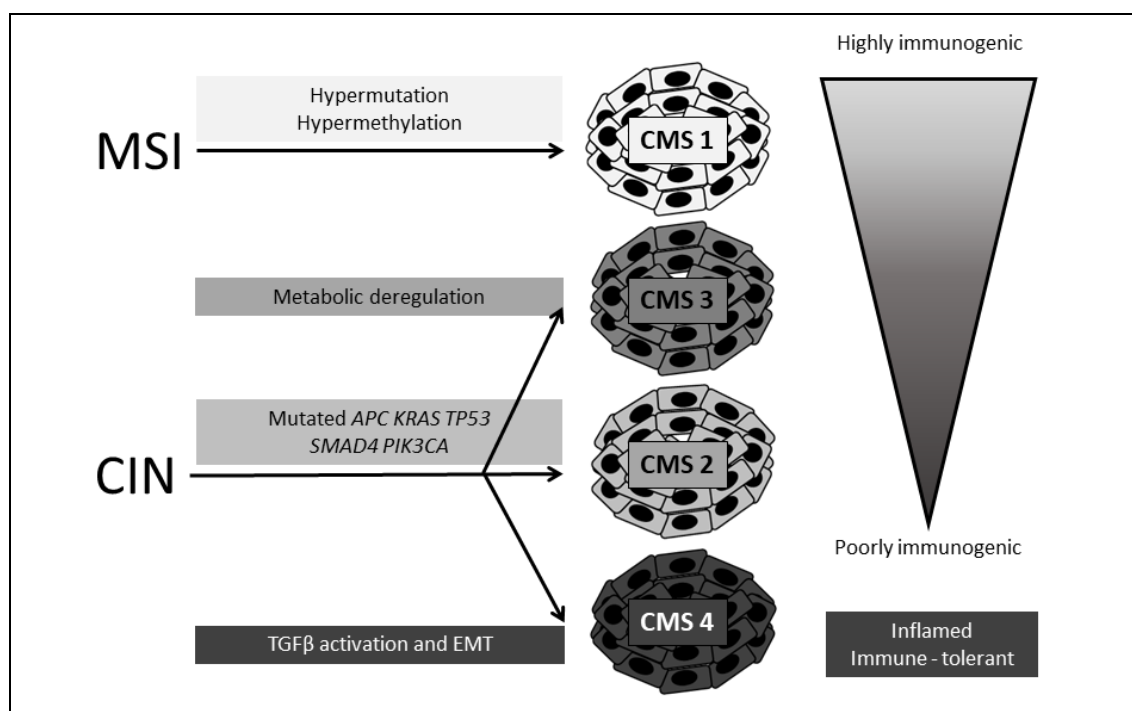


Figure 1.3. Consensus molecular subtypes of CRC

CMS classification criteria. MSI tumours are mostly CMS1. Tumours arising via CIN pathways are CMS 2, 3 and 4. A shift from CMS 2 carcinogenesis to CMS 3 is an early step in CRC pathogenesis, driven by metabolic deregulation and KRAS mutations. CMS 4 tumours are characterised by TGF- β activation which arises due to the stromal-enriched inflamed microenvironment and consequentially this facilitates epithelial-mesenchymal transition (EMT). Image adapted from (55).

1.2.3. CRC Treatments

There are no CRC treatments currently available that are considered the 'gold standard', with a treatment that would be able to be equally efficacious amongst all patients remaining elusive. Current best practise in determining treatment plans involve a multi-disciplinary team of medical professionals evaluating surgical, radiotherapy and

chemotherapeutic and/or biological agents on a case-by-case basis (57). These decisions are based upon evidence obtained by published RCTs. In addition to the RCT evidence, patient specific factors including; age, symptoms, medical history, co-morbidities, preferences (57, 58), treatment-specific factors including; efficacy and toxicity, and tumour-specific factors considered include; potential future operability, microsatellite and CIMP status, *EGFR*, *BRAF* and *RAS* mutations (57, 59).

There are three treatment types that may be used in isolation or combined regimens to treat CRC. First, early stage primary CRC can be removed by local excision. To remove later stage disease, major surgery can remove primary or metastatic tumours. Radiotherapy is also utilised as a localised treatment option, often in conjunction with surgery. Systemically administered oncological treatments (chemotherapy and / or targeted therapies) are available in neo-adjuvant and adjuvant settings.

1.2.3.1. Localised treatment: surgery and radiotherapy

In the colon, surgery to remove an early stage CRC and the margin can be completed which is termed 'local resection', or for later stage tumours a colectomy surgery can be performed in which a section or all of the bowel is removed (60). For rectal cancers there are two types of surgery; trans anal endoscopic microsurgery (TEM) and total mesorectal excision (TME), the latter of which is more invasive and involves the removal of part of the rectum, some healthy tissue and the fatty tissue that surrounds the rectum (61). Many patients will have a stoma following surgery which can be temporary or permanent (62). Between 80 % and 95 % of patients with stage 1 and 2 CRC treated with resection surgery without adjuvant chemotherapy, survive 5 years post-operatively (63, 64).

Surgery for advanced disease can include operating to remove blockages caused by tumour growth, either by inserting a stent or removing the blocked section of the bowel (65). In some cases, metastasectomy surgeries can be performed to remove small secondary tumours in the liver or lungs (65). For patients with liver metastases, survival rates depend upon the ability to resect the liver to remove the metastatic disease. If resection is possible, 25 – 40 % will survive 5 years post-diagnosis (65, 66). However, as three quarters of patients are not suitable for liver resection surgery, there are limited alternative treatment options for CRCLM and survival rates are lower, with a median survival of 5 to 20 months if left untreated (67).

Complications and risks associated with surgeries include some relating to age and co-existing morbidities, or anesthetic and operative risks. Common surgical complications

include bleeding, infection, and post-operative cardiac event. Patients with a stoma report problems with leakage and skin irritation (68). Long-term side-effects can include; altered and unpredictable bowel function, fatigue, impaired sleep and anal pain (68). There are associations between the side-effects of surgery and stoma and reports of patients having impaired physical, social, sexual and psychological function (68).

Radiotherapy is not commonly used to treat colon cancer (18, 69), with just 3% of patients receiving it as a primary treatment (23). However radiotherapy is more frequently used in combination with surgical and chemotherapeutic interventions to treat rectal cancer (18), with 41% of rectal cancer patients receiving radiotherapy as a primary treatment (23). Radiotherapy is recommended prior to surgery for locally advanced rectal cancers (neo-adjuvant radiotherapy) (18, 69), as it can improve surgical outcome by shrinking the tumour. Intraoperative radiation therapy (IORT) uses radiotherapy during surgery to kill remaining CRC cells (69). Additionally, radiotherapy can be used post-operatively to eradicate residual tumour cells at resection margins and is used in some cases to ease symptoms or target metastatic tumours (69). Side effects of radiotherapy include; skin, rectal and bladder irritation, nausea, bowel incontinence, fatigue and fibrosis, scarring or adhesion of the tissues in the treated area (69).

1.2.3.2. Chemotherapies

Chemotherapy is usually given post-operatively in order to minimise the risk of CRC recurrence (adjuvant chemotherapy), although as previously mentioned it is sometimes used prior to surgery (neo-adjuvant chemotherapy) (70, 71). It is rarely used to treat stage 1 cancers, but is frequently used to treat stage 2 and stage 3, and the drugs are administered in 'cycles' every 2 to 3 weeks for up to 8 cycles (70). For treatment of CRC, chemotherapy is usually a combination of drugs and may include:

1. Folinic acid (leucovorin, FA or calcium folinate), 5-fluorouracil (5-FU) and oxaliplatin (FOLFOX).
2. Oxaliplatin and capecitabine (XELOX, also known as CAPOX, CAPE-OX or OxCap)
3. Capecitabine (Xeloda[®])
4. 5-Fluoruracil (5-FU)
5. Irinotecan (Campto[®])

The severity of side effects is variable between patients and may be impacted by other treatments. Over 10 % of patients receiving FOLFOX therapy will report breathlessness,

fatigue, increased bruising and bleeding, nausea, pain, diarrhoea, sore mouth and also have increased risk of infection (72). Common side effects of XELOX treatment are similar to those for FOLFOX, with the addition of numbness and tingling in hands and feet, constipation and loss of appetite (73). Capecitabine treatment in addition to the aforementioned side-effects for FOLFOX and XELOX can result in mouth sores and ulcers (74). 5-FU may also cause heart problems, hair loss and an increased level of uric acid in the blood which causes stiff and painful joints (75). Irinotecan can result in the development of cholinergic syndrome which causes diarrhoea, increased sweating and chills, dizziness, increased saliva production, eye problems, blocked nose and abdominal cramps (76). It should be noted, that only a 3 – 4 % improvement in overall survival is attributed to adjuvant chemotherapy (64).

1.2.3.3. Targeted therapies

Targeted therapies are offered to patients with metastatic CRC, and side effects are the same as those for chemotherapy agents. These drugs target specific processes to stop cancer growth.

Bevacizumab (Avastin®), ramucirumab (Cyramza®) and zif-aflibercept (Zaltrap®) target vascular endothelial growth factor (VEGF) which limits angiogenesis (77). Metastatic CRC patients who received bevacizumab in combination with 5-FU, irinotecan or leucovorin had an increased 4.7 month survival compared to patients treated with placebo in place of bevacizumab (78). Cetuximab (Erbix®) and panitumumab (Vectibix®) target epidermal growth factor receptor (EGFR) can be used if the cancer does not contain mutations in *KRAS*, *NRAS* or *BRAF* (77). An improvement in survival of 3 months is attributed to cetuximab and panitumumab (79). Encorafenib (Braftovil®) targets abnormal BRAF proteins can be used in combination with cetuximab in metastatic disease treatment (77).

Immune checkpoint inhibitors can also be used for treatment of metastatic disease. PD-1 inhibitors pembrolizumab (Keytruda®) and nivolumab (Opdivo®) target PD-1 protein on T-cells which boosts the immune response to cancer cells. Pembrolizumab was approved for MSI CRC patients after 78 % patients obtained a beneficial response lasting more than 6 months (80). The CTLA-4 inhibitor ipilimumab (Yervoy®) can also be used, often in combination with nivolumab, in which an 84 % response rate has been reported for MSI patients (81, 82).

1.2.3.4. *Stratified medicine*

Achieving a fully 'personalised medicine' approach in conventional treatment of CRC has not been achieved. The Stratification in Colorectal Cancer: from biology to treatment prediction (S:CORT) (83) program was designed to expand the current understanding of the biology of CRC and validate biomarkers present in patient samples obtained from national studies and clinical trials. This study was designed to correlate molecular analysis of tumour samples with treatment response and clinical outcomes. One area it focused on was understanding response to oxaliplatin, which is only effective in 50 % of late stage CRC patients (83). It is hoped that findings the S:CORT study will ultimately provide a more detailed understanding of the fundamental biology of CRC and how this drives resistance to treatment, which could yield novel treatment strategies. In the UK the FOCUS 4 trial, a population-enriched molecularly-stratified multi-arm multi-stage phase II/III RCT, is evaluating first-line treatment of metastatic CRC (84). Molecular stratification criteria set for the trial was flexible and consisted of four molecularly defined cohorts with novel inhibitors selected for each subgroup: group A, BRAF mutant; group B, PI3 kinase mutant; group C, RAS mutant; and group D, all wild-type cohort (84).

Guidelines in the UK recommend testing to determine microsatellite stability, however, in clinical practice few patients are managed with full knowledge of these test results (85). Molecular markers considered and evaluated prior to treatment should include MMR/MSI status, RAS, BRAF and EGFR mutations (59). In addition, the site of primary tumour, and associations between this and the molecular phenotype, have shown differential treatment responses in the case of 5-FU. Right-sided MSI, CIMP+ tumours have a limited response to 5-FU compared to left-sided MSS tumours (86). In fact, left-sided CRC patients have better response to chemotherapy and targeted therapies compared with right-sided MSI tumours, which demonstrate responses to immunotherapeutic therapies (12).

CMS subgroups may be key to stratification of treatment, as it combines oncogenic expression, location, and microenvironment characteristics. Recent randomised controlled trials reported potential associations between CMS 1 and anti-VEGF1 benefit (87), CMS 2 and oxaliplatin benefit (88) and CMS 4 and anti-EGFR benefit (89). However, several criteria still need to be met before clinical use. There is an unmet need to improve laboratory and informatics utilised to classify tumours, and more clinical trials are required to corroborate CMS-associated therapeutic response (90). A summary diagram of associations between the primary site of CRC and clinical, molecular and treatment characteristics are displayed in the figure below [**Figure 1.4**].

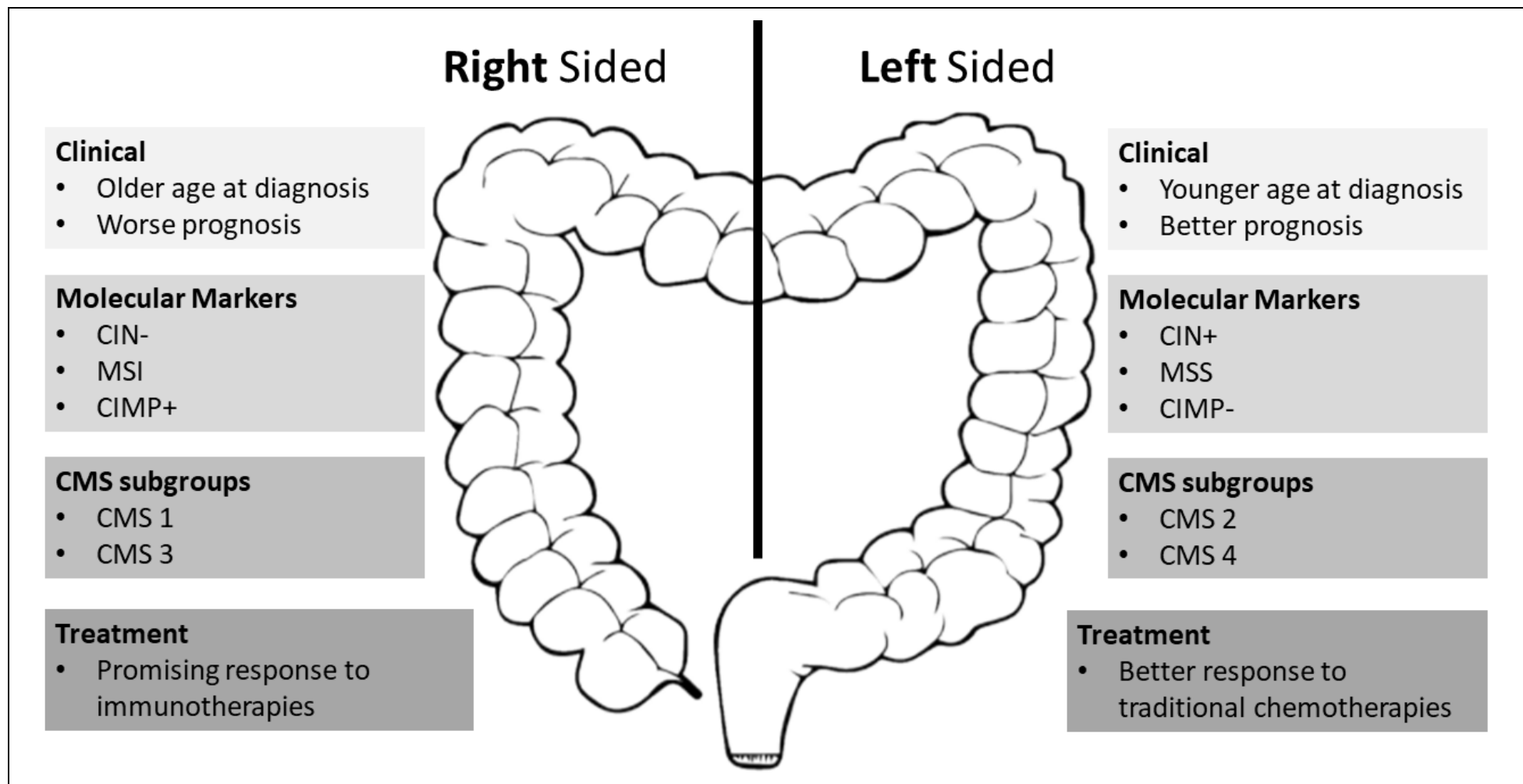


Figure 1.4. Clinical, molecular, CMS and treatment differences between CRC tumour sites

Current understandings of how CRC tumour location is associated with prognosis and treatment responses, and molecular phenotypes and CMS subtypes. Image adapted from (91, 92)

1.3. Omega-3 Polyunsaturated Fatty Acids

The link between cancer and lifestyle factors is an area of intense study, with large scale studies such as the Continuous Update Project (CUP) focused on definitively finding links between cancer prevention or survival data and lifestyle factors including diet and nutrition, physical activity and weight (93). The benefits of consuming a diet rich in fruit, vegetables and fish have been shown to correlate with reduced incidence of certain cancers including breast, prostate and CRC (94). In addition, the fruit, vegetable and fish-rich diet in cancer patients, has been shown to counteract treatment side effects, reduce incidence of secondary cancer and improve survivorship statistics (66, 94).

1.3.1. What are nutrients?

A nutrient is a substance or component of food that is utilised as an energy source by organisms to facilitate survival, growth, reproduction and maintenance of health (95). Nutrients and bioactive metabolic products of nutrient digestion including calcium, vitamin D, fibre, folate, vitamin B6, methionine, vitamins A, C and E, curcumin and omega-3 (*n*-3) polyunsaturated fatty acids (PUFAs) have been associated with colorectal cancer incidence, particularly in association with CRC prevention (96). Conventional treatment options are not efficacious for all CRC patients. In addition, there are limited treatment options for unresectable and metastatic tumours. Therefore, an unmet clinical need for alternative treatments exists. *N*-3 PUFAs are a potential CRC treatment.

1.3.2. Biochemistry of *n*-3 PUFAs

1.3.2.1. *Structure and key nomenclature*

N-3 PUFAs are lipids. Lipids are molecules, such as fatty acids (FAs), eicosanoids, phospholipids, and sphingolipids, found to be insoluble in water and soluble in organic solvents. Lipids have biological functions relating to energy storage, cell membrane structural components and signalling (97, 98).

FAs are carbon chains of varying lengths, with a methyl group at one end and a carboxyl group at the other. Saturated FAs contain only single bonds between carbon atoms. Monounsaturated and polyunsaturated FAs contain one or more double bonds between carbon atoms, respectively.

The two major classes of PUFAs are *n*-3 and omega-6 (*n*-6) fatty acids (99), examples of which are shown in **Figure 1.5**. These are long chain (containing 20 or more carbon atoms) FAs. The position of the first double bond in a carbon-carbon chain in *n*-3 PUFAs is at the third carbon from the methyl end, whilst the position of the first double bond in an *n*-6 PUFAs such as arachidonic acid (AA) is at the sixth carbon from the methyl end. PUFAs are often referred to using a shorthand nomenclature, C χ : γ (*n*-*z*) which denotes the number of carbon atoms (χ) followed by the number of double bonds (γ) and the position of the first double bond relative to the methyl carbon (*z*) (100).

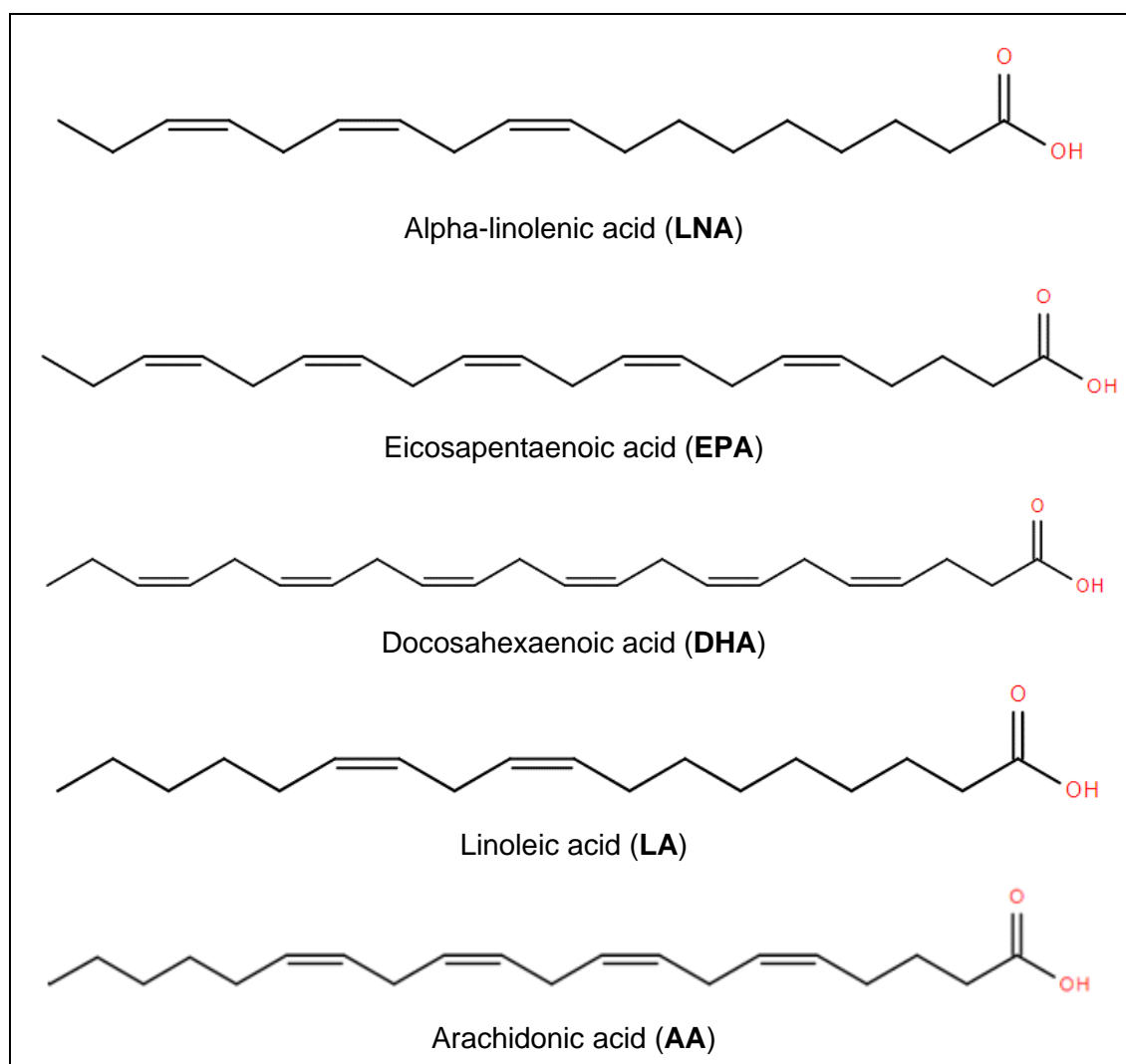


Figure 1.5. *N*-3 and *n*-6 polyunsaturated fatty acids (PUFAs)

Chemical structure of *n*-3 PUFAs; LNA, EPA, DHA and *n*-6 PUFAs; LA and AA. Image sources: (101-105).

N-3 PUFAs are essential nutrients, necessary to maintain regular physiological functions but unable to be synthesised in the body (106, 107). The majority of cancer-related scientific research focuses on three *n*-3 PUFAs: alpha-linolenic acid (LNA), eicosapentaenoic acid (EPA), and docosahexaenoic acid (DHA) (99). EPA (C20:5 *n*-3) and DHA (C22:6 *n*-3) are often referred to as marine FAs, as these *n*-3 PUFAs are found

in oily fish (108). The two major *n*-6 PUFAs commonly discussed in the literature are linoleic acid (LA, C18:2*n*-6) and AA (C20:4*n*-6) (109).

1.3.2.2. Sources and bioavailability

n-3 PUFAs can be found in cold-water, oily fish such as salmon and mackerel (110) although the content is dependent upon the dietary *n*-3 PUFA consumption of the fish, and consequently farmed fish typically has higher content (111). Some plant sources, including flaxseed, soybean and canola oil, contain LNA (99). Commercially available supplements are also available, typically containing a mixture of *n*-3 PUFAs and other FAs. There is a wide variation of composition of such supplements, but on average a 1000 mg fish oil supplement will contain 180 mg EPA and 120 mg DHA (99).

The naturally occurring forms of *n*-3 PUFA in a fish oil are natural triglyceride conjugates. However, there are different forms of *n*-3 PUFAs which can be found in dietary supplements. These include ethyl esters, which are synthesised from natural triglycerides and are made by removing the glycerol molecule and replacing this with ethanol. Free fatty acids, re-esterified triglycerides and phospholipids have been found to have a higher bioavailability than ethyl esters (112-114).

1.3.3. Cellular metabolism of *n*-3 PUFAs

Once *n*-3 PUFAs are in cells, there are multiple pathways through which they are metabolised. Many downstream metabolites are considered beneficial for human health and are thought to have anti-inflammatory and/or anti-neoplastic properties (100, 115).

1.3.3.1. Metabolism involving desaturase and elongase enzymes

PUFAs are metabolised by a series of desaturase (FADS1 and FADS2) and elongase (ELOVL-2 and ELOVL-5) enzymes. Membrane bound fatty acid desaturases, FADS, are a diverse superfamily of lipid-modifying enzymes that catalyse the introduction of double bonds into fatty acids, with a wide range of lipid substrate preferences including acyl-CoAs, sphingolipids and phospholipids (116). The FADS enzymes involved in the conversion of LA to docosapentaenoic acid (C22:5 *n*-6) or LNA to DHA are FADS1 and FADS2 which are sometimes referred to as desaturases Δ^5 and Δ^6 respectively (117).

Seven fatty acid elongase subtypes are identified in mouse, rat and human genomes, and function to add two-carbon units, lengthening the FA carbon backbone. ELOVL-2

and ELOVL-5 function alongside FADS 1 and FADS 2, generating end products of *n*-6 and *n*-3 PUFA synthesis (117, 118), as depicted in **Figure 1.6**.

It should be noted that this metabolic pathway is inefficient in humans, for example just 15 % of LNA is converted to DHA (99), and reports indicate 0-4 % conversion from EPA to DHA (119). Therefore, EPA and DHA are considered 'essential' and are mostly obtained directly from dietary sources. *n*-3 PUFAs are primarily degraded by β -oxidation, in order to produce energy for the cell (120).

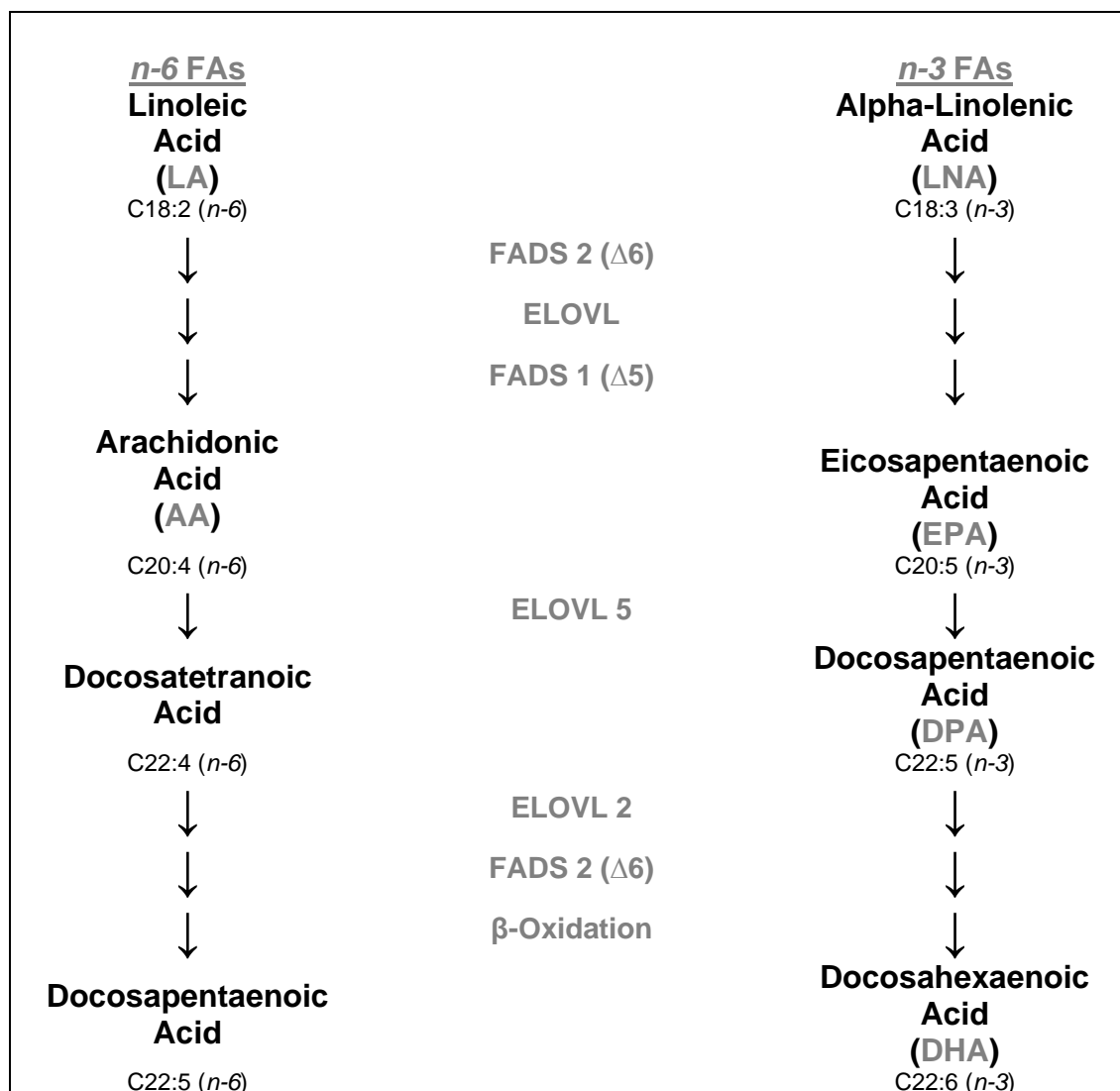


Figure 1.6. Activity of elongase and desaturase enzymes in the metabolism of LA and LNA

FAs are denoted as per IUPAC convention. ELOVL: elongase. FADS: desaturase. Diagram adapted from sources (117, 121)

When comparing mRNA expression of *ELOVL* and *FADS* between 38 healthy normal and 44 stage I – IV CRC tissues, *ELOVL*- 2,4,5 and *FADS*- 1,2 were found to have greater relative expression in CRC tissues (122). There are limited *in vitro* studies that examine expression of *ELOVL* and *FADS* genes in colorectal cancer cell lines. *ELOVL*4,

ELOVL5 and *FADS2* mRNA expression was found to be increased in cultured cancer cells (HT-29 and WiDr) when compared with normal colon cells (CCD 841 CoN) in a study by Mika *et al*, 2020 (122). The 'normal' colon cells do not have chromosomal rearrangements and mutations associated with CRC, however, are still immortalised. *ELOVL2* and *FADS1* expression was not detected in any cell lines (122).

1.3.3.2. Further metabolism of EPA, DHA and AA

EPA, DHA and AA can also be further metabolised [**Figure 1.7**] by cytochrome P450 (CYP450) monooxygenases, and cyclo-oxygenase (COX) 1 and 2 enzymes and lipoxygenase (LOX) enzymes (106). Their metabolic products are associated with generating an immune response in healthy individuals (123). *N*-3 PUFA metabolism results in formation of anti-inflammatory anti-neoplastic mediators; resolvins, protectins and maresins (106, 115), whilst *n*-6 PUFAs metabolism results in pro-inflammatory pro-cancer mediators (106, 115).

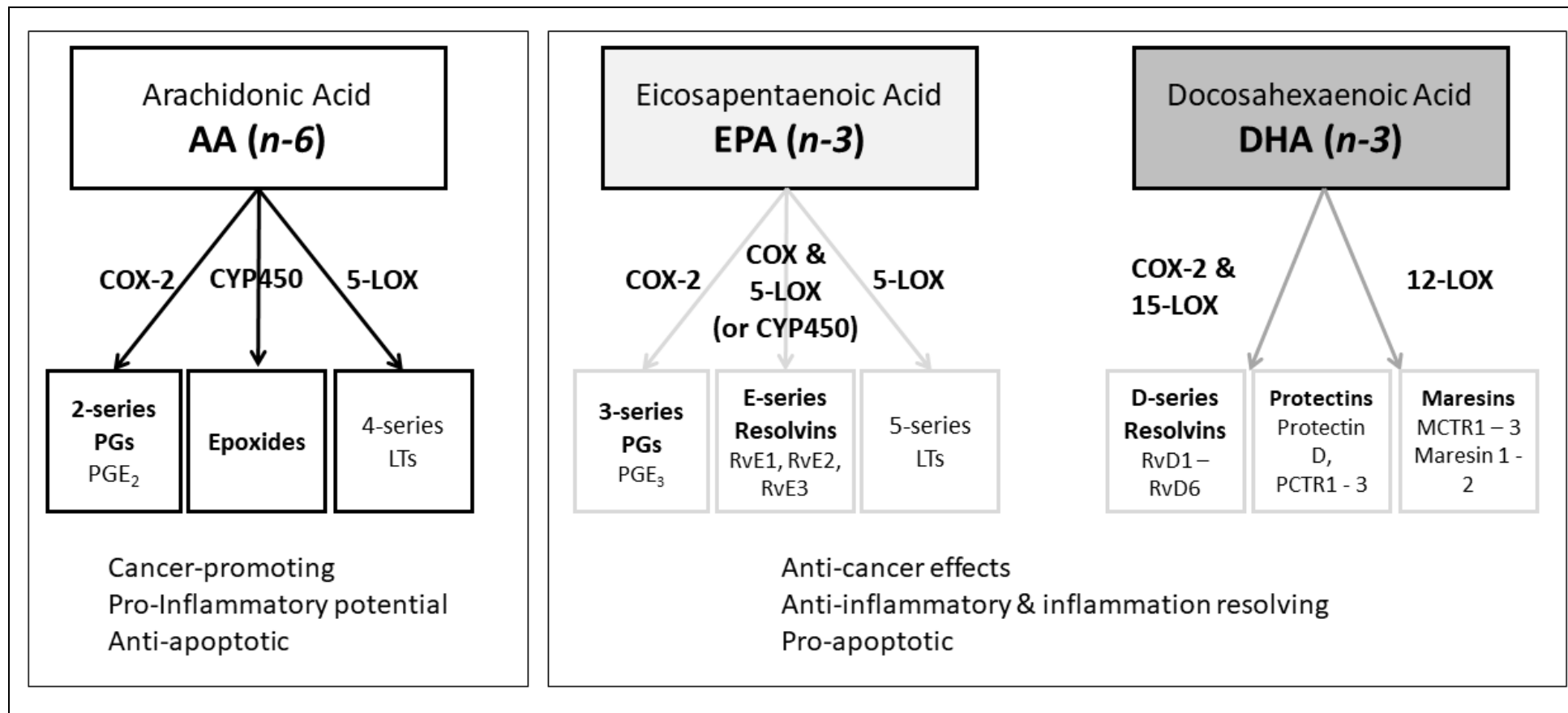


Figure 1.7. Metabolic fate of AA, EPA and DHA

Overview of the synthesis of lipid mediators produced from AA, EPA and DHA and the mediator effects on cancer and inflammation and apoptotic potential. COX, cyclooxygenase; CYP450, cytochrome P450; LOX, lipoxygenase; LT, leukotriene; MCTR, maresin conjugates in tissue regeneration; PG, prostaglandin; PCTR, protectin conjugates in tissue regeneration; Rv, resolvins. Image adapted from (115, 124)

1.3.4. Clinical use of *n*-3 PUFAs

N-3 PUFAs have demonstrated abilities in improving cardiovascular (125, 126) and inflammatory conditions (106, 115, 127). A major reason for the interest in using *n*-3 PUFAs medically is the excellent safety, tolerability profiles and limited side-effects (99). In pre-clinical and clinical settings, *n*-3 PUFAs are considered 'nutraceuticals'. Nutraceuticals are defined as 'nutritional products that provide health and medical benefits, including the prevention and treatment of disease' (128). The term, nutraceutical, implies that the nutritional component is a supra-physiological (pharmacological) dose and / or in a pharmaceutical form (capsule, tablet) (129). A systematic review of side effects attributed prescription *n*-3 PUFAs in 21 randomised controlled trials, found no reported serious adverse effects (130). Mild side-effects reported have included dysgeusia, gastrointestinal issues including diarrhoea and reflux, and skin abnormalities, such as itching or eczema (130). It was also noted that, in comparison to EPA-only prescription products, patients taking combination EPA/DHA products reported a greater number of gastrointestinal adverse effects.

1.4. Evidence supporting anti-CRC activity of *n*-3 PUFAs

n-3 PUFAs have demonstrated abilities to improve cardiovascular, rheumatological and inflammatory conditions (99, 106, 110) and *n*-3 PUFA attributed anti-cancer effects have been reported in studies including CRC, prostate and breast cancers. A growing body of evidence supports use of *n*-3 PUFAs for the prevention and/or treatment of CRC. The evidence comprises epidemiological studies that correlate increased *n*-3 PUFAs intake with reduced CRC risk, *in vitro* investigations that demonstrate *n*-3 PUFAs effects on human and murine cell lines, *in vivo* studies which show efficacy of *n*-3 PUFAs against carcinogenesis and more recently in clinical trials which have demonstrated potential chemopreventative properties of EPA and DHA. These are detailed below.

1.4.1. Epidemiological evidence supporting anti-cancer *n*-3 PUFA activity

The study of *n*-3 PUFAs in the context of CRC has shown a role in prevention of developing primary and metastatic tumours (131). The global distribution of CRC burden varies, but two thirds of all cases occur in countries with higher human development indices, indicating the link between Western lifestyle and colorectal cancer (132). The lowest incidence of cancer occurs in the Far East, where the diet has a higher *n*-3 PUFA content than Western diets (132). Findings from epidemiological studies are limited because of non-comparable study designs lacking statistical power to detect

associations and due to a high variability in interpretation of results. There is a dependence on food questionnaires to assess dietary intake, which do not always sub-categorise high *n*-3 PUFA sources and low *n*-3 PUFA sources. A study, in which *n*-3 and *n*-6 PUFA intake was estimated by in-depth one-to-one dietary interviews, collected data from 1872 patients in North Carolina (133). A significant reduction in CRC risk was identified in patients who consumed higher quantities of *n*-3 PUFAs, in a dose-dependent manner (133). In 2007 the World Cancer Research Fund and American Institute for Cancer Research acknowledged a probable association between dietary intake of oily fish and CRC risk and more recently in 2017 the CUP report concluded that there was 'limited yet suggestive' evidence supporting a link between decreased risk of CRC and fish intake (93).

1.4.2. Preclinical evidence supporting anti-cancer *n*-3 PUFA activity

Studies do not consistently use the same *n*-3 PUFAs, formulations or, in the case of *in vivo* work, administration mode and these differences must be considered when undertaking comparative interpretation of the data. Whilst *in vitro* studies use either EPA or DHA, EPA is more predominantly used in *in vivo* and clinical studies.

1.4.2.1. *In vitro* studies using CRC cell lines

A summary of pre-clinical studies utilising human CRC (hCRC) cell lines is shown in **Table 1.2**.

Work to identify mechanisms through which EPA and DHA act include a study by Volpato *et al*, which has shown that EPA decreased synthesis of a pro-inflammatory chemokine linked with carcinogenesis called chemokine C-C motif ligand (CCL2) in human HCA-7 and mouse MC38 CRC cells (134). D'Eliseo *et al* demonstrated that treating established human CRC cells; HT-29, HCT8 and HCT116 with DHA modulated epithelial-to-mesenchymal transition biomarkers and inhibited invasion (135). In combination with traditional CRC treatments, the effect of *n*-3 PUFA treatment has also been evaluated. A synergistic anti-cancer effect between EPA and a combined 5-FU / oxaliplatin (FuOx) treatment was found in HT-29 cell lines, with the combined dosage resulting in 6.05-times more cell death than in cells treated with FuOx alone (136).

Table 1.2. *In vitro* studies investigating *n*-3 PUFA activity in hCRC cells

CRC model	<i>n</i> -3 PUFA	<i>n</i> -3 PUFA formulation	Concentration / dose	Anti-cancer Effects	Reference
DLD-1, HT-29 and LIM-205	EPA DHA	FFAE	50 - 200 µM EPA 50 - 250 µM DHA	Significant loss of hCRC cell viability following 24 or 48h exposure with 200 µM <i>n</i> -3 PUFA ↑ reactive oxygen species present following 24h treatment with highest concentrations tested Activated caspase-3 and caspase-9	(137)
HCA-7, HT-29 and LoVo	EPA	FFA	25 - 100 µM	Induced hCRC apoptosis. COX-2-dependent “PGE ₂ -to-PGE ₃ switch”. PGE ₃ identified as a partial agonist of PGE ₂ EP4 receptor	(138)
LoVo and RKO	EPA DHA	Not specified	120 – 150 µM	↑ LXA ₄ , ↓ PGE ₂ , ↓ LTB ₄ Suppressed expression of COX-2, ALOX5 and mPGES ↑ LXA ₄ , ↑ PGE ₂ , ↓ LTB ₄ Suppressed expression of COX-2, ALOX5 and mPGES	(139)
LoVo and RKO	EPA DHA	Not specified	120 – 150 µM	Induced apoptosis mediated by a mitochondria-mediated pathway. ↓ mitochondrial membrane potential, ↓ ATP, ↑ ROS, ↑ intracellular Ca ²⁺ , ↑ Bax/Bcl2 expression, activated caspase-9 and caspase-3	(140)
LS174T	EPA DHA	Not specified	50 µM, 100 µM and 150 µM	Dose and time-dependent growth inhibition. Activated caspase-3 and ↓ expression of survivin mRNA	(141)
HT-29 and LoVo	EPA DHA	Not specified	25 - 100 µM	Inhibition of cell proliferation, induction of apoptosis via the Hippo pathway	(142)

CRC: colorectal cancer. hCRC: human CRC. FFA: Free fatty acid. FFAE: Free fatty acid extract (from krill oil). LT: leukotriene. LX: lipoxin. *N*-3 PUFA: omega-3 polyunsaturated fatty acid. PG: Prostaglandin. ROS: reactive oxygen species. ↓ Decrease. ↑ Increase.

1.4.2.2. *In vivo studies*

Animal models of CRC have shown that EPA can be used as a means of preventing CRC development. Nakanishi *et al*, recently assessed the chemopreventative efficacy of a new stable EPA compound, magnesium l-lysinate bis-eicosapentaenoate (TP-252) on intestinal tumour formation using *Apc*^{Δ14/+} mice (143). They observed that within the colonic mucosa, mice fed a diet supplemented with TP-252, there were decreased AA and increased EPA concentrations (143). In addition, TP-252 treatment resulted in reduced tumour size and number in the colon and small intestine, in a dose-dependent manner (143). A previous study within this research group demonstrated that CRCLM can be modeled in *BALB/c* mice through intrasplenic injection of murine MC26 CRC cells (144). Subsequent dietary supplementation with 5 % EPA-FFA (free fatty acid) led to a reduced liver tumour burden and increased EPA incorporation within tumour cells (144). In addition, this study showed that an increase in *n*-3 PUFA levels conversely affected *n*-6 PUFA concentration, reduced PGE₂ signaling and lowered proliferation and motility of CRC cells (131). DHA has been used in *in vivo* studies less frequently, however one study investigated differential gene expression in HT15 CRC xenografts grown in *BALB/c* nude mice fed a 7.5 % fish oil-based DHA-rich diet compared to those fed a normal (corn-oil lacking DHA) diet. It found that DHA inhibited tumour growth *in vivo* and genes related to metastatic behavior were downregulated following DHA supplementation (145).

1.4.3. Clinical evidence supporting anti-cancer *n*-3 PUFA activity

Supported by mounting evidence in epidemiological and preclinical work, clinical trials have been undertaken to investigate the effect of *n*-3 PUFA supplementation on CRC patients. In a trial (NCT00488904) involving 174 CRC patients randomly allocated *n*-3 PUFA treatment or standard isocaloric and isonitrogenous oral nutritional supplement, Sorensen *et al* reported that 2 g/day EPA and 1 g/day DHA 7 days pre- and post- CRC surgery had no effect on post-operative complications (146). However this study did not assess long-term CRC outcomes (146) .

In 2014, the EPA for Metastasis Trial (EMT) (NCT01070355) showed that in patients awaiting liver resection for CRCLM supplementation with 2 g EPA-FFA daily was safe and well-tolerated but also reduced tumour-supporting vasculature (131). Although the study was limited in statistical power to compare placebo *versus* treatment groups, pre-

operative EPA-FFA treatment was associated with a sustained benefit, increasing disease free survival (DFS) and overall survival (OS). Encouraged by such findings, a phase III RCT, EMT2 (NCT03428477), is in progress to assess the effect of long-term EPA treatment on CRC recurrence and patient survival after liver resection surgery for metastatic disease.

A randomised control clinical trial led by Professor Hull, known as the seAFOod Polyp Prevention trial (ISRCTN05926847), assessed 2 g EPA-FFA daily supplementation for sporadic CRC prevention. Participants with sporadic colorectal neoplasia detected by colonoscopy, were randomly assigned EPA alone, in combination with aspirin, or placebo. Participants who had received EPA were reported to have a reduction in number of total number of conventional adenomas in the left colorectum, and a lower number of detected adenomas present at the 1 year surveillance colonoscopy time point, when compared to the placebo treated patients. In comparison there was no effect of EPA noted for right-sided serrated lesions (147). These findings are indicative of differential EPA effects based on site and adenoma type.

In addition to this, a clinical trial which compared the clinical outcomes of CRC patients undergoing chemotherapeutic treatment who were receiving 2 g/day fish oil supplementation (containing 0.36 g/day EPA and 0.24 g/day DHA) with patients receiving no fish oil supplements, found that the tumour progression was longer in the supplemented group compared to the control group (593 ± 211.5 days versus 330 ± 135.1) and lower carcinoembryonic antigen (CEA) although neither finding was found to be significantly different. However the finding that *n*-3 PUFA treatment may result in delayed tumour progression when the quantities of EPA and DHA totalled just 0.6 g/day are encouraging, and these results were indicative of the ability of *n*-3 PUFAs to enhance antineoplastic action of the chemotherapy (148).

1.5. *N*-3 PUFAs anti-cancer mechanisms of action

The mechanisms through which *n*-3 PUFAs exert anti-cancer effects are not fully understood. By uncovering the mechanistic basis of anti-cancer activity, novel therapeutic targets and biomarkers of response could be discovered. Proposed mechanisms summarized in **Figure 1.8** are responsible for beneficial effects, including; maintaining cell-membrane fluidity, inhibition of inflammatory processes and decreasing secretion of pro-inflammatory cytokines and promoting anti-neoplastic processes (149).

It is also thought that *n*-3 PUFAs exert growth inhibitory and pro-apoptotic effects on cancerous cells, whilst allowing healthy cells to thrive (139), which is demonstrated in a mounting body of research.

1.5.1. Direct effects of *n*-3 PUFA on cellular response

DHA and EPA are molecularly and structurally different with distinct functional properties, with EPA being a precursor to DHA (150, 151). Therefore, the direct effects on cancer cells may differ between *n*-3 PUFA used, although this is not fully understood. It is unknown how the distinctive mechanisms of action of each *n*-3 PUFA, established using *in vitro* and *in vivo* models, contribute to anti-cancer *n*-3 PUFA activity in humans.

N-3 PUFAs can incorporate into the phospholipid bilayer of the cellular membrane and cause conformational changes which alter structure and function (106, 152). Cell surface receptors, are localized to lipid rafts or calveolae (153). DHA is more likely than EPA to incorporate into the cell membrane and disrupt lipid rafts (153), causing structural changes to the membrane. As a consequence of *n*-3 PUFA incorporation into the cell membrane, signalling pathways are impaired and effectively 'switch off' activated receptors. In human breast cancer MDA-MB-231 cells treated with 50 μ M DHA, incorporation into the membrane disrupted lipid-raft associated onco-proteins; EGFR, Hsp90, Akt and Src (154). This downregulates proliferation and inhibits pathways which evade apoptosis (106).

n-3 PUFAs metabolism produces reactive oxygen species (ROS) as a by-product (155), which can accumulate in cancer cells. ROS have been found to possess both detrimental and beneficial effects in the context of cancer (155). ROS cause DNA, lipid and protein damage, which consequentially can alter signalling pathways to promote cancer cell proliferation, survival, angiogenesis and metastasis (155, 156). However, a significant increase of ROS accumulation, following *n*-3 PUFA supplementation, was observed in LoVo and RKO CRC cell lines following exposure to 150 μ M and 120 μ M *n*-3 PUFA, respectively (140). ROS accumulation in this context may increase oxidative stress (155) and initiate an apoptotic signalling cascade pathway to eliminate cancerous cells.

1.5.2. Modulation of COX metabolism

COX-2 is overexpressed in many cancers including CRC and has a role in facilitating the enzymatic conversion of *n*-6 PUFAs such as LA and AA in to pro-inflammatory, tumour promoting PGE₂ (157, 158). In a study involving 1026 CRC specimens, 78 % expressed COX-2 detected by immunohistochemistry (IHC) (159). Expression of COX-2 in CRC has been associated with increased cell adhesion and resistance to apoptosis (160). COX-2 enzymatic conversion of AA into prostaglandin H₂ (PGH₂) leads to the production of a range of prostaglandins including tumour promoting prostaglandin E₂ (PGE₂) (157). PGE₂ causes aberrant signalling which promotes inflammation and tumour growth (152, 158) through interactions with EGFR-PI3K-Akt and Ras-MAPK pathways or PGE₂-EP₄ receptor signaling. Increased PGE₂ causes pro-tumourigenic CRC cell proliferation, invasion, motility and anti-apoptotic effects, as well as increased inflammatory signaling and immune evasion (138, 152, 157, 161)

COX-2 inhibition has been investigated in prevention and treatment of CRC, with over 100 observational studies confirming aspirin use in CRC cancer prevention (162). Aspirin elicits anti-cancer effects via COX-dependent pathways through the inhibition of COX-2 and reduced PGE₂ production, or COX-independent pathways (160). Reduced proliferation and increased apoptosis of human CRC cells following treatment with prostaglandin synthesis inhibitors (sulindac sulfide (an active metabolite of sulindac) and piroxicam) was independent of the cell lines COX-status or ability to produce prostaglandins as the cell lines compared were COX-negative (HCT-15) and COX-positive (HT-29) (163). Recently the follow up of the CAPP2 trial (ISRCTN59521990) which investigated the use of the non-steroidal anti-inflammatory drug (NSAID) 600 mg aspirin daily versus placebo in patients with Lynch syndrome and found that 9 % of patients who received aspirin developed CRC in comparison to 13 % who had received placebo (162). Celecoxib, a selective COX-2 inhibitor was also found to delay development of adenomas in patients with FAP (164).

EPA and DHA are substrates for COX-2, leading to the production of 3-series prostaglandins; prostaglandin E₃ (PGE₃) [Figure 1.7]. Whilst the affinity (K_M) does not differ between EPA and AA, EPA has a lower maximal rate of reaction (V_{MAX}) compared with AA (30 % of the AA rate) (138). Competition between substrates results in production of small quantities of PGE₃, reducing the amount of PGE₂ produced (165). PGE₃ is an anti-tumorigenic metabolic product and this may alter the cancer promoting

cellular environment utilised by the cancer cells (158, 165). It should be noted that EPA is an alternative substrate to AA for COX-2, however the structure of DHA renders it a poor substrate for COX-2.

In comparison to COX-2, the COX-1 isoform is less frequently studied. Constitutive expression of COX-1 is found in most tissues and it has a role in maintaining homeostasis through production of prostanoids (166). COX-1, like COX-2, may have a role in CRC tumourigenesis by synthesising cancer-promoting prostanoids via AA metabolism. A study in which COX-1 mRNA expression was compared between stage III CRC tumours and normal colonic mucosa, found elevated COX-1 expression in the tumours (167). COX-1 is irreversibly bound by aspirin, which inhibits AA metabolism and reduces synthesis of PGE₂ and other mediators (168, 169), and is being clinically evaluated for use as an adjunct to standard therapy in the Add-Aspirin trial, a phase 3 randomised placebo controlled trial (NCT02804815) (170). The trial involves patients who have had their primary CRC tumour surgically resected. COX-1, like COX-2, can metabolise EPA [Figure 1.7].

1.5.3. G protein coupled receptor signalling

EPA and DHA have been shown to act as ligands for cell surface G protein coupled receptors (GPCRs) (171). GPCRs are members of a large family of proteins, activated by a diverse range of ligands. Upon GPCRs are considered some of the most clinically relevant and promising targets for drug discovery (172). Binding of specific ligands to GPCRs initiates signal transduction pathways that are further detailed in **Chapter 6.1.3**.

n-3 PUFAs EPA and DHA are ligands for GPCRs, Gpr120 (also known as FFA4) (171, 173) and Gpr40 (also known as FFA1) (106). Whilst GPR120 has been found expressed in human CRC cell lines, GPR40 has not (174). Both are rhodopsin-like GPCRs (175), that upon ligand binding and activation, couple to the Gα_{q/11} subunit and mitigate a signal that causes the release of intracellular calcium (Ca²⁺) (175). In HT-29 and LoVo cell lines, EPA-induced agonism of the GPR120 receptor causes an increase of phosphorylation of downstream effectors YAP (yes-associated protein) which leads to the inactivation of YAP/TAZ (TAZ: WW-domain-containing transcription regulator 1) and activation of the Hippo pathway (142). In turn, this causes decreased proliferation and increased apoptosis of the CRC cells (142).

In murine models, activation of Gpr120 in response to *n*-3 PUFAs was shown to negatively affect tumour-associated macrophage pro-tumourigenic activity or modulate the systemic anti-tumour host response (171).

Determining if other GPCRs, expressed by CRC tumour cells, are activated upon EPA and DHA stimulation is therefore an important area of research. To identify molecular drivers of sensitivity and resistance, a whole mouse genome expression microarray was performed (prior to the start of this PhD project). The analysis investigated differential gene expression between murine CRC cells that were EPA-sensitive (MC38) or EPA-resistant (MC38r), further details of this are given in **Chapter 6.1.1**. This work identified *Mrgprf*, an orphan (no known ligand) GPCR, with a potential role in EPA sensitivity which is further described and investigated in **Chapter 6**.

1.5.4. Indirect anti-CRC effects of *n*-3 PUFAs

N-3 PUFAs activity is not limited to direct effects upon the cells to which they are exposed. Indirect activity, whereby *n*-3 PUFAs can alter the microbiome and tumour microenvironment, are areas that require further study to improve understanding. These are further discussed in **Chapter 7**, as detecting indirect activity was not possible in this thesis as it solely utilized *in vitro* CRC models.

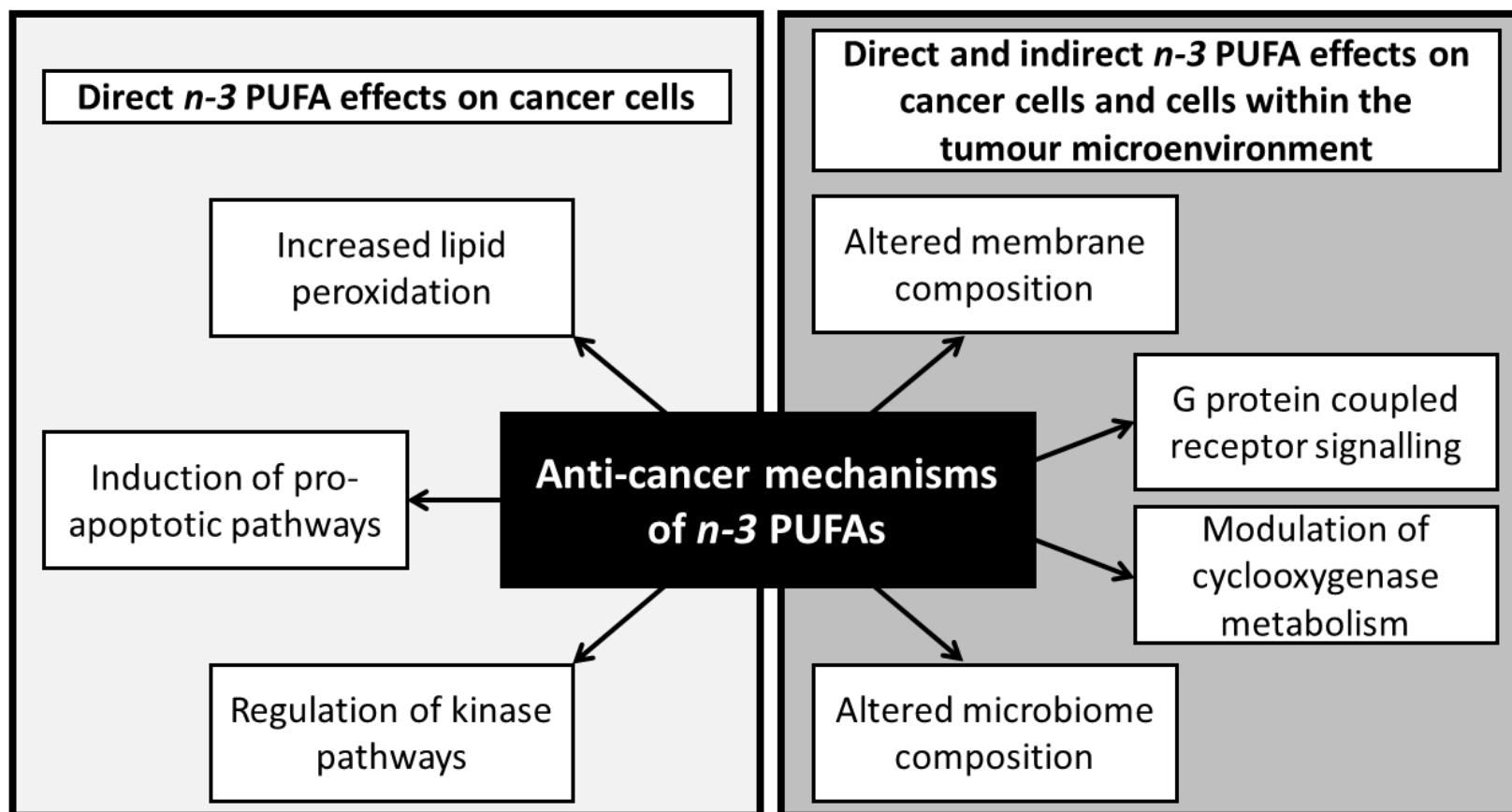


Figure 1.8. Mechanisms through which *n*-3 PUFAs exert anti-cancer effects on hCRC cells

Mechanisms through which *n*-3 PUFAs such as EPA and DHA exert anti-cancer effects are not fully understood. It is likely that mechanisms are interlinked or can occur concomitantly.

Chapter 2: Aims and hypotheses

Projected incidence of CRC suggests a 11 % reduction between 2014 and 2035 (23), but a clinical need for efficacious treatment options remains, as CRC accounts for the second most common (10 %) cause of cancer deaths in the UK (23). *N*-3 PUFAs are an attractive potential treatment, with EPA efficacy in CRCLM treatment being assessed by an ongoing phase III RCT (NCT03428477) (176). However, there are no biomarkers currently available to enable patient stratification. Previous studies show that different CRC cell lines have varied responses to EPA or DHA exposure (90, 106, 107, 110, 134-137, 139, 148, 150-152, 177-179). Predictive markers of intrinsic sensitivity or acquired resistance have yet to be investigated, especially in the context of human CRC molecular phenotypes. Further understanding of response to *n*-3 PUFAs will contribute to facilitating personalised therapeutic approaches.

2.1. Aim

The overall aim of this research was to identify and investigate markers, key drivers and pathways associated with sensitivity or resistance of colorectal cancer cell lines to the *n*-3 PUFAs; EPA and DHA. This work could identify phenotypes associated with, and predictive biomarkers of, response to *n*-3 PUFAs.

2.2. Hypotheses

In Chapters 4 and 5, I tested the following hypotheses to examine the intrinsic differences between *n*-3 PUFA sensitivity across a large panel of human CRC cell lines:

- I. CRC cell lines display inherent differences in sensitivity to EPA and DHA. These intrinsic differences are associated with key CRC molecular phenotypes (CIN, CIMP and microsatellite status) and/or enzymes involved in *n*-3 PUFA metabolism such as COX enzymes and/or FA content of cell lines.

To identify potential molecular markers associated with acquired *n*-3 PUFA resistance, in Chapter 6, I tested the following hypotheses:

- I. Reduced expression of orphan GPCR, *Mrgprf* (MRGPRF), in the EPA-resistant MC38r murine CRC cell line model compared to the parental EPA-sensitive MC38 counterpart, drives resistance to EPA.
- II. Comparison of EPA- or DHA- isogenic CRC cell line clones, generated from chronic exposure to these n-3 PUFAs, identifies phenotypic and genotypic alterations associated with *n*-3 PUFA sensitivity and/or resistance.

Chapter 3: Materials and Methods

3.1. Stock preparation

3.1.1. Fatty acids

Pure eicosapentaenoic acid in its free fatty acid form (referred to as EPA throughout) was gifted by SLA Pharma AG (Watford, UK). EPA oil (3.3 M) was extracted from capsules using a large gauge needle (21G) in a sterile environment and stored at 4°C for 1 month maximum. Working stock solutions (33 mM) were prepared fresh for each experiment, by diluting the oil in 100 % ethanol (Merck Life Science UK Ltd; Gillingham, UK).

Docosahexaenoic acid powder in its free fatty acid form (referred to as DHA throughout) was obtained from Cayman Chemical (Ann Arbor, USA; Item No: 90310). A 'master stock' solution (761 mM) was in 100 % ethanol. Working stock solutions (33 mM) were prepared fresh for each experiment, by further diluting the master stock solution in 100 % ethanol. Working stocks were stored at -20°C for a maximum of 1 month.

3.1.2. Epigenetic drugs

Epigenetic drugs were reconstituted in dimethyl sulfoxide (DMSO) (Merck Life Science UK Ltd; Gillingham, UK; cat No: 276855). Decitabine (DAC, Cell Guidance Systems Ltd; Cambridge, UK; Cat: SM46), was prepared to stock concentrations of 500 mM and 50 mM, 5-Azacytidine (AZA, Cayman Chemicals; Ann Arbor, USA; Cat: CAY11164), was prepared to a stock concentration of 10 mM and Temozolomide (TMZ, Cayman Chemicals; Ann Arbor USA; Cat: CAY14163) at a 25 mM concentration

3.2. Cell Culture

3.2.1. Cell Lines Used

Cell line details, including source and growth conditions, are summarised in **Table 3.1**. Cell lines were routinely tested for mycoplasma in house using MycoAlert Mycoplasma detection kit (Lonza; Basel, Switzerland). Cells were cultured in ThermoFisher Scientific (Massachusetts, USA) growth media and supplemented with 10 % (v/v) fetal calf serum (FCS) (Merck Life Science UK Ltd; Gillingham, UK). Culture medium used included: Roswell Park Memorial Institute 1640 media containing Glutamax® (RPMI) (cat No: 61870036), Dulbecco's Modified Eagle Media containing GlutaMAX™ (DMEM) (cat No: 10569010) and Gibco™ Ham's F-12 Nutrient Mix containing GlutaMAX™ (F12) (cat No: 31-765-035) and Leibovitz's L-15 (L15) (cat No: 11415049).

3.2.2. Routine passage and growth conditions

All cell lines were maintained at 37°C in a humidified atmosphere containing 5 % CO₂, with the exception of newly revived SW1116 and SW837 which were maintained under atmospheric air conditions in L-15 culture medium for 3 passages before being acclimatised to culture in RPMI medium with 5 % CO₂.

Cell lines were routinely sub-cultured once 70-80 % confluent, for a maximum of 18 passages. Sub-culturing was performed by removing medium, rinsing in Dulbecco's phosphate buffered saline (DPBS) (ThermoFisher Scientific; Massachusetts, USA; cat No: 14190-095), and resuspending cells by incubation with 2 ml of 0.25 % w/v trypsin-ethylenediaminetetraacetic acid (EDTA) (ThermoFisher Scientific; Massachusetts, USA) per T75 flask for 5 minutes at 37°C. Once cells had detached, trypsin was neutralised with 8 ml fresh complete medium, and an appropriate volume of cell suspension was transferred to a new flask containing fresh medium to a total volume of 10 ml. Subculture ratios are provided in **Table 3.1**.

3.2.3. Routine cell cryopreservation

Cell lines stocks were prepared for cryostore containment from early passage cultures. Following trypsinisation, cells were resuspended in appropriate cell media to give a total volume of 10 ml. Cells were centrifuged at 400 g for 5 minutes and media removed. Cell pellets were resuspended in media containing 10 % DMSO and transferred to cryovials

(Fisherbrand™; Loughborough, UK; cat No: 11777939). They were stored at -80°C for 24 hours in a freezing container (Nalgene® Mr Frosty; Merck Life Science UK Ltd; Gillingham, UK) containing 2-propanol before transfer into liquid nitrogen long-term storage.

Table 3.1. Cell line general information

Cell Line	Cell type	Organism	Source	Growth Media	Passage Ratio
HEK293	Embryonic Kidney	<i>Human</i>	ATCC	DMEM + 10 % FCS	1:20
MC38	Chemically induced CRC	<i>Mouse</i>	D. Beauchamp, Vanderbilt University, TN, USA	RPMI + 10 % FCS	1:10
MC38R	Chemically induced CRC	<i>Mouse</i>	Isolated in-house using TGF- β (5ng/ml) in a transwell migration assay	RPMI + 10 % FCS	1:10
CaCo-2	CRC	<i>Human</i>	ECACC	RPMI + 10 % FCS	1:10
Colo205	CRC	<i>Human</i>	ECACC	RPMI + 10 % FCS	1:10
DLD-1	CRC	<i>Human</i>	ATCC	RPMI + 10 % FCS	1:10
HCA7	CRC	<i>Human</i>	ATCC	RPMI + 10 % FCS	1:10
HCT116	CRC	<i>Human</i>	ATCC	RPMI + 10 % FCS	1:20
HRT18	CRC	<i>Human</i>	ECACC	RPMI + 10 % FCS	1:10
HT29	CRC	<i>Human</i>	ATCC	RPMI + 10 % FCS	1:10
LoVo	CRC	<i>Human</i>	ATCC	F12 + 10 % FCS	1:10
LS174T	CRC	<i>Human</i>	ECACC	DMEM + 10 % FCS	1:10
LS411N	CRC	<i>Human</i>	ATCC*	RPMI + 10 % FCS	1:10
SW48	CRC	<i>Human</i>	ATCC	RPMI + 10 % FCS	1:10
SW480	CRC	<i>Human</i>	ATCC	RPMI + 10 % FCS	1:20
SW620	CRC-LN	<i>Human</i>	ATCC	RPMI + 10 % FCS	1:20
SW837	CRC	<i>Human</i>	ATCC*	RPMI + 10 % FCS	1:5
SW1116	CRC	<i>Human</i>	ATCC*	RPMI + 10 % FCS	1:1
T84	CRC	<i>Human</i>	ATCC	F12 : DMEM (1:1) + 10 % FCS	1:10
TC71	CRC	<i>Human</i>	Prof Alex Duval, INSERM	DMEM + 10 % FCS	1:10

Cell lines marked with an asterisk were newly purchased for this study whereas stocks were available in-house for those without. CRC-LN: colorectal cancer derived from lymph node metastatic site. ATCC: American Type Culture Collection. ECACC: European Collection of Authenticated Cell Cultures.

3.3. Molecular Profiling of Cell Lines

3.3.1. Genomic DNA extraction

Genomic deoxyribonucleic acid (gDNA) was extracted using the PureLink™ Genomic DNA mini kit (Merck Life Science UK Ltd; Gillingham, UK; cat No: K182002) following manufacturer's instructions. 5×10^6 cells were harvested through trypsinisation and resuspended in 200 µl DPBS. 20 µl each of proteinase K and RNase A were added to the sample, vortexed and incubated at room temperature for 2 minutes. 200 µl of PureLink™ Genomic Lysis/Binding buffer was added to each sample and mixed thoroughly by vortex until the mixture was homogeneous. The reaction was incubated at 55°C for 10 minutes to promote protein digestion, and 200 µl of 100 % ethanol was added and mixed in until, once again, the resulting lysate mixture was homogenous.

Sample lysates were purified by adding the solution onto a PureLink™ spin column. Centrifugation at 10000 *g* for 1 minute was followed by discarding collected liquid and washing the column with 500 µl wash buffer 1. The sample was centrifuged at 10000 *g* for 1 minute. Once again, the collection tube was disposed of, 500 µl of wash buffer 2 was added and the column was centrifuged at a maximum speed of 16000 *g* for 3 minutes. The spin column was placed in a 1.5 ml microcentrifuge tube and 50 µl of PureLink™ genomic elution buffer was added to the column and left to incubate at room temperature for 1 minute. The column underwent centrifugation at 16000 *g* for 1 minute and resulting gDNA was quantified and purity assessed using a NanoDrop 1000 Spectrophotometer (ThermoFisher Scientific; Massachusetts, USA) using the 260 nm and 280 nm wavelengths.

3.3.2. Short tandem repeat profiling of human CRC cell lines

Short tandem repeat (STR) profiling was used to authenticate all human CRC cell lines (with the exception of the ones newly purchased from ATCC for this project, see **Table 3.1**) (180, 181). For each cell line, 50 µl gDNA samples (>20 ng/µl) were provided to Source Bioscience typing service (Nottingham, UK) for profiling using the Promega Powerplex 16HS assay. The following loci markers were analysed: AMEL, CSF1PO, D13S317, D16S539, D18S51, S21S11, D3S1358, D5S818, D8S820, D9S1179, FGA, PentaD, PentaE, TH01, HPOX and vWA.

Data was formatted using GeneMapper® ID and ID-X software by the service supplier before being returned. STR profile analysis was completed using Peak Scanner software (version: 3.0.3-PRC-build4; ThermoFisher Scientific; Massachusetts, USA) to confirm peak assignment. ATCC matching algorithm (181) was used to compare allele profiles with expected ATCC profiles. An authentication threshold was defined as >80 % match (181). Allele profiles were also compared to profiles listed on DSMZ, CLS and TKG databases.

3.3.3. Microsatellite Stability Testing

3.3.3.1. BAT25 and BAT26 primers

Amplifying and sizing BAT-25 and BAT-26 DNA markers, which are 2/5 of the Bethesda panel (45), have been shown to correctly identify 97 % of MSI-high samples (41). The oligonucleotide primers used for microsatellite status analysis are detailed in **Table 3.2**.

Table 3.2. Primer sequences for BAT-25 and BAT-26 microsatellite stability markers

Marker	Forward Primer F (5' – 3')	Reverse Primer R (5' – 3')	Product Size (bp)
BAT-25	[6FAM]CTCGCCTCCAAGAA TGTAAGT	CTATGGCTCTAAAATGCTC TGTTTC	114
BAT-26	[HEX]TGACTACTTTTGACTT CAGCC	AACCATTCAACATTTTAAAC CC	122

BAT-25 marker allows amplification of part of the *KIT* receptor tyrosine kinase. BAT-26 is a region of *MSH2* DNA mismatch repair gene.

Hydrophylised primers (Merck Life Science UK Ltd; Gillingham, UK) were reconstituted in nuclease free dH₂O at a concentration of 100 µM. BAT-25 and BAT-26 primers were stored at -20°C and kept away from light, as they were fluorescently tagged with 6FAM and HEX, respectively.

3.3.3.2. PCR Conditions

PCR reactions were performed in biological triplicate. gDNA was diluted to 10 ng/µl in 100 µl. For each experiment, an MSI primer master mix was prepared, comprising of 5 µM of each of the 4 primers and nuclease free water to give a final volume of 200 µl.

Polymerase chain reactions (PCR) were set up with a total reaction volume of 10 µl and constituting 5 µl Hot Shot Mastermix (Clent Life Science; Stourbridge, UK; cat No:

HS002), 1 µl MSI primer mastermix (giving a final individual primer concentration per reaction of 0.5 µM), 3 µl gDNA and 1 µl nuclease free water.

PCR was performed using the following cycles: initial denaturation at 95°C for 5 minutes, 40 cycles of (95°C for 30 seconds, 54°C for 42 seconds and 72°C for 60 seconds). The reaction ended with a final incubation at 72°C for 10 minutes.

3.3.3.3. PCR product analysis by DNA electrophoresis

To prepare samples for analysis by DNA electrophoresis, 1 µl of 6x loading buffer (Merck Life Science UK Ltd; Gillingham, UK; cat No: G2526) was added to 5 µl PCR product and briefly centrifuged at 4000 g to mix. Samples were loaded onto a 1.5 % w/v agarose (SeaKem® LG; Lonza; Basel, Switzerland; cat No: 50002) gel in 1x Tris-acetate EDTA (TAE) buffer [0.4 M tris acetate, 0.01 M EDTA] containing 15 µl ethidium bromide (Merck Life Science UK Ltd; Gillingham, UK; cat No: E1510).

The gel was loaded into gel tanks filled with 1X TAE buffer and samples were loaded alongside 10 µl 100 bp ladder (New England BioLabs; Massachusetts, USA; cat No: B7025) and run for 45 minutes at 120 V. The gel was visualised on the BioRad Molecular Imager® Gel Doc™ XR+ System (Bio-Rad, California, USA) using Image Lab 5.2.1 build 11 software to acquire images (Bio-Rad Laboratories, California, USA).

3.3.3.4. PCR product analysis by Sequencing

PCR product was diluted 1/10 with dH₂O and 0.5 µl of the diluted PCR product was mixed with 8.5 µl of HiDi™ Formamide (ThermoFisher Scientific; Massachusetts, USA; cat No: 4311320) and 1 µl Gene Scan ROX500 (ThermoFisher Scientific; Massachusetts, USA; cat No: 401734). Genotyping and sequence analysis were performed on the ABI3130xl Genetic Analyser (Applied BioSystems by Life Technologies; California, USA). The data was analysed using PeakHeights software (Ian Carr) (182). Sample traces were calibrated to the Gene Scan ROX500 standard and the analysis was focused on the region between 100 base pairs and 140 base pairs to include *BAT-25* and *BAT-26* PCR products. Calculation of the shift of the major peaks were performed manually upon visualisation of the peaks.

3.4. Cell viability assays

3.4.1. MTT Assay

This assay relies upon the principle that mitochondrially active cells have the ability to reduce 3-(4, 5-dimethylthiazol-2-yl)-2,5-diphenyl tetrazolium bromide salt (MTT, Invitrogen™; ThermoFisher Scientific; Massachusetts, USA; cat No: M6494) into formazan, which is a blue crystal salt [Figure 3.1], soluble in DMSO. Therefore, the amount of formazan product, determined by measuring absorbance at 620 nm, is proportional to the number of viable cells present.

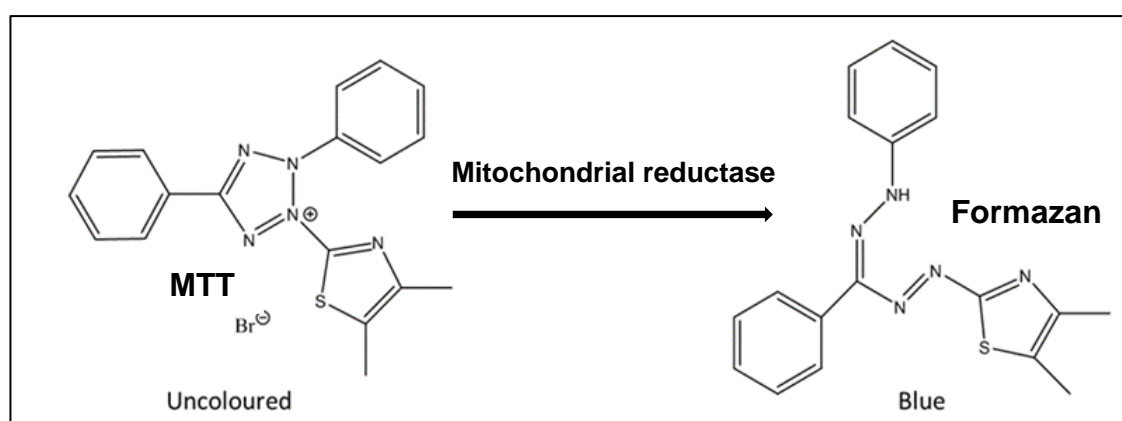


Figure 3.1. Reduction of MTT to crystal formazan salt.

Reduction of colourless MTT (3-(4,5-dimethylthiazol-2-yl)-2,5-diphenyl tetrazolium bromide salt) by mitochondrial reductase enzymes. This produces blue formazan crystals which can be quantified, after being dissolved in DMSO, by measuring absorbance at 620nm using a spectrometer. Image adapted from (183).

The assay was performed in a 96-well-plate. Four technical replicates per condition were included on each plate and between 3 and 18 independent replicates were conducted. More than 3 independent replicates were conducted for some cell lines due to their use in *n*-3 PUFA chronic exposure experiments (**Chapter 3.5**), as to assess altered sensitivity following chronic exposure, parental (non-chronically exposed) cells were used as a comparator. On each plate, the first column of cells was left blank. Cell lines were seeded at a density of 1000 cells / well, except for HCA-7, SW837 and SW1116, which were seeded at 5000 cells / well. Following seeding, cells were incubated for 24 hours at 37°C, 5 % CO₂. Culture media was removed and replaced with *n*-3 PUFA or epigenetic-drug containing media. Following 72-hour incubation, 20 µl of MTT solution (5 mg/ml) was added to each well and plates were incubated at 37°C, 5 % CO₂ for 4 hours, in the dark. The solution was removed and resulting formazan salt crystals were dissolved in 150 µl DMSO (Merck Life Science UK Ltd; Gillingham, UK; cat No: 276855).

Absorbance measurements at 620 nm wavelength, were made using the LB940 microplate reader (Berthold Mithras, UK) and visualised with MicroWin software.

3.4.2. Crystal Violet Assay (alternative to MTT)

SW1116 cells were observed to have a very slow doubling time, and repeat attempts to determine *n*-3 PUFA sensitivity using the MTT assay were unsuccessful, leading to the assumption that there is a lack of metabolic enzymatic activity which allows for the reduction process that converts MTT to formazan.

An alternative method to MTT involving use of crystal violet was utilised. Crystal violet is a chemical that binds to proteins and DNA (184). The protocol relies on the principle that dead cells lose adherence and are washed away, thus leading to a reduction in staining in culture (184).

SW1116 cells were seeded on day 1 at a density of 5.0×10^4 and left to incubate at 37°C, 5 % CO₂ until day 5. On day 5, cells were treated with media containing concentrations of EPA, DHA and combined EPA and DHA, and left to incubate in standard culture conditions until day 20. Media was aspirated and cells were washed under a gentle stream of tap water twice, before the plate was inverted on paper towels to remove excess liquid.

A 0.5 % crystal violet solution was prepared by dissolving 0.5 % w/v crystal violet powder (Alfa Aesar; Massachusetts, USA; cat No: B21932) in 80 ml dH₂O and 20 ml 100 % methanol (Merck Life Science UK Ltd; Gillingham, UK). 0.5 % crystal violet solution was stored at room temperature, in the dark, and kept for no longer than 2 months. In each well, 50 µl of 0.5 % crystal violet staining solution was added. Plates were then incubated for 20 minutes at room temperature on a benchtop rocker oscillating at a frequency of 20 oscillations per minute. Following the incubation period, cells were washed under a gentle stream of running water for 4 repeat washes, removing excess crystal violet stain. Plates were left overnight at room temperature to air dry, ensuring evaporation of all liquid. On day 21, 150 µl 100% methanol was added to each well and plates were incubated at room temperature for 20 minutes, on the bench rocker as per previous set up. Optical density was measured of each well using LB940 plate reader (Berthold Mithras, UK) at 570 nm.

3.4.3. Cell Treatments

3.4.3.1. *n-3 PUFA treatments*

Cell lines were exposed to EPA and/or DHA concentrations ranging from 1 μM to 500 μM , prepared as serial dilutions in culture medium as previously described (134, 144). For *n-3* PUFA concentrations below maximum, the ethanol volume was not adjusted to equal the v/v % in the maximum *n-3* PUFA concentration. In addition, control cells were treated with an ethanol carrier control equivalent to the maximum (500 μM) *n-3* PUFA exposure, which corresponded to a 1.5 % v/v 100 % ethanol in media. For determination of sensitivity to a combination treatment, EPA and DHA were mixed in a 2:1 ratio.

3.4.3.2. *Epigenetic drug treatments*

To determine sensitivity to individual epigenetic drugs, cells were exposed to a DAC range of 1 μM to 500 μM , AZA range of 0.03 μM to 8 μM and TMZ range of 1 μM to 500 μM . For epigenetic drug concentrations below maximum, the volume of DMSO was not adjusted to equal v/v % in maximum epigenetic drug concentrations. DMSO carrier control equivalent to the maximum DAC, AZA and TMZ was also prepared, corresponding to 0.1 % v/v DMSO, 0.08 % v/v DMSO and 0.05 % v/v DMSO respectively.

To examine the effect of epigenetic drug pre-treatment on *n-3* PUFA sensitivity, cells were exposed to either 1 μM or 2 μM DAC, 0.25 μM or 0.5 μM AZA, or 5 μM TMZ. Following 24 hours incubation at 37°C, 5 % CO_2 , cells were exposed to EPA and DHA concentrations ranging from 1 μM to 500 μM (prepared as previously described, in media containing DAC, AZA or TMZ corresponding to the initial 24 hour exposure dose).

3.4.4. Cell viability assay analysis

Data analysis was completed using Microsoft Excel for determining percentage growth compared to the untreated controls. First the mean absorbance was calculated for each set of 4 technical replicates. The mean 'blank' absorbance, measured across wells in which no cells were seeded, was subtracted from all mean absorbance values. The percentage compared to carrier control was calculated and the data was plotted on a semi-log x-axis in GraphPad Prism8™ (GraphPad Software; California, USA; software version 8.30 (328)). Regression 'Log (inhibitor) vs normalised response – variable slope'

or the 'biphasic' equation were used to determine IC₅₀ values. IC₅₀ are expressed as mean values ± standard error of the mean (SEM) for 3-18 independent experiments.

3.4.5. Growth rate of hCRC cell lines

Absorbance readings of control cells, treated for 72 hours with ethanol carrier and measured during MTT assays, were used as a surrogate marker of growth rate. This includes data for HCA-7, SW837 and SW1116 as the assay was initially attempted with 1000 cell/well seeding density before the protocol was optimised completely and the seeding density was increased.

3.4.6. EPA and DHA interaction analysis

Concentrations of independent EPA or DHA found in the combined EPA:DHA (2:1) mixture were calculated. In 50 µM combined treatment, corresponding concentrations of EPA and DHA were approximately 33 µM and 16 µM respectively. In 100 µM combined treatment, corresponding concentrations were 66 µM EPA and 33 µM DHA, respectively.

Cell viability was extrapolated from concentration response curves for cells exposed to 50 µM and 100 µM combined treatment, an example is shown in **Figure 4.6, Chapter 4.3.4.5**. Percent cell viability data for individual *n*-3 PUFAs at relevant corresponding concentrations was obtained from EPA and DHA concentration response curves. Percent change in viability was calculated for all treatment conditions, with a positive value indicating a growth benefit of treatment and a negative value indicative of growth inhibition).

Combined treatment was considered 'potentially antagonistic' if the percent growth change was smaller than the growth change expected by combining percent growth change for individual *n*-3 PUFAs. Combined treatment was considered 'potentially additive' if the percent growth change was equal to the growth change expected by combining percent growth change for individual *n*-3 PUFAs. If combined treatment caused a growth change that was larger than the growth change expected by combining percent growth change for individual *n*-3 PUFAs, the relationship was labelled 'potentially synergistic'. All the labels for the interaction between EPA and DHA in the combination mixture are considered 'potential' as further comprehensive studies would be required to confirm these interactions.

3.5. Generating Resistance: Chronic Exposure Experiments

To develop a relevant model to study the differences between *n*-3 PUFA sensitive and resistant cell lines, I set out to generate cell lines with acquired resistance to *n*-3 PUFAs.

3.5.1. IC₅₀ and escalating dose treatment

IC₁₀ and IC₅₀ concentrations [Table 3.3] were obtained by extrapolating EPA and DHA concentration response curves for the relevant cell lines [Figure 4.5, Chapter 4.3.4]. IC₁₀ in this instance is defined as the concentration of EPA / DHA at which 10% cells are viable (compared to carrier control). DLD-1, HCT116, HCA-7, HT29, LoVo and MC38 cells were seeded in T25 flasks and allowed to reach 30 % confluence. Cells were treated with IC₁₀ *n*-3 PUFA for 24 hours to sensitise the cells.

Cells were maintained in IC₅₀ μ M *n*-3 PUFA concentrations for 5 passages, PUFA-containing medium was refreshed every 2 days. After 5 passages, cell line's sensitivity to each *n*-3 PUFA was assessed by MTT as previously described [Chapter 3.4.1] and compared with the matched parental cell line.

Table 3.3. *n*-3 PUFA IC₁₀ and IC₅₀ concentrations

Cell Line	EPA concentration (μ M)		DHA concentration (μ M)	
	IC ₁₀	IC ₅₀	IC ₁₀	IC ₅₀
DLD-1	30	85	5	15
HCT116	5	90	5	30
HCA-7	55	140	5	25
HT29	5	120	15	55
LoVo	25	140	5	20
MC38	25	95	5	40

3.5.2. High concentration range selection

To increase selective pressure, cells were treated with a range of EPA or DHA concentrations. Cells were seeded in 6-well plates at 3.0×10^5 cells per well. At 70 % confluence, cells were treated with a range of EPA and DHA concentrations (100 to 200 μ M and 20 to 90 μ M respectively). Cell death was monitored, and regrowth of cells from cells surviving the highest possible concentration was observed. Microscope images

were acquired using a Nikon camera to document cell death and regrowth. Untreated and carrier (0.60 % v/v ethanol, equivalent to 200 μ M treatment dose) control treated cells were grown alongside high concentration treated cells. Once surviving cells were 80 % confluent, they were expanded into T25 flasks in the presence or absence of *n*-3 PUFA treated culture medium for 24 hours. Cells were maintained, in growth-selected conditions, for a further 5 passages. Sensitivity to EPA and DHA was tested by MTT assay as previously described in **Section 3.4.1**.

3.6. *PTGS1* and *PTGS2* gene expression model

3.6.1. Developing a *PTGS1* and *PTGS2* gene overexpression positive control

A lyophilised plasmid was synthesised by GeneWiz UK Ltd (UK) and reconstituted in Tris-EDTA (TE) Buffer (Invitrogen™; ThermoFisher Scientific; Massachusetts, USA; cat No: 12090015, 10 mM Tris-HCl (pH 8.0) and 0.1 mM EDTA), at a concentration of 100 ng/μl. The plasmid was based on a pUC57 vector backbone with Ampicillin resistance gene and a 565 base pair insert [Figure 3.2] containing the sequence of the expected qPCR product from my selected primers [Table 3.5] for human *PTGS1*, *PTGS2*^(a) and *IDO-1*, separated by specific restriction sites.

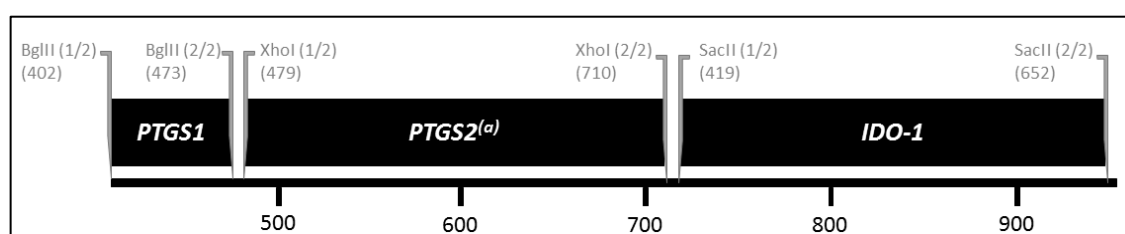


Figure 3.2. Vector insert containing selected amplicons

A schematic representation of the 565 base pair insert region of the cloning vector containing the specific sequences of the *PTGS1* and *PTGS2*.

PTGS2^(a) is denoted (a) as this was included in the plasmid design but was subsequently not utilised. This was due to inconsistent results obtained by primers designed to amplify this amplicon by RT-qPCR. The investigation into *IDO-1* expression in hCRC cell lines is not included in this thesis.

3.6.1.1. Plasmid Transformation

First, 50 μl of Subcloning Efficiency™ DH5α Competent cells [*E. coli*] (Invitrogen™, ThermoFisher Scientific; Massachusetts, USA; cat No: 18265017) were thawed on ice and 200 ng of plasmid added. The transformation mixture was incubated on ice for 30 minutes. The bacteria were heat-shocked at 42° for 45 seconds and cooled on ice for 2 minutes. 250 μl of super optimal broth with catabolite suppression (S.O.C) medium was added before incubating the reaction at 37°C for 1 hour, on a shaker (New Brunswick Scientific; New Jersey, USA; model: C25 Incubator Shaker, Classic Series) at 225 rpm.

Ampicillin stock solution was prepared to give a final concentration 50 mg/ml in 20 ml. 1 g of D-(-)- α -Aminobenzylpenicillin sodium salt was dissolved in 20 ml sterile deionized water, and aliquots containing 900 μ l were prepared and stored in -20°C. LB broth agar media and ampicillin plates were prepared by adding 8 g LB Broth powder, 8 g agar to 400 ml deionized water and 800 μ g ampicillin stock. The media was sterilized by autoclave and subsequently poured into plates and set. 125 μ l of the transformation mix was plated on a lysogeny broth (LB) plate containing 100 μ g/ml ampicillin. The plate was incubated overnight at 37°C.

3.6.1.2. Expansion of bacterial culture from frozen stocks

A sterile loop was used to inoculate a starter culture from a single colony in 3 ml of liquid LB medium supplemented with ampicillin (100 μ g/ml), for 8 hours. 200 μ l of this mixture was put into 20 ml LB ampicillin and incubated at 37°C overnight, shaking. This is now referred to as the 'overnight culture'.

3.6.1.3. Preparation of plasmid glycerol stocks

500 μ l of overnight culture was combined with 500 μ l of sterile glycerol (Merck Life Science UK Ltd; Gillingham, UK; cat No: G5516) and stored at -80°C. To expand a bacterial culture from frozen stocks, using a sterile loop, a small amount of the frozen plasmid glycerol was inoculated in a starter culture as described above.

3.6.1.4. Plasmid purification

Buffers (P1, P2, and P3) used during the plasmid purification process were provided in the QIAGEN Plasmid Midi Kit (QIAGEN; Hilden, Germany; cat No: 12143). The bacteria cells were harvested through centrifugation of the overnight culture at 4°C, 10 minutes at full speed (3220 g). Supernatant was removed. 200 μ l of cold (4°C) P1 buffer was added to the bacterial cell pellet and vortexed. 200 μ l of room temperature P2 buffer was added and gently mixed by inversion. 200 μ l of ice cold P3 buffer was added and mixed by inversion. The reaction was centrifuged for 10 minutes in a bench top centrifuge at maximum speed (16.1 g). The supernatant was discarded. The plasmid was washed in 300 μ l 70% ethanol and centrifuged for 5 minutes at maximum speed. The supernatant was removed, and the plasmid was air-dried for 10 minutes.

Purified vector DNA was resuspended in 50 µl 1x TE Buffer and quality and quantity was assessed by NanoDrop 1000 Spectrophotometer (ThermoFisher Scientific; Massachusetts, USA). The samples were stored at -20°C.

3.6.1.5. Restriction Digest

The details of the enzymes used, including the product that would release upon digestion, are listed in **Table 3.4** below.

Table 3.4. Restriction enzymes used

Restriction Enzyme	Source	Restriction Site	Digest Product
BglII	New England BioLabs (NEB), cat No: R0144	A [^] GATCT	<i>PTGS1</i>
XhoI	Promega, cat No: R6161	C [^] TCGAG	<i>PTGS2^(a)</i>
SacII	NEB, cat No: R0157	CCGC [^] GG	<i>IDO-1</i>

A: adenine. T: thymine. C: cytosine. G: guanine. The ^ notation indicates the cut site.

The buffers provided for each enzyme were as follows. 10x NEBuffer 3.1 (BglII), RE10x Buffer (XhoI) and 10x NEBuffer 4 (SacII).

For digestion involving NEB Enzymes / buffers, 5 µg of vector DNA, 3 µl enzyme and 2.5 µl 10x NEBuffer were added together, plus nuclease free water to give a total reaction mixture of 25 µl. For the Promega Enzyme / buffer, 5 µg of vector DNA, 1.5 µl enzyme and 3 µl RE10x Buffer and 0.3 µl were added together, plus nuclease free water to give a total reaction mixture of 25 µl. Reactions were mixed and briefly centrifuged before incubating at 37° for 1 hour. The digests were stopped by heating to 65°C for 20 minutes.

The digest products were run on agarose gels and visualised as previously described in **Section 3.3.3.3**, with the inclusion of a 1kb ladder (New England BioLabs; Massachusetts, USA; cat No: N3232L).

3.7. Mammalian cell MRGPRF overexpression model

To characterize and determine the role of Mrgprf in relation to CRC chemosensitivity to EPA, two stable Mrgprf-overexpressing cell lines were produced in 2016 during my Masters project (185). Brief details of this process are described here.

3.7.1.1. *Mrgprf* Vector

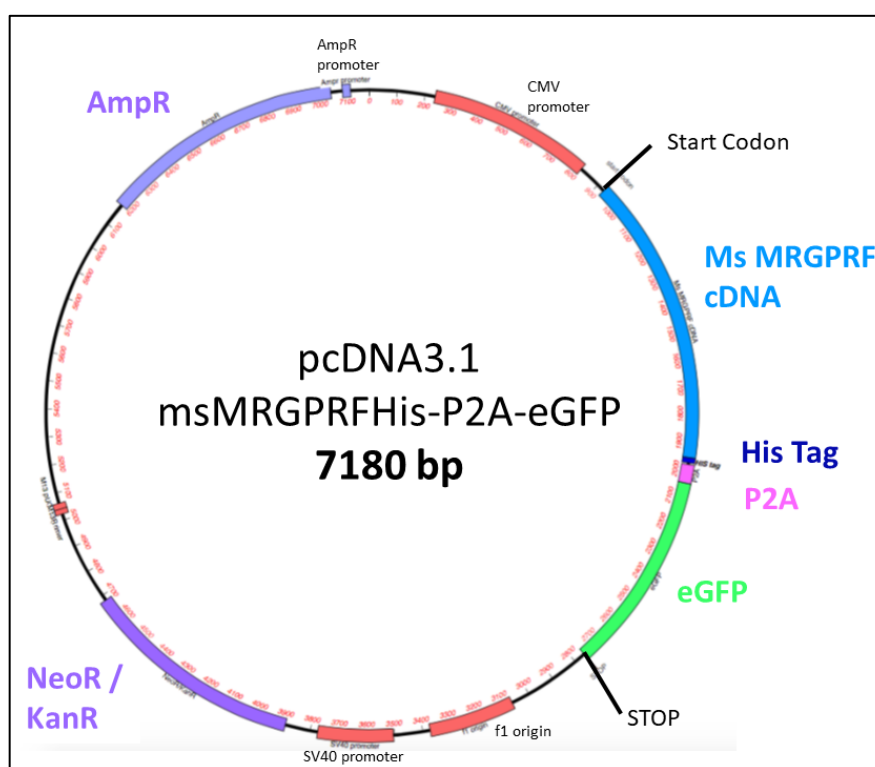


Figure 3.3. MRGPRF expression vector map

This diagram shows the MRGPRF vector plasmid. The His Tag could be used during protein purification and the P2A peptide enables simultaneous expression of MRGPRF and eGFP as it is a highly efficient cleavage site. Key features used during generation of transfected cell models labelled and outlined below.

Two expression vectors (10 µg/ml) were obtained from GenScript (USA); the first (pcDNA3.1 MRGPRF-His P2A-eGFP) containing msMRGPRF cDNA and the second (pcDNA3.1 P2A-eGFP) containing all the features of the first with the exception of msMRGPRF cDNA. A diagrammatic representation of the MRGPRF vector is shown in **Figure 3.3**. The notable key features include, eGFP tag, which was utilised to monitor transfection efficiency, an ampicillin resistance gene (AmpR) which allowed for selection of successfully transformed *E. coli* clones containing the vector which would grow on

ampicillin treated agar. The neomycin resistance (NeoR) gene was utilized in generation of stable clones, whereby cells transfected with the linear vector were cultured in media containing Geneticin®, also known as G-418 (Gibco by Life Technologies; Massachusetts, USA; cat No: 10131-019).

3.7.1.2. Generating stable Mrgprf Overexpressing Clones

The vector was linearised with the BglII restriction enzyme and stably transfected using lipofectamine in to two cell lines; HEK293 and MC38r. HEK293 cells are a human cell line known to readily take up vector DNA by transfection and were therefore used to maximize probability of a successfully transfected model. MC38r mouse cells were used to provide a more relevant model of CRC, with inherent resistance to EPA. Selective pressure by maintaining the transfected cell lines in G-418 was applied for a two-week period, to ensure that only cells encompassing the NeoR gene, and thus the vectors, survived. Following a cell sort (BD Influx 6-way cell sorter; BD Biosciences; UK), cells were gated on fluorescence intensity. Cells with highest fluorescence intensity were sorted into 96 well plates, 1 cell per well. Cells were maintained in G-418 treated media and expanded until populations of cells derived from original single cells were established. Stably transfected HEK293 and MC38r cells were cultured in 500 µM G-418.

3.7.1.3. Transient Mrgprf Overexpression Model

In a 6-well plate, cells were seeded at a density of 6.0×10^5 per well and incubated for 24 hours until 70 % confluent. Per transfection, a lipid mix containing 96 µl OptiMEM® medium (Invitrogen by Life Technologies™; Massachusetts, USA; cat No: 31985062) and 4 µl Lipofectamine® 2000 reagent (Invitrogen by Life Technologies™; Massachusetts, USA; cat No: 11668019) was incubated at room temperature for 5 minutes. Addition of OptiMEM® to 0.5 µg vector DNA stock to create a total 700 µl volume was completed. The DNA mixes and lipid mixes were combined in a 1:1 ratio and incubated at 37°C for 20 minutes. Finally, 400 µl of transfection mix was added per well after media was refreshed. Cells were incubated at 37°C, 5 % CO₂ for 24 hours.

Transfection efficiency was observed by microscopy, through visualizing the presence of green fluorescence emitted by eGFP contained within each vector. Transfection efficiency was expressed as an estimated percentage of cells positive for GFP in a field of view.

3.8. RNA Extraction Methods

Ribonucleic acid (RNA) extraction was completed using the RNeasy® Plus Mini Kit (QIAGEN; Hilden, Germany; cat No: 74134) as per manufacturer's instructions.

Cells were grown to 80 % confluence and prepared for RNA extraction by undergoing a DPBS wash then trypsinisation. 3×10^6 cells underwent centrifugation for 5 minutes at $400 \times g$. The resulting cell pellet was re-suspended in 350 μ l Buffer RLT+ plus 1% β -mercaptoethanol (Fisher Chemicals; Massachusetts, USA; cat No: O3446I-100). Samples were loaded on to a gDNA eliminator column and centrifuged at $8000 \times g$ for 30 seconds. 350 μ l of 70 % ethanol was added to the flow-through. The sample was transferred to an RNeasy MiniElute spin column, spun for 15 seconds and flow-through discarded, before addition of 700 μ l Buffer RW1 to the column. Samples again underwent centrifugation for 15 seconds, flow-through was discarded and 500 μ l Buffer RPE was added. Again, each column was spun for 15 seconds, flow-through removed and an additional 500 μ l Buffer RPE was added. The centrifugation step was repeated for 2 minutes and the column was transferred to a clean collection tube and spun at full speed for 1 minute. The column was placed in a 1.5 ml Eppendorf and 50 μ l RNase-free water was directly added to the column membrane. RNA was eluted by centrifugation of the column at $8000 \times g$ for 1 minute.

RNA was quantified using the NanoDrop 1000 Spectrophotometer (ThermoFisher Scientific; Massachusetts, USA).

3.9. Real-time PCR: quantitative polymerase chain reaction

Real-time quantitative PCR (qPCR) was used to measure gene expression of various targets against that of GAPDH in hCRC cell lines.

3.9.1. Primer details

Primers were ordered from Merck Life Science UK Ltd (Gillingham, UK) and reconstituted to give 100 mM stocks in nucleotide-free water. Details of all primers are provided in **Table 3.5** and **Table 3.6**.

All stock primers were stored at -20°C and further diluted before use in experiments. Final primer concentrations were; 0.2 µM for *β-actin* and *Mrgprf*; 0.3 µM for *GAPDH*, *PTGS1*, *PTGS2*^(a) and *IDO-1*, and 0.4 µM for *PTGS2*.

3.9.2. RNA processing for qPCR analysis

3.9.2.1. DNase Treatment of RNA

To eliminate genomic DNA contamination, 10 µg RNA was re-suspended in 1x DNase I Reaction Buffer (New England BioLabs; Massachusetts, USA; cat No: M0303) to a final volume of 50 µl. 2 units of DNase I (New England BioLabs; Massachusetts, USA; cat No: M0303S) was added to each sample, mixed and incubated at 37° for 10 minutes. The reaction was stopped by addition of 0.5 µl of 0.5 M EDTA and the DNase I heat inactivated by incubating the samples at 75°C for 10 minutes.

3.9.2.2. cDNA synthesis: Reverse transcription

The OmniScript® RT Kit QIAGEN; Hilden, Germany; cat No: 205113) was used to convert RNA into cDNA, following manufacturer's instructions.

In brief, 1 µg of template RNA was mixed with 2 µl 10x Buffer RT, dNTP mix, Oligo(dT) primers (Retroscript™ kit; ThermoFisher Scientific; Massachusetts, USA; cat No: 5730G) and 1 µl OmniScript reverse transcriptase and RNase inhibitor (RNaseOUT™, ThermoFisher Scientific; Massachusetts, USA; cat No: 10777019). After vortex, samples were incubated at 37°C for 1 hour. As a negative control, each RNA sample was also mixed with each component described above with the exception of reverse transcriptase.

For experiments involving the use of actin and *Mrgprf* primers, cDNA samples were diluted in nuclease free water before being added to the PCR reactions, 1:20 dilution for actin primers and 1:4 dilution for *Mrgprf* primers.

Table 3.5. Primers to amplify human target mRNA sequences

Primer Target	Forward Primer F: (5' → 3')	Reverse Primer R: (5' → 3')	Product Size (bp)	Reference
<i>GAPDH</i>	TCAACGACCACTTTGTCAAGC	CCAGGGGTCTTACTCCTTGG	110	(186)
<i>PTGS1</i>	GAGCAGCTTTTCCAGACGA	TCCTCGATGACAATCTTGATG	65	(187)
<i>PTGS2</i>^(a)	CAGGCTAATACTGATAGGAGAGA	AACTGTTGATAGTTGTATTTCTGGTCA	225	(186)
<i>PTGS2</i>	CCCTTGGGTGTCAAAGGTAA	GCCCTCGCTTATGATCTGTC	169	(188)

GAPDH: Glyceraldehyde 3-phosphate dehydrogenase. *PTGS1*: Prostaglandin-endoperoxide synthase 1. *PTGS2*: Prostaglandin-endoperoxide synthase 2. *IDO-1*: Indoleamine 2,3-dioxygenase. bp: base pair.

Table 3.6. Primers to amplify mouse target mRNA sequences

Primer Target	Forward Primer F: (5'→3')	Reverse Primer R: (5'→3')	Product Size (bp)	Primer Source
<i>β-Actin</i>	TTCTACAATGAGCTGCGTGTG	GGGGTGTTGAAGGTCTCAA	122	Dr James Thorne
<i>Mrgprf</i>	CCGTGATTGCTCTCCTGAACA	GCGTTCGATGCTAATGGCTG	134	Primer Bank ID 118130108c3

Mrgprf: MAS Related GPR Family Member F

3.9.3. qPCR: quantitative polymerase chain reaction

PCR reactions were performed in optical 96-well PCR reaction plate (Applied BioSystems by Life Technologies; ThermoFisher Scientific; Massachusetts, USA; cat No: N8010560).

Each well contained 20 μ l of the PCR reaction mixture, containing the following components: 12.5 μ l GoTaq® qPCR Master mix (Promega; Wisconsin, USA; cat No: A6002), 1 μ l primer forward, 1 μ l primer reverse, 0.25 μ l CXR dye and 5.25 μ l water. 5 μ l diluted cDNA was added per well. On each plate there were two technical replicates per sample.

The conditions of real-time PCR, performed on the QS5 Real Time PCR machine (ThermoFisher Scientific; Massachusetts, USA) were as follows. The initial pre-read stage heated the plate to 60.0°C for 30 seconds. This was followed by a holding stage whereby the sample was heated to 95.0°C for 10 minutes. During the PCR stage, samples underwent denaturation at 95°C for 15 seconds followed by annealing at 60°C for 1 minute and were cycled through this program 40 times. Upon completion of the PCR stage, a post-read stage concluded the reaction where samples were cooled to 60°C for 30 seconds.

Data was exported via QuantStudio Design and Analysis software (versions 3.2 – 4.2; ThermoFisher Scientific; Massachusetts, USA)

3.9.3.1. *PTGS1 and PTGS2 gene expression analysis*

Each cell line was assigned a gene expression score for *PTGS1* and *PTGS2* according to the respective ΔC_T value ($C_{T(PTGS)} - C_{T(GAPDH)}$). qPCR data, presented as ΔC_T values, are found in published work (189). The range of ΔC_T values were assigned to one of 4 scores. The first score was given a value of 0, corresponding to samples where the target gene Ct value was above 30 or undetermined. Next, the ΔC_T values calculated were divided into tertile groups, with ΔC_T values in the higher third being assigned a score of 1, mid values assigned 2 and low values assigned a score of 3 and therefore individual *PTGS1* and *PTGS2* scores ranged from 0 to 3. Therefore, scores were indicative of low *PTGS1 / 2* expression (1) to high *PTGS1 / 2* expression (3). This scoring method is like those used to report immunohistochemistry results (190). The combined *PTGS* score

was determined by adding together the gene expression scores for *PTGS1* and *PTGS2*, giving an overall score ranging from 0 to 6.

3.9.3.2. *Mrgprf* gene expression analysis

The relative quantification: $2^{-\Delta\Delta C_T}$ Method was used. First step of relative quantification analysis involved calculating the ΔC_T value [C_T (Gene-of-interest) – C_T (Housekeeper)] was calculated. Next, the difference in the ΔC_T value from a set 'comparator' was calculated to give $\Delta\Delta C_T$ values. The $2^{-\Delta\Delta C_T}$ method which has been previously described (191), converts the $\Delta\Delta C_T$ value to a relative fold expression values (relative to the comparator selected).

This method of quantification was used in the analysis of *Mrgprf*-transfected clones (where the comparator was untransfected HEK293 or MC38r as appropriate).

3.10. Fatty Acid Content Analysis by LC-ESI-MS/MS

The FA content of cells treated or not with EPA or DHA was measured by liquid chromatography tandem mass spectrometry technique (LC-ESI-MS/MS), in collaboration with the Institute of Cancer Therapeutics, University of Bradford (192).

3.10.1. Reagents

UHPLC-MS grade acetonitrile, methanol, 2-propanol, water, and chloroform were purchased from Merck Life Science UK Ltd, Gillingham, UK. Deionised purified water was generated using an Elga Maxima and Elga Purelab Option purifying system (18.2 MΩcm) (Veolia Water technologies; High Wycombe, UK.)

Derivatisation agents were purchased from Merck Life Science UK Ltd (Gillingham, UK). They were 1-Ethyl-3-(3-dimethylaminopropyl)-carbodiimide HCl (EDC) (cat No: E0388), 4-(dimethylamino) pyridine (DMAP) (cat No: 07700) and 4-[2-(*N,N*-dimethylamino)ethylaminosulfonyl]-7-(2-aminoethylamino)-2,1,3-benzoxadiazole (DAABD-AE) (cat No: 79291).

Table 3.7. Fatty acid standards

FA Standard	Abbreviation	Chemical formula	Reference (cat No)
Deuterated alpha-linolenic acid	LNA-d ₁₄	C18:3 <i>n</i> -3	CAY9000433
Alpha-linolenic acid	LNA	C18:3 <i>n</i> -3	CAY90210
Arachidonic Acid	AA	C20:4 <i>n</i> -6	CAY90010
Docosahexaenoic Acid	DHA	C22:6 <i>n</i> -3	CAY90310
Docosapentaenoic Acid	DPA	C22:5 <i>n</i> -3	CAY90165
Eicosapentaenoic Acid	EPA	C20:5 <i>n</i> -3	CAY90110
Linoleic Acid	LA	C18:2 <i>n</i> -6	CAY90150
Oleic Acid	OA	C18:1 <i>n</i> -9	CAY90260
Palmitic Acid	PA	C16:0	CAY10006627
Stearic Acid	SA	C18:0	CAY10011298

FA standards were purchased from Cambridge Bioscience (UK), **Table 3.7**. Pure FAs were diluted to a stock concentration of 1 mg/ml in 100 % ethanol. A stock of 50 µg/ml of LNA-d₁₄, used as the internal standard, was prepared by diluting 50 µl 1 mg/ml stock in 950 µl 100 % methanol. A combined 'FA standards' stock was prepared containing 100 µl of each non-deuterated 1 mg/ml FA and 100 µl methanol, giving a final concentration of each FA of 100 µg/ml.

3.10.2. Sample preparation

Cells seeded at a density of 3.0×10^5 per well of a 6 well plate were grown until 80 % confluent. Cells were treated with either ethanol carrier corresponding to the maximal EPA or DHA concentration, 5 μ M EPA or DHA and a cell-line-specific IC₅₀-equivalent concentration of EPA or DHA. After 24 h incubation, cells were washed twice with DPBS and harvested by trypsinisation (section 3.2.2). Cells were counted and the suspension centrifuged 500 *g* for 5 minutes at room temperature. Supernatant was discarded and the dry cell pellets were stored at -80°C until analysis.

The full process from sample preparation to FA extraction is depicted in **Figure 3.4**.

3.10.3. Fatty Acid Extraction

FAs were extracted from all the biological samples using an isopropanol / chloroform which has been previously developed by Rose *et al* in 1965 (193) and adapted by Volpato *et al* in 2017 (192). Samples were left to thaw at room temperature before starting the extraction protocol.

First, 4 μ l of 50 μ g/ml internal standard (IS) (LNA-d14; Cayman Chemical; Ann Arbor, USA) was added to each cell pellet and 50 μ l of UHPLC water was added. Samples were vortexed to mix and incubated at room temperature for 10 minutes. Next, 550 μ l of 2-propanol was added and mixed with the sample by vortex. Following a 1-hour incubation period, in which the tubes were briefly vortexed twice, 350 μ l chloroform was added. Following a 1-hour incubation, in which the tubes were briefly vortexed twice, samples underwent centrifugation for 5 minutes at 4000 *g* at room temperature. Solvent from the samples was collected and transferred to a Sirocco™ Protein Precipitation Plate (PP Plate) (Waters UK; Elstree, UK; cat No: 186002448).

Samples were evaporated to dryness in a rotary evaporator (EZ-2 plus rotary evaporator; Genevac Ltd; Suffolk, UK) at 50°C on a mixed low boiling point setting overnight.

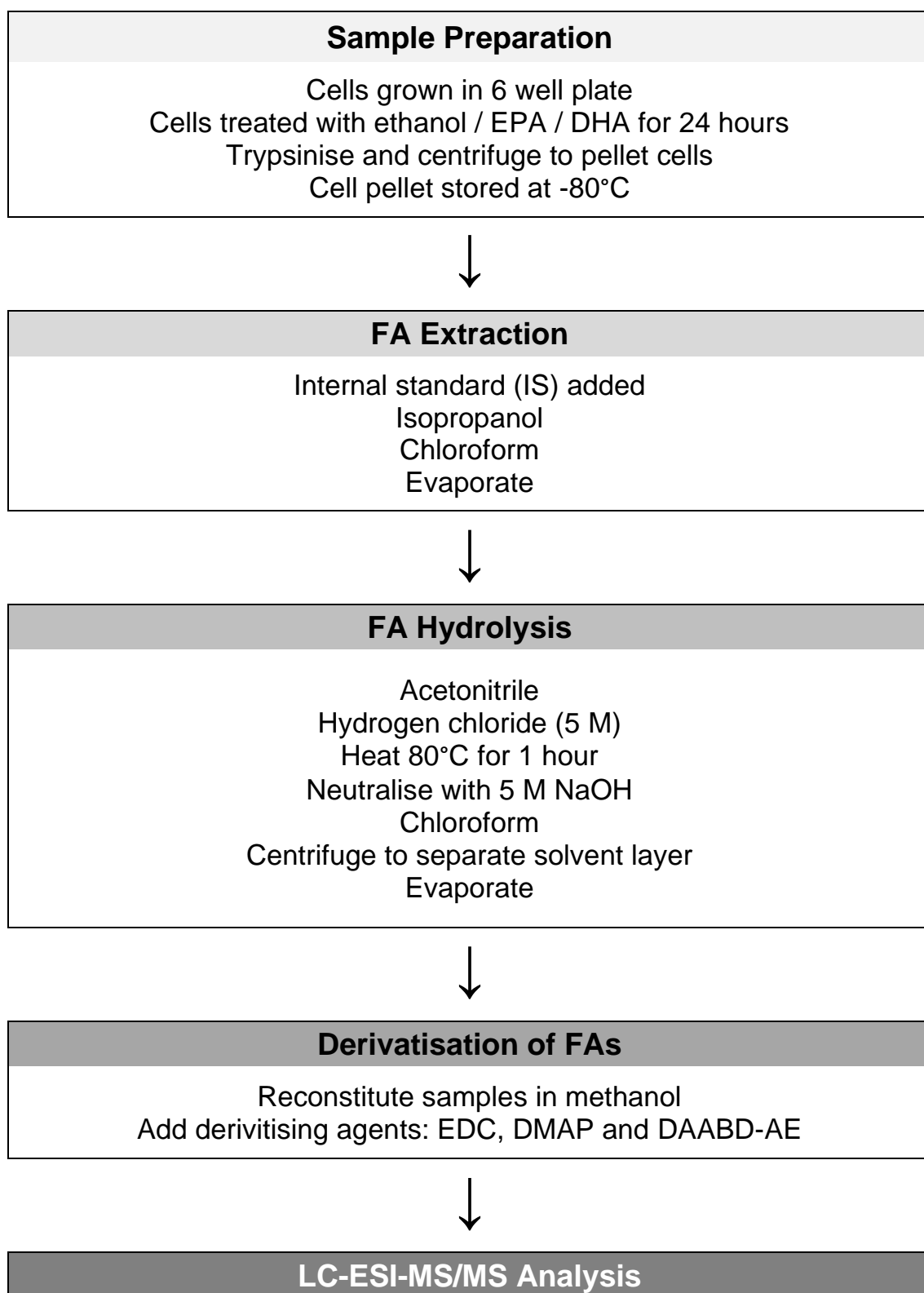


Figure 3.4. The process of sample preparation for FA analysis by LC-ESI-MS/MS

Stepwise depiction of the procedure followed for sample preparation. Image adapted from (192).

3.10.4. Fatty Acid Hydrolysis for total fatty acids

Acetonitrile (500 µl) was added to each well and samples were vortexed to reconstitute before 50 µl of 5 M hydrogen chloride (HCl) was added and samples were again vortexed to mix. Samples were transferred back to Eppendorf tubes and incubated at 80°C for 1 hour and allowed to cool. Following this, 50 µl of 5 M sodium hydroxide (NaOH) and 350 µl chloroform were added to each tube. Centrifugation resulted in the separation of solvent layers and the top 800 µl was manually transferred via pipette to a new PP collection plate. The samples were evaporated to dryness in a rotary evaporator (EZ-2 plus rotary evaporator; Genevac Ltd; Suffolk, UK) at 50°C overnight.

3.10.5. Derivatisation of Fatty Acids

Using electrospray ionisation (ESI), FAs exhibit low specificity when they ionise in the negative mode (194). Chemical derivatization allows for the incorporation of specific chemical features to a sample and derivatisation agent treated samples exhibit a unique fragmentation pattern that allows easy identification on chromatograms (195). Chemical derivatisation is a commonly used process which allows for an increased sensitivity of FA detection (194, 195).

Samples were reconstituted in 50 µl methanol and transferred to amber glass HPLC vials (ThermoFisher Scientific; Massachusetts, USA; cat No: 60180-560). For each sample, 0.5 mg of each derivatisation agent; EDC, DMAP and DAABD-AE was dissolved in 50 µl making solutions with a concentration of 10 mg/ml. The derivitising agents were added to the samples and vortexed to mix. The samples were incubated overnight at room temperature and the resulting FA derivatives were measured by LC-ESI-MS/MS.

3.10.6. Standard Curve Preparation

The standard curve dilution series was set up using the 'FA standards' stock described in section 3.12.1. By diluting the stock in 100 % methanol, 200 µl working stocks were prepared with concentrations of 10000 ng/ml, 1000 ng/ml, and 100 ng/ml. From this, a calibration curve was created by further diluting the working stocks in methanol. The final FA concentrations used for the curve were: 0 ng/ml, 50 ng/ml, 100 ng/ml, 200 ng/ml, 500 ng/ml, 1000 ng/ml, 2000 ng/ml, 5000 ng/ml, and 10000 ng/ml. The FA standard curve dilutions were transferred to HPLC vials and 150 µl of derivitising agent (prepared as previously described above) was added to each sample.

3.10.7. LC-ESI-MS/MS Sample Analysis

The samples were analysed as previously described (192). In summary, a Waters Alliance 2695 High Pressure LC separations module in combination with a Waters Micromass Quattro Ultima triple quadrupole mass spectrometer (Waters UK; Hertfordshire, UK) was used to analyse the FA content of the *n*-3 PUFA treated cell pellets. 2 µl of derivative sample was separated on a HiChrom RPB column (2.1 mm x 250 mm, 5 µm) (HiChrom Ltd; Berkshire, UK.) Mobile phase (MP)-A consisted of 90 % dH₂O, 10 % MeOH and 0.1 % formic acid and MP-B consisted of 90 % MeOH, 10 % dH₂O and 0.1 % formic acid. Gradient conditions started at 80 % MP-B changing to 83 % MP-B over 8 minutes, increasing to 95 % MP-B at 15 minutes, remaining at 95 % MP-B until 17 minutes before returning to the starting conditions at 18 minutes. The overall run time was 25 minutes. The flow rate was set at 0.5 ml/min and split post-column with 0.3 ml/min delivered to the mass spectrometer. Samples were analysed in MRM mode for the following FAs: LNA, AA, DHA, DPA, EPA, LA, OA, PA, SA, and the internal standard, LNA-d₁₄.

The instrument settings were as follows: capillary voltage, 3 kV; cone energy, 15 eV; collision energy, 25 eV; source temperature, 120°C and desolvation temperature, 300°C.

3.10.8. LC-ESI-MS/MS Data Analysis

Peak area for each FA, including the reference IS, in each FA standard sample and each cell pellet sample was measured. For each FA measured, the ratio to IS was calculated by dividing peak area of FA by peak area IS. For each sample, the total ratio was calculated by summing the 'ratio to IS' for all FAs measured. This allows a percentage ratio for each FA to be calculated in a sample, by dividing the FA ratio to IS by the total ratio and multiplying by 100.

To calculate the concentration of each FA in a sample, calibration curves for each individual FA are constructed plotting ratio to IS (y-axis) against known concentration (x-axis). The equation of the line was generated, and the gradient and y-intercept can be used to calculate the concentration of FA (ng/ml) for each sample as follows:

$$FA\ Concentration\ (ng/ml) = \frac{FA\ Ratio\ to\ IS - y\ intercept}{Gradient\ of\ FA\ standard\ curve}$$

The concentration values obtained were used to calculate the mass amount of FA (µg) in each sample. The data were then normalised to cell number.

Additional analyses have been conducted using fold change from baseline, and difference from baseline values. These were calculated as follows:

$$\textbf{Fold Change from Baseline (FC)} = \frac{\textit{Treated Pellet FA } \mu\textit{g/million cells}}{\textit{Ethanol control FA } \mu\textit{g/million cells}}$$

FA Difference from Baseline

$$= \textit{Treated FA } \mu\textit{g million cells} - \textit{Ethanol control FA } \mu\textit{g million cells}$$

3.11. MRGPRF protein analysis

3.11.1. Cell Lysate Preparation

Cell lysates were prepared from 80 % confluent T75 flasks. Following standard trypsinisation protocols, the cells were resuspended to a total of 10 ml media. The cell suspension was centrifuged at 400 g for 5 minutes and the resulting supernatant was discarded. Cells were lysed with 300 µl radio immunoprecipitation assay buffer (RIPA) buffer and placed to ice for a 30-minute incubation. Lysates were transferred onto a QIAshredder (QIAGEN; Hilden, Germany; cat No: 79654), centrifuged for 2 minutes at 16000 g. The eluate was stored at -80°C.

3.11.1.1. Quantifying protein concentration

Protein lysate concentrations were determined by Bio-Rad Protein Quantification Assay (BD Biosciences, UK). Protein standards were prepared by diluting 10 mg/ml bovine serum albumin (BSA) stock in RIPA buffer to give concentrations of; 2 mg/ml, 1 mg/ml, 0.5 mg/ml, 0.25 mg/ml, 0.13 mg/ml and 0.06 mg/ml. 'Working reagent A' (BD Biosciences; UK; cat No: 500-0113) was prepared by adding 'reagent S' (BD Biosciences; UK; cat No: 500-011) to 'reagent A' in a 2:100 ratio.

Cell lysates were diluted in RIPA buffer, 1 µl lysate in 19 µl RIPA buffer. In a 96-well plate 5 µl of each standard was added to duplicate wells, and 5 µl of each lysate sample was also added to duplicate wells. 25 µl 'working reagent A', followed by 200 µl of 'reagent B' (BD Biosciences; UK; cat No: 500-0114) was added to each well. Samples and

reagents were incubated for 30 minutes at room temperature and absorbance was read at 620 nm on the LB-940 plate reader (Berthold Mithras, UK).

The equation of the standard curve was obtained by plotting absorbance readings against BSA concentration and obtaining the equation of the line ($y = mx + c$). Cell lysate protein concentrations were calculated relative to the standard curve,

Protein expression analysis included use of the following buffers: TBS (Tris-buffered saline) and TBS-T (Tris-buffered saline with Tween-20™). TBS was prepared by mixing 60 ml 2.5 M NaCl (sodium chloride) and 20 ml 1M Tris HCl (hydrochloride) with 820 ml dH₂O. TBS-T was prepared by addition of 1.25 ml 10 % v/v Tween-20™ (ThermoFisher Scientific; Massachusetts, USA; cat No: 15825398) added per liter of solution.

3.11.2. MRGPRF protein expression detection by Immunofluorescence

To visualise the MRGPRF localization in stable transfected clones, immunofluorescence techniques were utilized. Immunofluorescence relies upon the principle of specific antibodies binding to specific antigens. In this case, the primary antibody to detect MRGPRF was unconjugated, and therefore a fluorophore-conjugated secondary antibody directed against the primary antibody was required.

Untransfected controls, and transfected clones, were seeded in 6-well-plates on circular coverslips at 3.0×10^5 cells per well, in 3 ml media. Following 24 hours of incubation at 37°C, medium was removed, and each coverslip was washed with 1 ml DPBS. Cells were fixed with 1 ml of ice-cold methanol and incubated at -20°C for 10 minutes. The methanol was removed, coverslips air-dried for 10 minutes and fixed coverslips were stored at 4°C, until required, in DPBS.

Per coverslip, 100 µl antibody diluent (Invitrogen™; Massachusetts, USA; cat No: 003218) followed by incubation at room temperature for 2 minutes, was undertaken to allow complete antigen blocking. The antigen diluent was removed before addition of the primary antibody.

The primary antibodies used to study Mrgprf were:

- anti-MRGPRF N-14 (Insight Biotechnology, Santa-Cruz Biotechnology © Inc; Texas, USA; cat No: sc138444 #C2111), which was used at a 1:50 dilution ratio

(referred to as N-14 henceforth). N-14 is an affinity purified rabbit polyclonal antibody raised against a peptide mapping within an N-terminal extracellular domain of MRGF of human origin (196).

- anti-MRGPRF HPA028811 (Atlas Antibodies; Stockholm, Sweden; cat No: R28217) was used at 2 µg/ml, for detection of protein. HPAMF is a purified polyclonal antibody raised to the following human antigen; MAGNCSWEAHPGNRNRMCPLSEAPELYSRGFLTIEQIAMLP which has 83 % sequence homology with mouse MRGPRF

Primary antibodies were diluted in antibody diluent to the relevant concentrations. 100 µl of antibody solution was added onto the coverslips. For each experiment, a no primary control sample was included where the antibody solution was replaced with antibody diluent. All coverslips were incubated at room temperature for 1 hour.

Coverslips were rinsed in TBS-T before washing for 2 x 5 minutes in 2 ml TBS-T and 1 x 5 minutes 2 ml TBS. Donkey anti-rabbit Alexa Fluor 594 secondary antibody (Invitrogen™; Massachusetts, USA; cat No: A21207) was diluted 1:300 in antibody diluent and added (100 µl) to the coverslip Following a 30 min incubation at room temperature, in the dark, the wash steps were repeated as described above. Coverslips were mounted on to Menzel Glaser Superfrost® Plus glass microscope slides (ThermoFisher Scientific; Massachusetts, USA; cat No: 090115), using ProLong Gold containing 4'-6-diamidino-2-phenylindole (DAPI) mounting reagent (Invitrogen™; Massachusetts, USA; cat No: P36931) and left to cure overnight at room temperature. Coverslips were hermetically sealed with nail varnish and images were acquired using the Zeiss AxioImager.Z1 fluorescence microscope, with ApoTome and at x100 objective magnification. Exposure times were kept consistent between all the sections within an experimental set to allow comparison of fluorescence intensities.

3.11.3. MRGPRF protein expression detection by dot blot

Protein concentration of cell lysates were quantified by BioRad protein assay as previously described. To compare native proteins and denatured proteins some of the lysate sample was first denatured by mixing it in a 3:1 ratio with Bolt™ LDS Sample buffer (Novex by Life Technologies; Massachusetts, USA; cat No: B0007). The subsequent mix was heated to 94°C for 4 minutes and spun down. The processing of native and denatured samples was as follows.

The polyvinylidene fluoride (PVDF) membrane (VWR™; Lutterworth, UK) was activated by soaking for 1 minute in 100 % methanol and rinsed 5 minutes in dH₂O and 5 minutes in DPBS. HEK293 derived protein lysates (10 µg) and MC38r derived protein lysates (20 µg) were added to separate areas of the membrane and the membrane was left to air dry, allowing the lysate to absorb into the membrane.

The membrane was blocked with in a 5 % w/v milk (Skim milk powder, Fluka Analytical; Buchs, Switzerland; cat No: 70166) in TBS-T solution for 30 minutes at room temperature. The blocking solution was discarded and replaced with primary antibodies diluted in 1 % w/v milk in TBS-T solution as follows: anti-MRGPRF N-14 diluted 1/100, anti-α-tubulin (clone B-5-1-2, monoclonal, produced in mouse, Merck Life Science UK Ltd; Gillingham, UK; cat No: 051M4771) and anti-β-actin (clone AC-15, monoclonal, produced in mouse, Merck Life Science UK Ltd; Gillingham, UK; cat No: A5441) diluted 1/2000. The membranes were incubated overnight at room temperature, overnight on a rocker (manufacturer and model).

The membranes were washed 3 times in TBS-T for 5 minutes. Secondary antibody, polyclonal goat anti-rabbit IgG/HRP (Cell Signalling Technology®; Massachusetts, USA; cat No: 7074) was prepared at a dilution of 1:2000 and the membranes were incubated in secondary antibody for 1 hour at 4°C, rocking. Membranes were again washed 3 times in TBS-T for 5 minutes and the membrane was tapped on blotting paper 703 (VWR™; Lutterworth, UK; cat No: 7320596) to remove excess wash. Super Signal West Pico Chemiluminescent Substrate (ThermoFisher Scientific; Massachusetts, USA; cat No: 34077) was prepared by mixing in a 1:1 ratio; Super Signal West Pico Lumi Enhancer solution with West Pico Stable Peroxide solution. Excess liquid was drained, and 2 ml Super Signal West Pico Chemiluminescent substrate was added to cover the membrane and left to develop for 5 minutes. The membrane was imaged on the BioRad Molecular Imager® Gel Doc™ XR+ System (Bio-Rad, California, USA).

3.11.4. MRGPRF Protein detection by Flow Cytometry

Cells were grown to confluence in T75 flasks. On the day of analysis, cells were harvested via trypsinisation and filtered through a cell strainer (MILLEX® GP Filter unit 0.22µm; Merck Life Science UK Ltd; Gillingham, UK; cat No: SLGP033RS) into universal tubes. Following 5-minute centrifugation at 400 g, cells were resuspended in PBS, 1 % v/v FCS, counted and placed on ice. 3.0×10^5 cell suspension was transferred to fluorescence activated cell sort (FACS) tubes and centrifuged for 5 minutes 400 g. The

cells were placed on ice. The staining was performed with and without fixation of the cells.

Unfixed cells were resuspended in PBS. Fixation was performed by decanting the supernatant and replacing it with 250 µl of fixation / permeabilisation solution for 20 minutes at 4°C (BD Cytfix / Cytoperm™ Kit (BD Biosciences; UK cat No: 554714)). Samples were washed twice with 1 ml of 1X BD Perm/Wash™ buffer (10X BD perm/wash buffer diluted in distilled water).

Samples were incubated in 1 ml FCS on ice for 20 minutes and spun 400 g for 5 minutes. N-14 was prepared as a serial dilution for optimisation (from 1:6.25 to 1:100) and then at a 1:50 dilution, in PBS for unfixed and 1X BD Perm/Wash buffer for fixed cells. 50 µl of primary antibody was added to each tube (or just PBS / 1X BD Perm/Wash buffer for no primary controls). Tubes were incubated for 1 hour at 4°C. Cells were washed in 2 ml PBS / 1X BD Perm/Wash buffer, spun at 400 g for 5 minutes and supernatant was discarded. Secondary antibody, donkey anti-rabbit Alexa Fluor 594 secondary antibody (Invitrogen™; Massachusetts, USA; cat No: A21207) dilution was prepared (1:100, 1:200 and 1:300 for optimisation, 1:100 dilution for final assays) in PBS / BD perm/wash buffer dependent upon unfixed or fixed conditions. 50 µl of secondary antibody was added to each tube (or PBS / 1X BD Perm/Wash buffer for no secondary controls). Tubes were incubated for 30 minutes at room temperature, in the dark. Cells were centrifuged at 400 g for 5 minutes and supernatant was discarded. Cells were resuspended in 500 µl PBS / 1X BD Perm/Wash buffer. Data (10000 events per samples, 'Standard Sensitivity mode at 100 µl/min) were acquired on the Attune® Acoustic Focusing Cytometer (ThermoFisher; Massachusetts, USA). Data was analysed using Attune Cytometric Software, version 2.1. Intact cellular bodies were gated by side scatter (SSC-A) and forward scatter (FSC-A). Baseline detection of fluorescence was detected by A604/48 band pass filter, with cell count plotted against BL2-AF594 (fluorescence). Finally, GFP expression was plotted against AF594 fluorescence to show the number of successfully transfected cells that were expressing MRGPRF.

3.11.5. Calcium Assay: Assessment of MRGPRF functionality in overexpression models.

The calcium assay is used to assess whether the overexpressing MRGPRF cell lines are producing a functional protein, which can trigger signalling via the calcium mediated pathways.

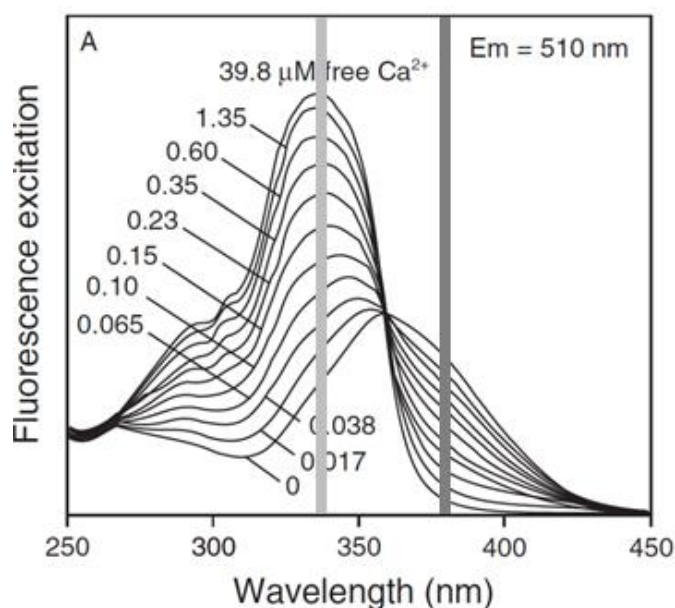


Figure 3.5. Fluorescence excitation spectrum of Fura2-AM

The fluorescence excitation spectra of Fura2 in solutions containing free Ca^{2+} . When higher concentrations of free Ca^{2+} are present in a sample, a higher level of fluorescence excitation at 340nm is measured, indicated by the intercept of the light grey line. A corresponding low level of fluorescence excitation measured at 380nm is denoted by the intercept of the dark grey line. Image adapted from (197).

Fura-2 is a fluorescent, charged, membrane impermeable, ratio-metric calcium indicator dye that has the ability to bind calcium with high affinity (198, 199). Masking the charge with an acetoxymethyl ester group allows membrane permeability however negates the calcium sensitivity of the compound (199). The acetoxymethyl ether (AM) form of Fura-2, referred to henceforth as Fura-2AM, upon entering the cell undergoes sequential cleavage of the AM group by esterases, leaving intracellular, calcium-sensitive Fura-2AM. Calcium (Ca^{2+}) binding to Fura-2 results in a spectral shift in Fura-2 absorption (at 510 nm emission), from 380 nm (unbound) to 340 nm (bound), which is proportional to the calcium concentration [Figure 3.5] (199). Therefore, the concentration of free intracellular Ca^{2+} is proportional to the ratio of fluorescence measured at 340/380.

3.11.5.1. Buffer preparation

Pluronic acid (Pluronic® F-127; Merck Life Science UK Ltd; Gillingham, UK; cat No: P2443) was prepared as a 10 % v/v concentration in DMSO, mixed thoroughly by shaking and incubated for 1 hour at 37°C in a water bath.

Standard buffer solution (SBS) containing 1.5 mM Ca^{2+} was prepared as per **Table 3.8**. In the absence of Ca^{2+} supplementation, the SBS buffer was prepared with 0.4 mM EGTA, a chelating agent selective for calcium ions, instead.

Table 3.8. Standard Buffer Solution (SBS)

Compound	SBS buffer with Ca^{2+}	SBS buffer without Ca^{2+}
Sodium Chloride (NaCl)	135 mM	135 mM
Potassium Chloride (KCl)	5 mM	5 mM
Magnesium Chloride (MgCl)	1.2 mM	1.2 mM
Glucose	8 mM	8 mM
HEPES	10 mM	10 mM
Calcium chloride (CaCl_2)	1.5 mM	-
EGTA	-	0.4 mM

HEPES: 4-(2-hydroxyethyl)-1-piperazineethanesulfonic acid. EGTA: ethylene glycol-bis(β -aminoethyl ether)-N,N,N',N'-tetraacetic acid

Fura2-AM (Merck Life Science UK Ltd; Gillingham, UK; cat No: F0888) was prepared at a 1 mM concentration in DMSO and stored at -20°C protected from light. In 1.5 mM Ca^{2+} SBS buffer, 10% Pluronic acid was added at a 1:1000 ratio and 1 mM Fura2-AM is added at a 1:500 ratio, giving a final concentration of 2 μM Fura2-AM.

3.11.5.2. Cell preparation

Following optimisation, HEK293 parental control, control vector and MRGPRF overexpressing cells were seeded at a density of 6.0×10^4 per well in 96-well PLA coated black plates (Greiner BioOne; Kremsmünster, Austria; cat No: 655077). 8 wells per cell line were seeded on one plate, with 3 total plates providing technical replicates for each run. During the assay, the 8 wells were exposed to the following conditions; (1) 0.1 % v/v DMSO, (2) 1 μM thapsigargin (Tg), (3) 0.38 % v/v ethanol, (4) 25 μM EPA, (5) 50 μM EPA, (6) 0.1 % v/v water and 2 wells (7 and 8) were used to test response to 20 μM ATP.

Once cells were confluent, medium was removed and replaced with 50 μl of 2 μM Fura2-AM – 1.5 mM Ca^{2+} SBS buffer mix. Plates were incubated for 1 hour in the dark at 37°C . Following incubation, the fura2-AM – 1.5mM Ca^{2+} SBS buffer mix was removed, and cells were washed twice with 50 μl 1.5 mM Ca^{2+} SBS. Cells were resuspended in 200 μl 1.5 mM Ca^{2+} SBS and incubated in darkness at room temperature for 30 minutes.

3.11.5.3. Positive controls

For these experiments, I used two positive controls. The first was thapsigargin, a sarco / endoplasmic reticulum calcium ATPase. Treating cells with Tg causes an increase in intracellular Ca^{2+} , $[\text{Ca}^{2+}]_i$ by blocking the ability of the cell to pump calcium back into the sarco / endoplasmic reticulum (200). Thapsigargin (Merck Life Science UK Ltd; Gillingham, UK; cat No: T9033), was prepared in DMSO to create 500 μM stock

The second positive control was ATP (adenosine triphosphate), which has been shown to increase $[\text{Ca}^{2+}]_i$. ATP activates P_2 -type purinoceptors, some of which are GPCRs (201). One such receptor is P_2Y_1 , which has been shown to be expressed in HEK293 (201, 202). Activation with ATP potentiates phospholipase C responses, catalysing IP_3 production that diffuses in to the cytoplasm and results in a release of calcium from intracellular stores (202, 203). ATP (Merck Life Science UK Ltd; Gillingham, UK; cat No: A2383) was diluted to create a stock concentration of 100 mM in nuclease free water.

3.11.5.4. Compound plate preparation

For each tested 'compound' a 1 ml preparation 5 times the desired final concentration was prepared in 1.5 mM Ca^{2+} SBS. Compound plate concentrations and final desired concentrations for positive controls, potential agonists, respective carrier controls, are shown below in **Table 3.9**. 200 μl of each 5x final concentration solution was added to the compound plate (Corning® Costar® Ultra-Low Attachment 96 Well Plate; Merck Life Science UK Ltd; Gillingham, UK; No: CLS7007).

It should be noted, that alongside the 33 mM EPA working stock (prepared as previously described), a 66 mM EPA working stock was prepared by adding 20 μl 3.3 M EPA to 980 μl 100 % ethanol. This allowed for addition of the same volume of 33 mM and 66 mM stock to create the 125 μM and 250 μM solutions, so the ethanol control was valid for both.

Table 3.9. Compound plate contents

Content	Compound plate concentration	Final desired concentration
DMSO	99.9 %	0.1 % v/v
Tg	5 µM	1 µM
Ethanol	99.9 %	0.38 % v/v
EPA - a	125 µM	25 µM
EPA - b	250 µM	50 µM
Water	99.9 %	0.1 % v/v
ATP	100 µM	20 µM

DMSO: dimethyl sulfoxide. Tg: Thapsigargin. EPA: eicosapentaenoic acid. ATP: adenosine triphosphate

Cell plates and compound plates were loaded onto the FlexStation machine (FlexStation III; Molecular Devices; California, USA; cat No: FV06118). The settings were as shown in **Table 3.10** below.

Table 3.10. Flex station settings

Condition	Setting (adjusted for experiment)
Flex	Fluorescence
Excitation wavelength	1 : 340 nm 2 : 380 nm
Emission	510 nm
Sensitivity	Medium
Timing (run time)	300 seconds 5 seconds between each reading
Compound transfer	Volume: 50 µl Time point: 30 seconds

The table presents the settings which were selected for each experimental repeat to ensure the conditions were identical. Compound transfer was initiated at 30s to allow for the baseline measurements to be made. The settings had been previously optimised by the Beech lab group.

3.11.5.5. Analysis of calcium flux data using PRISM Graph Pad

Data was exported to Microsoft Excel. For each well, fluorescence readings ($F_{340/380}$) were recorded at 5 second increments. Data was inputted into PRISM GraphPad and statistics on row function was used to calculate mean and standard error of the mean for 3 technical replicates. Line and symbol graphs were plotted. $F_{340/380}$ -fold changes of each condition to the appropriate carrier controls were calculated.

3.12. Exploitation of public databases

3.12.1. Development Therapeutics Program

The Development Therapeutics Program (DTP, <https://dtp.cancer.gov/>) was designed by the National Cancer Institute to facilitate discovery and development of new cancer therapeutic agents. 'DTP Databases and Search Tools' resource was used to predict cell responses to drug treatments (i.e.: AZA, DAC, TMZ) so that an appropriate concentration range was selected for cell viability assays involving these drugs.

3.13. Statistical analysis

Unless otherwise stated, statistical testing was undertaken using GraphPad Prism8™ (GraphPad Software; California, USA; software version 8.30 (328)). To test whether data fit a Gaussian distribution, the D'Agostino-Pearson Omnibus normality test was used.

Comparison of the data points in unpaired groups was determined by Mann-Whitney tests which was used to test statistical significance of median values. Comparison of mean values was determined by Student's t-test. To test whether one variable correlated with another Spearman-Rank correlation tests were performed. $P < 0.05$ was used as a cut off to determine significance.

Chapter 4: Characterising human colorectal cancer cell lines and response to EPA and DHA

4.1. Introduction

4.1.1. Sensitivity of CRC cell lines to *n*-3 PUFAs

EPA and DHA are both biologically active (100), however, to date, studies have been predominantly EPA-focused. This is in part due to the naturally occurring predominance of EPA in marine oils, in which it is found in the distinct ratio 3:2 (EPA/DHA), and the fact that DHA was purified later than EPA (204-206).

Studies report a range of *n*-3 PUFA sensitivity of hCRC cell lines. Concentrations greater than or equal to 150 µM EPA were required to inhibit proliferation in some cell lines, whilst 50 µM EPA or less is sufficient in others (131, 137, 179, 207, 208). A study by Hossain *et al* found sensitivity towards *n*-3 PUFAs, including EPA and DHA, was highest in HT29 cells and lowest in CaCo-2 and DLD-1 cells (207). The effect of both EPA and DHA have been assessed in hCRC cell line models in order to understand the mechanistic pathways involved in anti-cancer activity of *n*-3 PUFAs (131, 137, 179, 209). These are outlined in **Table 1.2, Chapter 1.4.2.1**.

4.1.1.1. Combined drug treatment interaction analysis

Most *in vitro* studies use single purified *n*-3 PUFAs, whilst *in vivo* and clinical studies evaluating the effect of *n*-3 PUFA have mostly used mixed formulations for supplementation, or use questionnaires to calculate dietary consumption (with varied *n*-3 PUFA compositions) (131, 207, 208). In this chapter, an initial assessment of interactions between EPA and DHA were investigated to determine whether a benefit (in terms of growth inhibitory effects) for combined or single *n*-3 PUFA treatments could be seen. Combination drug treatments are frequently used in the clinic in order to treat diseases, as previously described in **Chapter 1.2.3.2**, treatment of CRC often involves combination therapies including 5-FU, oxaliplatin and irinotecan. Drug combinations are often used to minimise toxic effects and reduce likelihood of acquiring resistance to a drug used in isolation (210). In addition, a benefit of combination drug treatments in some cases, can be the synergistic activity of the drugs (210). However, the definition of 'synergy' has long been debated (211, 212) and thus it is important that combination treatment experiments and analysis are carefully considered so that claims of synergistic interactions between 2 drugs are valid.

Practical and statistical challenges arise when multi-drug combination experiments are designed, as including multiple drugs and dose-levels to satisfy statistical requirements quickly renders a lab-bench based testing approach insufficient (213). Therefore, mathematical and computational approaches are often used to facilitate appropriate designs, and drug-combination experiments are completed in high-throughput formats (213, 214).

There are many ways in which drug-combination data can be analysed. Examples include; combination index (CI) analysis, isobologram analysis and curve shift analysis (215). Whilst both isobologram and curve shift analysis provide graphical outputs, CI analysis quantifies the interaction between drugs (215). The Chou-Talalay method is frequently used in drug combination experiments, and is a complex mathematical equation that allows the calculation of a CI (210). This can be used to describe drug-drug interactions whereby, additive drug-drug interactions have a CI equal to 1, synergistic interactions have a CI less than 1, and antagonistic interactions have a CI greater than 1 (210). As the work in this chapter was a preliminary analysis to determine whether further experimental work should be undertaken to assess interactions between EPA and DHA, experimental and analytical approaches were simplified.

4.1.2. Metabolism of *n*-3 PUFAs: *PTGS* activity

Although CRC cell lines have shown differential sensitivity to *n*-3 PUFAs, the mechanisms that facilitate cellular response to EPA and DHA are not known. Cyclooxygenase (COX) enzymes are the rate-limiting enzyme in the synthesis of prostanoids which are bioactive lipid messengers implicated in a range of physiological and pathological functions (216).

4.1.2.1. Cyclooxygenase inhibition and CRC prevention or treatment

As previously outlined in **Chapter 1.5**, COX-1 and COX-2 enzymes are involved in CRC carcinogenesis (157, 187) and metabolism of *n*-3 PUFAs (158). Studies to investigate the relationship between the two suggest that COX expression is associated with limited response to *n*-3 PUFAs. Such studies found that following combined treatment of hCRC cell lines with *n*-3 PUFAs and selective or non-selective COX-2 inhibitors (celecoxib or sulindac, respectively) a reduction in growth and increased apoptosis is observed (217, 218). This chapter investigated whether resistance to *n*-3 PUFAs was associated with increased *PTGS1* and *PTGS2* mRNA expression profiles.

4.1.3. Modelling CRC *in vitro*

CRC is not a homogeneous disease and genetic, morphological and epigenetic alterations are implicated in disease pathogenesis (33, 35, 219). The diversity of molecular subtypes of CRC is associated with heterogeneous clinical presentation of disease, response to treatment and patient prognosis (33, 219). However, the clinical relevance and suitability of *in vitro* preclinical models is repeatedly queried (41, 50, 220, 221), not limited to the setting of CRC studies.

Recent advances assessed whether CRC cell lines could be classified by molecular phenotypes (CIN, microsatellite stability, CIMP and CMS) described for patient tumours, and have confirmed that *in vitro* models recapitulate DNA, RNA and protein level characteristics (35, 41, 50, 54, 55). Therefore, using a panel of multiple CRC cell lines is representative of the mutational and transcriptional heterogeneity of primary tumours (35, 41, 222-224).

Drug sensitivity screening studies demonstrate that CRC cell lines recapitulate molecular alterations with similar frequencies and distribution of gene methylation between primary tumours and hCRC cell lines (225). Evidence suggests that pharmacogenomics of primary tumours is also recapitulated by hCRC cell lines (223, 225, 226) and response to chemotherapeutic drugs can be predicted in *in vitro* models. One study reported apoptosis resistance of CMS 4 subtype hCRC cell lines treated with oxaliplatin (227), for which a poor response has also been observed in CMS 4 patients (88). As the tumour microenvironment has implications on gene expression signals in tumour tissues, translation of the CMS classification to preclinical models, including cell lines and patient-derived xenografts (PDX) has major challenges. Sveen *et al* recently developed a cancer cell-adapted CMS classifier, which utilised data from primary CRCs, cell lines and PDX models, to assign a CMS classification to hCRC cells (50). Profiling cell lines by CIN, CIMP, microsatellite status (MSS / MSI) and CMS classifications facilitates comparisons to specific clinical tumours and provides characteristic features. This information enables careful selection of cell lines for the disease or therapeutic agent being investigated.

4.1.4. Associations between molecular phenotypes, CRC and response to *n*-3 PUFAs

Although there have been relationships established between response to chemotherapeutic agents and molecular phenotypes or CMS groups (55, 56, 227, 228), data surrounding *n*-3 PUFA response and phenotypes is limited. CIMP and CIN status have not previously been associated with sensitivity to *n*-3 PUFAs in clinical studies or

in vitro and *in vivo* studies in which the relationship has never been tested. Tumours obtained from the Nurses' Health Study and Health Professional Follow-up studies were classified by microsatellite status (941 cases were MSS and 184 cases were MSI-high) (108). An association between greater *n*-3 PUFA intake (from over-the-counter supplementation or acquired through the diet) and lower MSI-high CRC incidence was reported (≥ 0.3 grams / day was compared with < 0.1 grams / day: multivariable hazards ratio (HR) = 0.54, 95 % confidence interval (CI) = 0.35 to 0.83, $P_{\text{linearity}} = 0.03$) but the association was not observed for MSS cases (HR = 0.97, 95 % CI = 0.78 to 1.20, $P_{\text{linearity}} = 0.28$) (108). Additionally, a study to compare the efficacy of FOLFOX (folinic acid, 5-FU and oxaliplatin) combination therapy versus FOLFOX + cetuximab therapy in 1735 patients with stage 3 colon cancer, included a dietary questionnaire (229). Higher *n*-3 PUFA intake (EPA, DPA and DHA, obtained by fish sources) was associated with increased better 3-year disease free survival (DFS) in patients who had MSI tumours (72 % vs 67 %), but not in patients with MSS tumours (72 % vs 72 %) (229).

4.1.5. Epigenetics

Cell-cell differences are determined by variations in gene expression (230). Epigenetics is defined as heritable changes in gene expression associated with modifications of DNA, or chromatin proteins, that are not due to any alteration in the primary sequence (231). Epigenetics regulate gene expression in cell differentiation, growth, development, ageing and also cancer (232). Epigenetic mechanisms are regulatory processes which control gene expression at the transcriptional level by modifications which alter the transcription machinery accessibility to gene promoter regions (233). Colorectal carcinogenesis, at all stages from initiation to metastasis, has been associated with epigenetic aberrations including DNA methylation, histone modifications, chromatin remodelling, and non-coding RNAs (234).

4.1.5.1. DNA Methylation

DNA methylation is the reversible process of a covalent bond forming between a methyl ($-\text{CH}_3$) group and a cytosine DNA base (232). In humans, a majority of DNA methylation is restricted to cytosine base nucleotides adjacent to guanine nucleotides, known as CpG dinucleotides. Presence of CpGs are less than would be expected by chance (232), and there is an uneven distribution of CpG-rich regions. CpG enriched DNA appears most frequently in promoter regions and first exons of genes (235). The presence of CpG dinucleotides and methylation in the promoter and first exons is important for regulation and control of gene expression.

Cancer-associated global genomic hypomethylation activates oncogenes and regional hypermethylation inactivates genes including tumour suppressor genes (236). CIMP+ CRC tumours display regional hypermethylation of gene promoter regions, including DNA MMR genes (41). Chemotherapeutic drug response of CIMP+ and CIMP- tumours indicate that improved patient outcomes arose from irinotecan-based therapies compared to oxaliplatin-based treatment regimens (237).

4.1.5.2. *Altering methylation: epigenetic drug mechanisms*

Hypermethylation can be induced by treatment of cells with methylating agents such as Temozolomide (TMZ). TMZ has been utilised in treatment of astrocytomas, glioblastoma multiforme and melanomas since the 1990s (238). TMZ is a methylating triazene compound that is converted to its active form MTIC which alkylates DNA at the N⁷ position of guanine, N³ position of adenine and O⁶ position of guanine. Production of alkyl adducts, N⁷-methylguanine and N³-methyladenine do not induce cytotoxic effect, as the base excision repair system corrects the methylation (239). However, methylation of guanine (the most common site of methylation), results in single and double-strand DNA breaks and subsequent induction of apoptotic cell pathways (238). The repair of DNA damage caused by TMZ is facilitated by an enzyme, O⁶ methyl-guanine methyltransferase (MGMT) (240, 241). Promoter methylation of the *MGMT* gene (and subsequent epigenetic silencing of MGMT) is associated with reduced capability to repair DNA and better anti-cancer responses to TMZ (240).

Conversely, temporary demethylation of DNA can be achieved by use of epigenetic drugs known as demethylating agents, such as 5-azacytidine (5-AZA) and decitabine (DAC), both of which are nucleoside (cytidine) analogues. These incorporate into actively replicating DNA and covalently bond to DNA methyltransferases (DNMTs) (242), which targets DNMT proteins for proteasome degradation (243). Depletion of DNMT results in passive demethylation during cell division (242). This causes global hypomethylation (234). Effects of treating cells with low concentrations of decitabine, which include altered cell growth, differentiation and improved immunological responses to tumour-associated antigens, have been attributed to re-expression of critical genes which were silenced prior to DAC treatment (243).

4.2. Objectives

This chapter focused on the hypotheses that CRC cell lines display different *n*-3 PUFA sensitivity, and that sensitivity to *n*-3 PUFAs is associated with key CRC molecular characteristics, namely, CIN, CIMP, MSI/MSS status and *PTGS1/2* gene expression. It was hypothesised that exposing cell lines to 5-AZA, DAC and TMZ would alter molecular characteristics of the cells, and subsequently alter response to *n*-3 PUFAs. To test the hypotheses, the following objectives were set:

- Establish a panel of cell lines representative of key CRC molecular phenotypes
- Characterise *PTGS1* and *PTGS2* expression in hCRC cells
- Test CRC cell line sensitivity to *n*-3 PUFAs alone or in combination
- Identify associations between CRC cell response to *n*-3 PUFAs and molecular phenotypes.
- Determine the effect of epigenetic drug exposure on cell sensitivity to EPA

4.3. Results

4.3.1. Characterisation of the CRC cell line panel

Cell lines were authenticated by STR profile analysis to confirm correct identity [Appendix A4.1].

4.3.1.1. Cell line panel characterisation by molecular subtype

CRC cell lines were classified according to CIN status, microsatellite status and CIMP status. In addition, cell lines can be classified into 4 consensus molecular subtypes (CMS).

Table 4.1. Human colorectal cancer cell line molecular classifications

Cell Line	CIN status	CIMP status	Microsatellite status
CaCo-2	+	-	MSS
Colo205	+	+	MSS
DLD-1	-	+	MSI
HCA-7	+	+	MSI
HCT116	-	+	MSI
HRT18	-	+	MSI
HT29	+	+	MSS
LoVo	-	-	MSI
LS174T	-	-	MSI
LS411N	+	+	MSI
SW48	-	+	MSI
SW480	+	-	MSS
SW620	+	-	MSS
SW837	+	+	MSS
SW1116	+	-	MSS
T84	+	-	MSS
TC71	-	-	MSI

Classification of each CRC cell lines cell line is shown by; CIN: chromosomal instability, CIMP: CpG Island Methylator Phenotype, MS: microsatellite, I: unstable and S: stable. Data were compiled from the previous studies (35, 41, 50, 55, 56, 244, 245)

The panel comprised 10 CIN + and 7 CIN -, 9 CIMP + and 8 CIMP - and 9 MSI and 8 MSS cell lines [Table 4.1]. There were conflicting reports on the microsatellite status of HCA-7 cells. Microsatellite status of the cell lines was therefore tested in-house using an established method (41). Results show that HCA-7 cell line were MSI [Appendix A4.2].

CMS profiles used to characterise patient tumours combine these molecular phenotypes with tumour microenvironment properties (35, 50). As the models used in this study are all *in vitro*, I categorised cell lines by grouped CIN, MS and CIMP properties and discarded the CMS classification. No cell lines were 'CIN-, MSS, CIMP-' which was expected as there would be no genetic 'driver' of CRC development. The hCRC cell lines fell into the subgroups presented in **Table 4.2**.

Table 4.2. Cell line categorised by CIN, MSI and CIMP status

Molecular Property		CIMP -	CIMP +
CIN -	MSS		
CIN -	MSI	LoVo LS174T TC71	DLD-1 HCT116 HRT18 SW48
CIN +	MSS	CaCo-2 SW480 SW620 SW1116 T84	Colo205 HT29 SW837
CIN +	MSI		HCA-7 LS411N

CRC cell lines categorised by CIN, MS and CIMP status, providing comparative groups for downstream analysis. Data compiled from literature (35, 41, 50, 55, 56, 244, 245)

4.3.2. Optimisation of a gene expression assay to study *PTGS 1* and *2* expression in human CRC cell lines

It has been reported that 77.97 % CRC tumour samples overexpress COX-2 (159). The hCRC cell lines were therefore characterised for *PTGS1* and *PTGS2* gene expression using RT-qPCR.

4.3.2.1. *GAPDH* primers validation

GAPDH was selected as the 'housekeeper' gene. *GAPDH* primers were optimised using HEK293 cDNA. The standard curve shown in **Figure 4.1** demonstrated a linear relationship between amount of cDNA input and C_T value ($R^2 = 0.99$).

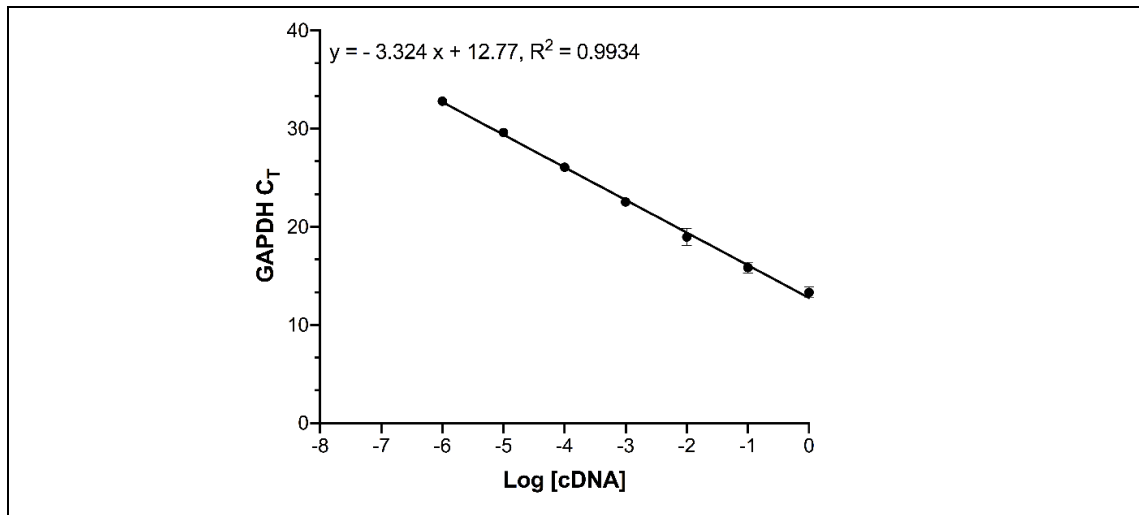


Figure 4.1 GAPDH Standard curve

GAPDH C_T values obtained by qPCR in serially diluted cDNA HEK293 samples ranging in quantity from 1μg to 10⁻⁶μg. GAPDH C_T data are expressed as the mean ± SD, for 4 independent experimental replicates.

4.3.2.2. PTGS1 primer validation

To assess the efficiency of the primers, a commercially synthesised plasmid [Figure 3.2, Chapter 3.6] containing the expected PCR product, was used to spike both water samples and HEK293 cDNA samples. HEK293 cells do not express *PTGS1* (246).

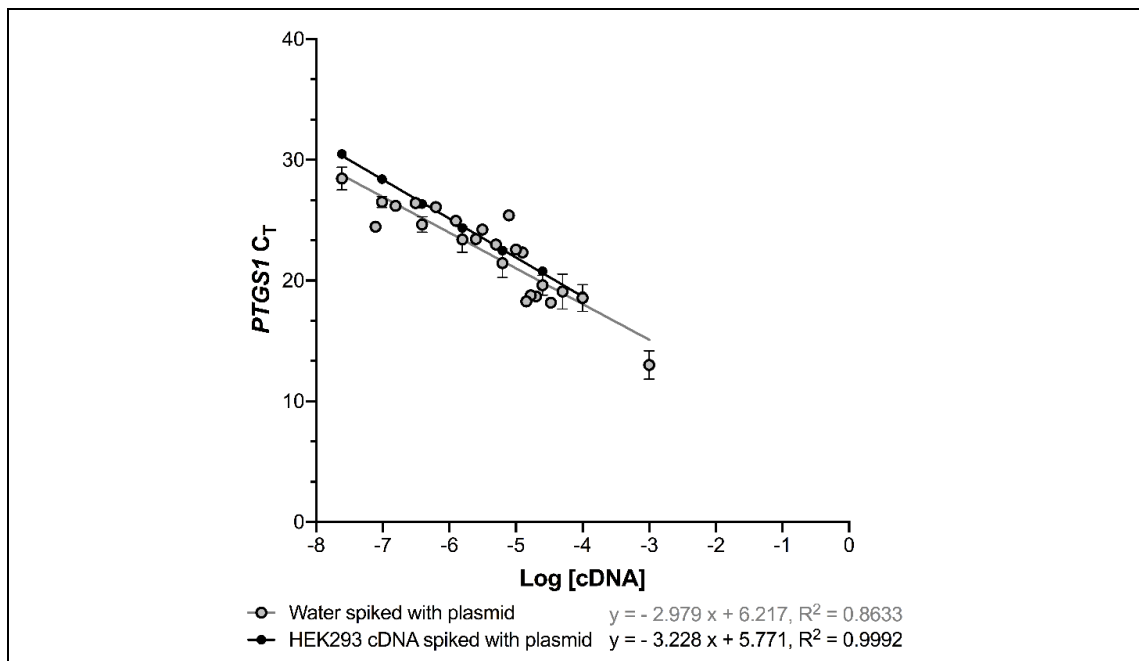


Figure 4.2 PTGS1 Standard curve

PTGS1 C_T values obtained by qPCR of serially diluted vector cDNA spiked into HEK293 cDNA or water, with the vector quantity ranging from 10⁻³ μg to 10⁻⁸μg. Each *PTGS1* C_T data point is representative of the duplicate well C_T mean ± SD, for 1 to 6 independent experimental replicates.

Vector DNA was diluted to a range between 10^{-3} and 10^{-8} μg , and *PTGS1* was measured with C_T values obtained that ranged from 13.01 to 30.49 [Figure 4.2]. The C_T value obtained for HEK293 with no spike was 31.09 ± 0.05 , confirming the cells did not express *PTGS1*. When comparing vector DNA spiked in water versus HEK293 cDNA, the gradient of the slopes (-2.98 and -3.23 respectively) were not shown to be statistically significantly different (F test; $F = 0.37$, $p = 0.54$). Primer efficiency was calculated using a pooled gradient, -2.99 and was found to have an efficiency of 115.72 %.

$10^{-5.81}$ μg of plasmid DNA was diluted in water as a positive control for further gene expression analyses.

4.3.2.3. *PTGS2* primer validation

I optimised the *PTGS2* primers using cDNA from HCA-7 cells, which are known to express COX-2 (247). The expected primer product was 169bp.

HCA-7 cDNA ranging from 1 to 10^{-6} μg was used. qPCR analysis found the C_T values ranged from 18.70 to 35.08 [Figure 4.3]. Primer efficiency was 126.59 %.

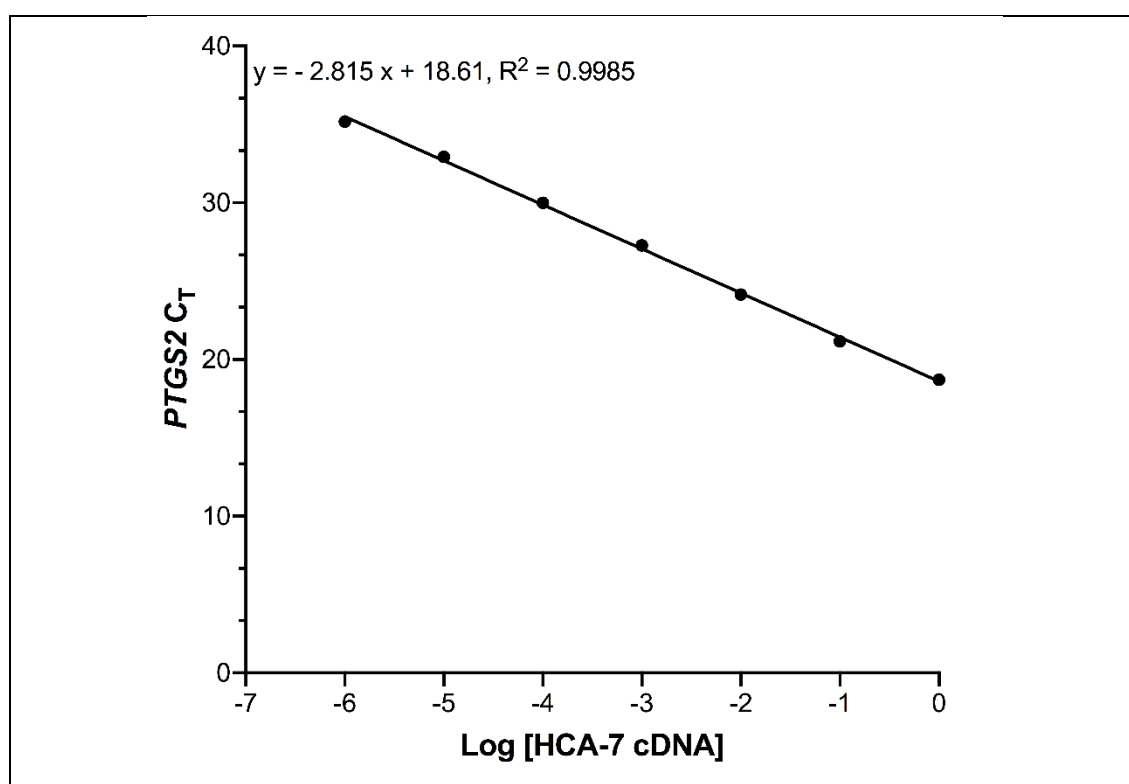


Figure 4.3 *PTGS2* Standard curve

PTGS2 C_T values obtained by qPCR in serially diluted cDNA HCA-7 samples ranging in quantity from $1\mu\text{g}$ to $10^{-6}\mu\text{g}$. *PTGS2* C_T data are expressed as the mean \pm SD, for 2 independent experimental replicates.

Having validated each primer pair, and established positive control for the assays, I proceeded with the analysis of *PTGS1* and *PTGS2* gene expression in the panel of CRC cell lines.

4.3.3. *PTGS1* and *PTGS2* gene expression in hCRC cell lines

Cyclooxygenase gene expression was measured in human CRC cell lines by RT-qPCR, and the measurements were converted in to a *PTGS* score as it enabled conversion of ΔC_T values (eliminating use of a comparator cell line) to a value in which a greater numerical score indicated greater expression of *PTGS1* or *PTGS2* [Chapter 3.9.3.1].

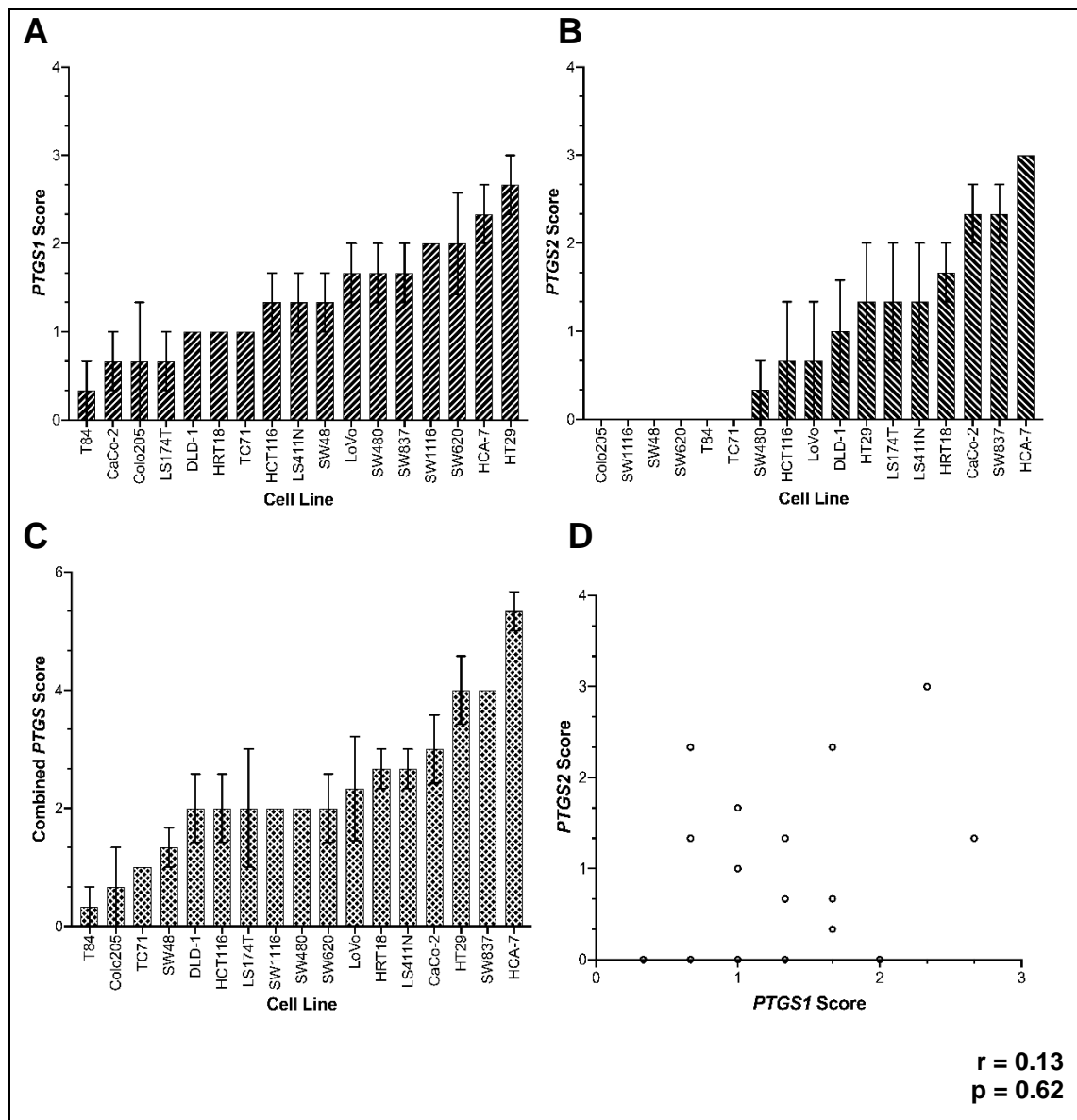


Figure 4.4 Expression of *PTGS1* and -2 genes in human CRC cell lines

Each figure presents cell lines in order of increasing gene expression for *PTGS1* (A), *PTGS2* (B) and combined *PTGS* (C). Scores are expressed as the mean \pm SD, for 3 independent replicates. No correlation between *PTGS1* expression and *PTGS2* expression was observed (D, Spearman correlation).

PTGS1 gene expression was detected in all cell lines [Figure 4.4 A], with lowest expression in T84 cells (*PTGS1* score: 0.33 ± 0.58) and highest expression in HT29 cells (*PTGS1* score: 2.67 ± 0.58). Colo205, SW1116, SW48, SW620, T84 and TC71 cells did not express *PTGS2* (as *PTGS2* Ct values were above 30 or undetermined). Lowest detectable expression of *PTGS2* was found in SW480 cells (*PTGS2* score: 0.33 ± 0.58), and highest expression was found in HCA-7 cells (*PTGS2* score: 3.00 ± 0.00) [Figure 4.4 B]. Combined PTGS score [Figure 4.4 C] values ranged from 0.33 ± 0.58 (T84) to 5.33 ± 0.58 (HCA-7). No correlation was found between *PTGS1* and *PTGS2*, giving no indication that expression of one *PTGS* isoform was associated with that of the other [Figure 4.4 D].

4.3.4. Sensitivity of CRC cell lines to *n*-3 PUFAs

The hCRC cell line response to EPA and/or DHA exposure was next examined and is presented in Table 4.3 below.

Table 4.3. Human colorectal cancer cell line sensitivity to *n*-3 PUFAs

Cell Line	EPA		DHA		EPA:DHA (2:1)	
	IC ₅₀ (μM)	<i>n</i>	IC ₅₀ (μM)	<i>n</i>	IC ₅₀ (μM)	<i>n</i>
CaCo-2	205.52 ± 1.51	3	54.21 ± 1.09	3	165.50 ± 1.11	3
Colo205	161.40 ± 1.16	3	5.57 ± 1.09	3	16.26 ± 1.29	3
DLD-1	85.91 ± 1.06	7	15.26 ± 1.07	10	53.06 ± 1.13	3
HCA-7	141.91 ± 1.05	9	23.31 ± 1.07	11	53.06 ± 1.13	3
HCT116	91.74 ± 1.08	18	31.09 ± 1.08	14	42.58 ± 1.13	3
HRT18	73.17 ± 1.13	3	41.95 ± 1.15	3	77.88 ± 1.19	3
HT29	118.60 ± 1.05	13	55.69 ± 1.05	13	83.52 ± 1.11	3
LoVo	141.10 ± 1.08	6	21.21 ± 1.08	8	41.03 ± 1.09	3
LS174T	228.23 ± 1.11	3	114.74 ± 1.06	3	194.00 ± 1.09	3
LS411N	84.33 ± 1.06	3	47.86 ± 1.21	3	75.75 ± 1.07	3
SW48	71.19 ± 1.16	3	35.44 ± 1.19	3	83.26 ± 1.12	3
SW480	77.84 ± 1.19	3	30.98 ± 1.08	3	54.73 ± 1.09	3
SW620	176.83 ± 1.18	3	24.72 ± 1.10	3	78.02 ± 1.11	3
SW837	138.33 ± 1.08	3	38.85 ± 1.13	3	104.40 ± 1.11	3
SW1116	224.52 ± 1.11	3	67.42 ± 1.11	3	254.80 ± 1.21	3
T84	137.00 ± 1.09	6	36.31 ± 1.09	6	62.54 ± 1.20	3
TC71	95.62 ± 1.25	3	43.12 ± 1.11	3	104.43 ± 1.10	3

Cell viability following exposure of cells to variable concentrations of *n*-3 PUFAs were measured by MTT assay or crystal violet assay. All IC₅₀ values are the mean ± SEM for *n* independent repeats. Independent repeats greater than 3 result from cell line use in chronic exposure experiments. Parental (non-chronically exposed) cells underwent *n*-3 PUFA concentration response MTT assays alongside chronically exposed cells to facilitate comparisons in *n*-3 PUFA sensitivity (IC₅₀ values) between parental and chronically exposed cells.

IC₅₀ values, determined using GraphPad Prism8™ as described in Chapter 3.4.4, were used as a measure of sensitivity, with a low IC₅₀ values indicative of a more sensitive cell line and high IC₅₀ values indicative of more resistant cells, relative to each other. The full concentration response curves are shown in **Figure 4.5**.

4.3.4.1. CRC cell lines had different sensitivities to EPA

Human CRC cell lines displayed a wide range of sensitivities to EPA with IC₅₀ values ranging from 71.19 ± 1.19 µM (SW48) to 228.23 ± 1.11 µM (LS174T) [**Table 4.3**]. Seven cell lines (DLD-1, HCT116, HRT18, LS411N, SW48, SW480, TC71) had IC₅₀ values below 100 µM, seven cell lines (Colo205, HCA-7, HT29, LoVo, SW620, SW837, T84) had IC₅₀ values between 100 and 200 µM and three cell lines had IC₅₀ values greater than 200 µM, namely CaCo-2, LS174T and SW1116.

As visual inspection of EPA, DHA and EPA:DHA (2:1) combination mixture concentration response curves indicated that biphasic responses were present. A biphasic response curve differs from a standard monotonic sigmoid shape, with a plateau evident between two distinct concentration-response phases (178). All concentration response curves were subsequently analysed using GraphPad Prism8™ (as described in Chapter 3.4.4). This indicated that four cell lines displayed a biphasic EPA concentration response curve, namely HCT116, HRT18, HT29 and T84 [**Figure 4.5, Table 4.4**]. The analysis of biphasic curves in GraphPad Prism8™ gave 2 IC₅₀ concentration outputs which are displayed in **Table 4.4**. No DHA or combination mixture concentration response curves were determined to be biphasic using the GraphPad Prism8™ software. Biphasic concentration response curves may indicate EPA acting via two different pathways.

Table 4.4. Cell lines exhibiting a biphasic response to EPA

Cell Line	EPA	
	IC _{50_1} (µM)	IC _{50_2} (µM)
HCT116	22.44 ± 0.17	141.58 ± 1.04
HRT18	7.59 ± 1.12	123.02 ± 1.02
HT29	0.85 ± 1.11	116.14 ± 1.12
T84	239.88 ± 0.01	371.53 ± 1.21

Concentration response curves were analysed in GraphPad Prism9™, using the biphasic equation curve analysis. Biphasic curves have two distinct concentration response phases. The half-maximal inhibitory concentrations (IC_{50_1} and IC_{50_2}) are expressed as the mean ± SEM.

However, whilst this software analysis eliminated subjective interpretation, it should be noted that there were limitations to type of analysis of the biphasic concentration

response. Indeed, some curves appear to be biphasic-curve in appearance (such as Colo205), but were not identified as such using this method. The GraphPad Prism8™ biphasic curve analysis is likely limited by the number concentrations that could be tested with the concentration-response range. The concentrations tested ranged from 1 to 500 μM *n*-3 PUFA and experimental set-up meant this was skewed towards the lower concentrations within the range. This could reduce the ability of the software to accurately model and identify biphasic curves.

4.3.4.2. CRC cell lines were more sensitive to DHA than EPA

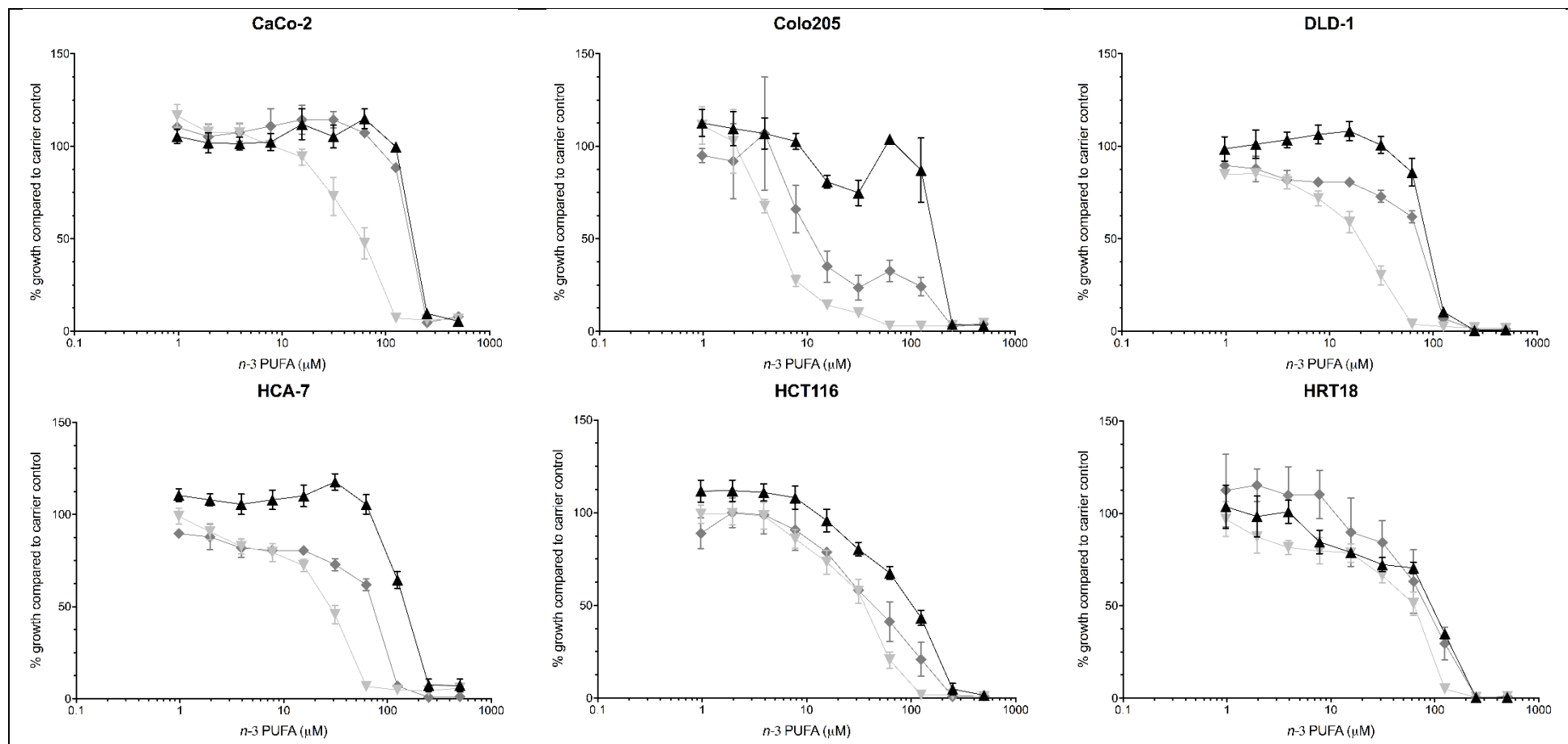
DHA IC_{50} values ranged from $5.57 \pm 1.09 \mu\text{M}$ (Colo205) to $114.74 \pm 1.06 \mu\text{M}$ (LS174T) [Table 4.3]. LS174T was the only cell line found to have an IC_{50} value greater than 100 μM . All cell lines, without exception, were more sensitive to DHA than EPA. Whilst LS174T cells were found to be the least sensitive to both EPA and DHA, the most sensitive cell lines were different for EPA and DHA.

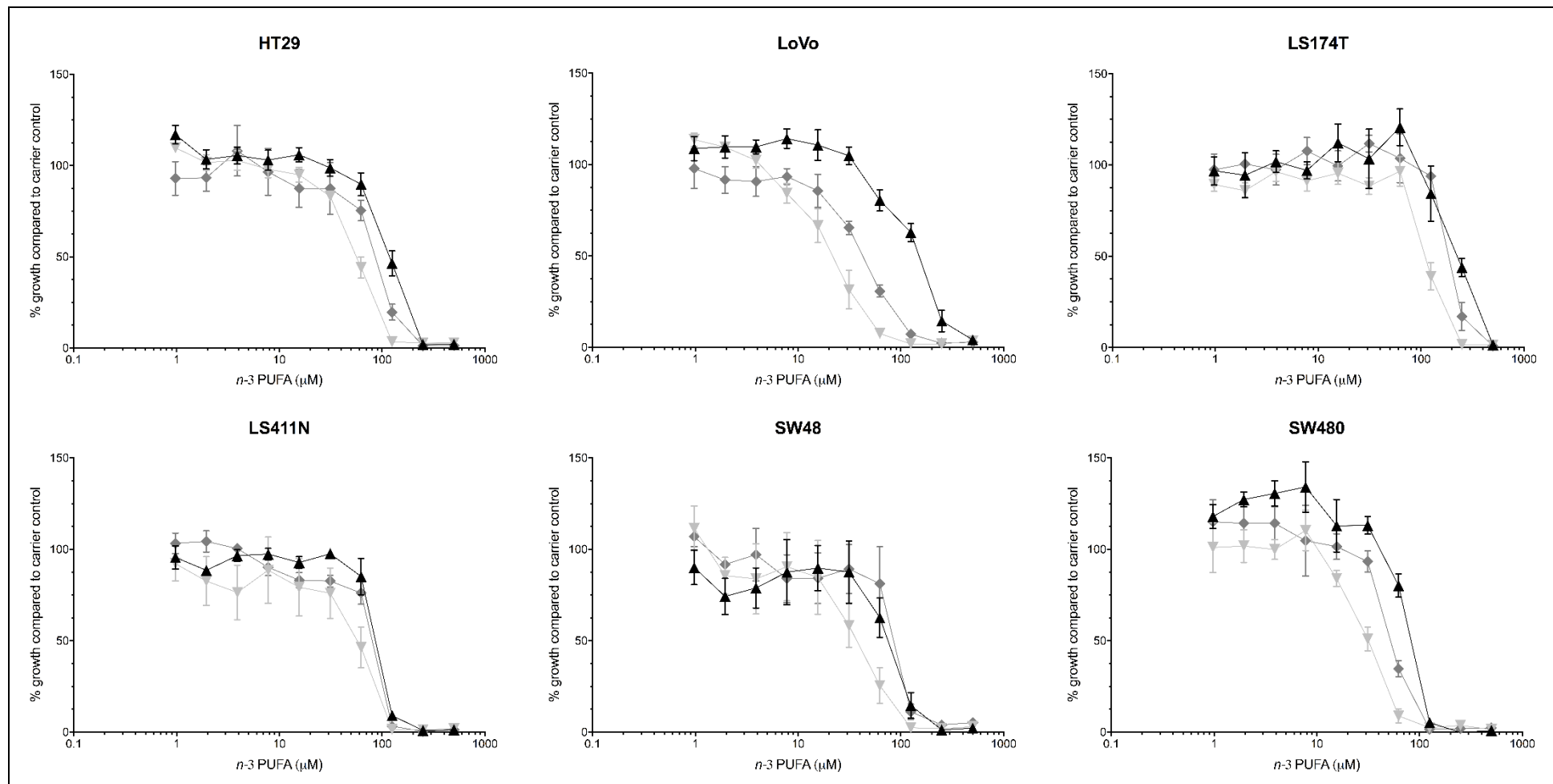
4.3.4.3. Combined EPA:DHA (2:1 ratio) sensitivity was varied in human CRC cells

The combined EPA:DHA (2:1) ratio was selected as this is the ratio commonly found in *n*-3 PUFA-rich food sources and over-the-counter *n*-3 PUFA supplement mixtures (99).

Colo205 cells were the most sensitive cells to combined *n*-3 PUFA treatment ($\text{IC}_{50} = 16.26 \pm 1.29 \mu\text{M}$), whilst the most resistant cell line was SW1116 ($\text{IC}_{50} = 254.80 \pm 1.21 \mu\text{M}$). Combined *n*-3 PUFA exposure resulted in an IC_{50} value greater than that of EPA or DHA alone in 4 cell lines; namely SW48, HRT18, TC71 and SW1116 [Table 4.3].

As all the data have been expressed as IC_{50} values, from hereon, the terms sensitive and resistant are relative.





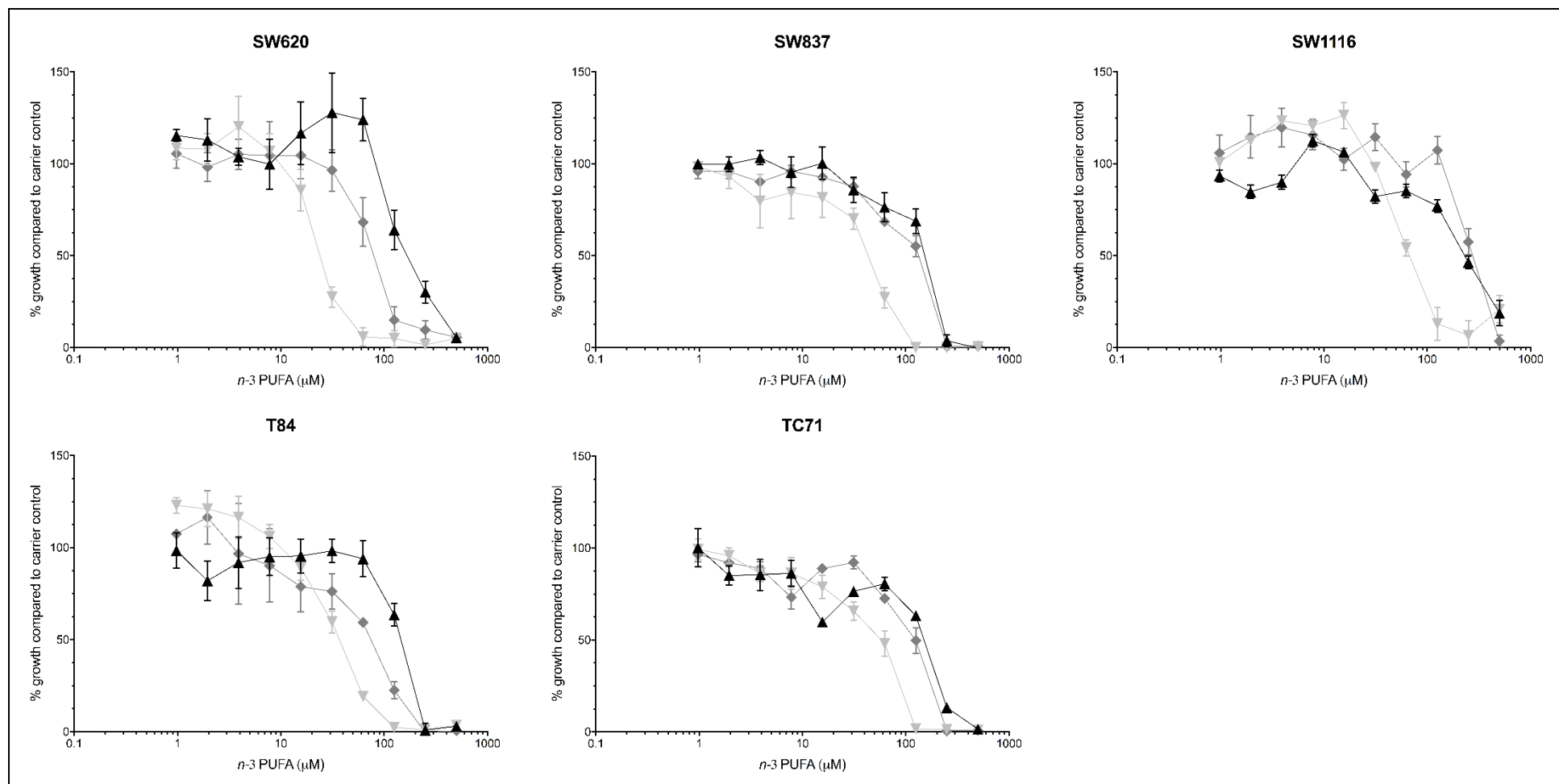


Figure 4.5 CRC cell line concentration response curves to *n*-3 PUFAs

Exponentially growing cells were cultured in presence of EPA ▲, DHA ▼ or combined EPA:DHA ◆ for 72 hours. Cell viability was measured by MTT assay or crystal violet assay. % growth inhibition was calculated relative to carrier control treated cells. Data are expressed as the mean +/- SEM of a minimum of 3 independent replicates.

4.3.4.4. *Sensitivity of a cell line to one n-3 PUFA was not indicative of sensitivity to a different n-3 PUFA*

The respective cell line responses to EPA and DHA were compared to establish whether sensitivity was comparable between *n*-3 PUFAs. No correlation was found between EPA and DHA sensitivity ($r = 0.19$, $p = 0.45$), nor was it found between EPA and combined EPA:DHA sensitivity ($r = 0.32$, $p = 0.21$). The lack of shared response was particularly evident in the case of Colo205 cells, which were resistant to EPA ($IC_{50} = 161.40 \pm 1.16 \mu M$), however were the most sensitive to DHA ($IC_{50} = 5.57 \pm 1.09 \mu M$). A strong positive correlation was found between DHA sensitivity and combined EPA:DHA sensitivity ($r = 0.86$, $p = 0.001$).

4.3.4.5. *Interactions between the individual n-3 PUFAs in EPA:DHA (2:1) treatment*

Whilst the sensitivity of a cell line to EPA was not associated with that of DHA, interactions between EPA and DHA were unknown in the combined mixture (EPA:DHA 2:1). To identify interactions, I compared EPA- and DHA-treatment induced % growth inhibition when *n*-3 PUFA were administered alone or in combination [Table 4.5], with examples of the curve extrapolation depicted in Figure 4.6.

Two distinct effects of combination *n*-3 PUFA treatment were obtained. For 6 cell lines, namely; CaCo-2, Colo205, LS174T, SW48, SW837 and TC71, a potentially antagonistic effect was observed at both concentrations tested. I have selected the DHA-sensitive cell line, Colo205, treated with 50 μM EPA:DHA (2:1) as an example. Exposure of Colo205 cells to 16 μM DHA alone resulted in an 85.9 % growth inhibition, and treatment with 33 μM EPA alone resulted in a 25.2 % growth inhibition [Table 4.5]. If a potentially additive effect were to be assumed, treatment with 50 μM EPA:DHA (2:1) exposure would result in no viable cells. However, the observed effect on cell viability following combined treatment was a growth inhibition of just 70% [Table 4.5], which was subsequently labelled potentially antagonistic. CaCo-2 and LS174T cell viabilities were greater following 50 μM *n*-3 PUFA combination treatment than when cells were treated with the corresponding concentration of individual *n*-3 PUFAs only.

Combination *n*-3 PUFA treatment produced an effect equal to (potentially additive), or greater than (potentially synergistic), the effect observed when the sum of individual EPA and DHA were measured, in 8 out of 16 cell lines. This was found at both concentrations of combination treatment tested in HCA-7, HCT116, HT29, SW480, SW620 and T84 cell

lines. In LoVo cells, 50 μM combination treatment had a potentially synergistic effect and 100 μM combination treatment had a potentially additive effect. 50 μM combination treatment had a potentially additive effect and 100 μM combination treatment had a potentially synergistic effect in LS411N cells. This could indicate that, for these cell lines, a benefit to using a combination treatment.

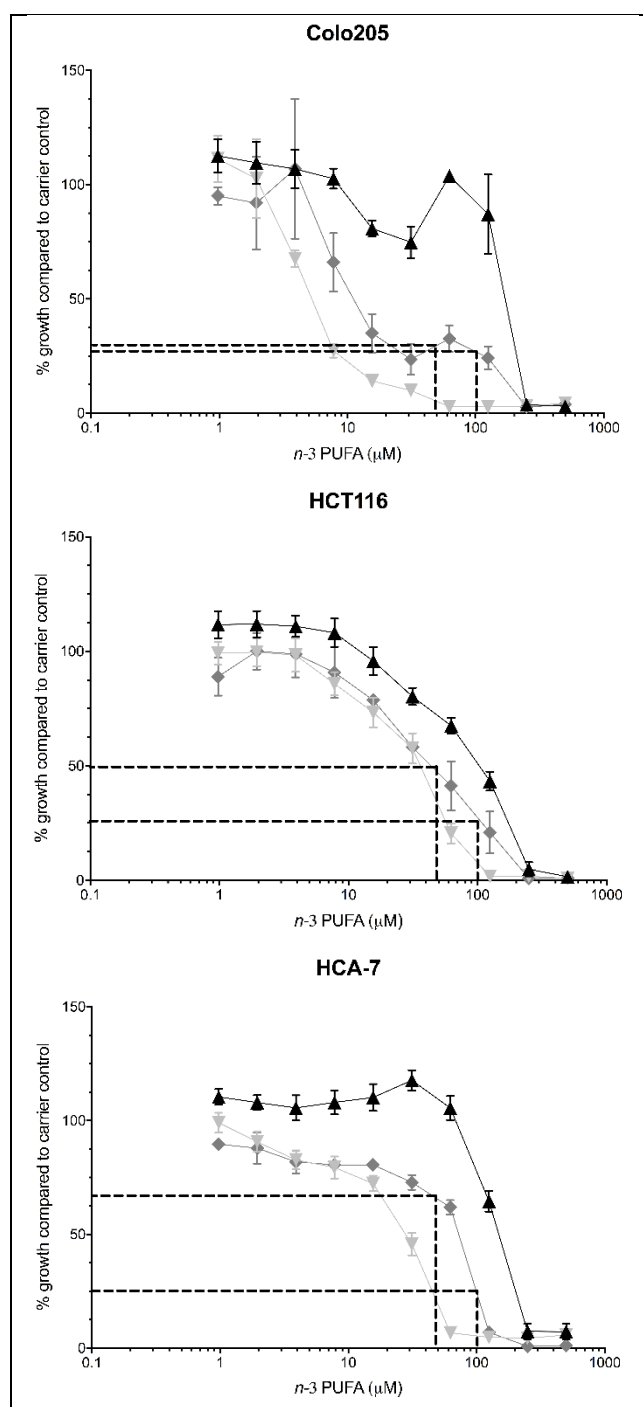


Figure 4.6 Extrapolation of *n*-3 PUFA concentration response curves

Extrapolating growth inhibition percentage following 50 μM and 100 μM combined EPA:DHA treatment in representative cell lines. Colo205, HCT116 and HCA-7 cells were grown in presence of EPA \blacktriangle , DHA \blacktriangledown or combined EPA:DHA \blacklozenge for 72 hours. Data are expressed as the mean \pm SEM of a minimum of 3 independent replicates. Dashed line shows the extrapolation of cell viability of cells treated with 50 μM or 100 μM of combination EPA:DHA (2:1) treatment.

Table 4.5. Cell viability in cells exposed to combination treatment and corresponding individual n-3 PUFA concentrations

Cell Line	Difference in Cell Viability compared to control (%)			Combined treatment interaction	Difference in Cell Viability compared to control (%)			Combined treatment interaction
	50 μ M EPA:DHA (2:1)	~ 33 μ M EPA	~ 16 μ M DHA		100 μ M EPA:DHA (2:1)	~ 66 μ M EPA	~ 33 μ M DHA	
CaCo-2	+ 12.5	+ 5.3	- 5.8	Antagonistic*	- 7	+ 14.9	- 27.0	Antagonistic*
Colo205	- 70	- 25.2	- 85.9	Antagonistic*	- 75	+ 3.9	- 90.0	Antagonistic*
DLD-1	- 37	- 0.7	- 41.1	Additive*	- 75	- 14.1	- 69.9	Antagonistic*
HCA-7	- 35	+ 17.7	- 27.6	Synergistic*	- 75	+ 5.5	- 54.3	Synergistic*
HCT116	- 50	- 19.7	- 26.7	Additive*	- 75	- 32.4	- 42.4	Additive*
HRT18	- 30	- 27.6	- 21.3	Antagonistic*	- 62.5	- 29.5	- 33.6	Additive*
HT29	- 20	- 1.2	- 5.0	Synergistic*	- 62.5	- 10.3	- 16.8	Synergistic*
LoVo	- 56	+ 4.8	- 33.5	Synergistic*	- 87.5	- 19.6	- 68.5	Additive*
LS174T	+ 5	+ 3.4	- 4.5	Antagonistic*	- 5	+ 20.7	- 11.5	Antagonistic*
LS411N	- 20	- 2.4	- 20.7	Additive*	- 75	- 14.8	- 24.0	Synergistic*
SW48	- 20	- 12.4	- 15.3	Antagonistic*	- 62.5	- 37.3	- 41.6	Antagonistic*
SW480	- 45	+ 13.1	- 15.9	Synergistic*	- 87.5	- 19.8	- 49.0	Synergistic*
SW620	- 20	+ 28	- 15.9	Synergistic*	- 62.5	+ 24.0	- 72.5	Synergistic*
SW837	- 25	- 14.2	- 18.5	Antagonistic*	- 40	- 23.6	- 29.8	Antagonistic*
SW1116	+ 5	- 17.8	+ 26.3	Additive*	+ 5	- 14.7	- 1.9	Antagonistic*
T84	- 37.5	- 1.7	- 10.9	Synergistic*	- 62.5	- 6.0	- 40.3	Synergistic*
TC71	- 20	- 23.5	- 21.1	Antagonistic*	- 40	- 19.4	- 34.3	Antagonistic*

Cell viabilities at 50 μ M and 100 μ M concentrations were extrapolated from the EPA:DHA (2:1) concentration-response curves. The corresponding cell viabilities of EPA and DHA at the concentrations within the mixture were obtained using the raw EPA (only) and DHA (only) concentration-response curves. Percentage of cells viable are displayed as the difference compared to ethanol carrier control, with positive values indicating the treatment increased growth and negative values indicating that growth was inhibited. Combined treatment interactions are described as antagonistic*, additive* and synergistic* with the asterisk to denote that these descriptions are potential interactions that require verification.

Two cell lines; DLD-1 and SW1116, exhibited a potentially additive effect when combination treatment was used at 50 μ M but a potentially antagonistic effect was shown when 100 μ M combination treatment was used.

The data suggests that mechanisms of action, through which EPA and DHA act, differ between cell lines and can change at different exposure concentrations. Potentially additive and potentially synergistic interactions may indicate that EPA and DHA exert their effects via different mechanisms, whereas potentially antagonist interactions could be the result of EPA and DHA competing for the same target. No key features identified for cell lines (in terms of sensitivity or molecular profile) were associated with potentially additive / synergistic EPA-DHA interactions or potentially antagonistic EPA-DHA interactions (data not shown). The interactions between EPA and DHA would need to be validated which could be achieved thorough studies utilising appropriate experimental set-up and analysis as discussed later in this chapter (**Chapter 4.4.1, Chapter 4.4.3**).

4.3.5. Relationships between cellular properties and *n*-3 PUFA sensitivity

To elucidate possible drivers of cellular response to *n*-3 PUFAs, I next explored the relationships between cell molecular characteristics and *n*-3 PUFA sensitivity.

4.3.5.1. Growth rate was correlated with EPA sensitivity

CRC cells were distinguishable by differing growth rates. Carrier treated cells used as a control in the MTT assay were used as a surrogate marker of growth rate (**Chapter 3.4.5**).

The relationship between growth rate and *n*-3 PUFA sensitivity was tested. There was a statistically significant negative correlation between sensitivity to EPA and growth rate (Spearman's correlation, $r = -0.40$, $p = 0.05$) [**Figure 4.7 A**]. No such relationship was found with respect to DHA or the combination treatment (Spearman's correlation, $r = 0.18$, $p = 0.25$ and $r = -0.30$, $p = 0.12$ respectively) [**Figure 4.7 B and C**].

An attempt to further investigate growth rate and cell lines' response to EPA was made by exposing cells to culture media containing low concentrations of FCS. It was theorised that growth rate of cell lines would decrease in low FCS conditions, and subsequent EPA sensitivity in 'slow' growing cells could be tested. However, the growth rate of cells tested was not reduced significantly, despite the reduction in FCS (data not shown).

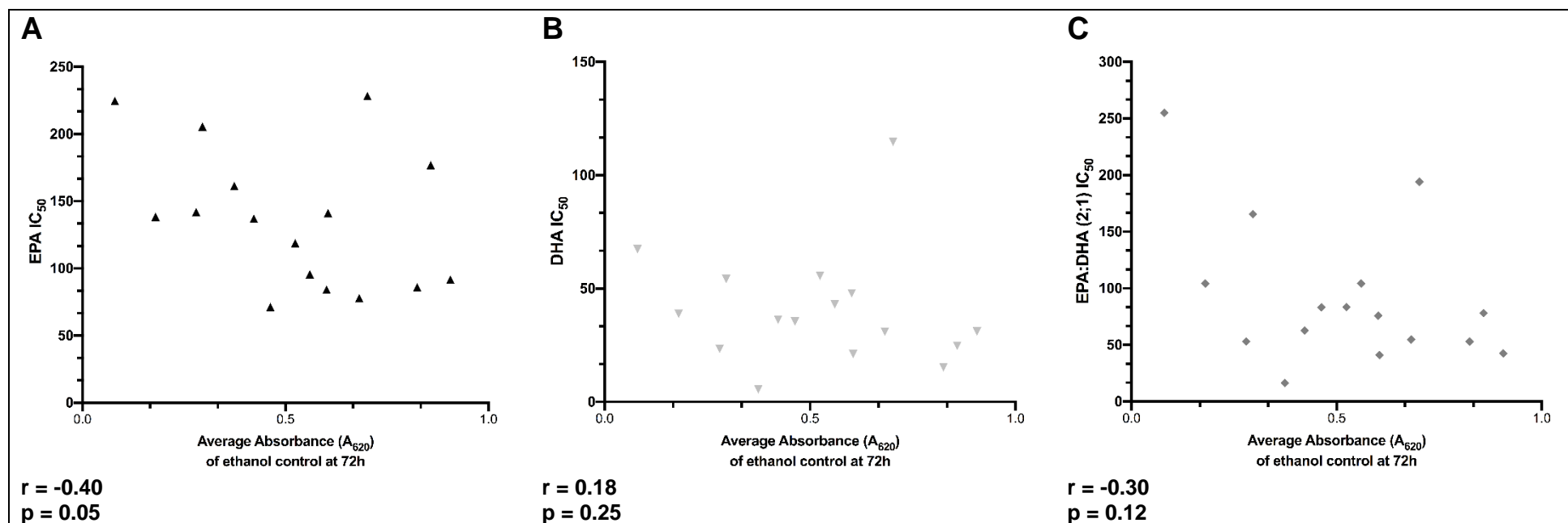


Figure 4.7 Correlation between growth rate and *n*-3 PUFA sensitivity

Absorbance readings were correlated with cell line sensitivity (IC₅₀) to EPA ▲ (A), DHA ▼ (B) and EPA:DHA ◆ (C). Absorbance data points are expressed as mean ± SD, for a minimum of n=3. Spearman correlation coefficient and p values are given below each graph.

4.3.5.2. *No strong trends between PTGS expression and n-3 PUFA sensitivity were identified*

Considering the key role of COX metabolism in *n*-3 PUFA bioactivity (158), it was hypothesised that less sensitive, more resistant, cell lines would have greater expression of *PTGS1* and / or *PTGS2*. Therefore, the relationship between *n*-3 sensitivity and *PTGS1* and *PTGS2* gene expression was tested in the human CRC cell line panel.

No statistically significant correlations were identified between *PTGS1* expression and EPA IC₅₀, DHA IC₅₀ or EPA:DHA (2:1) IC₅₀ [Figure 4.8], *PTGS2* expression and EPA IC₅₀, DHA IC₅₀ or EPA:DHA (2:1) IC₅₀ [Figure 4.9] or combined *PTGS* expression and EPA IC₅₀, DHA IC₅₀ or EPA:DHA (2:1) IC₅₀ [Figure 4.10].

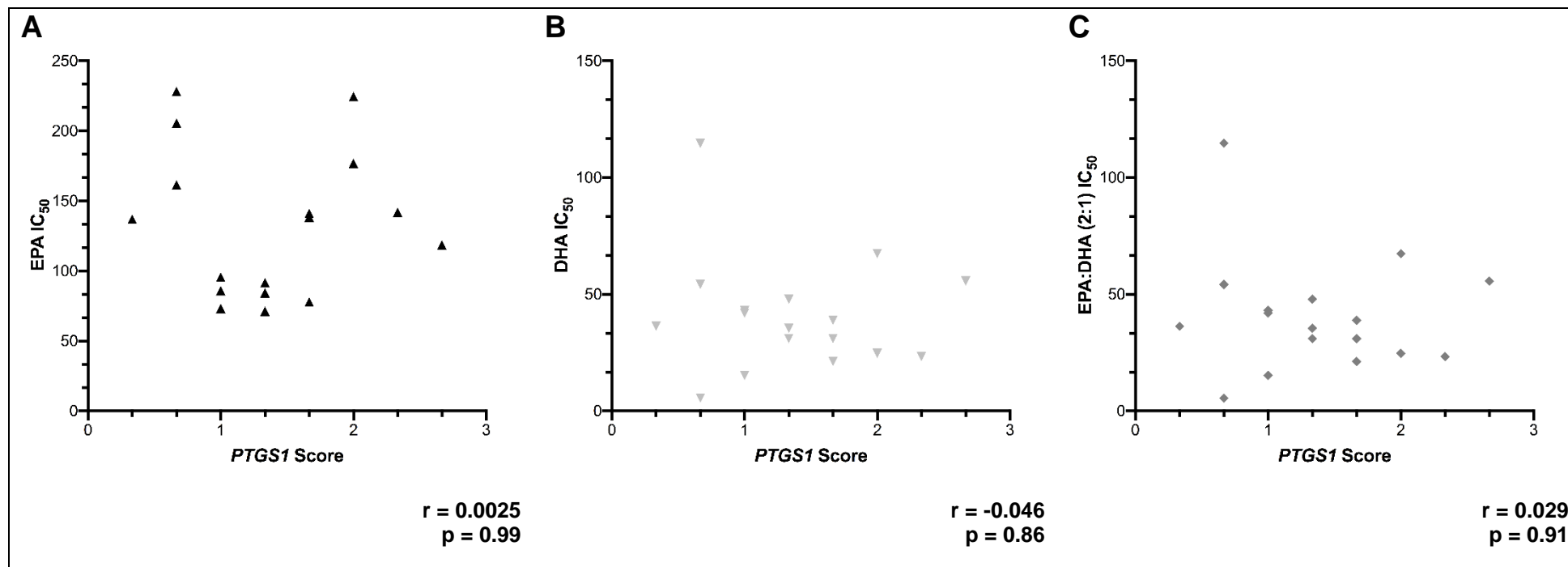


Figure 4.8 Associations between *PTGS1* expression and *n-3* PUFA sensitivity

The *PTGS1* mRNA transcript expression levels were measured in human CRC cell lines by RT-qPCR 3 independent replicates Expression levels were plotted against EPA (**A**), DHA (**B**) and EPA:DHA (2:1) (**C**) IC₅₀ values for with a minimum of 3 independent replicates. Associations were tested using Spearman's correlation, Spearman coefficients and p values are quoted below each graph.

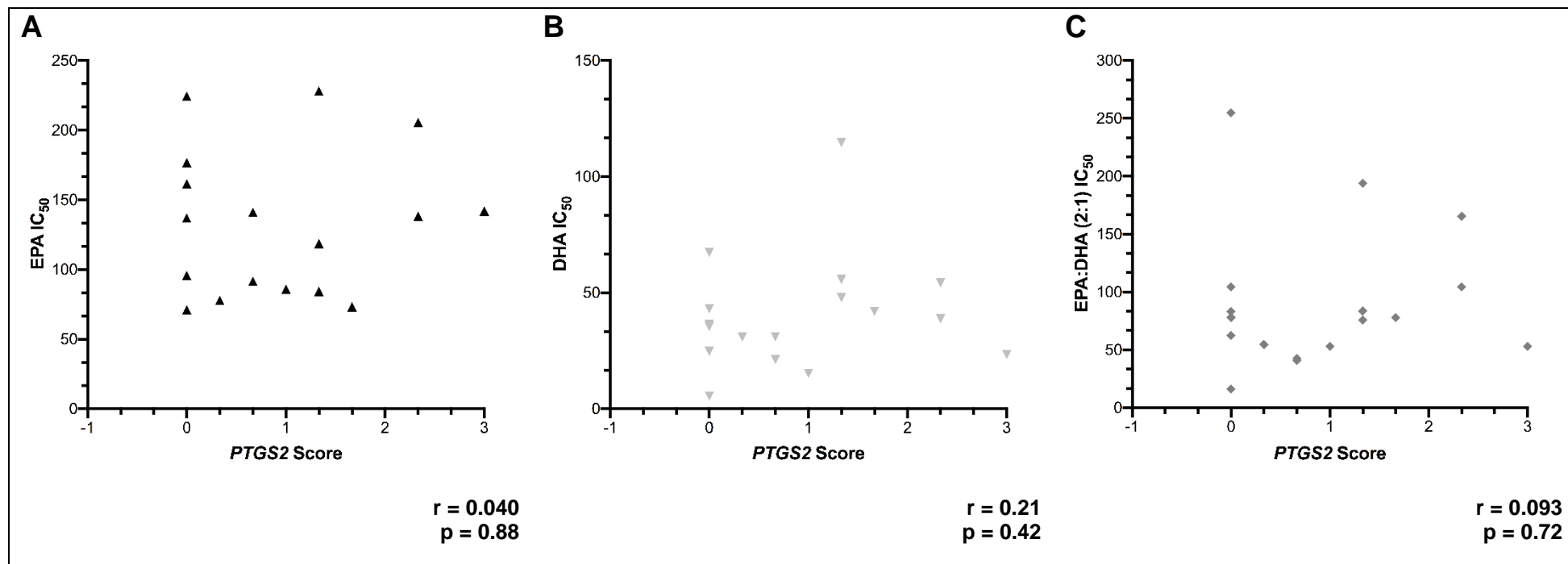


Figure 4.9 Associations between *PTGS2* expression and *n*-3 PUFA sensitivity

The *PTGS2* mRNA transcript expression levels were measured in human CRC cell lines by RT-qPCR 3 independent replicates Expression levels were plotted against EPA (**A**), DHA (**B**) and EPA:DHA (2:1) (**C**) IC₅₀ values for with a minimum of 3 independent replicates. Associations were tested using Spearman's correlation, Spearman coefficients and p values are quoted below each graph.

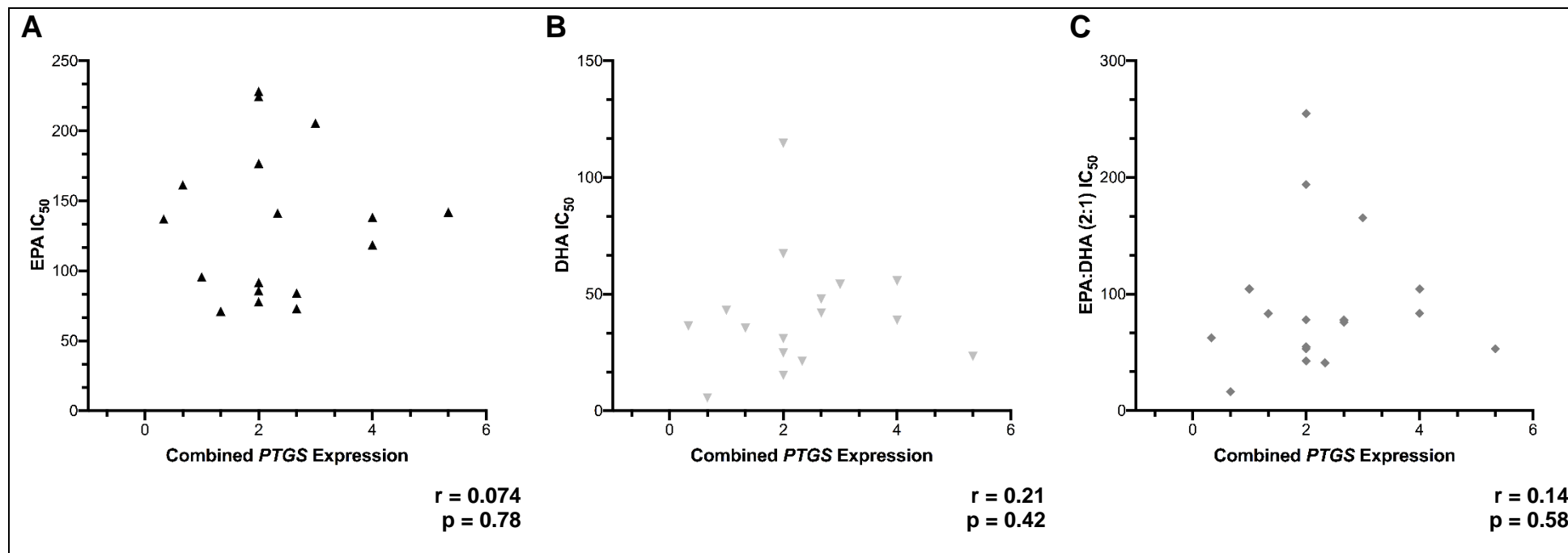


Figure 4.10 Associations between combined *PTGS* expression and *n*-3 PUFA sensitivity

The *PTGS1* and *PTGS2* mRNA transcript expression levels were measured in human CRC cell lines by RT-qPCR 3 independent replicates. Expression levels were plotted against EPA (**A**), DHA (**B**) and EPA:DHA (2:1) (**C**) IC₅₀ values for with a minimum of 3 independent replicates. Associations were tested using Spearman's correlation, Spearman coefficients and *p* values are quoted below each graph.

4.3.5.3. Associations between molecular phenotypes and *n*-3 PUFA sensitivity

Having established that the CRC cell lines in the panel displayed differential sensitivities to both EPA and DHA [Table 4.3], I tested whether molecular phenotypes of CRC cell lines [Table 4.1] could be associated with response to EPA or DHA. Associations between individual phenotypes and sensitivity were assessed.

4.3.5.3.1. Relationship between CIN status and cell sensitivity to *n*-3 PUFAs

There was no relationship between CIN status and *n*-3 PUFA sensitivity [Figure 4.11]. A potential trend was observed between CIN status and EPA IC₅₀ values, as five of the seven CIN- cell lines displayed IC₅₀ values below 100 µM (CIN- median value 91.74 µM, range 71.19 ± 1.16 µM (SW48) to 228.2 ± 1.11 µM (LS174T)). The median value for the CIN+ groups was greater at 140.2 µM (range 77.84 ± 1.19 µM (SW480) to 224.52 ± 1.11 µM). However, the difference between the two groups was not statistically significant.

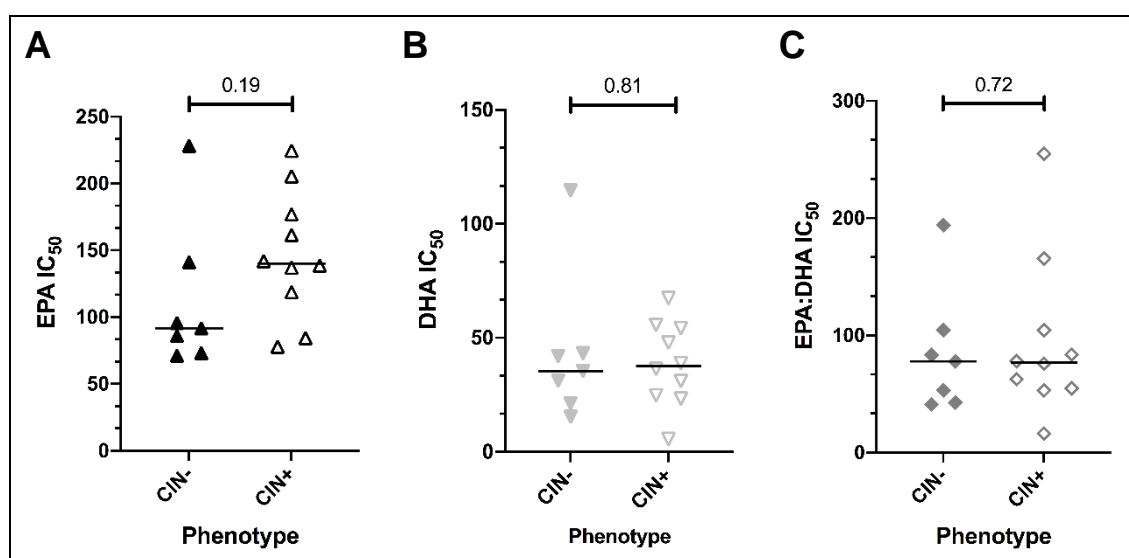


Figure 4.11 Associations between *n*-3 PUFA sensitivity and CIN status

EPA ▲△ (A), DHA ▼▽ (B), and combination ◆◇ (C) IC₅₀ values between CIN- (filled symbol) and CIN+ cell lines were compared. Mann-Whitney test was used to compare the groups.

4.3.5.3.2. Relationship between MSI status and cell sensitivity to *n*-3 PUFAs

No statistically significant relationship between microsatellite status and *n*-3 PUFAs was evident in this dataset [Figure 4.12]. Although a difference between median values was observed for EPA-treated cells, with MSS cells having a higher median IC₅₀ value (149.9 µM) than MSI cells (91.47 µM), this was not statistically significant.

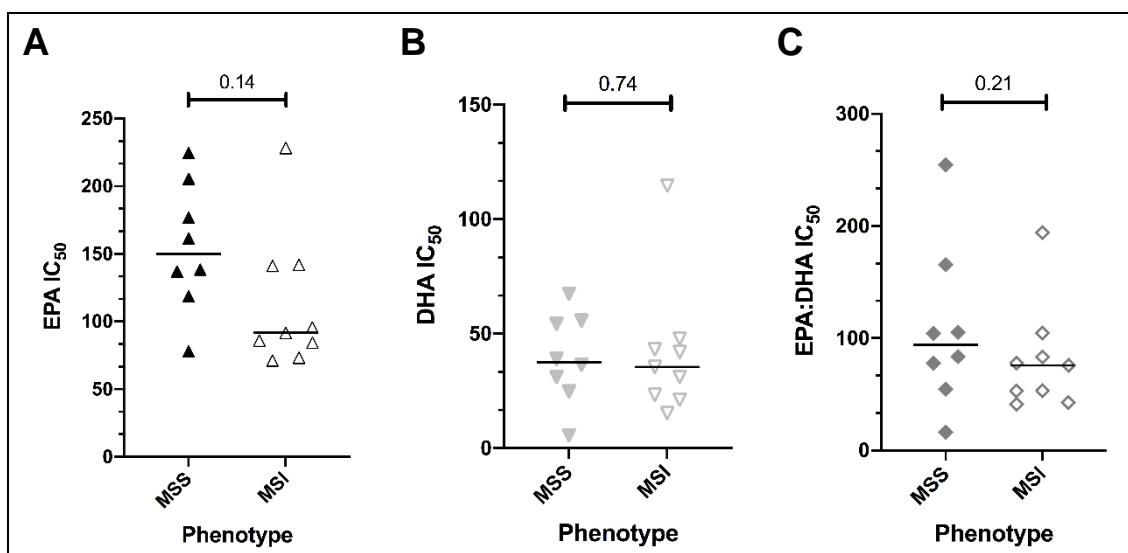


Figure 4.12 Associations between *n*-3 PUFA sensitivity and MS status

EPA ▲△ (A), DHA ▼▽ (B), and combination ◆◇ (C) IC₅₀ values between MSS (filled symbol) and MSI cell lines were compared. Mann-Whitney test was used to compare the groups.

4.3.5.3.3. Relationship between CIMP status and cell sensitivity to *n*-3 PUFAs

Although there was no association between CIMP status and cell sensitivity to DHA [Figure 4.13 B] or the combination [Figure 4.13 C], a statistically significant association between CIMP status and EPA sensitivity was identified [Mann-Whitney, $p = 0.05$, Figure 4.13 A].

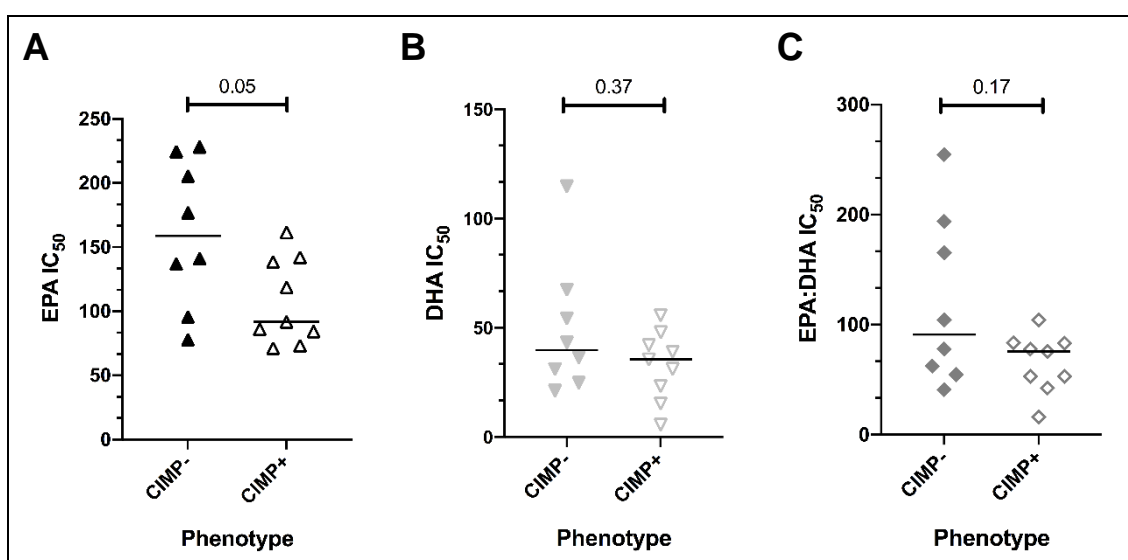


Figure 4.13 Associations between *n*-3 PUFA sensitivity and CIMP status

EPA ▲△ (A), DHA ▼▽ (B), and combination ◆◇ (C) IC₅₀ values between CIMP- (filled symbol) and CIMP+ cell lines were compared. Mann-Whitney test was used to compare the groups.

CIMP- cell lines were less sensitive to EPA than CIMP+ cell lines; median IC₅₀ 159.00 µM, range 77.84 ± 1.19 µM (SW480) to 228.23 ± 1.11 µM (LS174T). CIMP+ cells were more EPA sensitive (median IC₅₀ 91.74 µM, range 71.19 ± 1.16 µM (SW48) to 161.4 ± 1.16 µM (Colo205).

4.3.5.3.4. Relationship between grouped molecular subtypes and EPA sensitivity

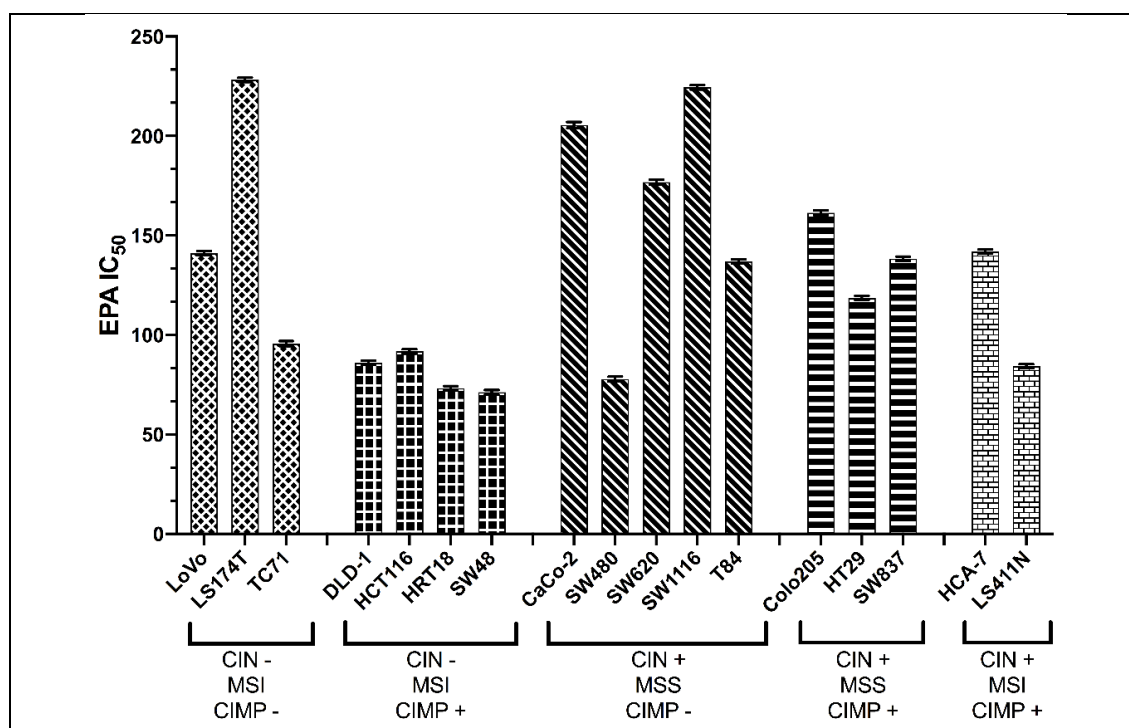


Figure 4.14 EPA sensitivity (IC₅₀) of cell lines grouped by molecular phenotype

EPA sensitivity of cell lines was measured by MTT assay and these were plotted against cell line molecular properties. Bar patterns are representative of molecular phenotypes. EPA IC₅₀ data is expressed as the mean ± SEM, for 3 to 18 independent repeats.

The subgroup most sensitive to EPA was CIN-, MSI and CIMP+ comprised of DLD-1, HCT116, HRT18 and SW48 cells. Within this group, all EPA IC₅₀ values were below 100 µM [Figure 4.14]. Four out of five cell lines classified as CIN+, MSS and CIMP-, had IC₅₀ values above 137 µM. The outlier in this subgroup was the SW480 cell line. This was interesting as, in comparison to SW620 cells (derived from a metastatic tumour from the same patient as SW480 cells), IC₅₀ values were 2.3-fold different (77.84 ± 1.19 versus 176.83 ± 1.18). Greater variation in EPA IC₅₀ values was found within the other phenotypic subgroups. Kruskal-Wallis test was used to compare distribution of IC₅₀ values between molecular phenotypic subgroups, with distributions not found to be significantly different (p = 0.19). The trend between high EPA sensitivity in CIN-, MSI, CIMP+ cell lines in comparison to the other subgroups was not seen when cells were exposed to DHA and EPA:DHA (2:1) [Appendix A4.3].

No trend was observed for DHA, whereas EPA sensitivity was found to be linked with CIN-, MSI and CIMP+ statuses. As EPA sensitivity and CIMP+ phenotypes were associated, an attempt to reverse CIMP phenotypes using epigenetic drugs was undertaken and presented next in this chapter.

4.3.6. Investigating the effect of epigenetic drug treatment on cell sensitivity to *n*-3 PUFAs

Having shown the link between CIMP+ cell lines and EPA sensitivity, I next used epigenetic drugs to establish that the association was linked to a molecular mechanism linked to DNA methylation. Treatment of CIMP- cells with a methylating agent should increase sensitivity to EPA and using demethylating agents should increase resistance in CIMP+ cell lines. The following cell lines were used: CIMP-; LS174T, TC71, LoVo and SW620 and CIMP+; HCT116, HCA-7, HRT18.

4.3.6.1. Optimisation of epigenetic drug pre-treatment of hCRC cells

The first objective was to establish a concentration of TMZ, DAC and 5-AZA that would maintain good cell viability to facilitate subsequent *n*-3 PUFA treatment. Literature searching found that previous studies had obtained TMZ IC₅₀ values over 100 μ M, with concentration ranges that included 50 – 400 μ M (248). It was determined that the concentration range to test in the hCRC cell lines should range from 1.25 μ M to 640 μ M.

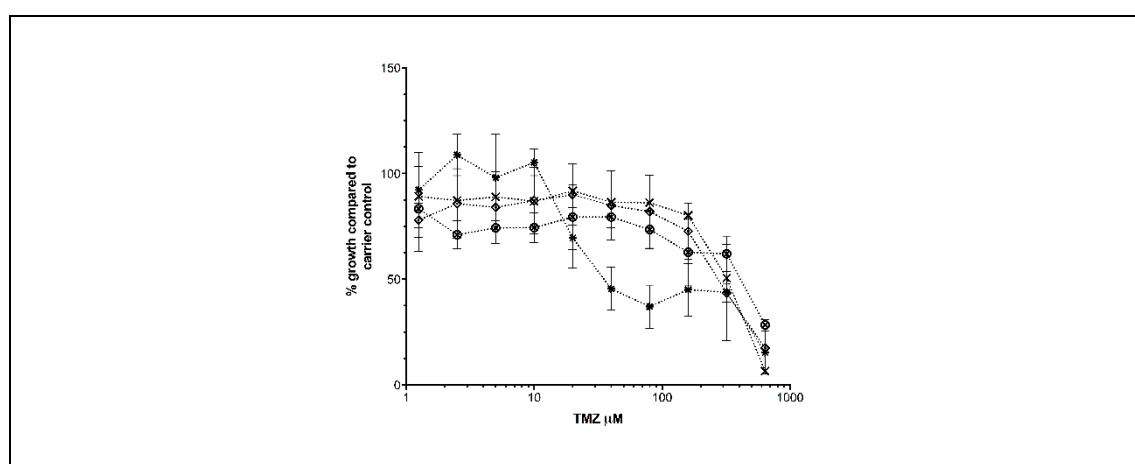


Figure 4.15 TMZ hCRC concentration response curves

Concentration-response curves obtained in LoVoX, LS174T⊗, SW620* and TC71◇ exposed to TMZ. Cell viability was measured by MTT assay, % growth inhibition data are expressed as the mean of 2 independent replicates, or mean \pm SEM of 3 independent replicates.

Four CIMP- cell lines were treated with varied concentrations of TMZ, the concentration response curves are presented in **Figure 4.15** above, and IC₅₀ values are shown in **Table 4.6** below.

Table 4.6. Sensitivity of hCRC cell lines to epigenetic agents TMZ, 5-AZA and DAC

Cell Line	<i>Temozolomide</i>		<i>5-Azacytidine</i>		<i>Decitabine</i>	
	IC ₅₀ (μM)	n	IC ₅₀ (μM)	n	IC ₅₀ (μM)	n
LS174T	560.10 ± 1.91	3			0.73 ± 1.29	2
TC71	254.40 ± 1.22	3			0.18 ± 0.47	2
SW620	85.04 ± 1.28	3				
LoVo	289.40 ± 1.21	2				
HCT116			0.51 ± 1.51	2	> 500	3
HCA-7			3.92 ± 1.27	2	> 500	3
HRT18					2.37 ± 0.22	2

Temozolomide (TMZ), 5-Azacytidine (5-AZA) and decitabine (DAC) IC₅₀ concentrations (μM) are expressed as mean +/-SEM for 3 independent replicates.

DAC and 5-AZA were screened as part of the Development Therapeutics Program (DTP) NCI-60 Human Tumour Cell Lines Screen (249) which included 9 hCRC cell lines (Colo205, HCT116, KM12, DLD-1, HCT-15, KM20L2, HCC-2998, HT29 and SW620). The publicly available data were used to determine the range of concentrations to use in the cell viability assays. DTP reported IC₅₀ values of approximately 40 μM (DAC) and 2 μM (5-AZA) for HCT116 cells. The concentration ranges tested were 0.96 – 500 μM (DAC) and 0.02 - 8.00 μM (5-AZA). IC₅₀ values obtained for 5-AZA and DAC are shown in **Table 4.6**. The concentration response curves show that in case of LS174T cells there was an increase in viability for concentrations above 3.90 μM [**Figure 4.16**].

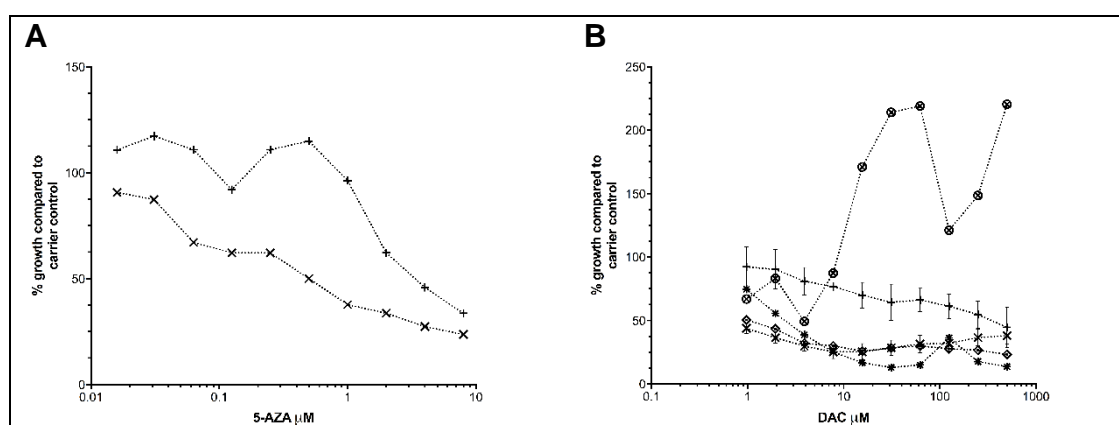


Figure 4.16 5-AZA and DAC hCRC concentration response curves

Concentration-response curves obtained in HCA-7+, HCT116x, HRT18*, LS174T ⊗ and TC71 ◇ exposed to varying concentrations of 5-AZA (A), or DAC (B). Cell viability was measured by MTT assay, % growth inhibition data are expressed as the mean of 2 independent replicates or mean +/- SEM of 3 independent replicates.

4.3.7. Impact of epigenetic drug pre-treatment on *n*-3 PUFA sensitivity of CIMP+ and CIMP- hCRC cell lines

To identify whether *n*-3 PUFA sensitivity was altered, EPA IC₅₀ concentrations of cells pre-treated for 24 hours with epigenetic drugs were compared to the EPA IC₅₀ concentration of cells that were not pre-treated.

4.3.7.1. Observing the effect of Temozolomide pre-treatment on sensitivity to EPA in CIMP- cell lines

Four CIMP- cell lines were exposed to methylating agent; Temozolomide, to see if this would increase cell sensitivity to EPA. Concentrations of TMZ, ranging from 5 µM to 90 µM were used to assess the impact of TMZ exposure on hCRC cell responses to EPA.

EPA IC₅₀ was compared between non-TMZ treated and TMZ-pre-treated cells [Table 4.7, Figure 4.17]. Treating SW620 cells with 5 µM TMZ caused a decrease in IC₅₀, from 141.00 ± 1.08 µM to 34.61 ± 1.15 µM, significantly different change ($p = 0.004$). However, the difference in EPA IC₅₀ between non-treated and 10 µM TMZ treated SW620 cells was not found to be statistically significantly different ($p = 0.52$). LS174T cells had an EPA IC₅₀ of 259.92 ± 1.04 µM and following treatment with 5 µM TMZ, an increased EPA IC₅₀ value of 365.09 ± 1.17 µM was obtained, a statistically significant increase ($p = 0.018$).

Table 4.7. Sensitivity of CIMP- cell lines to EPA following pre-treatment with TMZ

Cell Line	No Pre-treatment		TMZ Pre-treatment			T-test
	EPA IC ₅₀ (µM)	<i>n</i>	Concentration	EPA IC ₅₀ (µM)	<i>n</i>	<i>P</i> value
SW620	141.00 ± 1.08	5	5 µM	34.61 ± 1.15	3	0.004
			10 µM	125.52 ± 1.26	2	0.52
LS174T	259.92 ± 1.04	4	5 µM	365.09 ± 1.17	3	0.018
			90 µM	191.22	1	-
LoVo	111.78 ± 1.11	3	5 µM	110.04 ± 1.14	2	0.95
			90 µM	117.49	1	-
TC71	135.21 ± 1.04	5	5 µM	157.40 ± 1.12	3	0.15
			50 µM	172.90	1	-
			90 µM	233.00	1	-

IC₅₀ concentration (µM) expressed as mean ± SEM for *n* independent replicates. Comparison of EPA IC₅₀ values obtained in absence and presence of TMZ determined by t-test. For $n = 1$ data, no stats could be run (-) and more replicates were not undertaken as the initial experiment did not indicate increased sensitivity following TMZ exposure.

Two cell lines, LoVo and TC71, were not found to have EPA IC₅₀ values that did not differ between no pre-treatment and 5 µM TMZ pre-treated cells. The results indicate that TMZ activity is cell line specific. I next tested the effect of treating innately EPA-sensitive

CIMP+ cells with demethylating agents to investigate whether a decrease in sensitivity was obtained.

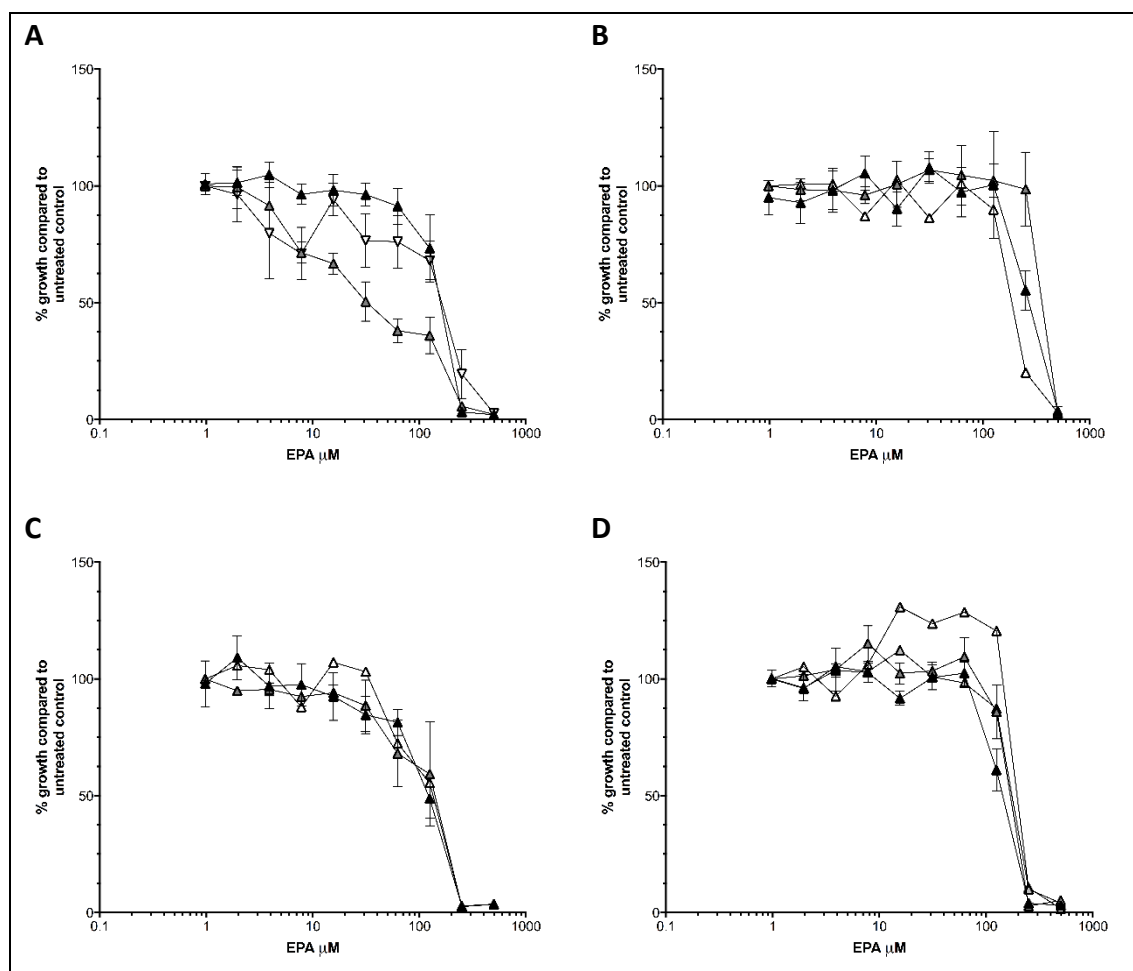


Figure 4.17 EPA concentration response curves in hCRC cell lines pre-treated with varied concentrations of TMZ

EPA concentration response curves obtained in CIMP- cell lines; SW620 (A), LS174T (B), LoVo (C) and TC71 (D). EPA concentration responses carrier control treated cells (▲) and cells pre-treated with 5μM TMZ (▲), 10 μM TMZ (▼) 50μM TMZ (△) and 90μM TMZ (△) were tested. Cell viability was measured by MTT assay. Data expressed as mean of 1 or 2 independent replicates, or +/- SEM of 3 independent replicates.

4.3.7.2. Observing the effect of 5-AZA and DAC pre-treatment on sensitivity to EPA in hCRC cell lines

5-AZA concentrations of 0.25 μM and 0.5 μM were used as these concentrations were well below the DTP reported IC₅₀ for HCT116 cells and there was good HCA-7 cell viability at these concentrations [Figure 4.16 A]. EPA IC₅₀ was found to be greater in cells pre-treated with 0.25 μM 5-AZA [Table 4.8]. The same relationship was observed when 1 μM and 2 μM DAC were the pre-treatment concentration, with EPA IC₅₀ for hCRC cells treated with 1 μM DAC being 299.41 ± 1.20 μM (HCT116) and 310.21 ± 1.19 μM (HCA-7) compared to 297.51 ± 1.19 μM (HCT116) and 244.75 ± 1.12 μM (HCA-7) when

2 μM DAC was used. EPA IC_{50} values of demethylating agent pre-treated cells were compared to those obtained in the absence of demethylating agent [Figure 4.18]. The biggest statistically significant difference in EPA IC_{50} was observed in cells pre-treated with 1 μM DAC, therefore this is the concentration that was used for further experiments.

Pre-treatment of CIMP+ hCRC cells with 1 μM DAC [Figure 4.18] resulted in EPA IC_{50} fold increases of 1.66 ± 0.33 (HCA-7), 2.12 ± 0.27 (HRT18) and 2.47 ± 0.66 (HCT116). DAC exposure resulted in significantly increased EPA IC_{50} values in CIMP+ cell lines [Table 4.8].

DAC exposure did not affect CIMP- hCRC cell line responses to EPA [Table 4.8, Figure 4.18], with LS174T cells treated with DAC obtaining an EPA IC_{50} of $221.72 \pm 1.17 \mu\text{M}$ compared with an EPA IC_{50} of $208.71 \pm 1.29 \mu\text{M}$ measured without DAC pre-treatment. Similarly, TC71 cells pre-treated had an EPA IC_{50} of $128.68 \pm 1.26 \mu\text{M}$ and $106.55 \pm 1.18 \mu\text{M}$ without DAC pre-treatment. These were not found to be significantly different. DAC exposure did not affect cell line sensitivity to DHA, regardless of CIMP status [Table 4.8. Appendix A4.4].

Table 4.8. Sensitivity of hCRC cell lines to EPA and DHA in presence and absence of 5-AZA and DAC

Cell Line	Pre-treatment		EPA			DHA		
	Drug	Concentration (μM)	IC ₅₀ (μM)	<i>n</i>	<i>p</i> -value	IC ₅₀ (μM)	<i>n</i>	<i>p</i> -value
HCT116	-	0	121.02 \pm 1.05	5		44.67 \pm 1.08	3	
	5-AZA	0.25	151.52 \pm 1.15	3	0.40			
	5-AZA	0.50	120.42 \pm 1.12	2	0.99			
	DAC	1.00	299.41 \pm 1.20	4	0.0012	27.83 \pm 1.09	3	0.11
	DAC	2.00	297.51 \pm 1.19	2	0.043			
HCA-7	-	0	186.42 \pm 1.07	4				
	5-AZA	0.25	295.29 \pm 1.91	2	0.10			
	5-AZA	0.50	187.74 \pm 1.10	3	0.43			
	DAC	1.00	310.21 \pm 1.19	3	0.02			
	DAC	2.00	244.75 \pm 1.12	2	0.10			
HRT18	-	0	116.73 \pm 1.11	3		32.92 \pm 1.05	3	
	DAC	1.00	247.02 \pm 1.09	3	0.0039	34.12 \pm 1.07	3	0.32
LS174T	-	0	208.71 \pm 1.17	3		95.46 \pm 1.13	3	
	DAC	1.00	221.72 \pm 1.29	3	0.68	121.29 \pm 1.01	3	0.28
TC71	-	0	128.68 \pm 1.26	3		56.71 \pm 1.06	3	
	DAC	1.00	106.55 \pm 1.18	3	0.90	59.12 \pm 1.07	3	0.69

Each IC₅₀ concentration (μM) is expressed as the mean \pm SEM for *n* independent replicates. Comparison of median IC₅₀ values obtained in cells that were treated with *n*-3 PUFA in absence and presence of pre-treatment was determined by t-test.

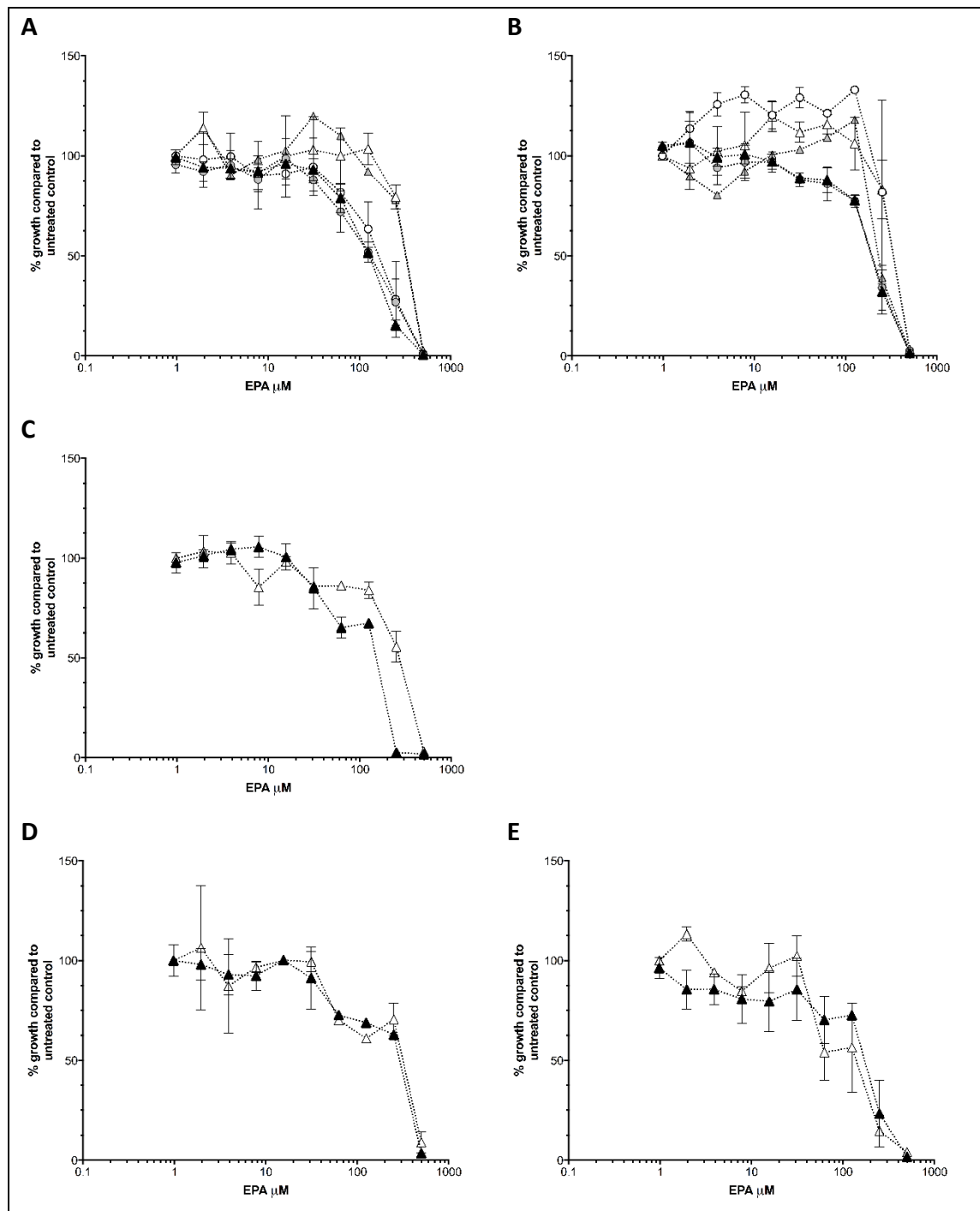


Figure 4.18 EPA concentration response curves in hCRC cell lines pre-treated with varied concentrations of demethylating drugs, 5-AZA and DAC

EPA concentration response curves obtained in CIMP+ cell lines; HCT116 (A), HCA-7 (B), HRT18 (C) and CIMP- cell lines; LS174T (D) and TC71 (E). EPA concentration response curves for cells that were pre-treated with control carrier (▲), 0.25 μM 5-AZA (○), 0.5 μM 5-AZA (●), 1 μM DAC (△) or 2 μM DAC (▲) are shown. Data are expressed as the mean of 2 independent replicates or mean \pm SEM of 3-5 independent replicates.

4.4. Discussion

This chapter focused on determining whether key CRC molecular characteristics were associated with hCRC cell line inherent sensitivity to *n*-3 PUFAs; EPA and DHA. Cell lines were selected to be representative of the diversity of CRC tumour types found in cancer patients, encompassing CIN status, microsatellite instability status, CIMP status, and cyclooxygenase gene expression. hCRC cell lines differential sensitivity to *n*-3 PUFAs has been shown in previous studies (131, 137, 179, 207, 208). This work aimed to compare EPA and DHA cell sensitivity, and identify molecular phenotypes of hCRC cell lines, that were predictive biomarkers of response *n*-3 PUFAs.

4.4.1. Key Findings

hCRC cell lines displayed a wide range of sensitivities to EPA. All cell lines, without exception, were more sensitive to DHA than EPA. This has been shown previously in a study comparing EPA and DHA cellular responses in HT29 and LS174T cells (179). Reduced cell viability following DHA treatment compared to EPA treatment has also been observed in breast cancer cell lines, MCF-7 and MDA-MB-231 (250). A potential explanation as to why cell lines were more sensitive to DHA, could be that the longer carbon chain and higher number of unsaturated bonds, cause greater disruption to the cell membrane. EPA and DHA have different effects in membrane models of atherosclerosis, with EPA associated with improved membrane stability and DHA responsible for increased membrane fluidity (251). DHA disruption of membrane integrity, can induce formation of pores via lysosomal damage or production of reactive oxygen species (ROS), causing oxidative stress that activates apoptotic pathways (252). Other studies have shown that DHA is more likely to incorporate into lipid rafts (153) and consequential altered cell signalling could induce cell death processes, which has been observed in breast cancer cells treated with DHA (252). The differential ability of EPA and DHA to incorporate into the cell membranes, and implications of this in relation to *n*-3 PUFA sensitivity, is examined in **Chapter 5**.

Although other studies have shown differential sensitivities of cell lines to EPA and / or DHA, comparison of sensitivity data obtained in this panel and in published data is challenging due to differences in experimental design, concentrations and type of *n*-3 PUFAs utilised (with studies using EE, FFA, TG and MAG formulations). The metabolic profiles are specific to the formulation used, with bioactivity reported to be greatest for FFA formulations and lowest for EE formulations (FFA > TG > EE) (253). Evidence suggests that mechanisms through which EPA and DHA exert their anti-cancer effects

differ (137, 179, 207, 209). As EPA does not disrupt the plasma membrane and lipid rafts as DHA does (153), it may be that EPA-supplementation relies on metabolism, and generation of metabolic products, to induce anti-proliferative effects. The data supports a case for trialling pure DHA supplementation, due to the greater CRC cell growth inhibitory effects.

After characterising hCRC cell line sensitivity to individual *n*-3 PUFAs, I next assessed the growth inhibition properties of an EPA:DHA combination, as *n*-3 PUFA-rich food sources, over-the-counter supplements and frequently formulations of *n*-3 PUFAs used in clinical studies, contain mixtures of *n*-3 PUFAs. Distinguishing whether purified single *n*-3 PUFA, or a combination mixture of *n*-3 PUFAs, induces greater anti-cancer effects will provide evidence to optimise *n*-3 PUFA formulations used in the clinic. Potentially antagonistic, additive, and synergistic effects of individual *n*-3 PUFAS were demonstrated when assessing combined treatment hCRC cell line responses to combined EPA:DHA. One study investigated a 1:1 combination mixture of EPA and DHA in LS174T cells, and reported growth inhibition compared to untreated cells of 80.3 ± 5.5 % (150 μ M DHA), 79.3 ± 5.0 % (150 μ M EPA) and 71.1 ± 1.0 % (75 μ M DHA and 75 μ M EPA) (141). The degree of growth inhibition was correlated with measured increases in caspase-3 activation and decreases in survivin mRNA expression (141). No other *in vitro* studies have investigated synergistic, additive, or antagonistic relationships between EPA and DHA.

The combination treatment data indicates that pure *n*-3 PUFA formulations will have the best growth inhibitory effects in some cases, and an *n*-3 PUFA mixture has greater growth inhibitory effects for others. Data did not indicate molecular properties associated with response to combined treatment. Analysis of epidemiological and clinical data in which combinations of EPA and DHA are used, could uncover biomarkers of response or resistance to combination treatments. Future studies using cell lines in which antagonistic effects were shown following combination treatment, could enable identification of biomarkers that could indicate that best treatment with an individual *n*-3 PUFA. Mechanisms through which EPA act to reduce toxicity of DHA need elucidating.

A negative correlation was identified between growth rate and EPA sensitivity. Whilst statistically this was a significant association, it should be stressed that this result utilised a surrogate measure of growth rate. One study has investigated the anti-proliferative effects of EPA in human melanoma cell lines that differ by doubling time (254). Doubling time for G361 cells ranged from 6 – 12 hours (255), A357 cells; 12 – 31 hours (255), A2058 cells; 27 hours (256) and C32 cells; 53 hours (256). Following 24 hours of culture

in media supplemented with 50 μ M EPA, cell viability compared to control cells ranged from 27.81 ± 4.09 % (G631) to 107.71 ± 2.86 % (C32) (254). This indicated that cell lines with slower doubling times were less sensitive to EPA, in agreement with my findings. A potential explanation for increased EPA sensitivity of rapidly dividing cells, may be an ability to incorporate or use EPA more efficiently. Cells with low doubling times may be more susceptible to EPA as the metabolic energy required for cell proliferation are met by other lipids. Conversely, cell lines with long doubling times may utilise exogenous EPA to proliferate (which could account for the increased cell viability following 50 μ M EPA treatment in C32 cells mentioned above) (254). An accumulation of EPA in sensitive cells would increase production of downstream metabolites that cause increased cellular toxicity.

When the relationships between cyclooxygenase expression and sensitivity to *n*-3 PUFAs were investigated, no associations were found. This suggests that EPA and DHA are exerting their effects through *PTGS*-independent mechanisms. The *in vitro* data presented here does not support our findings that COX-2 mediates resistance to EPA in mouse CRC cell lines and an *in vivo* model of CRC (178). EPA-resistant MC38r cells were found to have elevated COX-1 and COX-2 expression (quantified by Western blot) in comparison to EPA-sensitive MC38 cells (178). In an established syngeneic BALB/c-CT26 model of CRCLM, EPA diet was attributed to a significant 30 % reduction in COX^{low}-CT26 cell tumours compared to CT26 cell tumours (178). Differences may be dependent upon the fact that I measured mRNA expression compared to the study measuring protein COX-2 levels, differences between human and mouse derived cell lines or the difference between *in vitro* and *in vivo* context of the experiment.

There were varying levels of *PTGS2* gene expression in the panel of CRC cell lines, with 6 cell lines of the panel having no *PTGS2* expression. Studies have reported increased total cyclooxygenase activity in normal appearing mucosa in patients with colonic neoplasia and CRC (187, 257). Previous studies that investigated expression of *PTGS2*/COX-2 by RT-PCR and Western blot respectively in human CRC cells had found that, at mRNA and protein levels, there was no expression in poorly differentiated cell lines (including; HCT116, SW480, SW620, DLD-1, SW1116 and SW48) (258). Expression of *PTGS2*/COX-2 was found in well differentiated cell lines (HCA-7, LS174T, HT29, CaCo-2 and LoVo) (158, 163, 258, 259). However, my data contradicted the reports of no expression in HCT116, SW480, DLD-1 and SW1116 cell lines, perhaps attributed to a difference in primer targets or, as these studies were conducted between 1996 and 2000, cell lines may not have been confirmed by STR authentication. For all the cell lines which were previously reported to express *PTGS2*, my data corroborated

these findings and showed that the highest expression found in HCA-7 cells. COX-2 expression has reported in 90 % of colon tumours and premalignant colonic adenomas (260). In a study that analysed COX-2 expression in 1026 CRC surgical samples, 78.0 % scored positive, and an association between increased expression in highly invasive and metastatic cancers was shown (159). A higher percentage of cell lines were *PTGS2* negative compared to clinical settings, with 35 % cell lines being *PTGS2* negative. As there is a difference between *PTGS2* / COX-2 expression between *in vitro* and clinical samples, combined with the fact that our groups published *in vivo* data differs from the *in vitro* data (178), it indicates that using *in vitro* models may not be best suited for testing hypotheses related to *PTGS2* / COX-2 expression and *n*-3 PUFA sensitivity.

The association between molecular phenotypes of CRC cell lines and sensitivity to EPA and DHA was tested. CIMP+ cell lines were more sensitive to EPA than CIMP- cell lines, with cells assigned to the CIN-, MSI, CIMP+ subgroup displaying the greatest sensitivity. No other reports link sensitivity of a cell line to EPA with CIMP status directly in *in vitro*, *in vivo*, or clinical studies. EPA and DHA have been described as demethylating agents themselves, with increased expression of genes controlling cell cycle progression following treatment with EPA / DHA reported (236, 261). In human leukaemia cells, U937, EPA and DHA caused demethylation and subsequent increased expression of tumour suppressor gene, CCAAT-enhancer-binding proteins (C/EBP δ)(262). A study by Ceccarelli *et al*, found that 100 μ M EPA induced DNA demethylation in rat hepatoma cells (McRH-7777 / CRL-1601). Demethylation, facilitated by Ten-eleven translocation methylcytosine dioxygenase 1 (TET1) enzyme activity which converts 5-methylcytosine to 5-hydroxymethylcytosine (236, 261), induced expression of the gene p21^{Waf1/Cip1} which slows cell cycle progression (236). It is proposed that EPA could affect epigenetic gene regulation in hCRC cells, inducing expression of gene able to promote cell death or stop cell cycle progression and proliferation.

Epigenetic drugs were utilised to 'reverse' CIMP+ and CIMP- cell line properties. No previous studies have tested effects of the methylating agent, TMZ, in combination with EPA, and no clear effect was observed in this study. No studies report effects of combined EPA and DAC treatment in any pre-clinical or clinical context. I report that treatment of CIMP+ cells with 1 μ M DAC, prior to measuring an EPA concentration response, resulted in the biggest shift in EPA IC₅₀ compared to 5-AZA or a higher concentration of DAC. In a study that used genome scale Infinium analysis to characterise demethylation responses following treatment of HCT116 and the human leukaemia cell line HL60 with 5-AZA and DAC, non-random and reproducible patterns of DNA demethylation were observed (242). DAC and 5-AZA differ in their ability to

demethylate DNA. The study found that maximum levels of demethylation were achieved following treatment with 1 μ M DAC for between 24 and 36 hours, whereby a 60 % reduction of global DNA methylation was observed. The reduction in global DNA methylation was greater following DAC treatment than 5-AZA, which could facilitate a 50 % reduction (242). These data indicate that the altered EPA sensitivity following 1 μ M DAC exposure may be due to a better demethylating efficiency of DAC compared to 5-AZA, or as the demethylation patterns are specific, could be gene specific. In this case, comparing gene expression profiles following DAC and 5-AZA exposure, in presence and absence of EPA, would uncover target genes with a role in EPA-sensitivity.

DAC exposure caused altered EPA sensitivity of CIMP+ cell lines, but no change was observed in CIMP- cell lines. This could be indicative that there are genes with down-regulated expression in CIMP+ cell lines, that drive resistance to EPA, are pro-apoptotic or control cell cycle progression. Loss of CIMP+ cell EPA sensitivity after DAC exposure may indicate that global demethylation causes expression of genes that repress expression or inhibit activity of the gene targets activated by EPA-only exposure. Alternatively, as EPA is potentially a demethylating agent itself (236, 261, 262) the non-toxic concentration of DAC may compete with EPA and demethylate the same gene target more efficiently and thus render EPA demethylation activity ineffective. Whilst no studies have utilised DAC and EPA combination previously, one study found that reduced pro-apoptotic gene promoter methylation was associated with increased HCT116 cell apoptosis in a study that combined DHA treatment with butyrate, a short-chain FA with histone deacetylase inhibitory properties (263).

4.4.2. Strengths and Limitations

A major strength of this work was the number of hCRC cell lines used in the panel, which was larger than any other study characterising cellular responses to EPA and/or DHA. Although CRC cell lines have been characterised by consensus molecular subtype (CMS) (35, 41, 50), an important classification utilised in the study of resistance to chemotherapeutic drugs which enabled identification of subgroups that were predictive biomarkers of response (50), a lack of tumour stroma and microenvironment produces a major challenge for translation of CMS classifications in pre-clinical models to accurate modelling of clinical disease. Tumour stroma and microenvironment directly influence gene expression in bulk tumour tissue. *In vivo* studies will be necessary to further establish whether CMS classification can help stratify patients to EPA- (or DHA-) based therapies.

A limitation of determining IC₅₀ concentrations of both *n*-3 PUFAs and epigenetic drugs by MTT assay using 96-well plates was the limited space on the plate. The concentration range tested for EPA, DHA and DAC were 1 µM to 500 µM, for 5-AZA it was 0.02 µM to 8 µM and for TMZ it was 1.25 µM to 640 µM. In all cases due to experimental design and plate set up, 10 concentrations within the range could be tested. Therefore, when a greater range existed, fewer concentrations in the middle range were used, which resulted in less accurate IC₅₀ determination.

Combining the cell panel molecular data with sensitivity data was possible, and enabled identification of associations with sensitivity or resistance, although limitations when considering the small number of cell lines for specific subgroups impacted the strength of statistical analyses. Still, the data was still able to give indications of associations that warranted further study and investigation.

Analysis of the interaction between EPA and DHA in the combination mixture was limited by the number of concentrations utilised. To complete a full analysis of interactions between EPA and DHA in a combination mixture, specifically designed assays would be required. These would test a greater number of individual *n*-3 PUFAs concentrations and would ensure enough data to utilise software analysis programs. To determine the optimal combination mixture, varying the ratios within the combination and studying the interactions within such ratios would be necessary.

As previously mentioned, a surrogate marker for growth rate was used, and specific growth curve experiments to establish growth rates would be required to confirm the relationship between EPA sensitivity and growth rate. There was not time to utilise alternative techniques for slowing cell growth rates, which would rely on mutagenesis and therefore not target solely growth-related properties, a fact that would need careful consideration during data analysis.

A strength of the study was the use of 2 demethylating pre-treatments to establish an optimal treatment, as the difference between DAC and 5-AZA effects on EPA sensitivity indicates gene specificity. Use of TMZ needed further optimisation, as O⁶-methylguanine-DNA methyltransferase (MGMT) expression in cell lines may confound TMZ treatment effects. MGMT repairs the cytotoxic lesion induced by TMZ, and therefore resistance to TMZ occurs in the presence MGMT (240, 241). Expression of MGMT in hCRC cell lines is confirmed for DLD1, HCT116, HT29 cells (264, 265) and no MGMT expression was found SW620, SW48 (264) and SW480 cells (265). Lack of MGMT expression in SW620 may be linked with the noted effect of TMZ on EPA response

observed. In a study that included a panel of 32 CRC cell lines including LS174T, SW1116, SW480, DLD-1, HT29, SW620, SW48 and LoVo cells (265), MGMT protein was detected in 16 of the cell lines although full details aren't included in the paper, and no association was found between MGMT expression and microsatellite status (265). As there is an overlap between microsatellite status and CIMP status, it would suggest that no difference in MGMT expression between cells differing by CIMP subtype would be expected, although this has not been directly tested in published works. Without knowing MGMT status of the cell lines tested, no definitive conclusions about the ability of TMZ methylation of CIMP- restoring EPA sensitivity in CIMP- cells could be made.

Another limitation of this study was limited time in which to further investigate the effects of using global hypermethylating and hypomethylating drugs. Budget and time restrictions limited the confirmation of successful demethylation or methylation following DAC or TMZ treatment, which could have been achieved by various techniques such as Illumina's Infinium Human Methylation 450 BeadChip (HM450K) methylation array or whole genome bisulphite sequence (266). Alternatively, methylation specific-PCR or pyrosequencing could have been used to confirm DAC activity by showing reduced methylation in commonly hypermethylated genes in CRC cell lines. Studies that have used genes as markers of successful demethylation have used; *HIC1* (267), *Tnc* (268), *SFRP1* (269) and *UCHL1* (270).

4.4.3. Future directions

There are multiple aspects of this work that could be investigated in the future. Firstly, to strengthen cell line data, I would expand the number of CRC cell lines used to increase the number of cell lines present in each molecular subgroup. This would strengthen comparative statistical analyses performed in relation to *n*-3 PUFA sensitivity. Not only would I focus on expanding the number of CRC cell lines used, I would include primary cells from patients and would utilise 3D cell models incorporating stroma.

Deeper analysis into the combination treatments is another area which warrants further investigation. Assessing combination treatments in cell lines is challenging due to varied responses to, and multiple mechanisms of action utilised by, *n*-3 PUFAs. Identifying cell line properties associated with synergistic interactions between EPA and DHA, causing greater cancer cell growth inhibition, would facilitate downstream studies in patient-derived cell lines. This work could strengthen the rationale for patient stratified *n*-3 PUFA supplementation or using individual or combination treatments for optimal outcome.

Measuring *PTGS1* and *PTGS2* at an mRNA transcript level does not confirm the protein level expression and therefore I would confirm this to strengthen the data set and confirm that no associations between sensitivity and expression. To corroborate cell line findings, it would be beneficial to exploit clinical samples from *n*-3 PUFA supplementation trials. These would be characterised by COX-1 and COX-2 expression, which would confirm clinical translation of cell line data and identify potential relationships between COX-expression and response to EPA.

DAC demethylation would need to be confirmed by whole genome bisulphite sequencing. It would be beneficial to expand the number of cell lines in which combination DAC / EPA treatments were tested to increased statistical power. Utilising other agents to alter gene expression may further elucidate the relationship between methylation and EPA sensitivity, for example using combinations with butyrate or other histone deacetylation inhibitors.

Whole genome methylation and RNA sequencing following treatment of cells with epigenetic drugs could identify candidate genes associated with sensitivity to EPA. Interrogation of the expression patterns of *PTGS2*, *LOX-5* and *CRB1* in epigenetic drug treated and untreated cells, would be of interest as their roles in *n*-3 PUFA metabolism may have implications on EPA sensitivity. In addition, genes which are potentially mediating cell response to EPA could be investigated by comparing gene expression profiles of a panel including multiple inherently sensitive and resistant cell lines grown; in standard conditions, in EPA-supplemented media, in presence of DAC and in combined DAC and EPA supplemented media.

Once target EPA-sensitivity mediating genes are identified, further studies to establish the relationship between CIMP status and expression of identified genes would be undertaken. Targeted techniques to delete the gene (CRISPR-Cas9) or overexpression techniques (transfection) and subsequent EPA sensitivity tests would confirm the extent the target genes were involved in facilitating cellular response. Association between target genes, and their association to tumour response to EPA treatment and CIMP status, could also be investigated *in vivo* and in clinical samples.

In summary, this chapter has highlighted differences in cellular responses to EPA and DHA, with greater sensitivity to DHA. It demonstrated that cell line responses were cell-line specific. The data indicate multiple mechanisms of activity, with response to one *n*-3 PUFA not indicative of response to the other, or combination mixture. This chapter has

identified a relationship between CIMP+ status and EPA sensitivity, and examined the effect of combining demethylating agent and *n*-3 PUFA treatment on cell sensitivity.

The following results chapters endeavour to investigate potential reasons for differential sensitivity of EPA and DHA. Chapter 5 compares cell FA profiles following exposure to the *n*-3 PUFAs to provide insight into the role of FA storage on sensitivity. Chapter 6 focused on generating sensitive and resistant models to further examine cell response to *n*-3 PUFAs.

Chapter 5: Investigating the relationship between human CRC cell line sensitivity to *n*-3 PUFAs and cellular FA content

5.1. Using LC-ESI-MS/MS to measure fatty acid content in colorectal cancer cell lines

5.1.1. Presence of FAs in cells

Lipophilic fatty acids (FAs) are accessible for quantification and, following supplementation, localise to the cellular plasma membrane (192). Studies of the FA content in biological systems have revealed that the ratio of *n*-3 and *n*-6 PUFAs has direct implications on health, including through modification of mechanisms including inflammation, angiogenesis and lipid homeostasis (194). It is difficult to quote the expected baseline 'normal' range of EPA and DHA in adults as this has not been established, however reports have quoted a combined EPA and DHA content ranging from 3 – 4 % of total FAs in serum or plasma phospholipid (271, 272).

5.1.2. How FAs are measured in biological systems

Gas chromatography/mass spectrometry (GC/MS) is frequently used to analyse FAs and it has been shown that liquid chromatography (LC) in combination with electrospray ionisation triple quadrupole tandem mass spectrometry (ESI-MS/MS) can be used as an alternative to GC/MS (192). LC-ESI-MS/MS combines the separation of sample components by liquid chromatography and detection of charged ions by mass spectrometry (273) which can be converted to molecular weight, identify structural features and thus allows for determination of the analyte. LC-ESI MS/MS bypasses the heating required during sample preparation for GC-MS which can render a majority of organic compounds impossible to analyse (192, 273), and therefore can limit thermal degradation of PUFAs (192). FA measurements can allow for the potential of their use as a disease risk biomarker in observational studies or a predictive biomarker in intervention studies (192).

FAs can be measured in many sample types, not limited to; tumour or healthy tissue samples (147, 192, 274), red blood cells (274), cultured cells (192, 275), plasma, and culture medium (122). The most frequently used way of reporting FA data is % FA, whereby a FA is presented as the relative content proportional to all FAs measured. Another popular reporting style is use of the AA / EPA ratio. In a study by Tutino *et al*, 2019 in which they reported an increased AA / EPA ratio in 33 patients with metastatic CRC compared to the ratio measured in 35 patients with localised CRC (276). They

justified the analysis on the basis that AA / EPA ratio is an index to evaluate inflammation and nutritional status of cell membrane and has been used in multiple other sources as a biomarker for inflammation (277, 278). Less frequently, FA content is presented as an absolute amount. This is of interest as it allows a specific FA to be considered independently of other measured FAs in a dataset.

5.1.3. FA content measured in CRC cell lines

An *in vitro* study found a decrease in measured levels of PUFAs in culture medium of CRC cells (HT-29 and WiDr) compared to cell-free culture media, and no change in PUFA content in culture media in which normal colon cells (CCD 841 CoN) were incubated (122). This was particularly notable in the case of DHA. DHA content of control media measured 1.33 ± 0.23 % and was 1.40 ± 0.05 % in CCD 841 CoN culture media. DHA content of CRC cell culture media was 0.62 ± 0.07 % and 0.83 ± 0.09 %. The study measured a panel of 12 FAs including: *n*-6: 16:2, LA, 20:2, AA, dihomogamma-linolenic acid, *n*-6 DPA, adrenic acid; *n*-3: LNA, EPA, DPA, DHA and eicosatetraenoic acid and FA levels were presented as a percentage of the total FAs measured. Mika *et al* proposed that reduced PUFA content in culture media inoculated with CRC cell lines was due to an increased incorporation of *n*-3 PUFAs by CRC cell lines compared to normal colonic cells (122). The preferential *n*-3 PUFA uptake when CRC cells were compared to normal colon cells may be explained by the fact that *n*-3 PUFAs are required by rapidly proliferating cells, as they are a key component of the phospholipid cellular membranes (122). However, the study did not examine the FA content of the cells and thus failed to rule out alternative explanations as to the measured decrease in *n*-3 PUFA content of culture medium, such as β -oxidation.

In-house data, measuring the same FA panel used in this PhD work, have shown that when colorectal cancer cells were treated with 10 μ M EPA for 24 hours, the EPA content measured by LC-ESI-MS/MS and expressed as a percentage of the total FAs measured, ranged from 2.6 ± 1.0 % (MC38), 1.6 % (MC38r) to 0.3 ± 0.1 % HCA7 (275).

5.1.4. FA content measured in human CRC tissues

FA content differences between cancer tissues and normal tissues (44 CRC patients, 38 healthy controls) which had not been treated with *n*-3 PUFA supplementation, were measured by Mika *et al*, using the 12 FAs panel described above (122). The profiles measured by GC-MS show lower AA levels in healthy patients (6.4 ± 2.9 % CRC, $3.2 \pm$

1.9 % healthy), but significantly higher levels of EPA (0.4 ± 0.2 % CRC, 0.2 ± 0.1 % healthy) and DHA (1.0 ± 0.4 % CRC, 0.5 ± 0.2 % healthy) in CRC patients (122).

Another study measured FA content following *n*-3 PUFA supplementation. Tumour tissue from 37 patients with CRCLM, who had taken 2 g EPA-FFA daily for approximately 30 days prior to resection surgery as part of the EMT trial, was shown to have an EPA content of 1.8 ± 0.1 % (131). This was found to increase by 40 % following ingestion of daily EPA (131). EPA content of red blood cells for patients treated in the same trial was reported as; 2.7 ± 0.2 % and 2.1 ± 0.0 % for female and male participants respectively, which was a significant increase from baseline (274). These results are reported as a percentage of the same panel of FAs [Table 3.7, Chapter 3.10] used and reported in this chapter.

5.2. Chapter objectives

This chapter focuses on measurement of FA content in hCRC cells using a previously established liquid chromatography-tandem mass spectrometry (LC-ESI-MS/MS) technique (192). I hypothesised that FA content of cell lines, treated with *n*-3 PUFAs, would be associated with inherent cell line sensitivity to EPA or DHA and EPA sensitivity would correlate with ability of the cells to convert EPA to DHA. I also hypothesised that FA measurements would be altered following epigenetic drug treatment (DAC) in relation to the altered cell sensitivity. To address this, the following objectives were set:

- Analyse FA profiles of CRC cells treated with 5 μ M *n*-3 PUFA and a concentration capable of inducing a 50 % growth inhibition [Table 4.3, Chapter 4.3.4] to determine whether there are differences in how the cell lines' store EPA / DHA.
- Compare traditional reporting of percentage FA content data with FA amount quantified as amount per million cells.
- Identify associations between previously defined cell characteristics described in Chapter 4 and FA content measured following *n*-3 PUFA supplementation
- Compare FA profiles of non-treated cells with epigenetic drug treated cells

5.3. Results

5.3.1. Inter-assay variability

First the robustness of the method was verified by analysing data from replicate samples to determine the degree of inter-assay variability. To allow for FA quantification, standard curves were established. **Figure 5.1** shows the standard curves obtained for EPA and DHA, which both have R^2 values of 0.97. The standard curves for the remaining FAs (PA, SA, OA, LA, AA, LNA, EPA, DPA and DHA) are shown in **Appendix A5.1** and example chromatograms for standards and treated samples are shown in **Appendix A5.2**. It should be noted that the measured concentrations of FAs present, in many cases, exceeds the range measured for the standard curve. Due to the COVID-19 pandemic, further experimental work to confirm standard curve linearity was halted. Therefore, FA concentrations were determined on the basis of assumed linearity. Work is now ongoing.

Data obtained from independent replicate standard curves were used to assess inter-assay variability. Good inter-assay variability was shown by coefficients of variation below 30 %. Concentrations of FA measured were close to the concentration expected, indicative of good accuracy [**Table 5.1**]. FA concentrations measured across 5 preparations of FA standards were compared, replicate measurements of maximal concentration were comparable demonstrated by good coefficient of variations [**Table 5.1**].

Four FCS samples (two sets of technical duplicates) were analysed as an additional measure to assess inter-assay variability [**Table 5.2**]. I obtained coefficient of variation values ranging from 18.3 % to 37.9 %. Median concentrations for EPA and DHA measured were 7.1 $\mu\text{g/ml}$ (range 3.6 – 10 $\mu\text{g/ml}$) and 24.3 $\mu\text{g/ml}$ (range 12.0 – 28.8 $\mu\text{g/ml}$), respectively. The heat-inactivated FCS samples were collected from different production lot numbers of FCS hence some degree of variation would be expected.

All CRC cell lines were treated with EPA or DHA supplemented media for 24 hours. Different cell lines were grown in 3 different types of culture media and it was unknown as to whether the FA content of each was comparable. To ascertain the amount of FA introduced by each culture media type, FA content of FCS supplemented culture media was measured. The potential influence of differing media on FA profile of treated cells is shown in **Table 5.3**. In FCS supplemented media, the percentage of EPA, DPA and DHA in DMEM was greater than in RPMI and F-12 media.

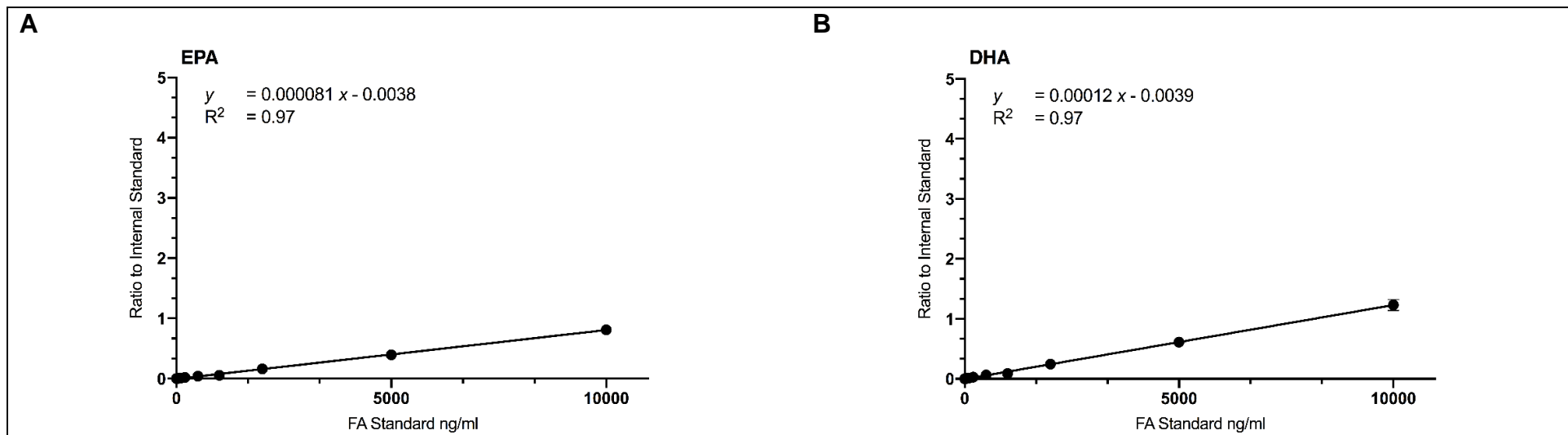


Figure 5.1. Standard curves for EPA and DHA quantification

Illustrative standard curves obtained by LC-ESI-MS/MS for (a) EPA and (b) DHA are shown, with R^2 values showing goodness of fit displayed on each plot. Ratio of FA peak area to internal standard LNA-d₁₄ peak area were calculated and presented as mean \pm SD for 5 independent biological replicates.

Table 5.1. Standard curve concentration measurements

	PA	SA	OA	LA	AA	LNA	EPA	DPA	DHA
Low concentration standard curve (1 μg/ml)									
Concentration (μg/ml)	0.6 \pm 0.2	1.1 \pm 0.7	0.7 \pm 0.3	0.8 \pm 0.3	0.7 \pm 0.4	0.7 \pm 0.3	0.7 \pm 0.3	0.7 \pm 0.4	0.7 \pm 0.4
Coefficient of Variation (%)	27.5	64.9	47.0	38.6	48.0	46.9	47.8	49.9	49.7
High concentration standard curve (10 μg/ml)									
Concentration (μg/ml)	10.2 \pm 0.2	9.8 \pm 0.7	10.0 \pm 0.3	10.1 \pm 0.2	10.0 \pm 0.2	10.1 \pm 0.2	10.1 \pm 0.2	10.1 \pm 0.2	10.1 \pm 0.2
Coefficient of Variation (%)	2.2	6.9	2.6	2.4	1.8	1.6	1.8	1.9	2.1

Each FA concentration was expressed as the mean \pm SD μ g/ml for 5 independent replicates. Percentage coefficient of variation (%) was calculated from these data.

Table 5.2. Fatty acid profile of fetal calf serum

	PA	SA	OA	LA	AA	LNA	EPA	DPA	DHA
FCS									
Concentration (µg/ml)	152.9 ± 28.0	169.6 ± 65.6	38.2 ± 11.6	5.8 ± 1.7	31.6 ± 9.7	0.5 ± 0.2	7.0 ± 2.7	5.4 ± 2.0	22.4 ± 8.0
Coefficient of Variation (%)	18.3	38.7	30.3	29.1	30.5	28.1	38.6	37.9	35.7
Median (µg/ml)	157.5	153.9	37.1	6.0	34.1	0.6	7.1	5.7	24.3
Range (µg/ml)	114.6 - 182.0	115.2 - 255.4	25.2 - 53.4	3.7 - 7.3	18.8 - 39.6	0.4 - 0.7	3.6 - 10.0	3.0 - 7.3	12.0 - 28.8

FA content FCS samples was measured by LC-ESI-MS/MS and quantified. Data is presented as the mean ± SD for 4 independent replicates. The median concentration and the range of values measured are also presented as the variation was expected between FCS samples prepared and analysed on different dates.

Table 5.3. FA concentration in different media supplemented with 10% FCS

Media	Fatty acid concentration (µg/ml)								
	PA	SA	OA	LA	AA	LNA	EPA	DPA	DHA
DMEM + 10% FCS	101.0 ± 5.0	98.0 ± 8.9	6.5 ± 0.7	1.2 ± 0.3	3.6 ± 1.1	0.0 ± 0.0	5.48 ± 4.3	2.6 ± 2.2	3.6 ± 0.5
RPMI + 10% FCS	132.8 ± 5.9	162.5 ± 20.7	6.7 ± 1.1	1.0 ± 0.1	3.6 ± 0.4	0.0 ± 0.0	0.6 ± 0.1	0.6 ± 0.0	2.3 ± 0.3
F-12 + 10% FCS	113.2 ± 4.7	200.0 ± 22.8	7.4 ± 0.8	1.2 ± 0.1	4.7 ± 0.7	0.1 ± 0.0	0.7 ± 0.1	0.7 ± 0.1	3.0 ± 0.3

FA content was measured by LC-ESI-MS/MS and quantified in samples containing DMEM, RPMI and F-12 media supplemented with 10% FCS. Data is represented as the mean ± SD for 2 technical replicates.

5.3.2. FA profiles of hCRC cell lines treated with EPA or DHA

I investigated whether hCRC cell lines displayed differences in FA content upon short term exposure to EPA or DHA. Short exposure times were used as the association between *n*-3 PUFA content and *n*-3 PUFA sensitivity was being investigated. In the following sections, 'carrier-treated' FA content signifies the FA content measured in the ethanol carrier control sample appropriate for the treatment group (EPA or DHA). The ethanol treatments ranged from 0.02 % v/v to 0.70 % v/v and were proportionate to the IC₅₀ [Appendix A5.3]. I will refer to the IC₅₀-equivalent treated samples as high-concentration *n*-3-treated (treatment concentrations are listed in Appendix A5.3). All cells were treated with 5 µM EPA or DHA. In addition, 'absolute' amount is referring to the quantified content expressed as µg / million cells. Unless otherwise stated, data presented henceforth are expressed as mean ± standard deviation (SD) for multiple independent replicates.

5.3.2.1. Association between concentration of *n*-3 PUFA used to treat cells and the amount of *n*-3 PUFA measured

To establish whether cellular response to exogenous supplementation of *n*-3 PUFA was an increase in the amount of that *n*-3 PUFA, the profiles of ethanol carrier treated, 5 µM *n*-3 PUFA treated and IC₅₀-equivalent treated were obtained by LC-ESI-MS/MS and subsequently compared.

Data were analysed as % FA to compare with published data in the first instance. For each cell line, the profile of FAs in cells treated with carrier controls were compiled, and these are available in the tables included in Appendix A5.4. It was found that the most abundant FAs were OA (40.9 ± 9.9 %), PA (23.1 ± 7.0 %) and SA (16.8 ± 5.8 %), and the least abundant was LNA (0.3 ± 0.2 %). The results showed that the EPA content of cells ranged from 0.9 ± 0.1 % (HCA7) to 2.8 ± 0.3 % (DLD-1) [Figure 5.2 A] and DHA content ranges from 2.6 ± 0.2 % (T84) to 7.9 ± 1.0 % (LoVo) [Figure 5.3 A]. Without exception, when reviewing percentage FA data, all cell lines had a higher DHA content than EPA content at baseline with DHA was found to be increased 1.34-fold to 4.76-fold more than EPA, for TC71 and HCA-7 cells, respectively.

When cells were treated with 5 µM *n*-3 PUFA, there were notable effects on the FA profiles. Full FA profiles are included in Appendix A5.4. Firstly, I confirmed that supplementing media with 5 µM of either EPA or DHA was associated with an increase in the measured content of that specific *n*-3 PUFA in all CRC cell lines tested.

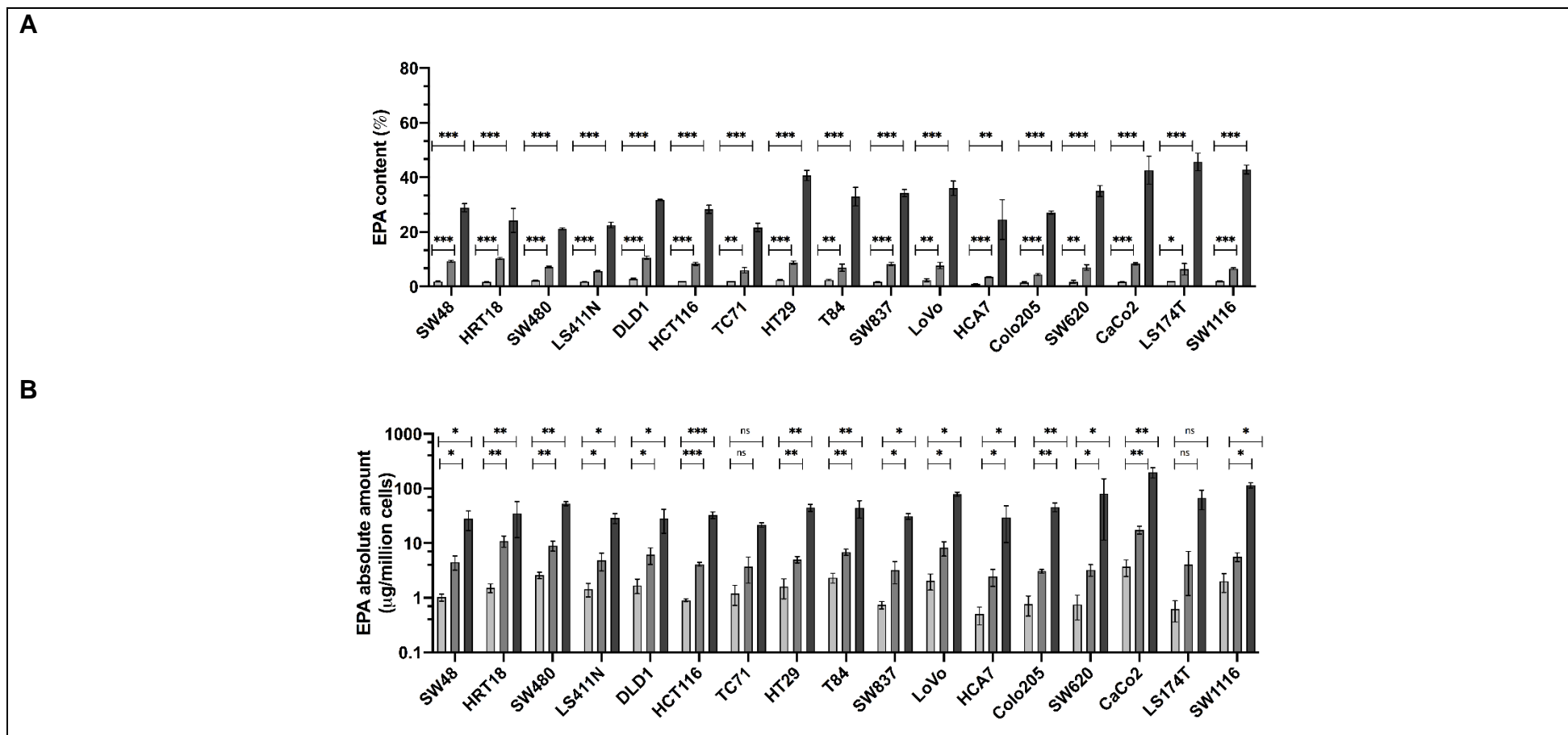


Figure 5.2. The effect of EPA exposure on EPA content of human colorectal cancer cell lines

Cells in culture were incubated for 24 hours in supplemented media containing ethanol carrier (white bar), 5µM EPA (light gray bar) or a high concentration of EPA (dark gray bar). EPA content is expressed as the mean \pm SD percentage of total fatty acids present (A) and mean \pm SD µg per million cells (B), for 3 independent replicates. Student's t-test compared EPA amount between ethanol control treated and EPA treated samples, with statistical significance denoted by (ns) not statistically significant, (*) $p < 0.05$, (**) $p < 0.005$, and (***) $p < 0.0005$.

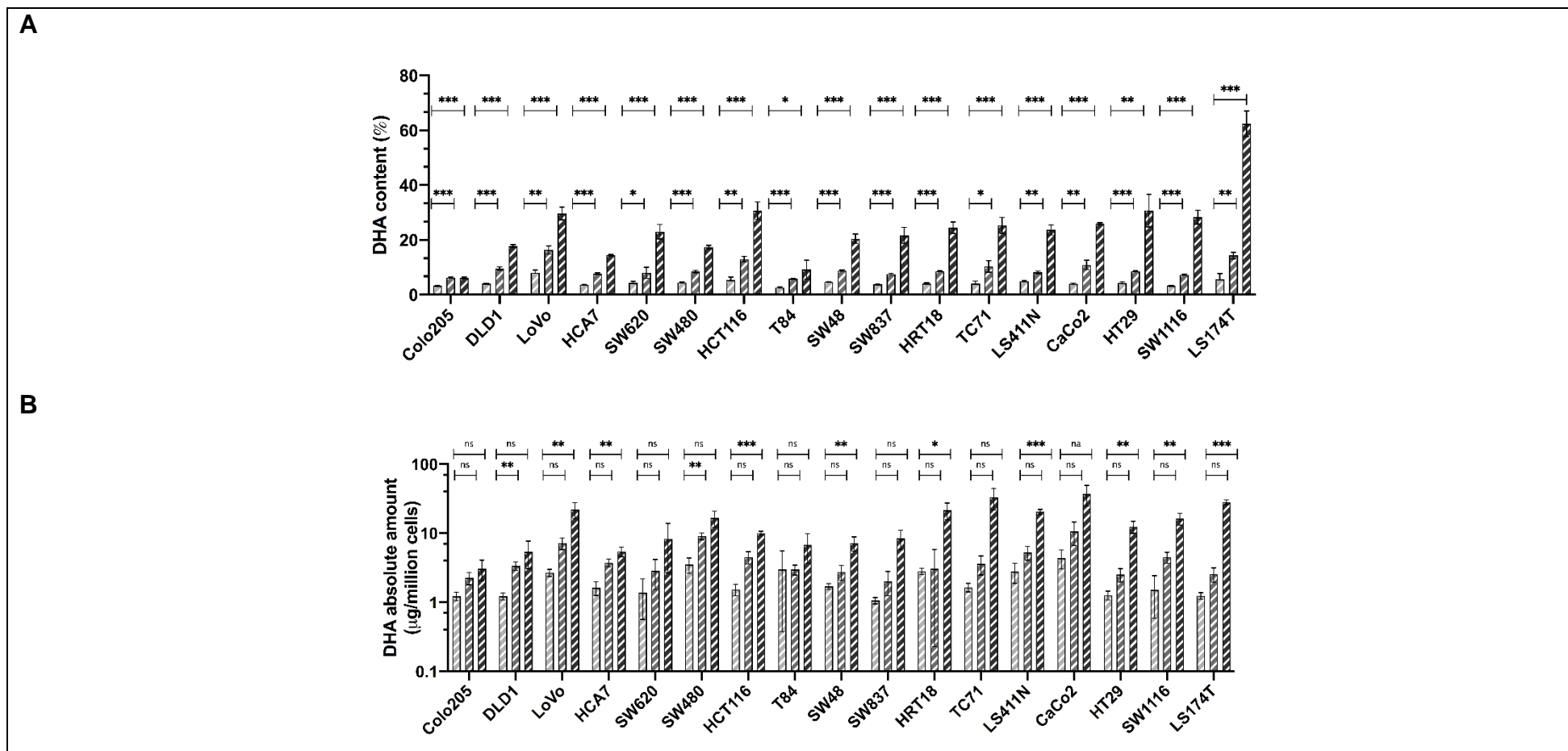


Figure 5.3. The effect of DHA exposure on DHA content of human colorectal cancer cell lines

Cells in culture were incubated for 24 hours in supplemented media containing ethanol carrier (white bar), 5µM DHA (hatched bar) or a high concentration of DHA (diagonal stripes bar). DHA content is expressed as the mean \pm SD percentage of total fatty acids present (A) and mean \pm SD µg per million cells (B), for 3 independent replicates. Student's t-test compared DHA amount between ethanol control treated and DHA treated samples, with statistical significance denoted by (ns) not statistically significant, (*) $p < 0.05$, (**) $p < 0.005$, and (***) $p < 0.0005$.

Following 5 μ M EPA-treatment, the lowest EPA content was 3.5 ± 0.1 % (HCA-7) and the highest EPA content was 10.6 ± 0.6 % (DLD-1) [Figure 5.2 A]. The difference between EPA content measured in carrier control treated and 5 μ M EPA-treated cells, when expressed as %FA, were all statistically significant (Student's t-test, $p \leq 0.05$). Whilst the cell lines for which the highest and lowest EPA percentages reported in carrier treated and 5 μ M EPA-treated were the same, relative EPA content measured in carrier treated cells did not predict relative EPA content between these same cell lines following treatment. For example, carrier-treated HRT18 had a relatively low EPA content (1.7 ± 0.1 %) but, following 5 μ M EPA treatment, the second highest content (10.3 ± 0.4 %) (Student's t-test, $p = 0.0000002$).

OA, PA, and SA were the most abundant FAs in carrier control cells. Following 5 μ M EPA-treatment, content ranged from; OA: 16.2 ± 2.9 % (T84) to 56.7 ± 0.9 % (SW620); PA: 9.3 ± 1.9 % (SW620) to 31.4 ± 1.9 % (T84) and SA: 8.0 ± 1.4 % (SW620) to 34.4 ± 4.3 % (T84). These were similar to carrier control measurements (16.3 ± 1.7 % (T84) to 61.5 ± 1.9 % (SW620), 10.9 ± 1.3 % (SW620) to 32.4 ± 0.4 % (T84) and 8.8 ± 2.2 % (SW620) to 37.2 ± 2.3 % (T84), for OA, PA and SA respectively).

A statistically significant increase in DHA content for all cell lines was measured following 5 μ M DHA-treatment (Student's t-test, $p \leq 0.05$), with DHA content ranging from 5.8 ± 0.2 % (T84) to 16.4 ± 1.8 % (LoVo) [Figure 5.3 A]. OA content ranged from 17.6 ± 0.8 % (T84) to 53.7 ± 7.5 % (SW620), PA content ranged from 9.8 ± 1.5 % (LS174T) to 30.3 ± 0.6 % (T84) and SA content measured 9.6 ± 0.9 % (HCT116) to 33.5 ± 1.0 % (T84).

Exposure of cell lines to high-concentration *n*-3 PUFA resulted in further increases in amount of FA to which they were exposed compared to carrier controls and 5 μ M-treated cells (see **Appendix A5.4** for full FA profiles for all cell lines and treatment groups). EPA content in high-concentration EPA-treated cells ranged from 21.2 ± 0.3 % (SW480) to 45.7 ± 3.2 % (LS174T) [Figure 5.2 A]. DHA content in high-concentration DHA-treated cells ranged from 6.1 ± 0.4 % to 62.3 ± 4.7 % (Colo205 and LS174T) [Figure 5.3 A]. Increased EPA or DHA content following high-concentration exposure, and compared to carrier control EPA or DHA content, was shown to be statistically significant ($p \leq 0.05$).

FA content was quantified as absolute amount of FA in each sample, normalised to cell number. Across all cell lines the least abundant FA remained LNA (undetectable to 0.2 μ g/million cells). As previously shown with the relative percentage data, PA, OA, and SA

were the most abundant FAs measured and the full profiles are shown in **Appendix A5.5**.

Absolute amount of EPA measured in carrier-treated cells ranged from 0.5 ± 0.2 $\mu\text{g}/\text{million cells}$ (HCA-7) to 3.7 ± 1.3 $\mu\text{g}/\text{million cells}$ (CaCo-2) [**Figure 5.2 B**]. DHA absolute amount measured in carrier-treated cells ranged from 1.1 ± 0.1 $\mu\text{g}/\text{million cells}$ (SW837) to 4.4 ± 1.4 $\mu\text{g}/\text{million cells}$ (CaCo-2) [**Figure 5.3 B**]. DLD-1, HT-29 and SW1116 cells had lower DHA content compared to EPA content when looking at absolute amounts ($\mu\text{g}/\text{million cells}$: DLD-1; EPA 1.7 ± 0.5 , DHA 1.2 ± 0.1 . HT29; EPA 1.6 ± 0.6 , DHA 1.3 ± 0.2 . SW1116; EPA 2.0 ± 0.8 , DHA 1.5 ± 0.9).

For all FAs measured across carrier-treated cells, with the exception of LNA, CaCo-2 cells contained higher absolute quantities of each FA than all other cell lines [**Appendix A5.5**], which was not detected when data were expressed as % FA. For instance, when the EPA content of CaCo-2 cells was compared to the content of the cells with the second highest (SW480) and lowest (HCA-7), CaCo-2 content was 1.4 to 7.4-fold higher. In a similar comparison, DHA content of CaCo-2 cells was 2.3-fold to 6.0-fold higher than in LoVo and Colo205 cell lines at baseline.

As shown with percentage FA data, *n*-3 PUFA supplementation resulted in an increased amount of that specific *n*-3 PUFA. EPA content of 5 μM EPA-treated cells ranged from 2.5 ± 0.8 $\mu\text{g}/\text{million cells}$ (HCA-7) to 17.6 ± 2.9 $\mu\text{g}/\text{million cells}$ (CaCo-2). When data were expressed as absolute amount, the EPA content between carrier treated and 5 μM EPA-treated were statistically significantly different (Student's t-test, $p \leq 0.05$), with the exception of TC71 and LS174T. DHA content of 5 μM DHA treated cells ranged from 2.0 ± 0.8 $\mu\text{g}/\text{million}$ (SW837) to 10.7 ± 4.0 $\mu\text{g}/\text{million}$ (CaCo-2) [**Figure 5.2 B**]. Following 5 μM *n*-3 PUFA treatment, the cell line with the highest measured EPA or DHA (respective of exposure) was consistently CaCo-2.

To further investigate relationships between *n*-3 supplementation and FA content, specifically for cells treated with 5 μM *n*-3 PUFA, I calculated fold change in FA absolute amount. EPA fold change ranged from 3.0 ± 0.3 (T84) to 7.5 ± 3.0 (HRT18) fold. DHA fold change ranged from 1.2 ± 1.1 (HRT18) to 3.8 ± 2.1 (SW1116) fold. When data was expressed as a difference between 5 μM *n*-3 PUFA treated and carrier-treated content, EPA content difference ranged from 1.9 ± 0.7 (HCA-7) to 13.9 ± 3.6 (CaCo-2) and DHA content difference ranged from -0.003 ± 3.0 (T84) to 6.3 ± 5.3 (CaCo-2).

High concentration exposure of cells to EPA or DHA also resulted in an increase in absolute amount of EPA or DHA measured. FA profiles of all cell lines and treatment groups are shown in **Appendix A5.5**. Cells treated with high EPA concentrations had absolute EPA quantities in the range of 21.6 ± 2.1 to 198.2 ± 42.1 $\mu\text{g}/\text{million cells}$ (TC71 and CaCo-2, respectively) [**Figure 5.2 B**]. When data were expressed as absolute amount, the EPA content between carrier treated and high concentration EPA-treated were statistically significantly different (Student's t-test, $p \leq 0.05$), with the exception of TC71 and LS174T. Following high-concentration DHA treatment, DHA content ranged from 3.1 ± 1.0 to 36.9 ± 12.4 $\mu\text{g}/\text{million cells}$ (Colo205 and CaCo-2, respectively) [**Figure 5.3 B**]. Once again, it was found that following high concentration *n*-3 PUFA treatment, the cell line with the highest measured quantity of EPA or DHA (relative to exposure FA) was CaCo-2.

In summary, the data so far indicated a 'concentration-response' between CRC cell treatments with EPA or DHA and the respective EPA or DHA cellular content measured [**Figure 5.2** and **Figure 5.3**]. The results show that at the lowest amount of EPA or DHA was measured in cells treated with ethanol carrier and the highest amount of *n*-3 PUFA was measured in the sample treated with high-concentration *n*-3 PUFA.

5.3.2.2. The impact of varying amounts of ethanol carrier upon the fatty acid profiles of cell lines

Carrier-treated cell data indicated that there were large variations in each FA absolute amount between cell lines, with the lowest and highest amount differing by 3.2 $\mu\text{g}/\text{million cells}$ and 3.3 $\mu\text{g}/\text{million cells}$ for EPA and DHA, respectively. However, the concentration of ethanol carrier was also variable between cell lines [**Appendix A5.3**]. Therefore, I tested whether changes in ethanol carrier concentration were associated with changes in the FA profiles.

I compared the FA profiles for cell lines with equivalent (LS411N) or different (Colo205 and LS174T) ethanol control carrier concentrations. The absolute amount of all FAs measured are shown in **Figure 5.4**. No statistically significant differences in any FA content between carrier control treated cells were found (independent Student's t-test)

It was concluded that there was no difference in FA profile dependent upon the concentration of ethanol carrier, and therefore the variation between FA profiles was dependent upon cell lines and was not related to ethanol exposure.

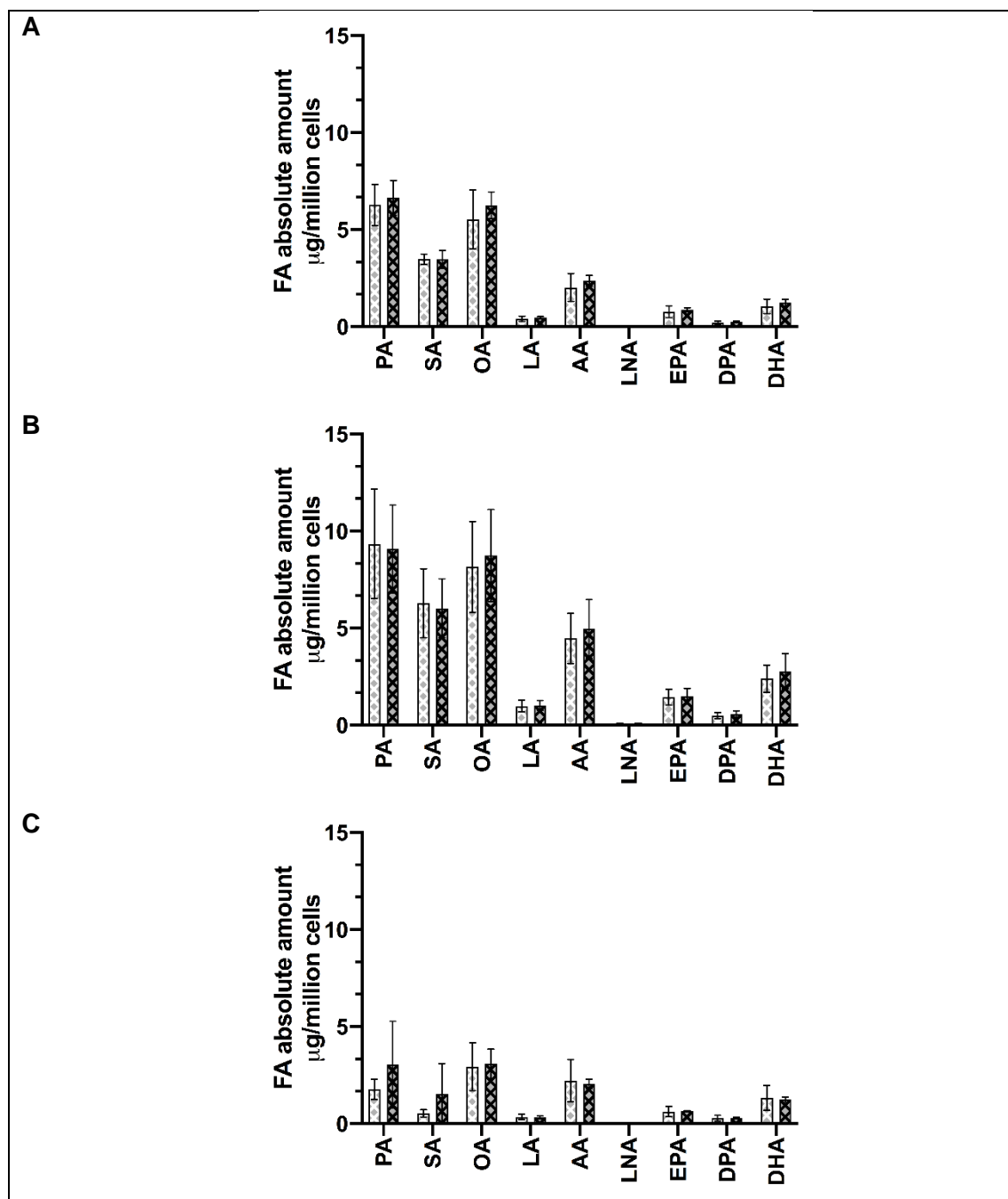


Figure 5.4. Fatty acid profile of ethanol control samples

FA profiles of cell lines following treatment with ethanol concentration equivalent to high-concentration EPA \square or DHA \boxtimes . (A) Colo205, 0.50 % v/v and 0.02 % v/v (B) LS411N, 0.30 % v/v and 0.20 % v/v and (C) LS174T, 0.70 % v/v and 0.40 % v/v. FA absolute quantity is expressed as mean \pm SD $\mu\text{g}/\text{million cells}$, for 3 independent biological replicates.

5.3.2.3. *Impact of EPA and DHA treatment on AA content in hCRC cell lines*

Studies have reported that supplementing cells with EPA causes a concomitant decrease in arachidonic acid (AA) in both *in vitro* (192) and human tissue samples (274). Having established that the profiles obtained were different depending on how the data was expressed (**Chapter 5.3.2.1**), I tested whether these differences also affected AA content. I compared the AA content percentage data with the measured absolute amount data ($\mu\text{g}/\text{million cells}$) following culture in media supplemented with EPA or DHA.

5.3.2.3.1. *Effect of EPA treatment on AA content in hCRC cell lines*

When expressed as relative FA content, the data obtained here [**Figure 5.5 A**] indicated that EPA supplementation was associated with a dose-dependent decrease in the relative AA content in all hCRC cell lines tested. For example, LoVo cells which had the highest AA %, 8.9 ± 0.9 % and following high-concentration EPA-treatment was 2.6 ± 2.3 % (Student's t-test, $p = 0.00023$). The data are comparable to published literature.

However, when the data are analysed further as the absolute amount values, the results are different depending on the cell line and none of the differences between AA content in carrier treated and EPA treated cell lines were shown to be statistically significant (Student's t-test). In 4 of the 17 cell lines (HRT18, DLD1, T84 and LoVo) analysed, EPA treatment was associated with a decrease in AA absolute amount [**Figure 5.5 B**], consistent with the relative data observed in **Figure 5.5 A**. For example, LoVo cells had an AA content that decreased following EPA exposure. Measurements of 6.6 ± 1.5 $\mu\text{g}/\text{million cells}$ (8.9 ± 0.9 %) AA in carrier-treated LoVo cells, and 4.8 ± 0.5 $\mu\text{g}/\text{million cells}$ (2.6 ± 0.1 %) AA in high-concentration EPA-treated LoVo cells, were reported (Student's t-test, $p = 0.14$). However, in 7 out of 17 cell lines (HCT116, TC71, HT-29, SW48, SW837, LS174T and CaCo-2) the AA content was stable following EPA treatment.

6 out of 17 cell lines were shown to have an increase in AA content following high-concentration EPA treatment, namely SW480, LS411N, HCA7, Colo205, SW620 and SW1116 cells. Using Colo205 cells as an example, when AA content is expressed as a relative percentage it decreases from 4.4 ± 0.7 % to 3.4 ± 1.2 % (Student's t-test, $p = 0.063$). However, the absolute quantities of AA measured were 2.0 ± 0.7 , 2.7 ± 0.2 (Student's t-test, $p = 0.19$) and 5.0 ± 0.9 $\mu\text{g}/\text{million cells}$ (Student's t-test, $p = 0.011$) for carrier-treated, 5 μM and high-concentration EPA-treated, respectively.

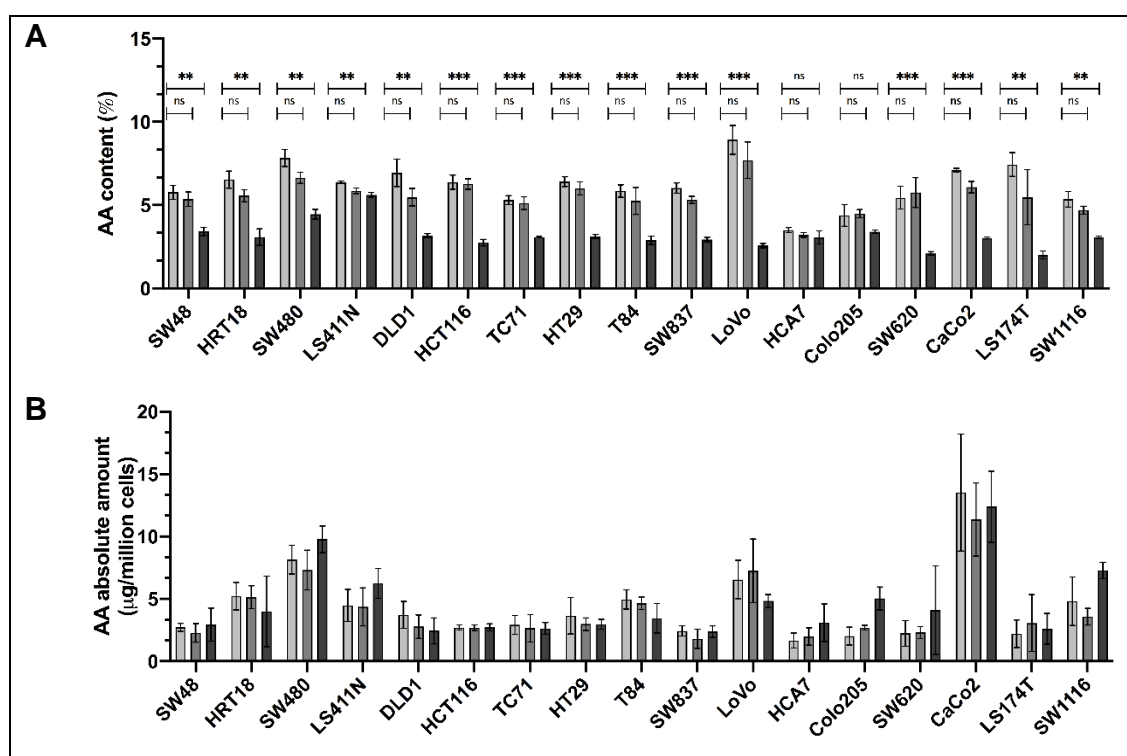


Figure 5.5. The effect of EPA supplementation on arachidonic acid (AA) content of CRC cell lines

The arachidonic acid (AA) content for cells cultured for 24 hours in supplemented media containing carrier (white bar), 5µM EPA (light grey bar) or high concentration EPA treatment (dark grey bar). AA content is expressed as mean \pm SD %AA (A) and mean \pm SD µg/million cells (B), for 3 independent biological replicates. Student's t-test compared AA amount between ethanol control treated and EPA treated samples, with statistical significance denoted by (ns) not statistically significant, (*) $p < 0.05$, (**) $p < 0.005$, and (***) $p < 0.0005$. No statistically significant differences in AA absolute content were shown following EPA supplementation.

5.3.2.3.2. Effect of DHA treatment on AA content in hCRC cell lines

A similar analysis was performed for DHA treated cells. In the case of LoVo cells, relative amount analysis suggested a decrease in AA relative content, but absolute amount analysis showed a non-statistically significant increase from 4.6 ± 0.7 µg/million cells (carrier-treated) to 5.3 ± 1.0 µg/million cells (5 µM DHA) (Student's t-test, $p = 0.37$) and 7.2 ± 1.7 µg/million cells (high concentration) (Student's t-test, $p = 0.068$) [Figure 5.6]. However, this increase in AA following DHA treatment was only observed in one other cell line, TC71.

Most cell lines (11/18) were found to have a decrease in AA content following high-concentration DHA treatment (DLD1, HCA7, SW620, SW480, HCT116, T84, SW48, HRT18, CaCo2, HT29 and SW1116) [Figure 5.6 B]. The greatest decrease was observed in T84 cells, for which carrier-treated AA content was 9.0 ± 7.7 µg/million cells and following high concentration DHA treatment was 3.7 ± 1.6 µg/million cells (Student's t-test, $p = 0.31$).

It is worth noting that at equivalent concentration (5 μ M) the effect of EPA and DHA supplementation on AA absolute amount in hCRC cells were different, potentially indicative of differential incorporation, storage, and biological activity.

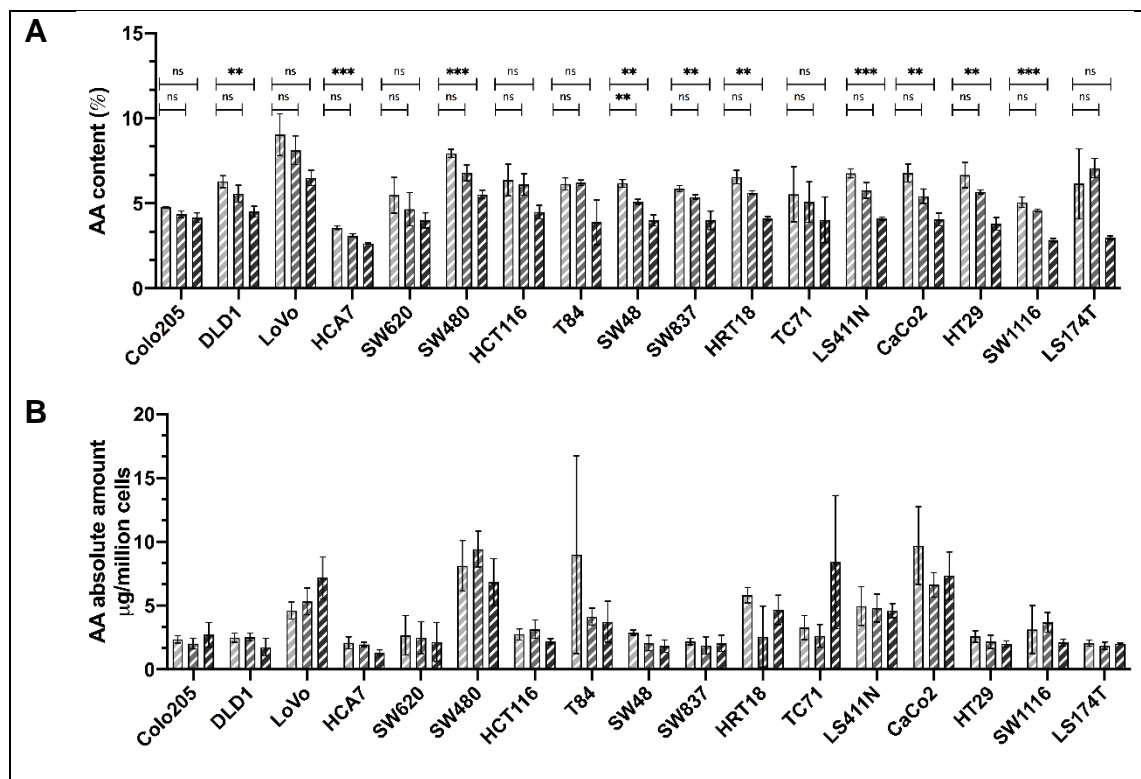


Figure 5.6. The effect of DHA supplementation on arachidonic acid (AA) content of CRC cell lines

The arachidonic acid (AA) content for cells cultured for 24 hours in supplemented media containing carrier (white bar), 5 μ M EPA (diagonal lines) or high concentration EPA treatment (cross-hatched). AA content is expressed as mean \pm SD %AA (A) and mean \pm SD μ g/million cells (B), for 3 independent biological replicates. Student's t-test compared AA amount between ethanol control treated and DHA treated samples, with statistical significance denoted by (ns) not statistically significant, (*) $p < 0.05$, (**) $p < 0.005$, and (***) $p < 0.0005$. No statistically significant differences in AA absolute content were shown following DHA supplementation.

Although there were differences in average AA content between *n*-3 PUFA treated and carrier treated cells, they were not sufficient to reach statistical significance (Student's t-test, $p > 0.05$). However, change in AA content could be explained in two ways. If the total amount of FA in each cell remains constant, *n*-3 PUFA supplementation could displace AA and reduce its overall content. If cells accumulate more FA upon supplementation, then addition of exogenous *n*-3 PUFA would increase overall amount of FA present, thus reducing the relative proportion of AA to the total. In any case, the relative amount of AA would decrease, but measuring absolute amount of AA or any other FA would be able to discriminate between the two phenomena. Hence, from hereon, further data analysis used absolute amount of each FA. This is, once again, presented with the caveat that all absolute amount data need further validation to confirm quantification of samples that were not within the range of the standard curve used.

5.3.3. Assessing the relationship between *PTGS1* and *PTGS2* gene expression and FA content

As COX enzymes metabolise *n*-3 PUFAs, their presence may affect the *n*-3 PUFA content in cells. I assessed whether *PTGS1* and *PTGS2* gene expression was correlated with FA content, using the gene expression data presented in **Chapter 4.3.3**.

5.3.3.1. *The relationship between PTGS expression and n-3 PUFA content*

Following treatment with respective carrier control, 5 μ M EPA or 5 μ M DHA supplementation no correlation was found between *PTGS1* expression, *PTGS2* or combined *PTGS* and EPA content [**Figure 5.7**] or DHA content [**Figure 5.8**].

As no relationship was found between *PTGS1* or *PTGS2* expression and *n*-3 PUFA content, I next tested whether the hCRC cell lines' sensitivity to EPA and/or DHA were associated with FA content.

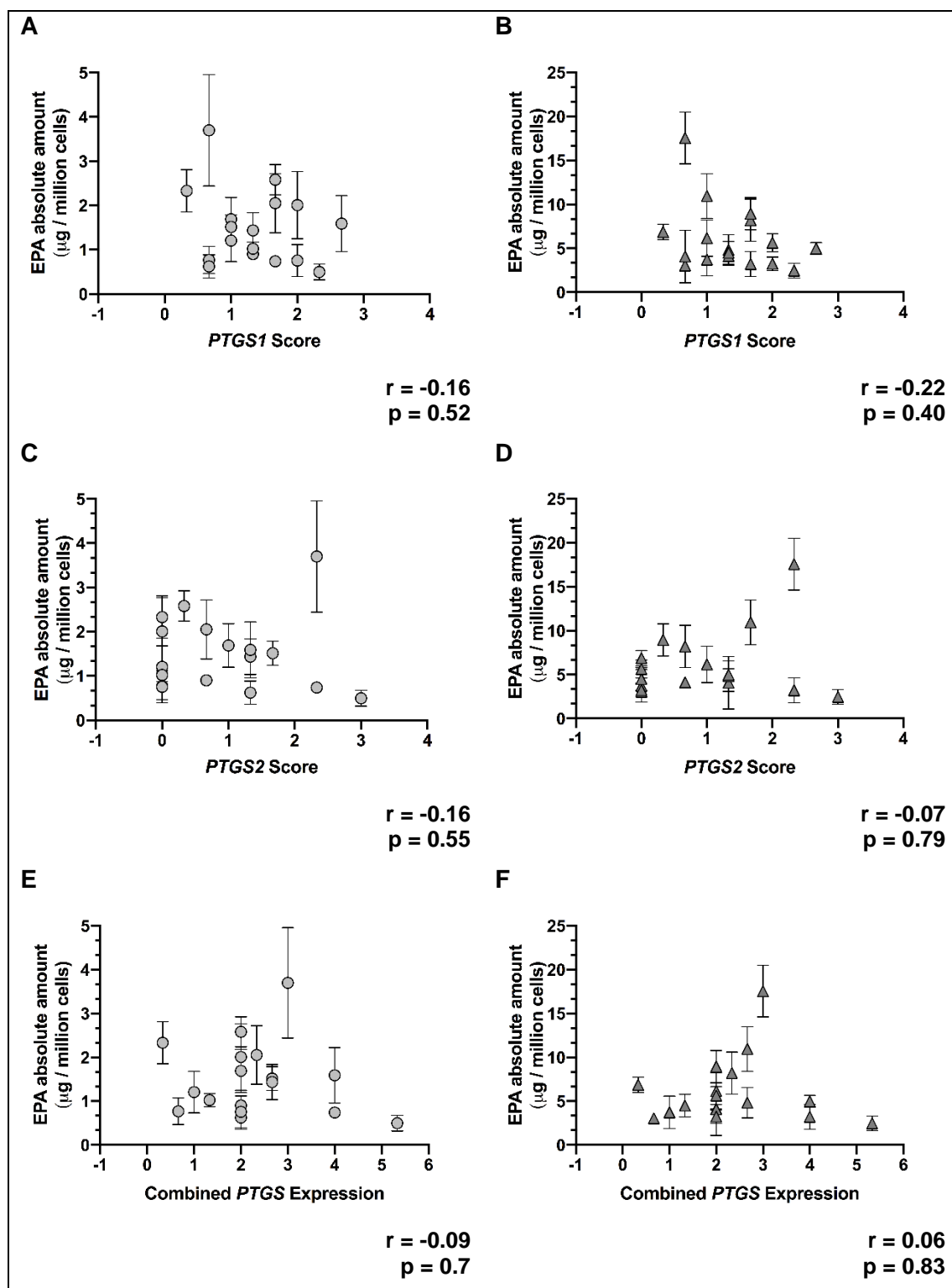


Figure 5.7. PTGS gene expression and EPA content in hCRC cells

Expression of *PTGS1* and *PTGS2* was measured in human CRC cell lines by RT-qPCR and converted to a *PTGS* score. EPA content was measured following treatment with carrier ● or 5μM EPA ▲ and is expressed as the mean ± SD μg per million cells, for 3 independent replicates. Spearman correlation coefficient and p values are given below each graph.

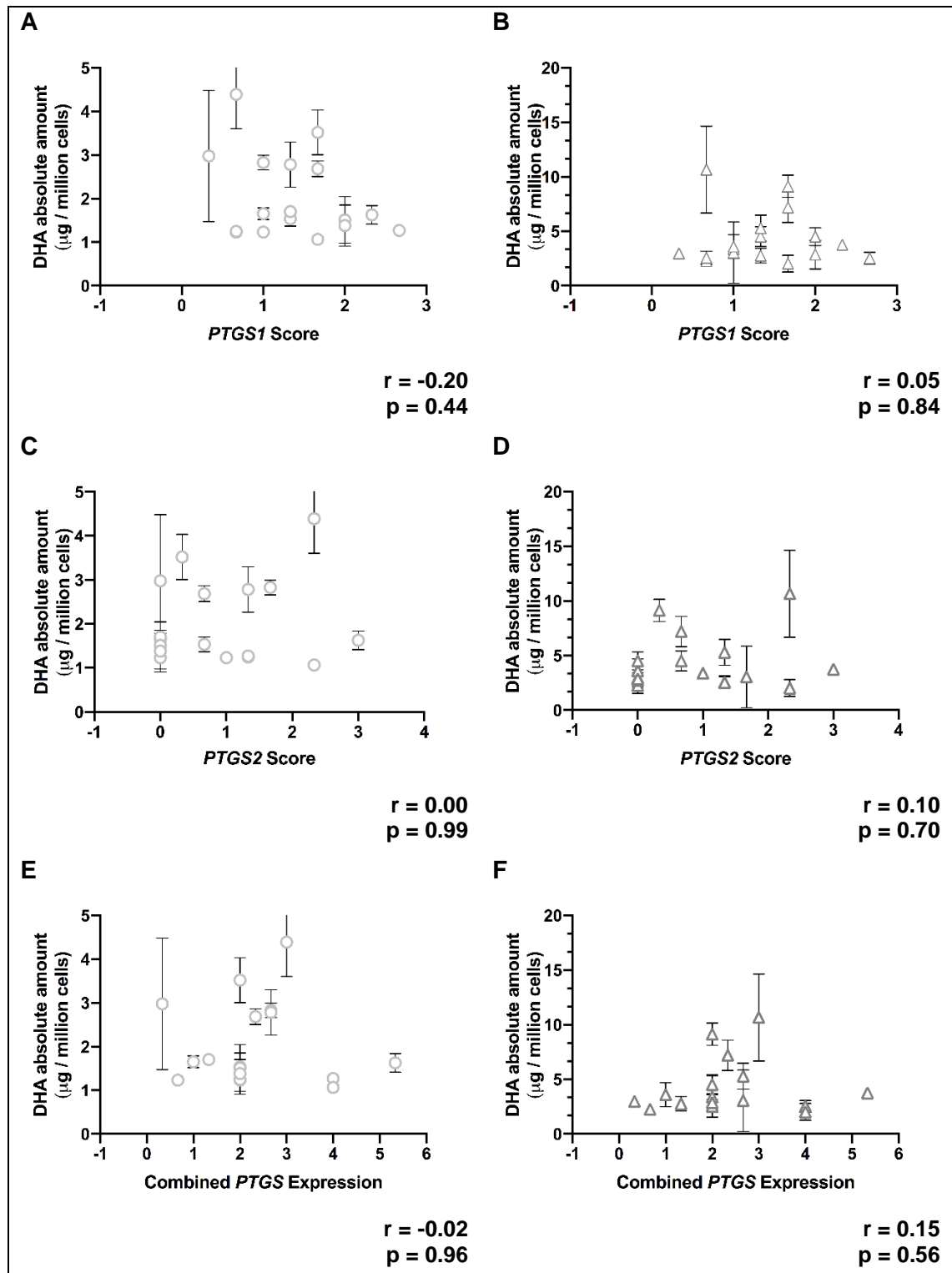


Figure 5.8. PTGS gene expression and DHA content in hCRC cells

Expression of *PTGS1* and *PTGS2* was measured in human CRC cell lines by RT-qPCR and converted to a *PTGS* score. EPA content was measured following treatment with carrier ○ or 5µM DHA △ and is expressed as the mean ± SD µg per million cells, for 3 independent replicates. Spearman correlation coefficient and p values are given below each graph.

5.3.4. Relationship between FA content and cell line sensitivity to *n*-3 PUFAs

5.3.4.1. The effect of high concentration *n*-3 PUFA treatment and measured *n*-3 PUFA amount

High-concentration treated cells were exposed to EPA or DHA concentrations equivalent to approximate IC₅₀. I tested whether a relationship between treatment concentration and FA content (absolute amount) existed. The aim was to establish whether cells had a threshold FA content that, once surpassed, would lead to growth inhibition outcome.

A trend was observed for both EPA and DHA treated cell lines, in that the higher concentrations of EPA or DHA corresponded with a higher absolute amount of *n*-3 PUFA (EPA or DHA) detected [Figure 5.9]. This indicated that cells were able to store the exogenous FA in a comparable manner when the exposure concentration was approximate to their individual IC₅₀.

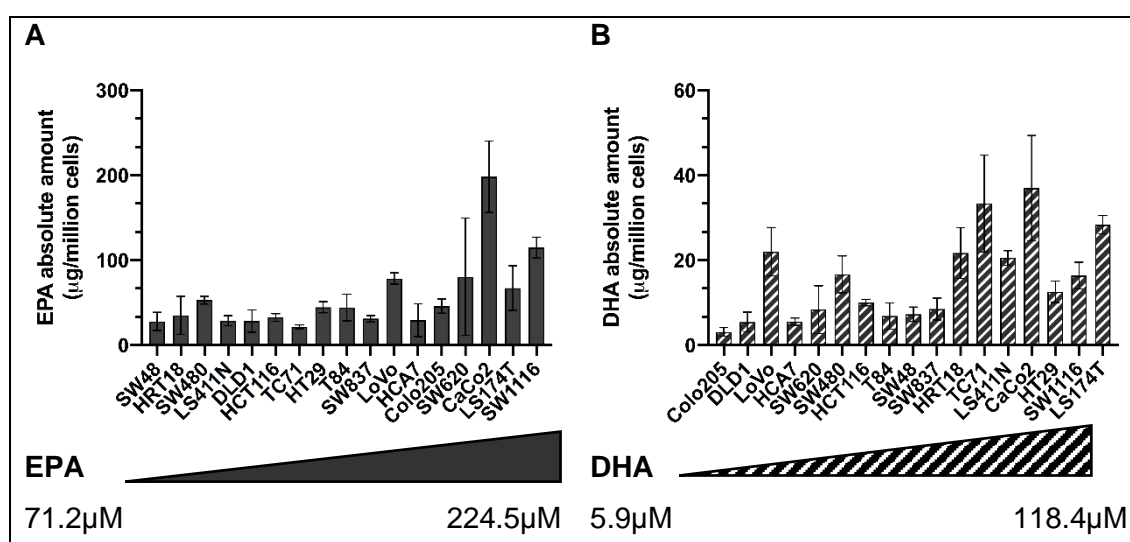


Figure 5.9. The effect of *n*-3 PUFA treatment concentration on absolute amount measured

Cells were treated with high concentrations of EPA (■) or DHA (▨) for 24 hours. *N*-3 content of EPA (A) and DHA (B), are expressed as the mean ± SD µg per million cells, for 3 independent replicates.

However, the data also showed some differences depending upon the cell lines and the *n*-3 PUFA used. For example, the absolute amount of EPA measured in HT-29 cells treated with a concentration of 118.4 µM EPA was over 1.5-fold greater than with the absolute amount of DHA measured in LS174T cells treated with the same concentration (118.4 µM) of DHA (44.6 ± 6.5 EPA µg/million and 28.3 ± 2.1 DHA µg/million respectively).

To assess further associations between FA content and sensitivities or molecular phenotypes, I focus on carrier-treated and 5 μ M *n*-3 PUFA treated samples as the exogenous addition is uniform and comparable between all cell lines and thus the confounding variation for high concentration treated cells would be avoided.

5.3.4.2. Assessing the relationship between EPA sensitivity and EPA content

I tested the relationship between sensitivity to EPA and EPA absolute amount measured in cell lines following treatment with carrier or 5 μ M EPA. **Figure 5.10** shows that there were variations in EPA content across the panel in either treatment group but there was no association found between EPA sensitivity and EPA content.

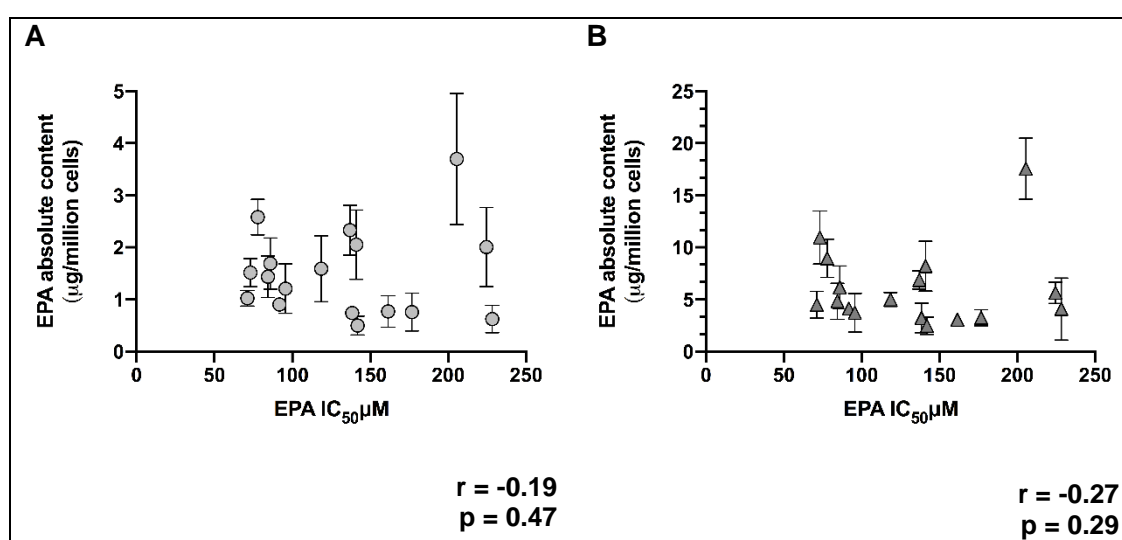


Figure 5.10. Correlation between EPA sensitivity and absolute EPA content

Absolute EPA content in cells cultured for 24 hours in media containing carrier \circ (A) or 5 μ M EPA \blacktriangle (B) plotted against EPA IC_{50} . EPA content is expressed as the mean \pm SD μ g per million cells, for 3 independent replicates. Spearman correlation coefficient and p values are given below each graph.

As variation in FA content at baseline had been observed between cell lines, I tested the relationship between EPA sensitivity and the increase in EPA content upon supplementation. This increase was expressed either as relative fold change [**Figure 5.11 A**] or as an absolute difference [**Figure 5.11 B**] between 5 μ M EPA treated and carrier-treated cell content.

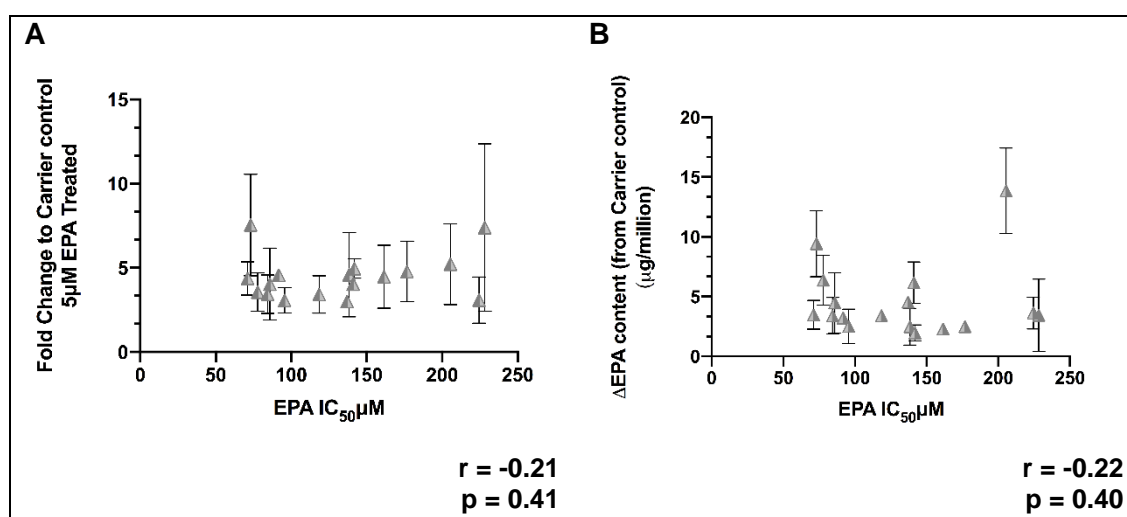


Figure 5.11. Correlation between EPA sensitivity and EPA content relative to content in carrier-treated controls

EPA content is expressed relative to carrier-treated cell content as mean \pm SD fold change \blacktriangle (A) and mean \pm SD absolute difference μg per million cells \blacktriangle (B). Spearman correlation coefficient and p values are given below each graph.

Figure 5.11 shows that when the change in EPA was expressed as either a fold change or difference compared to the content of carrier-treated cells, no statistically significant correlations between sensitivity and content were found.

As EPA and DHA are independent *n*-3 PUFAs, I also assessed the relationship between DHA sensitivity and DHA content. No significant relationships were identified [**Figure 5.12**, **Figure 5.13**]. DHA exposure, and storage of DHA, was not dependent on the inherent sensitivity.

In conclusion, EPA and DHA content did not correlate with EPA or DHA sensitivity, respectively. As absolute amount of *n*-3 PUFA or relative changes in their amount was not associated with hCRC cell sensitivity to *n*-3 PUFA, this suggests that sensitivity is not dependent on *n*-3 PUFA storage. I next tested whether any associations between FA content and enzymes linked with *n*-3 PUFA metabolism could be detected.

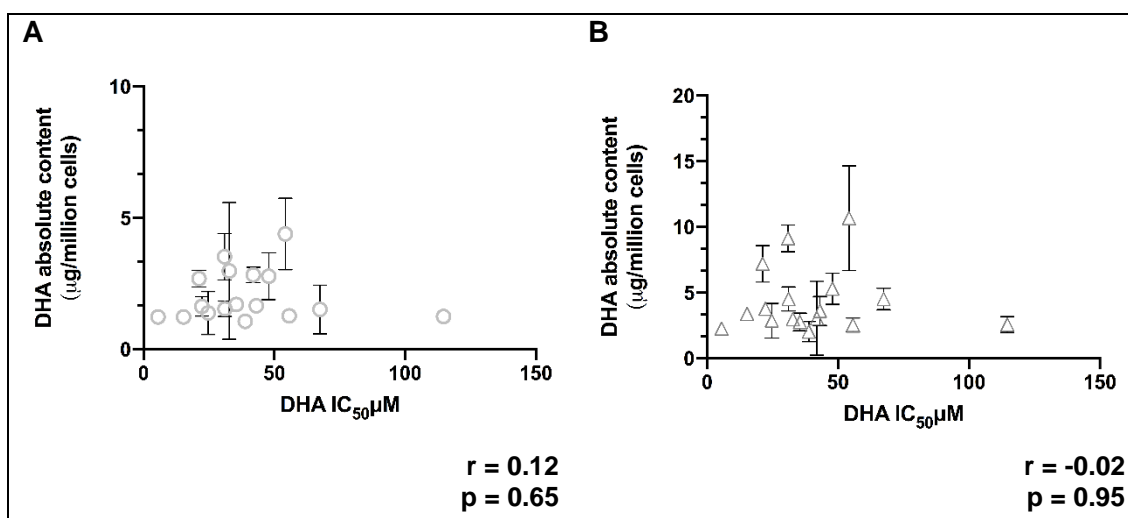


Figure 5.12. Correlation between DHA sensitivity and absolute DHA content

Absolute DHA content in cells cultured for 24 hours in media containing carrier \circ (A) or 5µM EPA \triangle (B) plotted against DHA IC₅₀. DHA content is expressed as the mean \pm SD µg per million cells, for 3 independent replicates. Spearman correlation coefficient and p values are given below each graph.

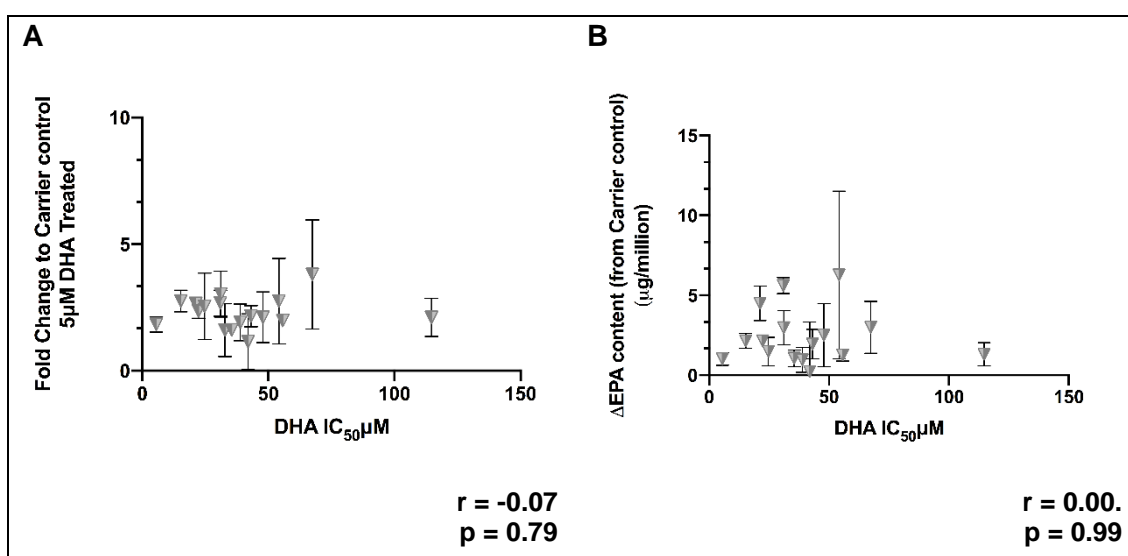


Figure 5.13. Correlation between DHA sensitivity and DHA content relative to carrier-treated cell content

DHA content is expressed relative to carrier-treated cell content as mean \pm SD fold change ∇ (A) and mean \pm SD absolute difference µg per million cells ∇ (B). Spearman correlation coefficient and p values are given below each graph.

5.3.5. Evaluating whether the cell ability to metabolise EPA to DPA and DHA has any effect on cell sensitivity

The conversion of EPA to DPA and DHA, involving the desaturase and elongase enzymes (FADS and ELOVL) **Figure 1.6 (Chapter 1.3.3.1)** (118), could provide an explanation as to the variable cellular *n*-3 PUFA sensitivities of the CRC panel. Indeed, as described previously (**Chapter 4.3.4**), hCRC cells were found to be more sensitive to DHA than EPA. I hypothesised that EPA-sensitive cell lines were able to convert EPA more efficiently to DHA than resistant cell lines.

In EPA-carrier-treated cells, DHA content ranged from 1.05 ± 0.38 $\mu\text{g}/\text{million cells}$ (Colo205) to 5.99 ± 2.08 $\mu\text{g}/\text{million cells}$ (CaCo-2). Cells treated with $5\mu\text{M}$ EPA had DHA content that ranged from 1.25 ± 0.06 $\mu\text{g}/\text{million cells}$ (Colo205) to 4.43 ± 1.03 $\mu\text{g}/\text{million cells}$ (CaCo-2). [**Figure 5.14**].

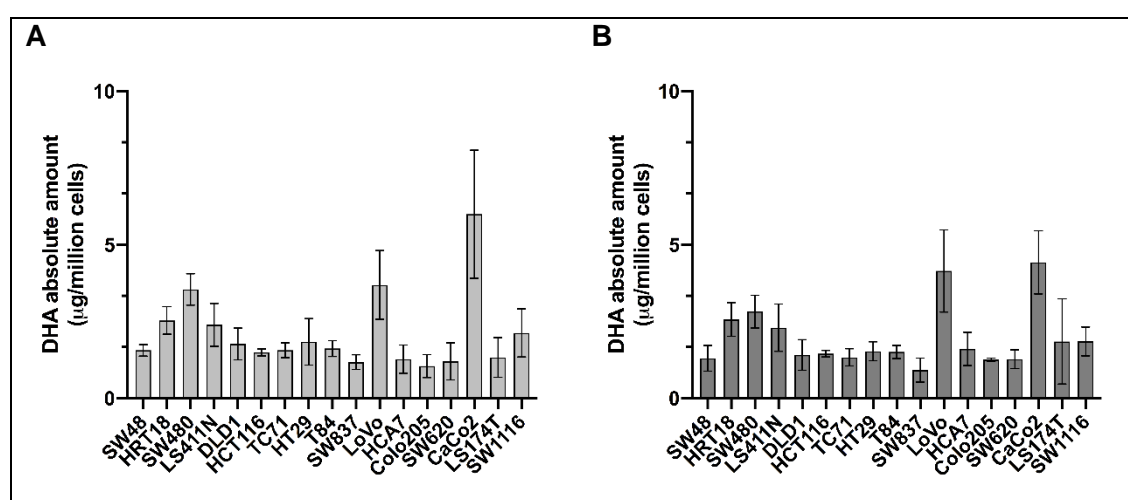




Figure 5.14. Impact of EPA supplementation on hCRC cell DHA absolute amount

DHA content is expressed as mean μg per million cells \pm SD, for 3 independent replicates, for (A) carrier treated cells  and (B) following treatment with EPA .

11 cell lines had a decreased DHA content following EPA treatment, with a 0.8-fold reduction in DHA content measured between CaCo-2 control and $5\mu\text{M}$ EPA treated cells. The largest fold change increase in DHA content from baseline was observed in LS174T cells, which had a DHA fold change compared to carrier-treated content of 1.6-fold [**Figure 5.15**]. For all cell lines, the measured amount of DHA in carrier-treated compared to $5\mu\text{M}$ EPA-treated cells was not statistically significantly different (Student's t-test, $p > 0.05$, data not shown). These findings did not support the hypothesis that more sensitive cells were converting EPA to the more cytotoxic DHA, but indicated that EPA-

sensitive cells were perhaps using DHA and causing a reduction in measured levels. Conversely, EPA-resistant cells were storing and accumulating DHA.

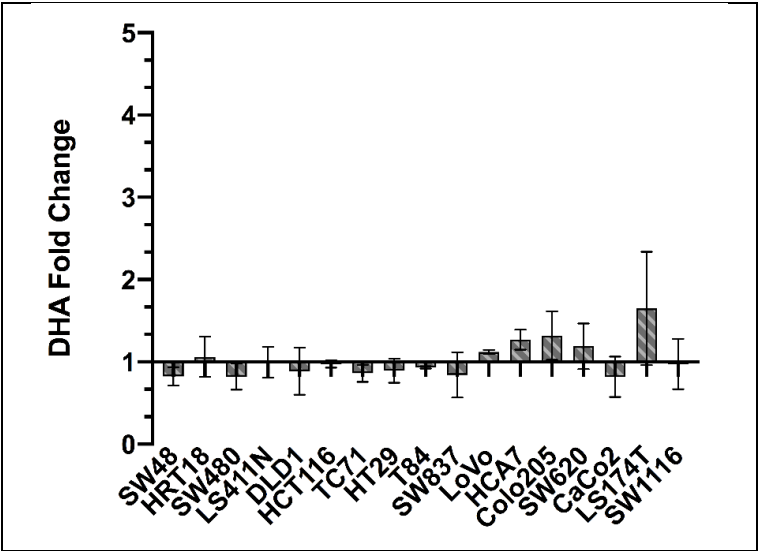


Figure 5.15. Impact of EPA supplementation on hCRC relative DHA content

DHA content of 5µM EPA treated CRC cell lines is expressed as mean ± SD fold change (FC) compared to carrier-treated cell DHA content. Cell lines are ordered by EPA sensitivity, from low to high IC₅₀ values.

I next tested whether any relationship could be found between EPA sensitivity and the absolute amount of DPA in hCRC cell lines. DPA was found to range from 0.15 ± 0.02 µg/million cells (SW837) to 1.30 ± 0.46 µg/million cells (CaCo-2) in carrier-treated cells, and 0.13 ± 0.06 µg/million cells (SW837) to 2.62 ± 0.56 µg/million cells (CaCo-2) following 5 µM EPA treatment for 24h [Figure 5.16].

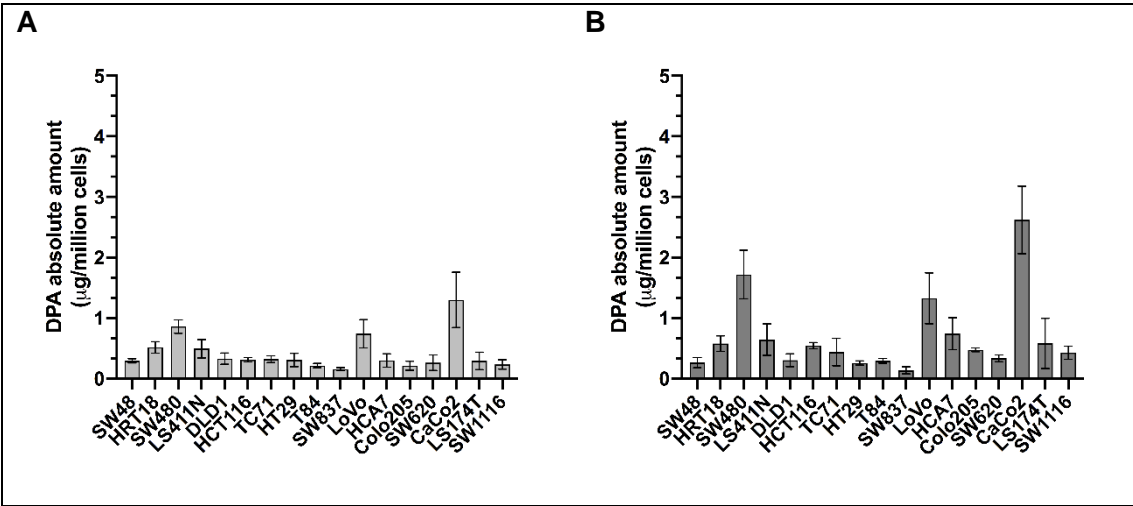


Figure 5.16. Impact of EPA supplementation on hCRC cell DPA absolute amount

DPA content expressed as mean µg per million cells ± SD, for 3 independent replicates in (A) carrier-treated and (B) in EPA treated cells.

Interestingly, 6 of 17 cell lines are shown to have a DPA content that increased over 2-fold, and of these 5/6 of these cell lines were less sensitive to EPA, with EPA IC₅₀ values over 140 μ M (HCA7, Colo205, CaCo-2, LS174T and SW1116) [Figure 5.17 A]. Spearman's rank correlation determined a positive correlation between EPA IC₅₀ and DPA content fold change, $r = 0.64$, $p = 0.007$ [Figure 5.17 B]. When DPA content fold change was grouped and compared with EPA IC₅₀, the mean values were shown to be statistically significantly different, unpaired Student's t-test, $p = 0.05$ [Figure 5.17 C]. A potential explanation as to the increased DPA content in EPA-resistant cells may be that the conversion from EPA to DPA, lowers EPA content. The production of DPA, an inactive metabolite, may reduce EPA bioactivity.

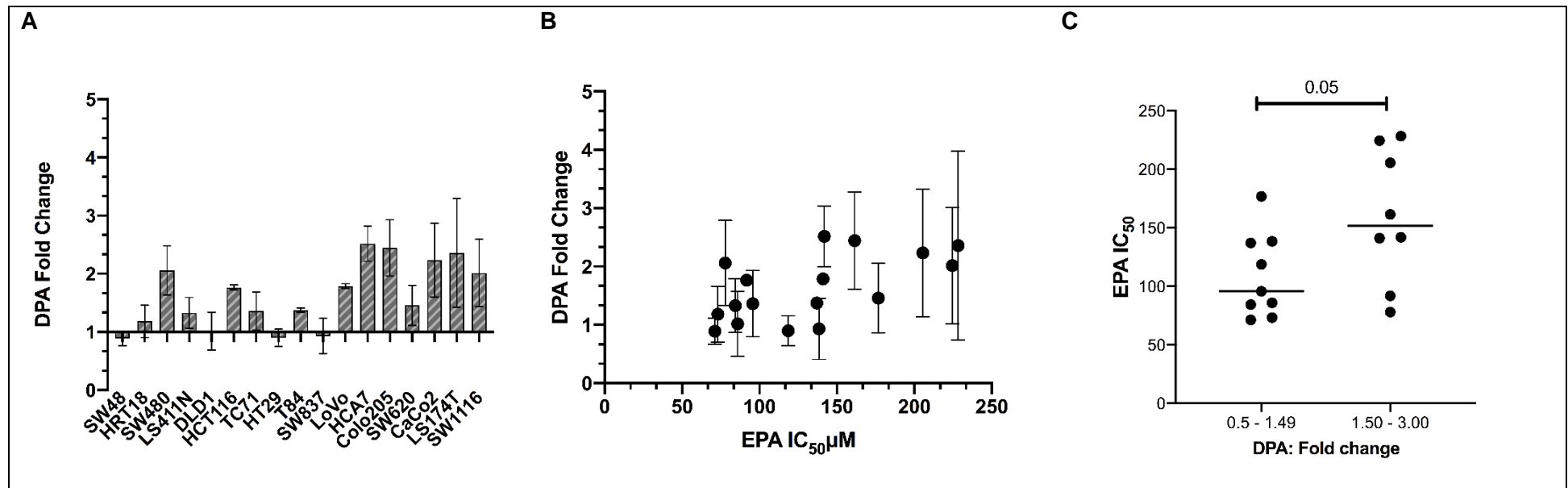
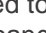


Figure 5.17. Impact of EPA supplementation on DPA content measured in hCRC cell lines

Assessing the impact of EPA supplementation on the change in DPA content in hCRC cell lines. (A) DPA content of 5μM EPA treated CRC cell lines is expressed as mean \pm SD fold change (FC)  compared to carrier-treated cell DPA content. Cell lines are ordered by EPA sensitivity, from low to high IC₅₀ values. (B) Correlation between EPA sensitivity and DPA fold change. (C) Based on the DPA fold change, the difference between EPA sensitivity is shown and assessed for statistical significance by unpaired Student's t-test.

5.3.6. Comparison of cells *n*-3 PUFA content in CIMP+ and CIMP- cell lines

As a relationship between high EPA sensitivity (low IC₅₀) and a CIMP+ status was identified [Chapter 4.3.5.3.3], the relationships between *n*-3 PUFA content and the molecular profiles (CIN, microsatellite status and CIMP status) were tested. This section focuses on the EPA, DPA and DHA absolute content in CIMP+ and CIMP- hCRC cell lines supplemented or not with 5 µM EPA. Relationships between other molecular profiles, and the relationship between DHA content of 5 µM DHA treated cells (and carrier controls) and molecular profiles, were also analysed, albeit with no statistically significant associations identified [Appendix A5.7].

A trend was identified between absolute EPA content and CIMP status with a lower EPA content in CIMP+ carrier-treated cells compared with CIMP- carrier-treated cells (Mann-Whitney, $p = 0.06$, **Figure 5.18 A**). No difference between CIMP+ and CIMP- cell line EPA content following 5µM EPA- cells was found (Mann-Whitney, $p = 0.12$, **Figure 5.18 B**).

Although no statistically significant associations were found between DPA content and CIMP status, in carrier-treated cells a greater range of DPA content was observed in CIMP- cells (0.24 – 1.30 µg / million cells) than in CIMP+ cells (0.15 – 0.30 µg / million cells) [**Figure 5.18 C**]. The same was observed following 5µM EPA treatment, with the DPA content in CIMP- cells ranging from 0.29 – 2.62 µg / million cells) and content in CIMP+ cells ranging from 0.13 – 0.74 µg / million cells) [**Figure 5.18 D**]. The relationship between DHA content and CIMP status mirrors that observed between CIMP status and DPA content, with no statistically significant associations identified [**Figure 5.18 E and F**].

I next tested the effect of DAC and EPA combined treatment on the FA content of cells.

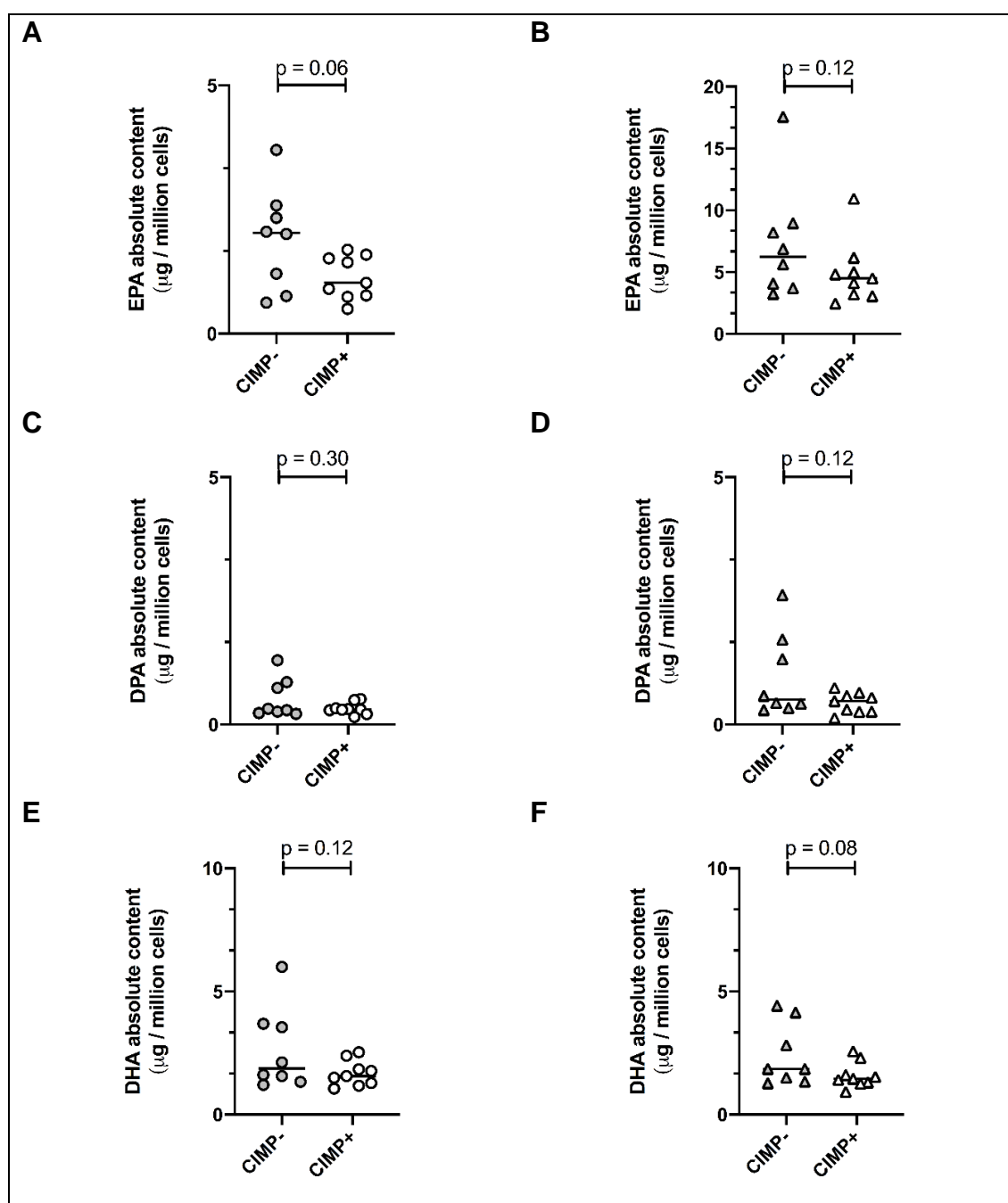


Figure 5.18. Relationship between CIMP status and *n*-3 PUFA content in hCRC cells

N-3 PUFA content of human CRC cells differing in CIMP status, obtained by LC-ESI-MS/MS. Baseline content of ethanol carrier control cells was measured for; EPA (A), DPA (C) and DHA (E). Following supplementation with 5 μM EPA, the content of EPA (B), DPA (D) and DHA (F) was measured. FA content in ethanol carrier control cells is represented by \bullet in CIMP- cells and \circ in CIMP+ cells, and in 5 μM EPA treated cells is represented by \blacktriangle in CIMP- cells and \triangle in CIMP+ cells. Content is presented as the mean μg /million cells for 3 independent biological replicates. Statistical analysis shown is Mann-Whitney comparison of median values which are indicated on each plot by the lines.

5.3.7. Impact of decitabine pre-treatment on *n*-3 PUFA content of hCRC cell lines in the presence or absence of EPA supplementation

To test the effect of DAC combination treatment on the *n*-3 PUFA content in CIMP+ and CIMP- cell lines, HCT116 CIMP+ and LS174T CIMP- cells were selected.

When HCT116 and LS174T cells were treated with carrier control or 1 μ M DAC alone there was no change in EPA, DPA or DHA absolute amount in cells (Student's T-test $p > 0.05$, **Appendix A5.7**), which confirmed that the carrier and DAC treatments were not altering FA content. As observed previously, untreated CIMP- LS174T cells displayed a greater amount of each *n*-3 PUFA than untreated CIMP+ HCT116 cells.

Following 5 μ M EPA exposure, the amount of EPA measured in the cells increased significantly as expected (carrier-treated cell content: HCT116 = 0.47 ± 0.43 μ g/million cells, LS174T = 1.33 ± 0.57 μ g/million cells; EPA treated cell content: HCT116 = 4.68 ± 0.79 μ g/million cells, LS174T = 4.43 ± 0.45 μ g/million cell) [**Figure 5.19 A and D**]. An increase in *n*-3 PUFA was also measured when cells were treated with 1 μ M DAC in combination with 5 μ M EPA compared to carrier-treated cells for both cell lines (Student's t-test = 0.005). However, there was less EPA (absolute amount) in CIMP+ HCT116 cells treated with the DAC/EPA combination compared with EPA alone ($p = 0.015$), but not in the CIMP- LS174T cells ($p = 0.12$) [**Figure 5.19 A and D**].

As EPA resistant cells were shown to have greater DPA content upon EPA supplementation, I proposed that DAC exposure would increase DPA content in CIMP+ cell lines following EPA treatment compared to EPA alone. Following treatment with 5 μ M EPA the increase in DPA content compared to carrier-treated cells was statistically significant (T-test, HCT116 $p = 0.005$ **Figure 5.19 B** and LS174T $p = 0.03$, **Figure 5.19 C**) as seen in previous experiments. DPA content was higher in HCT116 cells treated with combined DAC and EPA compared to carrier treated; 0.36 ± 0.09 μ g/million cells versus 0.14 ± 0.13 μ g/million cells respectively, Student's t-test $p = 0.04$). However, DPA content was significantly greater (Student's t-test, $p = 0.02$) in EPA only treated cells compared to the cells treated with DAC and EPA. In contrast, LS174T cells treated with combined DAC and EPA had similar DPA content to carrier treated cells (Student's t-test, $p = 0.48$), and lower DPA content than those treated with EPA only. This difference was not statistically different, Student's t-test, $p = 0.22$).

DAC exposure had no effect on DHA content following EPA supplementation in either cell line, as shown in **Figure 5.19 C and F**.

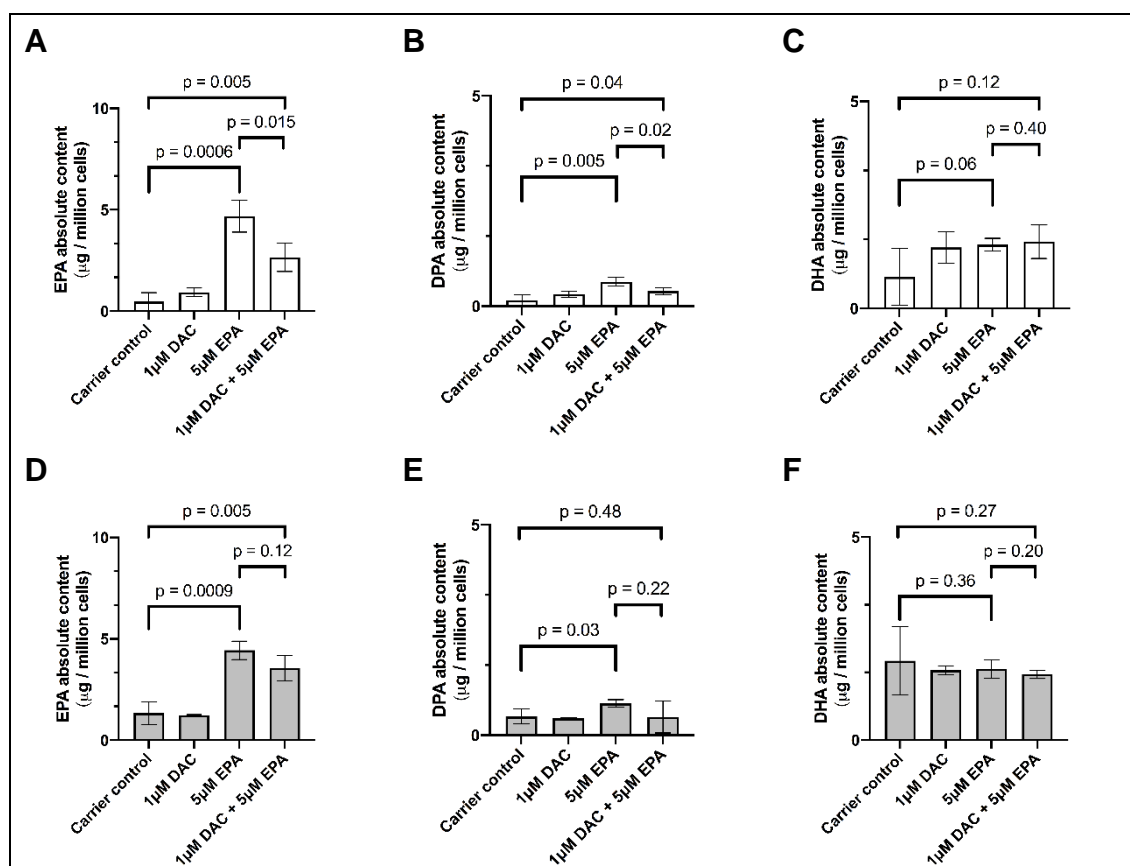


Figure 5.19. Effect of DAC pre-treatment on EPA, DPA and DHA content

N-3 PUFA content of CIMP+ HCT116 (□) and CIMP- LS174T (■) cells, obtained by LC-ESI-MS/MS. EPA (A, C), DPA (B,D) and DHA (E,F) absolute content of cells treated with carrier control, 1 μM DAC, 5 μM EPA and 1 μM DAC + 5 μM EPA was measured. Content is presented as the mean $\mu\text{g}/\text{million cells}$ for 3 independent biological replicates. T-tests were used to compare the groups.

To summarise, in comparison to the EPA amount in EPA-only treated cells, combination with DAC treatment resulted in a statistically significantly lower EPA content in CIMP+ cells. The difference between EPA content of EPA-only and DAC/EPA treated CIMP- cells was not statistically significant. This would suggest that CIMP+ cells treated with DAC/EPA were ‘using’ EPA, whereas the CIMP- cells were storing EPA.

I have shown that treating CIMP+ cells with DAC decreased sensitivity to EPA (**Chapter 4.3.7**) and that innately EPA-resistant cells had higher DPA content following EPA exposure (**Chapter 5.3.5**). DPA content of CIMP+ cells following DAC/EPA exposure was significantly less than in EPA-only treated cells. No significant difference in DPA content of CIMP- cells was detected between EPA-only and DAC/EPA treated cells. Therefore, the DPA content data does not indicate that CIMP+ cells were more resistant to EPA in the presence of DAC due to the conversion of EPA to DPA. It is therefore proposed that the presence of DAC facilitates expression of a gene with a role in EPA metabolism.

5.4. Discussion

This chapter aimed to examine the extent to which FA content of cells could explain intrinsic differences between *n*-3 PUFA sensitivity. I hypothesised that FA content of cell lines treated with *n*-3 PUFAs would be associated with inherent EPA or DHA sensitivity of the cell lines and that EPA sensitivity would be correlated with their ability of cells to convert EPA to DHA.

Using an established analytical method to measure FAs in CRC cell samples (192), I measured FA profiles of ethanol carrier-treated cells and following supplementation with different concentrations of EPA or DHA in 17 hCRC cell lines. Combining the FA profile data with defined cell line properties reported in Chapter 4 has allowed for associations to be tested between known cell properties including *PTGS* expression and *n*-3 PUFA sensitivities, and differences in cellular response to *n*-3 supplementation.

5.4.1. Key findings

The most prevalent FA measured across the cell line samples and all treatment groups was PA, with a mean content of 21.47 ± 7.40 %, comparable with the published data in human tissues. PA is the most common FA found in the human body, representative of between 20 and 30 % of total FAs measured in membrane phospholipids and adipose triacylglycerol (279).

I found that across the 17 hCRC cell lines for which EPA content was measured in ethanol treated pellets, the mean content was 1.93 ± 0.47 %. There was a higher baseline percentage of DHA, 4.36 ± 1.32 %. The data has shown a concentration dependent increase following culture in media containing varied EPA or DHA concentrations, seen previously in other studies (192, 280, 281). Previous work demonstrated MC38 mouse CRC cells displayed a concentration dependent increase in cellular EPA content, when treated with EPA-FFA. Low EPA levels were detected in carrier control treated MC38 cells, 1.98 ± 0.18 % (192), comparable to the mean content obtained in this study. A study to investigate the effects of 230 μ M EPA and 200 μ M DHA treatment on breast cancer cell lines MCF-7 and MDA-MB-231 analysed FA content by HPLC/GC. At baseline they found EPA content of 3.2 ± 1.0 % (MCF-7), 2.4 ± 0.7 % (MDA-MB-231), DHA content of 5.7 ± 2.4 % (MCF-7) and 7.7 ± 1.6 % (MDA-MB-231) and the effect of treating cells with EPA or DHA resulted in an increase in the respective content (281). These findings are comparable to the data presented in this chapter.

It should be stressed, that when comparing my data with other studies there are challenges due to no standardised reporting system for presenting GC-MS or LC-ESI-MS/MS data. Despite published best practice guidelines being developed specifically for trials involving FAs, it is not a mandatory requirement for publication (282). Implications of comparing results is complex due to; different formulations of FA used in different studies, differing FA extraction techniques, FA panel composition (which has implications specifically for relative quantities), analysis techniques and reporting of data.

Data were expressed as relative percentage and matched other published data. For example, treating cells with increasing concentrations of EPA or DHA results in a concomitant decrease in relative AA content (192, 274, 281). An example of this phenomenon was shown in breast cancer cell lines, MCF-7 and MDA-MB-231, whereby a reduced AA content was reported following treatment with EPA and DHA and subsequent HPLC/GC analysis of *n*-3 incorporation into the membrane. Baseline AA content was $14.4 \pm 2.9 \%$ and $12.7 \pm 2.9 \%$ for MDA-MB-231 cells and MCF-7 cells, respectively. Following 230 μM EPA treatment the AA content was $2.6 \pm 0.9 \%$ and $3.1 \pm 0.6 \%$ and following 200 μM DHA treatment AA content was $3.9 \pm 0.5 \%$ and $3.2 \pm 0.6 \%$ (for MDA-MB-231 and MCF-7, respectively) (281).

Although a decrease in AA content resulting from exogenous EPA or DHA addition was observed when AA content was expressed as relative FA percentage, expression of data as an absolute AA amount of AA did not identify this decrease in every cell line. Interestingly, the results showed that an individual cellular response to EPA and DHA are different in terms of AA content although the increase or decrease in AA contents measured were not shown to be statistically significant. Only 4/17 cell lines displayed a decrease in AA absolute quantity following EPA treatment, however DHA treatment in 11/17 cell lines corresponded with a decrease in AA content. Some cell lines were shown to have increased AA content following EPA / DHA supplementation, the cause is not known or previously reported. This highlights that for each of *n*-3 PUFAs tested, cells don't exhibit the same response, and AA levels are impacted differently. This could be indicative of the different mechanisms through which EPA and DHA are stored in the cell membrane, interact with and/or utilised and metabolised by cells. These findings are important and provide evidence to support the reassessment of AA % FA data particularly in the context of EPA-supplementation clinical trials and where AA/EPA ratios have been calculated.

No studies have reported a comparison between EPA and DHA effects on AA as an absolute quantity and therefore, as data has relied heavily on % FA data there are no

comparable studies for this work. The concept of presenting data as relative percentage versus absolute quantity has been addressed in other works, which confirm complexities of extrapolating and interpreting such data. One study reported that interpretation of FA data when compositions are reported as concentrations or as a percentage can differ. It stated that concentration dependent values having the benefit of showing amounts of individual FAs independent of each other (283). However, contradicting this, a more recent study by Miura *et al* investigated the differences in associations of plasma *n*-3 and *n*-6 PUFAs with all-cause mortality (284). The study measured baseline plasma phospholipid FA levels by gas chromatography and reported EPA, DPA, DHA, total long-chain omega-3 FAs, LA, AA, and total omega-6 FAs as both absolute (concentration) and relative (percentage) data. It found that the directions and magnitude of associations with all-cause mortality of absolute and relative amounts were comparable, with an inverse association between *n*-3 PUFA plasma content and risk of mortality. They suggested that expressing the data as absolute concentration was preferential to allow ease of comparison with other studies, and since relative units could be deduced from absolute values (284). However, that said, the relative units would only be comparable with other studies who have limited FA profiling to the same selected FAs.

There have been no *in vitro* studies that have assessed the relative sensitivity to an *n*-3 PUFA and the relationship with measured FA content. I have found that an association exists between cells with higher EPA or DHA IC₅₀ values and lower respective EPA or DHA content. This association was shown to be more pronounced in the context of EPA.

No associations between *PTGS1* and / or *PTGS2* gene expression and EPA or DHA content were identified. Although a study found a link between low *PTGS2* expression in HT29 cells and no growth effect following EPA treatment, and high *PTGS2* activity in CaCo-2 cells and inhibition of cell proliferation (158), this contradicts the EPA sensitivity data collected in this study previously presented in Chapter 4. Another study by Priman *et al*, found that despite a similar level of *PTGS2* expression in the non-small cell lung cancer (NSCLC) cell lines A549 and H596, the EPA content following 25 µM, 50 µM and 100 µM EPA treatment and measurement by matrix-assisted laser desorption/ionization (MALDI) mass spectrometry were different, with 4-fold greater EPA content in A549 cells (285). Published data identified a link between low *PTGS2* expression and sensitivity to EPA has been shown (178). Tumour growth was facilitated by CT26 and COX^{low}-CT26 (CRISPR-Cas9 targeted deletion of *Ptgs1* and *Ptgs2*) cell implantation in *Balb/c* mice, providing a model of CRCLM. The tumour burden was significantly reduced by 30 % in tumours derived from COX^{low}-CT26 compared to 10% for CT26-tumours, following a period in which the mice were fed an EPA-rich diet (178). In tumour tissue collected from

both tumour types, a similar EPA content was noted (178). My data agrees with Priman *et al*, no significant correlation was found between COX expression and EPA content.

hCRC cell lines following supplementation with DHA did not exhibit an increase in EPA, whereas an increase in EPA ranging from 49 % to 130 % following DHA supplementation has been measured in blood and tissue specimen, a proposed result of retro-conversion via β -oxidation (286). This highlights differences when comparing *in vitro* and human data. Despite observing greater sensitivity to DHA compared with EPA in all cell lines, I did not measure an accumulation of DHA in the more EPA-sensitive cell lines, which would indicate EPA to DHA conversion. However, this may be a method limitation and carbon isotope tracer studies may provide further insight. A RCT (NCT03378232) tested the effect of 3 g / day supplementation with purified EPA (containing a higher carbon-13 isotopic abundance ($\delta^{13}\text{C}$)-EPA than plasma EPA) for 12 weeks in 89 subjects. Whilst DHA plasma concentration, measured by GC-flame ionization detection, did not change following EPA supplementation, an increase in $\delta^{13}\text{C}$ -DHA was evident (287). They proposed that metabolic conversion of the EPA supplement was responsible for a majority of DHA present at the end of the trial period (287). In agreement with my finding that a higher DPA content was found in cells less sensitive to EPA, this study demonstrated a 200 % increase in DPA content following supplementation with EPA (287). Conversion of EPA to DPA by less EPA-sensitive cells suggests that they may metabolise EPA into the less biologically active metabolite DPA.

DPA has been less frequently studied as an individual *n*-3 PUFA in comparison to EPA and DHA, in part due to lower abundance in natural sources of *n*-3 PUFAs (288). Treatment of breast cancer cell lines MCF-7 and MDA-MB-231 with EPA also resulted in an increase of DPA content from a baseline content of 1.1 ± 0.7 % and 7.0 ± 1.1 % to 15.8 ± 3.3 % and 33.3 ± 1.8 % following EPA treatment (for MCF-7 and MDA-MB-231, respectively) (281). DPA content has been seen to significantly increase in mouse adenocarcinoma cell line CT26 following 50 μM EPA treatment (288), data which supports the finding that EPA-resistant cell lines, of which CT26 is one, accumulate DPA.

This chapter has shown a lower EPA content in CIMP+ cells at baseline, and following 5 μM EPA treatment, compared to the CIMP- cells. EPA sensitive cells store less EPA than EPA resistant cells. EPA resistant cells had increased DPA quantities. When FA content was measured in CIMP+ cells treated with combined EPA and DAC, which I have demonstrated are less sensitive to EPA, cells had lower EPA content compared with EPA only treated cells. DPA content also increased in combination treated cells compared to carrier-control treated cells but was lower than EPA only treated cells. This

contradicted previous findings, that found greater DPA content measured in cells with higher EPA IC₅₀ values. The results indicate that EPA sensitivity is controlled by multiple mechanisms, and that they differ between the inherently resistant cell lines and cell lines in which resistance has been acquired (through epigenetic drug exposure). It is hypothesised that DAC treatment of CIMP+ cell lines, results in a resistance-mediating gene being expressed. However, further study is required to elucidate the genes involved in increasing resistance to EPA treatment, which is discussed below.

5.4.2. Strengths and Limitations

A major challenge was that a wide range of IC₅₀ concentrations for EPA and DHA led to a complicated experimental design and difficulties in comparable analysis of data. By opting to treat cells with a 'high' concentration approximate to individual cell line IC₅₀ value, comparison between content is difficult as greater exogenous FA added results in a greater amount detected. However, the alternative of setting a universal 'high concentration' for which all cell lines were tested would also be confounded due to the inherent sensitivities of the cell line

As mentioned in **Section 5.3.1**, the measured concentrations of FAs present, in many cases, exceeded the range measured for the standard curve. Therefore, sample values were determined based on assumed standard curve linearity and thus the data reported within this chapter are subject to further validation. A strength of this work is the number of CRC cell lines analysed, using a concentration equivalent to clinical supplementation and a 'high' concentration, and using 2 independent *n*-3 PUFAs: EPA and DHA. This allowed for comparisons between *n*-3 PUFAs and confirmed that the cellular response to each FA is independent and cannot be predicted by response to a different FA.

Another strong attribute of this work is reporting the data as an absolute quantity, as this has enabled the discovery of new relationships between the effect of EPA or DHA treatment and FA profiles to be shown. Reporting absolute quantity relative to number of cells is not frequently used as it is time-consuming, especially when considering large numbers of samples. However, using absolute quantity data has shown particular importance in the identification of the differential relationships between EPA and DHA treatment on AA absolute content and EPA treatment effect on DPA content.

Finally, time and monetary expense of LC-ESI-MS/MS limited samples tested containing DAC and EPA treated cells to just 1 set of CIMP+ cells and 1 set of CIMP- cells and this data requires further validation.

5.4.3. Future Directions

Importantly, it is the priority to assess the linear range for each FA standard to confirm and corroborate FA quantification (this is in progress). Once achieved, the next step would be to expose the cell lines to a range of concentrations and assess the implications of supplementation based on the sensitivity profiles.

I would test many more types of cancer cell line to perhaps elucidate weak correlations identified. The first step would be to establish inherent sensitivity of cell lines and then compare cellular FA content following EPA and DHA supplementation.

In addition, metabolic properties of cell lines should be established, confirming expression of not only *PTGS* enzymes, but other enzymes involved in FA metabolism such as lipoxygenases (5-, 12-, 15-lipoxygenase) and cytochrome p450. This work could include measuring the relative ability of cell lines to break down FAs by β -oxidation, by use of a FA oxidation assay kit. Quantification of *ELOVL2*, *ELOVL5* and *FADS2* at an mRNA level, by RT-qPCR and at protein expression level by western blot would also be a next step. Tracer studies should be utilised in future work to quantify the proportion of exogenously added EPA or DHA that is incorporated versus metabolised as fuel or lipid mediators. Whilst tracer studies are predominantly found in *in vivo* study, there are reports of stable isotope-labelled tracers used in cell culture, for example detection of [U-¹³C] LNA metabolites in Y79 retinoblastoma cell lines (289). These investigations would potentially show why some cell lines convert EPA to DPA and may elucidated the relationship between EPA supplementation and subsequent DHA content.

Testing more cell lines to quantify AA content following treatment could corroborate the findings that not all cell lines see a decrease in AA content in response to *n*-3 PUFA supplementation. In addition, further data to support the relationship between EPA sensitivity and DPA content could be obtained. FA content analysis completed in a greater number of cell lines following treatment with relevant controls, and DAC in combination with EPA, would allow solid conclusions to be made.

I would test the associations, particularly between EPA supplementation, *n*-3 PUFA response and the absolute AA and DPA content in more *in vitro* and *in vivo* models and patient samples. FA profile and response data from the EMT study (274) could be utilised in the first instance to assess the relationship between response and specific EPA, DPA and AA profiles. Furthermore, the data from the ongoing EMT2 study (176) could be used to assess response, FA profiles and relationship to molecular phenotypes.

Chapter 6: Investigating CRC cell response to *n*-3 polyunsaturated fatty acids using isogenic clones with acquired resistance

6.1. Introduction

Chapters 4 and 5 identified trends in phenotypes and FA profiles that were potentially indicative of hCRC cellular responses to *n*-3 PUFAs. However, no specific molecular targets were associated with the response.

As previously described, sensitivity can be defined as ‘the ability of a population, an individual or a tissue, relative to the abilities of others, to respond in a qualitatively normal fashion to a particular drug dose’ (290). To understand why hCRC cells display differing sensitivities, and gain insight into molecular mechanisms underlying cellular response to *n*-3 PUFAs, I employed methods frequently used to understand drug-resistance, particularly to cancer chemotherapeutic agents. In this chapter, I aimed to identify molecular markers associated with *n*-3 PUFA sensitivity or resistance, using isogenic cell clones with acquired resistance

Section 6.2 is focused on investigating an orphan GPCR that was identified as differentially expressed in EPA-sensitive and EPA-resistant mouse CRC cells. Section 6.3 describes generation of hCRC cell lines resistant to EPA or DHA.

6.1.1. Identification of *Mrgprf*, a novel orphan G protein coupled receptor (GPCR)

I used a pair of established isogenic mouse CRC cell lines, to study molecular mechanisms underpinning the response of CRC cell lines to *n*-3 PUFAs *in vitro*. Previous work had shown that mouse colorectal cancer cell lines, MC26 and MC38, demonstrated differential EPA sensitivity and a concentration-dependent growth inhibition found in both an *in vitro* and *in vivo* setting. MC26 cells had a higher IC₅₀ of 241.8 ± 1.1 µM compared with MC38 cells, which had an IC₅₀ of 38.0 ± 3.4 µM (178). Transforming growth factor (TGF)-β was used to chemically attract a migrant population of MC38 cells, which led to isolation of a motile, EPA-resistant sub-population henceforth referred to as MC38r cells. MC38r cells were shown to be four-fold more resistant to EPA-FFA than parental MC38 cells (178)

To identify molecular drivers of sensitivity and resistance, a whole mouse genome expression microarray was performed (prior to the beginning of this PhD project),

combining comparative differences in gene expression between MC38 cells with and without EPA supplementation (array 1), and between MC38 (EPA-sensitive) and MC38r (EPA resistant) cell lines (array 2).

Table 6.1. Candidate genes identified by microarray analysis of mouse CRC cells

Gene	Name	Proposed Function	Array 1: EPA driven expression	Array 2: EPA resistance expression
<i>Lox</i>	Lysyl oxidase	Collagen cross-linking	↑	↓
<i>Col6a1</i>	Collagen	Extracellular matrix	↑	↓
<i>P4ha1</i>	Prolyl 4-hydroxylase α	Folding of collagen chain	↑	↓
<i>Mrgprf</i>	Mas-related GPCR F	Orphan GPCR	↑	↓
<i>Angpl6</i>	Angiopoietin-like 6	Chemo-attraction and inflammation	↓	↑
<i>PTGS-1</i>	Cyclooxygenase-1	PG metabolism	NSC	↑
<i>Erk1/2</i>	Extracellular signal regulated kinase	MAP kinase signalling	NSC	↑

Arrows indicate relative change in expression related to EPA driven or EPA resistance, namely ↑ (increase) ↓ (decrease), NSC; no significant change. GPCR; G protein coupled receptor. PG; prostaglandin. MAP; mitogen-activated protein.

By combining array datasets, it would strengthen the output genes to be selective to their possible roles in mitigating cellular response to EPA. The 7 top differentially expressed candidate genes, with a potential role in EPA sensitivity, are shown above in **Table 6.1**.

6.1.2. Mas-related G protein coupled receptor, F (*Mrgprf*)

In comparison to *Lox*, *Col6a1*, *P4ha1* and *Angptl6*, which are more likely linked to mechanisms associated with metastatic cell potential, such as epithelial-mesenchymal transition, *Mrgprf* is an orphan (no known ligand) GPCR. Therefore, *Mrgprf* was selected as a candidate gene with a likely role in EPA sensitivity. The microarray evidence shows a 2.2-fold increase in expression in MC38 EPA-treated cells compared to untreated, and a 3.4-fold downregulation of *Mrgprf* in MC38r cell compared with MC38 cells (291).

The gene, *Mrgprf*, is translated into the protein form which is denoted as MRGPRF. MRGPRF belongs to a GPCR family named MAS-related G protein coupled receptors (Mrgprs), comprising approximately 40 members (292). The literature currently suggests

that, although many of these *Mrgpr* family GPCRs are yet to be characterised, those which have been have a role in pruriception (sensation of itching) (293) and nociception (sensation of pain) (294) and are predominantly expressed in primary sensory neurons and mast cells (293).

MRGPRF has previously been detected in the small and large intestine (292), and it was recently reported that a different *Mrg* family member, *Mrgpr* C11, was found to have a role in the gut nociceptive innervation of the mouse colon (295).

6.1.3. G protein coupled receptors

GPCRs are a diverse range of proteins expressed on all cells of the body (296). Binding of specific ligands to their GPCRs leads to signal transduction. Upon binding, GPCRs undergo conformational changes that activate heterodimeric G $\alpha\beta\gamma$ guanine-nucleotide binding proteins (G proteins) (296-298). The α -subunit is bound by GDP, but upon ligand binding this is released and GTP can bind, physically displacing GDP and resulting in the detachment of the subunit from the complex. The resulting GTP-G α or G $\beta\gamma$ -complexes can alter activities or transduce signals depending on the environment they are present in, summarised in **Figure 6.1** (296, 297).

6.1.3.1. GPCR downstream signalling pathways

G α subunits are divided into four families; G $_s$, G $_i$, G $_q$ and G $_{12}/G_{13}$ which each produce signalling in different ways (296, 298). Activation of G $_s$ results in cyclic adenosine 3',5'-monophosphate (cAMP) production, which has multiple activities including protein kinase A (PKA) activation. cAMP activates Rap which are small guanosine triphosphatase (GTPase) molecules (299). G $_i$ activation inhibits adenylyl cyclase, which in turn inhibits cAMP production (299). Upon activation of G $_q$, which are coupled to phospholipase C, signal transduction mediated by calcium is stimulated (200, 299). Activation of calcium signalling, through stimulation of receptors coupled to phospholipase C (PLC), causes breakdown of phosphatidylinositol 4,5-bisphosphate to inositol 1,4,5-triphosphate (IP3), which, in turn, precedes a biphasic calcium ion (Ca $^{2+}$) signal (200). Diacylglycerol is also produced due to G $_q$ stimulations, and this recruits protein kinase C (PKC) (299). Signalling via the calcium pathway results due to a release of intracellular Ca $^{2+}$ stored within the endoplasmic reticulum (ER) of cells, and by enhanced entry across plasma membrane (200). G $_{12}/G_{13}$ activation regulates RhoGEF (Rho guanine nucleotide exchange factor) –mediated activation of RhoA (a small GTPase) (296).

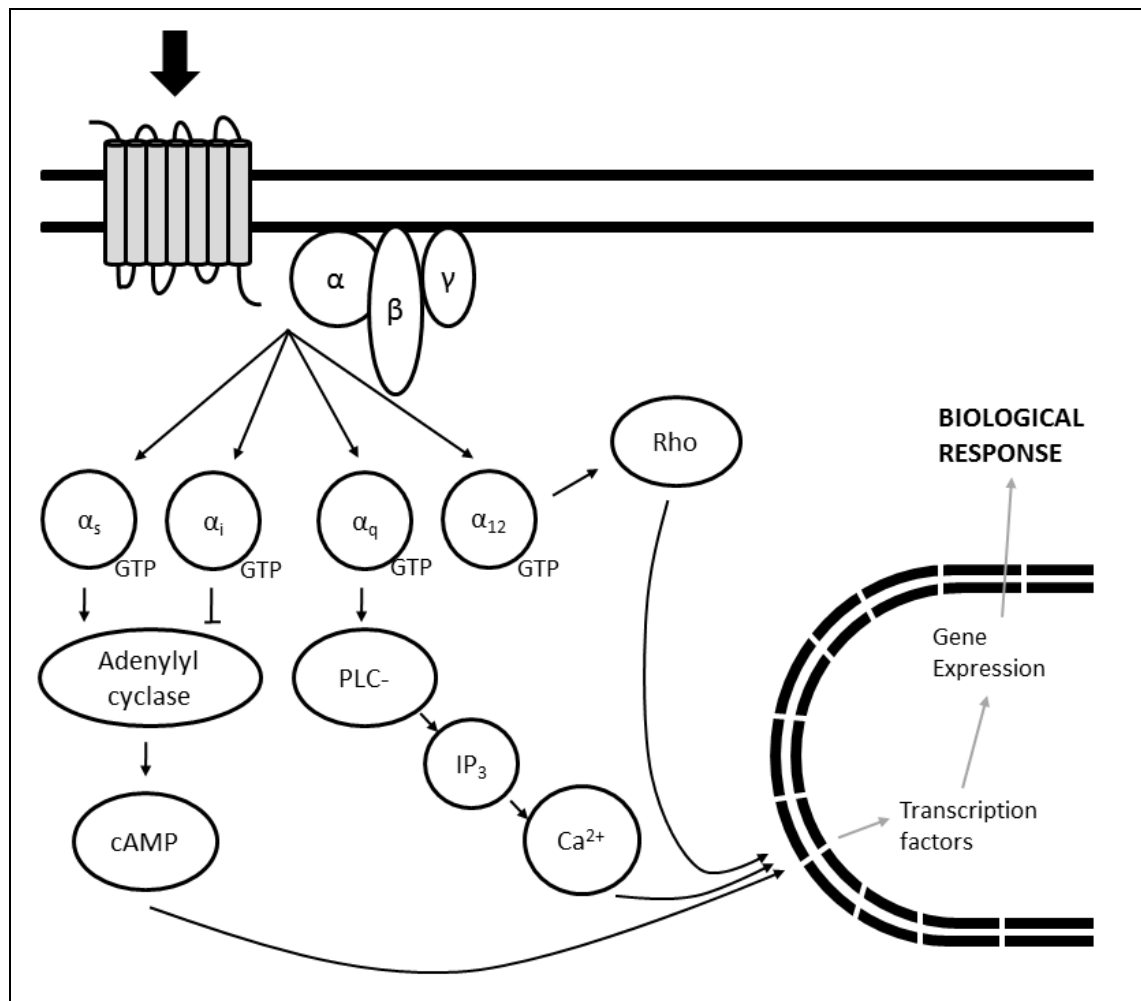


Figure 6.1 G protein coupled receptor signaling pathways

Ligands (↓) can bind GPCRs to stimulate membrane, cytoplasmic or nuclear targets. GPCRs interact with heterotrimeric G proteins composed of α , β and γ subunits. There are several G α subtypes (G α_s , G α_i , G α_q , G α_{12}) as shown in the diagram with multiple effectors that result in downstream signal transduction and leads to a plethora of biological responses. Ca²⁺: calcium, cAMP: cyclic adenosine 3',5'-monophosphate, GTP: guanosine triphosphate, IP₃: inositol 1,4,5-triphosphate, PLC: phosphatidylinositol 4,5-bisphosphate. Image adapted from Dorsam *et al*, 2007 (297).

6.1.4. Drug resistance in colorectal cancer

Standard treatments for CRC involve combinations of chemotherapies that involve the drugs; irinotecan or oxaliplatin in combination with the mainstay of treatment for CRC patients, 5-fluorouracil (5-FU). However, drug resistance frequently limits clinical efficacy of these treatments. Approximately 50 % of patients demonstrate resistance to 5-FU (300), and there is a reported 30 - 50 % objective response for combined therapies in patients with metastatic disease (301). Jensen *et al*, sought to establish and characterise cell line models of resistance; utilising HCT116, HT29 and LoVo cells and subjecting the cells to chronic exposure to oxaliplatin or SN-38 (the active metabolite of irinotecan) (301). Cells were continuously cultured in gradually increasing drug concentrations

ranging from 0.01 μM to 20 μM oxaliplatin, and 1 nM to 80 nM SN-38, for a period of 8 to 10 months, and subsequently drug sensitivities were measured for the parental and drug resistant cell lines (301). They found that the cell lines had acquired resistance to both drugs. Oxaliplatin resistant cell lines were between 13 and 107 times more resistant to the drug than parental cells, and SN-38 were 20 to 68 times more resistant than the cell line of origin (301). The generation of drug-resistant clones allowed for down-stream transcriptome analysis to identify resistance biomarkers. Other studies have also utilised these cell lines for work involving generating resistance to oxaliplatin and SN-38 (302, 303).

6.1.5. Investigating *n*-3 PUFA resistance in colorectal cancer cell lines

Although the literature does report variable sensitivity of CRC cell lines to *n*-3 PUFAs, as outlined in Chapters 1 and 4, it does not report any attempts at generating *n*-3 PUFA resistant counterparts to sensitive cells. I utilised the panel of hCRC cell lines, with variable sensitivities to EPA and DHA (Chapter 4), to generate resistance [Figure 6.2].

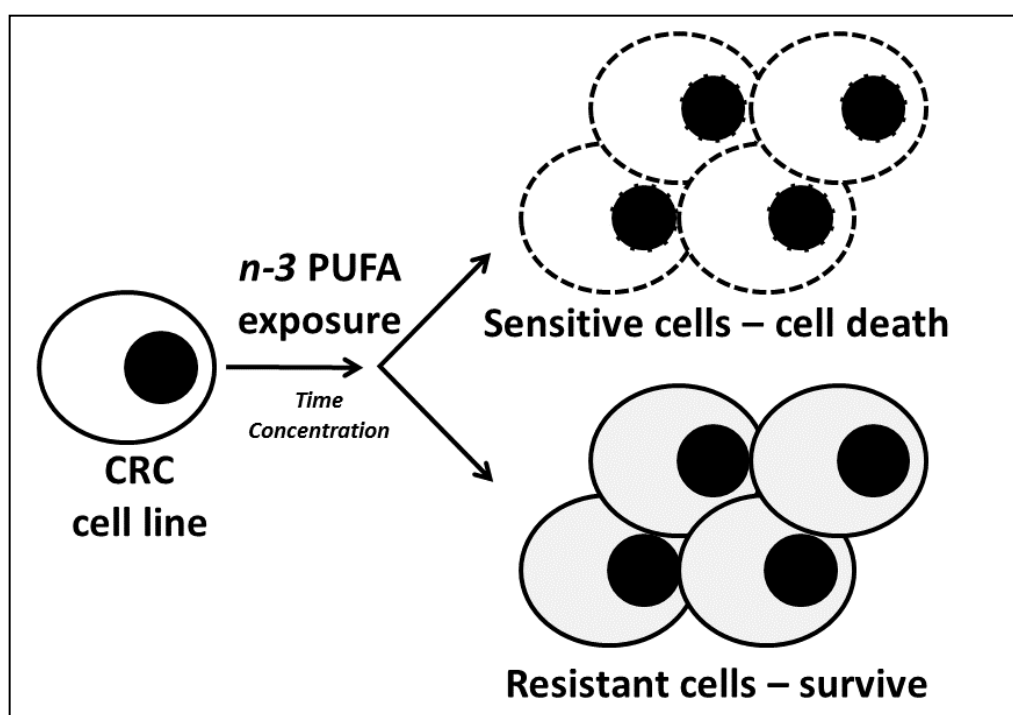


Figure 6.2 Generating *n*-3 PUFA resistant cell lines

A diagrammatic representation of generating a cell line resistant to *n*-3 PUFAs. Sensitive cells within a population would die, however any cells that adapt to conditions with increased *n*-3 PUFA would allow an established resistant population to develop.

6.2. Chapter Objectives:

The first aim was to establish whether MRGPRF had a role in determining EPA sensitivity. The second aim was to generate hCRC cell lines with acquired resistance to EPA and DHA; to both validate MRGPRF as a candidate gene, and to create comparable models in which to study similarities and differences in EPA and DHA sensitivity. To address these aims, the following objectives were set:

- To create *in vitro* models of MRGPRF overexpression in mouse CRC cell lines
- To validate MRGPRF overexpressing cell lines by confirming gene expression as well as protein functionality and EPA sensitivity
- To generate and characterise resistant clones of sensitive hCRC cell lines by chronic exposure to EPA (and DHA), in order to:
 - Confirm the MC38 / MC38r data in an EPA-specific human model
 - Expand the study of resistance to DHA

6.3. Results I: Investigating the potential role of MRGPRF in EPA sensitivity

I started the process of generating *Mrgprf* over-expression cell models during my MSc project (185). A summary is included in section 6.3.1, **Figure 6.3**. When discussing transient cell lines, the transfected vector will be denoted with a subscript 'V' (e.g.: CT_V or MF_V). When discussing stably transfected cell lines, the vector will be denoted by subscript 'VL' indicating that the vector is linearised in this model (e.g.: CT_{VL} and MF_{VL}).

6.3.1. Selection of MRGPRF overexpressing clones

Two cell lines were transfected with plasmid DNA, pcDNA3.1 msMRGPRFHis-P2A-eGFP [**Figure 3.3, Chapter 3.7**] (or empty control vector (pcDNA3.1 His-P2A-eGFP), following restriction enzyme digestion to create a linear DNA insert.) The cell lines used were HEK293 (human embryonic kidney cells, for ease of transfection) and MC38, a model of mouse CRC.

Following 24h incubation after lipofectamine transfection, efficiency of plasmid uptake was determined by observing the absence or presence of enhanced green fluorescent protein (eGFP) expression by fluorescence microscopy. More efficient transfection was seen for both cell lines containing control vector (CT_{VL}) as opposed to MRGPRF vector (MF_{VL}). When comparing transfection efficiency between cell lines, approximately 80 % HEK293 cells were found to express eGFP, in contrast to just 1 % of MC38r cells following vector transfection.

To create stable cell models in which MRGPRF was overexpressed, cells were cultured in media containing the antibiotic, G-418. This applied selective pressure and removed untransfected cells within the population to facilitate the expansion of the cells successfully containing vector. These originator cells, and any subsequent daughter cells, possess the neomycin resistance gene. The cells underwent a sterile cell sort, which gated cell populations by fluorescence intensity. This process finished with cells being plated in a 96 well plate containing 1000 cells, 200 cells or 1 cell per well. It was noted that the stress and isolation of cells seeded at 1 cell per well resulted in limited survival potential and thus a small number of clones that might be isolated.

Cell sort data were consistent with transfection efficiency observed fluorescence images. A greater number of HEK293 cells were shown to express eGFP when compared with

MC38r transfected cells. During the cell sort, MC38r cells had fluorescence detectable in 3 % of the population, but with a 1-2 log shift in measured fluorescence in transfected cells in relation to untransfected MC38r cells [Appendix A6.1]. Furthermore, once the cell sort was completed, the maintenance and survival of cells in 500 μ M G-418 treated media confirmed success of transfection.

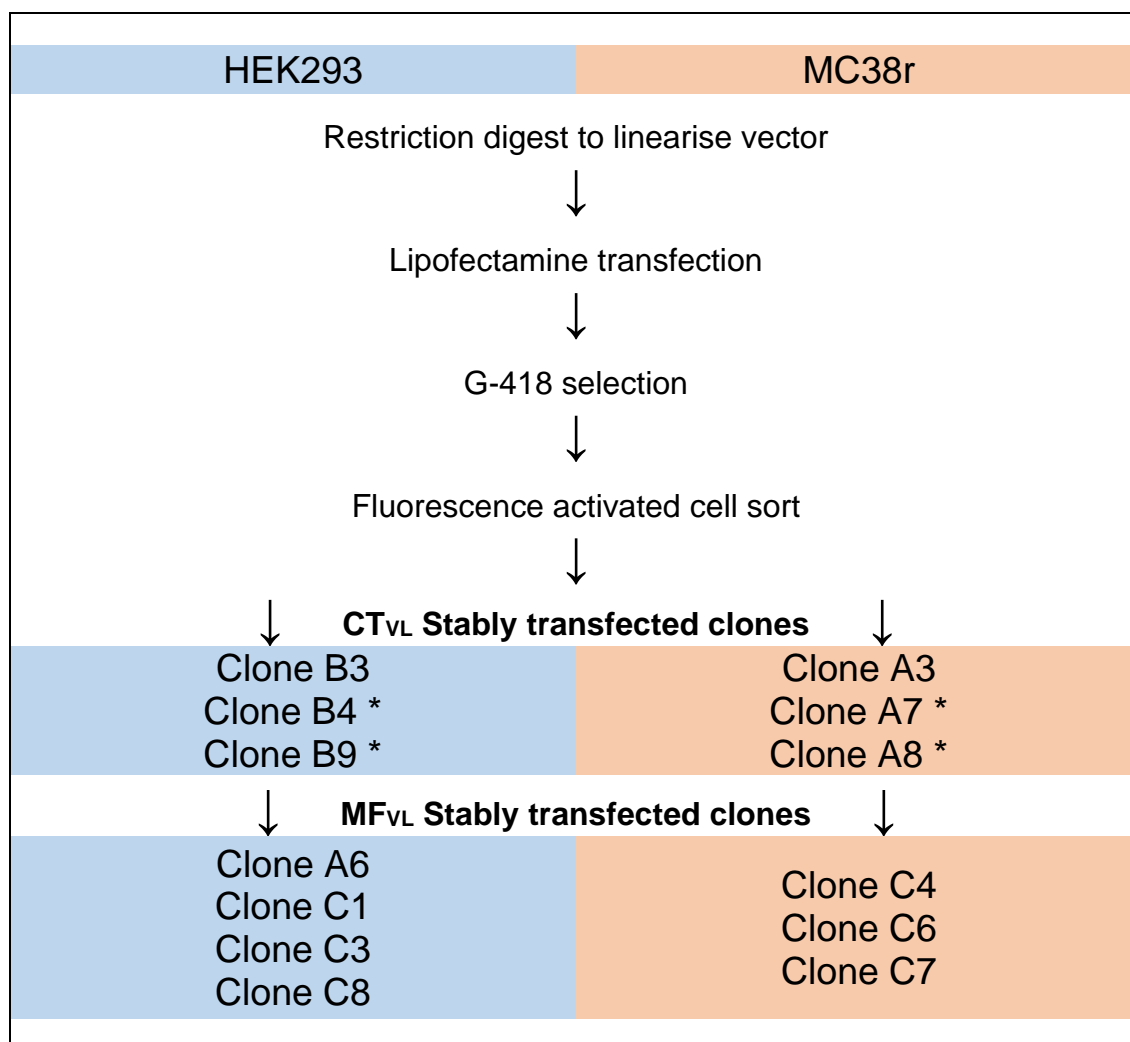


Figure 6.3 Generation of MRGPRF stable overexpressing cell lines

Schematic representation of the process by which stably transfected clones were created, with blue and pink labelling to signify HEK293 or MC38r transfectants, respectively. Clones were named according to the positioning on the 96 well plate following FACS. Clones denoted with an asterisk (*) were the product of a second cell sort in which a mixed population from the original cell sort was expanded before single cells were separated to give rise to single-cell clones.

Successful transfections and the subsequent cell sort resulted in single cell clones and mixed populations of cells containing control or MRGPRF vector. The mixed population was further utilised to generate additional single cell clones after it was noticed that the original HEK293-CT_{VL} clone B3 was displaying abnormal, clustered growth patterns. The figure above [Figure 6.3] shows single cell clones created during this process.

6.3.2. Characterisation of MRGPRF overexpressing clones

This section describes characterization of the stably transfected cell models with the aim of determining the clones which would be most suited for downstream studies. eGFP fluorescence intensity was the characteristic used as a marker for assessing that the vector DNA was being expressed. Characterisation of the vector transfected cell lines focused on cell morphology and growth rates, with the aim of selecting transfected cell lines which were not exhibiting different growth patterns to untransfected cells.

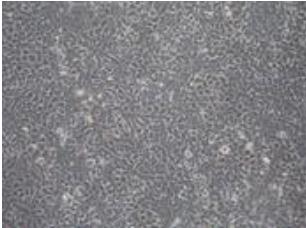
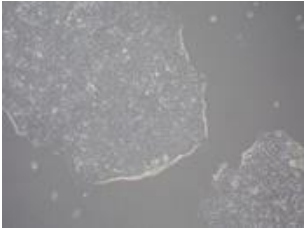
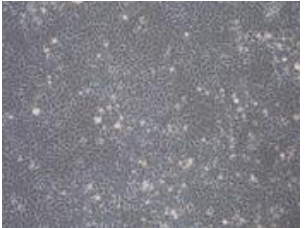
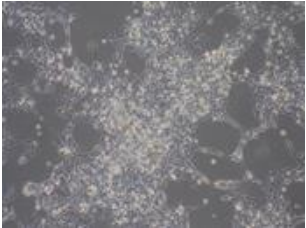

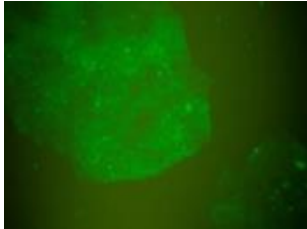
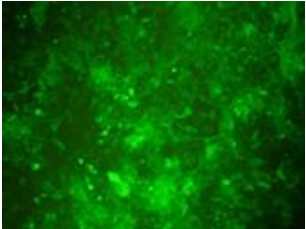
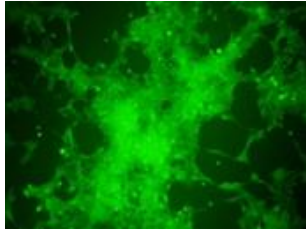
6.3.2.1. Phenotypic characterisation of HEK293 stable clones

All stably transfected HEK293 clones were phenotypically characterized through observation over a period of 4 months by microscopy to monitor growth rates, cell morphology patterns and the intensity of eGFP expression.

HEK293 cells are adherent epithelial cells that grow in a uniform monolayer and do not express eGFP, requiring passage two times a week; 10:1 split ratio. By visualising cells using light microscopy as shown in **Table 6.2**, morphology of HEK293-CT_{VL} clone B3 was shown to differ from that of untransfected HEK293 cells, growing in clustered 'islands', depicted clearly by the cluster edges showing a border marked by refractive light. Clone B3 also had the lowest intensity expression of eGFP when compared to the B4 and B9 clones. HEK293-CT_{VL} clone B4 and clone B9 displayed approximately similar growth rates on basis of subculture requirements, to untransfected HEK293 cells.

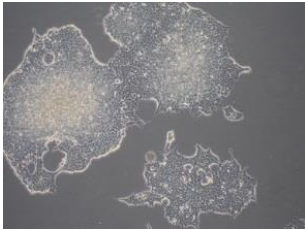
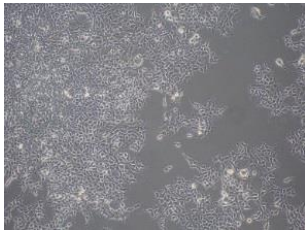
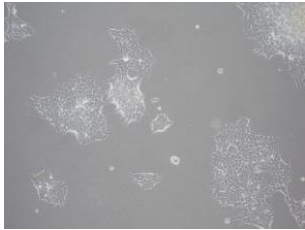
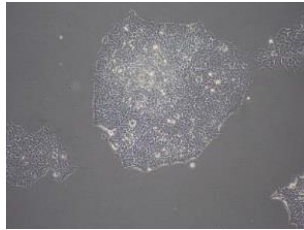
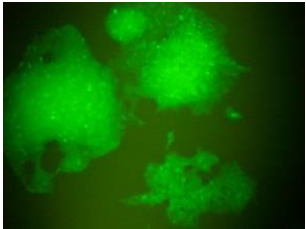
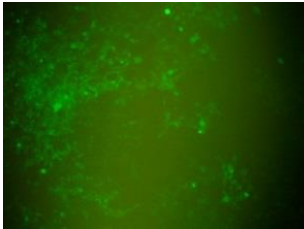
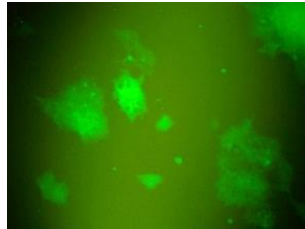
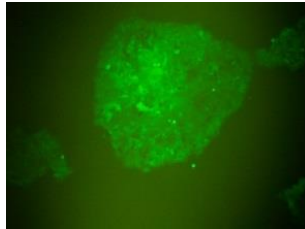
Stable MRGPRF-overexpressing HEK293 cells were also shown to have differing characteristics between clones, **Table 6.3**. Clones A6, C3 and C8 grew in clustered 'islands' unlike clone C1. However, when cells were imaged by fluorescent light microscopy clone C1 had the lowest expression of eGFP, whilst clustered cells derived from clone A6 had the brightest expression of eGFP. Clones C1 and C8 were observed to grow at a slower rate, and clone A6 at a quicker rate, than untransfected HEK293 cells. Cells derived from HEK293-MF_{VL} clone C3 were the only cells observed to grow at a similar rate to the untransfected HEK293 cells.

Table 6.2. Characteristics of HEK293-CT_{VL} clones and parental HEK293 cells

Clone	Untransfected	B3	B4	B9
Light microscopy				
Fluorescent Light microscopy				
Growth patterns	Monolayer	Clusters with light refractive edges	Monolayer	Clustered growth
Growth rate	-	Faster	Comparable	Comparable

B3, B4 and B9 are individual HEK293-CT_{VL} clones. Images were acquired by brightfield microscopy and fluorescent light microscopy at a 20x objective magnification. Growth rate of clones compared to untransfected cells was monitored based on subculture requirements.

Table 6.3. Characteristics of HEK293-MF_{VL} clones

Clone	A6	C1	C3	C8
Light microscopy				
Fluorescent Light microscopy				
Growth pattern	Clusters with light refractive edges	Monolayer	Clusters	Clusters
Growth rate	Faster	Slower	Comparable	Comparable

A6, C1, C3 and C8 are individual HEK293-MF_{VL} clones. Images were acquired by brightfield microscopy and fluorescent light microscopy at a 20x objective magnification. Growth rate of clones compared to untransfected cells was monitored based on subculture requirements

6.3.2.2. Phenotypic characterisation of MC38r stable clones

MC38r mouse colon carcinoma cells grow in a uniform monolayer [**Figure 6.4**]. MC38r stable clones, MC38r-CT_{VL} clones A3, A7 and A8 and MC38r-MF_{VL} clones C4, C6 and C7 had similar morphology and growth characteristics as parental MC38r cells. eGFP expression was not detected by low power fluorescence microscopy but was confirmed by FACS during the process of generation of the clones [**Appendix A6.1**].



Figure 6.4 MC38r cells in culture

MC38r cells were cultured in a T75 Corning tissue culture flask in RPMI media supplemented with 10 % fetal calf serum, 5 % CO₂ and at 37°. Cells grow in a monolayer and, although epithelial, are elongated and bipolar. The image was acquired by brightfield microscopy, with a 20x objective lens.

6.3.3. Validation of stable *Mrgprf* overexpressing clones by RT-qPCR

This section describes how stable clones were validated by quantifying mRNA expression of *Mrgprf* and by confirming protein expression and localisation.

6.3.3.1. Establishing a positive control for RT-qPCR gene expression studies

A transient transfection was used as a positive control for RT-qPCR gene expression studies. I previously confirmed that the method of transient transfection was efficient in HEK293 cells, and that using 0.5 µg as opposed to 1 µg maintained a higher cell viability (185).

Transfection efficiency of transiently transfected cells was monitored by observing and estimating the percentage of cells expressing eGFP. **Figure 6.5** shows that cells with control vector have higher transfection efficiency than those with *Mrgprf* vector (65 %

versus 40 % eGFP fluorescence measured at 36 hours, respectively). An increase in eGFP expression was observed at longer time points following transfection. To maximise the number of cells that were transiently transfected, cells were cultured for 48 hours post-transfection before RNA was extracted and subsequently reverse transcribed to provide positive control cDNA.

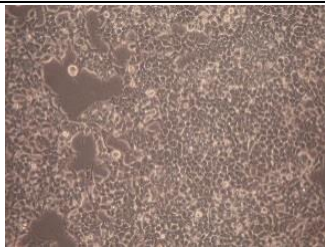
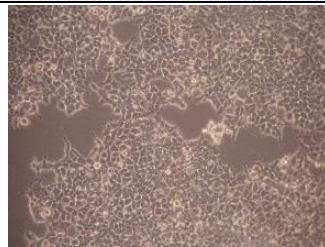
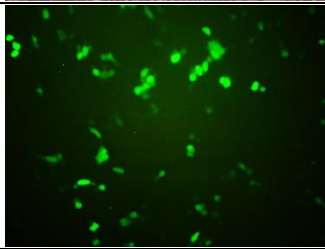
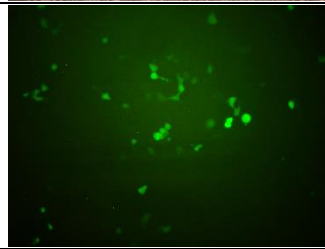
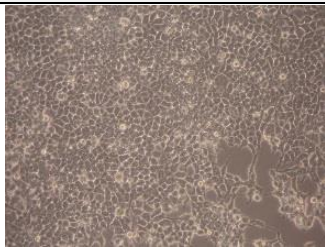
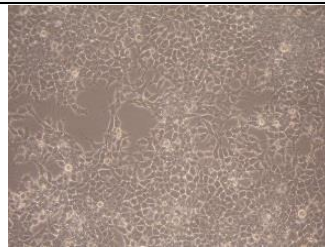
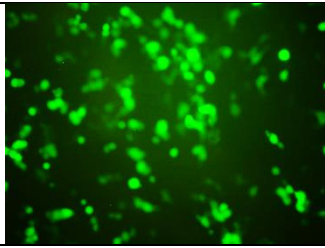
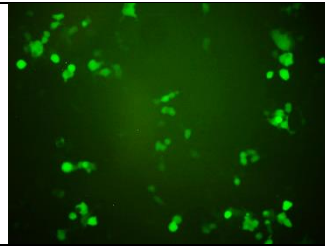
Cell type →	HEK29-CT _v				HEK293-MF _v			
12 hours								
Light Microscopy								
Fluorescent Light Microscopy								
eGFP Fluorescence	40 %				10 %			
36 hours								
Light Microscopy								
Fluorescent Light Microscopy								
eGFP Fluorescence	65 %				40 %			

Figure 6.5 Transient transfected HEK293 cell characteristics

HEK293 cells were transiently transfected with control (CT_v) or MRGPRF (MF_v) vector and incubated for 36 hours. Images were acquired at two time points; 12h and 36h. The images show that transfection efficiency (indicated by estimated percentage of cells expressing eGFP) was greater at 36 hours and was better for CT_v transfected cells.

6.3.3.2. Quantification of *Mrgprf* in transfected HEK293 cells by RT-qPCR

The transcript level of *Mrgprf* was quantified [**Figure 6.6**] and is reported as a relative quantity (RQ) in comparison to HEK293 cells, as detailed in **Chapter 3.9.3.2**. All sample mRNA quantity and quality plus C_T values are shown in **Appendix A6.2**.

Control vector and *Mrgprf* transfected cells had RQs of 4.24 ± 5.53 and 49554.25 ± 3817.84 , respectively. This difference in *Mrgprf* expression was found to be statistically significant (independent unpaired Student's t-test, $p = 0.02$).

The results show that all control vector transfected clones express low levels of endogenous *Mrgprf*, but the quantities of *Mrgprf* in all MF_{VL} clones was much greater. The clone expressing the highest relative quantity was HEK293-MF_{VL} clone C3 (RQ; 48227.83 ± 44249.16) and the lowest was HEK293-CT_{VL} clone B4 (RQ; 0.43 ± 0.33).

It should be noted that there are large standard deviations reported across the RQ values reported [**Figure 6.6**, **Appendix A6.2**]. This is due to the calculation in which RQ is determined, $2^{-\Delta\Delta C_T}$. A small difference in C_T value will produce a large difference in the RQ value generated. Therefore, over three, independent samples, variation in RQ values was large. Standard deviations for C_T values are shown in **Appendix A6.2** and shows that the difference from the mean value remains small across independent samples.

Significance of the differential *Mrgprf* expression between all clones was tested by the unpaired Student's t-test. No stable clones were found to express *Mrgprf* at a statistically significant level ($p \leq 0.05$), although this may be due to the large error bars, as **Figure 6.6** shows the *Mrgprf* RQ of all MF_{VL} clones were greater than CT_{VL} clones.

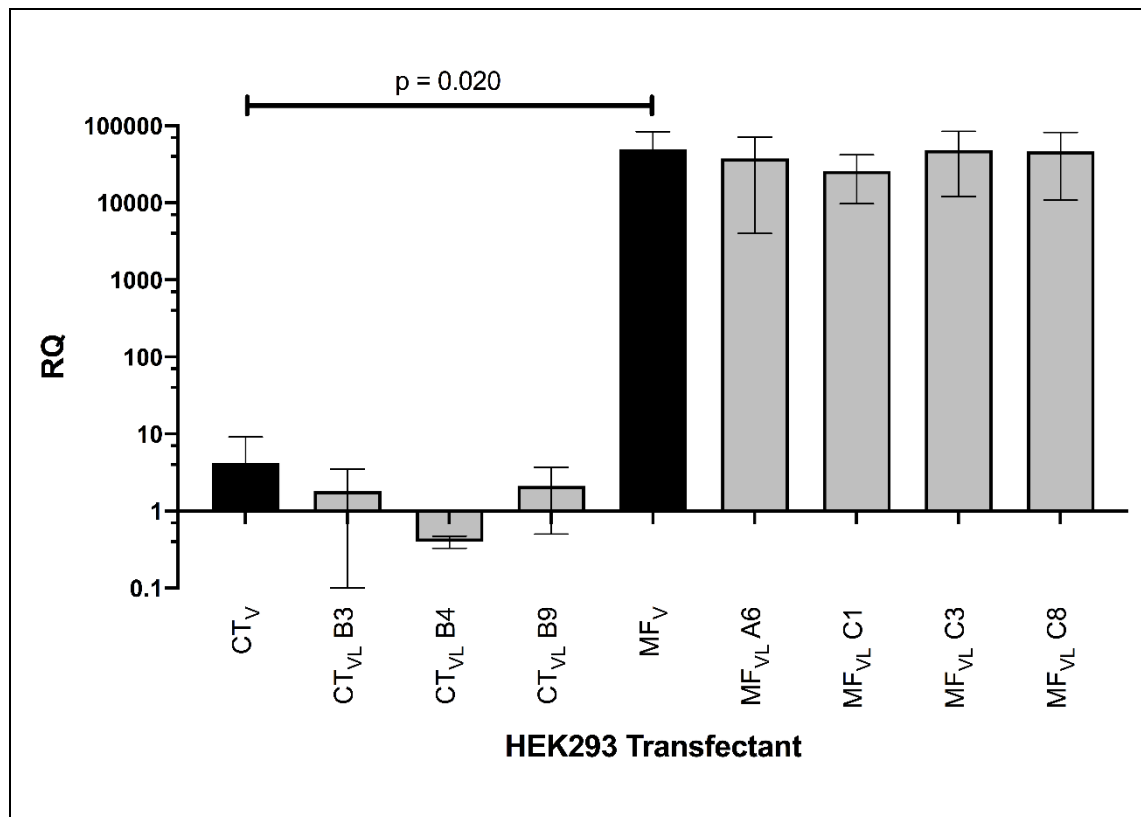


Figure 6.6 mRNA *Mrgprf* expression in transient and stably transfected HEK293 cells

Plasmid DNA was transfected directly for transient models (■; CT_V and MF_V) or was linearised before transfection and subsequent clonal selection for stable transfected models (□; CT_{VL} and MF_{VL}). *Mrgprf* was quantified by RT-qPCR, with β -actin used as the housekeeping gene. Relative quantity (RQ) to HEK293 untransfected cells was calculated. The results show that there is a greater quantity of *Mrgprf* in the overexpression models when compared to that measured in control vector transfectants, with a statistically significant difference between the transiently transfected cell lines shown, independent Student's t-test $p = 0.020$. Bars represent the mean \pm SD for 3 independent replicates.

6.3.3.3. Quantifying *Mrgprf* overexpression in MC38r stably transfected clones by RT-RT-qPCR

Mrgprf transcript was also measured in MC38r stably transfected clones and are reported as C_T and RQ (calculated in relation to untransfected MC38 cells) in **Table 6.4** and **Figure 6.7**.

Table 6.4. RNA quantity and RT-qPCR output data of MC38r stable clones

Sample	mRNA quality, purity, and transcript expression					
	ng/ μ l	260/280	β -Actin C_T	<i>Mrgprf</i> C_T	ΔC_T	RQ
MC38r	1226.0 303.2 271.7	2.10 2.07 2.10	17.3 ± 1.4	28.7 ± 0.9	11.3 ± 0.8	1.0
MC38r-CT _{VL} A3	491.8 758.9	2.09 2.10	17.6 ± 1.2	27.3 ± 2.1	12.0 ± 1.0	0.7 ± 0.1
MC38r-CT _{VL} A7	542.2 763.3 209.8 366.8	2.09 2.10 2.10 2.10	17.6 ± 1.0	28.6 ± 1.6	12.1 ± 0.9	0.7 ± 0.4
MC38r-CT _{VL} A8	620.5	2.10	16.8 ± 0.5	28.4 ± 0.6	11.6 ± 0.1	0.7 ± 0.4
MC38r-MF _{VL} C4	734.4	2.10	16.9 ± 0.8	29.5 ± 0.6	12.6 ± 0.2	0.4 ± 0.2
MC38r-MF _{VL} C6	501.3 492.1 311.4 636.5	2.10 2.10 2.09 2.10	17.4 ± 0.7	23.5 ± 1.1	6.64 ± 1.1	23.6 ± 19.6
MC38r-MF _{VL} C7	425.9 871.8	2.07 2.10	16.6 ± 0.5	28.7 ± 0.5	12.0 ± 0.7	0.9 ± 0.7

A3, A7 and A8 are individual MC38r-CT_{VL} clones. C4, C6 and C7 are individual MC38r-MF_{VL} clones. 260/280 is ratio of absorbance measured at 260 nm versus 280 nm. C_T : cycle threshold. RQ: relative quantity. All data are shown as mean \pm SD for a minimum 2 independent replicates.

β -actin transcript fluorescence reached the threshold for detection for all samples between cycle 16.6 and 17.6. C_T values obtained for MC38r *Mrgprf* stable clones ranged from 23.5 to 28.7.

Unlike HEK293-MF_{VL} clones, which all displayed increased *Mrgprf* mRNA levels in comparison to untransfected control, only one MC38r-MF_{VL} did – namely clone C6. MC38r-MF_{VL} clones C4 and C7 obtained RQ levels comparable to MC38r-CT_{VL} clones A3, A7 and A8. It should be noted that in comparison to stable HEK293-MF_{VL} clones, the relative expression increase is much lower for MC38r-MF_{VL} clone C6 (all HEK293-MF_{VL} clones have RQ values greater than 25000 versus the RQ of MC38r-MF_{VL} clone C6 which is 23.6 ± 19.57 .)

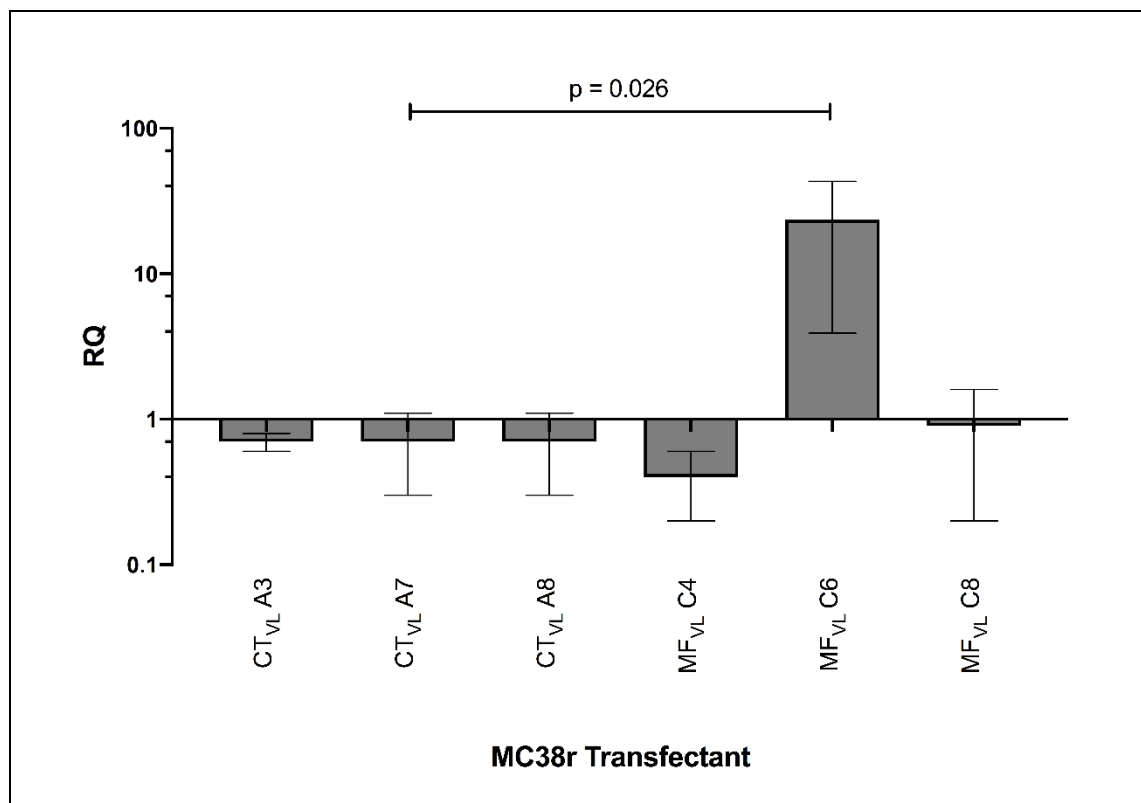


Figure 6.7 mRNA *Mrgprf* expression in transient and stably transfected MC38r cells

Mrgprf was quantified by RT-qPCR in MC38r stable transfectants, with β -actin used as the housekeeping gene. Relative quantity (RQ) to MC38r untransfected cells was calculated. The results show that there is a greater measured quantity of *Mrgprf* in MC38r-MF_{VL} clone C6 when compared to that measured in any of the other MC38r-MF_{VL} stable clones or control vector transfectants. A statistically significant difference between MC38r-CT_{VL} clone A7 and MC38r-MF_{VL} clone C6 is shown, unpaired independent Student's t-test $p = 0.026$. Bars represent the mean \pm SD for a minimum of 2 independent replicates.

Mrgprf expression was statistically significantly higher in MC38r-MF_{VL} clone C6 compared to MC38r-CT_{VL} clone A7 (unpaired Student's t-test, $p = 0.026$). Comparison between all remaining clones found no statistical significance when expression levels were compared.

6.3.3.4. Selection of stably transfected clones for protein expression, EPA sensitivity and functionality experiments

By combining the RT-qPCR relative *Mrgprf* expression data with observed phenotypic data (**Section 6.3.2**), clones were selected because of high *Mrgprf* expression and typical growth and morphology patterns following transfection. Clones identified in **Table 6.5** were selected for further validation and EPA sensitivity experiments.

Table 6.5. Clone selection for protein expression, EPA sensitivity and functionality studies

Clone	Justification
HEK293 Stable	
HEK293-CT _{VL} clone B4	<ul style="list-style-type: none"> • Low <i>Mrgprf</i> quantity • Similar rate and growth pattern to untransfected HEK293
HEK293-CT _{VL} clone B9	<ul style="list-style-type: none"> • Low <i>Mrgprf</i> quantity
HEK293-MF _{VL} clone C1	<ul style="list-style-type: none"> • Lowest <i>Mrgprf</i> quantity compared to HEK293-MF_{VL} clones A6, C3 and C8 • Monolayer growth like untransfected HEK293
HEK293-MF _{VL} clone C3	<ul style="list-style-type: none"> • Highest <i>Mrgprf</i> quantity compared to HEK293-MF_{VL} clones A6, C1 and C8
MC38r Stable	
MC38r-CT _{VL} clone A7	<ul style="list-style-type: none"> • Lowest <i>Mrgprf</i> quantity compared to clones A3 and A8
MC38r-MF _{VL} clone C6	<ul style="list-style-type: none"> • Highest <i>Mrgprf</i> quantity compared to clones C6 and C7

6.3.4. Validation of the stable *Mrgprf* overexpressing clones by interrogating protein expression

Having established that the selected clones [Table 6.5] express *Mrgprf* at the mRNA level, I investigated whether this was translated into protein expression. I compared two primary anti-*Mrgprf* antibodies; MRGF (N-14) and HPA02881 which will be referred to as N-14 and HPAMF henceforth.

6.3.4.1. N-14 antibody produced inconsistent MRGPRF detection by IF, flow cytometry and dot blot

To confidently characterise protein expression of MRGPRF in cells, the detection should be consistent upon multiple repeats of each experiment and ideally, would be consistent between techniques.

6.3.4.1.1. Using N-14 to detect MRGPRF by immunofluorescence

I used N-14 to visualise cellular location of MRGPRF. Antibody optimisation was completed previously (185) and thus N-14 was used to detect MRGPRF at a 1 in 50 μ l dilution. **Figure 6.8** (below) shows that I was unable to distinguish specific MRGPRF staining between HEK293 untransfected cells and HEK293-MF_{VL} clone C3, with the intensity of 'red' fluorescence being comparable. These images are representative of multiple experimental repeats. Although HEK293-MF_{VL} clone C3 immunofluorescent staining in **Figure 6.8** highlights some 'flecks' or brighter patches of staining, these were not present in each repeat.

As RT-qPCR data had shown a difference in *Mrgprf* expression, at an mRNA transcript level [Figure 6.6], between HEK293 and HEK293-MF_{VL} clone C3, it would be expected a difference in protein would be detectable. Using N-14, no increase in MRGPRF was found in the MF_{VL} overexpressing clones. This was contradictory to previous work in which I had found cytoplasmic and perinuclear localisation in HEK293-MF_{VL} and MC38r-MF_{VL} clones, respectively. With no differences in protocols or equipment used, I tested the antibody using two alternative protein detection techniques: flow cytometry and dot blot.

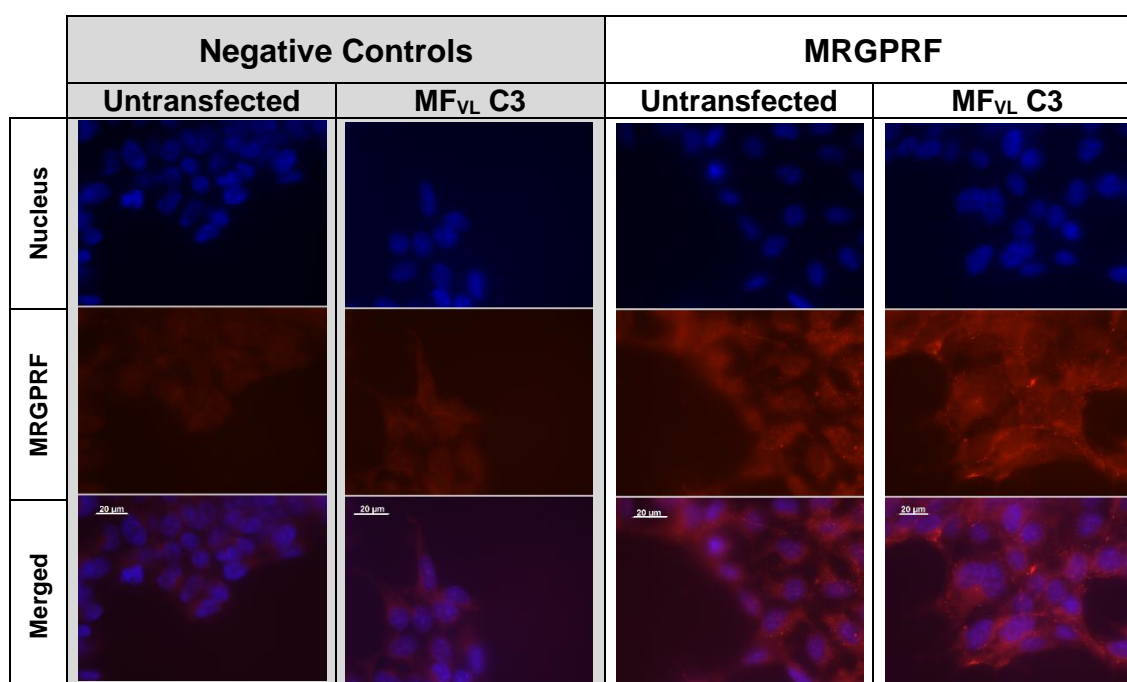


Figure 6.8 Using N-14 to detect MRGPRF protein expression in HEK293 and MF_{VL} clone C3 cells

Untransfected HEK293 and HEK293-MF_{VL} clone C3 cells were stained with anti-MRGPRF antibody, N-14 at dilution of 1 in 50 μ l and secondary antibody Alexa Fluor 594 at a 1 in 300 μ l dilution. Negative controls were incubated in antibody diluent containing no anti-MRGPRF antibody, and then in secondary antibody Alexa Fluor 594 (1 in 300 μ l). DAPI, a blue-fluorescent DNA stain, shows the nucleus. Images were acquired using the exposure time obtained for MRGPRF detection in HEK293-MF_{VL} clone C3 cells. The results show that no detectable difference in MRGPRF staining was seen between HEK293 and HEK293-MF_{VL} clone C3 cells. All images were acquired using x100 objective lens and are representative of a minimum of 3 independent replicates.

6.3.4.1.2. Using N-14 to detect MRGPRF by flow cytometry

I optimised a flow cytometry assay using N-14 anti-MRGPRF antibody to detect MRGPRF expression. Using unstained HEK293-CT_{VL} clone B4 and HEK293-MF_{VL} clone C3 cells, intact cells were gated by forward and side scatter, baseline detection of fluorescence was quantified and eGFP expression of these cells was confirmed [Figure 6.9]. Baseline detection of fluorescence measured using an A603/48 band pass filter shows that median fluorescence intensity between stable transfectants was comparable [Figure 6.9 B and E]. A higher percentage of HEK293-MF_{VL} clone C3 cells were intact compared to HEK293-CT_{VL} clone B4 cells, at 63.5 % and 57.8 % respectively. eGFP expression was quantified and confirmed that a higher percentage of HEK293-CT_{VL} clone B4 cells had detectable eGFP, with 75.0 % cells expressing the protein in comparison to 66.7 % of HEK293-MF_{VL} clone C3. Median fluorescence intensity was comparable between clones, measured to be 319 and 503 for HEK293-CT_{VL} clone B4 cells and HEK293-MF_{VL} clone C3 cells respectively.

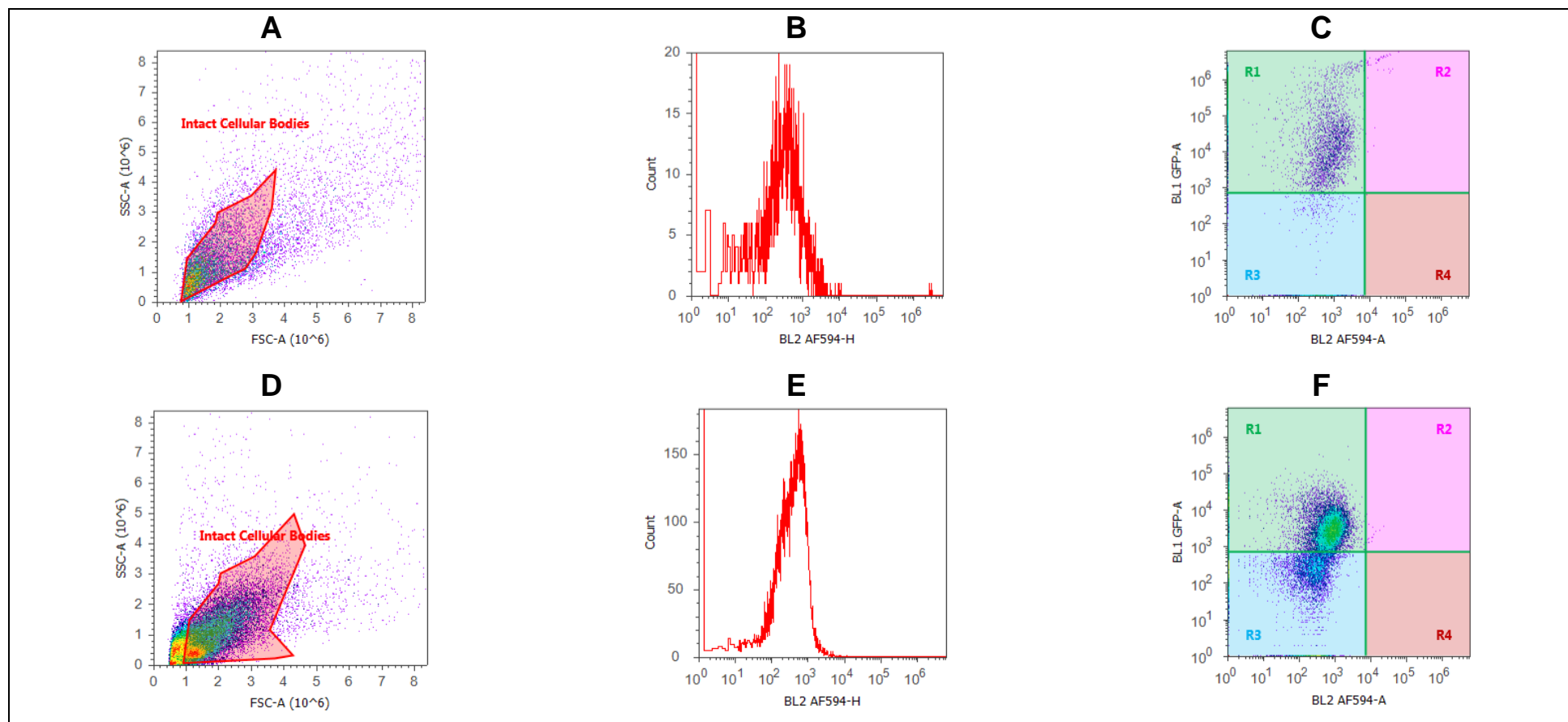


Figure 6.9 Confirmation of Stable transfectants GFP expression by flow cytometry

HEK293-CT_{VL} clone B4 (A-C) and HEK293-MF_{VL} clone C3 (D-F) cells were unstained. Intact cellular bodies were gated by side-scatter (SSC-A) and forward scatter (FSC-A) (A and D). Baseline detection of fluorescence was measured using an A603/48 band pass filter (B and E). C and F show that the cells were negative for AlexaFluor 594 detection, but both expressed GFP.

Eighteen experimental conditions were tested to optimise the primary and secondary antibody concentrations. In all conditions, both HEK293-CT_{VL} clone B4 and HEK293-MF_{VL} clone C3 were stained identically and changes in median fluorescent intensity were measured. Mean fluorescence shift was 5.1 and ranged from 1.1 to 17.3 [Figure 6.10]. The biggest shift in median fluorescent intensity was shown when the cells were stained with N-14 at a 1 in 50 dilution and AlexaFluor 594 at a 1 in 100 dilution [Figure 6.10 and Figure 6.11].

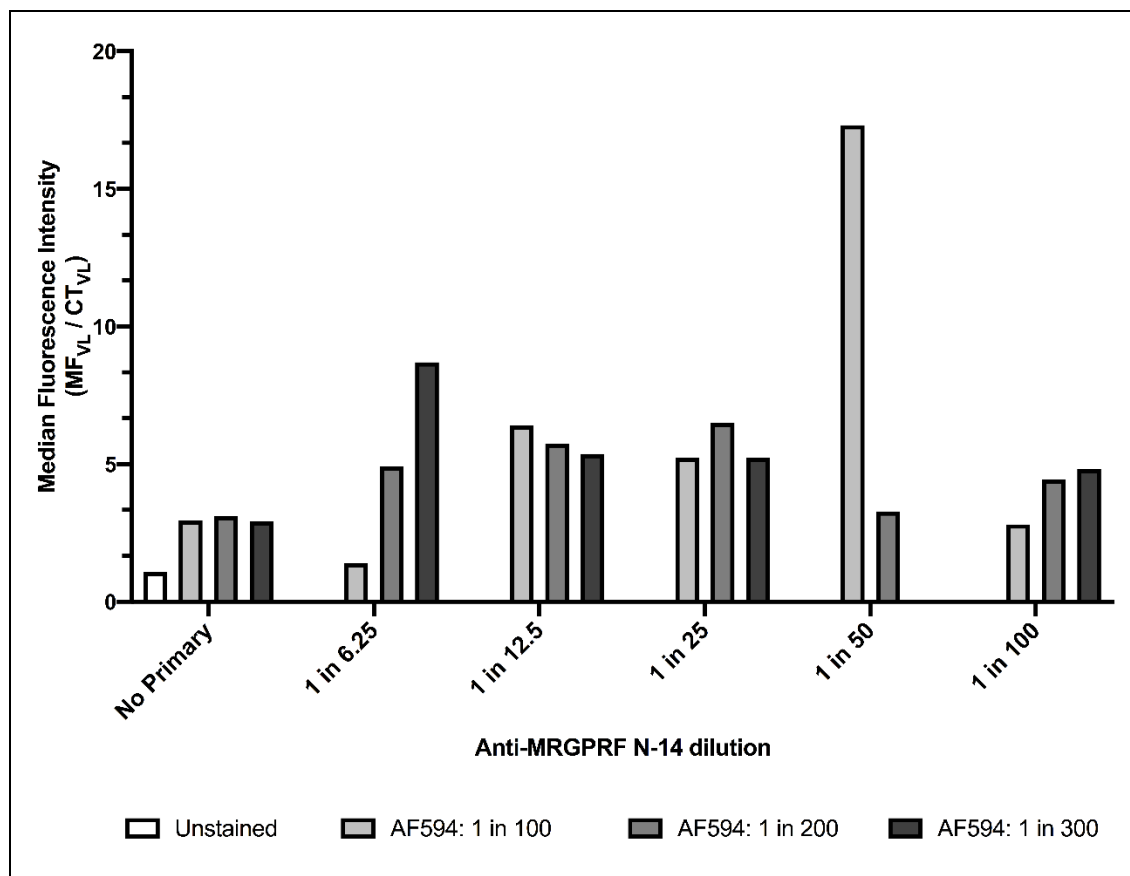


Figure 6.10 The effect of variable antibody concentrations on median fluorescent intensity shifts calculated between HEK293-CT_{VL} clone B4 and HEK293-MF_{VL} clone C3 cells

Stable HEK293 transfectants were incubated with no antibody, primary antibody (anti-MRGPRF, N-14) ranging in dilution from 1 in 6.25 to 1 in 100 and secondary antibody (AlexaFluor 594, AF594) ranging from 1 in 100 to 1 in 300. Flow cytometry detected shifts in median fluorescence intensity measured between stable transfectants that were quantified by showing the ratio of MF_{VL} to CT_{VL}. The greatest shift in median fluorescence intensity was found in cells incubated with 1 in 50 dilution of N-14 and 1 in 100 AF594. This data is representative of one experiment.

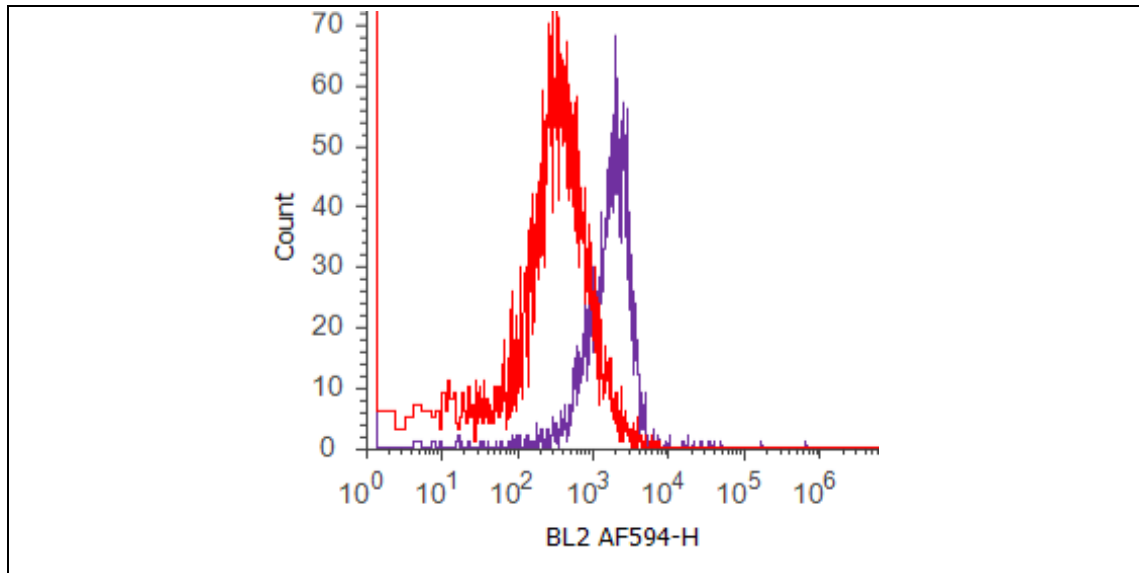


Figure 6.11 The effect of MRGPRF overexpression on fluorescence intensity

HEK293-CT_{VL} clone B4 (red) and HEK293-MF_{VL} clone C3 (purple) were stained with anti-MRGPRF N-14 (1 in 50 dilution) and AlexaFluor 594 (1 in 100 dilution). Fluorescence intensity was measured by flow cytometry and shows a shift in median intensity with a greater detection of fluorescence shown for HEK293-MF_{VL} clone C3 cells. This is representative of one experiment.

However, further optimisation to look at the difference between unfixed and fixed cells determined that this result was not reproducible as no fluorescent shift was detectable [Figure 6.12] in either unfixed or fixed cells. In addition, untransfected HEK293 cells were stained and fluorescence intensity was comparable with both stable transfectants.

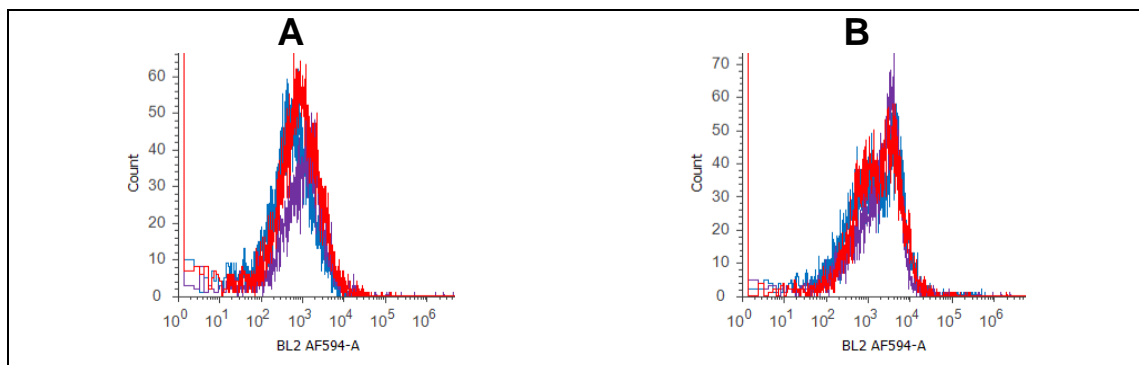


Figure 6.12 Comparison of fluorescence detected in unfixed and fixed cells

HEK293 (blue), HEK293-CT_{VL} clone B4 (red) and HEK293-MF_{VL} clone C3 (purple) were stained with anti-MRGPRF N-14 (1 in 50 dilution) and AlexaFluor 594 (1 in 100 dilution). (A) Cells were unfixed and (B) cells were fixed. Fluorescence intensity was measured by flow cytometry, and no shift in median intensity was detected for any cell line. This is representative of one experiment.

Using N-14 to detect MRGPRF by flow cytometry did not appear to be specific, and data was not reproducible, as I had previously shown when using it for immunofluorescence. An alternative protein detection method was therefore utilised next.

6.3.4.1.3. Using N-14 to detect MRGPRF by dot blot

The dot blot technique was used to establish whether denatured MRGPRF could be detected in lysates of stable transfectants. Dot blot was used to give an indication as to whether the antibody was more sensitive on denatured protein structures, perhaps due to increased epitope accessibility, in comparison to the folded protein structures which were investigated by immunofluorescence and flow cytometry.

Figure 6.13 is an image of one experiment, representative of three independent replicate experiments. There was no detection of the ‘housekeeping’ proteins selected (α -tubulin and β -actin) and the intensity of the ‘dots’ detecting MRGPRF were equal across all the stable HEK293 transfected cell lines. Each experimental repeat included additional variables, including new antibodies and fresh lysates (including those prepared from MC38r transfected cells) and lysates which had been boiled to denature the protein which could expose the epitope, but the output was consistent. Results were uninterpretable as the method had failed, indicated by the lack of housekeeper expression as these should be constitutively expressed in all cells.

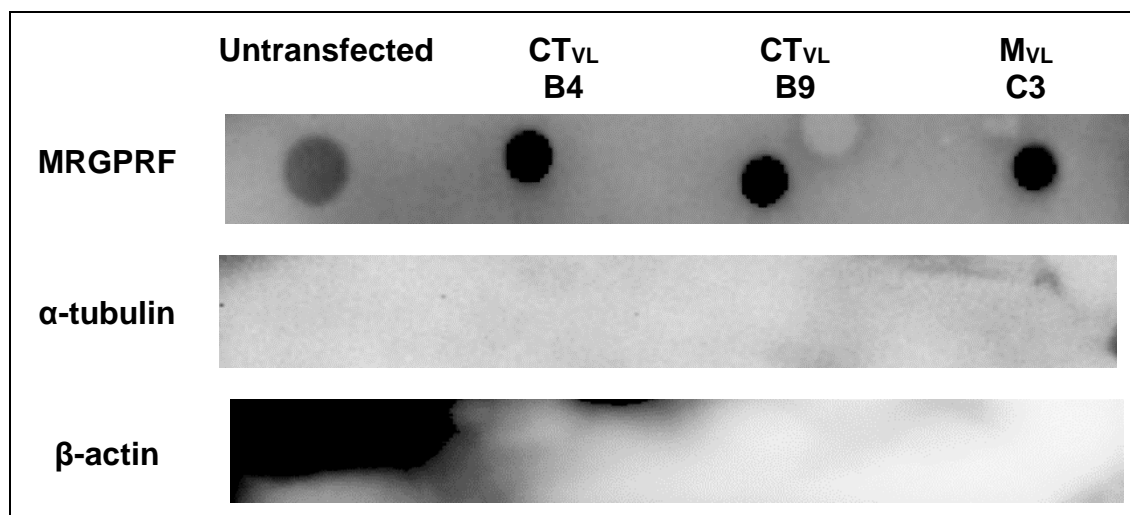


Figure 6.13 MRGPRF protein expression in stable transfectants

10 μ g of cell lysate was placed on a membrane which was blotted for MRGPRF, α -tubulin and anti- β -actin. As no α -tubulin or β -actin was detected in any lysate, the dot blot was uninterpretable.

As results using anti-MRGPRF N-14 in multiple techniques were non-specific, a new antibody was required. The new antibody (referred to throughout as HPAMF) was previously validated for use in cell lines and on human tissues by the Human Protein Atlas and publicly available data supports use.

6.3.4.2. Optimisation of the HPAMF antibody

To determine the optimal HPAMF antibody concentration, a range of primary antibody dilutions was tested on untransfected HEK293 cells and HEK293-MF_{VL} clone C3, on the basis that the mRNA transcript levels were low and high, respectively. HPAMF antibody has previously been used to show nuclear and plasma membrane MRGPRF protein localisation in the human BJ (foreskin fibroblast) cell line (304).

Figure 6.14 shows the staining patterns obtained by staining cells with 1 and 2 µg/ml HPAMF. It should be noted that C3 clone grew in clusters and thus imaging cells in a comparable field of view between untransfected and C3 clonal cells was difficult. Imaging the brightest cells, which were ascertained by visual inspection, confirmed exposure settings in which to image comparable cells. For cells stained with either antibody dilution, the cells which emitted greatest fluorescence were HEK293-MF_{VL} clone C3 cells. However, the longer exposure time required when imaging HEK293 cells treated with 1 µg/ml resulted in unspecific background staining seen in **Figure 6.14**. The absence of non-specific background staining or auto-fluorescence detection shown for HEK293 cells and the specific staining which appears to show the membranous localisation of MRGPRF in HEK293-MF_{VL} clone C3 cells supported use of the HPAMF antibody at a concentration of 2 µg/ml.

6.3.4.3. HPAMF immunofluorescent staining shows membranous staining in MRGPRF overexpressing HEK293 clones

Upon immunofluorescent staining of HEK293-CT_{VL} clones B4 and B9, and HEK293-MF_{VL} clones C1 and C3, a specific staining pattern was observed [**Figure 6.15**]. MRGPRF overexpressing cells, had distinct localisation of fluorescence indicative of membranous staining (indicated by arrows on **Figure 6.15**).

Untransfected and control vector transfected cells did not display this same staining pattern, and thus the results suggest that MRGPRF is a membrane-bound protein, with lower expression found in the cellular cytoplasm. It was also shown, in **Figure 6.15**, that protein expression between HEK293-MF_{VL} clones C1 and C3 mirrors the mRNA transcript expression. Consequently, more protein was detected (indicated by brighter fluorescence) in clone C3, suggesting that RNA and protein levels were proportionate to each other.

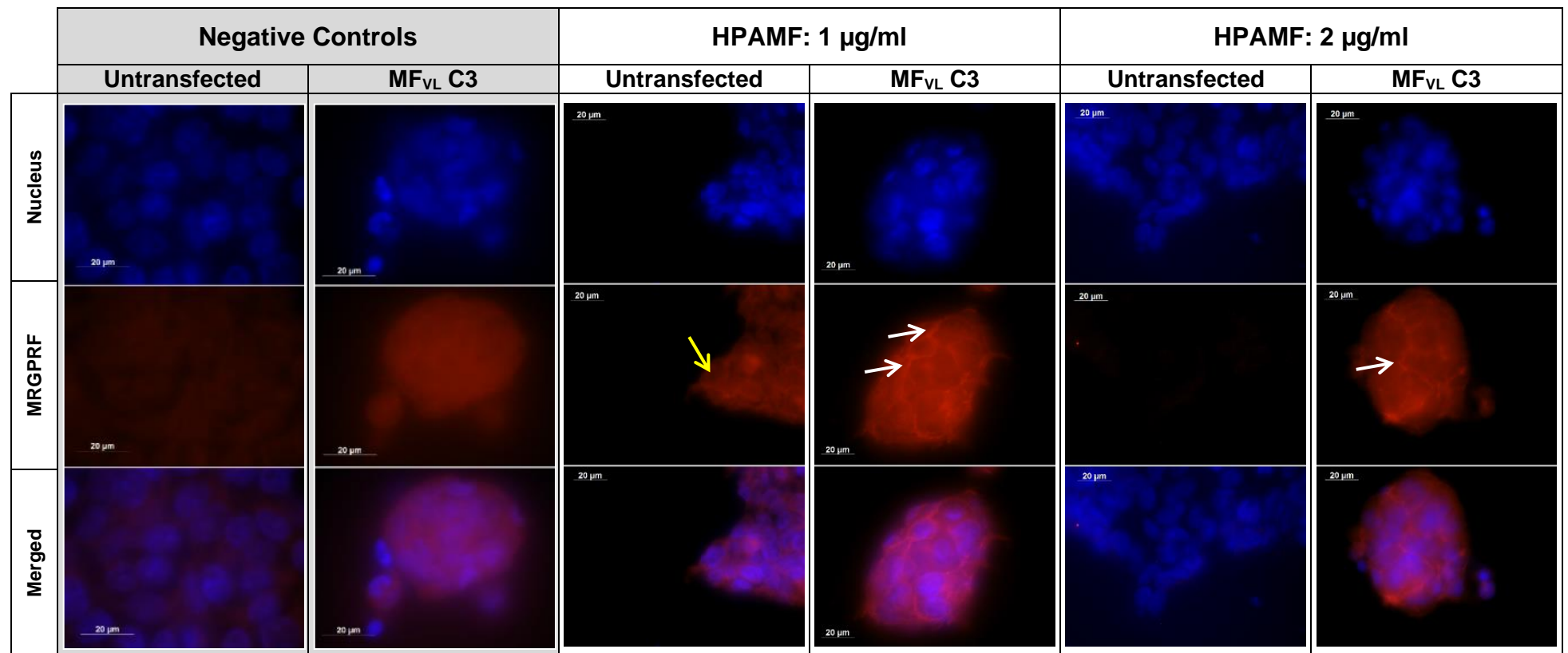


Figure 6.14 Antibody optimisation of anti-MRGPRF antibody, HPAMF to visualise MRGPRF protein in stable transfected cells

Untransfected HEK293 and HEK293-MF_{VL} clone C3 cells were stained with anti-MRGPRF antibody, HPAMF at concentrations of 1 and 2 $\mu\text{g/ml}$. Negative controls were incubated in antibody diluent containing no HPAMF antibody, and then in secondary antibody Alexa Fluor 594 (1 in 300 μl). Secondary antibody Alexa Fluor 594 was added at a 1 in 300 μl dilution. DAPI, a blue-fluorescent DNA stain, shows the nucleus. Long exposure times when cells were stained with HPAMF dilution 1 $\mu\text{g/ml}$ resulted in detection of auto-fluorescence and non-specific staining (indicated by yellow arrow). This was not seen for cells treated with 2 $\mu\text{g/ml}$; MRGPRF was not detected in untransfected cells, and membranous staining (white arrows) was found in HEK293-MF_{VL} clone C3 cells. All images were acquired on the Zeiss AxioImager.Z1 fluorescence microscope using x100 objective lens and are representative of $n = 1$, with the exception of HEK293 untransfected, 2 $\mu\text{g/ml}$, which is representative of $n=3$.

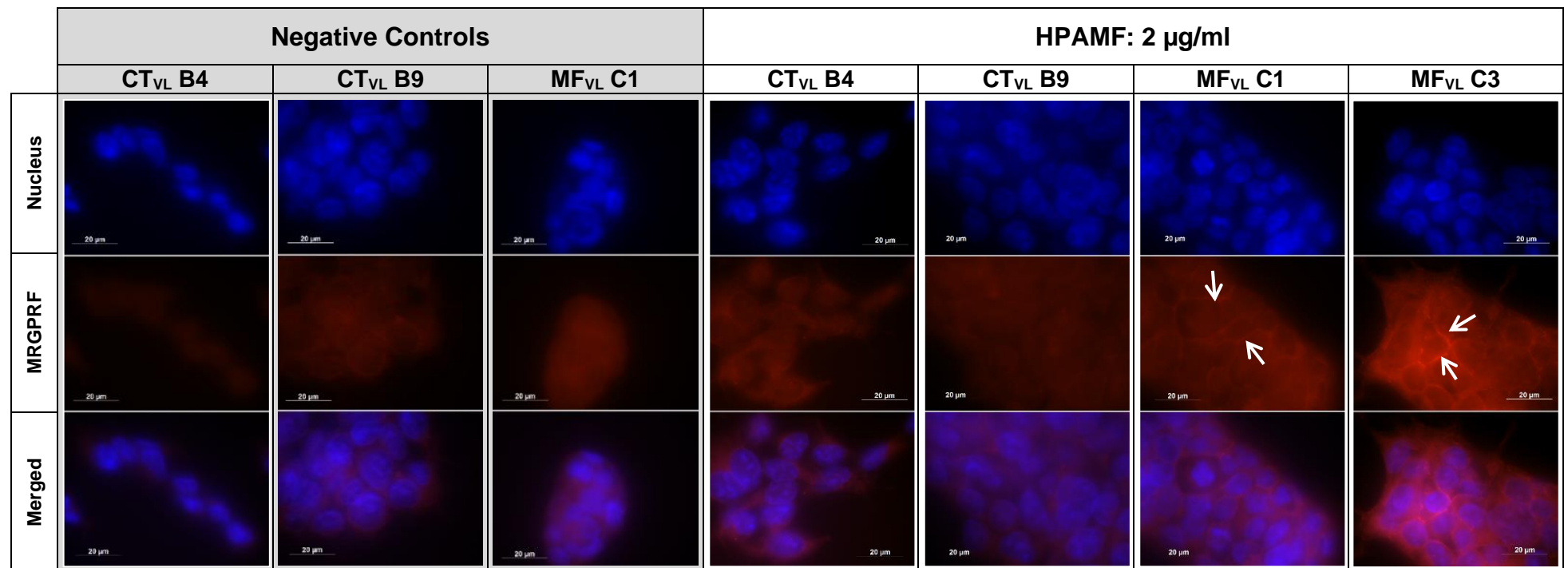


Figure 6.15 Immunofluorescent labelling of the MRGPRF receptor in HEK293 stably transfected clones

Immunofluorescence to detect MRGPRF in HEK293 stable clones was completed with HPAMF (2 µg/ml) and secondary antibody, Alexa Fluor 594 (1 in 300). Negative controls were not incubated with HPAMF. DAPI, a blue-fluorescent DNA stain, shows the nucleus. Control vector transfected clones did not show presence of MRGPRF, indicated by a lack of red fluorescence. The white arrows present on the MRGPRF overexpressing clones show that MRGPRF was localised to the cell membrane. Images are representative of 3 independent repeats, were acquired on the Zeiss Axio.Imager Z1 fluorescent microscope with the 'red' exposure set for HEK293-MF_{VL} clone C3. Each field of view presented is representative of the entire coverslip for which the image was taken, and all pictures were taken at x100 objective len

6.3.4.4. HPAMF immunofluorescent staining does not detect membranous staining in MRGPRF overexpressing MC38r clone

Unlike HEK293 clones, MC38r stable transfectants did not appear to demonstrate any specific staining using the HPAMF antibody, as shown in **Figure 6.16**. Unfortunately, due to limited availability of antibody, untransfected cells were not used. Red fluorescence of the same intensity was observed in negative control cells for both MC38r-CT_{VL} clone A7 and MC38r-MF_{VL} clone C6. There are potentially two reasons for this. First, mRNA transcript levels of MRGPRF for MC38r-MF_{VL} clone C6 was lower than any of the HEK293-MF_{VL} clones. Lower mRNA expression, assuming the ability of MC38r cells to translate RNA to protein expression, would mean corresponding protein levels were lower and thus less antigen to which the antibody could bind. When imaging the cells, the higher exposure times for obtaining an image of MC38r-MF_{VL} clone C6 results in detection of 'red' auto-fluorescence. Secondly, HPAMF may be detecting endogenous levels of MRGPRF present in the mouse CRC cells. However, as the signal was detected in all samples, results are uninterpretable.

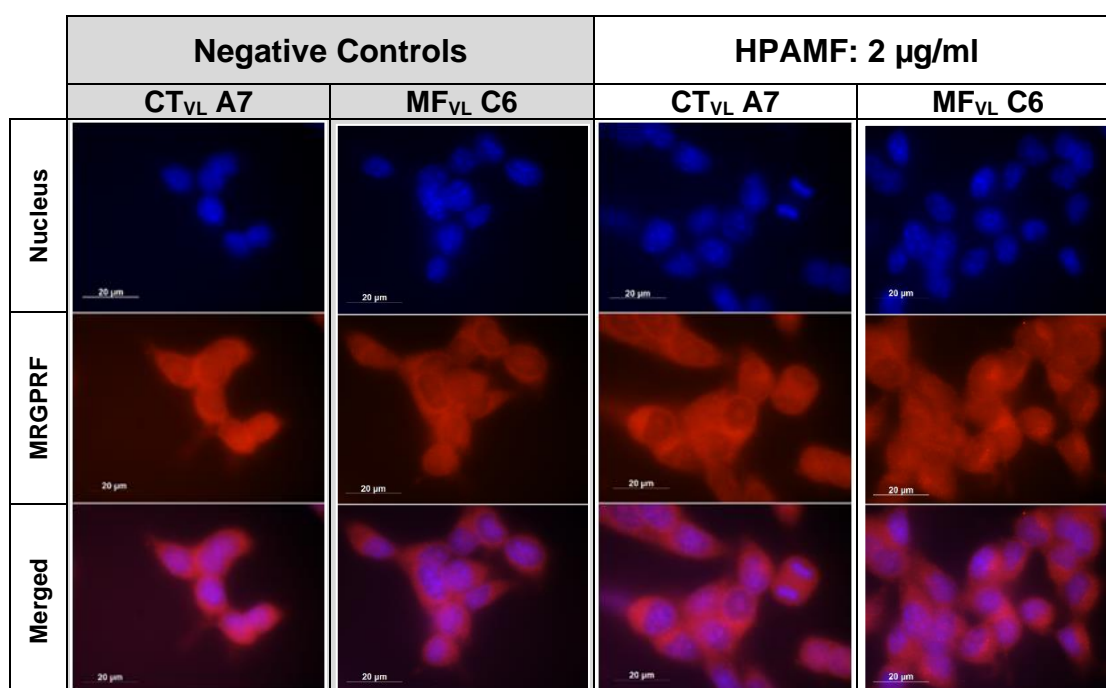


Figure 6.16 Immunofluorescent labelling of MC38r stably transfected clones

MC38r stable clones stained with HPAMF and secondary antibody, AlexaFluor594. No primary antibody was used for negative controls and the nucleus is depicted by the DAPI stain. Immunofluorescence images representative of 3 independent repeats, the field of view presented was representative of the entire coverslip and all pictures were taken at x100 objective lens.

In summary, immunofluorescent staining with HPAMF detected membranous MRGPRF protein expression proportionate to *Mrgprf* mRNA expression in HEK293 clones. However, no specific staining pattern was detected for MC38r clones.

6.3.5. MRGPRF overexpression does not alter CRC cell response to EPA

To investigate whether a link between MRPRF expression and sensitivity to EPA exists, EPA concentration response MTT cell viability assays were performed. As MRGPRF was decreased in MC38r EPA-resistant cells, it was hypothesised that increasing the expression of MRGPRF would increase sensitivity in HEK293-MF_{VL} clones or restore sensitivity in MC38r-MF_{VL} clones, and thus a lower IC₅₀ value would be shown relative to the untransfected or control vector transfected counterparts.

Figure 6.17 A shows that all stable HEK293 clones have concentration-response curves that are similar. EPA IC₅₀ values of HEK293 stable clones were compared, the most sensitive cells (HEK293-CT_{VL} clone B9, IC₅₀ = 90.41 ± 20.06 µM) and the most resistant cells (HEK293-CT_{VL} clone B4, IC₅₀ = 159.40 ± 39.49 µM) [**Figure 6.17 B**], were both CT_{VL} clones. IC₅₀ values were compared between all stable transfected clones, and no statistically significantly different IC₅₀ concentrations were identified (unpaired Student's t-test, **Figure 6.17**).

Figure 6.18 A shows comparable concentration response curves for MC38r cells and MC38r stable clones. MC38 cell curves had a greater loss of viability after ~30 µM EPA exposure compared with MC38r cells and MC38r stable clones.

IC₅₀ values obtained for MC38 and MC38r cells were 95.42 ± 12.87 µM and 161.71 ± 32.43 µM, respectively. These IC₅₀ concentrations were significantly different, unpaired Student's t-test, p = 0.05 [**Figure 6.18 B**]. MC38r-CT_{VL} clone A7 had an IC₅₀ of 142.66 ± 12.87 µM and MC38r-MF_{VL} clone C6 had an IC₅₀ of 146.41 ± 27.19 µM, the difference between the two was not found to be statistically significantly different (unpaired Student's t-test, p = 0.84). The observed difference in IC₅₀ values between MC38r and MC38r-MF_{VL} clone C3 shows that EPA sensitivity was not restored due to MRGPRF overexpression.

Overall, although *Mrgprf* overexpression was shown at transcript level in both HEK293 and MC38r overexpression clones, and at a protein level for HEK293-MF_{VL} cells, no observed alteration in cellular response to EPA was evident. It could not be concluded whether the transfected protein was functional, which would have implications on the result being a 'real negative' or a 'false negative'. Therefore, further validation of the model was undertaken.

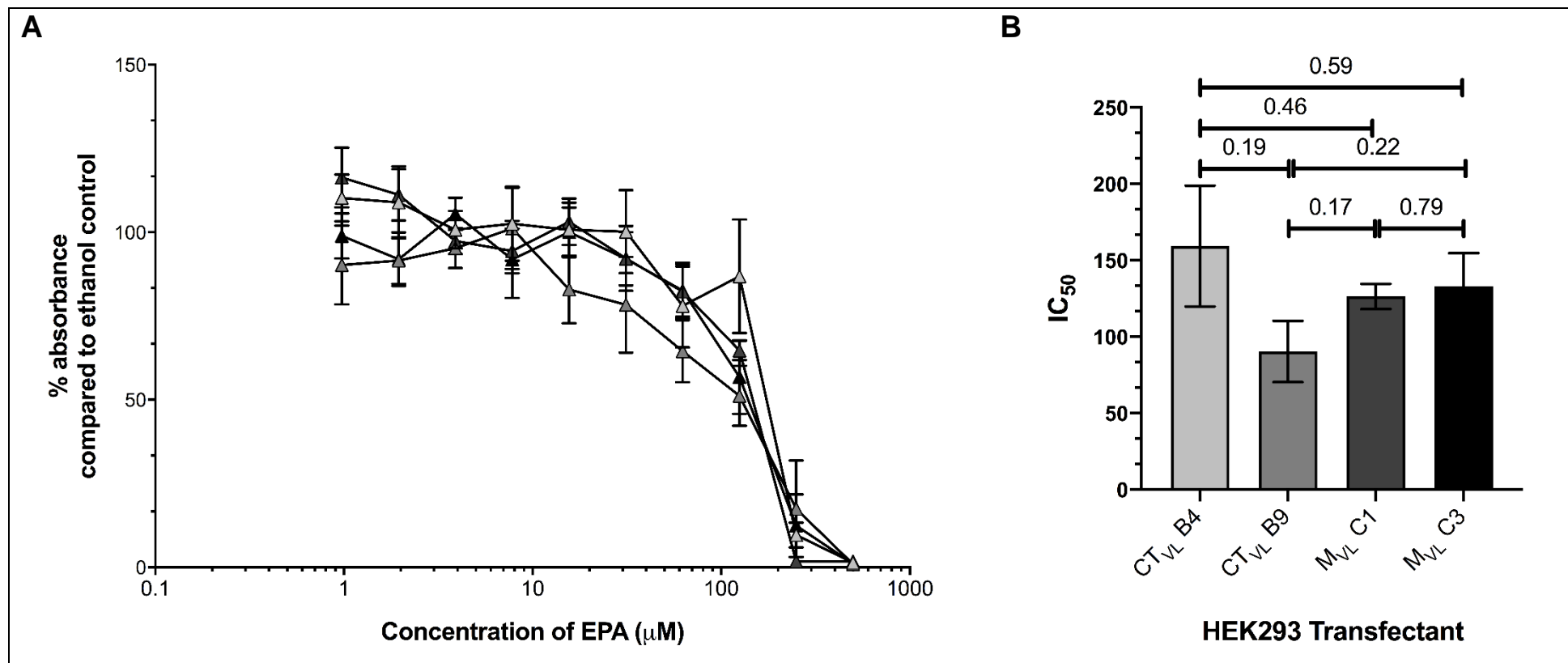


Figure 6.17 Sensitivity of stable HEK293 transfectants to EPA

Stable HEK293 transfected cell lines were treated with 1 to 500 μM EPA, and cells were left to grow for 72 hours and cell viability was determined by MTT assay, with absorbance at 620nm measured on the Berthold Mithras LB-940 plate reader. (A) EPA concentration response curves for HEK293-CT_{VL} clones B4 \blacktriangle and B9 \blacktriangle and HEK293-MF_{VL} clone C1 \blacktriangle and C3 \blacktriangle . (B) EPA IC₅₀ values of the clones. No statistically significant differences in IC₅₀ between MRGPRF overexpression models and control transfected cells, unpaired Student's t-test. All data presented as the mean of 3 independent repeats \pm SD.

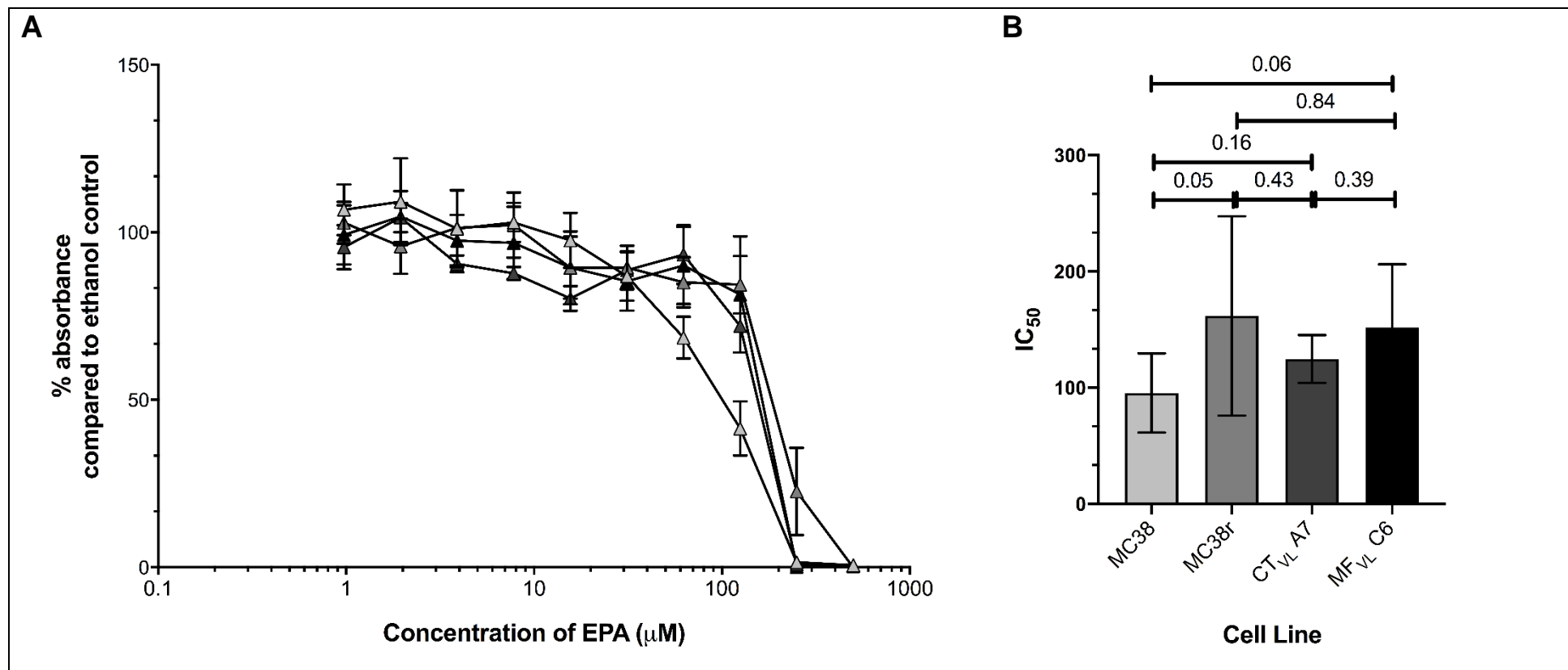


Figure 6.18 Sensitivity of stable MC38r transfectants cell lines to EPA

MC38, MC38r and stable MC38r transfectants cells were treated with 1 to 500 μ M EPA, and cells were incubated for 72 hours and cell viability was determined by MTT assay, with absorbance at 620nm measured on the Berthold Mithras LB-940 plate reader. (A) EPA concentration response curves for MC38 \triangle , MC38r \blacktriangle , MC38r-CT_{VL} clone A7 \blacktriangle and MC38r-MF_{VL} clone C6 \blacktriangle . (B) EPA IC_{50} values, statistically significant differences in IC_{50} between MC38 and MC38r cells were shown, unpaired Student's t-test. No other statistically significant differences were found. All data presented as the mean of 3 independent repeats \pm SD.

6.3.6. Assessing the effect of EPA exposure on calcium mediated signalling in MRGPRF overexpressing clones

As MRGPRF is an orphan receptor, it is not known how the signalling cascades are stimulated by its ligand. Previous data has shown that MRGPRF overexpression models did not increase cAMP levels compared with controls (data shown in **Appendix A6.3**).

To test whether MRGPRF overexpressing clones were signalling via calcium-mediated pathways, calcium flux assays were completed, using protocols developed and used frequently by the Professor David Beech lab group.

6.3.6.1. Thapsigargin exposure induces an increase in fluorescence ratio in HEK293 cells

To test that the assay detected an intracellular calcium increase in response to an external agent, Thapsigargin (Tg) was used as a positive control. Tg blocks the ability of the cell to pump Ca^{2+} into the sarco/endoplasmic reticulum. Prior to injection at 30s, cells treated with either DMSO or Tg were shown to have a normalised $F_{340/380}$ ratio of 0.0. **Figure 6.19** shows that, following the exposure of fura2-AM loaded HEK293 cells to 1 μM Tg, there was a steady increase in $F_{340/380}$. At 95s, the $F_{340/380}$ ratio was 0.16 ± 0.09 for DMSO treated cells, and 1.65 ± 0.43 for cells treated with Tg. The difference between the $F_{340/380}$ measurement at the 95s time-point, between DMSO and Tg treated cells, was shown by unpaired Student's t-test to have a p value 0.027.

The results show a reproducible and statistically significant change in fluorescence readings, validating the assay for detection of calcium flux changes in HEK293 cells upon Tg exposure. Next, I tested stable clones to determine whether exposure of MRGPRF-overexpression models to EPA resulted in increased intracellular calcium.

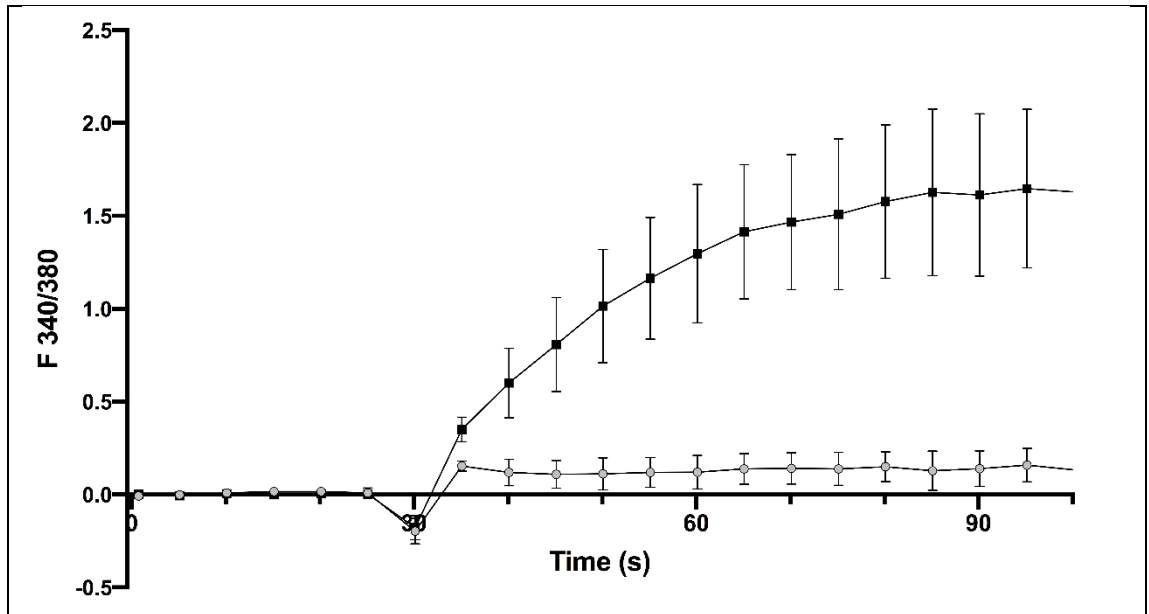


Figure 6.19 Intracellular Ca²⁺ response to Tg

HEK293 cells were loaded with 2μM Fura2-AM and 100μl 1.5mM Ca²⁺-SBS containing DMSO or 1μM Thapsigargin (Tg). F_{340/380} ratio was measured over a period of 100 seconds, with injections made at the 30s time point. The results show that there was an increase in F_{340/380} ratio measured for Tg treated cells that was not seen for DMSO treated cells, indicative of an increase in intracellular calcium. Data points are mean ± SD of 3 independent repeats. Student's t-test was used to compare F_{340/380} at the 95 s time-point, $p = 0.027$.

6.3.6.2. eGFP fluorescence does not affect F₃₄₀/F₃₈₀ ratio

To confirm that presence of eGFP in vector DNA did not affect fluorescence readings, and consequently the F_{340/380} ratio, I performed the calcium assay on cells with the brightest eGFP signal as shown by fluorescence microscopy; HEK293-CT_{VL} clone B4. I compared the raw fluorescence ratio reading (with no normalisation) in presence and absence of fura2-AM loading and included HEK293 cells which lack eGFP.

Comparable baseline readings for fura2-AM loaded cells are shown in **Figure 6.20**, with the mean F_{340/380} for HEK293 cells being 0.95 ± 0.04 and HEK293-CT_{VL} clone B4 cells being 0.76 ± 0.05 . In comparison, HEK293-CT_{VL} clone B4 cells with no fura2-AM had a mean F_{340/380} baseline of 0.38 ± 0.13 . All cells treated with DMSO show no increase in F_{340/380}, and cells loaded with fura2-AM that were treated with Tg display a detectable change in F_{340/380}. HEK293-CT_{VL} clone B4 cells not loaded with fura2-AM prior to Tg injection demonstrate no increase in F_{340/380} and the ratio remained constant for 200s.

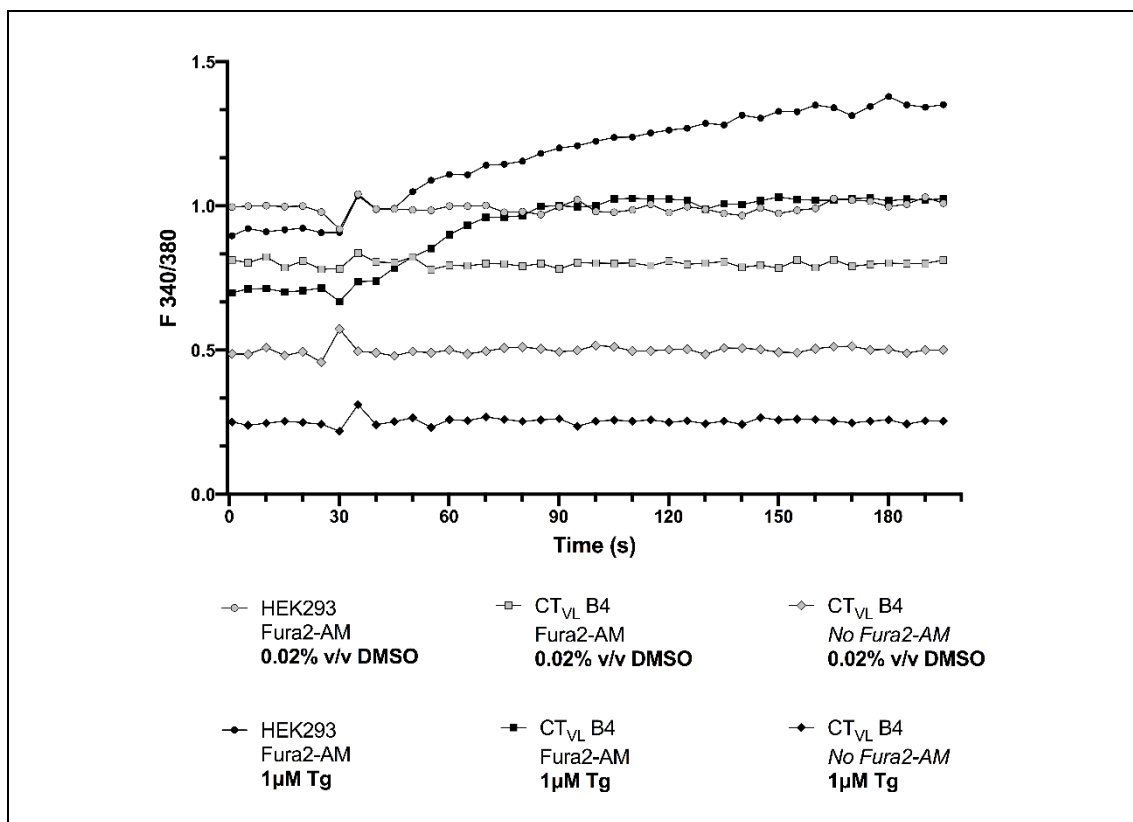


Figure 6.20 Comparing F_{340/380} in Fura-2AM loaded and non-loaded cells expressing eGFP

After 24h incubation, HEK293 and HEK293-CT_{VL} clone B4 (CT_{VL} B4) cells were incubated in 1.5mM Ca²⁺-SBS with or without Fura2-AM. The fluorescence ratio was measured for 200s, with an injection of DMSO or 1μM Tg at 30s. Raw F_{340/380} ratios are plotted, with no normalisation to show the effect of Fura-2AM loading versus no Fura-2AM. The results show that cells with no Fura2-AM loading had lower F_{340/380} ratios but the cells which were loaded have comparable ratios regardless of eGFP expression, with stable low fluorescence detected in eGFP expressing cells with no Fura-2AM. (n=1)

6.3.6.3. EPA exposure does not induce calcium mediated signalling

The biggest increases in F_{340/380} ratio fold change were shown for HEK293 cells as, following exposure to 1 μM Tg, an 11.2 ± 5.6 fold increase in F_{340/380} compared to DMSO control was shown, and after injection with 20μM ATP a fold increase of 11.3 ± 4.2 compared to water was observed [Figure 6.21]. In comparison to untransfected HEK293 cells, stable transfectants show lower F_{340/380}-fold changes in response to Tg and ATP. A 7.5-fold and 6.5-fold increase (Tg to DMSO) and a 5.2- and 4.0-fold increase (ATP to water) in F_{340/380} ratio is shown in Figure 6.21 for HEK293-CT_{VL} clone B4 and HEK293-MF_{VL} clone C3, respectively. For all cells, the increase in F_{340/380} in response to Tg was slow whereas there was a sharp increase in F_{340/380} in response to ATP [Figure 6.22]. Collectively, these results show that there was an increase in intracellular calcium in response to treating the cells with thapsigargin or ATP.

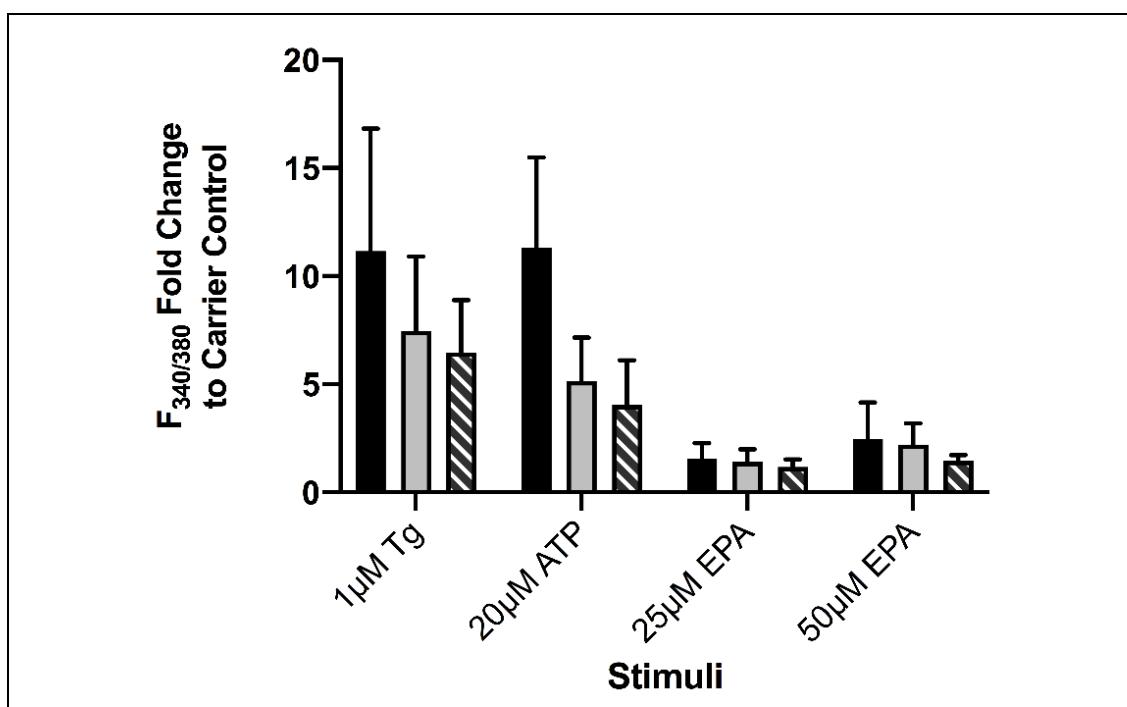


Figure 6.21 Effect of EPA exposure on intracellular calcium levels

HEK293 , HEK293-CT_{VL} clone B4 and HEK293-MF_{VL} clone C3 cells incubated following loading with 2µM Fura2-AM. 100µl 1.5mM Ca²⁺-SBS containing DMSO / 1µg Thapsigargin (Tg), water / 20µM ATP or ethanol / 25µM / 50µM EPA. F_{340/380} ratio was measured over a period of 200 seconds, with injections made at the 30s time point. The results show the F_{340/380} ratio measured for each agent in relation to their respective carrier control. Tg and ATP caused the biggest increase intracellular calcium. All data is representative of the mean ± SD of 3 independent replicates.

The fold change calculated for EPA exposed cells is in relation to ethanol carrier. Tg and ATP exposure resulted in the biggest increase in intracellular calcium for all cell lines [Figure 6.21, Figure 6.22], which would indicate that EPA exposure does not induce calcium signalling. Following injection of 25µM EPA the fold change was 1.6, 1.4 and 1.2 for HEK293, HEK293-CT_{VL} clone B4 and HEK293-MF_{VL} clone C3. Exposure to a higher concentration, 50 µM EPA, resulted in larger fold changes; 2.5, 2.2 and 1.5, for HEK293, HEK293-CT_{VL} clone B4 and HEK293-MF_{VL} clone C3. The smallest F_{340/380} fold-changes in MRGPRF overexpressing clones were shown in EPA treated cells.

This result indicates that the transfected cells were responding to stimuli such as Tg and ATP, however there is no known ligand for MRGPRF which could be used as a positive control. The results, in combination with the cAMP ELISA performed to show if the overexpressing cell lines were signalling via cAMP, were not able to confirm whether a functional MRGPRF protein was translated from the mRNA sequence. Therefore, the result shown in **Chapter 6.3.5**, whereby I reported that there was no change in CRC cell response to EPA as a result of MRGPRF overexpression, could potentially be a false negative.

To summarise, expression of *Mrgprf* mRNA transcript in HEK293-MF_{VL} clones and one MC38r-MF_{VL} clone was confirmed to be greater than *Mrgprf* expression measured in untransfected or control vector clones. Protein detection using the N-14 antibody was inconsistent and thus an alternative antibody, HPAMF was utilised. This identified membranous MRGPRF protein expression specific to HEK293-MF_{VL} clones that appeared to be proportional to the transcript expression detected. However, HPAMF was unable to detect protein expression in MC38r clones. EPA sensitivity was not altered as a result of *Mrgprf* / MRGPRF overexpression and the data were inconclusive as to whether the MRGPRF protein in stably transfected cells was functional. Therefore, the relationship between MRGPRF and EPA sensitivity remained unclear. To validate MRGPRF as a target, the next step was to generate hCRC cell lines with acquired EPA resistance and investigate MRGPRF expression between parental 'sensitive' cells and cells with resistance.

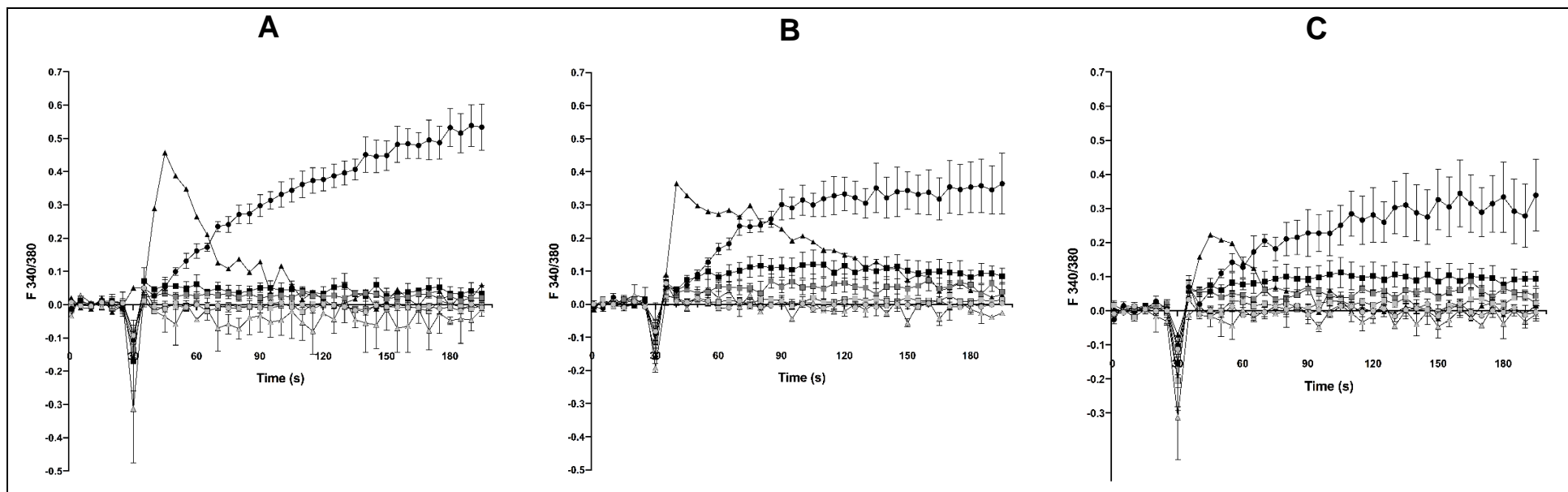


Figure 6.22 Measurement of F_{340/380} ratio for 200s to monitor response of cell lines to Thapsigargin, ATP and EPA.

HEK293 (A), HEK293-CT_{VL} clone B4 (B) and HEK293-MF_{VL} clone C3 (C) were loaded with 2 μ M Fura2-AM. They were injected with 100 μ l 1.5mM Ca²⁺-SBS containing; 0.02% v/v DMSO \circ , 1 μ g Thapsigargin (Tg) \bullet , 0.08% v/v water \triangle , 20 μ M ATP \blacktriangle , 0.20% v/v ethanol \square or 25 μ M \blacksquare / 50 μ M EPA \blacksquare . F_{340/380} ratio was measured for 200 seconds, with injections made at the 30s time point. The results show the F_{340/380} ratio measured at each time. Tg causes a steady increase in F_{340/380} whereas and ATP causes an initial spike that decreases over the time course. All carrier controls (DMSO, ethanol and water) are shown to not elicit any F_{340/380} response. No increase in intracellular calcium was detected following treatment with EPA at either concentration in any cell line. All data points are representative of duplicate wells \pm standard deviation.

6.4. Results II: Generating resistance to *n*-3 PUFAs in hCRC cell lines

6.4.1. CRC cell lines have variable sensitivities to EPA and DHA

Five human and 1 mouse CRC cell lines were used. Cell lines were chronically exposed to EPA or DHA to generate resistance. To maximise the chance of successful isogenic clone generation, I tested two methods for generating resistance; the first placed selective pressure on cells using high concentrations of *n*-3 PUFAs and the second was maintaining cells in media treated with an *n*-3 PUFA concentration equivalent to the IC₅₀ prior to a gradual incremental increase in exposure concentration. Although IC₅₀ values were reported for the full panel of cell lines in **Table 4.3, Chapter 4.3.4**, the data are repeated below [**Table 6.6**] for the relevant cell lines that subsequently underwent chronic exposure to *n*-3 PUFAs.

Table 6.6. Summary of EPA and DHA IC₅₀ data of CRC cell lines

Cell Line	EPA IC ₅₀	DHA IC ₅₀
DLD-1	85.9 ± 1.1 µM	15.3 ± 1.1 µM
HCA-7	141.9 ± 1.0 µM	22.3 ± 1.0 µM
HCT116	91.7 ± 1.1 µM	31.1 ± 1.1 µM
HT-29	118.6 ± 1.1 µM	55.7 ± 1.1 µM
LoVo	141.1 ± 1.1 µM	21.2 ± 1.1 µM
MC38	93.4 ± 1.1 µM	37.4 ± 1.1 µM

Data shown are the mean ± SD for a minimum independent 3 replicates.

6.4.2. The effect of ethanol exposure on cell morphology

Figure 6.23 shows normal morphology of each cell line grown under standard culture conditions. Most cell lines were epithelial-like, adherent, and polygonal in shape with regular dimensions. HCT116 and DLD-1 cells grow in a connected monolayer. HCA-7 and HT29 cells grow as cell colonies, although HT29 cells at confluence lose the island growth pattern to form a continuous monolayer [**Figure 6.23**]. LoVo cells were lymphoblast-like, spherical cells and MC38 cells had morphology resembling fibroblastic cells with bipolar, elongated shapes. Both LoVo and MC38 cells grow as a continuous monolayer, but it was found that MC38 cells at confluence would start to grow on top of each other in dense clusters.

EPA and DHA FFA were diluted in ethanol carrier. To establish whether chronic exposure to ethanol, at a volume equivalent to the volume added to media to give maximal *n*-3 PUFA concentration, resulted in any morphological changes to cell growth, I compared cell growth in regular conditions with growth in media containing 1.5 % v/v ethanol [Figure 6.23]. No differences in growth rates were objectively observed. Cell lines reached confluence on the same day irrespective of ethanol supplementation. Figure 6.23 shows cell lines at confluence, none show morphological differences.

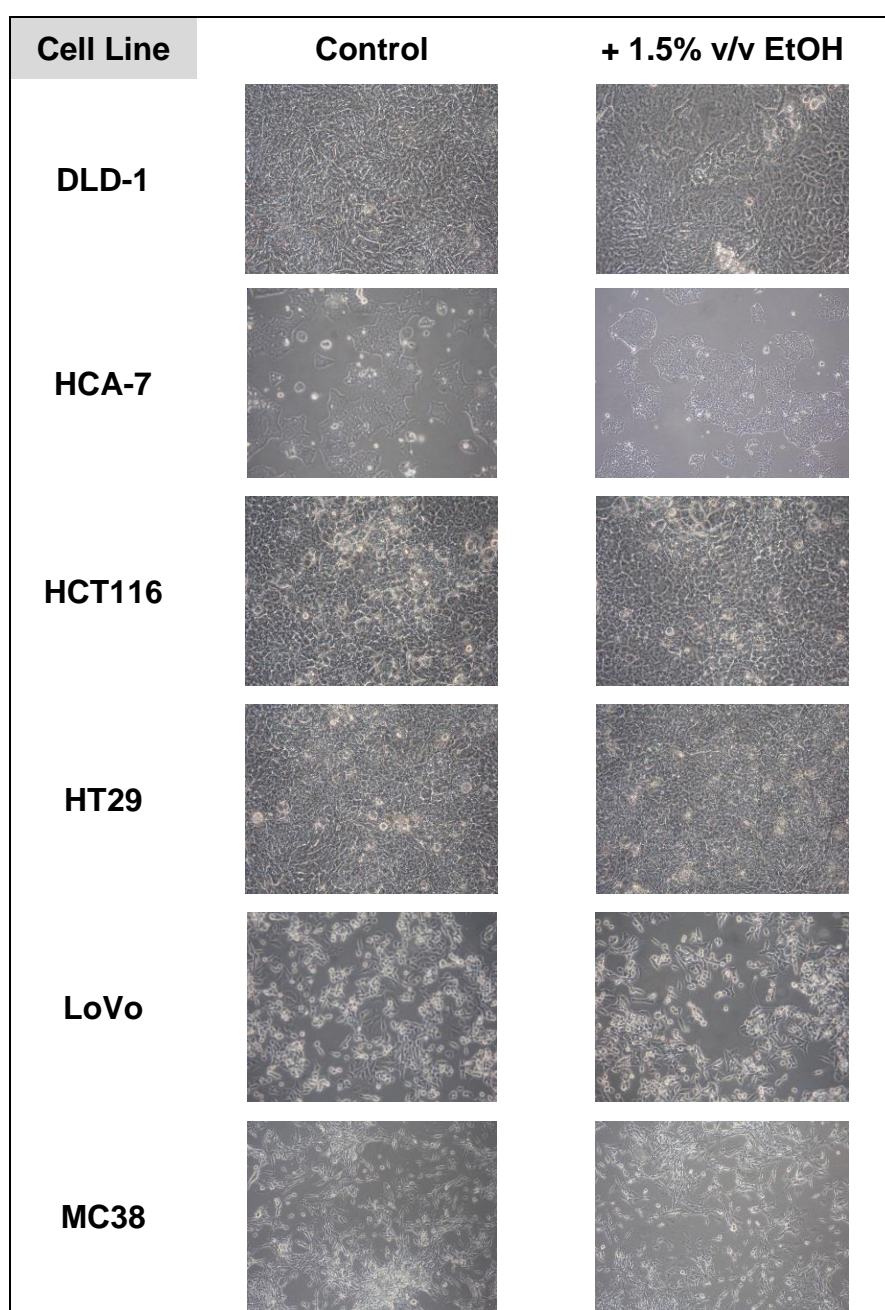


Figure 6.23 Impact of chronic ethanol exposure on cell growth

Illustrative images of cell lines to show morphological features. Cells were cultured in standard culture conditions (control) or in culture media containing 1.5% v/v ethanol (EtOH) for 5 days. Images were acquired on day 5 by light microscopy, obtained with the x20 objective lens.

6.4.3. Using high concentrations of *n*-3 PUFAs to place selective pressure on CRC cells to generate resistance

To test whether treating cells with high concentrations of *n*-3 PUFAs led to generation of resistance, I exposed cells to a concentration range of EPA and DHA and continued culture of cells that had survived the highest possible concentration.

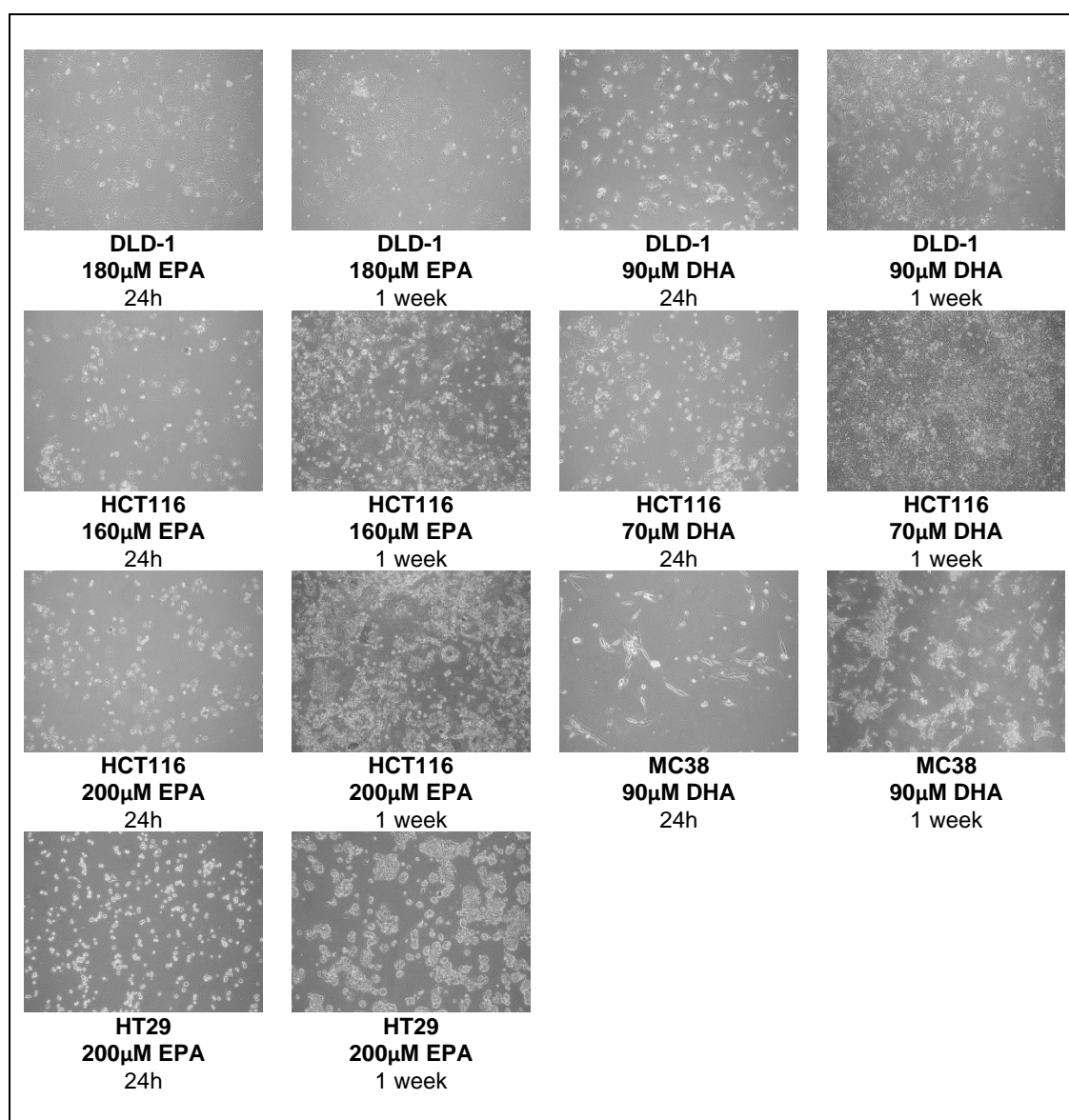


Figure 6.24 The impact of high concentration EPA and DHA exposure for 1 week on CRC cell lines

CRC cell lines were grown in concentrations of EPA that incrementally increased by 20µM from 100µM to 200µM and concentrations of DHA that ranged from 20µM to 90µM. Phase contrast images were obtained using the x10 objective lens at 2 time points; 24 hours and 1 week.

The cell lines had different responses to high concentration exposure of EPA and DHA [Figure 6.24] and these did not correspond to their measured IC₅₀ sensitivities. For example, both DLD-1 and MC38 cells were cultured and survived 1 week of chronic exposure to 90 µM DHA although the IC₅₀ values were 15.3 ± 1.1 µM and 37.4 ± 1.1 µM,

respectively [Table 6.7]. The highest concentrations in which cells survived were; DLD-1, 180 μ M EPA and 90 μ M DHA; HCT116 200 μ M EPA and 70 μ M DHA; HT29 200 μ M EPA and MC38 90 μ M DHA. With the exception of DLD-1 cells treated with 90 μ M DHA, all the cell lines survived passage after 1 week of *n*-3 PUFA exposure.

In the case of HCT116 cells, I maintained cells in two concentrations of EPA; 160 μ M and 200 μ M as the cells treated with 200 μ M began showing distinct morphological differences and appeared to accumulate excessive lipid droplets [Figure 6.25].

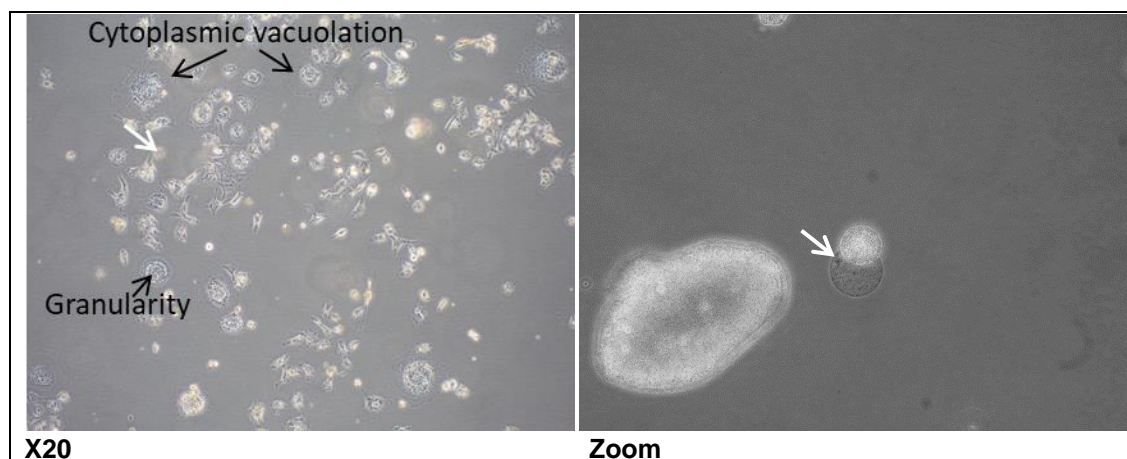


Figure 6.25 Impact of prolonged 200 μ M EPA on HCT116 cell morphology

Phase contrast images representative of the morphological changes in HCT116 cells which were cultured in media supplemented with 200 μ M EPA (refreshed every other day) for 1 week. The images show the effect high EPA exposure causing cells to develop granularity around the nucleus, cytoplasmic vacuolation and accumulate excessive lipid droplets (indicated by the white arrows).

When sensitivity to *n*-3 PUFAs was compared between untreated cells and high-concentration selected cells, all concentration response curves were very similar [EPA and DHA concentration response curves are shown in Figure 6.26 and Figure 6.27 respectively]. With the exception of MC38 cells exposed to 90 μ M DHA, the difference in IC₅₀ concentrations of parental cells and chronically exposed cells were not significantly different (unpaired Student's t-test) [Table 6.7 and Table 6.8].

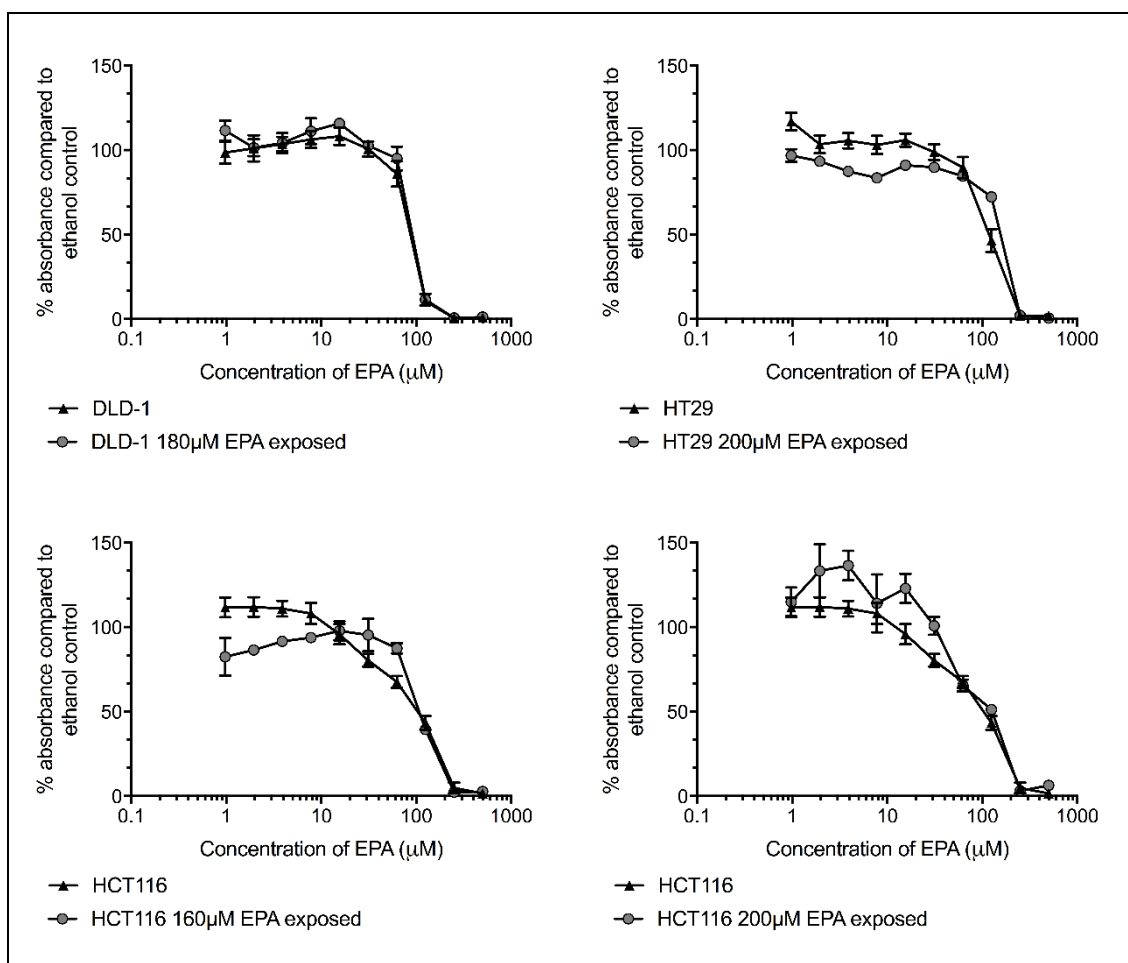


Figure 6.26 EPA concentration response curves of CRC cell lines which were selected following exposure to high concentrations of EPA

DLD-1, HT29 and HCT116 cells were viable in media containing high concentrations (160μM to 200μM of EPA) and subsequently underwent a concentration response MTT assay. Data is expressed as the mean \pm SD of 3 repeats.

Table 6.7. Effect of chronic EPA exposure upon EPA sensitivity (IC_{50})

Cell Line	EPA IC_{50}	p-value (t-test)
<i>DLD-1</i>	85.9 ± 1.1	
DLD-1 180μM EPA	94.4 ± 1.1	0.54
<i>HCT116</i>	91.7 ± 1.1	
HCT116 160μM EPA	109.5 ± 1.1	0.27
HCT116 200μM EPA	107.4 ± 1.2	0.31
<i>HT29</i>	118.6 ± 1.1	
HT29 200μM EPA	146.9 ± 1.1	0.07

IC_{50} : concentration of EPA in which 50% of cells were inhibited. P value was calculated by t-test, comparing chronically exposed cells with un-exposed cells. All data is the mean \pm SD of a minimum of 3 independent replicates.

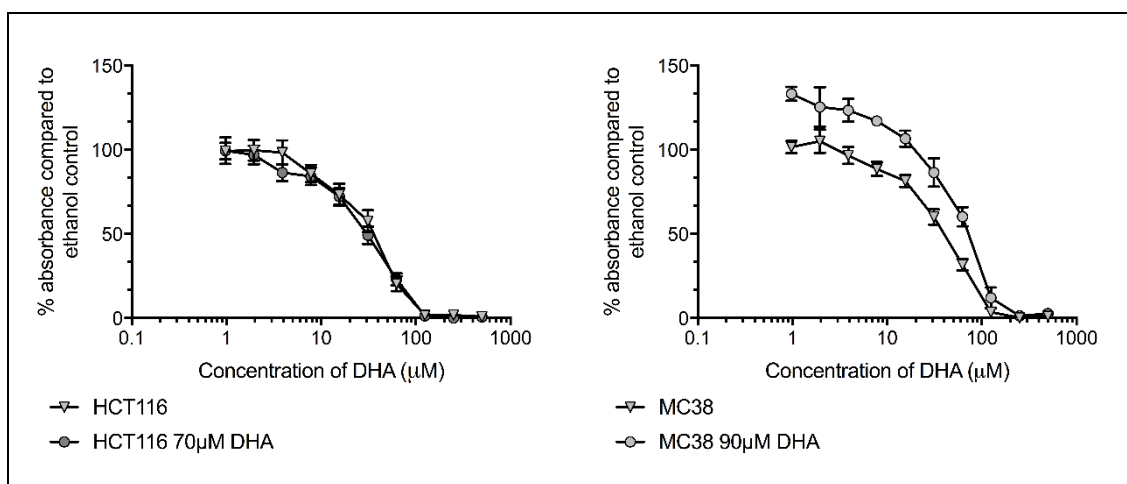


Figure 6.27 DHA concentration response curves of CRC cell lines which were selected following exposure to high concentrations of DHA

HCT116 and MC38 cells were viable in media containing high concentrations (70 µM to 90 µM of DHA) and subsequently underwent a concentration response MTT assay. Data is expressed as the mean \pm SD of 3 repeats.

Table 6.8. Effect of chronic DHA exposure upon DHA sensitivity (IC_{50})

Cell Line	DHA IC_{50}	p-value (t-test)
HCT116	31.1 ± 1.1	
HCT116 70µM DHA	27.5 ± 1.1	0.73
MC38	37.4 ± 1.1	
MC38 90µM DHA	69.4 ± 1.1	0.007

IC_{50} : concentration of DHA in which 50 % of cells were inhibited. P value was calculated by t-test, comparing chronically exposed cells with un-exposed cells. All data is the mean \pm SD of a minimum of 3 independent replicates

As many cell lines were changing morphologically, becoming filled with excess lipid droplets and not showing significant changes in sensitivity, I changed methods to facilitate a gentler approach, using lower concentrations of *n*-3 PUFAs and incremental increases.

6.4.4. Using incremental selective pressure to induce the emergence of a resistant population

I investigated the effect of placing a consistent selective pressure on CRC cells to determine whether an isogenic cell line could be established which would have greater resistance to EPA or DHA. Cells were treated with an IC_{10} concentration of EPA or DHA for 24 hours prior to being cultured in media containing EPA or DHA equivalent to the IC_{50} concentration [Table 6.7].

In general, cells were found to be less viable following passage. This was in part due to the intensive high volume tissue culture practises, including repeated handling in 6 well plates and daily media changes. This led to an increased frequency of infections.

DLD-1 and HCT116 cell lines were least affected by continued exposure to IC₅₀ EPA or DHA, with no differences in morphology seen and growth rates comparable to what was expected of cells in standard conditions. HCA-7 cells treated with 140 µM EPA were particularly difficult to culture as they began to show two signs of cellular stress: granularity around the cell nucleus and cytoplasmic vacuolation. They were therefore not able to be used for cell viability assays as they did not survive past the third passage [Figure 6.28]. HCA-7 cells treated with 20 µM DHA were very slow growing. LoVo cells were found to aggregate and form large clusters following chronic exposure to DHA, and length of time between passages increased. LoVo and MC38 cells treated with EPA were not viable after the third and fourth passage respectively, with LoVo cells detaching and remaining cells were so sparse that they didn't survive whereas MC38 cells grew in dense 3D cell colonies that were unable to be cultured in 96 well plates [Figure 6.28].

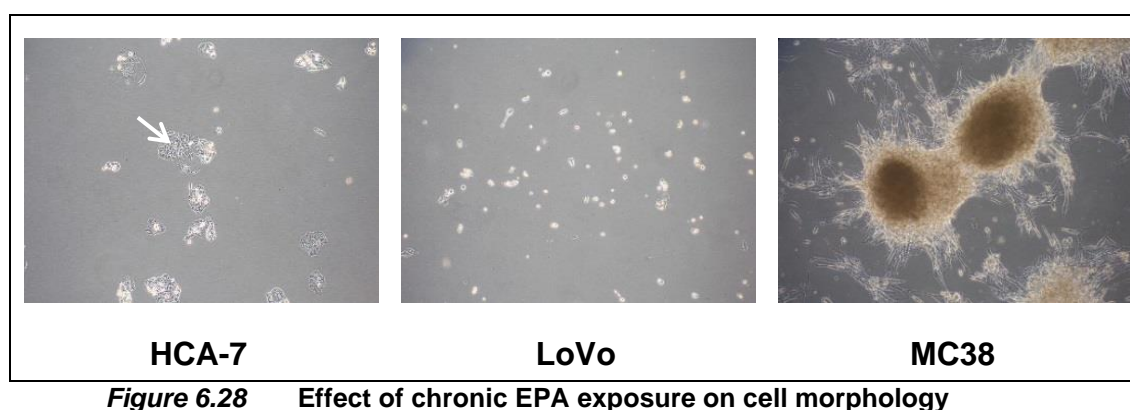


Figure 6.28 Effect of chronic EPA exposure on cell morphology

Illustrative images of HCA, LoVo and MC38 cells following multiple passages in culture media containing an IC₅₀-equivalent concentration of EPA. HCA-7 cells (p3) exhibit cytoplasmic vacuolation (indicated by the arrow). LoVo cells (p3) lost adherent properties and the sparse number of cells that survived failed to establish a new population. MC38 cells (p4) grew in dense clusters. Phase contrast images were obtained with x20 objective lens.

Only 3 cell lines (DLD-1, HCT116 and HT-29) were viable following 5 passages when maintained in IC₅₀ equivalent concentration EPA supplemented media. Images of DLD-1 [Figure 6.29 A], HCT116 [Figure 6.31 A] and HT29 [Figure 6.32 A] cells show that cell morphology did not change following maintained culture in respective IC₅₀ EPA supplemented media. No statistically significant differences in IC₅₀ were measured [Figure 6.29 C, Figure 6.31 C and Figure 6.32 C]. The biggest difference between treated and untreated cell line IC₅₀ values was seen for DLD-1 cells. Following chronic exposure, an increase in IC₅₀ from baseline 85.9 ± 1.06 µM to 109.0 ± 1.62 µM was

measured, although this was not significant (Student's t-test, p value = 0.38) [**Figure 6.29 B-C**].

All cell lines chronically exposed to DHA were able to be cultured in DHA-supplemented media and remained viable for 5 passages, with no observed changes in morphology [**Figure 6.29** to **Figure 6.34**]. Each chronic exposed cell line was shown to have an increased IC_{50} in comparison to their non-exposed counterparts, though none were found to be of statistical significance (unpaired independent Student's t-test) [**Figure 6.29 F** to **Figure 6.34 F**]. Comparing untreated and chronic exposed LoVo DHA IC_{50} showed an IC_{50} difference of 15 μ M (Student's t-test, p = 0.07) [**Figure 6.33 F**].

Sensitivity to the *n*-3 PUFA that was not used for chronic exposure was also assessed (i.e.: DHA sensitivity was tested in EPA-treated cells and EPA sensitivity was tested in DHA-treated cells), with no difference in sensitivity found between chronically exposed and untreated cells (data not shown). As multiple cell lines were found to be less viable following passage when maintained in constant IC_{50} -equivalent treated media, combined with the fact that the difference in sensitivity was not consistent and not determined to be statistically significant, the decision was made to stop using time and resources on this so that the work could focus on the investigation of inherent CRC *n*-3 PUFA sensitivity properties.

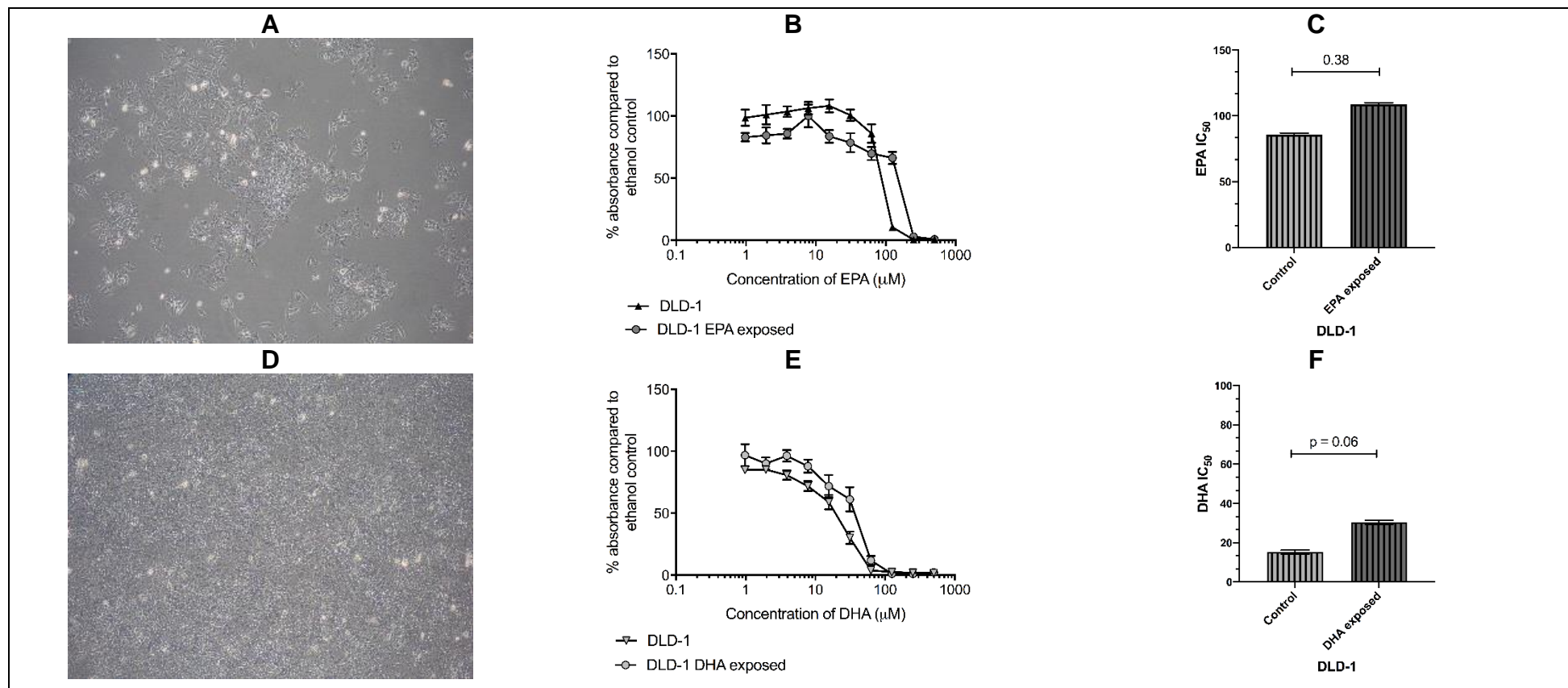


Figure 6.29 The effects of EPA and DHA chronic exposure on DLD-1 cells

DLD-1 cells were cultured in RPMI media containing an IC₅₀ equivalent concentration of EPA or DHA; DLD-1 cells morphology following growth in (A) EPA and (B) DHA respectively for 5 passages. All images acquired with x20 objective lens. Comparative (B) EPA and (E) DHA concentration response curves of untreated and chronically exposed cells, respectively. MTT concentration responses were plotted from a minimum of 3 independent replicates. (C) and (F) show EPA and DHA mean IC₅₀ \pm SD of untreated and chronic exposed cells. Statistical significance of the difference between the two was assessed by unpaired independent Student's t-test.

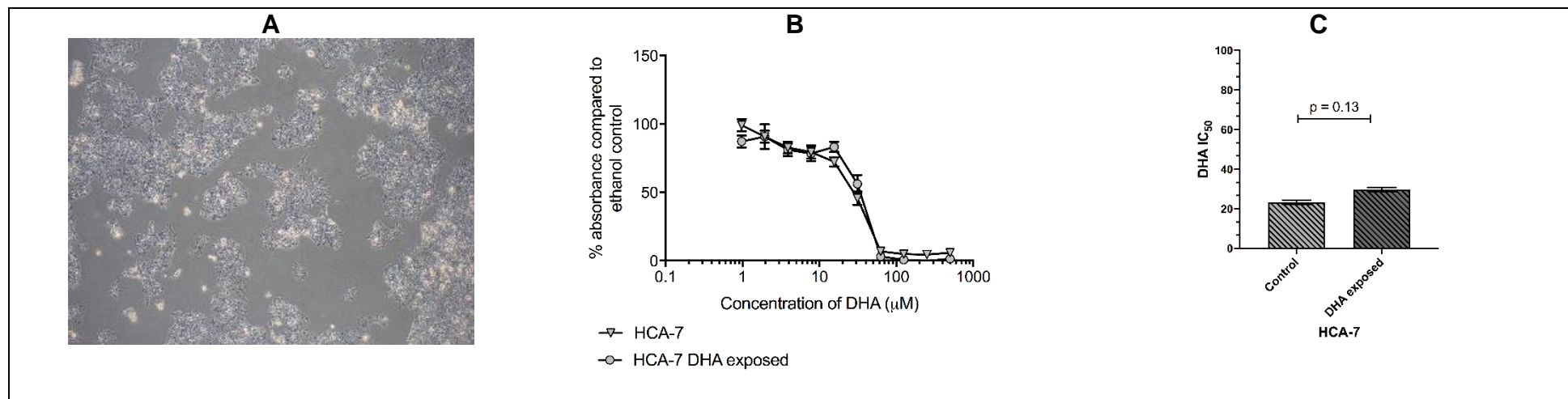


Figure 6.30 The effect of chronic DHA exposure on HCA-7 cells

HCA-7 cells were cultured in RPMI media containing an IC₅₀ equivalent concentration of DHA; HCA-7 cells morphology following growth in (A) DHA for 5 passages. All images acquired with x20 objective lens. Comparative (B) DHA concentration response curves of untreated and chronically exposed cells, respectively. MTT concentration responses were plotted from a minimum of 3 independent replicates. (C) Shows DHA mean IC₅₀ ± SD of untreated and chronic exposed cells. Statistical significance of the difference between the two was assessed by unpaired independent Student's t-test.

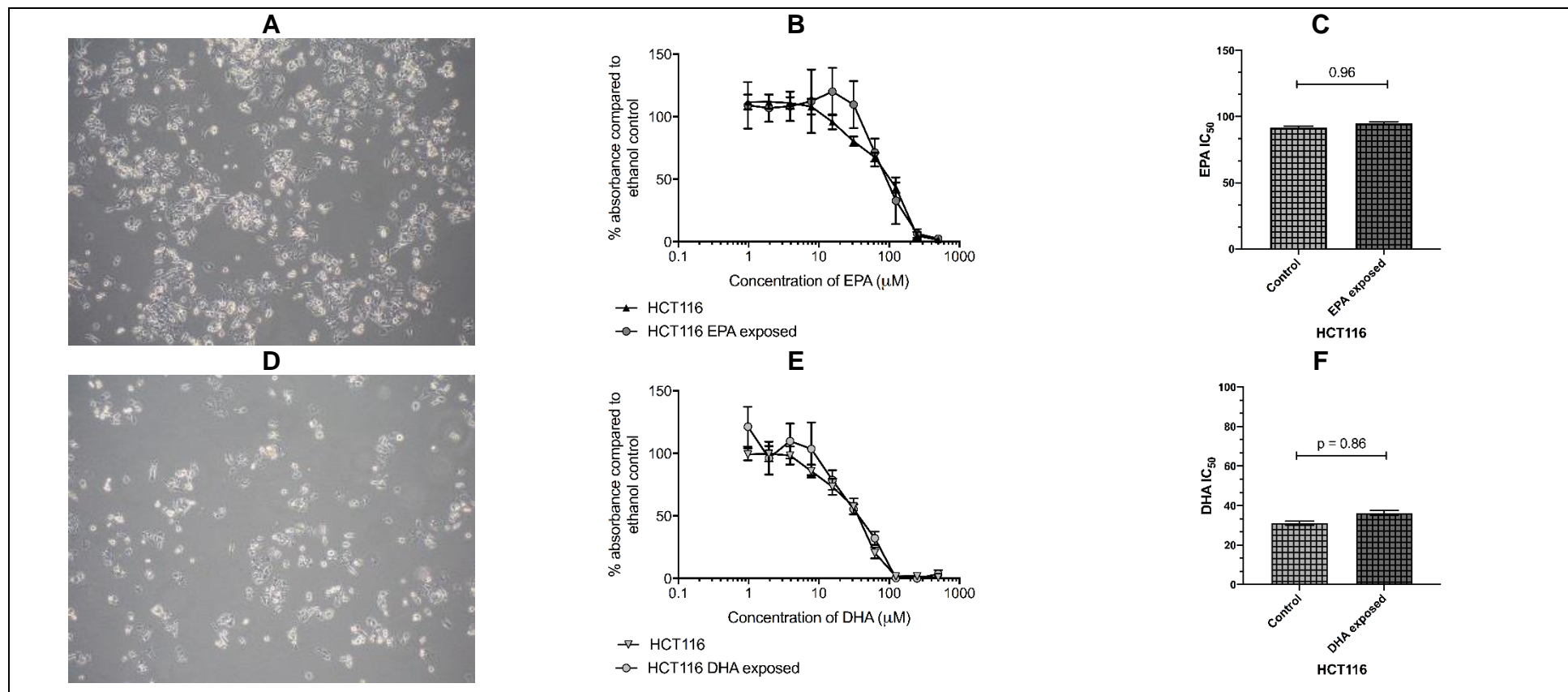


Figure 6.31 The effect of chronic EPA and DHA exposure on HCT116 cells

HCT116 cells were cultured in RPMI media containing an IC₅₀ equivalent concentration of EPA or DHA; HCT116 cells morphology following growth in (A) EPA and (B) DHA respectively for 5 passages. All images acquired with x20 objective lens. Comparative (B) EPA and (E) DHA concentration response curves of untreated and chronically exposed cells, respectively. MTT concentration responses were plotted from a minimum of 3 independent replicates. (C) and (F) show EPA and DHA mean IC₅₀ ± SD of untreated and chronic exposed cells. Statistical significance of the difference between the two was assessed by unpaired independent Student's t-test.

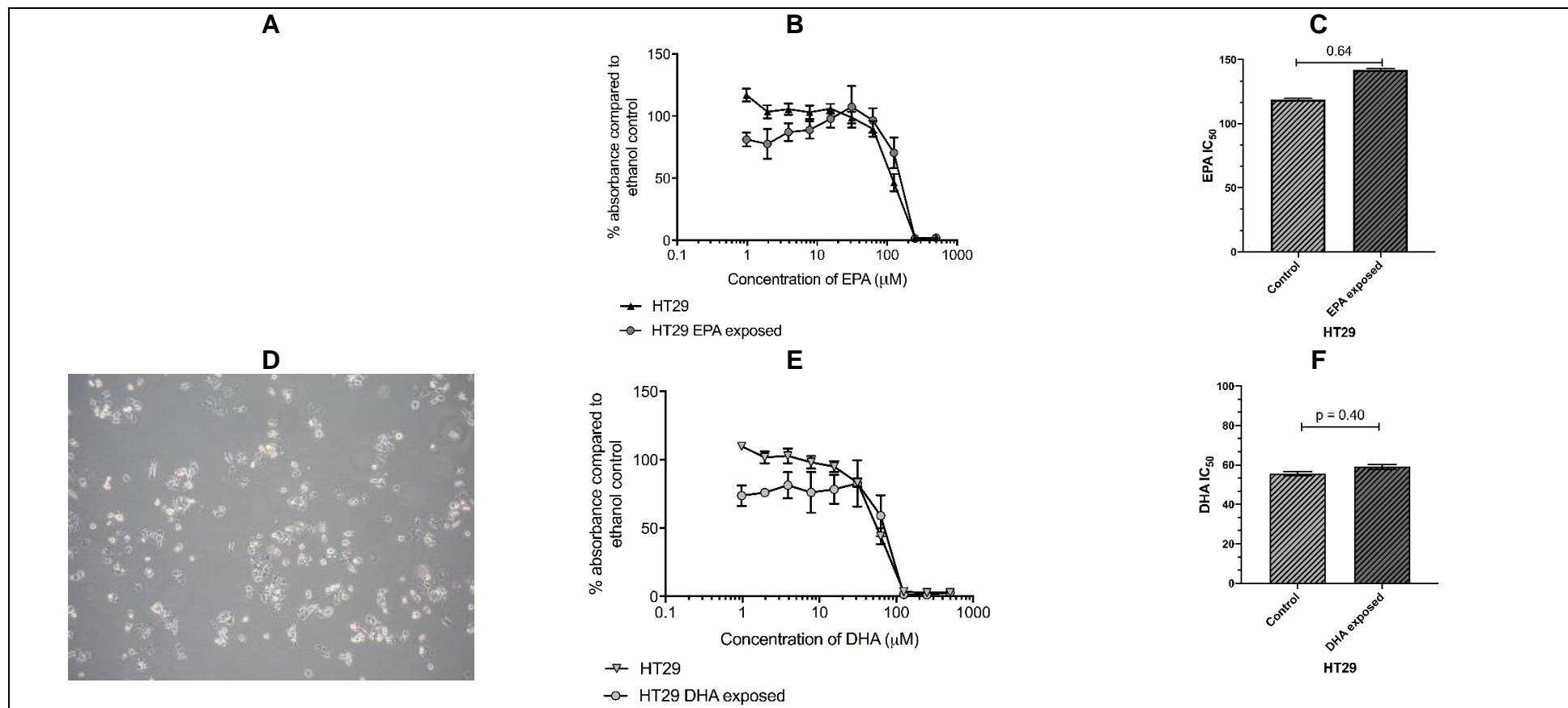


Figure 6.32 The effect of chronic EPA and DHA exposure on HT29 cells

HT29 cells were cultured in RPMI media containing an IC_{50} equivalent concentration of EPA or DHA; HT29 cells morphology following growth in (A) EPA and (B) DHA respectively for 5 passages. All images acquired with x20 objective lens. Comparative (B) EPA and (E) DHA concentration response curves of untreated and chronically exposed cells, respectively. MTT concentration responses were plotted from a minimum of 3 independent replicates. (C) and (F) show EPA and DHA mean $\text{IC}_{50} \pm \text{SD}$ of untreated and chronic exposed cells. Statistical significance of the difference between the two was assessed by unpaired independent Student's t-test.

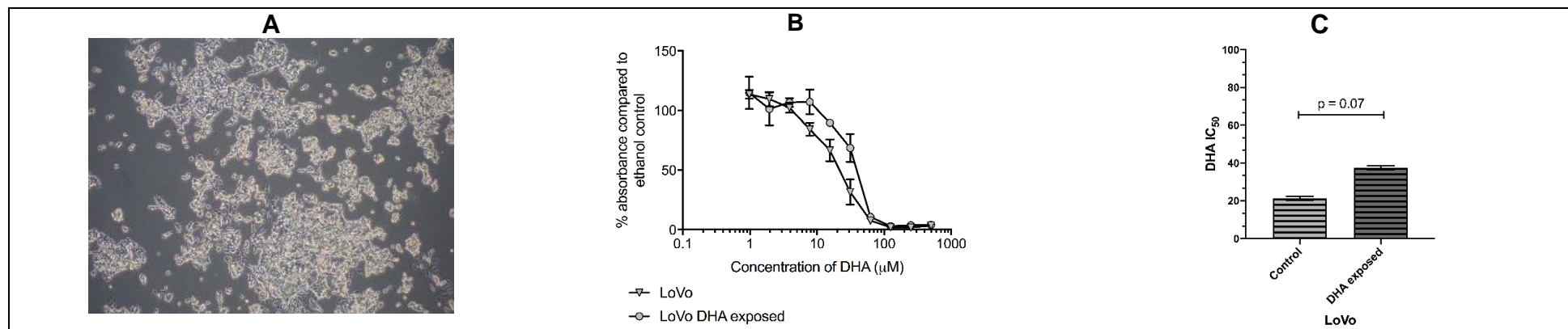


Figure 6.33 Chronic exposure of LoVo cells to IC₅₀ DHA

LoVo cells morphology following growth in (A) IC₅₀ equivalent concentration DHA for 5 passages. Image acquired with x20 objective lens. Comparative (B) DHA concentration response curves of untreated and chronically exposed cells. MTT concentration responses were plotted from a minimum of 3 independent replicates. (C) Shows DHA mean IC₅₀ ± SD of untreated and chronic exposed cells. Statistical significance of the difference between IC₅₀ assessed by unpaired Student's t-test.

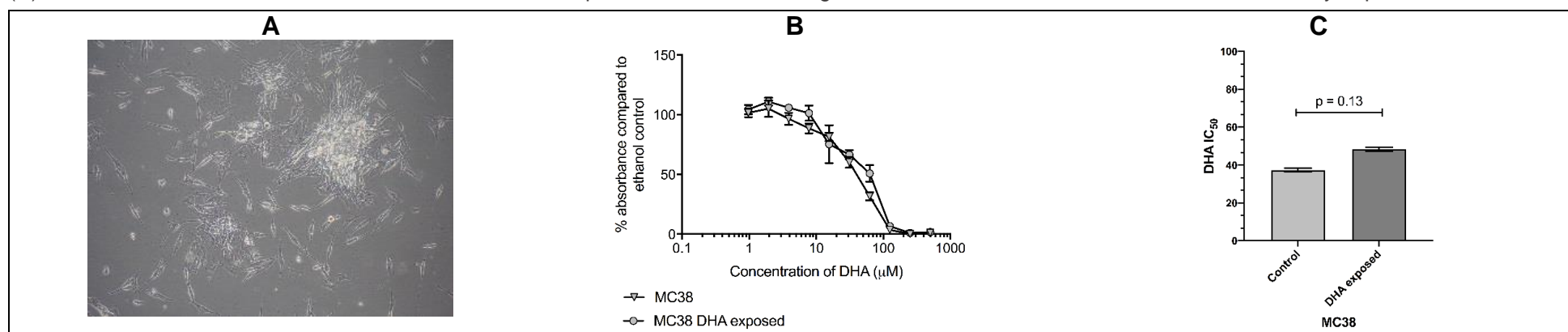


Figure 6.34 The effect of DHA chronic exposure on MC38 cells

MC38 cells morphology following growth in (A) IC₅₀ equivalent concentration DHA for 5 passages. Image acquired with x20 objective lens. (B) Comparative DHA concentration response curves of untreated and chronically exposed cells. MTT concentration responses were plotted from a minimum of 3 independent replicates. (C) Shows DHA mean IC₅₀ ± SD of untreated and chronic exposed cells. Statistical significance of the difference between IC₅₀ assessed by unpaired Student's t-test.

6.5. Discussion

Mechanism(s) of anti-cancer activity of *n*-3 PUFAs are still to be fully elucidated. To identify potential biomarkers or pathways associated with *n*-3 PUFA sensitivity, this work focused on comparison of isogenic sensitive and resistant cell lines.

6.5.1. MRGPRF

This chapter aimed to examine the role of MRGPRF EPA sensitivity. I hypothesised that increasing *Mrgprf* / MRGPRF expression in EPA-resistant MC38r cells would restore sensitivity to EPA.

6.5.1.1. Key findings

Using two cell lines, HEK293 and MC38r, I stably transfected an MRGPRF-vector and a control empty vector. HEK293 are well characterized cells of epithelial origin, and have been extensively used as a recombinant protein expression tool due to their amenability to transfection, high transfection efficiency and protein production rates and faithful translation and processing of proteins (305). Overexpression of two Mrg family members in HEK293 cells was used to investigate ligand selectivity and receptor signaling of MrgC11 and MrgA1 (306). hCRC cell lines can be used for transfection, an example of this is a study in which CaCo-2 and HT29 cells were transfected with calcium-sensing receptor, CaSR. CaSR, a GPCR, is a potential tumour suppressor found downregulated in highly malignant CRCs. Overexpression of CaSR was associated with reduced proliferation markers, and loss of CaSR correlated with poor tumour differentiation and a reduction in apoptotic potential (307). Cells used in this study were mouse derived colorectal cancer MC38r cells, as they were the most relevant model for study as they were interrogated in the original microarray that identified MRGPRF. However, MC38r cells (and the MC38 cells from which the 'r' strain is derived from) are not used as frequently for transfection and are therefore less well characterized in terms of expected transfection efficiencies and protein production ability.

My results show that HEK293 cells were easier to transfect. This is supported by the literature, which reports frequent use of HEK293 as transfection hosts, as the cells have the post-translational modification machineries, essential to ensure correct folding and subsequently optimal biological activity of the target protein (308). In addition, HEK293 cells have morphological, cell growth characteristics and capacity to express transgenic receptor proteins (308). These attributes may, or may not, be shared by CRC cell lines,

which are highly dysregulated by nature of their neoplastic origin. In comparison to the 80% of HEK293 cells with eGFP expression following transfection, only 1 % of MC38r transfected cells fluoresced. Despite this, more sensitive FACS data shows that single cell MRGPRF overexpression clones were generated using cells with greatest GFP fluorescence and flow cytometry data showed that cells were still GFP positive following multiple passages.

The stable overexpression clones were characterised, and it was observed that HEK293 cells displayed altered cellular properties (morphology and growth rates) in response to transfection, whereas MC38r cells did not. This could be due to the relative quantities of transcript, with HEK293-MF_{VL} clones containing vast relative quantities of *Mrgprf* transcript in comparison to MC38R-MF_{VL} clones, in which only MC38r-MF_{VL} clone C6 showed an increase in relative quantity. Relative quantity measurements indicate MC38r cells have lower transfection efficiency, less copies integrated and perhaps lack the biochemical machinery to incorporate vector DNA.

Characterising clones allowed for selection of cells with highest *Mrgprf*/MRGPRF expression, least growth disruption and cells least likely to have integrated the plasmid in a position where off-target effects unrelated to MRGPRF would render the model useless for this study.

Transcript *Mrgprf* was detected by RT-qPCR and immunofluorescence was used to determine whether this translated to give protein expression. Two anti-MRGPRF primary antibodies were used, both were raised against antigens which mapped to the N-terminal extracellular domain of human MRGPRF, although there is an 86 % sequence homology between human and mouse MRGPRF. The first antibody used, N-14, was found to be non-specific and produced inconsistent staining patterns and thus results were uninterpretable.

Immunofluorescent labeling with a second anti-MRGPRF antibody sourced from the Human Protein Atlas, HPAMF, allowed visualization of MRGPRF protein location in HEK293-transfectants. Results for MC38r transfectants showed no detectable intensity difference between unstained controls and stable clones. The staining pattern in HEK293-MF_{VL} clones was consistent between overexpressing clones and biological replicates, showing localisation of protein to the cellular membrane. In addition, by comparing HEK293-M_{VL} clone C1 and HEK293-M_{VL} clone C3, fluorescence intensity corresponded with quantity of *Mrgprf* as determined by RT-qPCR, with HEK293-M_{VL} clone C3 showing greater expression at both the mRNA and protein level. This

suggested that the antibody, HPAMF was specific and sensitive. My findings were consistent with data collected by the Human Protein Atlas (HPA) that predict MRGPRF localisation within the nuclear and plasma membrane (304) [Figure 35A] demonstrated by immunofluorescence using HPAMF antibody in human BJ cells [Figure 35B].

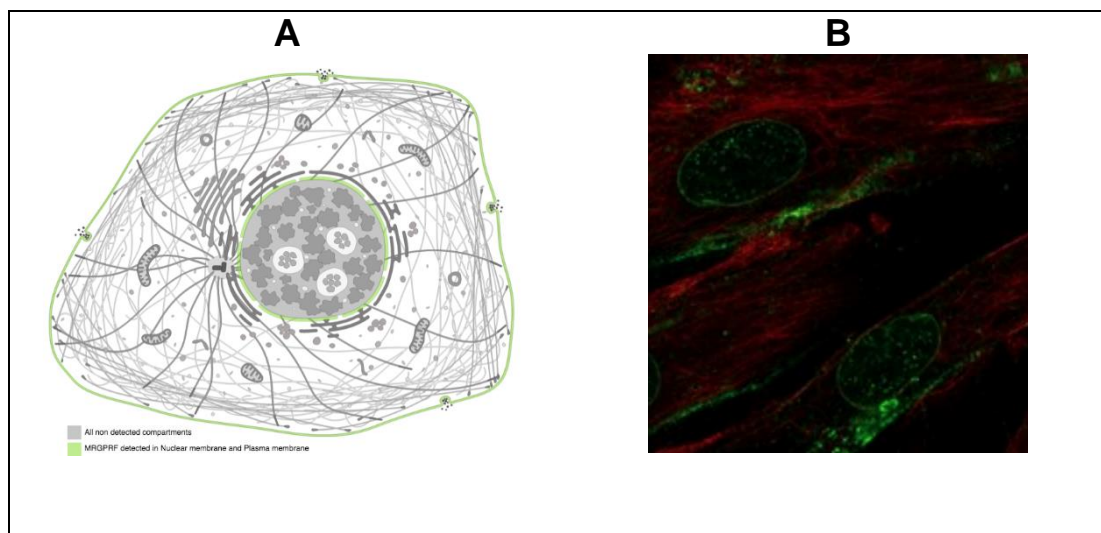


Figure 6.35 MRGPRF localization determined by Human Protein Atlas

The Human Protein Atlas have predicted and observed Mrgprf localisation to the nuclear and plasma membranes. Image reference: 70

Difficulties detecting consistent protein expression patterns between stable transfected cell lines required an alternative approach by which I could validate the vector expression. Anti-His antibody was therefore used to detect the His-tag present in MRGPRF transfected cells. His-tags are useful for protein purification and the size would be unlikely to have protein folding implications. However, detection of His-tags can be difficult due to; it's position (in this case C-terminal), cleavage, and accessibility of the epitope and specificity of the antibody or the technique used. In previous work (data not shown), immunofluorescence images of transiently transfected cells labelled with His-Tag (D3I10) XP rabbit monoclonal antibody (Cell Signalling Technology, #12698) were not found to show differential expression to untransfected control cells.

Altogether, data suggested that MRGPRF protein was present in HEK293-MF_{VL} stable clones and therefore EPA sensitivity and functionality assays were performed to determine whether the protein was able to signal, and by which pathway signaling was mediated.

A key finding of this project was that HEK293 cells overexpressing MRGPRF did not display increased sensitivity to EPA. My results were independently corroborated by work undertaken by Jordan Appleyard and Harriet Beal, who obtained IC₅₀ values of

184.6 \pm 0.83 μ M for HEK293-CT_{VL} clone B4, 129.2 \pm 0.79 μ M for HEK293-MF_{VL} clone C3 and 154.4 \pm 1.15 μ M for MC38r-CT_{VL} clone A7 and 159.1 \pm 1.17 μ M for MC38r-MF_{VL} clone C6 respectively (309, 310). A link between Mrgprf expression and EPA sensitivity could not be established in the stable transfectants. Therefore, confirming whether MRGPRF was functional in HEK293 and MC38r clones was necessary to allow a definitive conclusion as to whether the negative finding was real.

MRGPRF is a G protein coupled receptor and therefore activation of this receptor could lead to the production of second messenger molecules such as cyclic AMP (cAMP), diacylglycerol (DAG) and inositol 1,4,5-triphosphate (IP3) that can initiate and coordinate intracellular signaling pathways (200, 292, 298, 299). Algorithms to interrogate GPCR sequences in order to predict GPCR coupling preference is an area of research under development, with one method used to assess 282 GPCR sequences with known G-protein coupling patterns able to classify 89.7 % sequences correctly (311).

Mrgs are most closely related to MAS1, a proto-oncogene first identified in 1986 (294) for which Ang II metabolite Ang-(1-7) is an endogenous agonist (312). The MAS1 receptor has been shown to couple with G_{ai}, G_{aq} and G_{α12/13} proteins, and activation results in signalling via many pathways including activation of IP3/Akt, cAMP/PKA and calcium messenger release (313). Mrgs share up to 35 % sequence homology with MAS1 (294). Evidence suggests that many Mrg family members elicit response via calcium mediated signalling. In a study in which MrgA1 and MrgC11 were overexpressed in HEK293 cells, RF-amide neuropeptides FLRFa and γ2-MSH were used to activate MrgA1 and MrgC11 respectively. Transient intracellular calcium responses were detected (306). A study by Liu *et al*, 2009, reported that in response to chloroquine exposure a robust intracellular calcium increase was Mrgpr dependent (314). Calcium-mitigated signalling cascades were reported for *Mrgpr A1-4, A10, A12, A14, A16, A19, B4-5 and C11* (314). MRGPRD was shown to be G_{αq} coupled and thus signal via calcium (292, 293). In addition, activation of hMrgX1 resulted in calcium release (315). Therefore, performing a calcium assay allowed investigations as to whether the stable clones were signalling via the calcium pathway. Whilst the thapsigargin and ATP controls showed an increase in intracellular calcium, measured by the F_{340/380} ratio, no such response was observed for cells treated with 25 μ M or 50 μ M EPA.

Adenylyl cyclase is another target of an activated G protein. Upon activation, by interacting with GTP-bound G_α, adenylyl cyclase enzymatically catalyses cAMP second messenger production (298). Despite initial studies failing to identify Ang(1-7) induced calcium, IP3 or cAMP signalling responses in MAS1 transfected CHO cells (316, 317),

Ang(1-7) treatment activated MAS1 $G_{\alpha s}$ signalling that elevated cAMP in the kidney (313, 317). It was possible that MRGPRF was coupled to the $G_{\alpha_{i/o}}$ or to the G_{α_s} family of heterotrimeric G proteins. Thus, we measured cAMP production in the presence of EPA and presence or absence of forskolin. Work that was completed by Masters Students to determine whether cAMP production was triggered by EPA treatment shows that HEK293-MF_{VL} clone C3 and MC38r-M_{VL} clone C6 were not signalling through cAMP pathways [Appendix A6.3]. The results show that there was no increase in cAMP production upon EPA treatment when compared with untreated cells (309, 310)

It should be taken in to consideration that the homology between Mrgprs in humans and mice is notably lower than is observed for most other GPCRs, for example human MrgprX1 has two putative orthologues, mouse MrgprC11 and MrgprA3, which it shares only 54 % and 50 % amino acid identity, respectively (318, 319). This limits the development of animal models in which to study the MRG receptors to understand the function and identify ligands and response pathways. It has been shown that even amongst Mrg receptors in highly related species there are drastic differences in the genomic organization, therefore whilst the mouse genome contains 22 *MrgA* genes and 14 *MrgC* genes, the rat genome contains just one (320).

In conclusion, stable MRGPRF overexpression models were established and phenotypically characterized. The overexpression of *Mrgprf* has not resulted in increased EPA sensitivity. However, the functionality of the over-expressed protein was not definitively determined although it did not appear to cause downstream cAMP or calcium signaling.

6.5.1.2. Strengths and Limitations

The major strength of this work was the systematic approach taken. Once the MRGPRF cell line was established, steps were taken to both phenotypically characterize and validate the model. The work generated two stable transfected models of MRGPRF overexpression. However, there were limitations. The first limitation is the potential of clonally selected cells to accumulate additional genetic variation (passenger mutations) whilst in culture, which could alter the cellular phenotype and confound the effect of MRGPRF overexpression on EPA sensitivity. Whilst such passenger mutations may not drive sensitivity or resistance to EPA, they could impact upon pathways mediating the cells response to EPA.

Although there is a high level of sequence homology between human and mouse MRGPRF, there were no commercially available mouse specific anti-MRGPRF antibodies. Due to time and cost constraints, development and production of a mouse-specific antibody was not possible. A lot of the study involved use of N-14 primary antibody which was subsequently found to produce inconsistent results between experimental repeats and between techniques used. The fact that neither antibody was not mouse specific, could be related to the differences observed when comparing N-14 antibody with HPAMF antibody as they were targeting different epitopes, but were also both targeted to extracellular domains and validated against human epitopes. HPAMF epitope antigen sequence shared 83 % sequence similarity with the human protein sequence, however the peptide sequence to which N-14 was raised is not available. The different cell fixing methodologies required for optimal protein detection between techniques used for MRGPRF detection may also have implications for the inconsistent results seen between methods.

Another limitation is the lack of a known agonist for MRGPRF, as this would be beneficial stimulant that could be used as a marker for positive response in the calcium assay. Although ATP produces a positive response, indicating the presence of P₂-type purinoceptors, one of which has been found to be expressed in HEK293 cells; P₂Y₁ (201, 202), this only acts to confirm cell viability and reactive potential. The conformational protein structure of MRGPRF however is not known and cannot be determined from these assays. The size of GFP has been shown previously to alter localisation, structure and function of proteins to which it has been tagged when compared to native proteins (321). The effect of the GFP tag on MRGPRF protein structure and function is unknown, although *in vivo* studies investigating other Mrgpr family members have utilised GFP tags (322, 323) and have shown that there is no effect of GFP fusion on the normal function of Mrgprs (294, 306). Whilst I was not able to conclude as to whether the stable protein produced in MRGPRF transfectants was functional, there is precedent for successful development of MRG overexpressing clones in HEK293 cells with functionality of MrgA1 and MrgC11 confirmed to be coupled to Gα_q, but not to Gα_i or Gα_s signalling pathways (306).

6.5.1.3. *Future directions*

To further validate the current models of MRGPRF overexpression the structure of MRGPRF protein in stable transfectants would need to be ascertained, by X-ray crystallography, and compared to the known structure. Following confirmation of protein structure, production of a polyclonal mouse-specific antibody should be undertaken.

Polyclonal antibody production is relatively cheap and quick in comparison to production of a monoclonal antibody, resulting in an antibody that can recognise multiple epitopes (324). Antibody production would involve injection of the MRGPRF antigen into a host in order to stimulate B cell production of antibodies (324). It should be noted that there are challenges associated with producing antibodies to GPCRs, in fact only one anti-GPCR antibody is commercialised, namely mogamulizab which treats relapsed and refractory adult T-cell leukaemia-lymphoma (325). Challenges of antibody production relate to the difficulty in preparing and isolating homogenous GPCRs in solution, solubility concerns as detergents can alter protein conformation, limited exposed extracellular epitope region and highly variable extracellular regions (325).

Additionally, a ligand screen could be used to identify potential agonists and a positive response to MRGPRF stimulation. The deorphanisation of MRGPRF remains elusive, and the process of deorphanisation is challenging. Limited understanding as to physiological function and role within signal transduction pathways causes experimental designs confounded by lack of positive controls and signal transduction assays (326). Assays which focus on measurement of secondary messengers regulated by G proteins may be insufficient in deorphanisation studies, as GPCRs can activate a variety of signal transduction pathways (326). Detecting a signal being transmitted may be challenging as they are often expressed under specific conditions and for a limited duration of time (326).

Alternative strategies to interrogate the potential role of MRGPRF in cellular response to EPA could be used. This could include genetic deletion (via available technologies such as siRNA, shRNA or CRISPR-Cas9) of MRGPRF in MC38 cells and subsequent testing to see if the IC_{50} increased as cells became resistant to EPA. However, this would have been limited by low endogenous expression in many cell lines.

Finally, MRGPRF study could be strengthened by detecting differential expression of MRGPRF in the inherently sensitive and resistant human CRC cell line panel. In addition to further work investigating MRGPRF, the original microarray panel [Table 6.1] could be revisited to identify whether any of the targets identified warrant further investigation. If this comparison showed differential MRGPRF expression between sensitive and resistant human CRC cell lines, the MRGPRF vector could be re-designed with a human-derived sequence. The process of validating the model with anti-MRGPRF human antibodies would negate issues that have arisen when using such antibodies against a mouse epitope and in mouse CRC cells.

6.5.2. Generating resistance

Generating *n*-3 PUFA resistance in CRC cell lines was unsuccessful.

Morphological changes resulting from chronic exposure was observed in HCA-7, LoVo and MC38 cell lines. Previous work by Zhang *et al* compared effects of PUFAs and 5-FU treatments on LoVo and RKO hCRC lines (139). They found that the inhibition of cell growth and significant alterations in morphology were comparable between PUFA and 5-FU treatment, with notable morphological changes for LoVo cells reported following 48-hour treatment with 150 μ M EPA or DHA. Treatment of cells with EPA or DHA resulted in lower cell counts and distorted and 'rounded up' cell morphology(139). This was different to what I had observed in LoVo cells, where 140 μ M EPA chronic exposure rendered cells non-viable, and a much lower concentration of DHA (20 μ M) caused cells to grow in 'clumps'.

I found that cells lines chronically maintained in media containing high concentrations of *n*-3 PUFA had developed lipid bodies, organelles in which the excess lipid was stored (327). Weller *et al* found that other FAs; arachidonic acid (20:4 *n*-6) and oleic acid (18:1 *n*-9) stimulated dose-dependent formation of lipid bodies in human polymorphonuclear leukocytes (PMNs) over 30 to 60 minutes (328).

The data obtained were also difficult to interpret, as it is not known what shift in IC₅₀ would confirm altered sensitivity. In comparison to small molecules such as 5-FU, the multiple roles, metabolism profiles and signalling pathways of *n*-3 PUFAs create challenges when generating resistance as one single event is unlikely to confer resistance. 5-FU is a uracil analogue that is converted to active metabolites; fluorouridine triphosphate, fluorodeoxyuridine triphosphate, and fluorodeoxyuridine monophosphate, which interrupt RNA processing and functioning and cause DNA damage, initiating apoptosis (329). In a study in which CRC stem-like cells were treated with intermittent IC₅₀ drug dose or continuous treatment with escalating 5-FU doses, the former generated strong resistance (329). Aggressive tumours were grown from 5-FU resistant cells *in vivo*, and gene expression profiles indicative of upregulated *ID1* associated with resistance (329). Generating *n*-3 PUFA resistance to one target may not be specific to the dominant pathway used or cause cells to switch to alternative pathways or metabolism routes, resulting in limited effect sensitivity.

The strengths of this work included that an attempt to create resistant cell lines was trialled in multiple cell lines with differing inherent sensitivities. It was also not limited to

one protocol, the use of 2 approaches maximised the potential of developing a resistant strain. However, there were several limitations to this study. The process of generating cell lines resistant required a high amount of cell handling which increased likelihood of infections. In addition, the concentration of EPA or DHA that was required to apply enough selective pressure was unknown and therefore I used concentrations equal to or greater than the respective cell lines' IC₅₀. Methods, in anti-cancer therapeutic context, are reliant on the establishment of cancer drug resistant cell lines which are notoriously laborious and time-consuming to generate and establish (330). Studies in which cell lines were generated that were resistant to chemotherapies have shown success when the cells were incubated at very low start doses that gradually increased over time (301-303), or where cells have been treated with a higher dose but have taken 3 months to establish and overcome the initial selective pressure as seen during the development of a methotrexate-resistant HT-29 cell line (331). An attempt using lower concentrations of EPA or DHA and slowly increasing the exposure in small incremental amounts, was not finished due to time constraints, however could have potential for mitigating the cellular stress which has limited the progression of developing cell lines resistant to *n*-3 PUFAs.

6.5.2.1. *Future Directions*

A human CRC cell line with acquired *n*-3 PUFA resistance would still be a useful tool in which to study the differential cellular responses. Consequently, creating a cell line in which EPA or DHA was incrementally increased from a very low starting concentration over a period of many months could perhaps allow for slow adaptation to the *n*-3 PUFA presence and mitigate the issues with cells growing with altered morphology or dying. The alternative would involve mutagenesis techniques, however implications of this include the impact on many genes. Therefore, cells which could become resistant may be an artefact to alteration of a gene not related to cellular chemosensitivity to EPA or DHA.

Chapter 7: General Discussion

The overall aim of this research was to understand what drives response, sensitivity, or resistance in hCRC cells to *n*-3 PUFAs so that ultimately, personalised therapy can be developed and utilised in clinical practise for patient benefit.

Chapter 4 shows that hCRC cell line panel intrinsic sensitivity to *n*-3 PUFAs was variable and all cell lines were more sensitive to DHA than EPA. When testing the relationship between molecular phenotypes and *n*-3 PUFA sensitivity, no association with *PTGS* expression was found, but a relationship between CIMP+ status and EPA sensitivity was identified. Utilising demethylating treatment to 'reverse' the CIMP+ phenotype, an increase in EPA resistance was measured. **Chapter 5** investigated the relationship between sensitivity and FA profiles, in which data were expressed as both % FA and absolute quantities. As previously stated, as FA quantities measured in samples were greater than the limits of the standard curves, the data requires further validation, currently being undertaken by collaborators. Comparing % FA data with previous studies, similar trends were observed in relation to EPA or DHA supplementation and expected increases in EPA or DHA content, and concomitant decrease in AA content. However, preliminary analysis whereby data were expressed as an absolute quantity identified potential increased AA content in some EPA-treated cells. The relationship between EPA supplementation and conversion to DHA via DPA was examined. Whilst no relationship was found between EPA sensitivity and DHA content, less sensitive cells may have higher DPA content following EPA treatment. Finally, **Chapter 6** focused on cell line models, in which generation of, or previously established, acquired resistance was investigated. A role for MRGPRF in mediating cellular response to EPA was not confirmed, due to unconfirmed functionality of the over-expressed protein. Additionally, attempts to generate resistant cell lines following chronic exposure were unsuccessful due to morphological, growth changes and accumulation of lipid bodies in cells maintained in *n*-3 PUFA-containing culture media.

The overall result of this project was identification of an association between the CIMP+ molecular phenotype and EPA sensitivity. In contrast, no specific phenotype was associated with, or identified as a biomarker linked to, response of hCRC cells to DHA. This indicated that EPA and DHA act upon different molecular targets and exert effects through different mechanisms. EPA and DHA are essential non-toxic FAs and are well tolerated (even at high concentrations) and are thought to act through multiple mechanisms of action (**Chapter 1.5**). These properties of could contribute to challenges

faced when trying to determine biomarkers predictive of cell line response and generating models with acquired resistance.

There is an unmet clinical need to discover and develop CRC therapies that are efficacious, safe, have minimal side-effects and importantly, are accessible, to the global population of patients. The work contained within this thesis adds to the body of work that demonstrates the potential of *n*-3 PUFAs in CRC anti-cancer treatment.

7.1. Challenges of understanding resistance to *n*-3 PUFAs which act via multiple direct and indirect mechanisms of action

In contrast to targeted CRC therapies such as cetuximab® or panitumumab®, which are both used in treatment of metastatic CRCs, *n*-3 PUFAs target multiple pathways as outlined in **Chapter 1.5**. Mechanisms of *n*-3 PUFA activity can be cell or tissue specific, and how *n*-3 PUFAs mechanisms of action contribute to anti-cancer activity is not fully understood. Cetuximab® and panitumumab® act by targeting the epidermal growth factor receptor (EGFR), which blocks a signalling cascade that promotes cancer cell proliferation (332). 20 % patients who receive these treatments show clinical benefit from it (332). By genotyping circulating DNA to genotype CRC tumours that were resistant to anti-EGFR therapies, specific genomic alterations were identified that were causing the lack of response (332). Genes found altered in patients exhibiting resistance to anti-EGFR treatments include; *HER2*, *KRAS*, *EGFR* and *MAP2K1* (332). Identification of these genomic alterations led to alternative treatment recommendations. mCRC patients with *HER2* amplification are more likely to benefit from a treatment regimen containing trastuzumab (Herceptin®) in combination with pertuzumab or lapatinib (333), in order to downregulate the expression of *HER2*. As it is hypothesised that *n*-3 PUFAs act via multiple mechanisms, it is considered that this is a huge advantage in increasing their potential for efficacious anti-cancer activity in multiple tumour types. However, it also complicates delineating mechanisms of resistance.

Multiple mechanisms of *n*-3 PUFA activity may also limit the potential of cells to acquire resistance, as inhibition of one pathways and signalling cascades may activate an alternative pathway (334). Therefore, multiple pathways would need to be altered to reduce *n*-3 PUFA cell responses. This is not a novel phenomenon, in fact resistance to the chemotherapeutic agent Imatinib, a treatment for chronic myeloid leukaemia, develops through multiple pathways (335). Imatinib is a receptor tyrosine kinase (RTK) inhibitor, which targets the dysregulated, constitutively active RTK, BCR-ABL1 in order to inhibit proliferation and promote apoptosis (335). Mutations within the ABL-kinase

domain, amplification of active BCR-ABL1 and multi-drug resistant P-glycoprotein (MDR1) and development of alternative pathways independent of BCR-ABL1 signalling result in resistance to Imatinib (335). Overcoming resistance is a challenge, with second- and third- generation RTK inhibitors and combination therapies being clinically evaluated to maximise patient outcome (335, 336).

Aspirin and other non-steroidal anti-inflammatory drugs (NSAIDs) inhibit COX enzyme activity directly via COX-1 acetylation, which alters metabolism of AA and production of cancer-promoting and pro-inflammatory mediators (169). In addition, aspirin treatment causes COX-2 acetylation (though it demonstrates dose-dependent selectivity for COX-1) (337), PIK3CA pathway inhibition and can induce senescence of cancer cells (338). Aspirin is clinically relevant, with an ongoing phase 3 RCT currently assessing the effect of aspirin in preventing recurrence in patients following primary tumour resection, with the study expected to include an estimated 11000 participants with breast, colorectal, gastro-oesophageal and prostate cancers (339). Despite the initial results of the CAPP2 trial (ISRCTN59521990) which involved patients with high-MSI Lynch syndrome indicating limited aspirin protective effect on CRC incidence at 29 months (162, 340), a follow up at 56 months demonstrated a reduction in cancer incidence (341). In cardiovascular patients, aspirin bioavailability has been shown to be impacted by formulation and administration routes.

An *in vitro* study has shown that aspirin alone inhibited proliferation in HT29, HCA-7, SW480 and HCT116 cells, regardless of COX expression (342), highlighting the ability of aspirin to induce effects via COX-independent pathways. This mirrors the *n*-3 PUFA effects observed in this study, which indicated hCRC cell line *n*-3 PUFA sensitivity or resistance were independent of *PTGS* expression.

7.1.1. Studying direct effects using *in vitro* cell models of CRC

An objective of this project was to identify and investigate differences in inherent sensitivity of a human CRC cell line panel, representative of the molecular phenotypes clinically seen, to the *n*-3 PUFAs; EPA (alone), DHA (alone) and EPA:DHA mixture (2:1 combination). Cell lines have long been considered a valuable tool for studying cancer, with a major benefit being that unlimited growth provides an unlimited source of biological material (343). The work within this thesis builds on a body of data that investigates the direct *n*-3 PUFA anti-CRC activity *in vitro* (90, 106, 107, 110, 134-137, 139, 148, 150-152, 177-179).

7.1.2. Limitations of *in vitro* models for study of *n*-3 PUFA effects

It is thought that some cell lines are more valuable for *in vitro* studies than others, based on genetic similarity to tumour-derived cell profiles (219). Using a large panel of cell lines with varied genetic profiles is be beneficial for the study of associations between molecular features and drug response.

Although cell lines have repeatedly been shown to represent the molecular properties of tumours (35, 41, 50, 226), two-dimensional (2D) monolayer cell lines are unable to accurately mimic the environment and mechanisms of tumour growth in the body (221). One reason for this, is that there is a lack of heterogeneity, which does not arise solely as a result of genomic changes, but is also influenced by epigenetic changes and the tumour microenvironment (221, 344). Intra-tumour heterogeneity is genomic differences within the same tumour mass. Inter-tumour heterogeneity refers to differences between synchronous primary tumours or a primary tumour and matched metastases (344). There are some *in vitro* models for which there a matched cell lines derived from a primary and metastatic site, for example the CRC cell lines SW480 (primary tumour) and SW620 (metastases).

In contrast, intra-tumour heterogeneity refers to differences within the same neoplasm. Heterogeneity can also be sub-classified as spatial or temporal, where spatial heterogeneity describes variations in distinct regions of a tumour, and temporal heterogeneity refers to differences that develop within a given tumour over during time (344). The nature of cultured cells renders them unable to capture intra-tumour, spatial and temporal heterogeneity. In addition, use of mono-cultured cell lines cannot recapitulate the presence of cancer stem cells, which are thought to confer resistance to non-surgical cancer treatments (345). Although use of a single cell line is not sufficient for capturing the heterogeneity of CRC, a panel of cell lines is able to do so.

Molecular profiles of cancer cell lines are often found to be significantly different than tumour cell molecular profiles as different genomic alterations arise due to selective pressure placed on cells in culture compared to the tumour microenvironment (220, 346). Therefore, relationships between specific genes and responses to treatment may not translate from pre-clinical models to the clinic. As previously discussed in **Chapter 4.4.1**, COX-2 expression in tumour samples is reported between 78 % and 90 % (159) (260), whereas 65 % of cell lines in this panel expressed *PTGS2*. As described in **Chapter 1.5.2**, *n*-3 PUFAs are metabolised by cyclooxygenase (COX) enzymes. No associations between mRNA expression of *PTGS1* or *PTGS2* and sensitivity to *n*-3 PUFAs (**Chapter**

4.3.5.2) were identified. This differed from *in vivo* data which found that COX-2 expression was associated with EPA resistance (178), and contradicted published work in which the ability of aspirin to significantly increase sensitivity of COX-2-expressing MC38r and CT26 cells to EPA *in vitro* (178). No associations between *PTGS1* or *PTGS2* gene expression and FA content following *n*-3 PUFA supplementation (**Chapter 5.3.3**) were identified. This difference between published *in vivo* data, and the *in vitro* data could be linked with differential COX expression in *in vivo* and *in vitro* models.

7.2. Limitations of cell lines for studying indirect *n*-3 PUFA effects

Indirect effects arising due to *n*-3 PUFA treatment may increase the anti-cancer response. However, a limitation of the present study design would be the difficulty of translating into a clinical setting as the focus on *in vitro* cell line models of CRC. Cell lines cannot accurately portray the complexities of CRC in a clinical setting. As discussed in **Chapter 4.4.2**, there remain limitations when using molecular classification systems that are intended for use to stratify clinical samples, such as the CMS classification, to characterise *in vitro* models. The limitations arise from the fact that, although there are cell-line adapted CMS categories (35, 41, 50), mono-cultured cell lines cannot accurately model the tumour stroma, the microenvironment or the immune component, and consequently the impact of these can't be accurately assessed in *in vitro* models.

7.2.1. Tumour microenvironment

The tumour microenvironment influences development and heterogeneity within CRC tumours. Inflammation at the tumour site causes the accumulation of immune cells as shown in the figure [**Figure 7.1**] below, including; T cells (CD4+, CD8+ and Tregs), tumour-associated macrophages (TAM), myeloid-derived suppressor cells (MDSCs), natural killer (NK) cells, fibroblasts and dendritic cells (347, 348).

Cells within the microenvironment can be anti-tumourigenic and pro-tumourigenic dependent upon host and tumour factors (348). An anti-tumour immune response facilitate modifications that both activate antitumoural immunity and suppress tumour immune evasion (349). The effect of *n*-3 PUFA exposure could have implications on the tumour microenvironment. For example, the incorporation of *n*-3 PUFAs into plasma membranes of immune cells could disrupt lipid rafts and consequentially alter the signalling within this localised area surrounding the tumour to promote anti-inflammatory and anti-cancer activities (349). *n*-3 PUFAs are thought to alter the microenvironment by increasing phagocytosis and decreasing cytokine production of TAMs (350), inhibiting

dendritic cell activation (351) and suppressing cancer-associated fibroblast functions (352), decreasing activation of T cells and increasing Treg differentiation (115).

n-3 PUFA effects on the microenvironment are unable to be captured in 2D single cell line culture experiments and requires further investigation in the context of CRC. However, co-culture experiments could be utilised to investigate relationships between immune-cell rich tumour microenvironments and *n*-3 PUFAs. In a breast cancer study, Gionfriddo *et al* (350) investigated the effects of two DHA metabolites, *N*-docosahexaenoyl ethanolamine (DHEA) and *N*-docosahexaenoyl serotonin (DHA-5T) on human THP-1 macrophage cells. Although it was an *in vitro* study, the cells were altered to recapitulate cells present in the microenvironment. THP-1 macrophages were co-cultured with conditioned media collected from growth of MCF7 and MDA-MB-231 breast cancer cell lines resulting in an altered the phenotype of THP-1 cells which was TAM-like (350). Presence of DHEA and DHA-5-HT reduced cytokine secretion by the TAMs and was peroxisome proliferator-activated receptor gamma (PPAR γ)-dependent (350). PPAR γ activation by DHEA has been shown to inhibit proliferation of cancer cells (353). DHEA and DHA-5T activated PPAR γ receptors on both epithelial cancer cells and cells within the microenvironment, demonstrating the potential of multiple anti-cancer effects attributed to non-specific targeting *n*-3 PUFAs or their metabolites.

Song *et al* have hypothesised that decreased production of inflammatory eicosanoids and chemokines due to *n*-3 PUFA presence, causes immune suppression mediated by Treg and MDSCs to be reverted, facilitating enhanced anti-tumour immunity (349). Their 2016 cohort study identified an association between high *n*-3 PUFA intake and a lower risk of densely FoxP3⁺ T cell infiltrated CRC but not low FoxP3⁺ T cell infiltrated CRC (354). FoxP3 is a transcription factor expressed by Tregs and has been associated with supporting cancer development and reducing host anti-tumour immune responses (354). Song *et al* have also demonstrated that *n*-3 PUFA treatment reduced Treg suppressive activity and increased proliferation of T effector cells *in vitro* (349)

Volpato *et al* suggested in their 2018 review of *n*-3 PUFAs as adjuvant therapy for CRC (209), that *n*-3 PUFA inhibition of PGE₂ production within cancer cells, immune infiltrate (355) and blood vessels (356) reduces their ability to promote proliferative, inflammatory and angiogenic effects (209). Further reduction in PGE₂ production by MDSCs due to *n*-3 PUFA activity contributes to the anti-cancer and anti-inflammatory effects (357). The interaction of *n*-3 PUFAs with microenvironment cells may be of good benefit, contributing to the anti-neoplastic effects.

It is likely that the variation in tumour microenvironment between patients, and within a patient at different stages of CRC progression, and the degree of cross-talk between the neoplastic cells and immune component, will have implications on how effective *n*-3 PUFAs are. In addition, how *n*-3 PUFAs will interact with new immunotherapies will be an interesting future area of research.

7.2.2. The microbiome

The interaction between the gut microbiome and CRC and *n*-3 PUFA supplementation is another area that cannot be studied using the cell culture models, although new technology such as 'intestine-on-a-chip' allows for *in vitro* modelling of the microbiome (358). Evidence suggests that the microbiome can be regulated by increasing fibre PUFA, polyphenol and probiotic intake (359, 360). Therefore, modulation of the microbiome is being investigated as a potential mechanism in both a primary prevention setting and for enhancing response to conventional therapy.

The interactions between the microbiome, the host and the immune system contributes to all stages of CRC pathogenesis, with presence of invasive bacterial biofilms (mucin layers containing bacteria) (361) found on 89 % of right-sided tumours (362), contributing to pro-proliferative pathways (362). The microbiome can influence response to conventional CRC treatment (363, 364). Therefore, the microbiome is likely to impact upon response to *n*-3 PUFA supplementation and response to *n*-3 PUFAs will be influenced by microbiome composition.

Pre-clinical and clinical trials demonstrate the ability of *n*-3 PUFA supplementation to change the bacterial composition of the microbiome (365-369). The change in microbiome may explain some anti-CRC activity of *n*-3 PUFAs. A study involving 90-day treatment of UC patients with 2 g/day EPA reported outcomes of altered bacterial composition of the microbiome, a reduction in mucosal inflammation, and remission determined by endoscopy and histological examination (369). It is suggested that increased presence of certain bacteria (such as *Lactobacillus* and *Bifidobacterium*) could reduce inflammation (367), a known driver in CRC pathogenesis (24). Increased abundance of bacteria that produce short chain fatty acids (SCFA) (367), may also contribute to *n*-3 PUFA effects due to their ability to promote CRC cell apoptosis and host anti-tumour immune responses (349, 360).

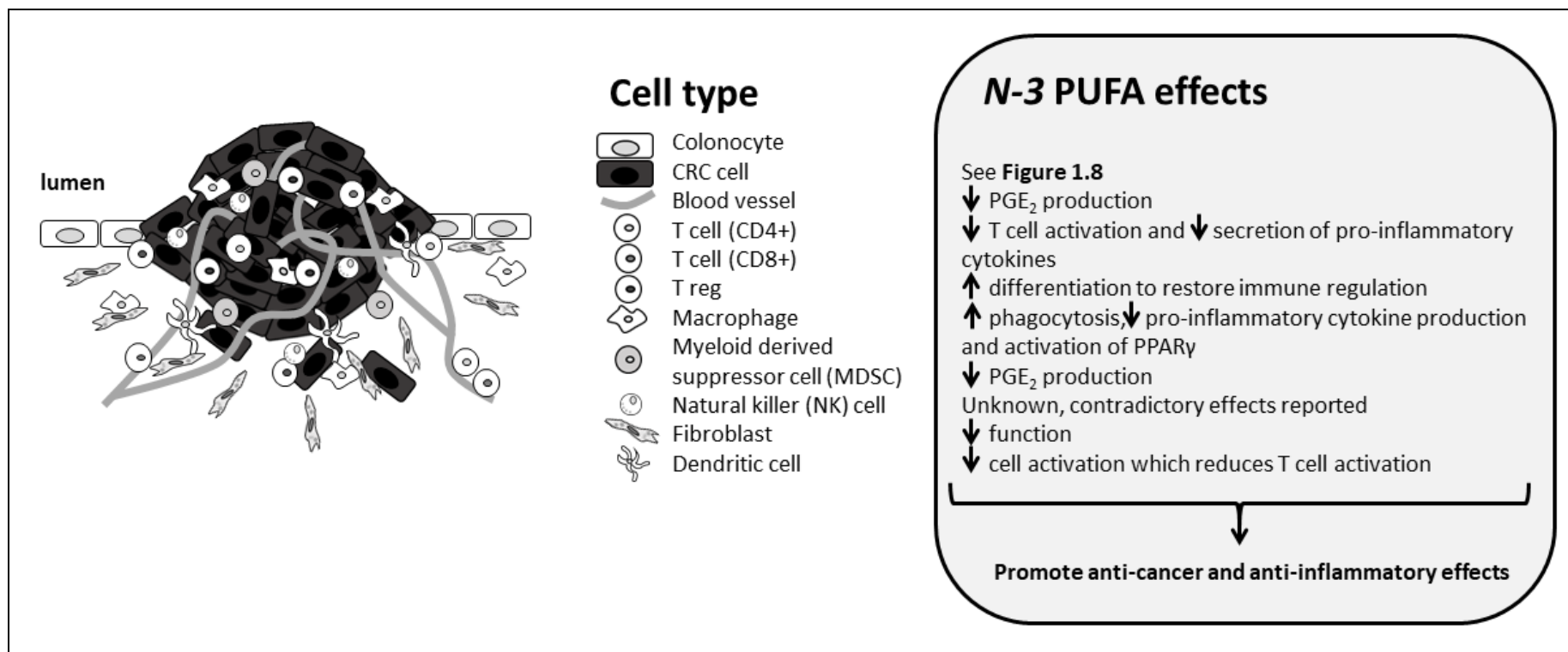


Figure 7.1. Key immune cells found in the microenvironment surrounding a CRC tumour

A diagrammatic representation of the tumour microenvironment made up of different tumour infiltrating immune cells that promote inflammation, angiogenesis (as shown by the presence of blood vessels within the tumour) and immunosuppression. The microenvironment ultimately facilitates the continued growth, and metastasis, of CRC tumours. Proposed effects of *n*-3 PUFAs are shown on the right side panel ↓ Decrease. ↑ Increase. Image adapted from (347, 348).

7.3. Biomarker discovery to improve CRC outcomes

One aim of this thesis was to identify markers and pathways that could provide the basis for identifying biomarkers of CRC cell response to *n*-3 PUFAs. Biomarkers are 'a characteristic that is objectively measured and evaluated as an indicator of normal biological processes, pathogenic processes or pharmacologic responses to a therapeutic intervention' as stated by the NIH Biomarkers Definitions Working Group (370). Biomarker development is a multi-step process that links initial discovery, validation, and clinical implementation. In brief the processes include: [1] biomarker discovery; [2] assay development and analytical validation; [3] clinical utility validation and [4] clinical implementation (371). Biomarkers are used in the context of CRC, with stool cancer DNA being used as a diagnostic biomarker (372), and the predictive biomarker of *KRAS*-activating mutations which is used to predict a lack of response to EGFR inhibitors such as cetuximab® or panitumumab® (373).

There have been few studies that investigate predictive markers of CRC response to *n*-3 PUFA in a translational setting. *In vitro* work by Volpato *et al* found that decreased CCL2 production and expression in human HCA-7 and murine MC38 CRC cells, was EPA-exposure dose dependent. These findings were corroborated in an *in vivo* setting, using an EPA-fed C576Bl/6 mouse MC38 xenograft model, in which there was a reduction in tumour burden associated with EPA-induced inhibition of CCL2 secretion (134, 374). In a clinical setting, plasma CCL2 levels were lower in CRCLM patients treated with EPA. CCL2 plasma levels were reported to increase in some patients, and this was associated with a significant decrease in DFS (134, 374).

Identification of biomarkers is advantageous as they offer the potential to speed up pre-clinical testing of drugs through high-throughput, high gain measurements of efficacy (375). Therefore quantitative data can be obtained which can be utilised for rational decision-making in drug development (375) and ultimately inform clinical decision-making to improve patient outcome (371). The work in this thesis contributes towards the first stage of the biomarker development process; biomarker discovery, as there was an association between CIMP+ cell lines and EPA sensitivity. Further studies to assess and corroborate the relationship between CIMP+ CRC and EPA sensitivity are required and are outlined in the discussion within Chapter 4 (**Chapter 4.4.3**).

7.3.1. Comparing *n*-3 PUFA measurements *in vitro* and patient samples

FA measurements are often used as biomarkers in studies involving *n*-3 PUFA supplementation to confirm incorporation of the FA into the desired tissue / blood. However, a biomarker does not correspond directly to response. The relevance of measuring the amount of EPA and DHA in cell line models of CRC and how this compares to quantities of FAs measured in tissue, was discussed in the **Chapter 5**. The FA content measured in human-derived samples is tissue, patient and time-point dependent. Several contributing factors influence FA content measurements. These factors include the expression of FA metabolising enzymes (including COX-1, COX-2, 5-LOX, 12-LOX, CYP450 and ELOVL and FADS enzymes) and consequent downstream bioactive lipid mediator production, personal diet and time between sample collection and meal times or supplementation. These variables cannot be accounted for using *in vitro* models, which in contrast, grow in a controlled environment. That said, FA profiles obtained for low concentration EPA / DHA treated cells in this study were relevant to levels observed in patient tissue levels reported previously in **Chapter 5**.

Furthermore, as *n*-3 PUFAs are distributed throughout the body, plasma and tissue levels of *n*-3 PUFAs will increase in an individual who is receiving supplementation in a non-specific manner (376), i.e.: the *n*-3 PUFAs are not targeted to the tumour. *N*-3 PUFA supplementation of media for culture hCRC cells grown do not go through digestion processes which facilitate distribution to plasma and alternative tissues like ingested *n*-3 PUFAs do. Consequently, *n*-3 PUFAs are directly incorporated into the target, mono-cultured hCRC cells. This again highlights a key difference between *in vitro* study and the translation to a human setting. Despite this, I have demonstrated that FA levels measured in hCRC cells were comparable with human CRC tissue samples (**Chapter 5.1**).

7.4. Towards clinical use of *n*-3 PUFAs for treatment of CRC

Currently, there are only 4 FDA-approved prescription *n*-3 PUFA products available [**Table 7.1**], used for the treatment of patients with severe hypertriglyceridemia (377-381). The recommended dose depends on the product, 4 g/day for LOVAZA® (378) and VASCEPA® (379), 2 g/day or 4 g/day for EPANOVA® (380) and 4.8 g/day for OMTRYG® (381). Three of the four are combination EPA:DHA mixtures, but VASCEPA® contains only EPA, icosapent ethyl. Whilst the benefits of *n*-3 PUFA treatment for hypertriglyceridemia, whereby triglyceride levels are lowered (377-381) are attributed to

a substantial increase in EPA tissue concentration, the impact of DHA is currently being evaluated in the mixed formulations (382).

Table 7.1. Prescription *n*-3 PUFA products for cardiovascular disease

Product	Formulation	<i>n</i>-3 PUFA content per 1 g capsule (g)	FDA Approval
LOVAZA®	Omega-3-Acid Ethyl Ester	EPA 0.465 DHA 0.375	2004
VASCEPA®	Icosapent Ethyl	EPA 1.0	2012 / 2019
EPANOVA®	Omega-3-Carboxylic Acids	EPA 0.550 DHA 0.2	2014
OMTRYG®	Omega-3-Acid Ethyl Esters A	EPA 0.465 DHA 0.375	2014

Prescription information sources: (378-381)

As shown by the FDA-approved products, different formulations and quantities were used to reduce triglyceride levels. In the case of VASCEPA®, it was originally approved to lower triglyceride levels of patients with hypertriglyceridemia in 2012. The additional approval of VASCEPA® to reduce risk of cardiovascular events in high risk patients, resulted from the findings of the Reduction of Cardiovascular Events with Icosapent Ethyl–Intervention Trial (REDUCE-IT) (NCT01492361) (383). REDUCE-IT involved 8179 patients with established cardiovascular disease (CVD) or with diabetes and high risk of CVD. Overall, they found that among patients with elevated levels of triglyceride, 4 g/day VASCEPA® significantly reduced the risk of ischemic events, including CVD-associated death (383). In 2019, VASCEPA® was FDA-approved for prescribing as an ‘adjunct to maximally tolerated statin therapy to reduce risk of myocardial infarction (MI), stroke, coronary revascularisation and unstable angina to require hospitalisation in adult patients with elevated triglyceride levels and (1) established CVD and (2) diabetes mellitus and 2 or more risk factors for CVD’ (379).

In the context of prescribed *n*-3 PUFAs for the treatment of CRC, optimisation of formulation, content and delivery mechanisms will require further research to determine the maximal anti-cancer effect. The impact of *n*-3 PUFA dose potentially explains conflicting outcomes between the aforementioned REDUCE-IT trial, and 2 further clinical trials in which *n*-3 PUFA effects for the primary prevention of CVD were assessed: VITamin D and OmegA-3 Trial (VITAL) (NCT01169259) (384) and A Study of Cardiovascular Events in Diabetes (ASCEND) (NCT00135226) (385). 1 g/day *n*-3 PUFA

formulations containing 480 mg EPA and 380 mg DHA) were used in both the VITAL and ASCEND trials (384, 385), with the VITAL trial also testing *n*-3 PUFA supplement with and without 2000 IU/day vitamin D (384). *n*-3 PUFA effects (compared to placebo controls) were assessed in different populations. 25871 individuals participated in the VITAL study, comprising males aged 50 and over and females aged 55 and over. No participants had previously suffered heart attacks, strokes or from cancer (384). ASCEND included 15480 diabetic participants aged 40 and older, who did not have CVD (385). In comparison to REDUCE-IT, in which a higher *n*-3 PUFA dose was used and significant CVD benefits were reported, VITAL and ASCEND found that 1 g/day *n*-3 PUFA supplementation did not significantly reduce the rate of major cardiovascular events (MI, stroke, death) after median and mean follow-up periods of 5.3 years (384) and 7.4 years (385), respectively. However, the VITAL study did report 1 g/day *n*-3 PUFA supplement associated benefits for some cardiovascular disease pathways (386). These included lower rates of fatal MI and total coronary heart disease, and a 28 % reduction in total MI rates which was deemed statistically significant (99, 384). Furthermore, the reduced total MI rates were more pronounced in two distinct subgroups. 40 % MI rate reduction was reported for participants who ate less than 1.5 fish servings weekly, and a 77 % reduction in MI rate was observed among African American participants (384). This highlights that the formulations, doses, study population and participant *n*-3 PUFA dietary intake could impact upon any trial in which the effects of *n*-3 PUFAs are being assessed.

VITAL also tested the effect of *n*-3 PUFA supplementation on invasive cancer of any type. 820 participants in the *n*-3 group, and 797 participants in the placebo control group, were diagnosed with invasive cancer (hazard ratio, 1.03; 95 % CI, 0.93 to 1.13, $p = 0.56$) (384). Of these diagnoses, 54 participants in the *n*-3 group, and 44 participants in the placebo control group, were diagnosed with CRC (hazard ratio, 1.23; 95 % CI, 0.83 to 1.83) (384). Further preliminary subgroup analysis does indicate a reduction in colorectal polyp recurrence following *n*-3 PUFA supplementation for African-American participants or individuals with low baseline plasma *n*-3 PUFA levels (387). This data indicates that subpopulations and baseline FA content of tissues could influence *n*-3 PUFA attributed CRC prevention or CRC response to *n*-3 PUFAs (129).

Whilst the findings within this thesis indicate that DHA exerts more potent anti-cancer cell effects, clinical trials assessing *n*-3 PUFA effects in CRC patients thus far by West *et al* (388), Cockbain *et al* (131) and Hull *et al* (147) involved capsules containing EPA-FFA or EPA-TG formulations. A trial by Bakker *et al*, is the only clinical trial involving *n*-3 PUFAs and CRC patients that have utilised a mixture of EPA and DHA. The study

investigated the effect of intravenous (IV) *n*-3 PUFAs on inflammatory cytokine markers following CRC surgery. The IV was a lipid emulsion containing 10 % fish oil, with every 10g fish oil containing 1.25 – 2.82 g EPA and 1.44 – 3.09 g DHA. Although within the *n*-3 PUFA group no definitive relationship between cytokines (including IL-6, IL-10 and c-reactive protein) was found, this study found that there was an increase in infection complications for patients who received perioperative IV *n*-3 PUFAs (389).

LOVAZA® is being assessed to determine its ability to prevent CRC development in patients with Lynch syndrome (NCT03831698) (390). A double-blind, placebo-controlled, randomised, phase II clinical trial (NCT03661047) is currently recruiting to assess the chemo-preventative effects of VASCEPA® by testing the composition of the colorectal tissue, tumour immune microenvironment and the gut microbiome (391). The EMT2 trial (NCT03428477) uses VASCEPA® in a randomised, double-blind, placebo-controlled, multi-centre, phase III trial in patients undergoing surgery for CRCLM (176). Although the high-doses of *n*-3 PUFA used for cardiovascular diseases were well tolerated, there have been a noted increase in atrial arrhythmias and an increase in bleeding and this need to be continually monitored, alongside other adverse effects, in CRC patients undergoing trials (392).

Estimations indicate that 50 % CRC cases are preventable, and in this setting modifications of lifestyle factors, including diet, could significantly reduce CRC risk. Nutraceuticals are likely to be more beneficial in an anti-cancer setting than dietary sources of specific nutrients as they provide concentrated exposure (129). However, it is unlikely that *n*-3 PUFAs would be a first-line treatment for CRC or CRCLM patients, and further studies are needed to determine their optimum use which may be in combination with chemotherapy or other nutraceutical agents. The potential implications of nutritional therapies for CRC on recurrence and overall survival, and the importance of diet, is becoming increasingly known. However, to identify optimal *n*-3 PUFA nutraceutical formulations and compositions further investigations are required, as *in vitro* and clinical studies indicate efficacy of single *n*-3 PUFAs, although comparisons between studies is challenging due to the differences in chemical formulations of the *n*-3 PUFAs utilised and a lack of comparing individual or combination treatments within the studies. Despite the benefit of single *n*-3 PUFAs, commercially available formulations are predominantly mixed and therefore my study has directly compared comparable concentrations of individual and combined formulations to assess ability to reduce cell viability.

7.4.1. Combination with traditional chemotherapy

The use of *n*-3 PUFAs in combination with traditional chemotherapy regimens is also an area for further investigation, with previous pre-clinical studies showing an improved anti-cancer effects by combining *n*-3 PUFA treatment with 5-FU (136, 208, 393-396) and increasing apoptosis in CRC cell lines treated with 5-FU, oxaliplatin and irinotecan (397). Investigations assessing the combination of *n*-3 PUFAs and traditional chemotherapies is not limited to a CRC setting. For example, one study tested the combination of EPA with paclitaxel, docetaxel and 5-FU in TE-1 oesophageal cancer cells proliferation (398). This resulted in a synergistic suppressive effect on TE-1 cellular proliferation (398). The work within this thesis identified CIMP+ cell lines as an EPA sensitive subtype. In addition, the benefit of 5-FU treatment for right-sided, CIMP+, CMS1 or CMS3 sided tumours has been reported (91). This may indicate the potential of *n*-3 PUFA to potentiate anti-tumour effects in combination treatment with 5-FU, although this would need further pre-clinical and clinical study. Incorporating FAs in treatment delivery modalities is an area of active research. A recent study used EPA and DHA to synthesise liposomes, created to deliver 5-FU to CRC cells (399). These liposomes were found to increase cytotoxicity in LS174T and HT-29 cell lines, compared to the effects of control liposomes containing 5-FU or EPA and DHA only. This is an approach that would be beneficial, if it is successfully translated to *in vivo* and clinical settings, as it could reduce rapid degradation of 5-FU in the bloodstream, enable lower therapeutic doses and reduce non-specific toxicity and mediate side-effects (399).

7.4.2. Combination with nutraceuticals

Other nutraceuticals are reported to exhibit potential anti-cancer activities, particularly when targeted against CRC, such as curcumin (400). A recent study involving a murine model of induced colonic carcinogenesis was used to assess the effect of *n*-3 PUFA and curcumin combination on the Lrg5+ stem cell population in the disease stages of tumour initiation and progression. The combination of *n*-3 PUFA and curcumin (diet was 4 % (w/w) Menhaden fish oil enriched in *n*-3 PUFA + curcumin) was shown to synergistically increase apoptosis in the stem cell population by 4.5-fold when compared to control diet (5 % corn-oil containing *n*-6 PUFA) (401).

7.5. Challenges of stratifying use of *n*-3 PUFAs for CRC treatment

This thesis is the first *in vitro* study that has investigated *n*-3 PUFA response based on CRC cell stratification by molecular phenotypes. Considering the molecular phenotypes

of CRC in relation to treatment response would provide evidence to support personalised therapy. Personalised medicine is a therapeutic approach involving the use of an individual's genetic and epigenetic information to tailor drug therapy or preventive care (402).

A truly personalised-medicine approach would require improved understanding of optimal dose needed to achieve the best clinical outcomes. This would likely be patient specific. Trials so far have treated patients with a uniform dose, with further work needed to assess how a suitable dose could be calculated. Calculating a dose will likely take in to account baseline FA measurements for each individual, as data (within this thesis and published) indicate that high concentrations of *n*-3 PUFA exposure are not always linked with increased anti-cancer and reduced cell proliferative activity. Consequently, it would be unlikely that uniform 'target' *n*-3 PUFA level would achieve desired anti-cancer effects across all patients.

7.6. Conclusion

Overall, data indicated potential benefits of using DHA to inhibit hCRC cell growth, and this needs to be assessed both *in vivo* and clinically. CIMP+ tumour responses to EPA require further investigation to identify mechanisms, or genes downregulated by methylation, that drive resistance. As understanding into the molecular pathology of CRC increases, further biomarkers of *n*-3 PUFA responses will be identified, which will facilitate personalised treatment regimens to improve patient outcome.

List of References

1. National Cancer Institute. *Glossary of Terms: large intestine*. [Online]. 2018. [Accessed 16.07.2019]. Available from: <https://www.cancer.gov/publications/dictionaries/cancer-terms/def/large-intestine?redirect=true>
2. Canadian Cancer Society. *The colon and rectum*. [Online]. 2019. [Accessed 16.07.2019]. Available from: <https://www.cancer.ca/en/cancer-information/cancer-type/colorectal/colorectal-cancer/the-colon-and-rectum/?region=on>
3. Siri, S., Zhao, Y., Maier, F., Pierce, D.M. and Feng, B. The Macro- and Micro-Mechanics of the Colon and Rectum I: Experimental Evidence. *Bioengineering* 2020, **7**(4), p.130.
4. Cancer Research UK. *TNM Staging*. [Online]. 2019. [Accessed 10.12.20]. Available from: <https://www.cancerresearchuk.org/about-cancer/bowel-cancer/stages-types-and-grades/TNM-staging>
5. Gill, S.R., Pop, M., Deboy, R. T., Eckburg, P. B., Turnbaugh, P. J., Samuel, B. S., Gordon, J. I., Relman, D. A., Fraser-Liggett, C. M., & Nelson, K. E. Metagenomic analysis of the human distal gut microbiome. *Science*. 2006, **312**(5778), pp.1355 - 1359.
6. Ternes, D., Karta, J., Tsenkova, M., Wilmes, P., Haan, S. and Letellier, E. Microbiome in Colorectal Cancer: How to Get from Meta-omics to Mechanism? *Trends in Microbiology*. 2020, **28**(5), pp.401 - 423.
7. Bhat, M.I.K., R. Dietary metabolites derived from gut microbiota: Critical modulators of epigenetic changes in mammals. *Nutr. Rev.* 2017, **75**, pp.374 - 389.
8. Jahani-Sherafat, S., Alebouyeh, M., Moghim, S., Amoli, H.A. and Safaei, H.G. Role of gut microbiota in the pathogenesis of colorectal cancer; a review article. *Gastroenterology and Hepatology from Bed to Bench*. 2018, **11**, pp.101 - 109.
9. Hanahan, D. and Weinberg, R.A. The Hallmarks of Cancer. *Cell*. 2000, **100**, pp.57 - 70.
10. Hanahan, D. and Weinberg, R.A. Hallmarks of cancer: the next generation. *Cell*. 2011, **144**(5), pp.646-674.
11. Centers for Disease Control and Prevention. *Colorectal (Colon) Cancer*. [Online]. 2021. [Accessed]. Available from: https://www.cdc.gov/cancer/colorectal/basic_info/what-is-colorectal-cancer.htm#:~:text=Colorectal%20cancer%20is%20cancer%20that,in%20the%20colon%20or%20rectum.
12. Baran, B., Mert Ozupek, N., Yerli Tetik, N., Acar, E., Bekcioglu, O. and Baskin, Y. Difference Between Left-Sided and Right-Sided Colorectal Cancer: A Focused Review of Literature. *Gastroenterology Research*. 2018, **11**(4), pp.264-273.
13. Hugen, N., Brown, G., Glynne-Jones, R., de Wilt, J.H. and Nagtegaal, I.D. Advances in the care of patients with mucinous colorectal cancer. *Nature Reviews Clinical Oncology*. 2016, **13**(6), pp.361 - 369.
14. Bordacahar, B., Barret, M., Terris, B., Dhooge, M., Dreanic, J., Prat, F. and Coriat, R. Sessile serrated adenoma: from identification to resection. *Digestive and Liver Disease*. 2015, **47**(2), pp.95 - 102.
15. Bosman, F.T., Carneiro, F., Hruban, R.H. and Theise, N.D. *WHO classification of tumours of the digestive system*. 4th Edition ed. WHO, 2010.
16. Murcia, O., Juárez, M., Hernández-Illán, E., Egoavil, C., Giner-Calabuig, M., Rodríguez-Soler, M. and Jover, R. Serrated colorectal cancer: Molecular classification, prognosis, and response to chemotherapy. *World Journal of Gastroenterology*. 2016, **22**(13), pp.3516 - 3530.
17. Marzouk O, S.J. Review of histopathological and molecular prognostic features in colorectal cancer. *Cancers (Basel)*. 2011, **3**(2), pp.2767 - 2810.
18. Roeder, F., Meldolesi, E., Gerum, S., Valentini, V. and Rödel, C. Recent advances in (chemo-)radiation therapy for rectal cancer: a comprehensive review. *Radiation Oncology*. 2020, **15**(1), p.262.
19. American Cancer Society. *Colorectal Cancer Signs and Symptoms*. [Online]. 2018. [Accessed 23.07.19]. Available from: <https://www.cancer.org/cancer/colon-rectal-cancer/detection-diagnosis-staging/signs-and-symptoms.html>
20. Cancer Research UK. *Cancer incidence for common cancers*. [Online]. 2019. [Accessed 22.07.19]. Available from: <https://www.cancerresearchuk.org/health-professional/cancer-statistics/incidence/common-cancers-compared#heading-Zero>
21. Siegel, R.L., Miller, K.D. and Jemal, A. Cancer Statistics, 2019. *CA Cancer J Clin*. 2019, **69**, pp.7-34.

22. Cancer Research UK. *Cancer Incidence by Age*. [Online]. 2019. [Accessed 22.07.19]. Available from: <https://www.cancerresearchuk.org/health-professional/cancer-statistics/incidence/age#heading-Two>
23. Cancer Research UK. *Bowel Cancer Statistics*. [Online]. 2019. [Accessed 22.07.2019]. Available from: <https://www.cancerresearchuk.org/health-professional/cancer-statistics/statistics-by-cancer-type/bowel-cancer#heading-Zero>
24. Thanikachalam, K. and Khan, G. Colorectal Cancer and Nutrition. *Nutrients*. 2019, **11**(1).
25. Rawla, P., Sunkara, T. and Barsouk, A. Epidemiology of colorectal cancer: incidence, mortality, survival, and risk factors. *Przegląd gastroenterologiczny*. 2019, **14**(2), pp.89 - 103.
26. Jaspersion, K.W., Tuohy, T.M., Neklason, D.W. and Burt, R.W. Hereditary and familial colon cancer. *Gastroenterology*. 2010, **138**(6), pp.2044 - 2058.
27. National Institute for Health and Care Excellence. *About: What we do*. [Online]. 2019. [Accessed 08.11.19]. Available from: <https://www.nice.org.uk/about/what-we-do>
28. National Institute for Clinical Excellence. *Pathways: Colorectal Cancer Overview*. [Online]. 2019. [Accessed 08.11.19]. Available from: <https://pathways.nice.org.uk/pathways/colorectal-cancer#content=view-node%3Anodes-staging>
29. Beating Bowel Cancer. *Secondary bowel cancer*. [Online]. 2016. [Accessed 03.03.2019]. Available from: <https://www.beatingbowelcancer.org/secondary-bowel-cancer>
30. Riihimäki, M., Hemminki, A., Sundquist, J. and Hemminki, K. Patterns of metastasis in colon and rectal cancer. *Scientific Reports*. 2016, **26756**, pp.1 - 9.
31. Wuan, D., Gallinger, S., Nhan, C., Auer, R.A., Biagi, J.J., Fletcher, G.G., Law, C.H.L., Moulton, C., Ruo, L., Wei, A.C. and McLeod, R.S. The role of liver resection for colorectal cancer metastases in an era of multimodality treatment: a systematic review. *Surgery*. 2012, **151**(151), pp.860 - 870.
32. Engstrand, J., Nilsson, H., Strömberg, C., Jonas, E. and Freedman, J. Colorectal cancer liver metastases - a population-based study on incidence, management and survival. *BMC Cancer*. 2018, **18**(1), p.78.
33. Brenner, H., Kloor, M. and Pox, C.P. Colorectal cancer. *The Lancet*. 2014, **383**(9927), pp.1490-1502.
34. Kinzler, K.W. and Vogelstein, B. Lessons from Hereditary Colorectal Cancer. *Cell*. 1996, **87**(2), pp.159 - 170.
35. Berg, K.C.G., Eide, P.W., Eilertsen, I.A., Johannessen, B., Bruun, J., Danielsen, S.A., Bjørnslett, M., Meza-Zepeda, L.A., Eknæs, M., Lind, G.E., Myklebost, O., Skotheim, R.I., Sveen, A. and Lothe, R.A. Multi-omics of 34 colorectal cancer cell lines - a resource for biomedical studies. *Molecular Cancer*. 2017, **16**(116).
36. Pino, M.S. and Chung, D.C. The Chromosomal Instability Pathway in Colon Cancer. *Gastroenterology*. 2010, **138**(6), pp.2059-2072.
37. Vogelstein, B., Fearon, E.R., Hamilton, S.R., Kern, S.E., Preisinger, A.C., Leppert, M., Nakamura, Y., White, R., Smits, A.M. and Bos, J.L. Genetic alterations during colorectal-tumor development. *New England Journal of Medicine*. 1988, **319**(9), pp.525 - 532.
38. Leslie, A., Carey, F.A., Pratt, N.R. and R.J.C., S. The colorectal adenoma-carcinoma sequence. *British Journal of Surgery*. 2002, **89**, pp.845-860.
39. Nguyen, H.T. and Nguyen, H.T. The molecular characteristics of colorectal cancer: Implications for diagnosis and therapy. *Oncology Letters*. 2018, **16**, pp.9 - 18.
40. Zhang, L. and Shay, J.W. Multiple Roles of APC and its Therapeutic Implications in Colorectal Cancer. *Journal of the National Cancer Institute*. 2017, **109**(8).
41. Ahmed, D., Eide, P.W., Eilertsen, I.A., Danielsen, S.A., Eknæs, M., Hektoen, M., Lind, G.E. and Lothe, R.A. Epigenetic and genetic features of 24 colon cancer cell lines. *Oncogenesis*. 2013, **2**(e71).
42. Chung, M.S.P.a.D.C. The Chromosomal Instability Pathway in Colon Cancer. *Gastroenterology*. 2010, **138**(6), pp.2059-2072.
43. Walther, A., Houlston, R. and Tomlinson, I. Association between chromosomal instability and prognosis in colorectal cancer: a meta-analysis. *Gut*. 2008, **57**(7), pp.941 - 950.
44. Deschoolmeester, V., Baay, M., Wuyts, W., Van Marck, E., Van Damme, N., Vermeulen, P., Lukaszuk, K., Lardon, F. and Vermorken, J.B. Detection of Microsatellite Instability in Colorectal Cancer Using an Alternative Multiplex Assay of Quasi-Monomorphic Mononucleotide Markers. *Journal of Molecular Diagnostics*. 2008, **10**(2), pp.154 - 159.
45. Murphy, K.M., Zhang, S., Geiger, T., Hafez, M.J., Bacher, J., Berg, K.D. and Eshleman, J.R. Comparison of the Microsatellite Instability Analysis System and the Bethesda Panel

- for the Determination of Microsatellite Instability in Colorectal Cancers. *Journal of Molecular Diagnostics*. 2006, **8**(3).
46. Gupta, R., Sinha, S. and Paul, R.N. The impact of microsatellite stability status in colorectal cancer. *Current Problems in Cancer*. 2018, **42**(6), pp.548 - 559.
 47. Issa, J.-P. CpG island methylator phenotype in cancer. *Nature Reviews: Cancer*. 2004, **4**, pp.988 - 993.
 48. Tapial, S., Olmedillas-López, S., Rueda, D., Arriba, M., García, J.L., Vivas, A., Pérez, J., Pena-Couso, L., Olivera, R., Rodríguez, Y., García-Arranz, M., García-Olmo, D., González-Sarmiento, R., Urioste, M., Goel, A. and Perea, J. CIMP-positive status is more representative in multiple colorectal cancers than in unique primary colorectal cancers. *Scientific Reports*. 2019, **9**(1), p.10516.
 49. Lao, V.V. and Grady, W.M. Epigenetics and colorectal cancer. *Nature reviews. Gastroenterology & hepatology*. 2011, **8**(12), pp.686 - 700.
 50. Sveen, A., Bruun, J., Eide, P.W., Eilertsen, I.A., Ramirez, L., Murumagi, A., Arjama, M., Danielsen, S.A., Kryeziu, K., Elez, E., Tabernero, J., Guinney, J., Palmer, H.G., Nesbakken, A., Kallioniemi, O., Dienstmann, R. and Lothe, R.A. Colorectal Cancer Consensus Molecular Subtypes Translated to Preclinical Models Uncover Potentially Targetable Cancer Cell Dependencies. *Clinical Cancer Research*. 2018, **24**(4), pp.794–806.
 51. Weisenberger, D.J., Siegmund, K.D., Campan, M., Young, J., Long, T.I., Faasse, M.A., Kang, G.H., Widschwendter, M., Weener, D., Buchanan, D., Koh, H., Simms, L., Barker, M., Leggett, B., Levine, J., Kim, M., French, A.J., Thibodeau, S.N., Jass, J., Haile, R. and Laird, P.W. CpG island methylator phenotype underlies sporadic microsatellite instability and is tightly associated with BRAF mutation in colorectal cancer. *Nature Genetics*. 2006, **38**(7).
 52. Juo, Y.Y., Johnston, F.M., Zhang, D.Y., Juo, H.H., Wang, H., Pappou, E.P., Yu, T., Easwaran, H., Baylin, S., van Engeland, M. and Ahuja, N. Prognostic value of CpG island methylator phenotype among colorectal cancer patients: a systematic review and meta-analysis. *Annals of Oncology*. 2014, **25**(12), pp.2314 - 2327.
 53. Ogino, S., Cantor, M., Kawasaki, T., Brahmandam, M., Kirkner, G.J., Weisenberger, D.J., Campan, M., Laird, P.W., Loda, M. and Fuchs, C.S. CpG island methylator phenotype (CIMP) of colorectal cancer is best characterised by quantitative DNA methylation analysis and prospective cohort studies. *Gut*. 2006, **55**(7), pp.1000 - 1006.
 54. Guinney, J., Dienstmann, R., Wang, X., de Reyniès, A., Schlicker, A., Soneson, C., Marisa, L., Roepman, P., Nyamundanda, G., Angelino, P., Bot, B.M., Morris, J.S., Simon, I.M., Gerster, S., Fessler, E., Melo, F.D.S.E., Missiaglia, E., Ramay, H., Barras, D., Homicsko, K., Maru, D., Manyam, G.C., Broom, B., Boige, V., Perez-Villamil, B., Laderas, T., Salazar, R., Gray, J.W., Hanahan, D., Tabernero, J., Bernards, R., Friend, S.H., Laurent-Puig, P., Medema, J.P., Sadanandam, A., Wessels, L., Delorenzi, M., Kopetz, S., Vermeulen, L. and Tejpar, S. The Consensus Molecular Subtypes of Colorectal Cancer. *Nature Medicine*. 2015, **21**(11), pp.1350 – 1356.
 55. Dienstmann, R., Vermeulen, L., Guinney, J., Kopetz, S., Tejpar, S. and Tabernero, J. Consensus molecular subtypes and the evolution of precision medicine in colorectal cancer. *Nature Reviews: Cancer*. 2017, **17**(2), pp.79 - 92.
 56. Mouradov, D., Sloggett, C., Jorissen, R.N., Love, C.G., Li, S., Burgess, A.W., Arango, D., Strausberg, R.L., Buchanan, D., Wormald, S., O'Connor, L., Wilding, J.L., Bicknell, D., Tomlinson, I.P.M., Bodmer, W.F., Mariadason, J.M. and Sieber, O.M. Colorectal Cancer Cell Lines Are Representative Models of the Main Molecular Subtypes of Primary Cancer. *AACR*. 2014, **74**(12), pp.1 - 10.
 57. Augestad, K.M., Merok, M.A. and Ignatovic, D. Tailored Treatment of Colorectal Cancer: Surgical, Molecular, and Genetic Considerations. *Clinical Medicine Insights. Oncology*. 2017, **11**(1).
 58. Goldwag, J., Marsicovetere, P., Scalia, P., Johnson, H.A., Durand, M.A., Elwyn, G. and Ivatury, S.J. The impact of decision aids in patients with colorectal cancer: a systematic review. *BMJ open*. 2019, **9**(9), p.e028379.
 59. Chiorean, E.G., Nandakumar, G., Fadelu, T., Temin, S., Alarcon-Rozas, A.E., Bejarano, S., Croitoru, A.E., Grover, S., Lohar, P.V., Odhiambo, A., Park, S.H., Garcia, E.R., Teh, C., Rose, A., Zaki, B. and Chamberlin, M.D. Treatment of Patients With Late-Stage Colorectal Cancer: ASCO Resource-Stratified Guideline. *JCO Global Oncology*. 2020, **6**, pp.414 - 438.

60. Cancer Research UK. *Surgery for Colon Cancer*. [Online]. 2020. [Accessed]. Available from: <https://www.cancerresearchuk.org/about-cancer/bowel-cancer/treatment/treatment-colon/surgery-colon>
61. Cancer Research UK. *Surgery for Rectal Cancer*. [Online]. 2020. [Accessed]. Available from: <https://www.cancerresearchuk.org/about-cancer/bowel-cancer/treatment/treatment-rectal/surgery-rectal/types-surgery-rectal>
62. Bowel Cancer UK. *Stomas*. [Online]. 2020. [Accessed]. Available from: <https://www.bowelcanceruk.org.uk/about-bowel-cancer/treatment/surgery/stomas/>
63. Fotheringham, S., Mozolowski, G.A., Murray, E.M.A. and Kerr, D.J. Challenges and solutions in patient treatment strategies for stage II colon cancer. *Gastroenterology Reports*. 2019, **7**(3), pp.151 - 161.
64. Quasar Collaborative Group, Gray, R., Barnwell, J., McConkey, C., Hills, R.K., Williams, N.S. and Kerr, D.J. Adjuvant chemotherapy versus observation in patients with colorectal cancer: a randomised study. *Lancet*. 2007, **370**(9604), pp.2020 - 2029.
65. Cancer Research UK. *Surgery for Advanced Cancer*. [Online]. 2020. [Accessed]. Available from: <https://www.cancerresearchuk.org/about-cancer/bowel-cancer/advanced/treatment/surgery>
66. Cancer Research UK. *Survival*. [Online]. 2017. [Accessed]. Available from: <http://www.cancerresearchuk.org/about-cancer/bowel-cancer/survival>
67. Misiakos, E.P., Karidis, N.P. and Kouraklis, G. Current treatment for colorectal liver metastases. *World Journal of Gastroenterology*. 2011, **17**(36), pp.4067 - 4075.
68. Rutherford, C., Müller, F., Faiz, N., King, M.T. and White, K. Patient-reported outcomes and experiences from the perspective of colorectal cancer survivors: meta-synthesis of qualitative studies. *Journal of Patient Reported Outcomes*. 2020, **4**(1), p.27.
69. American Cancer Society. *Radiation Therapy for Colorectal Cancer*. [Online]. 2020. [Accessed]. Available from: <https://www.cancer.org/cancer/colon-rectal-cancer/treating/radiation-therapy.html>
70. Cancer Research UK. *Chemotherapy treatment for colon cancer*. [Online]. 2020. [Accessed]. Available from: <https://www.cancerresearchuk.org/about-cancer/bowel-cancer/treatment/treatment-colon/chemotherapy-colon/chemotherapy-treatment-colon>
71. American Cancer Society. *Chemotherapy for Colorectal Cancer*. [Online]. 2020. [Accessed]. Available from: <https://www.cancer.org/cancer/colon-rectal-cancer/treating/chemotherapy.html>
72. Cancer Research UK. *Folinic acid, fluorouracil and oxaliplatin (FOLFOX)*. [Online]. 2020. [Accessed]. Available from: <https://www.cancerresearchuk.org/about-cancer/cancer-in-general/treatment/cancer-drugs/drugs/folfox>
73. Cancer Research UK. *Oxaliplatin and capecitabine (XELOX)*. [Online]. 2020. [Accessed]. Available from: <https://www.cancerresearchuk.org/about-cancer/cancer-in-general/treatment/cancer-drugs/drugs/oxaliplatin-capecitabine>
74. Cancer Research UK. *Capecitabine (Xeloda)*. [Online]. 2020. [Accessed]. Available from: <https://www.cancerresearchuk.org/about-cancer/cancer-in-general/treatment/cancer-drugs/drugs/capecitabine>
75. Cancer Research UK. *Fluorouracil (5FU)*. [Online]. 2020. [Accessed]. Available from: <https://www.cancerresearchuk.org/about-cancer/cancer-in-general/treatment/cancer-drugs/drugs/fluorouracil>
76. Cancer Research UK. *Irinotecan (Campto)*. [Online]. 2020. [Accessed]. Available from: <https://www.cancerresearchuk.org/about-cancer/cancer-in-general/treatment/cancer-drugs/drugs/irinotecan>
77. American Cancer Society. *Targeted Therapy for Colorectal Cancer*. [Online]. 2020. [Accessed]. Available from: <https://www.cancer.org/cancer/colon-rectal-cancer/treating/targeted-therapy.html>
78. Hurwitz, H., Fehrenbacher, L., Novotny, W., Cartwright, T., Hainsworth, J., Heim, W., Berlin, J., Baron, A., Griffing, S., Holmgren, E., Ferrara, N., Fyfe, G., Rogers, B., Ross, R. and Kabbinavar, F. Bevacizumab plus irinotecan, fluorouracil, and leucovorin for metastatic colorectal cancer. *New England Journal of Medicine*. 2004, **350**(23), pp.2335 - 2342.
79. US Food and Drug Administration. *FDA approves encorafenib in combination with cetuximab for metastatic colorectal cancer with a BRAF V600E mutation*. [Online]. 2020. [Accessed]. Available from: <https://www.fda.gov/drugs/resources-information-approved-drugs/fda-approves-encorafenib-combination-cetuximab-metastatic-colorectal-cancer-braf-v600e-mutation>

80. Marcus, L., Lemery, S.J., Keegan, P. and Pazdur, R. FDA Approval Summary: Pembrolizumab for the Treatment of Microsatellite Instability-High Solid Tumors. *Clinical Cancer Research*. 2019, **25**(13), pp.3753 - 3758.
81. American Cancer Society. *Immunotherapy for Colorectal Cancer*. [Online]. 2020. [Accessed]. Available from: <https://www.cancer.org/cancer/colon-rectal-cancer/treating/immunotherapy.html>
82. Overman, M.J., Lonardi, S., Wong, K.Y.M., Lenz, H.J., Gelsomino, F., Aglietta, M., Morse, M.A., Van Cutsem, E., McDermott, R., Hill, A., Sawyer, M.B., Hendlish, A., Neyns, B., Svrcek, M., Moss, R.A., Ledine, J.M., Cao, Z.A., Kamble, S., Kopetz, S. and André, T. Durable Clinical Benefit With Nivolumab Plus Ipilimumab in DNA Mismatch Repair-Deficient/Microsatellite Instability-High Metastatic Colorectal Cancer. *Journal of Clinical Oncology*. 2018, **36**(8), pp.773 - 779.
83. Maughan, T. *S-CORT Stratification in Colorectal Cancer*. [Online]. 2021. [Accessed]. Available from: <https://www.s-cort.org/>
84. Lawler, M., Kaplan, R., Wilson, R.H., Maughan, T. and Consortium, S.-C. Changing the Paradigm—Multistage Multiarm Randomized Trials and Stratified Cancer Medicine. *The Oncologist*. 2015, **20**(8), pp.849 - 851.
85. Wedden, S., Miller, K., Frayling, I.M., Thomas, T., Chefani, A., Miller, K., Hamblin, A., Taylor, J.C. and D'Arrigo, C. Colorectal Cancer Stratification in the Routine Clinical Pathway: A District General Hospital Experience. *Appl Immunohistochem Mol Morphol*. 2019, **27**(6), pp.e54 - e62.
86. Ribic, C.M., Sargent, D.J., Moore, M.J., Thibodeau, S.N., French, A.J., Goldberg, R.M., Hamilton, S.R., Laurent-Puig, P., Gryfe, R., Shepherd, L.E., Tu, D., Redston, M. and Gallinger, S. Tumour microsatellite-instability status as a predictor of benefit from fluorouracil-based adjuvant chemotherapy for colon cancer. *The New England Journal of Medicine*. 2003, **349**(3), pp.247-257.
87. Lenz, H.J., Ou, F.S., Venook, A.P., Hochster, H.S., Niedzwiecki, D., Goldberg, R.M., Mayer, R.J., Bertagnolli, M.M., Blanke, C.D., Zemla, T., Qu, X., Wirapati, P., Tejpar, S., Innocenti, F. and Kabbarah, O. Impact of consensus molecular subtyping (CMS) on overall survival (OS) and progression free survival (PFS) in patients (pts) with metastatic colorectal cancer (mCRC): analysis of CALGB/SWOG 80405 (Alliance). *Journal of Clinical Oncology*. 2017, **37**(22), pp.1876 - 1885.
88. Song, N., Pogue-Geile, K.L., Gavin, P.G., Yothers, G., Kim, S.R. and Johnson, N.L. Clinical outcome from oxaliplatin treatment in stage II/III colon cancer according to intrinsic subtypes: secondary analysis of NSABP C-07/NRG oncology randomized clinical trial. *JAMA Oncology*. 2016, **2**(1), pp.1162 - 1169.
89. Stintzing, S., Wirapati, P., Lenz, H.J., Neureiter, D., Fischer von Weikersthal, L., Decker, T., Kiani, A., Kaiser, F., Al-Batran, S., Heintges, T., Lerchenmüller, C., Kahl, C., Seipelt, G., Kullmann, F., Moehler, M., Scheithauer, W., Held, S., Modest, D.P., Jung, A., Kirchner, T., Aderka, D., Tejpar, S. and Heinemann, V. Consensus molecular subgroups (CMS) of colorectal cancer (CRC) and first-line efficacy of FOLFIRI plus cetuximab or bevacizumab in the FIRE3 (AIO KRK-0306) trial. *Annals of Oncology*. 2019, **30**(11), pp.1796 - 1803.
90. Buikhuisen, J.Y., Torang, A. and Medema, J.P. Exploring and modelling colon cancer inter-tumour heterogeneity: opportunities and challenges. *Oncogenesis*. 2020, **9**(7), p.66.
91. King, G.T., Lieu, C.H. and Messersmith, W.A. Frontline Strategies for Metastatic Colorectal Cancer: New Sides to the Story. *American Journal of Hematology and Oncology*. 2016, **12**.
92. Dekker, E., Tanis, P.J., Vleugels, J.L.A., Kasi, P.M. and Wallace, M.B. Colorectal cancer. *Lancet*. 2019, **394**(10207), pp.1467 - 1480.
93. World Cancer Research Fund International / American Institute for Cancer Research. Continouour Update Project Report: Diet, Nutrition, Physical Activity and colorectal cancer. 2017.
94. Davies, N.J., Batehup, L. and Thomas, R. The role of diet and physical activity in breast, colorectal and prostate cancer survivorship: a review of the literature. *The British Journal of Cancer*. 2011, **105**, pp.S52-S73.
95. British Nutrition Foundation. *Glossary*. [Online]. 2020. [Accessed]. Available from: <https://www.nutrition.org.uk/healthyliving/resources/glossary.html>
96. Song, M., Garrett, W.S. and Chan, A.T. Nutrients, Foods, and Colorectal Cancer Prevention. *Gastroenterology*. 2015, **148**(6), pp.1244 - 1260.
97. Dennis, E.A. Lipidomics joins the omics evolution. *Proceedings of the National Academy of Sciences of the United States of America*. 2009, **106**, pp.2089 - 2090.

98. Fahy, E., Subramaniam, S., Murphy, R., Nishijima, M., Raetz, C., Shimizu, T., Spener, F., van Meer, G., Wakelam, M. and Dennis, E.A. Update of the LIPID MAPS® comprehensive classification system for lipids. *Journal of Lipid Research*. 2009, **50**, pp.S9 - S14.
99. National Institutes of Health. *Omega-3 Fatty Acids*. [Online]. 2020. [Accessed 01.01.2020]. Available from: <https://ods.od.nih.gov/factsheets/Omega3FattyAcids-HealthProfessional/#en3>
100. Calder, P.C. Mechanisms of Action of (n-3) Fatty Acids. *The Journal of Nutrition*. 2012, **142**(3), pp.592S–599S.
101. LipidMaps. *Structure Database: EPA*. [Online]. 2020. [Accessed]. Available from: <https://www.lipidmaps.org/data/LMSDRecord.php?LMID=LMFA01030759>
102. LipidMaps. *Structure database: ALA*. [Online]. 2020. [Accessed]. Available from: <https://www.lipidmaps.org/data/LMSDRecord.php?LMID=LMFA01030152>
103. LipidMaps. *Structure database: DHA*. [Online]. 2020. [Accessed]. Available from: <https://www.lipidmaps.org/data/LMSDRecord.php?LMID=LMFA01030185>
104. LipidMaps. *Structure Database: Linoleic Acid*. [Online]. 2020. [Accessed]. Available from: <https://www.lipidmaps.org/data/LMSDRecord.php?LMID=LMFA01030120>
105. LipidMaps. *Structure Database: AA*. [Online]. 2020. [Accessed]. Available from: <https://www.lipidmaps.org/data/LMSDRecord.php?LMID=LMFA01030001>
106. Hull, M.A. Omega-3 polyunsaturated fatty acids. *Best Practice and Research: Clinical Gastroenterology*. 2011, **25**(4-5), pp.547-554.
107. Park, J.M., Kwon, S.H., Han, Y.M., Hahm, K.B. and Kim, E.H. Omega-3 polyunsaturated fatty acids as potential chemopreventative agent for gastrointestinal cancer. *Journal of Cancer Prevention*. 2013, **18**(3), pp.201 - 208.
108. Song, M., Nishihara, R., Wu, K., Qian, Z.R., Kim, S.A., Sukawa, Y., Mima, K., Inamura, K., Masuda, A., Yang, J., Fuchs, C.S., Giovannucci, E.L., Ogino, S. and Chan, A.T. Marine ω -3 polyunsaturated fatty acids and risk of colorectal cancer according to microsatellite instability. *Journal of the National Cancer Institute*. 2015, **107**(4).
109. Rich, M.R. Conformational analysis of arachidonic and related fatty acids using molecular dynamics simulations. *Biochim Biophys Acta*. 1993, **1178**(1), pp.87 - 96.
110. Singer, P., Wirth, M. and Singer, K. Canned seawater fish with declared content of omega-3 fatty acids: a novel benefit for dietary practice and research. *European Journal of Clinical Nutrition*. 2016, **70**(9), pp.1093 - 1094.
111. Miller, M.R., Nichols, P.D. and Carter, C.G. n-3 Oil sources for use in aquaculture–alternatives to the unsustainable harvest of wild fish. *Nutrition Resesearch Reviews*. 2008, **21**, pp.85 - 96.
112. Dyerberg, J., Madsen, P., Moller, J.M., Aardestrup, I. and Schmidt, E.B. Bioavailability of marine n-3 fatty acid formulations. *Prostaglandins, Leukotrienes and Essential Fatty Acids*. 2010, **83**, pp.137 - 141.
113. Cunningham, E. Are krill oil supplements a better source of n-3 fatty acids than fish oil supplements? *Journal of the Academy of Nutrition and Dietetics*. 2012, **112**, p.334.
114. Davidson, M.H., Kling, D. and Maki, K.C. Novel developments in omega-3 fatty acid-based strategies. *Current Opinion in Lipidology*. 2011, **22**, pp.437 - 444.
115. Calder, P.C. Omega-3 fatty acids and inflammatory processes. *Nutrients*. 2010, **2**(9), pp.355 - 374.
116. Li, D., Moorman, R., Vanhercke, T., Petrie, J., Singh, S. and Jackson, C.J. Classification and substrate head-group specificity of membrane fatty acid desaturases. *Computational and Structural Biotechnology Journal*. 2016, **14**, pp.341 - 349.
117. Jump, D.B. Mammalian Fatty Acid Elongases. *Methods Molecular Biology*. 2009, **579**, pp.375 - 389.
118. Leonard, A.E., Kelder, B., Bobik, E.G., Chuang, L.-T., Lewis, C.J., Kopchick, J.J., Mukerji, P. and Huang, Y.-S. Identification and Expression of Mammalian Long-Chain PUFA Elongation Enzymes. *Lipids*. 2002, **37**(8), pp.733 - 740.
119. Burdge, G.C., Jones, A.E. and Wootton, S.A. Eicosapentaenoic and docosapentaenoic acids are the principal products of α -linolenic acid metabolism in young men. *British Journal of Nutrition*. 2002, **88**(4).
120. Hou, L., Lian, K., Yao, M., Shi, Y., Lu, X., Fang, L., He, T. and Jiang, L. Reduction of n-3 PUFAs, specifically DHA and EPA, and enhancement of peroxisomal beta-oxidation in type 2 diabetic rat heart. *Cardiovascular diabetology*. 2012, **11**, p.126.
121. Robichaud, P.P., Munganyiki, J.E., Boilard, E. and Surette, M.E. Polyunsaturated fatty acid elongation and desaturation in activated human T-cells: ELOVL5 is the key elongase. *Journal of Lipid Research*. 2018, **59**(12), pp.2383 – 2396.

122. Mika, A., Kobiela, J., Pakiet, A., Czumaj, A., Sokołowska, E., Makarewicz, W., Chmielewski, M., Stepnowski, P., Marino-Gammazza, A. and Sledzinski, T. Preferential uptake of polyunsaturated fatty acids by colorectal cancer cells. *Scientific Reports*. 2010, **10**(1954).
123. Calder, P. Eicosapentaenoic and docosahexaenoic acid derived specialised pro-resolving mediators: concentrations in humans and the effects of age, sex, disease and increased omega-3 fatty acid intake. *Biochimie*. 2020.
124. Harris, R.C. and Breyer, M.D. *Brenner and Rector's The Kidney*. Philadelphia, USA: Elsevier, 2007.
125. Lai, H.T., de Oliveira Otto, M.C., Lemaitre, R.N., McKnight, B., Song, X., King, I.B., Chaves, P.H., Odden, M.C., Newman, A.B., Siscovick, D.S. and Mozaffarian, D. Serial circulating omega 3 polyunsaturated fatty acids and healthy ageing among older adults in the Cardiovascular Health Study: prospective cohort study. *British Medical Journal*. 2018, **363**(k4067).
126. Keaney, J.F. and Rosen, C.J. VITAL signs for dietary supplementation to prevent cancer and heart disease. *New England Journal of Medicine*. 2019, **380**(1), pp.91 - 93.
127. Im, D.S. Omega-3 fatty acids in anti-inflammation (pro-resolution) and GPCRs. *Progress in Lipid Research*. 2012, **51**(3), pp.232 - 237.
128. European Nutraceutical Association. *Science behind Nutraceuticals*. 594 Basel, Switzerland: European Nutraceutical Association (ENA), 2016.
129. Hull, M.A. Nutritional prevention of colorectal cancer. *Proceedings of the Nutrition Society*. 2020, **80**(1), pp.59 - 64.
130. Chang, C.H., Tseng, P.T., Chen, N.Y., Lin, P.C., Lin, P.Y., Chang, J.P., Kuo, F.Y., Lin, J., Wu, M.C. and Su, K.P. Safety and tolerability of prescription omega-3 fatty acids: A systematic review and meta-analysis of randomized controlled trials. *Prostaglandins Leukot Essent Fatty Acids*. 2018, **129**, pp.1 - 12.
131. Cockbain, A.J., Volpato, M., Race, A.D., Munarini, A., Fazio, C., Belluzzi, A., Loadman, P.M., Toogood, G.J. and Hull, M.A. Anticorectal cancer activity of the omega-3 polyunsaturated fatty acid eicosapentaenoic acid. *Gut*. 2014, **63**(11), pp.1760-1768.
132. Arnold, M., Sierra, M.S., Laversanne, M., Soerjomataram, I., Jemal, A. and Bray, F. Global patterns and trends in colorectal cancer incidence and mortality. *Gut*. 2016, **0** pp.1 - 9.
133. Kim, S., Sandler, D.P., Galanko, J., Martin, C. and Sandler, R.S. Intake of polyunsaturated fatty acids and distal large bowel cancer risk in whites and African Americans. *American Journal of Epidemiology*. 2010, p.9.
134. Volpato, M., Perry, S.L., Marston, G., Ingram, N., Cockbain, A.J., Burghel, H., Mann, J., Lowes, D., Wilson, E., Droop, A., Randerson-Moor, J., Coletta, P.L. and Hull, M.A. Changes in plasma chemokine C-C motif ligand 2 levels during treatment with eicosapentaenoic acid predict outcome in patients undergoing surgery for colorectal cancer liver metastasis. *Oncotarget*. 2016, **7**(19), pp.28139 - 28150.
135. D'Eliseo, D., Rocco, G.D., Loria, R., Soddu, S., Santoni, A. and Velotti, F. Epithelial-to-mesenchymal transition and invasion are upmodulated by tumour-expressed granzyme B and inhibited by docosahexaenoic acid in human colorectal cancer cells. *Journal of Experimental and Clinical Cancer Research*. 2016, **35**(24).
136. Vasudevan, A., Yu, Y., Banerjee, S., Woods, J., Farhana, L., Rajendra, S.G., Patel, A., Dyson, G., Levi, E., Maddipati, K.R., Majumdar, A.P.N. and Nangia-Makker, P. Omega-3 fatty acid is a potential preventive agent for recurrent colon cancer. *Cancer Prevention Research*. 2014, **7**(11), pp.1138 - 1148.
137. Jayathilake, A.G., Kadife, E., Luwor, R.B., Nurgali, K. and Su, X.Q. Krill oil extract suppresses the proliferation of colorectal cancer cells through activation of caspase 3/9. *Nutrition and Metabolism*. 2019, **16**(53).
138. Hawcroft, G., Loadman, P.M., Belluzzi, A. and Hull, M.A. Effect of eicosapentaenoic acid on E-type prostaglandin synthesis and EP4 receptor signaling in human colorectal cancer cells. *Neoplasia*. 2010, **12**(8), pp.618 - 627.
139. Zhang, C., Yu, H., Ni, X., Shen, S. and Das, U.N. Growth Inhibitory Effect of Polyunsaturated Fatty Acids (PUFAs) on Colon Cancer Cells via Their Growth Inhibitory Metabolites and Fatty Acid Composition Changes. *PLoS One*. 2015, **10**(4), p.e0123256.
140. Zhang, C., Yu, H., Shen, Y., Ni, X., Shen, S. and Das, U.N. Polyunsaturated fatty acids trigger apoptosis of colon cancer cells through a mitochondrial pathway. *Archives of medical science : AMS*. 2015, **11**(5), pp.1081 - 1094.
141. Sam, M.R., Ahangar, P., Nejati, V. and Habibian, R. Treatment of LS174T colorectal cancer stem-like cells with n-3 PUFAs induces growth suppression through inhibition of

- survivin expression and induction of caspase-3 activation. *Cellular Oncology*. 2016, **39**(1), pp.69 - 77.
142. Zhang, K., Hu, Z., Qi, H., Shi, Z., Chang, Y., Yao, Q., Cui, H., Zheng, L., Han, Y., Han, X., Zhang, Z., Chen, T. and Hong, W. G-protein-coupled receptors mediate ω -3 PUFAs-inhibited colorectal cancer by activating the Hippo pathway. *Oncotarget*. 2016, **7**(36), pp.58315–58330.
 143. Nakanishi, M., Hanley, M.P., Zha, R., Igarashi, Y., Hull, M.A., Mathias, G., Sciavolino, F., Grady, J.J. and Rosenberg, D.W. A novel bioactive derivative of eicosapentaenoic acid (EPA) suppresses intestinal tumor development in Apc Δ 14/+ mice. *Carcinogenesis*. 2018, **39**(3), pp.429 - 438.
 144. Hawcroft, G., Volpato, M., Marston, G., Ingram, N., Perry, S.L., Cockbain, A.J., Race, A.D., Munarini, A., Belluzzi, A., Loadman, P.M., Coletta, P.L. and Hull, M.A. The omega-3 unsaturated fatty acid EPA inhibits mouse MC-26 colorectal cancer liver metastasis via inhibition of PGE2-dependent cell motility. *British Journal of Pharmacology*. 2012, **166**, pp.1724 - 1737.
 145. Zou, S., Meng, X., Meng, Y., Liu, J., Liu, B., Zhang, S., Ding, W., Wu, J. and Zhou, J. Microarray analysis of anti-cancer effects of docosahexaenoic acid on human colon cancer model in nude mice. . *International journal of clinical and experimental medicine*. 2015, **8**(4), pp.5075 - 5084.
 146. Sorensen, L.S., Thorlacius-Ussing, O., Schmidt, E.B., Rasmussen, H.H., Lundbye-Christensen, S., Calder, P.C. and Lindorff-Larsen, K. Randomized clinical trial of perioperative omega-3 fatty acid supplements in elective colorectal cancer surgery. *The British Journal of Surgery*. 2014, **101**(2), pp.33 - 42.
 147. Hull, M.A., Sprange, K., Hepburn, T., Tan, W., Shafayat, A., Rees, C.J., Clifford, G., Logan, R.F., Loadman, P.M., Williams, E.A., Whitham, D. and Montgomery, A.A. Eicosapentaenoic acid and aspirin, alone and in combination, for the prevention of colorectal adenomas (seAFOod Polyp Prevention trial): a multicentre, randomised, double-blind, placebo-controlled, 2 \times 2 factorial trial. *The Lancet*. 2018, **392**(10164), pp.2583 - 2594.
 148. Camargo, C.Q., Mocellin, M.C., Silva, J., Fabre, M.E., Nunes, E.A. and Trindade, E.B. Fish oil supplementation during chemotherapy increases posterior time to tumor progression in colorectal cancer. *Nutrition and Cancer*. 2016, **68**, pp.70 - 76.
 149. Wiktorowska-Owczarek, A., Berezinska, M. and Nowak, J.Z. PUFAs: Structures, Metabolism and Function. *Advanced Clinical and Experimental Medicine*. 2015, **24**(6), pp.931 - 341.
 150. Hilleman, D. and Smer, A. Prescription omega-3 fatty acid products and dietary supplements are not interchangeable. *Managed Care*. 2016, **25**(1), pp.46 - 52.
 151. Swanson, D., Block, R. and Mousa, S.A. Omega-3 fatty acids EPA and DHA: health benefits throughout life. *Advances in Nutrition*. 2012, **3**, pp.1 - 7.
 152. Murray, M., Hraiki, A., Bebawy, M., Pazderka, C. and Rawling, T. Anti-tumor activities of lipids and lipid analogues and their development as potential anticancer drugs. *Pharmacology & Therapeutics*. 2015, **150**, pp.109 - 128.
 153. Pal, A., Methereel, A.H., Fiabane, L., Buddenbaum, N., Bazinet, R.P. and Shaikh, S.R. Do Eicosapentaenoic Acid and Docosahexaenoic Acid Have the Potential to Compete against Each Other? *Nutrients*. 2020, **12**(12), p.3718.
 154. Lee, E.J., Yun, U.J., Koo, K.H., Sung, J.Y., Shim, J., Ye, S.K., Hong, K.M. and Kim, Y.N. Down-regulation of lipid raft-associated onco-proteins via cholesterol-dependent lipid raft internalization in docosahexaenoic acid-induced apoptosis. *Biochim Biophys Acta*. 2014, **1841**(1), pp.190 - 203.
 155. Reczek, C.R. and Chandel, N.S. The Two Faces of Reactive Oxygen Species in Cancer. *Annual Review of Cancer Biology*. 2017, **1**(1), pp.79 - 98.
 156. Sabharwal, S.S. and Schumacker, P.T. Mitochondrial ROS in cancer: initiators, amplifiers or an Achilles' heel? *Nature Reviews Cancer*. 2014, **14**, pp.709 - 721.
 157. Wang, D. and DuBois, R.N. The role of COX-2 in intestinal inflammation and colorectal cancer. *Oncogene*. 2010, **29**, pp.781 - 788.
 158. Dommels, Y.E.M., Haring, M.M.G., Keestra, N.G.M., Alink, G.M., van Bladeren, P.J. and van Ommen, B. The role of cyclooxygenase in n-6 and n-3 polyunsaturated fatty acid mediated effects on cell proliferation, PGE2 synthesis and cytotoxicity in human colorectal carcinoma cell lines. *Carcinogenesis*. 2003, **24**(3), pp.385 - 392.
 159. Wu, Q.-B. and Sun, G.-P. Expression of COX-2 and HER-2 in colorectal cancer and their correlation. *World Journal of Gastroenterology*. 2015, **21**(20), pp.6206 - 6214.

160. Sostres, C., Gargallo, C.J. and Lanas, A. Aspirin, cyclooxygenase inhibition and colorectal cancer. *World journal of gastrointestinal pharmacology and therapeutics. World Journal of Gastrointestinal Pharmacology and Therapeutics*. 2014, **5**(1), pp.40 - 49.
161. Hawcroft, G., Ko, C.W.S. and Hull, M.A. Prostaglandin E2-EP4 receptor signalling promotes tumorigenic behaviour of HT-29 human colorectal cancer cells. *Oncogene*. 2007, **26**, pp.3006 - 3019.
162. Burn, J., Sheth, H., Elliott, F., Reed, L., Macrae, F., Mecklin, J.-P., Möslin, G., McDonald, F.E., Bertario, L., Evans, D.G., Gerdes, A.-M., Ho, J.W.C., Lindblom, A., Morrison, P.J., Rashbass, J., Ramesar, R., Seppälä, T., Thomas, H.J.W., Pylvänäinen, K., Borthwick, G.M., Mathers, J.C., Bishop, D.T., Boussioutas, A., Brewer, C., Cook, J., Eccles, D., Ellis, A., Hodgson, S.V., Lubinski, J., Maher, E.R., Porteous, M.E., Sampson, J., Scott, R.J. and Side, L. Cancer prevention with aspirin in hereditary colorectal cancer (Lynch syndrome), 10-year follow-up and registry-based 20-year data in the CAPP2 study: a double-blind, randomised, placebo-controlled trial. *The Lancet*. 2020, **395**(10240), pp.1855 - 1863.
163. Hanif, R., Pittas, A., Feng, Y., Koutsos, M.I., Qiao, L., Staiano-Coico, L., Shiff, S.I. and Rigas, B. Effects of nonsteroidal anti-inflammatory drugs on proliferation and on induction of apoptosis in colon cancer cells by a prostaglandin-independent pathway. *Biochemistry and Pharmacology*. 1996, **52**(2), pp.237 - 245.
164. Kim, B. and Giardiello, F.M. Chemoprevention in familial adenomatous polyposis. *Best Practise Res Clin Gastroenterology*. 2011, **25**(0), pp.607-622.
165. Yang, P., Cartwright, C., Chan, D., Ding, J., Felix, E., Pan, Y., Pang, J., Rhea, P., Block, K., Fischer, S.M. and Newman, R.A. Anticancer activity of fish oils against human lung cancer is associated with changes in formation of PGE2 and PGE3 and alteration of Akt phosphorylation. *Molecular Carcinology*. 2014, **53**(7), pp.566 - 577.
166. Pannunzio, A. and Coluccia, M. Cyclooxygenase-1 (COX-1) and COX-1 Inhibitors in Cancer: A Review of Oncology and Medicinal Chemistry Literature. *Pharmaceuticals*. 2018, **11**(4), p.101.
167. Church, R.D., Yu, J., Fleshman, J.W., Shannon, W.D., Govindan, R. and McLeod, H.L. RNA profiling of cyclooxygenases 1 and 2 in colorectal cancer. *British Journal of Cancer*. 2004, **91**, pp.1015 - 1018.
168. Rothwell, P.M., Wilson, M., Price, J.F., Belch, J.F., Meade, T.W. and Mehta, Z. Effect of daily aspirin on risk of cancer metastasis: a study of incident cancers during randomised controlled trials. *Lancet*. 2012, **379**(9826), pp.1591 – 1601.
169. Block, R.C., Kakinami, L., Jonovich, M., Antonetti, I., Lawrence, P., Meednu, N., CalderonArtero, P., Mousa, S.A., Brenna, J.T. and Georas, S. The combination of EPA+DHA and low-dose aspirin ingestion reduces platelet function acutely whereas each alone may not in healthy humans. *Prostaglandins, leukotrienes, and essential fatty acids*. 2012, **87**(4-5), pp.143–151.
170. Coyle, C., Cafferty, F.H., Rowley, S., MacKenzie, M., Berkman, L., Gupta, S., Pramesh, C.S., Gilbert, D., Kynaston, H., Cameron, D., Wilson, R.H., Ring, A. and Langley, R.E. Add-Aspirin i ADD-ASPIRIN: A phase III, double-blind, placebo controlled, randomised trial assessing the effects of aspirin on disease recurrence and survival after primary therapy in common non-metastatic solid tumours. *Contemporary Clinical Trials*. 2016, **51**, pp.56 - 64.
171. Oh, D.Y., Talukdar, S., Bae, E.J., Imamura, T., Morinaga, H., Fan, W., Li, P., Lu, W.J., Watkins, S.M. and Olefsky, J.M. GPR120 is an omega-3 fatty acid receptor mediating potent anti-inflammatory and insulin-sensitizing effects. *Cell*. 2010, **142**(5), pp.687 - 698.
172. Hutchings, C.J., Koglin, M., Olson, W.C. and Marshall, F.H. Opportunities for therapeutic antibodies directed at G-proteincoupled receptors. *Nature Reviews: Drug Discovery*. 2017, **16**, pp.787-810.
173. Dranse, H.J., Kelly, M.E.M. and Hudson, B.D. Drugs or diet? - Developing novel therapeutic strategies targetting the free fatty acid family of GPCRs. *The British Journal of Pharmacology*. 2013, **170**, pp.696 - 711.
174. Senatorov, I.S. and Moniri, N.H. The role of free-fatty acid receptor-4 (FFA4) in human cancers and cancer cell lines,. *Biochemical Pharmacology*. 2018, **150**, pp.170 - 180.
175. Moran, B.M., Flatt, P.R. and McKillop, A.M. G protein-coupled receptors: signalling and regulation by lipid agonists for improved glucose homeostasis. *Acta Diabetol*. 2016, **53**(2), pp.177 - 188.
176. ClinicalTrials.gov. *EPA for Metastasis Trial 2 (EMT2)*. [Online]. 2018. [Accessed]. Available from: <https://clinicaltrials.gov/ct2/show/NCT03428477>

177. D'Eliseo, D. and Velotti, F. Omega-3 fatty acids and cancer cell cytotoxicity: implications for multitargeted cancer therapy. *Journal of Clinical Medicine*. 2016, **5**(15), pp.1 - 29.
178. Volpato, M., Ingram, N., Perry, S.L., Spencer, J., Race, A.D., Marshall, C., Hutchinson, J.M., Nicolaou, A., Loadman, P.M., Coletta, P.L. and Hull, M. Cyclooxygenase activity mediates colorectal cancer cell resistance to the omega-3 polyunsaturated fatty acid eicosapentaenoic acid. *Cancer Chemotherapy and Pharmacology*. 2020, DOI: **10.1007/s00280-020-04157-2**.
179. Cai, F., Sorg, O., Granci, V., Lecumberri, E., Miralbell, R., Dupertuis, Y.M. and Pichard, C. Interaction of u-3 polyunsaturated fatty acids with radiation therapy in two different colorectal cancer cell lines. *Clinical Nutrition*. 2014, **33**, pp.164-170.
180. Mastersa, J.R., Thomson, J.A., Daly-Burns, B., Reid, Y.A., Dirks, W.G., Packer, P., Toji, L.H., Ohno, T., Tanabe, H., Arlett, C.F., Kelland, L.R., Harrison, M., Virmani, A., Ward, T.H., Ayres, K.L. and Debenham, P.G. Short tandem repeat profiling provides an international reference standard for human cell lines. *PNAS*. 2001, **98**(14), pp.8012 - 8017.
181. ATCC. *STR: Understanding the Matching Algorithm*. [Online]. 2019. [Accessed 20.08.2019]. Available from: https://www.lgcstandards-atcc.org/understanding_the_matching_algorithm.aspx?geo_country=gb
182. Carr, I. *PeakHeights: A program for collecting peak signal intensity levels from ABI genotype files*. [Online]. 2018. [Accessed 07.03.2018]. Available from: <http://dna.leeds.ac.uk/peakheights/guide/>
183. Riss, T.L., Moravec, R.A., AL, N. and al, e. *Cell Viability Assays*. Bethesda (MD): Eli Lilly & Company and the National Center for Advancing Translational Sciences; 2004, May 2013 [Updated 2016].
184. Feoktistova, M., Geserick, P. and Leverkus, M. Crystal Violet Assay for Determining Viability of Cultured Cells. *Cold Spring Harbour Laboratory Press*. 2016, pp.343-346.
185. Marshall, C. *Can an orphan G coupled protein receptor be key in improving colorectal cancer patient responses to EPA and personalising therapy?* Leeds: University of Leeds, 2016.
186. Hennequart, M., Pilotte, L., Cane, S., Hoffmann, D., Stroobant, V., De Plaen, E. and Van den Eynde, B.J. Constitutive IDO1 Expression in Human Tumors Is Driven by Cyclooxygenase-2 and Mediates Intrinsic Immune Resistance. *Cancer Immunology Research*. 2017, **5**(8), pp.695 - 709.
187. Jensen, T.S.R., Mahmood, B., Damm, M.D., Backe, M.B., Dahllof, M.S., Poulsen, S.S., Hansen, M.B. and Bindslev, N. Combined activity of COX-1 and COX-2 is increased in non-neoplastic colonic mucosa from colorectal neoplasia patients. *BMC Gastroenterology*. 2018, **18**(31).
188. Mann, J.R., Backlund, M.G., Buchanan, F.G., Daikoku, T., Holla, V.R., Rosenberg, D.W., Dey, S.K. and DuBois, R.N. Repression of Prostaglandin Dehydrogenase by Epidermal Growth Factor and Snail Increases Prostaglandin E2 and Promotes Cancer Progression. *Cancer Research*. 2006, **66**(13), pp.6649-6656.
189. Chisamore, M.J., Cunningham, M. E., Flores, O., Wilkinson, H. A., & Chen, J. D. Characterization of a novel small molecule subtype specific estrogen-related receptor alpha antagonist in MCF-7 breast cancer cells. *PLoS One*. 2009, **4**(5), p.e5624.
190. Fedchenko, N. and Reifenrath, J. Different approaches for interpretation and reporting of immunohistochemistry analysis results in the bone tissue - a review. *Diagnostic pathology*. 2014, **9**(221), pp.1 - 12.
191. Applied Biosystems. *Guide to Performing Relative Quantitation of Gene Expression Using Real-Time Quantitative PCR*. [Online]. AB, 2004.
192. Volpato, M., Spencer, J.A., Race, A.D., Munarini, A., Belluzzi, A., Cockbain, A.J., Hull, M.A. and Loadman, P.M. A liquid chromatography–tandem mass spectrometry method to measure fatty acids in biological samples. *Journal of Chromatography B*. 2017, **1055-1056**, pp.125-134.
193. Rose, H.G. and Okland, M. Improved procedure for the extraction of lipids from human erythrocytes. *Journal of Lipid Research*. 1965, **6**, pp.428-431.
194. Serafim, V., Tiugan, D.A., Andreescu, N., Mihailescu, A., Paul, C., Velea, I., Puiu, M. and Niculescu, M.D. Development and Validation of a LC–MS/MS-Based Assay for Quantification of Free and Total Omega 3 and 6 Fatty Acids from Human Plasma. *Molecules*. 2019, **24**(2), p.360.
195. Yang, W.-C., Adamec, J. and Regnier, F.E. Enhancement of the LC/MS Analysis of Fatty Acids through Derivatization and Stable Isotope Coding. *Analytical Chemistry*. 2007, **79**(14), pp.5150 – 5157.

196. Santa Cruz Biotechnology, I. *MRGF (N-14)*: sc-138444. 2014.
197. Invitrogen. *A Guide to Fluorescent Probes and Labeling Technologies*. Online, 2010.
198. ThermoFisher Scientific. *Fura-2 Calcium Indicator*. [Online]. 2017. [Accessed 14.07.2017]. Available from: <https://www.thermofisher.com/uk/en/home/industrial/pharma-biopharma/drug-discovery-development/target-and-lead-identification-and-validation/g-protein-coupled-html/cell-based-second-messenger-assays/fura-2-calcium-indicator.html>
199. Patel, A., Hirst, R.A., Harrison, C., Hirota, K. and Lambert, D.G. *Calcium Signaling Protocols. Methods in Molecular Biology (Methods and Protocols)*. Totowa, NJ: Humana Press, 2013.
200. Bird, G.S., DeHaven, W.I., Smyth, J.T. and Putney Jr, J.W. Methods for Studying Store-Operated Calcium Entry. *Methods*. 2008, **36**(3), pp.204-212.
201. Erb, L. and Weisman, G.A. Coupling of P2Y receptors to G proteins and other signaling pathways. *Wiley Interdiscip Rev Membr Transp Signal*. 2012, **1**(6), pp.789-803.
202. Jones, S., Evans, R.J. and Mahaut-Smith, M.P. Ca²⁺ Influx through P2X1 Receptors Amplifies P2Y1 Receptor-Evoked Ca²⁺ Signaling and ADP-Evoked Platelet Aggregation. *Molecular Pharmacology*. 2014, **86**(3), pp.243 – 251.
203. Rafehi, M. Screening of GPCR antagonists using the calcium mobilisation assay. *Berthold Technologies: Application Note*. 2016, **08**.
204. Ghasemi Fard, S., Wang, F., Sinclair, A.J., Elliott, G. and Turchini, G.M. How does high DHA fish oil affect health? A systematic review of evidence. *Critical Reviews in Food Science and Nutrition*. 2019, **59**(11), pp.1684 - 1727.
205. Mori, T.A., Burke, V., Puddey, I.B., Watts, G.F., O'Neal, D.N., Best, J.D. and Beilin, L.J. Purified eicosapentaenoic and docosahexaenoic acids have differential effects on serum lipids and lipoproteins, LDL particle size, glucose, and insulin in mildly hyperlipidemic men. *American Journal of Clinical Nutrition*. 2000, **71**(5), pp.1085 - 1094.
206. Gorjão, R., Azevedo-Martins, A.K., Rodrigues, H.G., Abdulkader, F., Arcisio-Miranda, M., Procopio, J. and Curi, R. Comparative effects of DHA and EPA on cell function. *Pharmacology & Therapeutics*. 2009, **122**(1), pp.56 - 64.
207. Hossain, Z., Hosokawa, M. and Takahashi, K. Growth Inhibition and Induction of Apoptosis of Colon Cancer Cell Lines by Applying Marine Phospholipid. *Nutrition and Cancer*. 2008, **61**(1), pp.123 - 130.
208. De Carlo, F., Witte, T.R., Hardman, W.E. and Claudio, P.P. Omega-3 Eicosapentaenoic Acid Decreases CD133 Colon Cancer Stem-Like Cell Marker Expression While Increasing Sensitivity to Chemotherapy. *PLoS One*. 2013, **8**(7), p.e69760.
209. Volpato, M. and Hull, M. Omega-3 polyunsaturated fatty acids as adjuvant therapy of colorectal cancer. *Cancer and Metastasis Reviews*. 2018, **37**, pp.545–555.
210. Chou, T.-C. Drug Combination Studies and Their Synergy Quantification Using the Chou-Talalay Method. *Cancer Research*. 2010, **70**(2), pp.440 - 446.
211. Goldin, A. and Mantel, N. The employment of combinations of drugs in the chemotherapy of neoplasia: a review. *Cancer Research*. 1957, **17**, pp.635 - 654.
212. Grec, W.R., Bravo, G. and Parsons, J.C. The search for synergy: a critical review from response surface perspective. *Pharmacological Reviews*. 1995, **47**, pp.331 - 385.
213. Huang, H., Fang, H.B. and Tan, M.T. Experimental design for multi-drug combination studies using signaling networks. *Biometrics*. 2018, **74**(2), pp.538 - 547.
214. He, L., Kuleskiy, E., Saarela, J., Turunen, L., Wennerberg, K., Aittokallio, T. and Tang, J. Methods for High-throughput Drug Combination Screening and Synergy Scoring. *Methods in Molecular Biology*. 2018, **1711**, pp.351 - 398.
215. Zhao, L., Au, J.L. and Wientjes, M.G. Comparison of methods for evaluating drug-drug interaction. *Frontiers in bioscience*. 2010, **2**, pp.241 - 249.
216. Zidar, N., Odar, K., Glavač, D., Jerše, M., Zupanc, T. and Štajerc, D. Cyclooxygenase in normal human tissues – is COX-1 really a constitutive isoform, and COX-2 an inducible isoform? *Journal of Cellular and Molecular Medicine*. 2009, **13**(9b), pp.3753 - 3763.
217. Swamy, M.V., Cooma, I., Patlolla, J.M., Simi, B., Reddy, B.S. and Rao, C.V. Modulation of cyclooxygenase-2 activities by the combined action of celecoxib and decosahexaenoic acid: novel strategies for colon cancer prevention and treatment. *Molecular Cancer Therapeutics*. 2004, **3**(2), pp.215 - 221.
218. Lim, S.J., Lee, E., Lee, E.H., Kim, S.Y., Cha, J.H., Choi, H., Park, W., Choi, H.K., Ko, S.H. and Kim, S.H. Docosahexaenoic acid sensitizes colon cancer cells to sulindac sulfide-induced apoptosis. *Oncology Reports*. 2012, **27**(6), pp.2023 - 2030.
219. Ronen, J., Hayat, S. and Akali, A. Evaluation of colorectal cancer subtypes and cell lines using deep learning. *Life Science Alliance*. 2019, **2**(6), pp.1 - 16.

220. Gillet, J.-P., Varma, S. and Gottesman, M.M. The Clinical Relevance of Cancer Cell Lines. *J Natl Cancer Inst.* 2013, **105**(7), pp.452 – 458.
221. Bartlett, R., Everett, W., Lim, S., G, N., Loizidou, M., Jell, G., Tan, A. and Seifalian, A.M. Personalized in vitro cancer modelling - fantasy or reality? *Translational Oncology.* 2014, **7**(6), pp.657 – 664.
222. Sadanandam, A., Lyssiotis, C.A., Homicsko, K., Collisson, E.A., Gibb, W.J., Wullschlegel, S., Ostos, L.C.G., Lannon, W.A., Grotzinger, C., Del Rio, M., Lhermitte, B., Olshen, A.B., Wiedenmann, B., Cantley, L.C., Gray, J.W. and Hanahan, D. A colorectal cancer classification system that associates cellular phenotype and responses to therapy. *Nature Medicine.* 2013, **19**(5), pp.619 - 625.
223. Medico, E., Russo, M., Picco, G., Cancelliere, C., Valtorta, E., Corti, G., Buscarino, G., Isella, C., Lamba, S., Martinoglio, B., Veronese, S., Siena, S., Sartore-Bianchi, A., Beccuti, M., Mottolese, M., Linnebacher, M., Cordero, F., Nicolantonio, F.D. and Bardelli, A. The molecular landscape of colorectal cancer cell lines unveils clinically actionable kinase targets. *Nature Communications.* 2015, **6**(7002).
224. Mouradov, D., Sloggett, C., Jorissen, R.N., Love, C.G., Li, S., Burgess, A.W., Arango, D., Strausberg, R.L., Buchanan, D., Wormald, S., O'Connor, L., Wilding, J.L., Bicknell, D., Tomlinson, I.P.M., Bodmer, W.F., Mariadason, J.M. and Sieber, O.M. Colorectal cancer cell lines are representative models of the main molecular subtypes of primary cancer. *Cancer Research.* 2014, **74**(12).
225. Lind, G.E., Thorstensen, L., Løvig, T., Meling, G.I., Hamelin, R., Rognum, T.O., Esteller, M. and Lothe, R.A. A CpG island hypermethylation profile of primary colorectal carcinomas and colon cancer cell lines. *Molecular Cancer.* 2004, **3**(28).
226. Barretina, J., Caponigro, G., Stransky, N., Venkatesan, K., Margolin, A.A. and Kim, S. The cancer cell line encyclopedia enables predictive modelling of anticancer drug sensitivity. *Nature.* 2012, **483**, pp.603 - 607.
227. Linnekamp, J.F., Hooff, S., Prasetyanti, P.R., Kandimalla, R., Buikhuisen, J.Y., Fessler, E., Ramesh, P., Lee, K., Bochove, G., de Jong, J.H., Cameron, K., Leersum, R.V., Rodermond, H.M., Franitza, M., Nürnberg, P., Mangiapane, L.R., Wang, X., Clevers, H., Vermeulen, L., Stassi, G. and Medema, J.P. Consensus molecular subtypes of colorectal cancer are recapitulated in in vitro and in vivo models. *Cell death and differentiation.* 2018, **25**(3), pp.616 - 633.
228. Okita, A., Takahashi, S., Ouchi, K., Inoue, M., Watanabe, M., Endo, M., Honda, H., Yamada, Y., & Ishioka, C. Consensus molecular subtypes classification of colorectal cancer as a predictive factor for chemotherapeutic efficacy against metastatic colorectal cancer. *Oncotarget.* 2018, **9**(7), pp.18698 - 18711.
229. Song, M., Ou, F.S., Zemla, T.J., Hull, M.A., Shi, Q., Limburg, P.J., Alberts, S.R., Sinicrope, F.A., Giovannucci, E.L., Van Blarigan, E.L., Meyerhardt, J.A. and Chan, A.T. Marine omega-3 fatty acid intake and survival of stage III colon cancer according to tumor molecular markers in NCCTG Phase III trial N0147 (Alliance). *International Journal of Cancer.* 2019, **145**(2), pp.380 - 389.
230. Hoopes, L. Introduction to the gene expression and regulation topic room. *Nature Education.* 2008, **1**(1), p.160.
231. Feinberg, A. Epigenetics at the Epicenter of Modern Medicine. *JAMA.* 2008, **299**(11), pp.1345-1350.
232. Barros, S.P. and Offenbacher, S. Epigenetics: connecting environment and Genotype to Phenotype and disease. *Journal of Dental Research.* 2009, **88**(5), pp.400 - 408.
233. Gupta, R.C. *Reproductive and Developmental Toxicology.* Second Edition ed. United States: Elsevier, 2017.
234. Patnaik, S. and Anupriya. Drugs Targeting Epigenetic Modifications and Plausible Therapeutic Strategies Against Colorectal Cancer. *Frontiers in Pharmacology.* 2019, **10**(588).
235. Larsen, F., Gundersen, G., Lopez, R. and Prydz, H. CpG islands as gene markers in the human genome. *Genomics.* 1992, **13**(4).
236. Ceccarelli, V., Valentini, V., Ronchetti, S., Cannarile, L., Billi, M., Riccardi, C., Ottini, L., Talesa, V.N., Grignan, F. and Vecchini, A. Eicosapentaenoic acid induces DNA demethylation in carcinoma cells through a TET1-dependent mechanism. *The FASEB Journal.* 2018, **32**, pp.5990–6001.
237. Zhang, X., Zhang, W. and Cao, P. Advances in CpG Island Methylator Phenotype Colorectal Cancer Therapies. *Frontiers in Oncology.* 2021, **11**(629390).
238. Neyns, B., Tosoni, A., Hwu, W.-J. and Reardon, D.A. Dose-Dense Temozolomide Regimens. *Cancer.* 2010, **116**, pp.2868–2877.

239. Belter, A., Barciszewski, J. and Barciszewska, A.M. Revealing the epigenetic effect of temozolomide on glioblastoma cell lines in therapeutic conditions. *PLoS One*. 2020, **15**(2), p.e0229534.
240. Hegi, M.E., Diserens, A.C., Gorlia, T., Hamou, M.F., de Tribolet, N., Weller, M., Kros, J.M., Hainfellner, J.A., Mason, W., Mariani, L., Bromberg, J.E., Hau, P., Mirimanoff, R.O., Cairncross, J.G., Janzer, R.C. and Stupp, R. MGMT gene silencing and benefit from temozolomide in glioblastoma. *New England Journal of Medicine*. 2005, **352**(10), pp.997 - 1003.
241. Pietrantonio, F., Lobefaro, R., Antista, M., Lonardi, S., Raimondi, A., Morano, F., Mosconi, S., Rimassa, L., Murgioni, S., Sartore-Bianchi, A., Tomasello, G., Longarini, R., Farina, G., Petrelli, F., Gori, S., Randon, G., Corallo, S., Pagani, F., Guarini, V., Palermo, F., Martinetti, A., Macagno, M., Barault, L., Perrone, F., Tamborini, E., Milione, M., Di Nicolantonio, F., Di Maio, M., Fucà, G., Di Bartolomeo, M. and de Braud, F. Capecitabine and Temozolomide versus FOLFIRI in RAS-Mutated, MGMT-Methylated Metastatic Colorectal Cancer. *Clinical Cancer Research*. 2020, **26**(5), pp.1017 - 1024.
242. Hagemann, S., Heil, O., Lyko, F. and Brueckner, B. Azacytidine and Decitabine Induce Gene-Specific and Non-Random DNA Demethylation in Human Cancer Cell Lines. *PLoS One*. 2011, **6**(3), p.e17388.
243. Hesson, L.B., Patil, V., Sloane, M.A., Nunez, A.C., Liu, J., Pimanda, J.E. and Ward, R.L. Reassembly of nucleosomes at the MLH1 promoter initiates resilencing following decitabine exposure. *PLoS genetics*. 2013, **9**(7), p.e1003636.
244. Burgess, A.W., Love, C.G., Sloggett, C., Buchanan, D., Bicknell, D., Arango, D., Mouradov, D., Tomlinson, I.P., Wilding, J., Mariadason, J.M., O'Connor, L., Sieber, O.M., Strausberg, R.L., Jorissen, R.N., Wormald, S., Li, S. and Bodmer, W. *E-GEOD-55832 - Colorectal cancer cell lines are representative models of the main molecular subtypes of primary cancer*. [Online]. 2015. [Accessed]. Available from: https://www.ebi.ac.uk/arrayexpress/experiments/E-GEOD-55832/?query=p53&page=1&pagesize=500&sortby=releasedate&sortorder=descending&s_page=1&s_pagesize=501&s_sortby=col_5&s_sortorder=ascending
245. Knutsen, T., Padilla-Nash, H.M., Wangsa, D., Barenboim-Stapleton, L., Camps, J., McNeil, N., Difilippantonio, M.J. and Ried, T. Definitive Molecular Cytogenetic Characterization of 15 Colorectal Cancer Cell Lines. *Genes, Chromosomes and Cancer*. 2010, **49**(3), pp.204-223.
246. Sood, R., Flint-Ashtamker, G., Borenstein, D. and Barki-Harrington, L. Upregulation of Prostaglandin Receptor EP1 Expression Involves Its Association with Cyclooxygenase-2. *PLoS One*. 2014, **9**(3).
247. Sheng, H., Shao, J., Kirkland, S.C., Isakson, P., Coffey, R.J., Morrow, J., Beauchamp, R.D. and DuBois, R.N. Inhibition of human colon cancer cell growth by selective inhibition of cyclooxygenase-2. *The Journal of Clinical Investigation*. 1997, **99**(9), pp.2254 - 2259.
248. Wickstrom, M., Dyberg, C., Milosevic, J., Einvik, C., Calero, R., Sveinbjornsson, B., Sanden, E., Darabi, A., Siesjo, P., Kool, M., Kogner, P., Baryawno, N. and Johnsen, J.I. Wnt/B-catenin pathway regulates MGMT gene expression in cancer and inhibition of Wnt signalling prevents chemoresistance. *Nature Communications*. 2015, **6**(8904).
249. National Cancer Institute. *NCI-60 Human Tumor Cell Lines Screen*. [Online]. 2020. [Accessed 01/06/2019]. Available from: <https://dtp.cancer.gov/services/nci60data/colordoseresponse/pdf/102816>
250. Brown, I., Lee, J., Sneddon, A.A., Cascio, M.G., Pertwee, R.G., Wahle, K.W.J., Rotondo, D. and Hey, S.D. Anticancer effects of n-3 EPA and DHA and their endocannabinoid derivatives on breast cancer cell growth and invasion. *Prostaglandins, Leukotrienes and Essential Fatty Acids*. 2020, **156**(102024).
251. Mason, R.P., Jacob, R.F., Shrivastava, S., Sherratt, S.C.R. and Chattopadhyay, A. Eicosapentaenoic acid reduces membrane fluidity, inhibits cholesterol domain formation, and normalizes bilayer width in atherosclerotic-like model membranes. *Biochimica et Biophysica Acta*. 2016, **1858**(12), pp.3131 - 3140.
252. Pizato, N., Luzete, B.C., Kiffer, L.F.M.V., Corrêa, L.H., Santos, I.d.O., Assumpção, J.A.F., Ito, M.K. and Magalhães, K.G. Omega-3 docosahexaenoic acid induces pyroptosis cell death in triple-negative breast cancer cells. *Scientific Reports*. 2018, **8**(1952).
253. Ghasemifard, S., Turchini, G.M. and Sinclair, A.J. Omega-3 long chain fatty acid "bioavailability": a review of evidence and methodological considerations. *Progress in Lipid Research*. 2014, **56**, pp.92 - 108.

254. Zajdel, A., Wilczok, A., Chodurek, E., Gruchlik, A. and Dzierzewicz, Z. Polyunsaturated fatty acids inhibit melanoma cell growth in vitro. *Acta Poloniae Pharmaceutica n Drug Research*. 2013, **70**(2), pp.365 - 369.
255. Benga, G. Basic studies on gene therapy of human malignant melanoma by use of the human interferon beta gene entrapped in cationic multilamellar liposomes. 1. Morphology and growth rate of six melanoma cell lines used in transfection experiments with the human interferon beta gene. *Journal of Cellular and Molecular Medicine*. 2001, **5**(4), pp.402 - 408.
256. Cowley, G.S., Weir, B.A., Vazquez, F. and et al. Parallel genome-scale loss of function screens in 216 cancer cell lines for the identification of context-specific genetic dependencies. *Scientific Data*. 2014, **30**(1).
257. Kaltoft, N., Tilotta, M.C., Witte, A.B., Osbak, P.S., Poulsen, S.S., Bindsløv, N. and Hansen, M.B. Prostaglandin E2-induced colonic secretion in patients with and without colorectal neoplasia. *BMC Gastroenterology*. 2010, **10**(9).
258. Shao, J., Sheng, H., Inoue, H., Morrow, J.D. and DuBois, R.N. Regulation of constitutive cyclooxygenase-2 expression in colon carcinoma cells. *Journal of Biological Chemistry*. 2000, **275**, pp.33951 - 33956.
259. Hsi, L.C., Baek, S.J. and Eling, T.E. Lack of cyclooxygenase-2 activity in HT-29 human colorectal carcinoma cells. *Experimental Cell Research*. 2000, **256**(2), pp.563 - 570.
260. Eberhart, C.E., Coffey, R.J., Radhika, A., Giardiello, F.M., Ferrenbach, S. and DuBois, R.N. Up-regulation of cyclooxygenase 2 gene expression in human colorectal adenomas and adenocarcinomas. *Gastroenterology* 1994, **107**, pp.1183 - 1188.
261. Tahiliani, M., Koh, K.P., Shen, Y., Pastor, W.A., Bandukwala, H., Brudno, Y., Agarwal, S., Iyer, L.M., Liu, D.R., Aravind, L. and Rao, A. Conversion of 5-methylcytosine to 5-hydroxymethylcytosine in mammalian DNA by MLL partner TET1. *Science*. 2009, **324**(5929), pp.930 - 935.
262. Ceccarelli, V., Racanicchi, S., Martelli, M.P., Nocentini, G., Fettucciari, K., Riccardi, C., Marconi, P., Di Nardo, P., Grignani, F., Binaglia, L. and Vecchini, A. Eicosapentaenoic Acid Demethylates a Single CpG That Mediates Expression of Tumor Suppressor CCAAT/Enhancer-binding Protein in U937 Leukemia Cells. *The Journal of Biological Chemistry*. 2011, **286**(31).
263. Cho, Y., Turner, N.D., Davidson, L.A., Chapkin, R.S., Carroll, R.J. and Lupton, J.R. Colon cancer cell apoptosis is induced by combined exposure to the n-3 fatty acid docosahexaenoic acid and butyrate through promoter methylation. *Experimental Biology and Medicine*. 2014, **293**(3), pp.302 - 310.
264. Branch, P., Hampson, R. and Karran, P. DNA mismatch binding defects, DNA damage tolerance, and mutator phenotypes in human colorectal carcinoma cell lines. *Cancer Research*. 1995, **55**(11), pp.2304 - 2309.
265. Halford, S., Rowan, A., E, S., Talbot, I. and Tomlinson, I. O6-methylguanine methyltransferase in colorectal cancers: detection of mutations, loss of expression, and weak association with G:C>A:T transitions. *Gut*. 2005, **54**, pp.797 - 802.
266. Yong, W.S., Hsu, F.M. and Chen, P.Y. Profiling genome-wide DNA methylation. *Epigenetics & Chromatin*. 2016, **9**(26).
267. Graule, J., Uth, K., Fischer, E., Centeno, I., Galván, J.A., Eichmann, M., Rau, T., Langer, R., Dawson, H., Nitsche, U., Traeger, P., Berger, M.D., Schnüriger, B., Hädrich, M., Studer, P., Inderbitzin, D., Lugli, A., Tschan, M.P. and Zlobec, I. CDX2 in colorectal cancer is an independent prognostic factor and regulated by promoter methylation and histone deacetylation in tumors of the serrated pathway. *Clinical Epigenetics*. 2018, **10**(1), p.120.
268. Yu, G., Wu, Y., Wang, W., Xu, J., Lv, X., Cao, X. and Wan, T. Correction to: Low-dose decitabine enhances the effect of PD-1 blockade in colorectal cancer with microsatellite stability by re-modulating the tumor microenvironment. *Cellular & molecular immunology*. 2020, **17**(1), pp.111 - 112.
269. Lo, P.K., Mehrotra, J., D'Costa, A., Fackler, M.J., Garrett-Mayer, E., Argani, P. and Sukumar, S. Epigenetic suppression of secreted frizzled related protein 1 (SFRP1) expression in human breast cancer. *Cancer Biology and Therapy*. 2006, **5**(3), pp.281 - 286.
270. Xiang, T., Li, L., Yin, X., Yuan, C., Tan, C., Su, X., Xiong, L., Putti, T.C., Oberst, M., Kelly, K., Ren, G. and Q, T. The ubiquitin peptidase UCHL1 induces G0/G1 cell cycle arrest and apoptosis through stabilizing p53 and is frequently silenced in breast cancer. *PLoS One*. 2012, **7**(1), p.e29783.

271. Brasky, T.M., Till, C., White, E., Neuhausser, M.L., Song, X., Goodman, P., Thompson, I.M., King, I.B., Albanes, D. and Kristal, A.R. Serum phospholipid fatty acids and prostate cancer risk: results from the prostate cancer prevention trial. *American Journal of Epidemiology* 2011, **173**(12), pp.1429-1439.
272. Harris, W.S., Sands, S.A., Windsor, S.L., Ali, H.A., Stevens, T.L., Magalski, A., Porter, C.B. and Borkon, A.M. Omega-3 fatty acids in cardiac biopsies from heart transplantation patients: correlation with erythrocytes and response to supplementation. *Circulation*. 2004, **110**(12), pp.1645-1649.
273. Agilent. *Basics of LC/MS: A primer*. USA, 1998.
274. Watson, H., Cockbain, A.J., Spencer, J., Race, A., Volpato, M., Loadman, P.M., Toogood, G.J. and Hull, M.A. Measurement of red blood cell eicosapentaenoic acid (EPA) levels in a randomised trial of EPA in patients with colorectal cancer liver metastases. *Prostaglandins, Leukotrienes and Essential Fatty Acids*. 2016, **115**, pp.60 - 66.
275. Volpato, M. *GC-MS versus LC-MS - Internal Communication*, 2019.
276. Tutino, V., De Nunzio, V., Caruso, M.G., Veronese, N., Lorusso, D., Di Masi, M., Benedetto, M.L. and Notarnicola, M. Elevated AA/EPA Ratio Represents an Inflammatory Biomarker in Tumor Tissue of Metastatic Colorectal Cancer Patients. *International Journal of Molecular Sciences*. 2019, **20**(8), p.2050.
277. Kitagawa, M., Haji, S. and Amagai, T. Elevated serum AA/EPA ratio as a predictor of skeletal muscle depletion in cachexic patients with advanced gastro-intestinal cancers. *In Vivo*. 2017, **31**, pp.1003–1009.
278. Tutino, V., De Nunzio, V., Caruso, M.G., Bonfiglio, C., Franco, I., Mirizzi, A., De Leonardis, G., Cozzolongo, R., Giannuzzi, V., Giannelli, G., Notarnicola, M. and Osella, A.R. Aerobic physical activity and a low glycemic diet reduce the aa/epa ratio in red blood cell membranes of patients with nafld. *Nutrients* 2018, **10**(9), p.1299.
279. Carta, G., Murru, E., Banni, S. and Manca, C. Palmitic Acid: Physiological Role, Metabolism and Nutritional Implications. *Frontiers in Physiology*. 2017, **8**, p.902.
280. Njoroge, S.W., Laposata, M., Katrangi, W. and Seegmiller, A.C. DHA and EPA reverse cystic fibrosis-related FA abnormalities by suppressing FA desaturase expression and activity. *Journal of Lipid Research*. 2012, **53**(2), pp.257 - 265.
281. Corsetto, P.A., Montorfano, G., Zava, S., Jovenitti, I.E., Cremona, A., Berra, B. and Rizzo, A.M. Effects of n-3 PUFAs on breast cancer cells through their incorporation in plasma membrane. *Lipids in Health and Disease* 2011, **10**(73).
282. Brenna, J.T., Plourde, M., Stark, K.D., Jones, P.J. and Lin, Y.-H. Best practices for the design, laboratory analysis, and reporting of trials involving fatty acids. *The American Journal of Clinical Nutrition*. 2018, **108**(2), pp.211–227.
283. Schwertner, H.A. and Mosser, E.L. Comparison of lipid fatty acids on a concentration basis vs weight percentage basis in patients with and without coronary artery disease or diabetes. *Clinical Chemistry*. 1993, **39**(4), pp.659 - 663.
284. Miura, K., Hughes, M.C.B., Ungerer, J.P.J., Smith, D.D. and Green, A.C. Absolute versus relative measures of plasma fatty acids and health outcomes: example of phospholipid omega3 and omega6 fatty acids and allcause mortality in women. *European Journal of Nutrition*. 2018, **57**(2), pp.713 - 722.
285. Pirman, D.A., Efuet, E., Ding, X.-P., Pan, Y., Tan, L., Fischer, S.M., DuBois, R.N. and Yang, P. Changes in Cancer Cell Metabolism Revealed by Direct Sample Analysis with MALDI Mass Spectrometry. *PLoS One*. 2013, **8**(4), p.e61379.
286. Metherel, A.H. and Bazinet, R.P. Updates to the n-3 polyunsaturated fatty acid biosynthesis pathway: DHA synthesis rates, tetracosahexaenoic acid and (minimal) retroconversion. *Progress in Lipid Research*. 2019, **76**.
287. Metherel, A.H., Irfan, M., Klingel, S.L., Mutch, D.M. and Bazinet, R.P. Compound-specific isotope analysis reveals no retroconversion of DHA to EPA but substantial conversion of EPA to DHA following supplementation: a randomized control trial. *The American Journal of Clinical Nutrition*. 2019, **110**(4), pp.823 - 831.
288. Dijk, F.J., van Dijk, M., Dorresteyn, B. and van Norren, K. DPA shows comparable chemotherapy sensitizing effects as EPA upon cellular incorporation in tumor cells. *Oncotarget*. 2019, **10** (57).
289. Huang, M.-C., Muddana, S., Horowitz, E.N., McCormick, C.C., Infante, J.P. and Brenna, J.T. High-Precision Isotope Ratio Mass Spectrometry and Stable Isotope Precursors for Tracer Studies in Cell Culture. *Analytical Biochemistry*. 2000, **287**(1), pp.80 - 86.
290. Pelikan, E.W. *Glossary of Terms and Symbols Used in Pharmacology*. [Online]. 2004. [Accessed]. Available from: <https://www.bumc.bu.edu/busm-pm/academics/resources/glossary/#s>

291. Volpato, M. *MC38 and MC38r Microarray Data - Internal Communication*, 2016.
292. Solinski, H.J., Gudermann, T. and Breit, A. Pharmacology and signalling of MAS-Related G Protein-Coupled Receptors. *Pharmacological Reviews*. 2014, **66**(3), pp.570-597.
293. Bader, M., Alenina, N., Andrade-Navarro, M.A. and Santos, R.A. Mas and Its Related G Protein-Coupled Receptors, Mrgprs. *Pharmacological Reviews*. 2014, **66**(4), pp.1080 - 1105.
294. Dong, X., Han, S., Zylka, M.J., Simon, M.I. and Anderson, D.J. A diverse family of GPCRs expressed in specific subsets of nociceptive sensory neurons. *Cell*. 2001, **106**(5), pp.619-632.
295. Remoortel, S.V., Ceuleers, H., Arora, R., Nassauw, L.V., Man, J.G.D., Buckinx, R., Winter, B.Y.D. and Timmermans, P. 3 Mas-related G protein-coupled receptor C11 (Mrgprc11) induces visceral hypersensitivity in the mouse colon: A novel target in gut nociception? *Neurogastroenterology and Motility*. 2019, **31**(8), p.e13623.
296. Becker, W.M., Kleinsmith, L.J., Hardin, J. and Bertoni, G. *The World of The Cell*. Seventh Edition ed. San Francisco, USA: Pearson/Benjamin Cummings, 2009.
297. Dorsam, R.T. and Gutkind, J.S. G Protein Coupled Receptors and Cancer. *Nature Reviews: Cancer*. 2007, **7**, pp.79 - 94.
298. K, M. *Janeway's Immunobiology*. 8th Edition ed. New York: Garland Science, 2012.
299. Neves, S., Ram, P. and Iyengar, R. G Protein Pathways. *Science*. 2002, **296**.
300. Van der Jeught, K., Xu, H.-C., Li, Y.-J., Lu, X.-B. and Ji, G. Drug resistance and new therapies in colorectal cancer. *World Journal of Gastroenterology*. 2018, **24**(34), pp.3834 - 3848.
301. Jensen, N.F., Stenvang, J., Beck, M.K., Hanáková, B., Belling, K.C., Do, K.N., Viuff, B., Nygård, S.B., Gupta, R., Rasmussen, M.H., Tarpgaard, L.S., Hansen, T.P., Budinská, E., Pfeiffer, P., Bosman, F., Tejpar, S., Roth, A., Delorenzi, M., Andersen, C.L., Rømer, M.U., Brünner, N. and Moreira, J.M. Establishment and characterization of models of chemotherapy resistance in colorectal cancer: Towards a predictive signature of chemoresistance. *Molecular Oncology*. 2015, **9**(6), pp.1169 - 1185.
302. Boyer, J., McLean, E.G., Aroori, S., Wilson, P., McCulla, A., Carey, P.D., Longley, D.B. and Johnston, P.G. Characterization of p53 Wild-Type and Null Isogenic Colorectal Cancer Cell Lines Resistant to 5-Fluorouracil, Oxaliplatin, and Irinotecan. *Clinical Cancer Research*. 2004, **10**(6), pp.2158 - 2167.
303. Candeil, L., Gourdier, I., Peyron, D., Vezzio, N., Copois, V., Bibeau, F., Orsetti, B., Scheffer, G.L., Ychou, M., Khan, Q.A., Pommier, Y., Pau, B., Martineau, P. and Del Rio, M. ABCG2 overexpression in colon cancer cells resistant to SN38 and in irinotecan-treated metastases. *International Journal of Cancer*. 2004, **109**(6), pp.848-854.
304. Human Protein Atlas. *Anti-MRGPRF Antibody*. [Online]. 2016. [Accessed]. Available from: <https://www.atlasantibodies.com/products/antibodies/primary-antibodies/triple-a-polyclonals/mrgprf-antibody-hpa028811/?q=HPA028811&t=at7RN659jP3tfDFkSRDmOw==>
305. Thomas, P. and Smart, T.G. HEK293 cell line: A vehicle for the expression of recombinant proteins. *Journal of Pharmacological and Toxicological Methods*. 2005, **51**(3), pp.187 - 200.
306. Han, S.K., Dong, X., Hwang, J.I., Zylka, M.J., Anderson, D.J. and Simon, M.I. Orphan G protein-coupled receptors MrgA1 and MrgC11 are distinctively activated by RF-amiderelated peptides through the G_q/11 pathway. *Proceedings of the National Academy of Sciences USA*. 2002, **99**(23), pp.14740–14745.
307. Aggarwal, A., Prinz-Wohlgenannt, M., Tennakoon, S., Höbaus, J., Boudot, C., Mentaverri, R., Brown, E.M., Baumgartner-Parzer, S. and Kállay, E. The calcium-sensing receptor: A promising target for prevention of colorectal cancer. *Biochimica et Biophysica Acta - Molecular Cell Research*. 2015, **1853**.
308. Ooi, A., Wong, A., Esau, L., Lemtiri-Chlieh, F. and Gehring, C. A Guide to Transient Expression of Membrane Proteins in HEK-293 Cells for Functional Characterization. *Frontiers in Physiology*. 2016, **7**(300).
309. Appleyard, J. *Can an orphan G protein coupled receptor be key in improving patient response to eicosapentaenoic acid and personalising therapy?* Leeds, UK: University of Leeds, 2017.
310. Beal, H. *Can an orphan G protein coupled receptor be key in improving patient response to eicosapentaenoic acid and personalising therapy?* Leeds: University of Leeds, 2017.
311. Sgourakis, N.G., Bagos, P.G., Papasaikas, P.K. and Hamodrakas, S.J. A method for the prediction of GPCRs coupling specificity to G-proteins using refined profile Hidden Markov Models. *BMC bioinformatics*. 2005, **22**(6), p.104.

312. Canals, M., Jenkins, L., Kellett, E. and Milligan, G. Up-regulation of the angiotensin II type 1 receptor by the MAS proto-oncogene is due to constitutive activation of Gq/G11 by MAS. *Journal of Biological Chemistry*. 2006, **281**(24), pp.16757 - 16767.
313. Karnik, S.S., Singh, K.D., Tirupula, K. and Unal, H. Significance of angiotensin 1-7 coupling with MAS1 receptor and other GPCRs to the renin-angiotensin system: IUPHAR Review 22. *British Journal of Pharmacology*. 2017, **174**(9), pp.737 - 753.
314. Liu, Q., Tang, Z., Surdenikova, L., Kim, S., Patel, K.N., Kim, A., Ru, F., Guan, Y., Weng, H.J., Geng, Y., Undem, B.J., Kollarik, M., Chen, Z.F., Anderson, D.J. and Dong, X. Sensory neuron-specific GPCR Mrgprs are Itch Receptors Mediating Chloroquine-Induced Pruritus. *Cell*. 2009, **139**(7), pp.1353 – 1365.
315. Lembo, P.M.C., Grazzini, E., Groblewski, T., O'Donnell, D., Roy, M.-O., Zhang, J., Hoffert, C., Cao, J., Schmidt, R., Pelletier, M., Labarre, M., Gosselin, M., Fortin, Y., Banville, D., Shen, S.H., Ström, P., Payza, K., Dray, A., Walker, P. and Ahmad, S. Proenkephalin A gene products activate a new family of sensory neuron-specific GPCRs. *Nature Neuroscience*. 2002, **5**(3), pp.201 - 209.
316. Bikkavilli, R.K., Tsang, S.Y., Tang, W.M., Sun, J.X., Ngai, S.M., Lee, S.S., Ko, W.H., Wise, H. and Cheung, W.T. Identification and characterization of surrogate peptide ligand for orphan G protein-coupled receptor mas using phage-displayed peptide library. *Biochemical Pharmacology*. 2006, **71**(3), pp.319 - 337.
317. Shemesh, R., Toporik, A., Levine, Z., Hecht, I., Rotman, G. and Wool, A. Discovery and validation of novel peptide agonists for G-protein-coupled receptors. *Journal of Biological Chemistry*. 2008, **283**, pp.34643 - 34649.
318. McNeil, B. and Dong, X. *Itch: Mechanisms and Treatment*. 2014 ed. Boca Raton (FL): Taylor & Francis, 2014.
319. Subramanian, H., Gupta, K. and Ali, H. Roles of MAS-related G protein coupled receptor-X2 (MRGPRX2) on mast cell-mediated host defense, pseudoallergic drug reactions and chronic inflammatory diseases. *Journal of Allergy and Clinical Immunology*. 2016, **138**(3), pp.700–710.
320. Burstein, E.S., Ott, T.R., Feddock, M., Ma, J.-N., Fuhs, S., Wong, S., Schiffer, H.H., Brann, M.R. and Nash, N.R. Characterization of the Mas-related gene family: structural and functional conservation of human and rhesus MrgX receptors. *British Journal of Pharmacology*. 2006, **147**.
321. Palmer, E. and Freeman, T. Investigation into the use of C- and N-terminal GFP fusion proteins for subcellular localization studies using reverse transfection microarrays. *Comparative and functional genomics*. 2004, **5**(4), pp.324 - 353.
322. Li, Z., Tseng, P.-Y., Tiwari, V., Xu, Q., He, S.-Q., Wang, Y., Zheng, Q., Han, L., Wu, Z., Blobaum, A.L., Cui, Y., Tiwari, V., Sun, S., Cheng, Y., Huang-Lionnet, J.H.Y., Geng, Y., Xiao, B., Peng, J., Hopkins, C., Raja, S.N., Guan, Y. and Dong, X. Targeting human MRGPRX1 to inhibit persistent pain. *Proceedings of the National Academy of Sciences of the United States of America*. 2017, **114**(10), pp.E1996 - E2005.
323. Dussor, G., Zylka, M. J., Anderson, D. J., & McCleskey, E. W. Cutaneous sensory neurons expressing the Mrgprd receptor sense extracellular ATP and are putative nociceptors. *Journal of neurophysiology*. 2008, **99**(4), pp.1581 - 1589.
324. Leenaars, M. and Hendriksen, C.F. Critical steps in the production of polyclonal and monoclonal antibodies: evaluation and recommendations. *ILAR Journal*. 2005, **46**(3), pp.269 - 279.
325. Jo, M. and Jung, S.T. Engineering therapeutic antibodies targeting G-protein-coupled receptors. *Experimental & molecular medicine*. 2016, **48**(2), p.e207.
326. Tang, X.I., Wang, Y., Li, D.I. and et al. Orphan G protein-coupled receptors (GPCRs): biological functions and potential drug targets. *Acta Pharmacol Sin*. 2012, **33**, pp.363 - 371.
327. Guo, Y., Cordes, K.R., Farese, R.V. and C., W.T. Lipid Droplets at a Glance. *Journal of Cell Science*. 2009, **122**, pp.749 - 752.
328. Weller, P., Ryeom, S.W., Picard, S., Ackerman, S.J. and Dvorak, A.M. Cytoplasmic Lipid Bodies of Neutrophils: Formation Induced by cis-Unsaturated Fatty Acids and Mediated by Protein Kinase C *The Journal of Cell Biology*. 1991, **113**(1), pp.137-146.
329. Francipane, M.G., Bulanin, D. and Lagasse, E. Establishment and Characterization of 5-Fluorouracil-Resistant Human Colorectal Cancer Stem-Like Cells: Tumor Dynamics under Selection Pressure. *International Journal of Molecular Sciences*. 2019, **20**(8), p.1817.

330. Xavier, C.P.R., Pesic, M. and Vasconcelos, M.H. Understanding Cancer Drug Resistance by Developing and Studying Resistant Cell Line Models. *Current Cancer Drug Targets*. 2016, **16**(3).
331. Lesuffleur, T., Barbat, A., Dussaulx, E. and Zweibaum, A. Growth adaptation to methotrexate of HT-29 human colon carcinoma cells is associated with their ability to differentiate into columnar absorptive and mucus-secreting cells. *Cancer Research*. 1990, **50**(19), pp.6334 - 6343.
332. Siravegna, G., Mussolin, B., Buscarino, M., Corti, G., Cassingena, A., Crisafulli, G., Ponzetti, A., Cremolini, C., Amatu, A., Lauricella, C., Lamba, S., Hobor, S., Avallone, A., Valtorta, E., Rospo, G., Medico, E., Motta, V., Antoniotti, C., Tatangelo, F., Bellosillo, B., Bardelli, A. Clonal evolution and resistance to EGFR blockade in the blood of colorectal cancer patients. *Nature Medicine*. 2015, **21**(7), pp.795 - 801.
333. Li, Q.H., Wang, Y.Z., Tu, J., Liu, C.W., Yuan, Y.J., Lin, R., He, W.L., Cai, S.R., He, Y.L. and Ye, J.N. Anti-EGFR therapy in metastatic colorectal cancer: mechanisms and potential regimens of drug resistance. *Gastroenterology Reports*. 2020, **8**(3), pp.179 - 191.
334. Xie, L. and Bourne, P.E. Developing multi-target therapeutics to fine-tune the evolutionary dynamics of the cancer ecosystem. *Frontiers in Pharmacology*. 2015, **6**(209).
335. Milojkovic, D. and Apperley, J. Mechanisms of Resistance to Imatinib and Second-Generation Tyrosine Inhibitors in Chronic Myeloid Leukemia. *Clinical Cancer Research*. 2009, **15**(24), pp.7519-7527.
336. Mitchell, R., Hopcroft, L.E.M., Baquero, P., Allan, E.K., Hewit, K., James, D., Hamilton, G., Mukhopadhyay, A., O'Prey, J., Hair, A., Melo, J.V., Chan, E., Ryan, K.M., Maguer-Satta, V., Druker, B.J., Clark, R.E., Mitra, S., Herzyk, P., Nicolini, F.E., Salomoni, P., Shanks, E., Calabretta, B., Holyoake, T.L. and Helgason, G.V. Targeting BCR-ABL-Independent TKI Resistance in Chronic Myeloid Leukemia by mTOR and Autophagy Inhibition. *Journal of the National Cancer Institute*. 2018, **110**(5), pp.467 - 478.
337. Chiang, N. and Serhan, C.N. Aspirin triggers formation of anti-inflammatory mediators: New mechanism for an old drug. *Discovery Medicine*. 2004, **4**(24), pp.470 - 475.
338. G, S.R. The role of aspirin in colorectal cancer chemoprevention. *Critical Reviews in Oncological Hematology*. 2016, **104**, pp.87 - 90.
339. ClinicalTrials.gov. *Add-Aspirin: A Trial Assessing the Effects of Aspirin on Disease Recurrence and Survival After Primary Therapy in Common Non Metastatic Solid Tumours*. [Online]. 2021. [Accessed]. Available from: <https://clinicaltrials.gov/ct2/show/NCT02804815>
340. Burn, J., Bishop, D.T., Mecklin, J.P. and et al. Effect of aspirin or resistant starch on colorectal neoplasia in the Lynch syndrom. *New England Journal of Medicine*. 2009, **359**(24), pp.2567 - 2578.
341. Burn, J., Gerdes, A.M., Macrae, F. and CAPP2 Investigators. Long-term effect of aspirin on cancer risk in carriers of hereditary colorectal cancer: an analysis from the CAPP2 randomised controlled trial. *Lancet*. 2011, **378**(9809), pp.2081 - 2087.
342. Smith, M.L., Hawcroft, G. and Hull, M.A. The effect of non-steroidal anti-inflammatory drugs on human colorectal cancer cells: evidence of different mechanisms of action. *The European Journal of Cancer*. 2000, **36**(5), pp.664 - 674.
343. Mirabelli, P., Coppola, L. and Salvatore, M. Cancer Cell Lines Are Useful Model Systems for Medical Research. *Cancers*. 2019, **11**(8), p.1098.
344. Blank, A., Roberts, D.E., 2nd, Dawson, H., Zlobec, I. and Lugli, A. Tumor Heterogeneity in Primary Colorectal Cancer and Corresponding Metastases. Does the Apple Fall Far From the Tree? *Frontiers in Medicine*. 2018, **5**(234).
345. Reya, T., Morrison, S.J., Clarke, M.F. and Weissman, I.L. Stem cells, cancer, and cancer stem cells. *Nature*. 2001, **414**(6859), pp.105 - 111.
346. Ben-David, U., Siranosian, B., Ha, G., Tang, H., Oren, Y., Hinohara, K., Strathdee, C., Dempster, J., Lyons, N.J., Burns, R., Nag, A., Kugener, G., Cimini, B., Tsvetkov, P., Maruvka, Y.E., O'Rourke, R., Garrity, A., Tubelli, A.A., Bandopadhyay, P., Tsherniak, A., Vazquez, F., Wong, B., Birger, C., Ghandi, M., Thorner, A.R., Bittker, J.A., Meyerson, M., Getz, G., Beroukhir, R. and Golub, T.R. Genetic and transcriptional evolution alters cancer cell line drug response. *Nature*. 2018, **560**(7718), pp.325 - 330.
347. Peddareddigari, V.G., Wang, D., & Dubois, R. N. The tumor microenvironment in colorectal carcinogenesis. *Cancer microenvironment : official journal of the International Cancer Microenvironment Society*. 2010, **3**(1), pp.149 - 166.

348. Markman, J.L. and Shiao, S.L. Impact of the immune system and immunotherapy in colorectal cancer. *Journal of gastrointestinal oncology*. 2015, **6**(2), pp.208 - 223.
349. Song, M. and Chan, A.T. The potential role of exercise and nutrition in harnessing the immune system to improve colorectal cancer survival. *Gastroenterology* 2018, **155**, pp.596 - 600.
350. Gionfriddo, G., Plastina, P., Augimeri, G., Catalano, S., Giordano, C., Barone, I., Morelli, C., Giordano, F., Gelsomino, L., Sisci, D., Witkamp, R., Andò, S., van Norren, K., & Bonofiglio, D. Modulating Tumor-Associated Macrophage Polarization by Synthetic and Natural PPAR γ Ligands as a Potential Target in Breast Cancer. *Cells*. 2020, **9**(1), p.174.
351. Zeyda, M., Säemann, M.D., Stuhlmeier, K.M., Mascher, D.G., Nowotny, P.N., Zlabinger, G.J., Waldhäusl, W. and Stulnig, T.M. Polyunsaturated fatty acids block dendritic cell activation and function independently of NF-kappaB activation. *Journal of Biological Chemistry*. 2005, **280**(14), pp.293 - 301.
352. Taguchi, A., Kawana, K., Tomio, K., Yamashita, A., Isobe, Y., Nagasaka, K., Koga, K., Inoue, T., Nishida, H., Kojima, S., Adachi, K., Matsumoto, Y., Arimoto, T., Wada-Hiraike, O., Oda, K., Kang, J. X., Arai, H., Arita, M., Osuga, Y., & Fujii, T. Matrix metalloproteinase (MMP)-9 in cancer-associated fibroblasts (CAFs) is suppressed by omega-3 polyunsaturated fatty acids in vitro and in vivo. *PLoS One*. 2014, **9**(1).
353. Rovito, D., Giordano, C., Vizza, D., Plastina, P., Barone, I., Casaburi, I., Lanzino, M., De Amicis, F., Sisci, D., Mauro, L., Aquila, S., Catalano, S., Bonofiglio, D. and Andò, S. Omega-3 PUFA ethanolamides DHEA and EPEA induce autophagy through PPAR γ activation in MCF-7 breast cancer cells. *Journal of Cellular Physiology*. 2013, **228**(6), pp.1314 - 1322.
354. Song, M., Nishihara, R., Cao, Y., Chun, E., Qian, Z.R., Mima, K., Inamura, K., Masugi, Y., Nowak, J.A., Nosho, K., Wu, K., Wang, M., Giovannucci, E., Garrett, W.S., Fuchs, C.S., Ogino, S. and Chan, A.T. Marine ω -3 Polyunsaturated Fatty Acid Intake and Risk of Colorectal Cancer Characterized by Tumor-Infiltrating T Cells. *JAMA Oncology*. 2016, **2**(9), pp.1197 - 1206.
355. Zelenay, S., van der Veen, A.G., Bottcher, J.P., Snelgrove, K.J., Rogers, N., Acton, S.E., Chakravarty, P., Girotti, M., Marais, R., Quezada, S., Sahai, E. and Reis e Sousa, C. Cyclooxygenase-dependent tumor growth through evasion of immunity. *Cell*. 2015, **126**(6), pp.1257 - 1270.
356. Szymczak, M., Murray, M. and Petrovic, N. Modulation of angiogenesis by omega-3 polyunsaturated fatty acids is mediated by cyclooxygenases. *Blood*. 2008, **111**(7), pp.3514 - 3521.
357. Veglia, F., Perego, M., & Gabrilovich, D. Myeloid-derived suppressor cells coming of age. *Nature Immunology*. 2018, **19**(2), pp.108 - 119.
358. Tang, L. In vitro intestine model for gut microbiome. *Nature Methods*. 2019, **16**(578).
359. Zeng, H., Lazarova, D.L. and Bordonaro, M. Mechanisms linking dietary fiber, gut microbiota and colon cancer prevention. *World Journal of Gastroenterology*. 2014, **6**, pp.41 - 51.
360. Song, M. and Chan, A.T. Environmental Factors, Gut Microbiota, and Colorectal Cancer Prevention. . *Clinical Gastroenterology and Hepatology*. 2019, **17**(2), pp.275 - 289.
361. Flemer, B., Lynch, D.B., Brown, J.M., Jeffery, I.B., Ryan, F.J., Claesson, M.J., O'Riordain, M., Shanahan, F. and O'Toole, P.W. Tumour-associated and non-tumour-associated microbiota in colorectal cancer. *Gut*. 2017, **66**(4), pp.633 - 643.
362. Dejea, C.M., Wick, E.C. and Hechenbleikner, E.M. Microbiota organization is a distinct feature of proximal colorectal cancers. *Proceedings of the National Academy of Sciences of the United States of America*. 2014, **111**, pp.18321 - 18326.
363. Chung, H., Pamp, S.J., Hill, J.A., Surana, N.K., Edelman, S.M., Troy, E.B., Reading, N.C., Villablanca, E.J., Wang, S., Mora, J.R., Umesaki, Y., Mathis, D., Benoist, C., Relman, D.A. and Kasper, D.L. Gut immune maturation depends on colonization with a host-specific microbiota. *Cell*. 2012, **149**(7), pp.1578 - 1593.
364. Wong, S.H. and Yu, J. Gut microbiota in colorectal cancer: Mechanisms of action and clinical applications. . *Nature Reviews: Gastroenterology & Hepatology*. 2019, **13**, pp.691 - 706.
365. Caesar, R., Tremaroli, V., Kovatcheva-Datchary, P., Cani, P.D. and Backhed, F. Crosstalk between gut microbiota and dietary lipids aggravates WAT inflammation through TLR signaling. *Cell Metabolism*. 2015, **22**(4), p.658 650 668.
366. Robertson, R.C., Seira Oriach, C., Murphy, K., Moloney, G.M., Cryan, J.F., Dinan, T.G., Paul Ross, R. and Stanton, C. Omega-3 polyunsaturated fatty acids critically regulate

- behaviour and gut microbiota development in adolescence and adulthood. *Brain, Behavior, and Immunity*. 2017, **59**, pp.21 - 37.
367. Watson, H., Mitra, S., Croden, F.C., Taylor, M., Wood, H.M., Perry, S.L., Spencer, J.A., Quirke, P., Toogood, G.J., Lawton, C.L., Dye, L., Loadman, P.M. and A., H.M. A randomised trial of the effect of omega-3 polyunsaturated fatty acid supplements on the human intestinal microbiota. *Gut*. 2018, **67**(11), pp.1974 - 1983.
 368. Noriega, B.S., Sanchez-Gonzalez, M.A., Salyakina, D. and Coffman, J. Understanding the Impact of Omega-3 Rich Diet on the Gut Microbiota. *Case Reports Medicine*. 2016, **3089303**.
 369. Prossomariti, A., Scafoli, E., Piazzzi, G., Fazio, C., Bellanova, M., Biagi, E., Candela, M., Brigidi, P., Consolandi, C., Balbi, T., Chieco, P., Munarini, A., Pariali, M., Minguzzi, M., Bazzoli, F., Belluzzi, A. and Ricciardiello, L. Short-term treatment with eicosapentaenoic acid improves inflammation and affects colonic differentiation markers and microbiota in patients with ulcerative colitis. *Scientific Reports*. 2017, **7**(1), p.7458.
 370. Group, B.D.W. Biomarkers and surrogate endpoints: preferred definitions and conceptual framework. *Clinical Pharmacology & Therapeutics*. 2001, **69**, pp.89 - 95.
 371. Goossens, N., Nakagawa, S., Sun, X. and Hoshida, Y. Cancer biomarker discovery and validation. *Translational cancer research*. 2015, **4**(3), pp.256 – 269.
 372. Imperiale, T.F., Ransohoff, D.F. and Itzkowitz, S.H. Multitarget stool DNA testing for colorectal-cancer screening. *New England Journal of Medicine*. 2014, **371**(12), pp.187 - 188.
 373. Van Cutsem, E., Köhne, C.H., Hitre, E., Zaluski, J., Chang Chien, C.R., Makhson, A., D'Haens, G., Pintér, T., Lim, R., Bodoky, G., Roh, J.K., Folprecht, G., Ruff, P., Stroh, C., Tejpar, S., Schlichting, M., Nippgen, J. and Rougier, P. Cetuximab and chemotherapy as initial treatment for metastatic colorectal cancer. *New England Journal of Medicine*. 2009, **360**(14), pp.1408 - 1417.
 374. Volpato, M., Cockbain, A.J., Perry, S.L., Marston, G., Ingram, N., Mann, J., Burghel, H., Wilson, E., Randerson-Moor, J., Droop, A., Coletta, P.L. and Hull, M.A. B84: Increased in CCL2 levels is a negative prognostic marker in colorectal liver metastasis patients treated with eicosapentaenoic acid. In: *NCRI Cancer Conference, Liverpool, UK*. 2015.
 375. Freeman, W.M., Bixler, G.V., Brucklacher, R.M., Lin, C.M., Patel, K.M., Van Guilder, H.D., LaNoue, K.F., Kimball, S.R., Barber, A.J., Antonetti, D.A., Gardner, T.W. and Bronson, S.K. A multistep validation process of biomarkers for preclinical drug development. *Journal of Pharmacogenomics*. 2010, **10**(5), pp.385 - 395.
 376. Arterburn, L.M., Hall, E.B. and Oken, H. Distribution, interconversion, and dose response of n-3 fatty acids in humans. *The American Journal of Clinical Nutrition*. 2006, **83**(6), pp.1467 - 1476.
 377. Kastelein, J.J., Maki, K.C., Susekov, A., Ezhov, M., Nordestgaard, B.G., Machielse, B.N., Kling, D. and Davidson, M.H. Omega-3 free fatty acids for the treatment of severe hypertriglyceridemia: the EpanoVa for Lowering Very high triglycerides (EVOLVE) trial. *Journal of Clinical Lipidology*. 2014, **8**(1), pp.94 - 108.
 378. GlaxoSmithKline. *Lovaza prescribing information*. [Leaflet]. Research Triangle Park, North Carolina, 2014.
 379. Amarin Pharma Inc. *Vascepa - Prescribing Information*. [Leaflet]. Dublin, Ireland, 2019.
 380. AstraZeneca Pharmaceuticals LP. *Epanova prescribing information*. [Leaflet]. Wilmington, Delaware, 2014.
 381. Trygg Pharma Inc. *Omtryg prescribing information*. [Leaflet]. Arlington, Virginia, 2014.
 382. Superko, H.R., Superko, S.M., Nasir, K., Agatston, A. and Garrett, B.C. Omega-3 fatty acid blood levels: clinical significance and controversy. *Circulation*. 2013, **128**(19), pp.2154 - 2161.
 383. Bhatt, D.L., Steg, P.G., Miller, M., Brinton, E.A., Jacobson, T.A., Ketchum, S.B., Doyle Jr, R.T., Juliano, R.A., Jiao, L., Granowitz, C., Tardif, J.C. and Ballantyne, C.M. Cardiovascular Risk Reduction with Icosapent Ethyl for Hypertriglyceridemia. *New England Journal of Medicine*. 2019, **380**(1), pp.11 - 12.
 384. Manson, J.E., Cook, N.R., Lee, I.M., Christen, W., Bassuk, S.S., Mora, S., Gibson, H., Albert, C.M., Gordon, D., Copeland, T., D'Agostino, D., Friedenberg, G., Ridge, C., Bubes, V., Giovannucci, E.L., Willett, W.C., Buring, J.E. and VITAL Research Group. Marine n-3 Fatty Acids and Prevention of Cardiovascular Disease and Cancer. *New England Journal of Medicine*. 2019, **380**(1), pp.23 - 32.
 385. Bowman, L., Mafham, M., Wallendszus, K., Stevens, W., Buck, G. and ASCEND Study Collaborative Group. Effects of n-3 Fatty Acid Supplements in Diabetes Mellitus. *New England Journal of Medicine*. 2018, **379**, pp.1540 - 1550.

386. Kris-Etherton, P.M., Richter, C.K., Bowen, K.J., Skulas-Ray, A.C., Jackson, K.H., Petersen, K.S. and Harris, W.S. Recent Clinical Trials Shed New Light on the Cardiovascular Benefits of Omega-3 Fatty Acids. *Methodist DeBakey Cardiovascular Journal*. 2019, **15**(3), pp.171 - 178.
387. Song, M., Lee, I. M., Manson, J. E., Buring, J. E., Dushkes, R., Gordon, D., Walter, J., Wu, K., Chan, A. T., Ogino, S., Fuchs, C. S., Meyerhardt, J. A., Giovannucci, E. L., VITAL Research Group,. Effect of Supplementation With Marine ω -3 Fatty Acid on Risk of Colorectal Adenomas and Serrated Polyps in the US General Population: A Prespecified Ancillary Study of a Randomized Clinical Trial. *JAMA Oncology*. 2020, **6**(1), pp.108 - 115.
388. West, N.J., Clark, S.K., Phillips, R.K., Hutchinson, J.M., Leicester, R.J., Belluzzi, A. and Hull, M.A. Eicosapentaenoic acid reduces rectal polyp number and size in familial adenomatous polyposis. *Gut*. 2010, **59**(7), pp.918 - 925.
389. Bakker, N., van den Helder, R.S., Stoutjesdijk, E., van Pelt, J. and Houdijk, A.P.J. Effects of perioperative intravenous ω -3 fatty acids in colon cancer patients: a randomized, double-blind, placebo-controlled clinical trial. *American Journal of Clinical Nutrition*. 2020, **111**(2), pp.385 - 395.
390. ClinicalTrials.gov. *Omega 3 Fatty Acids in Colorectal Cancer (CRC) Prevention in Patients With Lynch Syndrome (COLYNE)*. [Online]. 2019. [Accessed]. Available from: <https://clinicaltrials.gov/ct2/show/NCT03831698>
391. ClinicalTrials.gov. *OMega-3 Fatty Acid for the Immune Modulation of Colorectal Cancer (OMICC)*. [Online]. 2018. [Accessed]. Available from: <https://clinicaltrials.gov/ct2/show/NCT03661047>
392. Nelson, A.J.a.N., S. J. Translating evidence from clinical trials of omega-3 fatty acids to clinical practice. *Future Cardiology*. 2020, **16**(4), pp.343 - 350.
393. Rani, I., Sharma, B., Kumar, S., Kaur, S. and Agnihotri, N. Apoptosis mediated chemosensitization of tumor cells to 5-fluorouracil on supplementation of fish oil in experimental colon carcinoma. *Tumour Biology*. 2017, **39**(3).
394. Sebe, M., Tsutsumi, R., Yamaguchi, S., Horikawa, Y.T., Harada, N., Oyama, T., Kakuta, N., Tanaka, K., Tsutsumi, Y.M., Nakaya, Y. and Sakaue, H. The synergistic effects of omega-3 fatty acids against 5-fluorouracil-induced mucosal impairment in mice. *BMC Nutrition*. 2016, **2**(1), p.17.
395. Rani, I., Vaiphei, K. and Agnihotri, N. Supplementation of fish oil augments efficacy and attenuates toxicity of 5- fluorouracil in 1,2-dimethylhydrazine dihydrochloride/dextran sulfate sodium induced colon carcinogenesis. *Cancer Chemotherapy and Pharmacology*. 2014, **74**, pp.309 - 322.
396. Siddiqui, R.A., Harvey, K.A., Xu, Z., Bammerlin, E.M., Walker, C. and Altenburg, J.D. Docosahexaenoic acid: a natural powerful adjuvant that improves efficacy for anticancer treatment with no adverse effects. *BioFactors*. 2011, **37**, pp.399 - 412.
397. Granci, V., Cai, F., Lecumberri, E., Clerc, A., Dupertuis, Y.M. and Pichard, C. Colon cancer cell chemosensitisation by fish oil emulsion involves apoptotic mitochondria pathway. *The British Journal of Nutrition*. 2013, **109**(7), pp.1188 - 1195.
398. Ogo, A., Miyake, S., Kubota, H., Higashida, M., Matsumoto, H., Teramoto, F. and Hirai, T. Synergistic Effect of Eicosapentaenoic Acid on Antiproliferative Action of Anticancer Drugs in a Cancer Cell Line Model. *Annals of Nutrition and Metabolism*. 2017, **71**, pp.247 - 252.
399. Dupertuis, Y.M., Boulens, N., Angibaud, E., Briod, A.S., Viglione, A., Allémann, E., Delie, F. and Pichard, C. Antitumor Effect of 5-Fluorouracil-Loaded Liposomes Containing n-3 Polyunsaturated Fatty Acids in Two Different Colorectal Cancer Cell Lines. *AAPS PharmSciTech*. 2021, **22**(1), p.36.
400. Howells, L.M., Mitra, A. and Manson, M.M. Comparison of oxaliplatin- and curcumin-mediated antiproliferative effects in colorectal cell lines. *International Journal of Cancer*. 2007, **121**(1), pp.175 - 183.
401. Kim, E., Davidson, L. A., Zoh, R. S., Hensel, M. E., Salinas, M. L., Patil, B. S., Jayaprakasha, G. K., Callaway, E. S., Allred, C. D., Turner, N. D., Weeks, B. R., & Chapkin, R. S. Rapidly cycling Lgr5+ stem cells are exquisitely sensitive to extrinsic dietary factors that modulate colon cancer risk. *Cell death & disease*. 2016, **7**(11).
402. Nature. *Personalized medicine*. [Online]. 2020. [Accessed]. Available from: <https://www.nature.com/subjects/personalized-medicine>
403. ATCC. *HCT 116 (ATCC (R) CCL-247TM)* [Online]. 2019. [Accessed 02.10.2019]. Available from: <https://www.lgcstandards-atcc.org/en/Products/All/CCL-247.aspx#generalinformation>

404. Butler, J. *STRBase (SRD-130): Overview of STR Fact Sheets*. [Online]. 2020. [Accessed 15.05.2020]. Available from: https://strbase.nist.gov/str_fact.htm
405. Cellosaurus. *CLASTR: The Cellosaurus STR Similarity Search Tool*. [Online]. 2020. [Accessed 15.05.2020]. Available from: <https://web.expasy.org/cellosaurus-str-search/>

List of Abbreviations

A		CRC-LN	colorectal cancer derived from lymph node metastases
AA	arachidonic acid	CRCSC	CRC Subtyping Consortium
AmpR	ampicillin resistance gene	C_T	Cycle threshold
APC	Adenomatous polyposis coli	CT	computed tomographic
ATCC	American Type Culture Collection	CTLA-4	cytotoxic T-lymphocyte-associated protein 4
ATP	adenosine triphosphate	CUP	Continuous Update Project
AZA	5-Azacytidine	CYP450	cytochrome P450
B		D	
bp	Base pair	DAABD-AE	4-[2-(<i>N,N</i> -dimethylamino)ethylaminosulfonyl]-7-(2-aminoethylamino)-2,1,3-benzoxadiazole
BRAF	B-Raf Proto-Oncogene	DAC	Decitabine
C		DAG	diacylglycerol
Ca²⁺	calcium	DFS	disease free survival
cAMP	cyclic adenosine 3',5'-monophosphate	DHA	docosahexaenoic acid
CCL2	chemokine C-C motif ligand	DMAP	4-(dimethylamino) pyridine
cDNA	complementary DNA	DMEM	Dulbecco's Modified Eagle Media
CEA	carcinoembryonic antigen	DMSO	dimethyl sulfoxide
CGH	comparative genomic hybridization	DNA	deoxyribonucleic acid
CI	confidence interval	dNTPs	deoxynucleotide triphosphates
CIMP	CpG island methylation phenotype	DPA	docosapentaenoic acid
CIN	chromosomal instability	DPBS	Dulbecco's phosphate buffered saline
CMS	consensus molecular subtypes	DTP	Development Therapeutics Program
CO₂	Carbon dioxide		
COX	cyclo-oxygenase		
CRC	colorectal cancer		
CRCLM	CRC liver metastases		

E		GAPDH	Glyceraldehyde 3-phosphate dehydrogenase
ECACC	European Collection of Authenticated Cell Cultures	GC/MS	gas chromatography/mass spectrometry
EDC	1-Ethyl-3-(3-dimethylaminoropyl)-carbodiimide HCl	GDP	Guanosine diphosphate
EDTA	trypsin-ethylenediaminetetraacetic acid	gDNA	Genomic deoxyribonucleic acid
eGFP	Enhanced Green Fluorescent Protein	GPCRs	G protein coupled receptors
EGFR	epidermal growth factor receptor	GTP	Guanosine-5'-triphosphate
ELISA	enzyme-linked immunosorbent assay		
ELOVL-2	Fatty Acid Elongase 2	H	
ELOVL-5	Fatty Acid Elongase 5	HCl	hydrogen chloride
EMT	EPA for Metastasis Trial	hCRC	human colorectal cancer
emt	epithelial mesenchymal transition	HNPCC	hereditary nonpolyposis colorectal cancer
EPA	eicosapentaenoic acid	HPA	Human Protein Atlas
ESI	electrospray ionisation	HR	hazards ratio
EtOH	ethanol		
F		I	
F12	Ham's F-12 Nutrient Mix	IBD	inflammatory bowel diseases
FA	Fatty acid	IC₅₀	Half maximal inhibitory concentration
FACS	fluorescence activated cell sort	IHC	immunohistochemistry
FADS1	Fatty Acid Desaturase 1	INSERM	Institut national de la santé et de la recherche médicale
FADS2	Fatty Acid Desaturase 2	IP₃	inositol 1,4,5-triphosphate
FAP	familial adenomatous polyposis	IS	Internal Standard
FC	fold change	IUPAC	International Union of Pure and Applied Chemistry
FCS	fetal calf serum		
FFA	free fatty acid	K	
FISH	fluorescent in situ hybridization	KRAS	Kirsten ras
5-FU	5-Fluoruracil	L	
G		L-15	Leibovitz's L-15
		LA	linoleic acid

LC	liquid chromatography	PDX	patient-derived xenografts
LOH	loss of heterozygosity	PD-1	Programmed cell death protein 1
LOX	lipoxygenase	PG	prostaglandin
LNA	alpha-linolenic acid	PGE₂	Prostaglandin E2
LT	leukotriene	PGE₃	Prostaglandin E3
M		PGH2	Prostaglandin H2
MgCl₂	magnesium chloride	PKC	protein kinase C
MLH1	MutL Homolog 1	PMS2	PMS1 Homolog 2
MMR	mismatch repair	PTGS	prostaglandin-endoperoxide synthase
MRGPRF	MAS Related GPR Family Member F	PUFA	polyunsaturated fatty acid
MRI	Magnetic resonance imaging	Q	
mRNA	messenger RNA	qPCR	quantitative PCR
MS	Mass spectrometry	R	
MSH2	MutS Homolog 2	RCT	randomised controlled trial
MSH6	MutS Homolog 6	RhoGEF	Rho guanine nucleotide exchange factor
MSI	microsatellite instability	RIPA	
MTT	3-(4,5-dimethylthiazol-2-yl)-2,5-diphenyl tetrazolium bromide salt	RNA	Ribonucleic acid
N		ROS	reactive oxygen species
<i>n</i>-3	omega-3	RPMI	Roswell Park Memorial Institute
<i>n</i>-6	omega-6	RQ	relative quantity
NeoR	neomycin resistance gene	S	
NICE	National Institute for Health and Care Excellence	SA	Stearic Acid
O		SD	standard deviation
OA	Oleic Acid	seAFOod	Systemic evaluation of Aspirin and Fish oil
OS	overall survival	SEM	standard error of the mean
P		S/ER	sarco/endoplasmic reticulum
PA	Palmitic Acid	STR	short tandem repeat
PCR	Polymerase chain reaction		

T

TAE	tris acetate ethylenediaminetetraacetic
TBS	Tris-buffered saline
TE	Tris-EDTA
TEM	trans anal endoscopic microsurgery
Tg	thapsigargin
TGF-β	Transforming growth factor beta
TME	total mesorectal excision
TMZ	Temozolomide
TNM	Tumour Node Metastases
TP53	Tumour protein P53

U

UC	Ulcerative colitis
UK	United Kingdom

V

VEGF	vascular endothelial growth factor
-------------	---------------------------------------

Appendix

A4.1. STR profiling

The cell line HCT116, which is frequently used in CRC *in vitro* studies, was immortalised from the tumour of an adult male patient (403). According to the ATCC and Cellosaurus database have an expected profile of XY at the amelogenin marker (181). However, my data shows an amelogenin marker profile of X, with the loss of the Y marker. This has been seen in the literature, following repeat passage the amplification of the Y marker product is lost.

Table A4.1. Loci detected by STR profiling and the expected base pair ranges

Fluorescein labelled loci	Base Pair Range (bp)	JOE labelled loci	Base Pair Range (bp)	TMR labelled loci	Base Pair Range (bp)
D3S1358	99 – 147	D5S818	115 – 163	AMEL	
TH01	152 – 196	D13S317	157 – 205	vWA	123 – 183
D21S11	155 – 273	D7S820	211 – 251	D8S1179	203 – 255
D18S51	286 – 373	D16S539	260 – 308	TPOX	254 – 302
pentaE	379 - 484	CSF1PO	317 – 361	FGA	308 – 464
		PentaD	370 – 454		

Expected size range (base pair) of amplified PCR products for each locus. Promega Powerplex 16HS assay was used, and therefore these sizes are specific to the expected sizes when samples are analysed by this assay. The data was sourced from reference (404).

Table A4.2. Summary STR trace matches to database profiles

Cell Line	ATCC	Cellosaurus
CaCo-2	100	100
Colo205	100	100
DLD-1	100	100
HCA7		94.55
HCT116	67	96.77
HRT18	78	98.04
HT29	100	100
LoVo	67	90
LS174T	81.3	100
SW48	93.8	96.43
SW480	100	100
SW620	100	100
T84	100	100
TC71	85.7	93.88

Scores were compared to the scores recorded on the following databases; ATCC (181) and Cellosaurus (405). The comparison was made by calculating percentage match, with scores above 80% being accepted as the threshold for confirming the cell line identity.

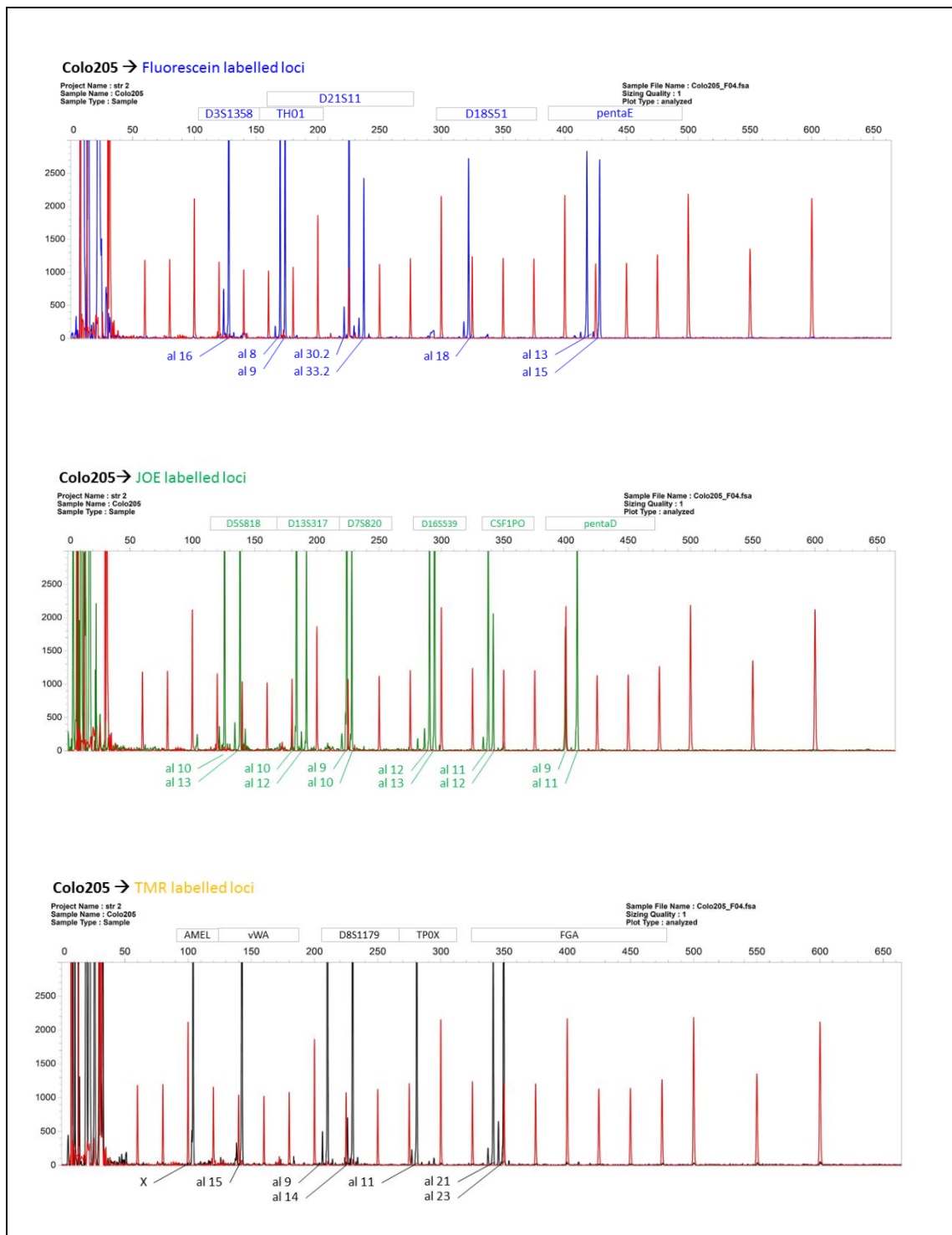


Figure A4.1 Representative STR trace for Colo205 cells

A representative amplification traces for Colo205 cells are shown: A: Fluorescein labelled loci (D3S1358, TH01, D21S11, D18S51, pentaE). B: JOE labelled loci (D5S818, D13S317, D7S820, D16S539, and CSF1PO). C: TMR labelled loci (AMEL, vWA, D8S1179, TP0X, and FGA). Called alleles are notated below each trace.

A4.2. Microsatellite status confirmed of HT29, HCT116 and HCA-7 cells

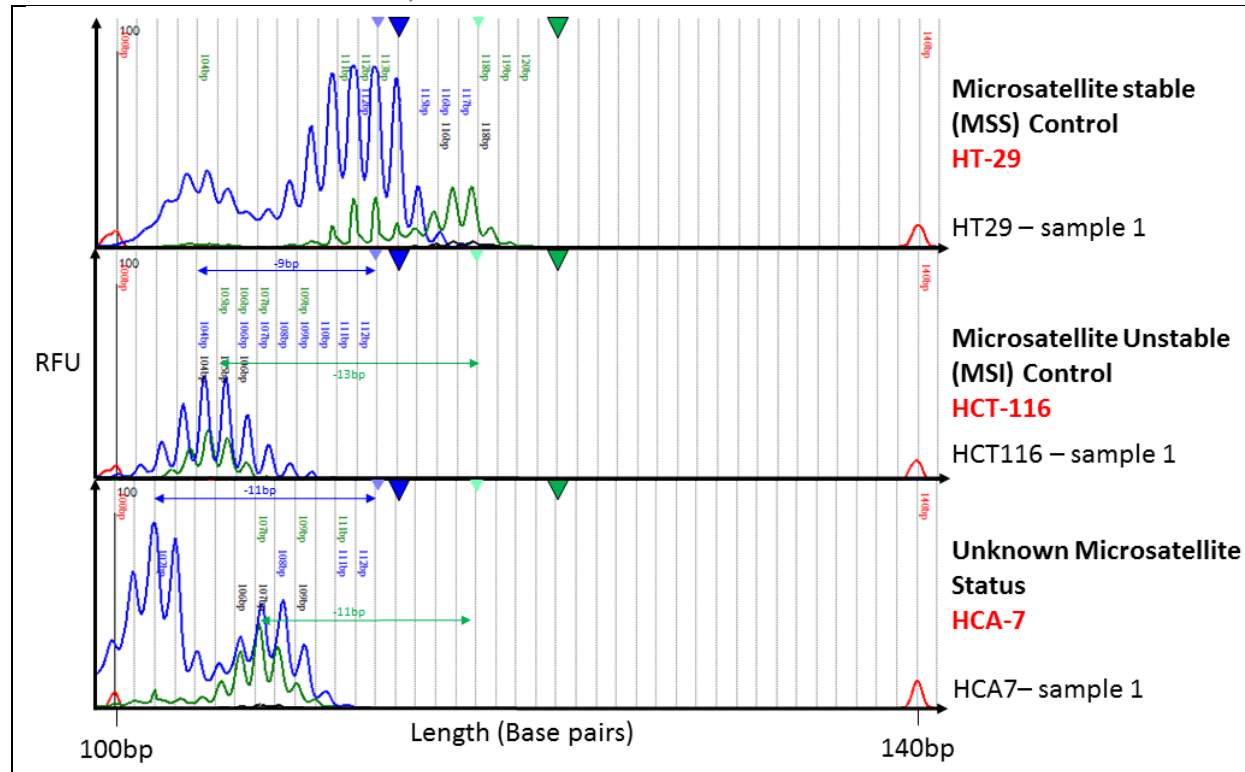


Figure A4.2 Representative traces of HT29, HCT116 and HCA-7 cells

gDNA was collected from each cell line, and PCR reactions to amplify *BAT-25* and *BAT-26* and the PCR products were sequenced (ABI3130xl) using Gene Scan ROX500 as the marker reference. The blue trace is representative of peaks attributed to the *BAT-25* and green trace is *BAT-26*. Expected product sizes are shown at 114bp (*BAT-25*), 122bp (*BAT-26*). For analysis the used 'peak' to calculate difference in major peak are denoted by: small blue triangle at 113bp (*BAT-25*) and small green triangle (*BAT-26*) at 118bp as these were the major peaks identified for the known MSS sample used for this analysis (HT29). HCT116 was the known MSI sample, and the difference from expected peak size was calculated and shown on the plots (*BAT-25*: -9bp, *BAT-26*: -13bp). HCA-7 was found to have an 11bp difference in major peak expected product size for both markers. Data representative of 3 independent repeats.

A4.3. Associations between molecular phenotypes and *n*-3 PUFA sensitivity

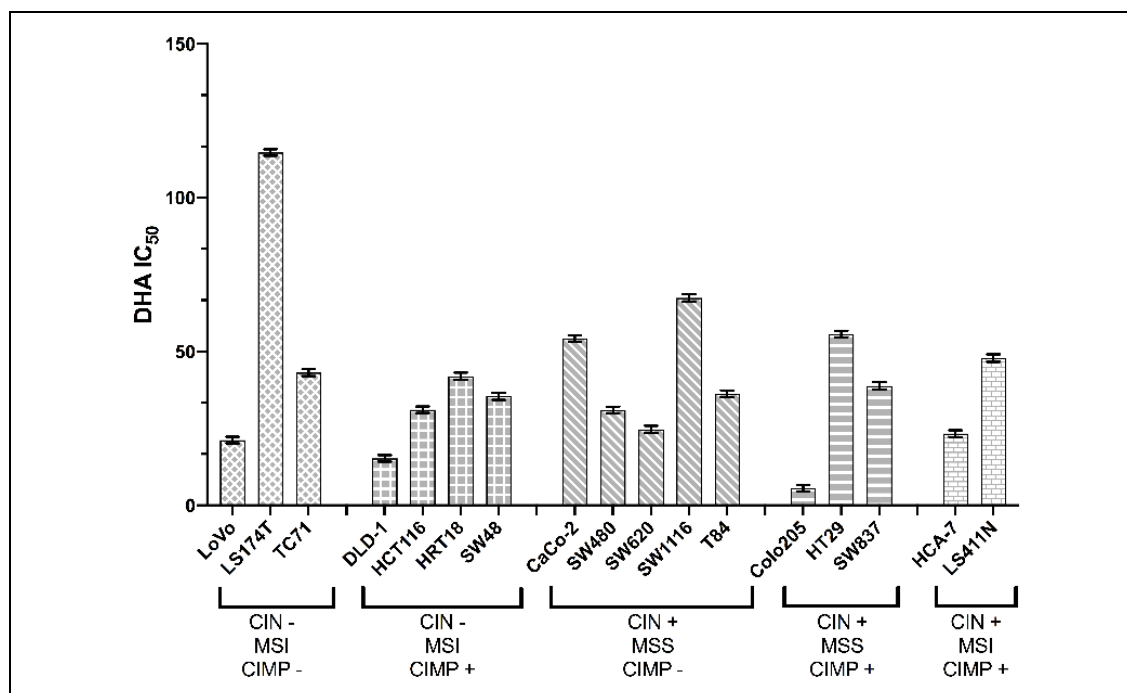


Figure A4.3 DHA IC₅₀ sensitivity of cell lines grouped by molecular phenotype

DHA sensitivity of cell lines were measured by MTT assay and IC₅₀ was plotted against cell line molecular properties. Bar patterns are representative of subgroups. DHA IC₅₀ data is expressed as the mean ± SEM, for 3 to 14 independent repeats.

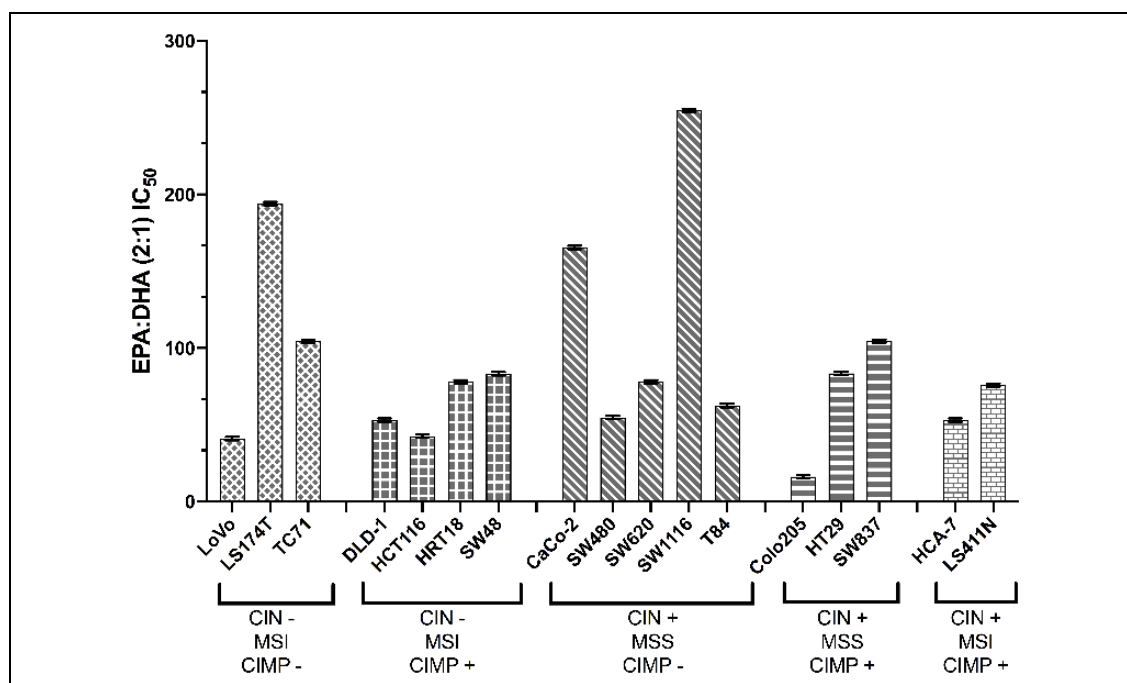


Figure A4.4 EPA:DHA (2:1) sensitivity of cells grouped molecular phenotype

EPA:DHA (2:1) sensitivity of cell lines was measured by MTT assay and IC₅₀ was plotted against cell line molecular properties. Bar patterns are representative of subgroups. EPA:DHA IC₅₀ data is expressed as mean ± SEM, for 3 independent repeats.

A4.4. DAC pre-treatment effect on DHA concentration response curves

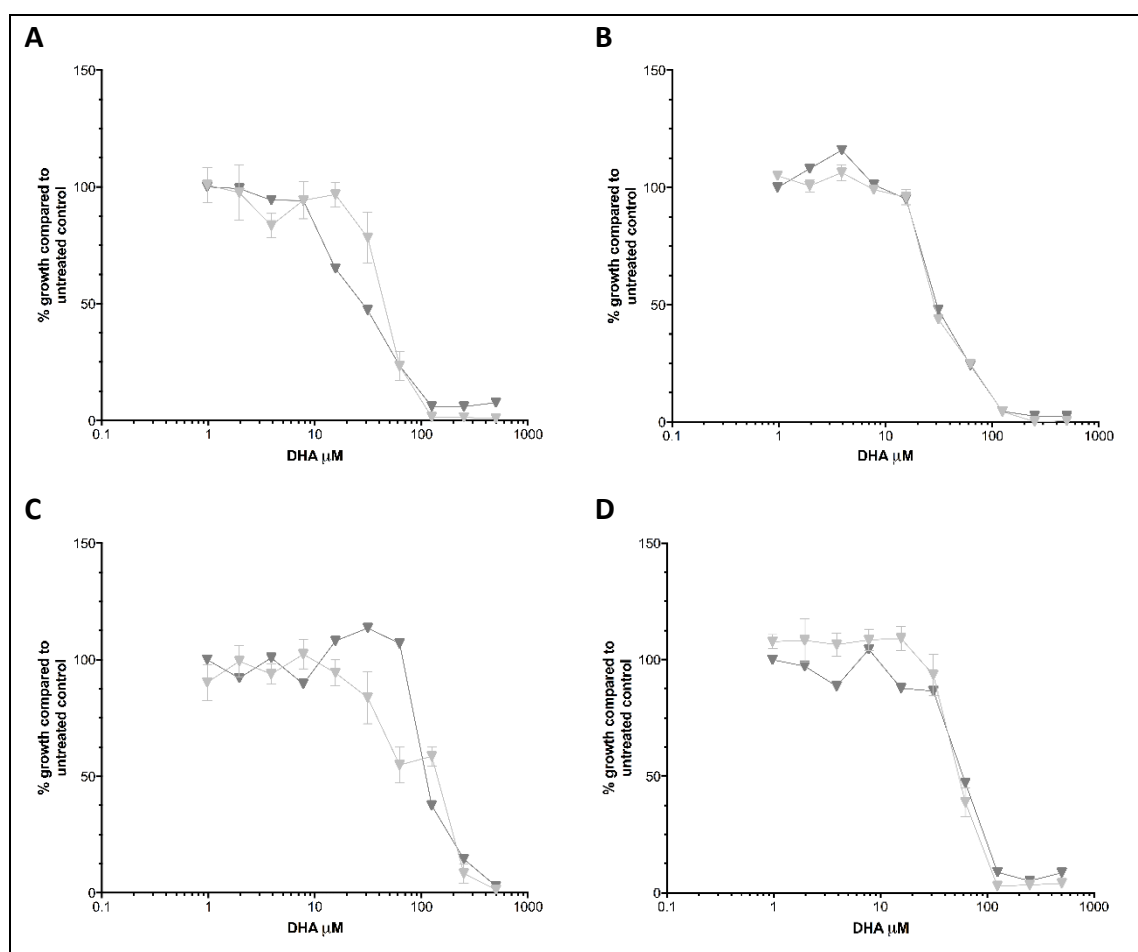


Figure A4.5 DHA concentration response curves for cells following DAC pre-treatment

DHA concentration response curves obtained in CIMP+ cell lines; HCT116 (A), HRT18 (B) and CIMP- cell lines; LS174T (C) and TC71 (D). DHA concentration responses in non-DAC treated cells (▼) and cells pre-treated with 1 μM DAC (▲) were tested. Cell viability was measured by MTT assay, % growth inhibition was calculated relative to carrier control treated cells. Data are expressed as the mean \pm SEM of a 3 independent replicates.

A5.1. Standard Curves

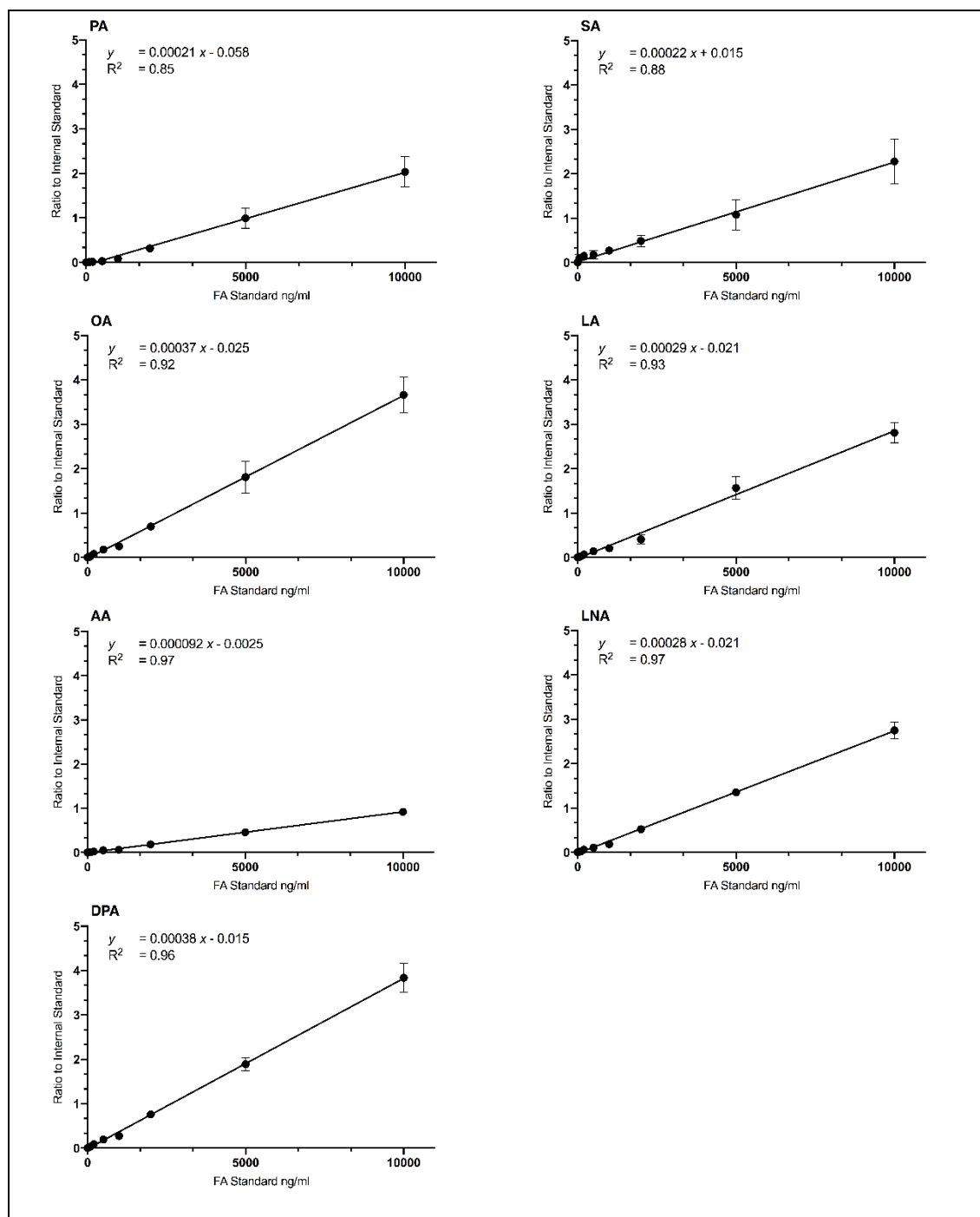


Figure A5.1 Standard curves for all FAs measured

Fatty acid standards were prepared, with a calibration range from 0 to 10000 ng/ml and analysed by LC-ESI-MS/MS. LNA-d14 was used as the internal standard and the ratio of standard FA peak area to internal standard was calculated. The standard curves for PA, SA, OA, LA, AA, LNA and DPA are shown. Data is representative of mean $5 \pm \text{SD}$ for independent biological replicates. Equations for the linear regression and R² values are displayed on each plot.

A5.2. LC-ESI-MS/MS Chromatograms

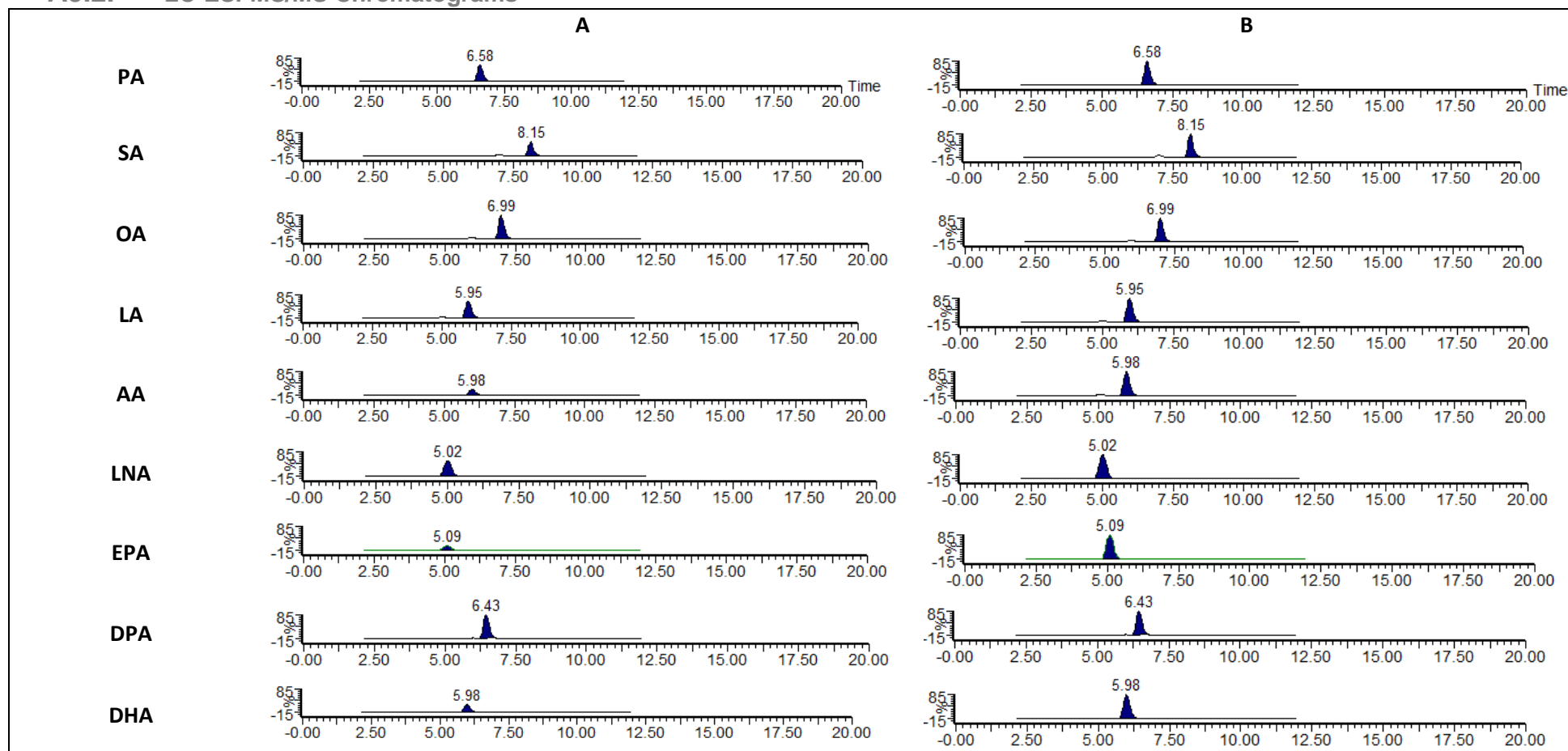


Figure A5.2 Chromatograms of 10000 ng/ml standard

Fatty acid standards were prepared, with a calibration range from 0 to 10000 ng/ml and analysed by LC-ESI-MS/MS. Traces are shown (A) scaled to the highest peak from all traces (A), and scaled to its own highest peak (B).

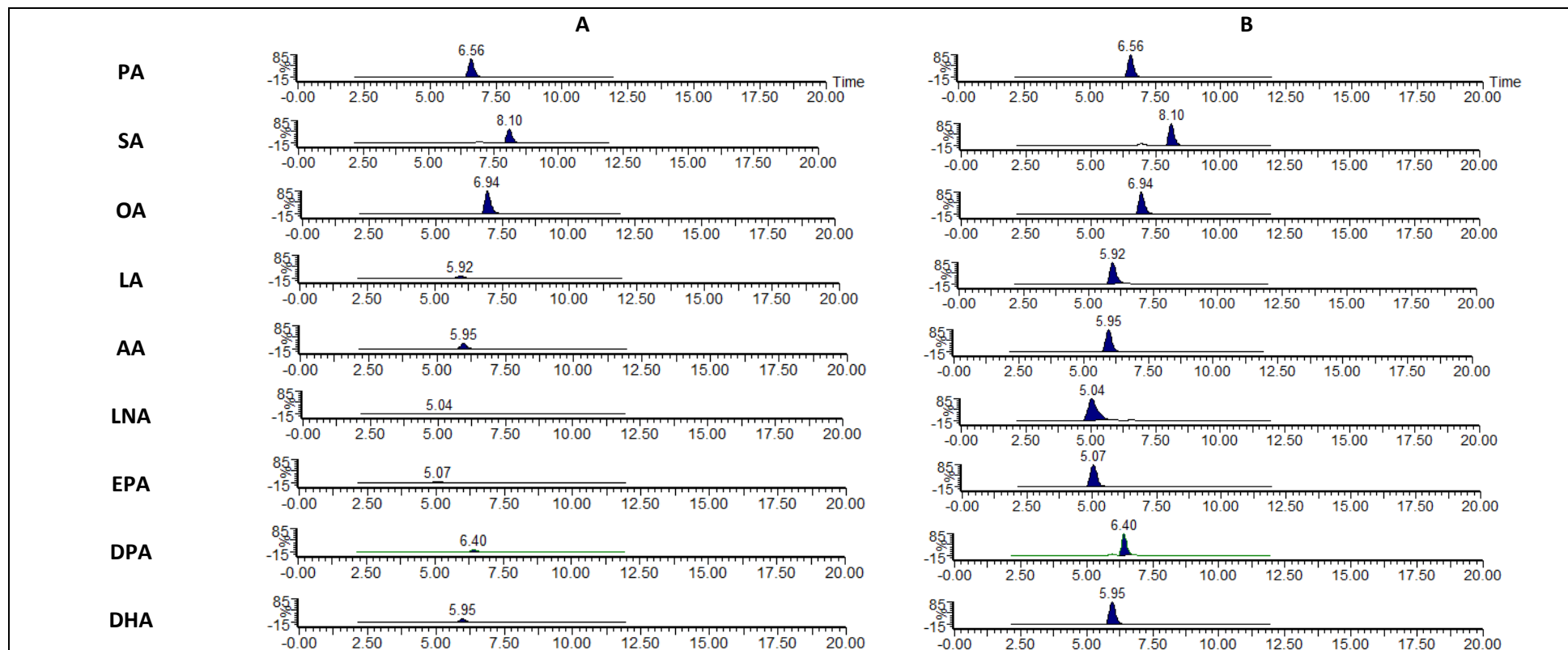


Figure A5.3 Chromatograms of ethanol treated HT29 cells

Cells were treated with ethanol as a control for EPA exposure and analysed by LC-ESI-MS/MS. Traces are shown (A) scaled to the highest peak from all traces (A), and scaled to its own highest peak (B).

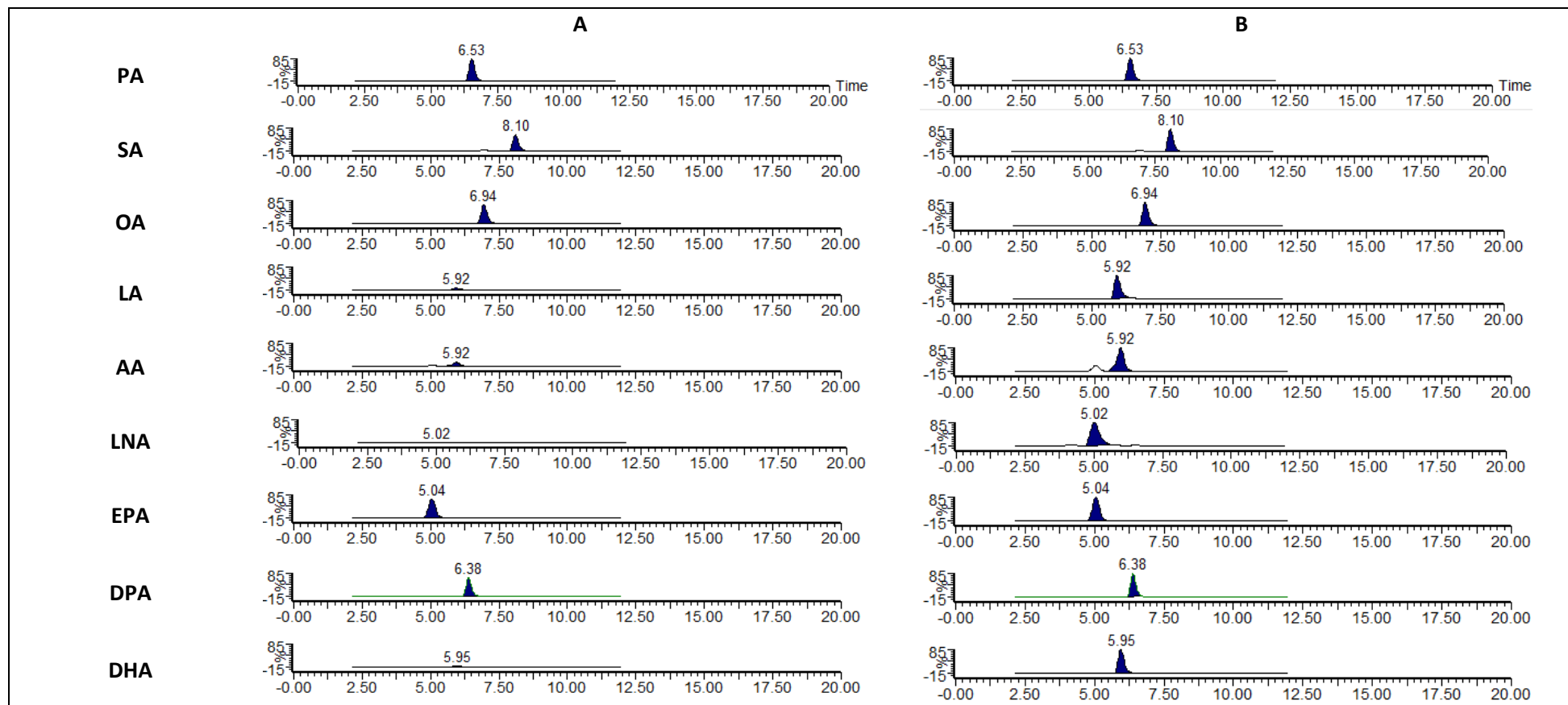


Figure A5.4 Chromatograms of high concentration EPA treated HT29 cells

Cells were treated with a high concentration of EPA (equivalent to EPA IC_{50}) and analysed by LC-ESI-MS/MS. Traces are shown (A) scaled to the highest peak from all traces (A), and scaled to its own highest peak (B).

A5.3. IC₅₀ concentrations.

Table A5.1. Cell line dependent IC₅₀ equivalent concentrations

Cell Line	EPA			DHA		
	IC ₅₀ (μ M)	High-concentration Treatment (μ M)	% V/V ethanol carrier	IC ₅₀ (μ M)	High-concentration Treatment (μ M)	% V/V ethanol carrier
CaCo-2	205.52 \pm 1.51	196	0.60	54.21 \pm 1.09	66	0.20
Colo205	161.40 \pm 1.16	164	0.50	5.57 \pm 1.09	7	0.02
DLD-1	85.91 \pm 1.06	99	0.30	15.26 \pm 1.07	33	0.10
HCA-7	141.91 \pm 1.05	131	0.40	23.31 \pm 1.07	33	0.10
HCT116	91.74 \pm 1.08	99	0.30	31.09 \pm 1.08	33	0.10
HRT18	73.17 \pm 1.13	66	0.20	41.95 \pm 1.15	33	0.10
HT29	118.60 \pm 1.05	131	0.40	55.69 \pm 1.05	66	0.20
LoVo	141.10 \pm 1.08	131	0.40	21.21 \pm 1.08	33	0.10
LS174T	228.23 \pm 1.11	230	0.70	114.74 \pm 1.06	131	0.40
LS411N	84.33 \pm 1.06	98	0.30	47.86 \pm 1.21	66	0.20
SW48	71.19 \pm 1.16	66	0.20	35.44 \pm 1.19	33	0.10
SW480	77.84 \pm 1.19	66	0.20	30.98 \pm 1.08	33	0.10
SW620	176.83 \pm 1.18	197	0.60	24.72 \pm 1.10	26	0.08
SW837	138.33 \pm 1.08	131	0.40	38.85 \pm 1.13	33	0.10
SW1116	224.52 \pm 1.11	230	0.70	67.42 \pm 1.11	66	0.20
T84	137.00 \pm 1.09	131	0.40	36.31 \pm 1.09	33	0.10
TC71	95.62 \pm 1.25	99	0.30	43.12 \pm 1.11	33	0.10

IC₅₀ data is mean \pm SD for a minimum of 3 independent replicates.

A5.4. FA profiles (%) of all cell lines

Table A5.2. Relative percentage FA profile of EPA ethanol control treated cells

Cell Line	Fatty acid content (%)*								
	PA	SA	OA	LA	AA	LNA	EPA	DPA	DHA
CaCo-2	29.4 ± 0.5	14.8 ± 0.5	37.1 ± 0.7	3.1 ± 0.1	7.1 ± 0.1	0.2 ± 0.0	1.7 ± 0.1	2.6 ± 0.1	4.1 ± 0.1
Colo205	28.4 ± 1.8	17.1 ± 2.6	41.3 ± 2.5	2.5 ± 0.3	4.4 ± 0.7	0.2 ± 0.03	1.4 ± 0.3	1.7 ± 0.3	2.9 ± 0.5
DLD-1	25.2 ± 2.6	18.9 ± 3.4	35.5 ± 3.7	3.7 ± 0.4	6.9 ± 0.8	0.5 ± 0.1	2.8 ± 0.3	2.3 ± 0.3	4.3 ± 0.5
HCA-7	27.4 ± 0.5	16.2 ± 1.2	43.5 ± 1.6	2.5 ± 0.1	3.5 ± 0.2	0.1 ± 0.01	0.9 ± 0.1	2.4 ± 0.1	3.5 ± 0.2
HCT116	15.1 ± 0.7	12.6 ± 2.1	50.8 ± 1.8	4.0 ± 0.1	6.4 ± 0.4	0.3 ± 0.01	1.8 ± 0.1	3.8 ± 0.4	5.3 ± 0.4
HRT18	27.2 ± 1.2	17.6 ± 0.4	37.0 ± 0.9	3.2 ± 0.1	6.5 ± 0.5	0.4 ± 0.0	1.6 ± 0.1	2.5 ± 0.1	4.1 ± 0.2
HT29	26.4 ± 0.6	15.7 ± 0.4	38.8 ± 0.6	3.6 ± 0.03	6.4 ± 0.3	0.5 ± 0.0	2.4 ± 0.1	2.1 ± 0.04	4.2 ± 0.2
LoVo	13.8 ± 1.4	17.0 ± 3.1	39.1 ± 1.1	5.9 ± 0.3	8.9 ± 0.9	0.3 ± 0.1	2.4 ± 0.3	5.2 ± 0.5	7.4 ± 0.9
LS174T	11.1 ± 1.4	9.2 ± 0.7	54.0 ± 0.7	4.4 ± 0.4	7.4 ± 0.7	0.2 ± 0.1	1.8 ± 0.1	5.2 ± 0.5	6.7 ± 0.5
LS411N	27.1 ± 0.4	13.3 ± 0.4	40.0 ± 0.8	4.0 ± 0.1	6.4 ± 0.1	0.3 ± 0.01	1.8 ± 0.0	2.7 ± 0.1	4.4 ± 0.0
SW1116	23.6 ± 0.5	19.5 ± 0.4	43.1 ± 0.9	2.2 ± 0.1	5.4 ± 0.5	0.1 ± 0.0	2.0 ± 0.1	1.0 ± 0.03	3.1 ± 0.2
SW48	28.0 ± 1.3	17.0 ± 1.1	36.9 ± 0.8	3.3 ± 0.1	5.8 ± 0.4	0.4 ± 0.0	1.9 ± 0.1	2.4 ± 0.2	4.3 ± 0.3
SW480	26.6 ± 1.0	18.6 ± 0.5	33.7 ± 0.5	3.3 ± 0.1	7.8 ± 0.5	0.2 ± 0.0	2.2 ± 0.1	3.2 ± 0.2	4.4 ± 0.3
SW620	10.9 ± 1.3	8.8 ± 2.2	61.5 ± 1.9	3.8 ± 0.1	5.5 ± 0.7	0.3 ± 0.1	1.6 ± 0.1	3.3 ± 0.4	4.3 ± 0.4
SW837	27.7 ± 0.9	16.7 ± 1.0	36.3 ± 0.8	5.0 ± 0.2	6.0 ± 0.3	1.4 ± 0.1	1.6 ± 0.1	1.5 ± 0.1	3.8 ± 0.3
T84	32.4 ± 0.4	37.2 ± 2.3	16.3 ± 1.7	2.1 ± 0.2	5.8 ± 0.4	0.3 ± 0.0	2.4 ± 0.2	1.0 ± 0.1	2.5 ± 0.2
TC71	13.3 ± 4.2	16.5 ± 11.8	51.7 ± 15.5	3.7 ± 0.2	5.3 ± 0.3	0.2 ± 0.08	1.9 ± 0.3	3.1 ± 0.4	4.3 ± 0.4

* FA content is expressed as the mean percentage of total fatty acids present ± SD for 3 independent replicates.

Table A5.3. Relative percentage FA profile of 5µM EPA treated cells

Cell Line	Fatty acid content (%)*								
	PA	SA	OA	LA	AA	LNA	EPA	DPA	DHA
CaCo-2	28.6 ± 0.4	14.4 ± 0.4	31.4 ± 0.8	2.5 ± 0.1	6.1 ± 0.3	0.1 ± 0.0	8.3 ± 0.4	5.4 ± 0.3	3.1 ± 0.1
Colo205	27.2 ± 1.2	16.5 ± 0.7	38.8 ± 1.0	2.6 ± 0.1	4.5 ± 0.3	0.2 ± 0.01	4.5 ± 0.3	3.0 ± 0.2	2.7 ± 0.1
DLD-1	25.6 ± 1.9	21.2 ± 2.4	27.8 ± 2.3	3.0 ± 0.2	5.5 ± 0.5	0.5 ± 0.04	10.6 ± 0.6	2.2 ± 0.3	3.6 ± 0.3
HCA-7	27.4 ± 0.5	15.8 ± 1.2	39.8 ± 1.3	2.3 ± 0.1	3.2 ± 0.1	0.1 ± 0.01	3.5 ± 0.1	4.5 ± 0.3	3.4 ± 0.2
HCT116	13.3 ± 0.6	10.2 ± 0.8	45.7 ± 0.7	4.3 ± 0.3	6.3 ± 0.3	0.3 ± 0.04	8.2 ± 0.6	6.7 ± 0.9	5.0 ± 0.3
HRT18	26.0 ± 1.0	18.1 ± 1.4	31.2 ± 1.5	2.6 ± 0.1	5.6 ± 0.4	0.3 ± 0.02	10.3 ± 0.4	2.4 ± 0.1	3.6 ± 0.1
HT29	24.5 ± 1.2	14.9 ± 1.0	35.9 ± 0.9	3.4 ± 0.2	6.0 ± 0.4	0.5 ± 0.05	8.8 ± 0.6	2.0 ± 0.1	4.0 ± 0.3
LoVo	12.7 ± 1.6	16.3 ± 4.0	36.3 ± 0.8	5.1 ± 0.3	7.7 ± 1.1	0.5 ± 0.1	7.6 ± 1.3	7.5 ± 1.4	6.7 ± 0.9
LS174T	14.2 ± 5.6	15.7 ± 9.7	44.7 ± 8.1	3.1 ± 0.5	5.5 ± 1.6	0.1 ± 0.0	6.3 ± 2.0	5.6 ± 1.8	4.9 ± 1.4
LS411N	27.6 ± 0.5	14.4 ± 0.4	35.5 ± 0.2	3.5 ± 0.2	5.9 ± 0.2	0.3 ± 0.02	5.7 ± 0.2	3.3 ± 0.2	4.0 ± 0.1
SW1116	22.5 ± 0.5	18.1 ± 0.8	40.7 ± 0.9	2.0 ± 0.1	4.7 ± 0.2	0.2 ± 0.02	6.6 ± 0.3	2.2 ± 0.3	3.2 ± 0.4
SW48	26.0 ± 1.4	16.8 ± 0.6	32.7 ± 0.6	3.2 ± 0.2	5.4 ± 0.4	0.4 ± 0.02	9.3 ± 0.3	2.4 ± 0.2	4.0 ± 0.3
SW480	26.0 ± 1.1	18.5 ± 0.3	29.2 ± 0.4	3.0 ± 0.1	6.6 ± 0.3	0.2 ± 0.01	7.1 ± 0.3	6.0 ± 0.4	3.3 ± 0.1
SW620	9.3 ± 1.9	8.0 ± 1.4	56.7 ± 0.9	3.9 ± 0.3	5.8 ± 0.9	0.3 ± 0.02	7.0 ± 1.2	4.4 ± 0.6	4.7 ± 0.8
SW837	27.2 ± 0.6	16.2 ± 1.7	32.5 ± 1.5	4.2 ± 0.2	5.3 ± 0.2	1.1 ± 0.1	8.3 ± 0.6	1.6 ± 0.1	3.5 ± 0.1
T84	31.4 ± 1.9	34.4 ± 4.3	16.2 ± 2.9	2.0 ± 0.3	5.3 ± 0.8	0.3 ± 0.0	6.9 ± 1.3	1.3 ± 0.3	2.2 ± 0.4
TC71	12.1 ± 3.4	15.6 ± 12.2	48.9 ± 16.3	3.6 ± 0.4	5.1 ± 0.4	0.2 ± 0.07	6.1 ± 1.1	4.4 ± 0.8	4.1 ± 0.7

* FA content is expressed as the mean percentage of total fatty acids present ± SD for 3 independent replicates.

Table A5.4. Relative percentage FA profile of high concentration EPA treated cells

Cell Line	Fatty acid content (%)*								
	PA	SA	OA	LA	AA	LNA	EPA	DPA	DHA
CaCo-2	13.4 ± 3.5	6.3 ± 2.3	15.0 ± 0.8	1.3 ± 0.04	3.0 ± 0.1	0.1 ± 0.0	42.6 ± 5.1	17.1 ± 1.5	1.1 ± 0.05
Colo205	22.3 ± 0.7	13.3 ± 1.1	18.0 ± 0.9	1.5 ± 0.1	3.4 ± 1.2	0.2 ± 0.01	27.1 ± 0.5	13.1 ± 0.3	1.2 ± 0.02
DLD-1	21.1 ± 0.2	17.5 ± 0.4	17.8 ± 0.3	2.2 ± 0.05	3.2 ± 0.1	0.4 ± 0.01	31.7 ± 0.2	4.4 ± 0.1	1.8 ± 0.1
HCA-7	20.1 ± 1.5	12.5 ± 1.6	21.2 ± 3.2	1.5 ± 0.5	3.1 ± 0.4	0.2 ± 0.05	24.5 ± 7.3	15.3 ± 9.8	1.7 ± 0.5
HCT116	8.3 ± 1.1	5.7 ± 1.3	22.1 ± 0.5	2.5 ± 0.3	2.8 ± 0.2	0.2 ± 0.1	28.3 ± 1.7	27.7 ± 1.1	2.4 ± 0.3
HRT18	23.9 ± 1.8	16.5 ± 0.9	20.0 ± 1.5	1.6 ± 0.4	3.1 ± 0.5	0.2 ± 0.03	24.2 ± 4.4	3.4 ± 0.1	1.8 ± 0.4
HT29	17.4 ± 1.6	12.4 ± 2.1	18.2 ± 1.3	1.9 ± 0.1	3.1 ± 0.1	0.3 ± 0.02	40.7 ± 1.9	4.5 ± 0.3	1.6 ± 0.03
LoVo	7.8 ± 1.2	10.1 ± 2.6	15.3 ± 1.1	2.6 ± 0.1	2.6 ± 2.3	0.2 ± 0.03	36.0 ± 2.3	23.2 ± 1.8	2.2 ± 0.1
LS174T	4.0 ± 1.0	2.5 ± 1.2	14.4 ± 2.1	1.3 ± 0.2	2.0 ± 3.1	0.1 ± 0.02	45.7 ± 3.2	28.2 ± 1.0	2.0 ± 0.2
LS411N	21.2 ± 0.8	11.7 ± 0.7	21.7 ± 0.7	2.1 ± 0.1	5.6 ± 0.1	0.4 ± 0.02	22.6 ± 1.1	12.1 ± 0.7	2.5 ± 0.02
SW1116	12.4 ± 0.3	8.9 ± 0.7	18.7 ± 1.1	1.0 ± 0.03	3.1 ± 0.1	0.2 ± 0.0	42.9 ± 1.6	11.7 ± 0.4	1.1 ± 0.04
SW48	21.4 ± 1.1	14.7 ± 0.9	21.9 ± 0.3	2.1 ± 0.06	3.4 ± 0.2	0.3 ± 0.01	28.9 ± 1.5	4.9 ± 0.1	2.3 ± 0.3
SW480	21.8 ± 0.4	14.7 ± 0.8	17.9 ± 0.8	1.9 ± 0.1	4.5 ± 0.3	0.2 ± 0.01	21.2 ± 0.3	16.5 ± 0.3	1.4 ± 0.1
SW620	5.3 ± 1.6	3.6 ± 1.1	21.0 ± 1.6	1.7 ± 0.2	2.1 ± 0.1	0.2 ± 0.03	35.3 ± 2.0	29.2 ± 2.4	1.5 ± 0.1
SW837	20.8 ± 0.5	12.3 ± 0.2	20.6 ± 0.8	2.5 ± 0.1	2.9 ± 0.1	0.5 ± 0.01	34.2 ± 1.3	4.4 ± 0.1	1.8 ± 0.05
T84	22.9 ± 2.0	24.2 ± 3.3	11.3 ± 1.0	1.4 ± 0.1	2.9 ± 0.2	0.2 ± 0.0	32.9 ± 3.4	3.0 ± 0.5	1.3 ± 0.1
TC71	8.9 ± 3.3	10.1 ± 8.5	28.5 ± 9.1	2.2 ± 0.1	3.1 ± 0.04	0.2 ± 0.03	21.9 ± 1.9	22.9 ± 1.8	2.2 ± 0.5

* FA content is expressed as the mean percentage of total fatty acids present ± SD for 3 independent replicates.

Table A5.5. Relative percentage FA profile of DHA ethanol control treated cells

Cell Line	Fatty acid content (%)*								
	PA	SA	OA	LA	AA	LNA	EPA	DPA	DHA
CaCo-2	30.0 ± 0.9	14.5 ± 1.0	37.3 ± 0.9	3.0 ± 0.06	6.8 ± 0.5	0.1 ± 0.0	1.7 ± 0.2	2.6 ± 0.2	4.0 ± 0.3
Colo205	27.3 ± 0.8	15.2 ± 0.7	43.1 ± 0.4	2.8 ± 0.1	4.8 ± 0.02	0.2 ± 0.01	1.5 ± 0.03	1.9 ± 0.04	3.2 ± 0.1
DLD-1	27.0 ± 0.9	21.3 ± 0.9	32.8 ± 1.0	3.3 ± 0.1	6.3 ± 0.3	0.5 ± 0.0	2.5 ± 0.1	2.2 ± 0.1	4.0 ± 0.2
HCA-7	27.5 ± 0.7	16.0 ± 0.2	43.1 ± 1.0	2.7 ± 0.1	3.6 ± 0.1	0.1 ± 0.01	0.9 ± 0.04	2.5 ± 0.1	3.6 ± 0.1
HCT116	14.9 ± 2.3	11.6 ± 2.7	51.0 ± 2.0	4.1 ± 0.2	6.4 ± 0.9	0.3 ± 0.02	2.2 ± 0.3	4.2 ± 0.9	5.3 ± 0.8
HRT18	27.0 ± 0.5	18.3 ± 1.0	36.5 ± 1.4	3.2 ± 0.03	6.5 ± 0.4	0.4 ± 0.0	1.6 ± 0.1	2.4 ± 0.1	4.1 ± 0.2
HT29	25.1 ± 3.3	14.3 ± 4.4	40.5 ± 5.4	3.8 ± 0.5	6.7 ± 0.7	0.5 ± 0.06	2.6 ± 0.3	2.2 ± 0.3	4.3 ± 0.4
LoVo	13.7 ± 1.5	15.2 ± 2.8	39.9 ± 0.5	6.0 ± 0.3	9.0 ± 1.2	0.2 ± 0.0	2.5 ± 0.4	5.6 ± 0.9	7.9 ± 1.0
LS174T	13.1 ± 5.2	17.3 ± 12.8	47.9 ± 11.2	3.5 ± 0.8	6.2 ± 2.1	0.1 ± 0.0	1.7 ± 0.8	4.7 ± 1.6	5.6 ± 1.9
LS411N	25.6 ± 0.5	12.3 ± 0.7	41.3 ± 0.7	4.0 ± 0.1	6.8 ± 0.3	0.3 ± 0.0	1.8 ± 0.04	3.0 ± 0.1	4.9 ± 0.3
SW1116	23.6 ± 1.1	18.2 ± 2.0	44.5 ± 2.0	2.3 ± 0.2	5.1 ± 0.3	0.1 ± 0.0	2.0 ± 0.3	1.1 ± 0.2	3.1 ± 0.2
SW48	26.9 ± 0.2	17.1 ± 1.6	37.0 ± 0.9	3.4 ± 0.2	6.2 ± 0.2	0.4 ± 0.04	1.8 ± 0.1	2.5 ± 0.06	4.7 ± 0.1
SW480	26.5 ± 0.6	18.5 ± 1.1	33.5 ± 1.0	3.5 ± 0.1	7.9 ± 0.2	0.2 ± 0.01	2.2 ± 0.04	3.3 ± 0.1	4.4 ± 0.2
SW620	11.8 ± 2.1	8.4 ± 2.2	61.4 ± 1.7	3.8 ± 0.1	5.5 ± 1.1	0.2 ± 0.1	1.5 ± 0.3	3.3 ± 0.9	4.2 ± 0.8
SW837	28.3 ± 0.2	16.7 ± 1.7	35.9 ± 1.4	5.1 ± 0.1	5.9 ± 0.2	1.3 ± 0.05	1.7 ± 0.02	1.5 ± 0.1	3.7 ± 0.1
T84	32.4 ± 0.6	36.1 ± 2.3	16.6 ± 1.9	2.1 ± 0.2	6.1 ± 0.3	0.3 ± 0.02	2.5 ± 0.2	1.1 ± 0.1	2.6 ± 0.2
TC71	12.0 ± 2.8	14.7 ± 8.9	54.4 ± 15.5	3.8 ± 0.2	5.5 ± 1.6	0.2 ± 0.1	2.1 ± 1.4	3.1 ± 0.6	4.2 ± 0.7

* FA content is expressed as the mean percentage of total fatty acids present ± SD for 3 independent replicates.

Table A5.6. Relative percentage FA profile of 5µM DHA treated cells

Cell Line	Fatty acid content (%)*								
	PA	SA	OA	LA	AA	LNA	EPA	DPA	DHA
CaCo-2	29.7 ± 0.2	15.4 ± 0.7	31.9 ± 1.3	2.5 ± 0.1	5.4 ± 0.4	0.2 ± 0.0	2.3 ± 0.2	1.9 ± 0.2	10.9 ± 1.7
Colo205	27.4 ± 1.0	16.5 ± 0.9	38.7 ± 1.2	2.5 ± 0.1	4.4 ± 0.2	0.3 ± 0.01	2.7 ± 0.1	1.4 ± 0.04	6.3 ± 0.2
DLD-1	26.7 ± 1.7	21.8 ± 2.0	28.0 ± 1.6	3.0 ± 0.2	5.6 ± 0.5	0.5 ± 0.03	3.6 ± 0.3	1.4 ± 0.1	9.6 ± 0.6
HCA-7	27.5 ± 0.5	16.5 ± 1.1	39.6 ± 1.1	2.2 ± 0.1	3.1 ± 0.1	0.1 ± 0.0	1.2 ± 0.04	2.1 ± 0.1	7.6 ± 0.3
HCT116	13.1 ± 0.8	9.6 ± 0.9	47.7 ± 2.1	4.0 ± 0.1	6.1 ± 0.6	0.3 ± 0.0	2.8 ± 0.4	3.3 ± 0.5	13.1 ± 1.4
HRT18	26.3 ± 0.4	17.5 ± 0.12	35.1 ± 0.1	2.9 ± 0.0	5.6 ± 0.1	0.4 ± 0.0	1.7 ± 0.1	2.0 ± 0.02	8.6 ± 0.1
HT29	26.4 ± 0.5	16.6 ± 1.7	34.6 ± 1.8	3.2 ± 0.1	5.7 ± 0.1	0.5 ± 0.0	3.0 ± 0.04	1.5 ± 0.1	8.6 ± 0.2
LoVo	12.4 ± 1.3	13.9 ± 2.1	35.7 ± 0.6	5.6 ± 0.2	8.1 ± 0.8	0.2 ± 0.04	3.2 ± 0.2	4.5 ± 0.3	16.4 ± 1.8
LS174T	9.8 ± 1.5	9.9 ± 1.0	48.0 ± 0.4	3.8 ± 0.5	7.1 ± 0.6	0.1 ± 0.04	2.0 ± 0.1	4.9 ± 0.6	14.4 ± 1.3
LS411N	27.2 ± 2.0	14.2 ± 2.0	36.5 ± 2.4	3.6 ± 0.3	5.8 ± 0.5	0.3 ± 0.0	2.0 ± 0.1	2.3 ± 0.2	8.2 ± 0.5
SW1116	22.3 ± 0.8	17.1 ± 1.6	43.2 ± 2.3	2.0 ± 0.1	4.6 ± 0.1	0.2 ± 0.01	2.6 ± 0.2	0.8 ± 0.1	7.3 ± 0.2
SW48	28.1 ± 0.8	17.5 ± 0.7	33.2 ± 0.8	3.0 ± 0.1	5.1 ± 0.1	0.4 ± 0.0	2.0 ± 0.1	1.9 ± 0.05	8.8 ± 0.2
SW480	26.4 ± 1.0	19.0 ± 1.9	29.8 ± 1.6	3.1 ± 0.1	6.8 ± 0.5	0.2 ± 0.01	3.7 ± 0.2	2.6 ± 0.2	8.5 ± 0.4
SW620	13.0 ± 4.5	12.6 ± 7.8	53.7 ± 7.5	3.4 ± 0.8	4.7 ± 1.0	0.2 ± 0.1	1.4 ± 0.5	2.0 ± 1.0	8.2 ± 2.2
SW837	27.4 ± 0.2	16.0 ± 0.5	34.9 ± 0.4	4.6 ± 0.1	5.4 ± 0.1	1.2 ± 0.03	1.7 ± 0.1	1.3 ± 0.05	7.5 ± 0.3
T84	30.3 ± 0.6	33.5 ± 1.0	17.6 ± 0.8	2.2 ± 0.1	6.2 ± 0.2	0.3 ± 0.02	3.2 ± 0.3	1.0 ± 0.05	5.8 ± 0.2
TC71	12.0 ± 3.0	14.0 ± 7.8	49.9 ± 13.2	3.5 ± 0.4	5.1 ± 1.2	0.2 ± 0.07	2.2 ± 1.0	2.7 ± 0.6	10.5 ± 2.4

* FA content is expressed as the mean percentage of total fatty acids present ± SD for 3 independent replicates.

Table A5.7. Relative percentage FA profile of high concentration DHA treated cells

Cell Line	Fatty acid content (%)*								
	PA	SA	OA	LA	AA	LNA	EPA	DPA	DHA
CaCo-2	26.3 ± 0.9	13.3 ± 0.2	23.8 ± 0.4	1.8 ± 0.08	4.1 ± 0.4	0.1 ± 0.0	3.0 ± 0.1	1.7 ± 0.1	25.9 ± 0.4
Colo205	27.7 ± 1.3	17.7 ± 1.7	37.9 ± 2.0	2.4 ± 0.1	4.2 ± 0.3	0.2 ± 0.01	2.5 ± 0.2	1.3 ± 0.1	6.1 ± 0.4
DLD-1	25.3 ± 1.1	22.8 ± 0.6	22.2 ± 0.8	2.4 ± 0.1	4.5 ± 0.3	0.4 ± 0.02	3.6 ± 0.1	1.1 ± 0.1	17.8 ± 0.5
HCA-7	26.7 ± 0.8	16.4 ± 0.3	33.3 ± 0.8	1.9 ± 0.1	2.6 ± 0.04	0.1 ± 0.0	2.5 ± 0.1	2.0 ± 0.03	14.5 ± 0.2
HCT116	11.9 ± 1.4	10.2 ± 3.1	32.7 ± 0.2	3.1 ± 0.1	4.5 ± 0.4	0.2 ± 0.03	4.9 ± 0.5	2.8 ± 0.4	30.7 ± 3.4
HRT18	24.5 ± 1.3	17.3 ± 0.8	24.3 ± 0.7	2.0 ± 0.1	4.1 ± 0.1	0.3 ± 0.01	1.8 ± 0.07	1.3 ± 1.4	24.5 ± 2.1
HT29	21.0 ± 3.5	14.8 ± 5.5	23.8 ± 2.2	2.2 ± 0.2	3.8 ± 0.4	0.4 ± 0.03	2.2 ± 0.1	1.2 ± 0.2	30.7 ± 6.0
LoVo	11.6 ± 1.4	13.5 ± 2.2	27.3 ± 0.5	4.4 ± 0.2	6.5 ± 0.4	0.2 ± 0.02	3.6 ± 0.4	3.3 ± 0.3	29.7 ± 1.9
LS174T	4.5 ± 1.2	4.2 ± 1.4	20.2 ± 2.1	1.6 ± 0.1	3.0 ± 0.2	0.1 ± 0.02	2.3 ± 0.2	2.1 ± 0.1	62.3 ± 4.7
LS411N	25.4 ± 0.8	14.4 ± 1.2	25.8 ± 0.4	2.3 ± 0.02	4.1 ± 0.1	0.3 ± 0.0	2.5 ± 0.1	1.7 ± 0.1	23.6 ± 1.8
SW1116	20.1 ± 1.1	15.6 ± 1.8	28.5 ± 0.8	1.2 ± 0.1	2.8 ± 0.1	0.2 ± 0.0	2.5 ± 0.01	0.7 ± 0.1	28.3 ± 2.6
SW48	25.9 ± 2.0	16.9 ± 1.8	25.8 ± 1.8	2.3 ± 0.2	4.0 ± 0.3	0.4 ± 0.02	3.0 ± 0.2	1.3 ± 0.1	20.4 ± 1.8
SW480	25.8 ± 0.6	19.3 ± 1.5	23.1 ± 1.1	2.3 ± 0.1	5.5 ± 0.3	0.2 ± 0.01	4.4 ± 0.2	2.1 ± 0.1	17.3 ± 0.7
SW620	10.0 ± 2.1	7.9 ± 2.4	46.9 ± 0.8	2.9 ± 0.1	4.0 ± 0.4	0.2 ± 0.03	2.4 ± 0.3	2.4 ± 0.4	23.3 ± 2.6
SW837	25.1 ± 3.9	13.8 ± 2.5	28.3 ± 2.3	3.3 ± 0.4	4.0 ± 0.5	0.9 ± 0.1	1.9 ± 0.2	0.9 ± 0.1	21.7 ± 2.9
T84	31.8 ± 2.8	38.0 ± 8.0	12.8 ± 4.3	1.5 ± 0.4	3.9 ± 1.3	0.2 ± 0.07	2.0 ± 0.9	0.7 ± 0.2	9.2 ± 3.4
TC71	11.7 ± 1.3	13.2 ± 5.4	38.3 ± 10.7	2.7 ± 0.3	4.0 ± 1.2	0.2 ± 0.0	2.6 ± 1.2	2.1 ± 0.5	25.1 ± 2.7

* FA content is expressed as the mean percentage of total fatty acids present ± SD for 3 independent replicates.

A5.5. FA profiles (absolute amount) of all cell lines

Table A5.8. FA profile of EPA ethanol control treated cells expressed as absolute amount

Cell Line	Fatty acid content (µg/million cells)*								
	PA	SA	OA	LA	AA	LNA	EPA	DPA	DHA
CaCo-2	27.3 ± 9.6	18.9 ± 6.2	20.4 ± 6.7	2.1 ± 0.7	13.5 ± 4.7	0.1 ± 0.0	3.7 ± 1.3	1.3 ± 0.5	6.0 ± 2.1
Colo205	6.3 ± 1.1	3.5 ± 0.3	5.5 ± 1.5	0.4 ± 0.1	2.0 ± 0.7	0.0 ± 0.0	0.8 ± 0.3	0.2 ± 0.1	1.0 ± 0.4
DLD-1	7.0 ± 3.4	5.0 ± 2.7	5.6 ± 2.0	0.7 ± 0.2	3.7 ± 1.1	0.1 ± 0.0	1.7 ± 0.5	0.3 ± 0.1	1.8 ± 0.5
HCA-7	6.4 ± 2.6	3.6 ± 1.6	6.1 ± 2.6	0.4 ± 0.1	1.7 ± 0.6	0.0 ± 0.0	0.5 ± 0.2	0.3 ± 0.1	1.3 ± 0.5
HCT116	3.7 ± 0.1	1.1 ± 0.2	4.0 ± 0.2	0.5 ± 0.0	2.7 ± 0.2	0.0 ± 0.0	0.9 ± 0.1	0.3 ± 0.0	1.5 ± 0.1
HRT18	10.5 ± 1.4	9.4 ± 1.5	8.5 ± 1.0	0.9 ± 0.1	5.2 ± 1.1	0.1 ± 0.0	1.5 ± 0.3	0.4 ± 0.1	2.5 ± 0.4
HT29	7.3 ± 2.6	4.1 ± 1.5	6.5 ± 2.4	0.7 ± 0.3	3.7 ± 1.5	0.1 ± 0.0	1.6 ± 0.6	0.3 ± 0.1	1.8 ± 0.8
LoVo	5.9 ± 2.2	2.5 ± 0.5	5.4 ± 1.6	1.2 ± 0.4	6.6 ± 1.5	0.1 ± 0.0	2.1 ± 0.7	0.7 ± 0.2	3.7 ± 1.1
LS174T	1.8 ± 0.5	0.5 ± 0.2	2.9 ± 1.2	0.3 ± 0.1	2.2 ± 1.1	0.0 ± 0.0	0.6 ± 0.3	0.3 ± 0.1	1.3 ± 0.6
LS411N	9.3 ± 2.8	6.3 ± 1.8	8.2 ± 2.3	1.0 ± 0.3	4.5 ± 1.3	0.1 ± 0.0	1.4 ± 0.4	0.5 ± 0.2	2.4 ± 0.7
SW1116	11.5 ± 3.4	9.8 ± 3.2	11.0 ± 3.3	0.7 ± 0.2	4.8 ± 1.9	0.0 ± 0.0	2.0 ± 0.8	0.2 ± 0.1	2.1 ± 0.8
SW48	6.5 ± 1.0	5.4 ± 0.5	5.1 ± 0.7	0.5 ± 0.1	2.7 ± 0.3	0.1 ± 0.0	1.0 ± 0.2	0.3 ± 0.0	1.6 ± 0.2
SW480	13.6 ± 2.9	13.1 ± 2.0	10.2 ± 2.0	1.2 ± 0.2	8.1 ± 1.2	0.1 ± 0.0	2.6 ± 0.3	0.9 ± 0.1	3.5 ± 0.5
SW620	2.5 ± 0.9	0.7 ± 0.2	4.7 ± 2.1	0.4 ± 0.2	2.2 ± 1.0	0.0 ± 0.0	0.8 ± 0.4	0.3 ± 0.1	1.2 ± 0.6
SW837	6.2 ± 0.6	3.8 ± 0.4	4.2 ± 0.6	0.7 ± 0.1	2.4 ± 0.4	0.2 ± 0.0	0.7 ± 0.1	0.2 ± 0.0	1.2 ± 0.2
T84	15.1 ± 1.8	17.8 ± 2.1	4.0 ± 0.8	0.6 ± 0.1	4.9 ± 0.8	0.1 ± 0.0	2.3 ± 0.5	0.2 ± 0.0	1.6 ± 0.3
TC71	4.4 ± 2.4	2.0 ± 1.9	5.1 ± 0.8	0.5 ± 0.1	2.9 ± 0.8	0.0 ± 0.0	1.2 ± 0.5	0.3 ± 0.1	1.6 ± 0.2

* FA content is expressed as the mean absolute of total fatty acids present; µg/million cells ± SD for 3 independent replicates.

Table A5.9. FA profile of 5µM EPA treated cells expressed as absolute amount

Cell Line	Fatty acid content (µg/million cells)*								
	PA	SA	OA	LA	AA	LNA	EPA	DPA	DHA
CaCo-2	25.9 ± 5.1	17.9 ± 3.5	17.0 ± 3.7	1.7 ± 0.4	11.4 ± 2.9	0.1 ± 0.0	17.6 ± 2.9	2.6 ± 0.6	4.4. ± 1.0
Colo205	8.0 ± 1.0	4.6 ± 0.5	6.8 ± 0.5	0.5 ± 0.0	2.7 ± 0.2	0.0 ± 0.0	3.1 ± 0.2	0.5 ± 0.0	1.3 ± 0.1
DLD-1	6.3 ± 2.0	4.9 ± 1.5	4.1 ± 1.4	0.5 ± 0.2	2.8 ± 0.9	0.1 ± 0.0	6.2 ± 2.1	0.3 ± 0.1	1.4 ± 0.5
HCA-7	8.5 ± 3.4	4.7 ± 2.2	7.3 ± 2.6	0.5 ± 0.2	2.0 ± 0.7	0.0 ± 0.0	2.5 ± 0.8	0.7 ± 0.3	1.6 ± 0.5
HCT116	3.3 ± 0.4	0.9 ± 0.1	3.7 ± 0.4	0.5 ± 0.1	2.7 ± 0.2	0.0 ± 0.0	4.1 ± 0.3	0.5 ± 0.1	1.4 ± 0.1
HRT18	11.9 ± 3.5	11.4 ± 3.0	8.4 ± 2.1	0.7 ± 0.5	5.1 ± 0.9	0.1 ± 0.1	10.9 ± 2.5	0.6 ± 0.1	2.6 ± 0.6
HT29	6.0 ± 1.3	3.4 ± 0.9	5.2 ± 0.9	0.6 ± 0.1	3.0 ± 0.5	0.1 ± 0.0	5.0 ± 0.7	0.3 ± 0.0	1.5 ± 0.3
LoVo	6.9 ± 2.9	3.1 ± 1.3	6.4 ± 2.0	1.3 ± 0.5	7.3 ± 2.6	0.0 ± 0.0	8.2 ± 2.4	1.3 ± 0.4	4.1 ± 1.3
LS174T	7.4 ± 9.8	3.3 ± 4.7	5.2 ± 4.6	0.5 ± 0.5	3.1 ± 2.3	0.0 ± 0.0	4.1 ± 3.0	0.6 ± 0.4	1.8 ± 1.4
LS411N	10.1 ± 3.8	7.2 ± 2.5	7.7 ± 2.7	0.9 ± 0.3	4.4 ± 1.5	0.1 ± 0.0	4.8 ± 1.7	0.6 ± 0.3	2.3 ± 0.8
SW1116	9.4 ± 1.2	7.8 ± 0.9	9.0 ± 1.2	0.5 ± 0.1	3.6 ± 0.7	0.0 ± 0.0	5.6 ± 1.0	0.4 ± 0.1	1.9 ± 0.5
SW48	5.3 ± 1.3	4.7 ± 1.1	4.0 ± 1.1	0.5 ± 0.1	2.3 ± 0.7	0.1 ± 0.0	4.5 ± 1.3	0.3 ± 0.1	1.3 ± 0.4
SW480	14.0 ± 3.1	13.7 ± 3.2	9.3 ± 1.9	1.1 ± 0.3	7.3 ± 1.6	0.1 ± 0.0	9.0 ± 1.8	1.7 ± 0.4	2.8 ± 0.5
SW620	2.1 ± 0.5	0.7 ± 0.2	4.2 ± 0.5	0.4 ± 0.1	2.3 ± 0.5	0.0 ± 0.0	3.2 ± 0.8	0.3 ± 0.1	1.3 ± 0.3
SW837	5.0 ± 1.9	3.0 ± 1.0	3.2 ± 1.3	0.5 ± 0.2	1.8 ± 0.8	0.1 ± 0.1	3.2 ± 1.4	0.1 ± 0.1	0.9 ± 0.4
T84	15.5 ± 2.2	17.4 ± 3.1	4.2 ± 0.6	0.6 ± 0.1	4.7 ± 0.5	0.1 ± 0.0	6.9 ± 0.9	0.3 ± 0.0	1.5 ± 0.2
TC71	3.8 ± 2.4	1.9 ± 2.1	4.4 ± 1.0	0.5 ± 0.2	2.6 ± 1.1	0.0 ± 0.0	3.7 ± 1.9	0.4 ± 0.2	1.3 ± 0.3

* FA content is expressed as the mean absolute of total fatty acids present; µg/million cells ± SD for 3 independent replicates.

Table A5.10. FA profile of high concentration EPA treated cells expressed as absolute amount

Cell Line	Fatty acid content (µg/million cells)*								
	PA	SA	OA	LA	AA	LNA	EPA	DPA	DHA
CaCo-2	26.8 ± 9.4	17.4 ± 7.7	17.9 ± 4.5	1.8 ± 0.4	12.4 ± 2.8	0.2 ± 0.0	198.2 ± 42.1	18.3 ± 4.3	3.5 ± 0.8
Colo205	16.1 ± 2.1	9.0 ± 1.3	7.8 ± 1.6	0.7 ± 0.1	5.0 ± 0.9	0.1 ± 0.0	45.9 ± 8.4	5.1 ± 0.8	1.3 ± 0.2
DLD-1	8.1 ± 3.7	6.3 ± 3.0	4.1 ± 1.8	0.6 ± 0.3	2.4 ± 1.0	0.1 ± 0.0	28.4 ± 13.1	0.9 ± 0.4	1.1 ± 0.5
HCA-7	9.5 ± 2.7	5.5 ± 1.2	6.3 ± 3.4	0.6 ± 0.4	3.1 ± 1.5	0.1 ± 0.0	29.4 ± 19.1	3.4 ± 1.8	1.3 ± 0.9
HCT116	4.7 ± 0.7	1.1 ± 0.3	4.1 ± 0.5	0.7 ± 0.0	2.7 ± 0.3	0.1 ± 0.0	32.7 ± 4.5	5.2 ± 0.6	1.6 ± 0.1
HRT18	14.3 ± 8.1	13.8 ± 8.4	7.3 ± 4.6	0.7 ± 0.5	4.0 ± 2.8	0.1 ± 0.1	35.1 ± 22.5	2.0 ± 1.2	1.8 ± 1.3
HT29	8.1 ± 0.7	5.4 ± 0.7	5.1 ± 0.7	0.6 ± 0.1	3.0 ± 0.4	0.1 ± 0.0	44.6 ± 6.5	1.1 ± 0.2	1.2 ± 0.1
LoVo	8.5 ± 2.6	4.0 ± 1.7	5.4 ± 0.9	1.3 ± 0.2	4.8 ± 0.5	0.1 ± 0.0	78.4 ± 6.7	8.3 ± 0.8	2.8 ± 0.2
LS174T	2.7 ± 0.3	0.6 ± 0.3	3.3 ± 1.0	0.4 ± 0.1	2.6 ± 1.2	0.0 ± 0.0	67.1 ± 26.1	6.8 ± 2.6	1.7 ± 0.6
LS411N	11.5 ± 1.9	8.8 ± 1.6	7.0 ± 1.0	0.8 ± 0.1	6.3 ± 1.2	0.2 ± 0.0	28.7 ± 6.0	3.5 ± 0.7	2.2 ± 0.4
SW1116	16.4 ± 2.0	12.1 ± 1.9	12.9 ± 1.5	0.8 ± 0.1	7.3 ± 0.7	0.2 ± 0.0	114.8 ± 12.4	7.0 ± 0.6	2.1 ± 0.2
SW48	8.7 ± 3.1	8.3 ± 3.2	5.4 ± 2.2	0.6 ± 0.3	2.9 ± 1.3	0.1 ± 0.0	27.8 ± 10.8	1.1 ± 0.4	1.6 ± 0.7
SW480	23.4 ± 2.2	21.7 ± 2.5	11.4 ± 0.9	1.4 ± 0.1	9.8 ± 1.1	0.1 ± 0.0	53.0 ± 4.5	9.4 ± 0.9	2.3 ± 0.1
SW620	5.0 ± 3.0	1.2 ± 0.6	7.2 ± 5.5	0.8 ± 0.7	4.1 ± 3.5	0.1 ± 0.1	80.5 ± 69.2	11.0 ± 9.4	2.0 ± 1.7
SW837	9.3 ± 1.5	5.7 ± 0.7	4.8 ± 0.9	0.7 ± 0.1	2.4 ± 0.5	0.1 ± 0.0	31.1 ± 3.8	0.9 ± 0.1	1.1 ± 0.2
T84	14.8 ± 4.1	15.8 ± 3.9	3.9 ± 1.4	0.6 ± 0.2	3.4 ± 1.2	0.1 ± 0.0	44.2 ± 15.6	0.9 ± 0.4	1.2 ± 0.4
TC71	4.5 ± 2.4	1.9 ± 1.8	4.5 ± 1.2	0.5 ± 0.1	2.6 ± 0.5	0.0 ± 0.0	21.6 ± 2.1	3.7 ± 0.4	1.2 ± 0.1

* FA content is expressed as the mean absolute of total fatty acids present; µg/million cells ± SD for 3 independent replicates.

Table A5.11. FA profile of DHA ethanol control treated cells expressed as absolute amount

Cell Line	Fatty acid content (µg/million cells)*								
	PA	SA	OA	LA	AA	LNA	EPA	DPA	DHA
CaCo-2	20.7 ± 4.5	13.7 ± 2.5	15.4 ± 4.2	1.5 ± 0.4	9.7 ± 3.0	0.1 ± 0.0	2.7 ± 1.0	1.0 ± 0.3	4.4 ± 1.4
Colo205	6.6 ± 0.9	3.5 ± 0.5	6.3 ± 0.7	0.5 ± 0.0	2.4 ± 0.3	0.0 ± 0.0	0.9 ± 0.1	0.2 ± 0.0	1.2 ± 0.2
DLD-1	5.2 ± 0.3	3.9 ± 0.2	3.8 ± 0.4	0.5 ± 0.1	2.5 ± 0.4	0.1 ± 0.0	1.1 ± 0.1	0.2 ± 0.0	1.2 ± 0.1
HCA-7	7.9 ± 1.7	4.3 ± 0.8	7.3 ± 1.3	0.5 ± 0.1	2.1 ± 0.5	0.0 ± 0.0	0.6 ± 0.1	0.4 ± 0.1	1.6 ± 0.4
HCT116	3.8 ± 1.1	1.1 ± 0.4	4.1 ± 0.7	0.5 ± 0.1	2.7 ± 0.4	0.0 ± 0.0	1.1 ± 0.3	0.3 ± 0.1	1.5 ± 0.3
HRT18	11.7 ± 0.5	10.9 ± 0.9	9.4 ± 0.5	1.0 ± 0.1	5.8 ± 0.6	0.1 ± 0.0	1.6 ± 0.1	0.6 ± 0.0	2.8 ± 0.3
HT29	4.8 ± 1.1	2.6 ± 1.0	4.6 ± 0.7	0.5 ± 0.1	2.6 ± 0.4	0.1 ± 0.0	1.2 ± 0.2	0.2 ± 0.0	1.3 ± 0.2
LoVo	4.1 ± 0.9	1.6 ± 0.4	3.8 ± 0.6	0.8 ± 0.1	4.6 ± 0.7	0.0 ± 0.0	1.5 ± 0.2	0.5 ± 0.1	2.7 ± 0.3
LS174T	3.0 ± 2.2	1.5 ± 1.6	3.1 ± 0.7	0.3 ± 0.1	2.1 ± 0.2	0.0 ± 0.0	0.6 ± 0.0	0.3 ± 0.0	1.2 ± 0.1
LS411N	9.1 ± 2.3	6.0 ± 1.5	8.7 ± 2.4	1.0 ± 0.3	5.0 ± 1.5	0.1 ± 0.0	1.5 ± 0.4	0.6 ± 0.2	2.8 ± 0.9
SW1116	7.9 ± 4.2	6.2 ± 3.1	7.9 ± 4.7	0.5 ± 0.3	3.1 ± 1.9	0.0 ± 0.0	1.4 ± 0.9	0.2 ± 0.1	1.5 ± 0.9
SW48	6.1 ± 0.5	5.4 ± 0.8	5.0 ± 0.4	0.5 ± 0.0	2.9 ± 0.2	0.1 ± 0.0	1.0 ± 0.0	0.3 ± 0.0	1.7 ± 0.2
SW480	13.2 ± 2.5	12.6 ± 2.0	10.0 ± 2.4	1.2 ± 0.3	8.1 ± 2.0	0.1 ± 0.0	2.5 ± 0.6	0.9 ± 0.2	3.5 ± 0.9
SW620	3.1 ± 1.9	0.8 ± 0.6	5.4 ± 2.9	0.5 ± 0.3	2.7 ± 1.6	0.0 ± 0.0	0.9 ± 0.5	0.3 ± 0.2	1.4 ± 0.8
SW837	5.8 ± 0.5	3.5 ± 0.1	3.9 ± 0.5	0.7 ± 0.1	2.2 ± 0.3	0.2 ± 0.0	0.7 ± 0.1	0.1 ± 0.0	1.1 ± 0.1
T84	25.3 ± 20.2	28.4 ± 21.6	7.2 ± 6.4	1.1 ± 1.0	9.0 ± 7.7	0.1 ± 0.1	4.2 ± 3.7	0.4 ± 0.4	3.0 ± 2.6
TC71	4.1 ± 1.0	1.8 ± 1.1	6.0 ± 1.8	0.6 ± 0.0	3.3 ± 0.9	0.0 ± 0.0	1.4 ± 1.0	0.4 ± 0.1	1.7 ± 0.2

* FA content is expressed as the mean absolute of total fatty acids present; µg/million cells ± SD for 3 independent replicates.

Table A5.12. FA profile of 5µM DHA treated cells expressed as absolute amount

Cell Line	Fatty acid content (µg/million cells)*								
	PA	SA	OA	LA	AA	LNA	EPA	DPA	DHA
CaCo-2	17.9 ± 4.5	12.8 ± 2.9	11.4 ± 2.0	1.1 ± 0.2	6.6 ± 1.0	0.1 ± 0.0	3.2 ± 1.0	0.6 ± 0.1	10.7 ± 4.0
Colo205	6.2 ± 0.8	3.5 ± 0.4	5.3 ± 1.1	0.4 ± 0.1	2.0 ± 0.4	0.0 ± 0.0	1.4 ± 0.3	0.2 ± 0.0	2.3 ± 0.5
DLD-1	6.0 ± 0.3	4.6 ± 0.8	3.8 ± 0.5	0.5 ± 0.1	2.5 ± 0.3	0.1 ± 0.0	1.9 ± 0.2	0.2 ± 0.0	3.4 ± 0.5
HCA-7	8.5 ± 0.7	4.8 ± 0.2	7.4 ± 0.9	0.5 ± 0.0	2.0 ± 0.2	0.0 ± 0.0	0.8 ± 0.1	0.3 ± 0.0	3.8 ± 0.5
HCT116	4.0 ± 1.5	1.0 ± 0.4	4.7 ± 1.7	0.6 ± 0.2	3.1 ± 0.7	0.0 ± 0.0	1.7 ± 0.3	0.3 ± 0.1	4.5 ± 0.9
HRT18	8.8 ± 2.4	8.1 ± 2.3	7.0 ± 2.1	0.7 ± 0.2	3.9 ± 1.2	0.1 ± 0.0	1.4 ± 0.5	0.3 ± 0.1	4.6 ± 1.4
HT29	5.0 ± 1.0	2.9 ± 0.5	3.9 ± 1.0	0.4 ± 0.1	2.2 ± 0.5	0.1 ± 0.0	1.3 ± 0.3	0.2 ± 0.0	2.5 ± 0.5
LoVo	4.7 ± 0.9	1.8 ± 0.3	4.4 ± 0.8	1.0 ± 0.2	5.3 ± 1.0	0.0 ± 0.0	2.4 ± 0.4	0.6 ± 0.1	7.2 ± 1.4
LS174T	1.5 ± 0.3	0.5 ± 0.1	2.4 ± 0.4	0.3 ± 0.0	1.9 ± 0.3	0.0 ± 0.0	0.6 ± 0.1	0.2 ± 0.0	2.6 ± 0.6
LS411N	11.2 ± 3.1	8.0 ± 2.1	8.9 ± 2.1	1.0 ± 0.3	4.8 ± 1.1	0.1 ± 0.0	1.9 ± 0.4	0.5 ± 0.1	5.3 ± 1.2
SW1116	10.0 ± 2.2	7.9 ± 2.2	10.1 ± 1.9	0.6 ± 0.1	3.7 ± 0.8	0.0 ± 0.0	2.3 ± 0.4	0.2 ± 0.0	4.3 ± 0.8
SW48	5.6 ± 1.5	4.8 ± 1.5	3.9 ± 1.1	0.4 ± 0.1	2.1 ± 0.6	0.1 ± 0.0	0.9 ± 0.2	0.2 ± 0.1	2.8 ± 0.7
SW480	17.9 ± 2.5	17.7 ± 2.2	12.0 ± 1.2	1.5 ± 0.1	9.4 ± 1.4	0.1 ± 0.0	5.9 ± 0.7	0.9 ± 0.1	9.1 ± 1.0
SW620	5.1 ± 5.3	1.9 ± 2.4	5.5 ± 3.1	0.5 ± 0.2	2.5 ± 1.3	0.0 ± 0.0	0.8 ± 0.4	0.3 ± 0.1	2.9 ± 1.3
SW837	5.3 ± 1.9	3.1 ± 1.0	3.5 ± 1.3	0.6 ± 0.2	1.9 ± 0.7	0.1 ± 0.1	0.7 ± 0.2	0.1 ± 0.0	2.0 ± 0.8
T84	11.2 ± 1.3	12.7 ± 1.6	3.4 ± 0.5	0.5 ± 0.1	4.1 ± 0.7	0.1 ± 0.0	2.4 ± 0.5	0.2 ± 0.0	3.0 ± 0.5
TC71	3.7 ± 1.6	1.6 ± 1.1	4.7 ± 1.2	0.5 ± 0.1	2.6 ± 0.9	0.0 ± 0.0	1.4 ± 0.8	0.3 ± 0.0	3.6 ± 1.1

* FA content is expressed as the mean absolute of total fatty acids present; µg/million cells ± SD for 3 independent replicates.

Table A5.13. FA profile of high concentration DHA treated cells expressed as absolute amount

Cell Line	Fatty acid content (µg/million cells)*								
	PA	SA	OA	LA	AA	LNA	EPA	DPA	DHA
CaCo-2	23.7 ± 8.4	16.5 ± 5.7	12.7 ± 4.3	1.2 ± 0.3	7.3 ± 1.9	0.1 ± 0.0	6.3 ± 1.9	0.8 ± 0.2	36.9 ± 12.4
Colo205	8.8 ± 2.7	5.2 ± 1.2	7.3 ± 2.7	0.6 ± 0.2	2.7 ± 1.0	0.1 ± 0.0	1.9 ± 0.7	0.2 ± 0.1	3.1 ± 1.0
DLD-1	4.9 ± 2.0	4.1 ± 1.6	2.5 ± 1.1	0.3 ± 0.1	1.7 ± 0.7	0.1 ± 0.0	1.6 ± 0.7	0.1 ± 0.0	5.4 ± 2.3
HCA-7	6.5 ± 1.4	3.7 ± 0.7	4.8 ± 0.7	0.3 ± 0.1	1.3 ± 0.2	0.0 ± 0.0	1.4 ± 0.3	0.3 ± 0.0	5.5 ± 0.9
HCT116	3.4 ± 1.1	1.1 ± 0.5	3.0 ± 0.6	0.4 ± 0.1	2.2 ± 0.2	0.0 ± 0.0	2.3 ± 0.1	0.3 ± 0.0	10.0 ± 0.8
HRT18	13.5 ± 3.1	13.2 ± 3.2	8.1 ± 2.2	0.8 ± 0.2	4.7 ± 1.1	0.1 ± 0.0	2.3 ± 0.5	0.4 ± 0.1	21.6 ± 5.9
HT29	5.5 ± 1.2	3.6 ± 1.5	3.7 ± 0.4	0.4 ± 0.0	2.0 ± 0.2	0.1 ± 0.0	1.3 ± 0.1	0.2 ± 0.0	12.5 ± 2.5
LoVo	7.3 ± 1.6	3.0 ± 0.7	5.6 ± 1.2	1.3 ± 0.4	7.2 ± 1.7	0.1 ± 0.0	4.6 ± 1.1	0.7 ± 0.2	22.0 ± 5.7
LS174T	1.8 ± 0.5	0.6 ± 0.2	2.6 ± 0.2	0.3 ± 0.0	2.0 ± 0.1	0.0 ± 0.0	1.8 ± 0.1	0.3 ± 0.0	28.3 ± 2.1
LS411N	14.0 ± 2.1	10.9 ± 2.3	8.4 ± 1.0	0.9 ± 0.1	4.6 ± 0.5	0.1 ± 0.0	3.2 ± 0.4	0.5 ± 0.1	20.5 ± 1.7
SW1116	8.3 ± 1.2	6.7 ± 1.2	6.3 ± 0.7	0.3 ± 0.0	2.1 ± 0.3	0.0 ± 0.0	2.1 ± 0.3	0.1 ± 0.0	16.3 ± 3.2
SW48	5.7 ± 0.9	5.1 ± 0.5	3.4 ± 0.9	0.4 ± 0.1	1.8 ± 0.5	0.1 ± 0.0	1.6 ± 0.4	0.2 ± 0.0	7.2 ± 1.7
SW480	15.5 ± 3.3	15.8 ± 2.7	8.3 ± 2.1	1.5 ± 0.1	6.8 ± 1.8	0.1 ± 0.0	6.2 ± 1.7	0.7 ± 0.2	16.6 ± 4.3
SW620	2.8 ± 1.1	0.8 ± 0.3	4.6 ± 2.8	0.4 ± 0.2	2.2 ± 1.5	0.0 ± 0.0	1.5 ± 1.0	0.2 ± 0.1	8.3 ± 5.6
SW837	6.9 ± 1.1	3.9 ± 0.7	4.2 ± 1.0	0.6 ± 0.2	2.0 ± 0.6	0.2 ± 0.0	1.1 ± 0.3	0.1 ± 0.0	8.5 ± 2.6
T84	16.3 ± 0.7	19.8 ± 1.7	3.6 ± 1.5	0.5 ± 0.2	3.7 ± 1.6	0.1 ± 0.0	2.1 ± 1.1	0.2 ± 0.1	6.8 ± 3.1
TC71	13.6 ± 5.3	5.7 ± 3.9	13.5 ± 1.8	1.4 ± 0.6	8.4 ± 5.2	0.1 ± 0.0	6.6 ± 4.9	0.8 ± 0.4	33.3 ± 11.4

* FA content is expressed as the mean absolute of total fatty acids present; µg/million cells ± SD for 3 independent replicates.

A5.6. DPA and DHA content at following treatment with ethanol carrier control and 5μM EPA

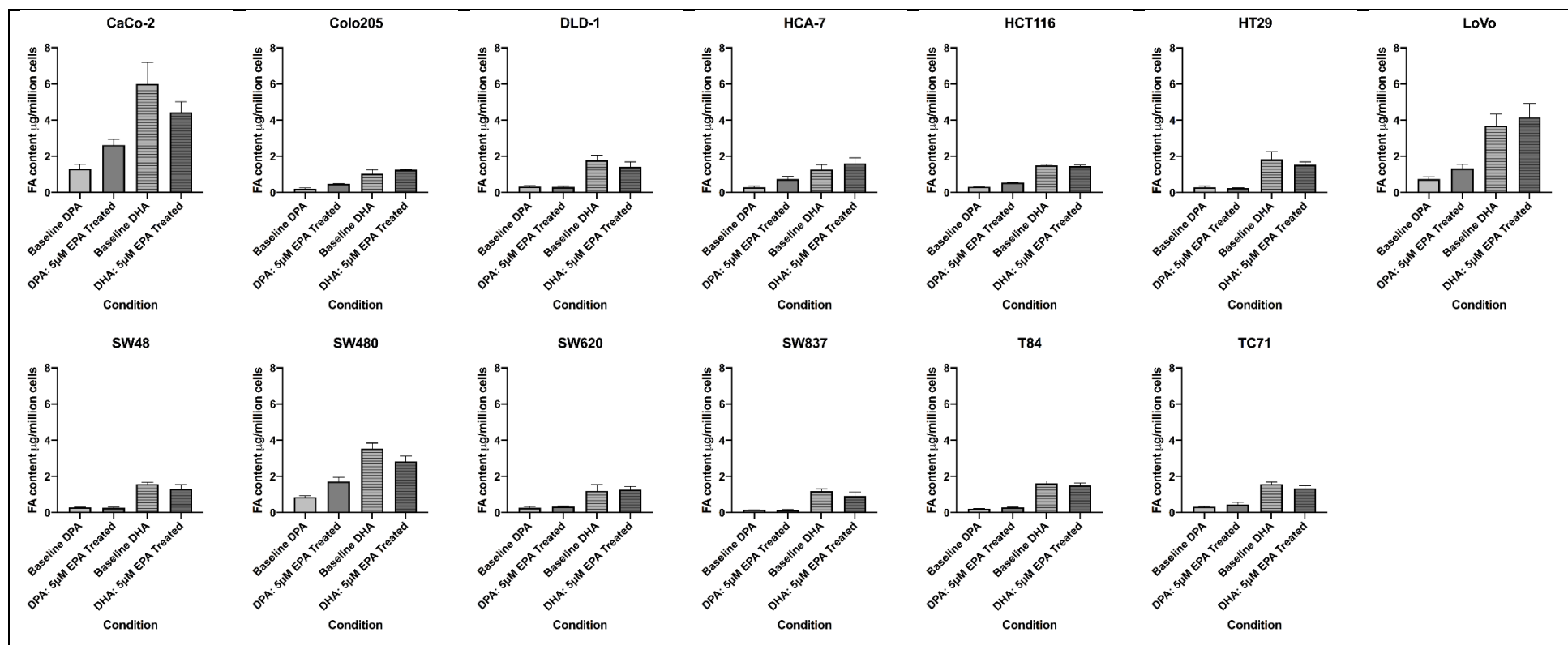


Figure A5.5 Absolute content of DPA and DHA following treatment with ethanol carrier and 5 μM EPA

DPA content following treatment with EPA carrier , 5 μM EPA and DHA content following treatment with DHA carrier and 5 μM EPA . All FA content is expressed as mean \pm SD μg per million cells, for 3 independent replicates.

A5.7. Statistical analysis of FA content analysis by molecular subgroup and following DAC exposure

Table A5.14. Differences in *n*-3 PUFA content of carrier and 5μM EPA (or 5μM DHA) treated CRC cells between molecular subtypes

Cell Treatment	<i>n</i> -3 Content	<i>P</i> value (Mann-Whitney)		
		CIN- vs CIN+	MSS vs MSI	CIMP- vs CIMP+
EPA ethanol control treated	EPA	0.37	0.14	0.06
5μM EPA treated	EPA	0.33	0.41	0.12
EPA ethanol control treated	DPA	0.13	0.08	0.30
5μM EPA treated	DPA	0.48	0.19	0.12
EPA ethanol control treated	DHA	0.41	0.44	0.12
5μM EPA treated	DHA	0.49	0.31	0.08
DHA ethanol control treated	DHA	0.44	0.44	0.08
5μM DHA treated	DHA	0.48	0.24	0.08

Table A5.15. Differences in *n*-3 PUFA content of carrier, DAC, EPA, and combined DAC + EPA treated HCT116 and LS174T cells

Treatment	<i>P</i> value (t-test)					
	HCT116: EPA content	HCT116: DPA content	HCT116: DHA content	LS174T: EPA content	LS174T: DPA content	LS174T: DHA content
Carrier control v 1μM DAC	0.08	0.10	0.10	0.38	0.35	0.33
Carrier control v 5μM EPA	0.0006	0.005	0.06	0.0009	0.03	0.36
Carrier control v 1μM DAC + 5μM EPA	0.005	0.04	0.06	0.005	0.48	0.27
5μM EPA v 1μM DAC + 5μM EPA	0.015	0.02	0.40	0.12	0.22	0.20

A6.1. Fluorescence Activated Cell Sorting: GFP gating

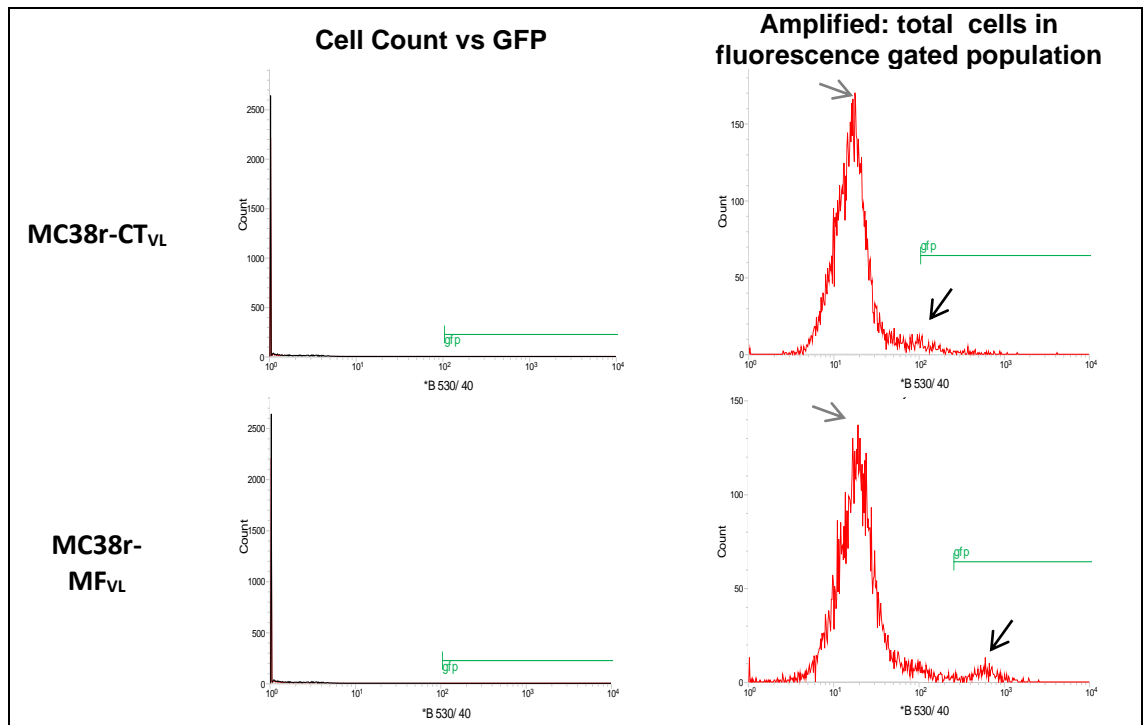


Figure A6.1 eGFP gating in MC38r stable transfectants

MC38r cells had fluorescence detectable in 3% of the population, but with a 1-2 log shift in measured fluorescence in transfected cells in relation to untransfected MC38r cells. Peaks in fluorescence (B530/40) are highlighted on the plots below in grey (untransfected cells) and in transfected cells with black arrows.

A6.2. RNA quantity and RT-qPCR output data for HEK293 clones

Table A6.1. RNA quantity and RT-qPCR output data of HEK293 stable clones

Sample	mRNA quality, purity, and transcript expression					
	ng/ μ l	260/280	β -Actin C_T	<i>Mrgprf</i> C_T	ΔC_T	RQ
HEK293	487.5 297.2 299.5 401.7	2.10 2.10 2.10 2.07	17.9 ± 1.6	30.5 ± 2.1	13.5 ± 1.0	1.0
HEK293-CT _v *	240.1	2.10	18.4 ± 1.1	31.1 ± 2.0	11.2 ± 1.8	4.2 ± 4.9
HEK293-M _v *	305.1	2.10	17.9 ± 1.5	16.3 ± 1.2	-1.7 ± 0.7	49554 ± 34139
HEK293-CT _{vL} B3	387.9 427.1 327.1	2.10 2.09 2.10	17.1 ± 0.3	30.0 ± 1.4	12.9 ± 1.1	1.8 ± 1.7
HEK293-CT _{vL} B4	230.4 346.4 223.3	2.07 2.04 2.03	18.2 ± 0.3	34.4 ± 1.3	16.2 ± 0.7	0.4 ± 0.1
HEK293-CT _{vL} B9	527.0 204.1 516.6	2.07 2.08 2.10	18.7 ± 0.2	30.6 ± 0.3	11.9 ± 0.1	2.1 ± 1.7
HEK293-MF _{vL} A6	318.5 510.6 381.1 361.9	2.10 2.10 2.09 2.08	18.0 ± 1.3	17.9 ± 1.1	-0.1 ± 1.9	37563 ± 33572
HEK293-MF _{vL} C1	372.8 162.4 179.1	2.10 2.10 2.09	16.9 ± 0.1	18.0 ± 0.6	1.1 ± 1.5	25848 ± 16140
HEK293-MF _{vL} C3	518.3 1367.8 477.1 361.1	2.10 2.10 2.10 2.08	17.5 ± 0.9	15.5 ± 1.2	-2.0 ± 0.7	48227 ± 36129
HEK293-MF _{vL} C8	626.4 238.1 542.2	2.08 2.10 2.09	18.4 ± 0.2	18.4 ± 2.3	-0.1 ± 2.1	46536 ± 35650

RNA was extracted from HEK293 and transfected clones and was measured on the NanoDrop. The results are displayed as a concentration; ng/ μ l, with purity shown by the 260/280 ratio. C_T and RQ are shown as mean \pm SD for 3 independent samples with the exception samples denoted with (*) in which transcript levels were measured for one sample over 3 experimental repeats.

A6.3. Assessing whether EPA stimulation of MRGPRF clones induced cAMP signalling

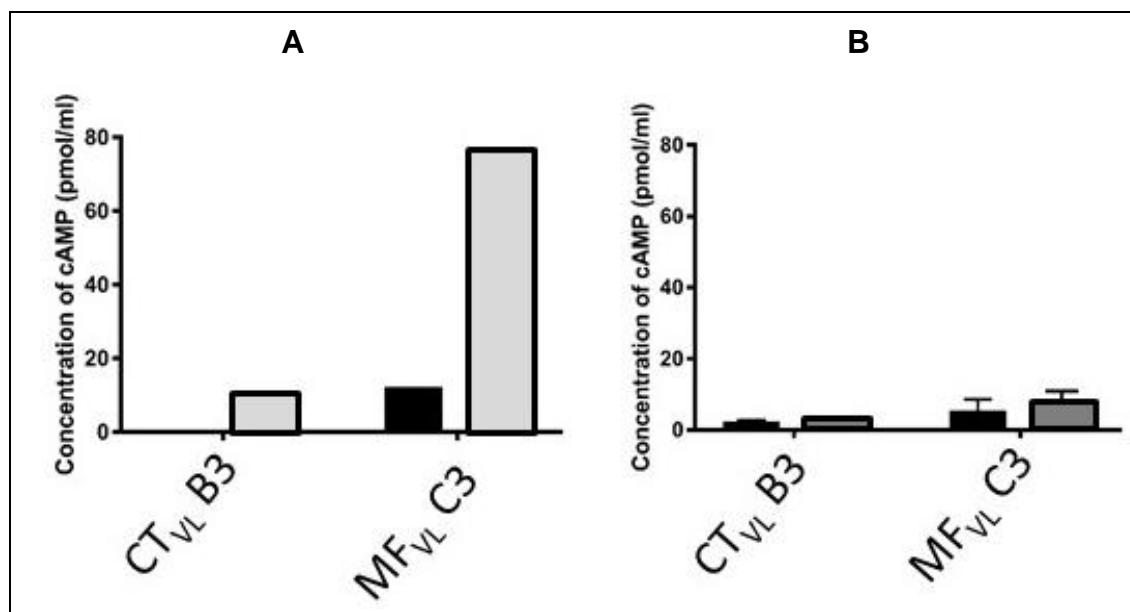


Figure A6.2 cAMP production in stable transfectants

ELISAs to detect presence of cAMP were completed by Jordan Appleyard and Harriet Beal.

A: HEK293-CT_{VL} clone B3 and HEK293-M_{VL} clone C3 produce cAMP, with MF_{VL} C3 producing a greater amount in presence of 10 μ M forskolin (grey) compared to DMSO carrier control (black) and compared to CT_{VL} B3. Forskolin is a pharmacological agent often used to study cAMP production as it activates adenylyl cyclase in a rapid and reversible manner. B: No cAMP response was observed when HEK293 stable clones were treated with ethanol control (black) and 75 μ M EPA (grey) as no increase in cAMP concentration was shown.